LASER SURFACE TREATMENT OF NYLON 6,6 FOR THE MODIFICATION OF WETTABILITY CHARACTERISTICS AND SUBSEQUENT ENHANCEMENT OF OSTEOBLAST CELL RESPONSE

by

David Garreth Waugh (MPhys., MSc.)

A Doctoral Thesis

Submitted in fulfillment of the requirements
for the award of

Doctor of Philosophy

of Loughborough University

June 2010

Wolfson School of Mechanical and Manufacturing Engineering
Loughborough University

Certificate of Originality

This is to certify that I am responsible for the work submitted in this thesis, that the original work is my own except as specified in acknowledgments or in footnotes, and that neither the thesis nor the original work contained therein has been submitted to this or any other institution for a degree.

…… (Signed)

…… (Date)

Abstract

The control of cell adhesion to synthetic polymers is a key factor in tissue engineering, resting on the ability to direct specific cell types to adhere and proliferate in order to stimulate tissue reconstruction. But often the surface properties are compromised for the sake of the bulk properties, leading to surfaces that do not support sufficiently the level of bioactivity required and accordingly the polymeric biomaterial will fail clinically. Laser treatment offers a unique means of enhancing the osteoblast cell response of the surface of a polymeric biomaterial, whilst keeping the already sufficient bulk properties intact. To this end, infra-red (IR) and ultraviolet (UV) lasers have been employed to modify the wettability characteristics of nylon 6,6, as wetting is often the primary factor dictating the adhesion and bonding potential of materials, as a route to enhancing the surface in terms of osteoblast cell response. What is more, modifying wettability characteristics in this way is a highly attractive means of estimating the biofunctionality of a polymer.

IR (CO_2) and UV (F_2 and KrF excimer) lasers were employed to carry out two different processes: laser whole area irradiative processing and laser-induced patterning. With both CO_2 and the excimer lasers changes in the wettability characteristics could be effected with subsequent enhancement of osteoblast cell response. This was also the case with both laser-induced patterning and laser whole area irradiative processing. Essentially, an approach has been established whereby the osteoblast cell response on the surfaces of laser treated nylon 6,6 can be predicted through the laser-induced wettability characteristics modification, particularly for the laser whole area irradiative processed nylon 6,6. This ultimately allows one to determine the osteoblast cell response of the laser surface treated nylon 6,6 surfaces directly from the laser operating parameters.

In concurrence with established wetting theory the laser whole area irradiative processing of the nylon 6,6 surfaces caused increased surface roughness, increased surface oxygen content, increased polar component, γ^P, and increased total surface energy, γ^T; thereby generating surfaces displaying reduced contact angle, θ, making the nylon 6,6 surfaces more hydrophilic. The laser-induced patterned samples differed from current theory insofar as the nylon 6,6 surfaces became less hydrophilic due to an increase in θ despite an increase in surface roughness, an increase in surface oxygen content, an increase in γ^P and an increase in γ^T. This phenomena can be explained by the transition in wetting regimes from a Wenzel regime to a mixed-state wetting regime. Nevertheless, collation of the wettability characteristics results revealed that θ was a strong correlative decreasing function of both γ^P and γ^T, indicating that surface energy played a large role in determining the wetting nature of the nylon 6,6.

It was found that for all laser whole area irradiative processed nylon 6,6 surfaces the osteoblast cell response was an increasing correlative and therefore predictive function of θ and was a decreasing function of γ^P. To an extent, the surface oxygen content and surface roughness could be used indirectly to foretell the osteoblast cell response of the nylon 6,6 surfaces. This is on account of the CO_2 and KrF excimer laser whole area irradiative processing bringing about increased surface

toxicity, which above a certain level hindered the osteoblast cell response. For the laser-induced patterned nylon 6,6 samples there did not appear to be any particular correlative trend between the modified surface parameters and osteoblast cell response. This can be accounted for by the transition in wetting regimes. Another important factor is that cell morphologies were modulated over all samples which suggests that varying surface parameters on account of laser surface treatment gave rise to variations in cell signaling.

It was determined that θ, γ^P and γ^T all had very strong correlative relationships with the cytotoxicity. The cytotoxicity reduced upon an increase in θ until a minimum constant was achieved, whereas the cytotoxicity remained constant at low γ^P and γ^T until a point at which the cytotoxicity began to increase. These results are noteworthy as they allow one to deduce that, with constant cytotoxicity levels, the osteoblast cell response appeared to be modulated by the wettability characteristics. But once the cytotoxicity increased, the toxicity began to dominate and so negated the identified positive wettability characteristic correlations with osteoblast cell response. Practically, the surface roughness and surface oxygen content could be implemented indirectly to estimate the cytotoxicity. Increase in cytotoxicity was the result of the laser processing with higher fluences generating excessive melting. As a result of this, it is possible to deduce that there was a maximum threshold fluence, beyond which the toxicity of the nylon 6,6 began to dominate, giving rise to a less enhanced osteoblast cell response.

On account of the correlative trends which have been identified between the laser surface treatment, wettability characteristics and osteoblast cell response of nylon 6,6 it is likely for one to have the ability to estimate the osteoblast cell response *in vitro*. This is significant as it indicates that laser surface modification of polymeric materials could have tremendous potential for application within the field of regenerative medicine.

Acknowledgements

I would like to thank my supervisor, Dr. Jonathan Lawrence and our collaborators Directed Light Inc., East Midlands NHS Innovation Hub, Nobel Biocare and Photomachining Inc. for all of their much appreciated help and support.

I would also like to thank the University of Hull, Cardiff University, Manchester University and Exeter University for accommodating me by giving access to equipment without which wouldn't have allowed me to complete my research.

I greatly acknowledge the Access to Research Equipment Initiative funded by the EPSRC, (grant number EP/F019823/1). Furthermore, I would like to thank the EPSRC for financially supporting my research (grant number EP/E046851/1).

Lastly but by no means least, I thank my family, in particular Diana, my Parents, my Brother and my Nana whose love and support has helped me get through the last three years.

List of Publications

Conference Papers

1. Waugh D.G., Lawrence J., Walton C.D., Zakaria R.B., (2008) Investigation into the efficacy of CO_2 lasers for modifying the factors influencing biocompatibility of a polymeric biomaterial in comparison with an F_2 excimer laser. *ICALEO 2008 Proceedings*, Pechanga, CA, USA.

2. Waugh D.G., Lawrence J. (2008) Wettability characteristics variation of nylon 6,6 by means of CO_2 laser generated surface patterns. *ICALEO 2008 Proceedings*, Pechanga, CA, USA.

3. Waugh D.G., Lawerence J., Morgan D.J. (2009) Investigation into time dependant degradation and atmospheric conditions on the wettability of nylon 6,6 which has undergone CO2 laser surface modification. *ICALEO 2009 Proceedings*, Orlando, FL, USA.

4. Waugh D.G., Lawrence J. (2009) Wettability characteristics variation of PMMA by means of CO2 laser generated surface patterns. *ICALEO 2009 Proceedings*, Orlando, FL, USA.

5. Waugh D.G., Lawrence J. (2010) Wettability analysis of CO_2 laser surface patterned nylon 6,6 samples soaked in simulated body fluid (SBF). **Submitted to and accepted** *MATADOR 2010*, Manchester, Lancashire, UK.

6. Waugh D.G., Lawrence J. (2010) A comparative study between large area and CO_2 laser patterning of nylon 6,6 and the effect thereof on osteoblast cell response in relation to wettability. S**ubmitted to and accepted** *ICALEO 2010*, Anaheim, CA, USA.

7. Waugh D.G., Lawrence J. (2010) Using UV laser surface treatment to modify the wettability of polyamide 6,6 and its effects on cytotoxicity and alkaline leukocyte phosphatase activity of osteoblast cells. **Submitted to and accepted** *ICALEO 2010*, Anaheim, CA, USA.

Journal Papers

1. Waugh D.G., Lawrence J., Morgan D.J., Thomas C.L. (2009) Interaction of CO_2 laser-modified nylon with osteoblast cells in relation to wettability. *Materials Science and Engineering C* **29** 2514-2524.

2. Waugh D.G., Lawrence J., Walton C.D., Zakaraia R.B. (2009) On the effects of using CO_2 and F_2 lasers to modify the wettability of a polymeric biomaterial. *Optics and Laser Technology* **42** 347-356.

3. Waugh D.G., Lawrence J. (2010) On the use of CO_2 laser induced surface patterns to modify the wettability of poly(methyl methacrylate) (PMMA). *Optics and Lasers in Engineering* **48** 707-715.

4. Waugh D.G., Lawrence J. The effect of infra-red (IR) laser surface treatment of nylon 6,6 on cytotoxicity and alkaline leukocyte phosphatase (ALP) activity of osteoblast cells. *Colloids and Surfaces B: Biointerfaces*, **submitted 15/03/10**.

5. Waugh D.G., Lawrence J. (2010) The enhancement of biomimetic apatite coatings by means of KrF excimer laser surface treatment of nylon 6,6. *Lasers in Engineering*, **submitted 20/03/10.**

6. Waugh D.G., Lawrence J. (2010) A comparative study of CO_2 laser patterning and whole area processing of nylon 6,6 and the effects on wettability and osteoblast cell response. *Journal of Biomedical Materials Research B: Applied Biomaterials*, **submitted 28/04/2010**.

7. Waugh D.G., Lawrence J. (2010) Wettability modification of nylon 6,6 via CO_2 laser surface treatment and the effects thereof on biomimetic apatite coatings. *Journal of Biomedical Materials Research A*, **submitted 05/05/2010**.

8. Waugh D.G., Lawrence J. (2010) The modulation of cytotoxcity and alkaline leukocyte phosphatase (ALP) activity of osteoblast cells seeded onto excimer laser surface treated polyamide 6,6. *Cell Death and Differentiation*, **submitted 28/05/2010.**

9. Waugh D.G., Lawrence J. (2010) A comparative study into modifying the biofunctionality of nylon 6,6 by means of excimer laser processing. *Journal of Biomaterial Applications*, **submitted 28/05/2010**.

Books

1. Waugh D.G., Lawrence J. (2010) *Chapter 10 - Laser Surface Processing of Polymeric Materials for Biomedical Applications*, In: *Laser Assisted Fabrication of Materials*, **submitted to editor March 2010**.

Table of Contents

PART 1 - LITERATURE REVIEW

PART 2 - METHODOLOGY

PART 3 - POLYMERIC LASER-INDUCED SURFACE MODIFICATION AND WETTABILITY CHARACTERISTICS

PART 4 - BIOACTIVITY OF LASER PROCESSED NYLON 6,6

List of Figures

List of Tables

Glossary of Terms

CO_2 - Carbon dioxide

N_2 - Nitrogen

AFM - Atomic force microscope

ANOVA - Analysis of variance

ArF - Argon fluoride

CO – Carbon monoxide

cw - Continuous wave

DBD - Dielectric barrier discharge

DLC - Diamond-like carbon

DLVO - Derjauim Landau Verwey Overbek

DOE - Diffractive optical element

e - Electron

EB - Electron beam

EDX - Energy-dispersive X-ray spectroscopy

FIB - Focused ion beam

HAZ - Heat affected zone

HCN – Hydrogen Cyanide

IAR - Ion assited reaction

IBAD - Ion beam-assisted deposition

IBT - Ion beam texturing

In vitro - Within glass (denotes testing without living organisms)

In vivo - Within living (denotes testing which takes place inside a living organism)

IR - Infra-red

KrF - Krypton fluoride

LB - Langmuir-Blodgett

LSV - Liquid-solid-vapour line

MAPLE - Matrix-assisted pulsed laser deposition

MDW - MAPLE direct write

N.A. - Numerical aperture

Nd:YAG - Neodymium-doped yttrium aluminium garnet

PVC - Polyvinyl chloride

PVD - Pulsed vapour deposition

RFU - Relative fluorescence units

SAMs - Self assembled monolayers

SBF - Simulated body fluid

TCPS - Tissure culture polystyrene

TEM - Transverse electromagnetic

UV - Ultra-violet

XeCl - Xenon chloride

XeF - Xenon fluoride

XPS - X-ray photoelectron spectroscopy

Yb - Ybbertium

Nomenclature

SYMBOL	NAME	SI UNITS
λ	Wavelength	M
ν	Frequency	Hz
τ_c	Temporal coherence	S
M^2	Diffraction limited beam quality	Dimensionless
M_D	Demagnification	%
η	First-order diffraction efficiency	%
α	Absorption coefficient	m^{-1}
F_T	Threshold fluence	Jm^{-2}
t_p	Characteristic pulse duration	s
k_{opt}	Extinction coefficient	Dimensionless
ρ	Density	Kgm^{-3}
ΔT	Temperature rise	K
θ	Contact angle	◦
γ_{sv}	Solid surface energy	Jm^{-2}
γ_{lv}	Liquid surface energy	Jm^{-2}
γ_{sl}/γ^T	Solid-liquid interfacial energy	Jm^{-2}
θ_A	Advancing angle	◦
θ_R	Receding angle	◦

SYMBOL	NAME	SI UNITS
F_{lsv}	Force along the liquid-solid-vapour line	N
W_{ad} / W_{adv}	Work of adhesion/	Jm^{-2}
W_{im}	Immersion work of adhesion	Jm^{-2}
r_a	Roughness factor	M
θ_w	Characteristic angle for wetting	◦
D_R	Wenzel type roughness parameter	M
F_R	Cassie-Baxter type roughness parameter	M
D_s	Distance to a flat solid surface	M
ΔF_{adh}	Interfacial free energy of adhesion	Jm^{-2}
a	radius	m
Ra	Arithmetical mean roughness	µm
Sa	Mean roughness value over a given area	µm

SYMBOL	NAME	SI UNITS
c	Speed of light in a vacuum	ms^{-1}
D	Thermal diffusivity	m^2s^{-1}
f	Focal length	f
F	Fluence	Jm^{-2}
H	Hamaker constant	J
I	Irradiance	WM^{-2}
R	Surface reflectivity	%
S	Spreading coefficient	Jm^{-2}
t	Time	s
u	Object distance	m
v	Image distance	m
w	Resolution	m
x	Amount of material removed per pulse	m
Z	Depth of focus	m
Z	Depth	m

Introduction

Research Background

Lasers

Numerous laser types have been developed and discovered since the advent of the ruby laser by Maiman in the early 1960s [1]. Two of the main types of laser are the excimer ultra violet (UV) and the infrared (IR) and along with other variations it can be seen that there is a wide choice of operating wavelengths for laser processing of materials. Each type of laser has its own unique advantages and disadvantages in comparison to other laser families including parameters such as pulse duration, operating wavelength and even fundamental parameters such as cost. UV laser (excimer laser) wavelengths range between 10 and 1000 nm with the main UV lasers being: XeF (351 nm), XeCl (308 nm), KrF (248 nm) and ArF (193 nm). Excimer lasers can also be seen to emit in the visible spectrum; however, they typically do emit in the UV spectrum [2]. It has been realized that excimer lasers offer pulsed outputs ranging from 10 to 50 ns with pulse energies ranging between 0.1 and 1 J and repetition rates of up to several hundred hertz have been achieved [1,2]. When taking into account laser processing of materials it can be seen that excimer lasers offer many advantages over other laser types due to the small wavelength and high energies per pulse. For instance it has been seen that for materials processing irradiances of up to 10^{13} Wm^{-2} are required which can easily be achieved using an excimer laser [2]. In addition to this, it should also be noted here that it has been realized that the absorption coefficients are considerably greater for UV wavelengths in comparison to the other laser types on offer. As a result of this, the material dependant absorption depth of the light is shorter for these materials with high absorption coefficients leading to sharper edges being achievable.

There are numerous laser types that can emit in the IR spectrum ranging between 1 µm and 1000 µm, with the main laser types being: carbon dioxide (CO_2) lasers (9.4 to 10.6 µm), Nd:YAG lasers (1.064 µm) and fiber lasers (1.06 to 1.56 µm). One of the main advantages offered by the CO_2 laser is that they can be operated both continuously (cw) and pulsed, with cw powers up to 100 kW and large pulse energies up to 10 kJ [1,2]. It has been seen in industry that CO_2 lasers are extensively used for materials processing as they can be used for an extremely intense heating source that can be applied to a very small area. When using this type of laser in cw mode the materials processing has been determined to be due to thermal interactions in which the laser beam can be seen as a heating or cutting tool. On the other hand pulsed operations give rise to the necessity of irradiances of 10^{13} Wm^{-2} from the laser beam and can be achieved using this type of laser. For Nd:YAG and fiber lasers the parameters and features are a result of the various types of laser structure that can be utilized to produce such a laser. The main variation in structure for this type of laser is the way in which the laser is pumped and has been seen to affect the various laser parameters. Nd:YAG lasers are also used extensively within industry formaterials processing and offer very accurate results due to the fact that the beam can be focused to a very small spot [3].

Laser-Induced Surface Treatment

It has been realized that the wettability of many different materials can be altered by the means of laser-induced surface treatment [4]. This can be done in two main ways; firstly it is possible to change the chemical properties of the sample by allowing the laser beam to melt the surface and allow resolidification to take place and secondly the topography can be varied on either a micro or nano-scale [5] which, as a result, will affect the value of the contact angle, θ [4]. It should be noted here that typically a hydrophylic surface (also known as the Anti-Lotus effect) has a θ with water less than 30° in which the surface can be seen to be 'wet' [6]. In addition, research into the wettability of materials has been increasing over the past years due to the fact that this parameter is usually used as a primary test to estimate whether materials will bond to a substrate sample.

Biomedical Cell Growth

With biotechnology having the potential to improve quality of life it can be seen that there is ever increasing interest in this field with many of those within the industry predicting that growth will lead from the development of inexpensive polymeric biomaterials. It has been seen that there usually has to be a compromise between bulk and surfaces properties when determining the best polymeric materials to use. Where, in most cases the bulk properties are seen more in favour over those surface properties required [4]. As a result of this it has been realized that the surface properties are not sufficient in some situations due to the bioactivity required giving rise to clinical failure of the implant. This results in one being able to see the necessity of changing the surface properties of the polymer enhancing the osteoblast cell response to improve biological cell adhesion and proliferation. When analysing any implant surface it has been seen that there are two main considerations: cell adhesion and blood coagulation [7]. Controlling cell adhesion is an extremely important factor when reconstructing tissue and supporting cellular architecture with the importance resting on how the implant surface can manipulate the appropriate cells. It has been seen through prior research that other methods such as gas plasmas, photochemical techniques and wet chemical etching offer the ability to vary the physiochemical properties of the polymer surface without changing the bulk properties. These various techniques have the ability to improve cell growth and adhesion on polymeric biomaterials; however controlled, precise modification is lacking from the methods named. Laser-induced surface treatment offers the ability to vary the physiochemical surface properties with considerably more control and accuracy in comparison to the other possible techniques resulting in an ever increasing interest in polymeric surface treatment utilizing laser technology.

Research Objectives

The objectives (●) along with sub-objectives (○) for the research project are:

- To determine how the wettability (hydrophilic) characteristics of nylon 6,6 are modified by using various laser parameters such as different wavelengths (UV and IR):
    - Altering the chemical properties of specific polymeric biomaterials by using melting and resolidification techniques.

    - Using various different laser types for surface treatment to achieve micro-scale (using UV and IR lasers) features.
- To determine the correlation between the modified surface wettability characteristics and bioactivity of the nylon 6,6.
    - Investigate into how bioactivity varies on the laser surface treated surfaces by using in vitro testing with osteoblast cells and simulated body fluid (SBF).
    - Allow relationships to be investigated between the various laser parameters, surface parameters and cell response.
- To determine how the biofunctionality of the nylon 6,6 affects cell adhesion and spreading.
    - Achieve quantification of the generic nature of the discovered relationships arising between laser parameters, surface parameters and cell response.

It is possible to see from those objectives set out above that a framework can be established such that each factor of the research can be linked and can be seen in the schematic diagram shown in Figure A.

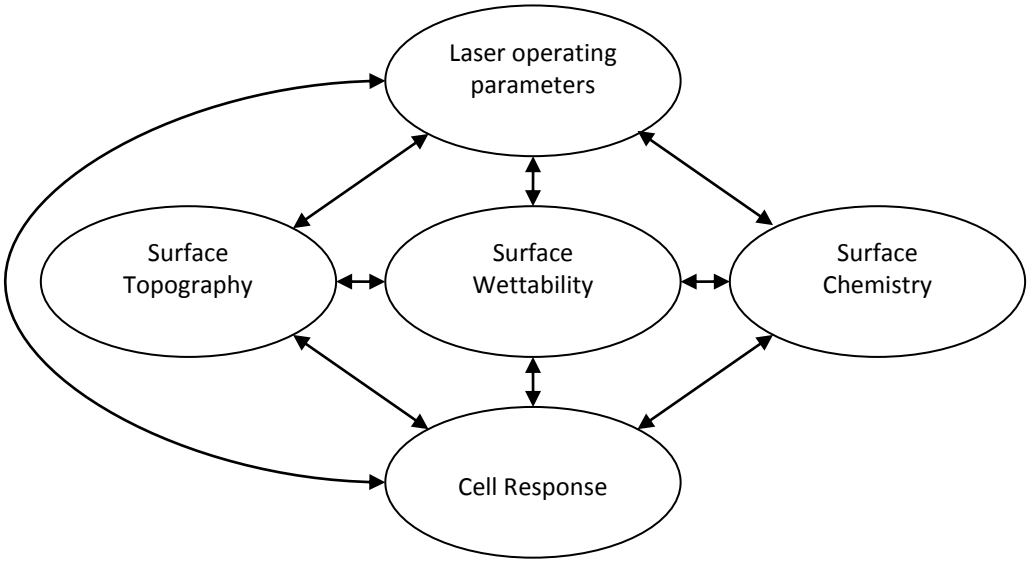

Figure A – Schematic diagram showing the deduced links between the factors arising throughout the research.

By achieving these objectives stated, it may be possible to determine if polymeric surfaces can be produced using laser-induced surface treatment in order to increase the bioactivity and as a result decrease the failure rate of implants to improve the quality of life for those who may require them. In addition to this it may also be possible to ascertain whether a technique could be easily repeated and cost effective enough to allow the biotechnology industry to undertake the method for producing biocompatible implants.

Thesis Organization

This thesis elaborates on the investigations into the characterization of nylon 6,6 which has undergone various to laser surface treatments. Leading on from this, studies into the biofunctionality of the

polymer are also considered and evaluated. To carry out an organized and efficient evaluation the thesis is set out into five parts which are described in brief below:

Part 1 – Literature Review

This part of the thesis primarily sets out the current state of the biomedical industry in regards to biocompatible implants and laser surface treatment. This allows one to see a comprehensive collection of work carried out by others within this area in previous years including factors such as wettability, bioactivity and alternative techniques to surface modification. In addition, the objectives of the project are set out within this part allowing clear milestones to be determined. This part is covered by Chapters 1, 2, 3 and 4.

Part 2 – Methodology

This part details how the experimentation was carried out to obtain the results given in Parts 3 and 4. This includes the procedures for laser surface modification, use of the white light interferometer (WLI), use of the sessile drop device and the methods implemented for biological testing of the samples. This part is covered by Chapter 5.

Part 3 – Polymeric Laser-Induced Surface Modification and Wettability Characteristics

This part of the thesis will incorporate the experimental research into the wettability characteristics of nylon 6,6 which has undergone various laser surface treatments ranging from different wavelengths employed to using both patterned and large area processing. In particular it has been realized in this part what may be the dominant parameters in terms of driving force for the characteristic wettability of nylon 6,6. This part is covered by Chapters 6, 7, 8, 9 and 10.

Part 4 – Bioactivity of Laser Processed Nylon 6,6

This part of the thesis allows one to see the direct link between the wettability characteristics of a polymeric biomaterial and bioactivity. Through experimentation it has been realized whether various laser types have the ability to improve the biofunctionality of nylon 6,6 by studying the response of osteoblast cells and SBF *in vitro*. Furthermore, links between surface functionalities, topography, wettability and bioactivity are taken into account. Leading on from this an optimum method for improving the bioactivity of the nylon 6,6 is discussed. This part is covered by Chapters 11, 12, 13 and 14.

PART 1 – LITERATURE REVIEW

1
Lasers, Beam Delivery and Irradiation Techniques

This chapter details different laser types that can be implemented in laser materials processing and gives a brief description as to how they are manufactured. Furthermore, this chapter discusses the methods which can be utilized to guide the laser beam to the target material as this can have a large impact on laser-material interactions.

1.1 - Introduction

It has been realized worldwide within the scientific community and various industries that lasers offer major advantages over alternative techniques for materials processing. Some of the main advantages of using a laser for materials processing are:

- Relative cleanliness.
- Accurate processing.
    - Allows much control over the Heat Affected Zone (HAZ) due to the ability of relative precise control over the thermal profile and thermal penetration/absorption.
- Precise placement of the beam onto the target material allowing user specified areas of the target material to be processed.
- Post-processing techniques required are usually minimal.
- Non-contact processing.
- Automation (repeatability) of the various processing techniques using a laser is relatively easy to implement.

There are many applications within materials processing in which lasers can be employed such as welding, drilling, cutting and peening (shock hardening) [8,9]. With a large number of different lasers now commercially available it is possible for one to deduce that almost all materials can be processed using a laser due to the wide range of laser parameters that can be utilized. To visualize the possible processing applications using a laser it is possible to graph the power density/irradiance (Wmm^{-2}) as a function of interaction time as seen in Figure 1.1 [8].

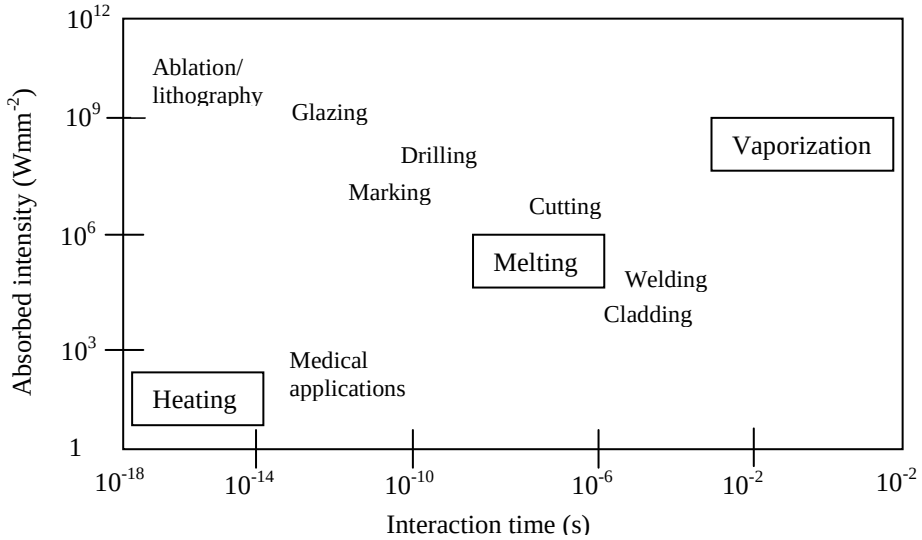

Figure 1.1 – Graphical diagram indicating the laser beam-material interaction spectrum.

Even though lasers offer many advantages over alternative techniques one of the main disadvantages of laser processing is the ability to process large areas of the target material. Allowing the process to be automated would ultimately speed up the processing time; however, this would still hinder this technique to be utilized for large area processing of materials. To attempt and improve on this issue, it should be noted here that in some cases the laser system has been adapted for large area processing for such applications as the production of lens arrays for large visual displays [10,11].

1.2 – Laser Types

With many families of lasers being discovered and developed it can be seen that lasers are usually commonly grouped using the lasing medium. As a result there are three main groups of laser: gas, liquid and solid state. It should also be noted here that there are groups such as excimer lasers which are a sub-group of the gas lasers. A number of laser types will be used for this research and will be discussed in this section to give an understanding and insight into the different aspects of each laser.

1.2.1 – CO_2 Laser (Gas Laser)

The CO_2 laser is one of the most used lasers throughout the scientific world and within many industries due to this laser being one of the most versatile. It is capable of emitting radiation within the IR region of the electromagnetic spectrum on rotational-vibrational transitions with wavelengths ranging from 9 to 11 μm [2]. This laser gives rise to the possibility of operating in either continuous wave (cw) or pulsed using different types of gas discharge configurations. The gases generally used to achieve these configurations are CO_2, N_2 and He with ratios of CO_2:N_2 usually being around 0.8:1 with commonly more helium then nitrogen and gas pressures ranging from 50 to 760 torr [2]. Each gas within this type of laser plays a distinct role to the production of population inversion. The CO_2 is the gas which allows the laser light to be emitted and is firstly excited such that the molecules vibrate

in an asymmetrical stretching mode. After a time the CO_2 molecules begin to lose their excitation energy by dropping to one of two lower vibrational energy states which can be seen to be two of the main principal laser transitions for this system [1]. The nitrogen is utilized within the system to allow more efficient excitation of the CO_2 molecules up to the upper laser level. This is done efficiently due to the fact that the lowest vibrational energy state of the nitrogen molecules is equivalent to that of the upper laser level for the CO_2 molecules giving rise to a high probability of energy transfer between the two different molecules. It should be noted here that the CO_2 molecules can be excited in other ways such as directly absorbing the energy from electrons; however, with the presence of the nitrogen the system becomes considerably more efficient. The Helium on the other hand has two distinct roles to the functioning of the CO_2 laser with the first being that it acts as a buffer gas to aid in heat transfer within the system and secondly to efficiently attempt and relax the CO_2 molecules back down to the ground state in the attempt to achieve efficient population inversion. To fully understand the way in which a CO_2 laser functions it is possible to take an energy level diagram into consideration showing the energy transfers as seen in Figure 1.2.

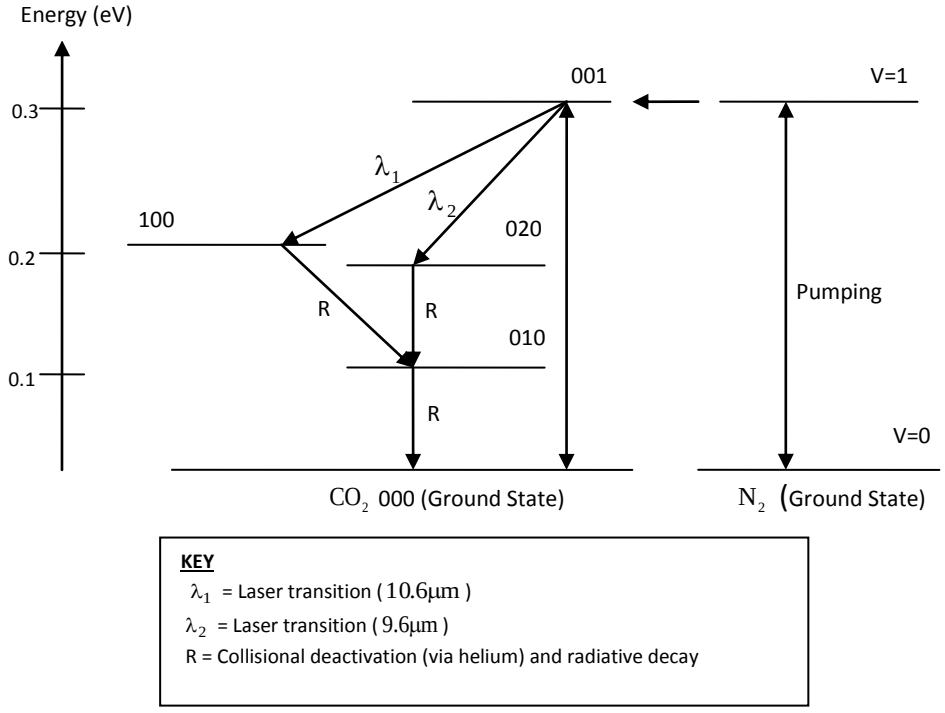

Figure 1.2 – An energy level diagram showing the main energy transfers and laser transitions for the CO_2 laser.

Elaborating on Figure 1.2, it can be seen that the upper laser level excitation can be achieved *via* direct electron collisional excitation in the form:

$$e + CO_2(000) \rightarrow e + CO_2(001)$$

However, this process is not particularly selective giving rise to many other vibrational modes of CO_2 becoming populated. As it has been discussed and can be visualized in Figure 1.2 the lasing process can be made more efficient by vibrational energy transfer from the nitrogen present in the form of:

$$e + N_2(V = 0) \rightarrow e + N_2^*(V = 1,...8)$$
$$N_2^*(V = 1) + CO_2(000) \Leftrightarrow N_2(V = 0) + CO_2(001)$$

The second step in the vibrational energy transfer from the nitrogen is more commonly known as the V-V resonant Transfer and is very selective due to the close coincidence of the nitrogen (V=1) and CO_2 (001) levels allowing very efficient population of the upper laser level. To allow for efficient lasing, the lower level relaxation must be taken into account and in this case the (100) level shares energy rapidly with the (020) level due to the fact that they are mixed-states as a result of a Fermi resonance. From this it can then be seen that the relaxation proceeds via:

$$CO_2(020) + CO_2(000) \rightarrow CO_2(010) + CO_2(010)$$
$$CO_2(010) + He \rightarrow CO_2(000) + He$$

It should be noted here that the deactivation of the (010) state to the (000) ground state is vital for recycling molecules for re-excitation in the attempt to prevent degrading population inversion.

For cw CO_2 lasers, powers of 100 kW and pulse energies of up to 10 kJ can easily be achieved [1,2]. In addition to this there are a number of different laser structures that have been developed for this laser type. These being sealed-off tube, longitudinal flow, waveguide and transversely excited [2]. Due to the versatility and high powers that this laser can achieve it has been implemented for many years in the general field of materials processing from cutting to alloying.

1.2.2 – KrF Laser (Excimer Laser)

The KrF laser or krypton fluoride laser is one of a series of lasers that come under the sub-group of excimer lasers which emit in the ultraviolet (UV) region of the electromagnetic spectrum. The term excimer originates from the contraction of the phrase excited dimer in which is a term given to a molecule that consists of two identical atoms which can only exist in an excited state due to the fact that the ground state lifetime is very short as a result of the repulsive force that arises between the two atoms in the non-excited state. KrF lasers operate at a wavelength of 248 nm with pulse durations ranging between 30 ns and 50 ns, total gas pressures of approximately 2 atmospheres and pulse energies of 0.1 to 1 J [2]. The gas mixtures within the lasing system differ from laser to laser; however, generally the bulk of the gas mixture (90 to 99%) is a buffer gas usually in the form of helium or neon and is used in order to allow for more efficient energy transfer. The buffer gas does not contribute to the actual lasing process but a rare gas and a halogen donor gas are present to give rise to the process in which the concentrations are very small at approximately 1 to 9% for the rare gas and 0.1 to 0.2% for the halogen donor gas [1]. It should be noted here that for these lasers to function efficiently it has been realized that a pre-ionization pulse is required to provide the initial electrons in the region between the two electrodes. This is done to ensure that there is a uniform excitation allowing the electrical conductivity of the gaseous medium to be increased prior to the lasing process. As discussed for the CO_2 laser it is possible to achieve a more complete understanding of excimer lasers by considering the potential energy diagram for the lasing process as seen in Figure 1.3.

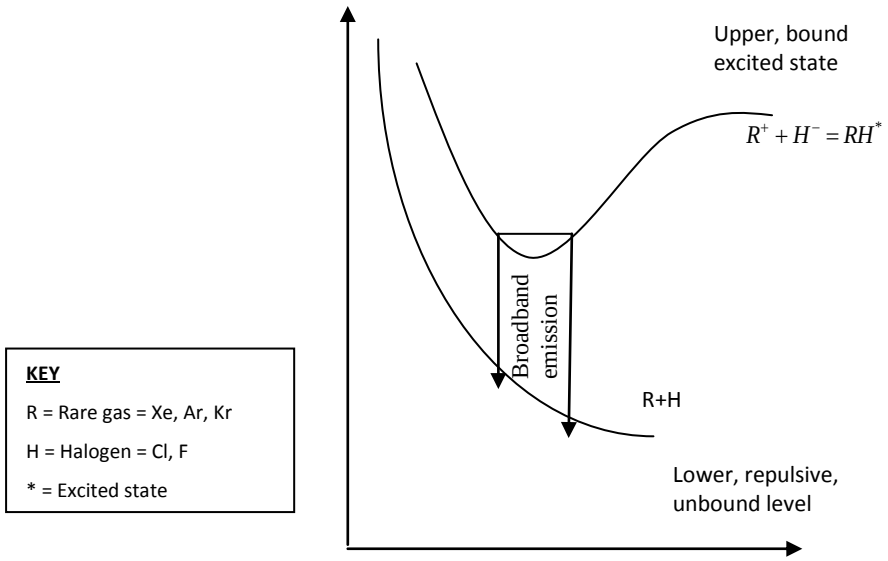

Figure 1.3 – Potential energy diagram for excimer lasers showing the laser transition.

From Figure 1.3 one can seen that the there is a broadband emission at the laser transition allowing a range of photon energies to be emitted. This gives rise to a large frequency band, $\Delta\nu$,and a low temporal coherence, τ_c:

$$\tau_c = \frac{1}{\Delta\nu} \tag{1.1}$$

with τ_c being the time over which the electromagnetic waves associated with the beam oscillate as well defined sine waves of approximate constant amplitude. Due to the UV operating wavelength and high energy per pulse available these lasers have also been employed for materials processing over a number of years but they also have other applications in such areas as medical applications, photolithography and the pumping of dye lasers.

1.2.3 – Other Laser Types

The following laser types are available for use as a laser materials processing tool and as a result have been discussed in brief. However, it should be noted that these lasers offer the least efficiency for surface modification of nylon 6,6 owed to the fact that most polymers are highly transparent around wavelengths of 1 μm.

1.2.3.1 – Nd:YAG Laser (Solid State)

The Nd:YAG laser is one of the most common lasers within the solid state family with a fundamental operating wavelength of 1.064 μm. This type of laser incorporates a four-level system resulting in a low pumping threshold. All solid state lasers which incorporate neodymium crystals rely on light from an external source to excite the Nd atoms to the upper laser levels. Through development of this technology it has been realized that this can be done in three main structures: flashlamp-pumped Q-

switched, flashlamp-Pumped cw and diode-pumped [1-3]. As a result of the compactness and relatively lower cost compared to other laser types it has been seen that Nd:YAG lasers have many applications with one of the major ones being various areas of materials processing such as drilling, spot welding and laser marking. Also, due to the fact that the beam can be focussed to very small spot, applications which require a high degree of accuracy can take advantage of this laser.

1.2.3.2 – Fiber Laser (Solid State)

High power fiber lasers are a relatively new technology and it is being realized that they can be utilized for many applications within the industry of materials processing. For instance, a comprehensive literature review has been produced by Canning [12] on fiber lasers and the related technologies. From this review, Canning found that it is possible for one to see that high power lasers are attractive for use within numerous industries. He also indicated that extensive research had been undertaken to understand the way in which these lasers operate and can also be seen throughout published literature [13-17]. This research has covered many areas of fiber laser technology ranging from large mode area fibers [13,16], to internal thermal effects [14], to the investigation of utilizing different materials for the construction of high power fiber lasers [17]. In addition to this, others have already researched into the possibility of using these high power fiber lasers for welding and cutting various materials; for example, Quintino *et al* [18] have recently carried out preliminary studies to determine the quality of welding pipeline steel with an 8 kW fiber laser.

1.3 – Laser Beam Delivery and Laser Irradiation Techniques

For laser materials processing one of the main important factors within the laser system is the way in which the beam is delivered to the target material in order to achieve the anticipated outcome. Many methods and techniques have been researched and developed in order to achieve this efficiently and effectively. Within this chapter the main techniques for beam delivery and laser irradiation techniques will be discussed allowing one to see the major advantages and disadvantages of each method considered.

1.3.1 – Direct Write, Flying Optics and Scanning Optics

Direct writing requires good quality beams (near TEM_{00}) that hold the ability to be focused for point by point processing. In order to achieve the required processing pattern on the target material either the work piece or the beam itself can be translated; however, both have advantages and disadvantages which need to be taken into account. Moving the beam is more advantageous for heavy bulky target materials, but maintaining the optimum spot size can prove to be problematic as it reduces the overall precision of the laser processing system. This disadvantage can be eliminated if one was to move the workpiece, though; this may give rise to the velocity/acceleration of the system to be limited allowing processing rates to be potentially lower than expected.

In order to translate the beam onto the target material it may be necessary to manipulate the beam using reflection and deflection techniques. One popular technique for doing this is that of

galvanometer scanning. This technique incorporates low mass mirrors that are attached to moving coil rotary actuators (or moving magnet rotary actuators). The angular movement of the mirrors is controlled by computer software and offers very high speed processing. This method, however, can be limited in laser power handling and also has high costs as the scan lens can be expensive if a flat field is required.

Two deflection techniques that can be utilized are that of rotating prisms and rotating polygons. The rotating prisms method involves using a wedge shaped prism that gives angular deflection of the beam. By rotating the prism it can be seen that this causes a circular motion of the beam and using two prisms together would allow more control over the radius of the circular motion. As a result of the motion of the beam that arises it has been found that this technique is usually used for trepanning applications. The rotating polygon method utilizes a highly polished polygon which is rotated at high speeds resulting in the beam being deflected in a scanned line. This technique can be used as pre or post objective scanning and the number of facets, along with rotation rate control ultimately allows the scan and velocity of the system to be controlled. If this rotating polygon method was used in conjunction with movement of the target material then this would allow 2-D scans to be made possible. Both these techniques that incorporate deflection are useful within many applications, yet these systems can require high maintenance by re-alignment to ensure accuracy of the systems.

A reflecting technique that is becoming highly used within materials processing industries is that of flying optics. This method uses two mirrors fixed onto a moving gantry and has the ability to direct the beam in orthogonal directions. As the conjugate ratio of the system is constantly changing specific mirrors or lenses should be incorporated. These are usually deformable mirrors (hydraulic actuators) or zoom lenses. Flying optics are very useful for heavy bulky target materials and the height of the gantry can be controlled by capacitive monitor or triangulation allowing various different sized materials to be processed using this system. This technique can be very efficient for large area processing; however, like the two deflection methods described previously the maintenance required is high due to re-alignment and ensuring that the system is functioning appropriately.

1.3.2 – Large Area Beams, Projection Etching and Masks

Lasers that produce large area beams are not suitable for focusing to a small spot in order to carry out materials processing. Nevertheless, it has been seen that they can be applied in materials processing for illuminating masks (or stencils). This can be done by using a technique known as projection etching where the simplest form can be visualised in Figure 5.

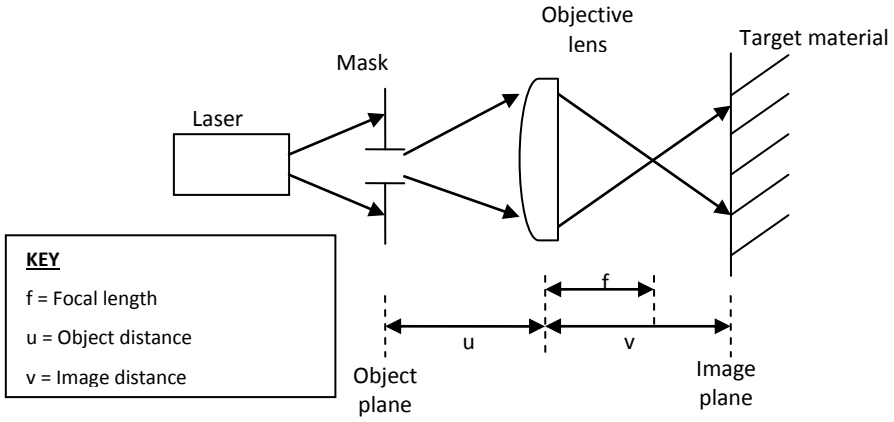

Figure 1.4 – Schematic diagram showing the simplest form of projection etching.

Projection etching, the simplest form as seen in Figure 1.4, is a useful tool to manipulate the beam shape in order to process the target material with the required etch. The three variables (*f, u* and *v*) shown in Figure 5 can be related using the Gaussian Lens Formula seen in Equation (2.1) which is a more simple version of the Lensmakers Formula [19].

$$\frac{1}{f} = \frac{1}{u} + \frac{1}{v} \tag{1.2}$$

where the demagnification, M_D , resolution, *w*, and depth of focus, *z*, of an optical system can be calculated using Equations (1.3), (1.4) and (1.5) respectively:

$$M_D = \frac{u}{v} \tag{1.3}$$

and

$$w = \frac{0.6\lambda}{N.A.} \tag{1.4}$$

and

$$z = \frac{0.8\lambda}{N.A.^2} \tag{1.5}$$

with *N.A.* being the numerical aperture of the objective lens. It should also be noted here that the constants shown in Equations (1.4) and (1.5) depend on the level of coherence and only represent typical values. It can be seen that the resolution can be improved by reducing λ or increasing the *N.A.*; however, this ultimately results in a reduction of depth of focus (also known as the depth of field and the working distance). Usually the depth of focus z is determined by the topography of the target material, how deep the processing needs to be and the mechanics of the target material positioning. The main advantages of this system are that it is non-contact (which will be discussed further in Section 1.3.2.2) and that it offers variable magnification. This leads to the fact that the fluence at the target can easily be controlled and the fluence at the mask can be reduced leading to longer lifetimes.

Disadvantages associated with this technique are that it can be a complicated system with high costs and long setup times.

1.3.2.1 – Contact Masks

Contact masks allow the target to come into close proximity to the mask in order to etch the required pattern or shape into the material. This type of setup is a simple arrangement for materials processing; however the mask used needs to have the ability to withstand the fluence at the target material. The minimum feature of this type of system is controlled by the size of the hole in the mask and diffraction (if the mask was not in absolute direct contact with the target material). Due to restrictions in the manufacturing of contact masks it is difficult to produce a contact mask to produce features less than 5 μm. There are three main types of contact mask that can be utilized for materials processing these are free standing masks (stencils), conformal masks and semi-transparent liquid contact masks.

Free standing masks are usually manufactured using thin metal that are patterned with holes and can be used on several target materials. It can be found that it is extremely difficult to achieve the distance between the mask and the material to tend towards zero without damaging the target material. As a result of this, the minimum feature size can be highly affected due to diffraction. In addition to this it has been seen on numerous occasions that the mask can become clogged with ablation products from the target materials resulting in a reduction of processing efficiency. Also, one major disadvantage is that intricate features incorporated inside the mask pattern must be supported if they are required. For example the two middle sections of a capital “B” must be supported in the mask shape to achieve the required pattern. It should be noted here that in order to eliminate the supports on the etch in the target material, each support should be smaller than the resolution of the laser system. However, with mechanical constraints it can be seen that it may not be possible to produce these small features in the mask.

Conformal masks necessarily contaminate the target material to produce the required pattern such that the distance between the mask and the material tends towards zero. Therefore, the conformal mask would be deposited onto the target material and could be used for a number of applications. The mask could be in place to perform differential etching in which the mask etches slower than the target to produce the required pattern. Alternatively, the applied mask could be utilized as a sacrificial layer to remove debris. It has also been realized that the conformal mask may already be part of the target material itself. For example two layer circuit boards manufactured from copper with a polymeric sandwich layer can be processed using an Nd:YAG laser such that the beam etches the copper but is poorly absorbed by the polymer allowing only one side of the circuit board to be manipulated at a time. If the same circuit board was to be processed with a CO_2 laser after removal of a section of one of the copper layers then the polymer would be etched until it reached the copper layer on the opposite side. At this point the beam would be reflected by the copper and not be etched allowing the process to be self terminating.

1.3.2.2 – Non-Contact Masks

Non-contact masks, as discussed previously, are utilized within projection etching systems to produce the required pattern in the target material. These masks offer advantages over contact masks as they can be positioned anywhere within the optical system and they are less likely to be contaminated/congested with debris from the processing of the target material. In addition to this, as the non-contact mask can be placed anywhere within the optical system it can be seen that the fluence at the mask can be greatly reduced leading to a longer lifetime of the mask. They can be manufactured as free standing stencils or opaque on transparent substrates. The free standing stencils are similar to those seen used as contact masks but constitute larger features. With this method and free standing masks it can also be seen that supports for complex features can be manufactured small enough not to be resolved at the target material. This can be done easier than contact masks due to less of a demand on the size of features in the mask. Opaque on transparent substrate masks are robust and are usually manufactured using chromium on quartz; but, they are less commonly used in comparison to using dielectric reflectors on quartz. It has been seen that non-contact masks offer several advantages over contact masks, although, the optical system required for projection etching can be more complex as demagnification, image and object distances need to be taken into account. In addition, to illuminate non-contact masks a larger beam is required and could require more components to be included in the optical system; for instance, a beam forming telescope may be required to increase the beam size whilst reducing the beam divergence. Also, a beam homogenizer or random phase plate may be required within the system to create a flatter irradiance distribution and reduce spatial coherence to reduce speckle in the image plane.

1.3.3 – Mask and Work Piece Scanning (Dragging)

In order to process large target materials or cover large area masks it is possible to utilize mask and/or work piece scanning which involves moving either the mask or the work piece to create the required pattern in the material. It can be deduced from this that if the mask and work piece were scanned in opposite directions a large pattern can be produced in large bulky materials. The ratio of relative velocities for the mask and the work piece are set by the magnification of the system. In addition to this it should be noted that the precision/resolution required for the movement of the mask is somewhat lower than that of the work piece. This is due to the fact that the movement of the work piece determines where the pattern will be etched in the material and this can require the highest accuracy. Although, these methods can be very useful there are limits on quality that involve optical resolution such as alignment and beam non-uniformities. Another factor that can limit the quality of the processing is material properties such as heat diffusion which require to be taken into account when considering these systems. The mechanics of the translational stage can also give rise to limits on quality as it may not be possible to achieve both high accuracy and high repeatability with the system.

2
Polymers as Biomaterials and Surface Modification Techniques

This chapter details how polymers, namely nylon 6,6, have previously been employed for use as biomaterials. In addition, some of the main surface modification techniques and attempts to identify the advantages and disadvantages of using laser surface modification techniques over competing technologies are discussed.

2.1 – Introduction

The three main material families that are usually used throughout the biomaterials industry can be seen as metals, ceramics and polymers. Polymers is the name given to materials that include plastics, gels, rubbers and even fluids which are typically large, long chain molecules produced from molecules named monomers [20]. It has been realized that polymers can be broadly grouped into two categories; thermoplastic polymers and thermosetting polymers. Thermoplastic polymers are named such that they become soft when heat is applied, can be shaped and upon cooling will retain the given shape. Reshaping of thermoplastic polymers is possible due to the fact that the process can be repeated by reapplying heat. Thermosetting polymers is the term given to those materials which have a chemical cross-linking such that the polymeric chains are connected together in a three dimensional network. These types of polymers differ from thermoplastics as they do not become soft upon the application of heat and are also insoluble; however, it is possible for these polymers to swell when they are exposed to organic solvents [20].

It has been realized that unprocessed polymeric biomaterials posses poor adhesion characteristics that allow one to deduce that they are hydrophobic in which they are difficult to wet. So, in order to increase the wettability of polymers for use in biological environments, a vast number of techniques and methods have been developed. These techniques range from surface topography modification [21-23] to surface chemistry modification [24-26] and have given rise to the increased interest in using polymers as biomaterials [27-34].

2.2 - Applications of Polymeric Biomaterials

Polymers are long chain molecules which constitute a large number of small repeating units more commonly known as monomers. As a result of the fact that a vast amount of materials come under the title of polymers, it can be seen that there are numerous applications within the biological industry in which these materials can be used. Table 2.1 shows some of the main polymeric biomaterials indicating their most common uses within the biomaterials industry.

Table 2.1 – Some of the main polymeric biomaterials with their most common applications within the biomaterials industry.

POLYMER	APPLICATION
Nylon	Gastrointestinal segments, Tracheal tubes.
Polyethylene (PE)	Acetabular cup of hip prosthesis, Heart pacemakers.
Polymethyl methacrylate (PMMA)	Dental restorations, Intraocular lenses, Joint replacement.
Polypropylene	Heart valves.
Polyurethane	Heart pacemakers, Maxillofacial prosthesis.
Polyvinyl chloride (PVC)	Gastrointestinal segments, Maxillofacial prosthesis.
Ultrahigh molecular weight polyethylene (UHMWPE)	Total joint replacement- usually hip, knee and shoulder joints.

Advantages of using polymers can be seen to be the fact they are able to be easily fabricated to various complex shapes and structures and provide a large range of bulk compositions and physical properties which could be applied to a number of applications. Disadvantages have been identified such as they can be difficult to sterilize, can easily absorb water and may leach out harmful substances to the body under *in vivo* circumstances [35].

Nylon is a family of semi-crystalline engineering thermoplastics which are generally fabricated using straight chain aliphatic acids and amines. The most common nylons are that of nylon 6 and nylon 6,6 where the numbers correspond to the number of carbon atoms donated to the amine and acid monomer chain. Nylon 6,6 is an off-white engineering thermoplastic which has been found to be the strongest and most abrasive resistant unreinforced nylon. Owed to the material properties nylon 6,6 possesses it can be seen that this polymer has been used for such biological applications as sutures, tracheal tubes and gastrointestinal segments [35]. With regards to orthopedic applications it can be seen that nylon is not commonly employed due to the hygroscopic nature having a large effect on the mechanical properties over long periods of time [36]. As a result of this, PMMA and UHMWPE are two of the most common polymeric materials to be used as orthopedic implants [35]. Having said that, the use of nylon 6,6 within this work gives high value experimentally insofar as to ascertain generic factors for polymeric materials which could be used to predict the osteoblast cell response. Also, by modifying the surface of polymeric materials it may be possible to identify other biological applications as this may enhance the osteoblast cell response and biocompatibile properties. On account of nylon 6,6 being a relatively inexpensive polymer when compared to other polymer types, by identifying other applications for this material the biological industry would benefit by being able to implement cheaper, more economic bio-implant materials.

2.2.1 – The Hygroscopic Nature of Polymeric Materials

For most polymeric materials it has been found that the hygroscopic nature (water absorption) plays an important role in the material properties [35-40]. In most instances it has been identified that the water uptake for polymers is diffusion-controlled and that an increase in water uptake generally leads to a polymeric material to become softer as a result of a plasticizing effect or the scission of water-sensitive bonds such as hydrogen bonds [37].

On account of amide groups (-NHCO-) in the nylon 6,6 backbone it has been shown that these groups favour water absorption with the formation of hydrogen bonded water molecules owing to its higher polarity [36]. One can then deduce that the extent of water uptake of the nylon 6,6 material would be dependent on the amide group concentration in the molecular chain. As a result of the hygroscopic nature of nylon 6,6 it has been shown that that the water absorption can have a large effect upon the chemistry of the material in addition to giving rise to considerable swelling [36,40]. These modifications have then been found to have detrimental effects upon the mechanical properties; for instance, Rajesh *et al.* [36] concluded that for nylon 6 the erosive wear and mechanical properties had been influenced by the water uptake on account of the deterioration in strength properties. On account of water uptake for any polymeric material this is likely to have a large effect upon the osteoblast cell response over a long period of time due to topographical dimensional and surface chemistry changes. Furthermore, owed to water absorption over a period of time it is likely that the bioactive nature of the nylon 6,6, in terms of osteoblast cell response, would vary over the time in which the water absorption took place. This could have a negative effect on the ability to predict how the osteoblast cells would respond to such an environment. However, by keeping the time between surface processing and biological analysis constant, generic parameters that determine the osteoblast cell response would likely be more identifiable.

Excessive water uptake can lead to the breakdown of the polymer and in terms of biological applications, can lead to the ingress of unwanted microorganisms which can contribute to the failure of a biomedical implant [39]. However, it should be noted here that the water uptake for a polymeric material is not always detrimental to the bioactive nature. For example, water absorption is sometimes beneficial for dental filling materials in that the arising swelling from the water uptake compensates for the shrinkage arising due to polymerization [39]. In addition to this, it has been determined that water absorption from a range of biological fluids had reduced to 1.5 to 3% [38] which would have a large impact upon the implant performance *in vivo*. Therefore, when the polymeric material is ready to be tested *in vivo* a precise evaluation of the water absorption characteristics for the intended application is clearly imperative.

2.2.2 – Sterilization of Bio-Implant Polymeric Materials

Another important factor which can be a disadvantage for polymeric materials, for use in biological applications, is that of the need for sterilization. In order to avoid subsequent infection that can lead to illness and discomfort to the patient it should be ensured that the material be sterile. Sterility is defined as the absence of all living organisms [41] and even if one viable bacterium is present on a bio-implant, it is rendered non-sterile. As a result of the hygroscopic nature of materials as discussed in Section 2.2.1 water uptake can lead to the ingress of microorganisms and due to this, polymeric materials can be seen to be difficult to sterilize.

In order to achieve a sterile surface prior to implantation a number of techniques have been developed such as cold solution, dry heat, moist heat, gas, gas plasma and gamma radiation [7]. It is reported that some of these sterilization methods can affect the material properties, especially for polymers [7] and

as a result of this great care should be taken when sterilizing a material for *in vivo* applications as the sterilization technique could have detrimental effects of the resulting cell response.

Even though, with respect to nylon 6,6 and other polymeric materials, water absorption and sterilization can be seen to be two of the main potential constraints to biological applications, polymers are beginning to be widely used throughout the biomedical industry due to being cheap and relatively easy to fabricate. With this in mind, it would be beneficial to the industry to have the ability to modify polymeric materials to optimize the surface for the intended application. Also, through experimental conditions it may be possible to identify generic factors for polymeric materials to hold the ability to estimate the performance of a polymeric material in a given biological application. Furthermore, through the surface modification of polymeric materials it may be found within future work that the hygroscopic and sterilization properties could be modified.

2.3 - Alternatives to Laser Surface Treatment of Polymeric Biomaterials

In order to gain broader knowledge of the subject area of polymeric biomaterials and how they can be processed it is necessary to take into account the techniques that can be employed that do not incorporate the use of laser technology. Some of the methods detailed within this chapter have been used for many years to produce biomaterials manufactured from numerous materials such as ceramics and metals [4] in addition to polymers. These techniques have already been tried and tested and it can be seen that they offer some advantageous results to allowing the bioactivity to be dramatically improved.

2.3.1 – Radiation Grafting

Radiation grafting and photografting are techniques that are widely used throughout the biomaterials industry. In respect to polymers the radiation can be applied in many forms such as high energy electrons, gamma radiation, UV and visible light and is used to allow the chemical bonds of the polymer to be broken. This gives rise to the formation of free radicals and, in the presence of a monomer, react to produce a free radical chain reaction allowing other monomers to be incorporated to ultimately construct a surface-grafted polymer. With regards to the bioactivity of a material this technique allows one to selectively place chemical molecules onto the material surface to improve the biointeraction for such things as cell adhesion and water absorption [42]. This was reconfirmed by Mao *et al.* [27] as they carried out *in vitro* studies on blood compatibility of nylon films that had been radiation grafted with *O*-butyrylchitosan. From this work it was realized that radiation grafting in this manner would give rise to enhanced bioactivity of the nylon films and was a suitable method to tailoring custom nylon films for a required biological application. It has also been found that this technique has a major advantage as it is a very clean method [24] and allows for indirect, cost-effective sterilization of those materials that will be required to function within a biological environment [42]. In addition, it has been realized that radiation grafting with a source such as 172 nm UV light can provide a uniform nanoscale layer to be produced on the surface of the material promoting advantages that include durability [43] and improvement of the load bearing components [42]. Radiation grafting can also be used to produce lamination, allowing a high mechanical strength

and selective barrier properties to be achieved [44]. Through research also carried out by Ranby *et al.* [45], they found that the primary reaction mechanism of the photografting arose due to the excitation of the initiator which in their case was benzophenone. Furthermore, they determined that slow photografting between two LDPE sheets gave rise to both of the sides becoming photografted.

2.3.2 – Plasma Surface Modification

Plasma surface modification techniques are dry methods which have been found to possess the ability to vary the surface properties of numerous materials without the bulk properties becoming modified. With regards to plasma surface modification of polymers there are numerous examples of industrial applications such as the automobile, microelectronics, packaging and biomedical. From the work carried out by Arefi-Khonsari *et al.* [46] it was found that certain polymers such as OTS-SAM are much more resistant to this technique compared to PE. This is due to the fact that the amorphous structure of PE allows them to be less resistant than the crystalline structure of the OTS-SAM. It has also been deduced by Milde *et al* [47] that ECR plasma treatment of polymer films can give rise to enhanced adhesion behaviour for PVD coatings. The enhancement of adhesion properties of polyimide and FEP using ECR plasma was reconfirmed by Abdul majeed *et al.* [48] which indicated that the exposure of atomic oxygen ions to the polymeric materials induced significant variations in surface chemistry and topography in order to improve upon the surface wettabilities. Furthermore, it has been seen that extensive research has been carried out on how the hydrophilic and hydrophobic tendencies of numerous polymers can be manipulated using plasma based technologies [32,49,50]. Each of these works have allowed one to see that using plasma based technologies can extensively manipulate variations in surface morphology in order to be used in certain applications. In addition to this, an important piece of analysis that has arose from such work came from Lai *et al.* [49]who concluded that their results indicated that the C=O double bond ratio was the most important aspect when considering θ and wettability of polymeric surfaces.

The technique itself involves the production of a glow discharge plasma which can be created by evacuating a vessel, usually quartz due to it being inert, and then refilling the vessel with a low pressure gas. It is then required that the gas be energized and can be done using various techniques such as microwaves, radiofrequency energy, alternating current and direct current. This gives rise to energetic species within the gas plasma in which they can take many forms. For instance these energetic species could be ions, electrons, radicals, metastables and short-wave ultra-violet UV) photons [4]. This produces energy transfers to the surface of the material to occur via chemical and physical processes which gives rise to the surface modification. It has been shown that it is possible to utilize these induced surface modifications for numerous biomaterials. Chu [51-53] has undertook an extensive amount of research into this field and has shown that it is possible to use plasma based surface modification to enhance the bioactivity of diamond-like carbon. From research such as this, it is possible to foresee that plasma-based technologies could potentially be used for polymeric biomaterials in order to improve upon their bioactivity for use in biological environments.

2.3.3 – Ions, Ion Beam and Electron Beam Processing

Ion beam processing techniques are one of the most popular methods of biomaterial surface modification due to the fact that they can be used to produce surface layers incorporating the required modified properties with negligible affects on the bulk properties. Through research it has been found that there are two main types of ion beam processing; these are ion implantation [54] and ion beam assisted deposition (IBAD) [34]. The ion implantation technique is carried out by injecting accelerated ions with energies ranging between 10^1 and 10^6 eV into the surface of the target material giving rise to alterations in the properties of the surface. It has been seen that this technique gives rise to many advantageous modifications such as hardness (wear), lubricity, toughness, corrosion, conductivity and bioreaction properties [34]. This process is highly selective; however, there are high costs involved and the depth in which modification can occur is relatively shallow. One major advantage that this technique poses as discussed by Lau [55] is that it is possible to surface modify large area materials in relatively quick processing times. With this in mind, it is feasible to realize that using this particular method for processing polymers for enhancing wettability and bioactivity characteristics is attractive to many of those within the industry. As a result, much research has been carried out such as that of Cho *et al.* [56] who used ion assisted reactions (IAR) to produce sufficient surface modifications of numerous polymers to increase the hydrophilic tendencies. In addition to this, through the work of Aubry *et al.* [57] it was determined that by using a focused ion beam (FIB) it was possible to produce effective surface reliefs that could rise to the efficient production of DOEs. This highlights the high selectivity that this method offers as discussed earlier and also indicates that FIB could potentially be used to produce variations in the topography of various polymers in order to modify the wettability and bioactivity characteristics. Leading on from this, it has also been seen through the research of Porte-Durrieu *et al.* [54] that the utilization of heavy ion grafting can be implemented when producing polymeric biomaterials in the aim to increase the absorption of biological proteins. This in turn would lead to increased bioactivity of the polymeric biomaterials.

IBAD is a vacuum deposition process that combines physical vapour deposition (PVD) with the bombardment of ions. The main feature incorporated within IBAD processing is that an ion beam is used with energies ranging from several hundred to several thousand eV during the deposition of a coating. IBAD is primarily used in applications such as hydroxyapatite coatings, diamond-like carbon (DLC) film, C-N film and other coatings [34]. In addition to this, another ion beam process is that of ion beam texturing (IBT) in which this method holds the ability to produce micro and macrofeatures on the surfaces of biomaterials to meet requirements set by bioactivity *in vivo* [34].

It has been realized that it is possible to utilize an electron beam (EB) in the production of biomaterials. Through the work carried out by Iwanaga *et al.* [58] they found that it was possible to use EB polymerization to graft polyacrylamide onto tissue culture polystyrene (TCPS). Using this technique along with a pre-treatment of UV excimer ablation they found that micropatterned surfaces could be formed which incorporated hydrophilic PAAm and hydrophobic basal polystyrene layers. From the results it was determined that these modified surfaces allowed for increased cell adhesion and proliferation indicating that this technique could be used to produce cell-based biosensors and tissue engineering devices.

2.3.4 – Other Common Methods

There are other less common methods that can be utilized for the surface modification of materials. Even though they are seen to be less common process it can be realized that they can offer relatively good results and are briefly discussed here.

2.3.4.1 – Coatings

There are two main types of coatings that can be used for surface modification; these are conversion and parylene coatings. Conversion coatings modify the surface of a material in such a way that it allows the surface to become oxide-rich improving properties such as corrosion, adhesivity and lubricity. Parylene (para-xylene) coatings hold a unique niche within surface modification due to the good quality thin film coatings that can be formed. Through the work carried out by Lord *et al.* [59] it has been seen that using silica nanoparticulate coatings on biomaterials gives rise to the influence of cell attachment and spreading. This has also been confirmed by others such as Gross *et al.* [60] which highlighted the possibility of using plasma sprayed hydroxyapatite coatings for controlling the *in vitro* response to biological implants. Additionally, it has been observed by Harnett *et al.* [61] that by using adhesion molecule coatings such as fibronection and poly-D-lysine on various materials the polarity of those materials could be manipulated in such a way that could influence cell adhesion and proliferation. Apatite coatings have also been realized to produce sufficient bioactive tendencies on oxidized titania as found by Song *et al.* [62]. This work indicated that the induced apatite coatings on titania gave rise to enhanced bioactivity in the simulated body fluid.

It is widely accepted that for some biomedical applications, such as biocompatible coatings, the necessity of high quality thin films is essential for the optimization of the application. For instance, through the work carried out by Bloisi *et al.* [63] it was found that high quality polyethylene glycol thin films could be produced using the MAPLE technique for biomaterial applications. In addition to this, Mei *et al.* [64] employed a spin coating method to produce sorbitol-containing polyesters thin films and highlighted through their results that these films had attractive biocompatible characteristics. This led them to conclude that sorbitol-containing polyester shows potential for use within tissue engineering, cell adhesion and proliferation. It should also be noted here that alternative work has been carried out by Zhao *et al.* [65] which shows that metal-polymer coatings can be used to produce surfaces that hinder the process of bacterial adhesion. From the literature one can then deduce that coatings could play an important role within enhancing the bioactivity of materials; however, it should be noted here that some of the methods mentioned for coating technology can be time consuming, costly and, in some cases, require high maintenance.

2.3.4.2 – Silanization [4]

Silanization processes involve silane reactions that can be utilized to modify surfaces that are hydroxylated or amine-rich. This type of process is useful for surface modification for materials such

as glass, silicon, germanium, alumina, and quartz due to the fact that they have rich hydroxylated surfaces.

2.3.4.3 – Langmuir-Blodgett Deposition [4]

Langmuir-Blodgett (LB) deposition allows a surface to be covered with a highly ordered layer with each of the molecules that assemble into this layer having a polar head group and a non-polar region.

2.3.4.4 – Self-Assembled Monolayers [4]

Self-assembled monolayers (SAMs) are primarily surface coating films that form spontaneously to produce highly ordered structures (two-dimensional crystals) on specific substrates.

2.3.4.5 – Surface-Modifying Additives [4]

It is possible to include certain components in low concentrations to the material during the production which can give rise to the production of required surface properties. But, it must be added here that this may affect the bulk properties of the material and it should be ensured that low concentrations are used.

2.4 – Laser Surface Treatment of Polymeric Biomaterials

For many years laser processing of polymeric materials has been used widely throughout many industries and has been extensively researched. It has been found that Nd:YAG and CO_2 lasers offer relatively good quality processing and can be used for such applications as cutting [66], welding and engraving [67]. Following on from the early research carried out, both the laser technology and processing techniques have been improved giving rise to the possibility of micro processing to produce surface patterning using direct beam scanning [21]. This gives rise to considerably smaller features being achievable with an improved quality of surface modification.

With the many benefits of using lasers for materials processing it has been found that the interest in laser-induced surface treatment has grown, especially within the biomedical industry. This is due to the fact that lasers offer the user a highly selective, rapid technique to induce surface modification in both organic and inorganic materials [4]. From this it has been found that the utilization of laser technology for surface modification can be brought about in many forms such as annealing, polymerization, etching and deposition.

2.4.1 – Laser-Induced Surface Patterning

It can be seen that surface patterning due to laser irradiation arises from the ability to focus the laser beam onto specific areas of the target material allowing evaporation of the material to take place. With most lasers it is seen that the smallest possible features that can be achieved are on the micron scale; however, it has been realized that it is possible to achieve nano-structures by using a laser

emitting at a wavelength of 157 nm. With the work carried out by Sarantopoulou *et al.* [22] it was deduced that the mixture of nano and micro-structures present on the polymer surface was due to a localized thermal instability which occurred at the poly trifluoroethyl methacrylate (PTFEMA) film and gold silicon substrate interface. It was also determined that the thermal instabilities that occur within this process resolves itself resulting in well-ordered structures to be produced on the surface of the polymer.

Much of the research that has been carried out in the past few years in the laser patterning of polymers has been done utilizing excimer lasers that operate within the UV spectrum, this is due to the fact UV ablation is very powerful, flexible and can be used to irriadiate a various number of materials. It has been realized that the interaction between UV irradiation and organic polymers gives rise to ablative photo-decomposition, which ultimately leads to etching of the polymeric surface and an explosive ejection of the ablated products at supersonic velocities. It can then be deduced from workings of those such as Callewaert *et al.* [23] that this system allows direct writing of the polymer and eradicates the necessity for photo-masks. In addition to this it was shown from the individual workings of Pfleging *et al.* [29] and Duncan *et al.* [68] that two and three dimensional topographies can be efficiently achieved using excimer lasers. From both workings it was then found that these laser-induced micro-patterns had potential applications in cell applications. Alternatively, it is possible to utilize diffractive phase masks to produce the required surface pattern. This method allows fast fabrication of 3-D topographies to be achievable and any non-linearities within the polymer response can be compensated for in the mask design [69]. It should be noted here, however, that for ablation of any material to take place the ablation threshold must either be met or exceeded [8,70]. By carrying out etch rate analysis it can be seen that Beer Lambert's law of absorption [8] together with a thermal mechanism leads to a prediction of the amount of material removed per pulse, *x*:

$$x = \alpha^{-1} ln\left(\frac{F}{F_T}\right) \tag{2.1}$$

where, α is the absorption coefficient, F is the fluence and F_T is the threshold fluence. From Equation 2.1 it can then be deduced that the threshold fluence for a given material can be estimated by drawing a graph of etch rate against the natural logarithm of the fluence and extrapolating the resulting straight line to where it crosses the x-axis. This can be visualized in Figure 2.1.

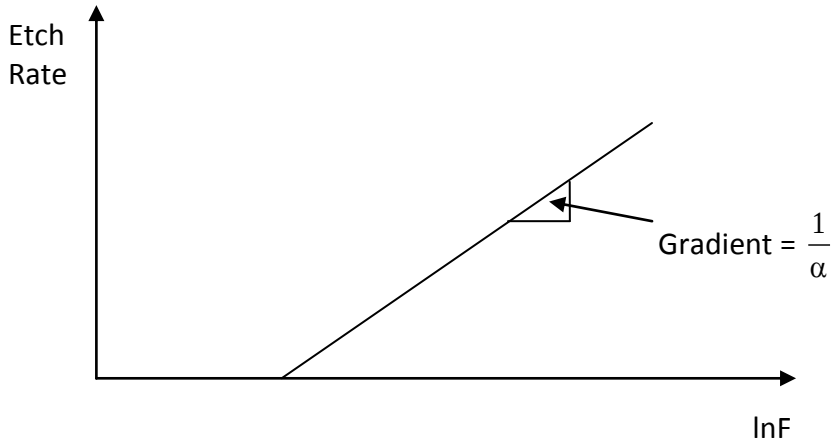

Figure 2.1 – Example graph showing how the threshold fluence, F_T , can be estimated using etch rate and the natural logarithm of the fluence.

From Figure 2.1 it can then be seen that by carrying out various experiments by changing the fluence and measuring the resulting etch rate, the ablation threshold by means of the fluence can be determined. However, it should be noted here that it is assumed the irradiance of the incident beam is not high enough to modify the material properties. If the irradiance was high enough then this could modify the properties inducing higher absorption and deeper etches than expected and gives rise to the possibility of incubation in which the absorption coefficient increases over a number of pulses.

It has been seen that laser types other than UV excimer lasers can be used to produce microstructure patterns within polymers. For instance, Chan *et al.* [71] and Tiaw *et al.* [21] realized that using the 4th and 3rd harmonic of an Nd:YAG laser, respectively, allowed periodic linear and dot patterns to be generated within polymer surfaces without the use of photo-mask or a focusing lens. It has also been indicated by Yu *et al.* [28,72] that it is possible to use Nd:YAG lasers to produce linear micropatterns for the manipulation of cell adhesion to polymers by using laser interference lithography (LIL) which employs two or more coherent laser beams to selectively ablate the polymer surface. Furthermore, other laser types such as CO_2 and femtosecond lasers have been employed to produce laser-induced surface patterns. For example, Dadbin [26] showed that it was possible to modify the surface wettability of LDPE film by using a pulsed CO_2 laser, inducing both topography and surface chemistry variations. The research carried out by Aguilar *et al.* [73] allows one to see that direct micro-patterning of biodegradable polymers can be carried out by both excimer and femtosecond lasers indicating that femtosecond lasers give results equivalent to that achieved by the excimer. A number of comparative studies between the different laser types have been undertaken to determine the effects each laser has upon surface patterning. Skordoulis *et al.* [74] carried out laser ablation using XeCl, CO_2 and Nd:YAG lasers and concluded that it was not recommended to utilize any of the three lasers for ablating nylon 6,6 due to the induced thermal damages that arises from the laser processing. This recommendation is contradicted by Lawrence and Li [75] who carried out research into varying the wettability characteristics of PMMA using CO_2 , Nd:YAG, excimer and high power diode lasers (HPDL) as no thermal damages are mentioned. This indicates that it is possible for one to

see that the laser processing of polymers could specifically be material dependant. In addition to this, the process of laser patterning of polymers can be optimized by producing polymers specifically for the task. These optimized polymers are manufactured such that they are more sensitive to the incident laser beam and through the work carried out by Lippert *et al.* [76] it has been found that the sensitivity was considerably higher in comparison with those equivalent commercially available polymers.

2.4.2 – Pulsed Laser Deposition of Polymeric Biomaterials

Pulsed laser deposition has now become relatively widely used in order to form thin materials for numerous applications. Many various materials can be used using this method and it has been proven through experimental research that it is possible to use pulsed laser deposition to produce thin films of polymeric materials [77,78]. Excimer lasers appear to be the most commonly used laser for this technique due to the fact that most materials have strong absorption over the UV spectral range [79]. This is due to the fact that the absorption coefficients tend to increase as shorter wavelengths are used giving rise to corresponding reduced penetration depths. This can be seen as a major benefit towards controlling the system as thinner layers can be ablated along with the fact that ablation thresholds decrease for shorter wavelengths [79]. Furthermore, through the workings of Rebollar *et al.* [80] it was determined that it is possible to utilize a Ti:Sapphire laser to produce thin films of PMMA doped with fluorescent probes that hold the ability to serve as environmental sensors. With regards to polymers it has been determined that smooth thin films of PMMA can be produced using relatively high fluences [77]; it has also been realized that pulsed laser deposition at high fluences can change the chemical structure during the process [77,78] and could have a detrimental effect to the bioactivity. This has been observed by Cristescu *et al.* [80] as they compared pulsed laser deposition with matrix-assisted pulsed laser evaporation (MAPLE) and concluded that pulsed laser deposition of pullulan (a polymeric biomaterial) could not be used with this technique as resulting thin films had a different composition. Furthermore, they also concluded that the MAPLE technique was more viable for that specific polymeric biomaterial. From this it can then be seen that pulsed laser deposition does not seem to be the most optimum technique to produce polymeric biomaterials to increase the wettability characteristics resulting in improved bioactivity. However, it may be possible to utilize this technique to change the polymer composition in such a way that would allow for improved bioactivity.

2.4.3 – Laser-Induced Surface Chemistry Modification and Laser Grafting

It has been seen that the surface chemistry of polymers can be relatively easily modified by laser processing of the surface. Even when processing is carried out in air it has been found that the surface can become oxidized where the surface oxygen content has increased along with the polar component of the surface energy giving rise to improved wettability characteristics [26,71,75]. With this increase in O_2 it has been determined that oxidized groups are formed on the surface of the irradiated materials such as through the workings of Mirzadeh and Dadsetan [30] that theorized the drop in θ of CO_2 irradiated PET could be attributed to these oxidized groups which arise from chain scission and contact with the ambient air. Following on from this, the research into the debris formation from PET as a result of KrF excimer laser irradiation carried out by Shin *et al.* [81] allowed them to conclude

that the photochemical bond-breaking which leads to carbonization arises from the UV absorption of the benzoate present in the PET. In addition, it has been proven experimentally that laser surface processing with various different ambient gases can be used to modify the surface chemistry of the polymer surfaces to improve the wettability characteristics [26,29,82]. For instance Niino *et al.* [82] allowed PTFE film to be UV laser processed whilst being present in a pressure chamber filled with hydrazine vapour which allowed the surface chemistry of the film to be modified such that the adhesion for a metal layer was sufficiently increased. Following on, work carried out by Pfleging *et al.* [29] allows one to see a comparison in the processing of polystyrene surfaces using three different processing gases (air, O_2 and He). Furthermore, they were able to draw up a table indicating the best parameters for improving cell adhesion, the hydrophilicity and the hydrophobicity for polystyrene surfaces. From this it can then be seen that the modification of surface chemistry of polymeric biomaterials can be crucial to improving the wettability techniques.

Another effective way in which the surface chemistry of a material is that of laser-induced grafting which allows additives to be either placed onto the surface or imbedded [83] into the surface prior to laser irradiation. This allows radicals to form giving rise to chemical reactions that allow the surface chemistry to be modified. Charbonnier *et al.* [84] carried out research into laser grafting nitrogen atoms onto the surface of polycarbonate and showed that UV laser irradiation could efficiently carry out this process. Also, they were able to conclude that increasing the laser fluence allowed for the increase of nitrogen to be grafted onto the polycarbonate surface until a limit was reached, which arose from the equilibrium state between nitrogen grafting and the induced bond breaking. Much research using CO_2 lasers as an excitation source has been carried out by Mirzadeh *et al.* [31,84,85] which grafted HEMA, NVP, AAm onto ethylene-propylene rubber (EPR) for use as an enhanced biomaterial. From these works it was found that the modified EPR gave rise to sufficiently enhanced bioactivity in comparison to unmodified EPR; however, it was also seen that the process of cell spreading was highly dependent on the amount of hydrophilic chains grafted onto the samples [31]. In addition, they carried out *in vivo* studies to AAm and HEMA grafted EPR which showed that that CO_2 laser irradiation could be utilized to improve upon the bioactivity of EPR [85].

2.4.4 – Matrix-Assisted Pulsed Laser Evaporation and MAPLE Direct Write

As it has already been discussed, MAPLE techniques have been found to produce sufficiently better results with regards to improving the wettability characteristics of certain polymers in comparison to pulsed laser deposition. This is due to the fact that this technique is more appropriate for preserving the chemical structure and functionality of the molecules [78] as the laser irradiation energy is absorbed only by those molecules that require it [63]. It can also be seen that MAPLE is an advantageous method to produce polymeric biomaterials due to the fact that this technique is reliable and allows the user to have sufficiently greater control over the deposition parameters in comparison to other deposition techniques that are available. The basics of the MAPLE technique is to allow the target material to become a frozen matrix which consists of a dilute solution of the required material to be deposited in an appropriate solvent [63]. With the laser irradiation, it has been seen that the plume given off incorporates solvent molecules which are in different phases. As the plume reaches the substrate the volatile substance, which ideally would be a material that has no tendency to form a

thin film, is removed using a vacuum system. This allows the organic/polymer molecules to be deposited onto the substrate free of the volatile solvent [63].

A similar technique can be used for directly depositing material onto the substrate which is known as MAPLE direct writing (MDW). This method is carried out by placing the matrix of the solution onto a ribbon which is transparent to the laser irradiation. As the ribbon is transparent, when a laser pulse is incident on it the beam passes through the ribbon allowing thermal excitation to take place of the solution matrix. This thermal excitation results in thermal expansion of the matrix allowing the required material to be propelled and deposited onto the substrate. With this technique it has been observed that resolutions of around 10 μm can be achieved [86]. From an applications perspective, it has been determined by Ringeisen *et al.* [87] that it is possible to produce mesoscopic patterns of viable *Escherichia coli* onto various materials using MDW. From this research it can then be seen that it may be possible to use MDW for various other cell types and could lead to allowing the bioactive nature of a material to be greatly enhanced.

Both MAPLE and MDW can be seen to have many advantages compared to other deposition techniques to produce polymeric biomaterials; however, the possibility of producing thicker or multilayer films can be difficult as these methods are process intensive and are limited to specific materials [86]. In addition, it can also be seen that MAPLE techniques are highly laser wavelength dependant and in some cases it has been realized that slightly longer wavelengths than UV, for instance 532 nm in the visible has given the optimal results [63]. Even though there appears to be some limitations to using this technique, the advantages that it does offer allows one to see that this is a very attractive method in order to produce thin film polymeric biomaterials.

2.4.5 – Laser Surface Modification for Improving Corrosion Properties

Even though there does not currently appear to be many publications regarding improving the corrosion properties of polymeric biomaterials it has been recognized that these properties can be improved for various other biomaterials such as ceramics and metals. For instance it has been seen that by inducing a temperature rise by means of laser irradiation surface/laser hardening can take place. This gives rise to improvements in such properties as hardness, strength, wear, fatigue and lubrication [9]. By using laser technology to induce the temperature rise to carry out this process the shape and location of the HAZ can be very accurately controlled allowing specific areas of the target material to be modified. Furthermore, another benefit is that of the speed of processing in which a laser offers flexibility and the potential to have high manipulation of the beam. To determine whether or not current methods can be applied to improving the corrosion/dissolution properties of polymeric biomaterials more research into this field may be required.

3
Wettability: Contact Angle, Surface Energy and System Parameters

Current understanding and progress made to date in the field of wettability and the factors that arise through the investigation of the wettability characteristics of materials are presented in this chapter. ϑ, surface energy and other potential system parameters are discussed at length, as required by any wettability study.

3.1 – Introduction

When considering the subject of hydrophilic surfaces and the wettability of materials the term 'wetting' is a fundamental phenomena that should always initially be taken into account. The understanding of the wetting of a surface by liquids leading to the spreading of those liquids over the surface can be seen to be a crucial factor that is incorporated within surface chemistry. The process of wetting has been recognized and researched for many years by many scientists; however, like many subjects within the scientific community the process is still not fully understood [4,88]. Even though this process is still not fully understood, many breakthroughs have occurred in this subject area in order to gain a more thorough understanding between the interactions of surfaces, interfaces and the biological environment. Through this work it is possible to see that allowing modification of the wettability characteristics of biomaterials gives an attractive means to evaluate the degree of the bioactivity of those materials used prior to implementing them within the intended biological environment. Leading on, various laser-based techniques for altering the wettability characteristics of numerous materials have been developed [88,89]. It should also be noted here that various other methods, discussed previously in Chapter 2, have been developed. One such example is the research carried out by Dumitrascu *et al.* [90] highlighted the possibility of using a pulsed dielectric barrier discharge (DBD) to modify the roughness of surfaces for various materials. As a result of this, they found that DBD could be used to induce a controlled roughness throughout various material types in order to manipulate the wettability by changing the θ.

3.2 – Contact Angle and Wettability: Theoretical Background

Since the first description of θ and wettability by Young in 1805, much research has been carried out on the wetting of various materials. For instance, the Lotus Effect was discovered in 1997 by Barthlott [91] indicating that when rain falls onto a Lotus leaf water droplets form, producing a θ of approximately 160° which is highly hydrophobic (superhydrophobic). As the droplets roll off the leaf dirt is picked up along the way allowing for the leaves to have clean surfaces [92]. Discoveries such as this have given rise to increased interest into the wettability of materials such as polymeric biomaterials, with the complex mathematics regarding wettability also being researched and discussed [93-99]. Experimentally, there has also been extensive research into wettability of materials. The

work done by Bico *et al.* [100] allows one to see how the designed roughness of a textured surface can be utilized in order to manipulate the wettability characteristics of a material. Within this work these workers also allude to the implications of applying wettability methods to porous media by showing that such a material cannot be considered as an array of capillary tubes when attempting to explain the complex phenomenon of wettability. In addition, research has also been carried out into the parameters that govern the transition between the Cassie-Baxter to Wenzel wetting types. Such work has been undertaken by Jung *et al.* [101] who concluded that the droplet size has a major influence on the transition between the two wetting types. In some cases it has been seen that it may be possible for a hydrophilic surface to give rise to some form of Cassie-Baxter wetting or Cassie-Baxter/Wenzel mixed intermediate wetting regime owed to the roughness and topographical pattern on the surface [102-104]. In this instance it is seen in some cases that increasing the surface roughness, through the patterning of a surface, can give rise to an increase in θ for hydrophilic materials.

3.2.1 - Contact Angle

It has been observed extensively that when a drop of liquid is left in free space it has a tendency to be drawn into a spherical shape as a result of the tensile forces from the surface tension. This is a resultant that arises from the attractive and repulsive forces that exist between the molecules within the liquid. If the same drop of liquid were to be brought into contact with a solid flat surface the final outcome of the droplet (as to what shape it would undertake or whether the liquid would wet the surface) would be dependant on the relative magnitudes of the molecular forces that exist within the cohesive and adhesive parameters. This phenomenon is quantified utilizing θ, which is the angle that the liquid subtends with the solid and can be visualised in the schematic diagram of a droplet of liquid on a flat solid surface shown in Figure 3.1.

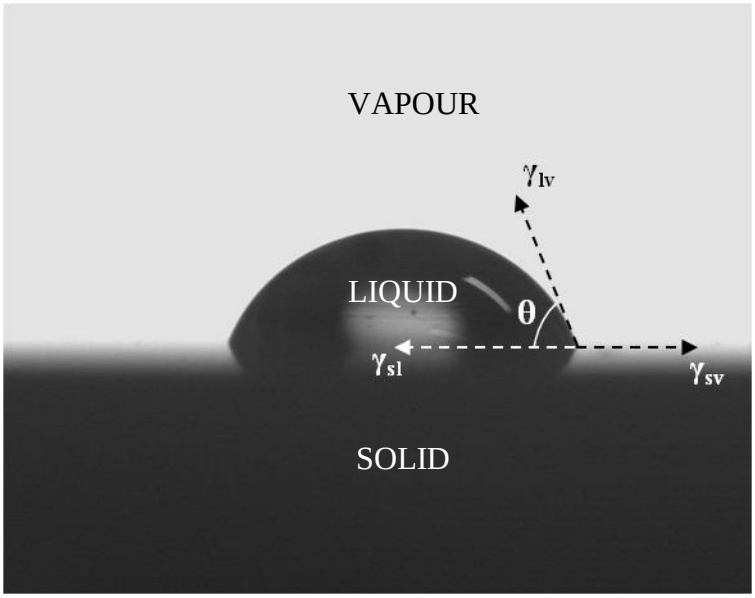

Figure 3.1 – Photograph showing a liquid droplet at rest on a flat solid surface

It is understood that in a generalized sense, for wetting to take place θ, shown in Figure 3.1, has to be less than 90°. From this it can then be deduced that wetting of the solid surface will not occur if θ was to be greater than 90° resulting in adhesion not taking place [105].

From observation and experimentation it has been found that θ is closely related to three specific energies; the solid and liquid surface energies, γ_{sv} and γ_{lv}, respectively, and the solid-liquid interfacial energy denoted by γ_{sl}. Through the work carried out by Young it was realized that these parameters were related as shown in Young's equation:

$$\gamma_{sv} = \gamma_{lv} \cos\theta + \gamma_{sl} \tag{3.1}$$

It can then be seen that if the liquid droplet, shown in Figure 10, was to be in a state of equilibrium then Young's equation shown in Equation (3.1) could be rearranged to give

$$\cos\theta = \frac{\gamma_{sv} - \gamma_{sl}}{\gamma_{lv}} \tag{3.2}$$

From Equation (3.2) it is then possible to deduce some basic understanding of what is required to achieve wetting; that is, if wetting was to be required then γ_{sv} would have to be large in comparison to that of γ_{sl} and γ_{lv}. This scenario then indicates that those liquids that have comparatively low surface tensions would almost always spread over the solid surface in the attempt to reduce the total free energy within that system [106,107]. This arises from the molecular adhesion between the solid and liquid being greater than that of the cohesion between the molecules within the liquid [105]. It has been seen that a sessile drop device is the main technique to measure θ and as a result much research has been employed into this technology.

3.2.1.1 – Contact Angle Hysteresis

For almost all liquid-solid interface systems that are numerous angles that can be measured in which the droplet is stable. There are two important angles which allow θ hysteresis to be determined. These are the advancing angle, θ_A , and the receding angle, θ_R [108]. The advancing angle is the largest possible θ that can be obtained and is usually achieved by advancing the margin of the sessile drop which is a result from the addition of more liquid. This indicates that the height of the droplet on the surface would be increased whilst the base width remains constant resulting in a greater θ to be achieved. On the other hand the receding angle is usually achieved by removing liquid from the droplet thereby allowing the height to be reduced whilst the width of the base still remains constant. This allows the smallest possible θ to be achieved allowing the θ hysteresis to be determined by calculating the difference between the two angles.

Leading on from this, much research has been recently carried out into this phenomenon and it has been widely accepted that amorphous polymers give rise to greater hysteresis in comparison to polymers that consist of ordered molecular chains. This research has been advanced by the work done by Tavana *et al.* [109] which investigated θ hysteresis achieved by fluoropolymers. From their research it was indicated that using a function containing both the advancing and receding θ,

suggested by Chibowski [96,110], is unsuitable for determining solid surface tensions of polymer materials. Tavana *et al.* [109] propose that these tensions should be determined using the advancing angle alone due to processes such as reorganization of polymer chains, that give rise to the receding angle, allow for the properties of the polymer surface to be changed. Each theory possesses good, relevant reasoning; however, it should be noted here that only through continued research into this area will an overall conclusion to this phenomenon be achieved.

3.2.1.2 – Static and Dynamic Contact Angles

In general terms it can be seen that there are two categories that θ can fall under. These are static and dynamic θ. Θ can be defined as 'static' if the angle remains constant over time giving rise to the system being in a state of equilibrium in which they would either be stable or metastable [88]. Alternatively, if the system has not reached an equilibrium state, where θ varies over time and form both advancing and receding, then the θ formed are known as dynamic angles.

In order to illustrate static and dynamic angles it is necessary for one to think of a simple system in which a liquid droplet comes into contact with a flat solid surface. At the point of contact the liquid-vapour interface taken at the liquid-solid-vapour line (LSV) will begin to proceed over the solid due to self-spreading until an equilibrium state is achieved. This results in an equilibrium θ_e to be produced [111]. Additionally, it can also be seen that a constant shape and minimum area for the droplet will be achieved over the time it would take to give the equilibrium state. This process can be seen diagrammatically in Figure 3.2.

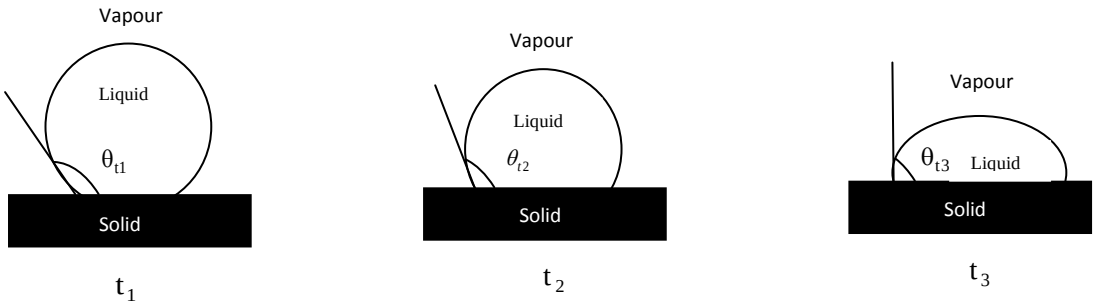

Figure 3.2 – Schematic diagram showing how a liquid droplet forms on a solid surface over time, t, with $t_1 < t_2 < t_3$.

From Figure 3.2 it can be seen that at time t_1 the liquid droplet has just come into contact with the flat solid surface producing θ_{t1} of up to180°. After some time has elapsed, at t_2, the droplet has slightly spread giving a smaller contact angle of θ_{t2} until at a time t_3 in which the droplet system reaches an equilibrium state. At t_3 it can then be seen that due to the state of equilibrium the LSV line does not move giving rise to a constant contact angle of θ_{t3} [105]. For completeness it should also be noted here that the angles θ_{t1} and θ_{t2} arising from the movement of the LSV line in the non-equilibrium are known as dynamic angles and will be denoted as θ_d in all future references. Considerable amounts of research have been undertaken in regards to static and dynamic wetting angles for various surfaces and solutions [112-114]. For instance, Michalski *et al.* [112] highlighted that it was possible to utilize

the sessile drop method and the Wilhelmy method to determine the static and dynamic contact angles of triglycerides on solid surfaces. Furthermore, the research undertaken by Sikalo *et al.* [113] investigated into a verified theory for the dynamic contact angle. The results they achieved highlighted two important factors. Firstly, they were able to verify that, in addition to the contact line speed, the flow field in close proximity to the contact line was closely related to the dynamic contact angle, as previously discussed by Blake *et al.*[115]. The second concluding factor was that the effect of the static contact angle on the dynamic contact angle appeared to be material and surface inclination dependant [113]. In addition, research carried out by Wei *et al.* [114] studied the variations of dynamic wetting of PET fibers arising from plasma treatment. The results obtained from this research allows one to see that the hysteresis can be manipulated by roughening the PET fiber surface. In fact, the plasma treatment allowed for an increase in the hysteresis which is attributed to the roughened PET surface, which allowed for the conclusions produced by Wang *et al.* [116] to be verified.

Due to the schematic diagram shown in Figure 3.2 being a very simplistic view, it can be seen that the assumption of the constant curvature, minimum energy shape, at the liquid-vapour interface throughout the elapsed time can only hold true if the motion of the LSV is very slow. By taking a more realistic view it is possible to see from this that the liquid-vapour interface will have a variable curvature as the droplet moves towards a state of equilibrium. Therefore, a more detailed schematic diagram can be seen in Figure 3.3 indicating how the curvature changes over time.

Figure 3.3 – Schematic diagram showing the change of curvature of the liquid droplet over time with $t_1<t_2$.

From Figure 9 it is possible to visualize that at time t_1 the droplet has just recently come into contact with the surface and the attraction of the solid-vapour interface has given rise to a thin layer of liquid to be pulled from the main bulk of the droplet (denoted as *Y* in Figure 3.3). It has been realized that the attraction from the solid-vapour interface is unable to be extended any further than a few molecular diameters from the surface. This arises to the layer of liquid, *Y*, being extremely thin and in some instances may not even possess liquid properties [105]. After a time t_2 is reached then a second layer region arises (denoted as *B* in Figure 3.3) with this layer being thick enough to possess liquid properties. It should be noted here that once the equilibrium state has been reached the regional layers Y and B are eradicated as they are absorbed by the droplet bulk.

As the liquid spreads across the surface in order to achieve an equilibrium state the driving forces are more commonly referred to as self-spreading forces and can be evaluated in utilising the Young's equation Equation (3.1). From this, the force along the LSV line, F_{lsv}, with γ_{sv} and γ_{sl} in equilibrium and $\theta_d > \theta_e$, can be deduced to be

$$F_{lsv} = \gamma_{lv}(\cos\theta_e - \cos\theta_d) \quad (3.3)$$

3.3 – Wetting, Spreading and Adhesion

In order to gain a complete understanding of wettability it is necessary for one to understand the definition of the wetting process. In general terms the term 'wetting' is applied to the resulting displacement of air from a liquid or solid surface in the presence of water, any aqueous or any molten solution [111]. From observations, when a liquid is allowed to come into contact with any solid surface leading to a solid-liquid interface to be formed, three resulting situations can occur:

i. The surface could be highly hydrophilic allowing the liquid to spread over the solid surface displacing the air giving rise to complete wetting of the surface to be achieved;
ii. The surface could be highly hydrophobic giving rise to the liquid not having the ability to spread across the surface. This results in no wetting of the surface occurring by the liquid; or
iii. The surface could hold a mixture of hydrophobic and hydrophilic properties allowing the liquid to partially spread over the surface. This would allow an intermediate contact angle to be formed with the solid surface.

Also, from observations, it has been determined that there are several variations of wetting in which a solid-liquid interface can be formed. These are adhesional, immersional and spreading wetting [88]. The types of wetting discussed here result from different combinations of the system parameters such as the kind of free energy change, the work which is performed and the way in which the interface is brought about. It should also be noted here that wetting can be classed into two broad categories, these being physical and chemical wetting. Physical wetting involves the reversible physical forces, such as Van der Waals and dispersion forces, to provide the attractive energy required. Chemical wetting incorporates reactions occurring between the two surfaces in contact which lead to the production of chemical bonds.

3.3.1 – Adhesional Wetting

This form of wetting arises when a liquid not in contact with the solid surface makes contact with that surface in which adhesion takes place. In simplest terms this can be seen as one unit of solid surface and one unit of liquid being removed in order to create a liquid-solid interface. The driving force which gives rise to this specific type of wetting is that of the work of adhesion, W_{ad}. The work of adhesion parameter is defined as the amount of work that is required to remove one unit area of liquid away from one unit area of the solid surface and can be calculated using the Young-Dupre equation:

$$W_{ad} = \gamma_{lv}(1 + \cos\theta) \quad (3.3)$$

where γ_{lv} is the liquid surface energy. From Equation (3.3) it can be deduced that the adhesional wetting can be augmented by increasing the surface energy. In addition to this it can also be seen that an increase in contact angle after the occurrence of wetting would not necessarily imply that adhesion is less likely to occur.

It has been determined that the Young-Dupre equation (shown in Equation 3.3) is not strictly true as it can be seen that it is possible that liquid vapour can be adsorbed at the interface, which in turn results in an additional parameter to be considered. This additional parameter is the change in surface free energy due to adsorption of vapour, π_{sv} [117], and is included into the Young-Dupre equation giving the real work of adhesion, W_{adv} , as

$$W_{adv} = \pi_{sv} + \gamma_{lv}(1 + \cos\theta) \tag{3.4}$$

In most materials π_{sv} is usually small enough to be negligible since the majority of theoretical and experimental research has proven that it is not possible to reduce the surface energy of a material by the adsorption of high energy materials [118]. Then, this gives rise to the fact that $W_{ad} \approx W_{adv}$. As a general rule of thumb it can be seen that adhesional wetting occurs when the value of Equation (3.4) is positive when $\theta < 180°$, which gives rise to spontaneous adhesion wetting when $\cos\theta > -1$ [88]. It has also been observed that this specific type of wetting is the most common compared to the other types.

3.3.2 – Immersional Wetting

Immersional wetting can be defined as a solid-vapour interface being exchanged for a solid-liquid interface with the degree of the solid-liquid interface remaining unaltered. The driving force which gives rise to this variation of wetting is the quantity $\gamma_{sv} - \gamma_{sl}$. Leading on from this it can be seen that if a finite contact angle was to be given from the immersion of the solid in the liquid then the energy change, W_{im}, can be calculated from

$$W_{im} = \gamma_{lv} \cos\theta \tag{3.5}$$

where θ can be determined by measuring the angle that results with the solid and the liquid-air interface. Generally, this type of wetting can be seen to occur $\theta < 90°$, with spontaneous immersional wetting occurring when $\cos\theta > 0$ [88].

3.3.3 – Spreading Wetting

Spreading wetting arises from corresponding areas of solid-liquid and liquid-vapour interfaces replacing the solid-vapour interface. It is known that for this process to arise spontaneously the surface free energy, W_{sp}, which can be calculated using Equation (3.6), must decrease during the time in which the spreading process takes place.

$$W_{sp} = \gamma_{lv}(\cos\theta - 1) \tag{3.6}$$

This phenomenon occurs when $\theta = 0$ and as a result spontaneous spreading occurs for $\cos\theta > 1$ which allows one to see that this condition can never be satisfied unless external work is carried out on the liquid [88].

3.3.4 – The Spreading Coefficient

In order to analyse spreading and the spreading coefficient effectively it is primarily necessarily to take into account the work of adhesion that would be required to sever the attraction that arises between the dissimilar molecules of the solid-liquid interface. By considering this it can be found that the W_{ad} required to break this attraction (see Equation (3.3) can be simplified to

$$W_{ad} = \gamma_{sv} + \gamma_{lv} - \gamma_{sl} \tag{3.7}$$

where all the parameters shown in Equation (3.7) have their usual meaning. Following on from this it is then required to consider the amount of energy that would be required to separate the molecules of the spreading substrate. This amount of energy is known as the work of cohesion, W_{co}, and is given by:

$$W_{co} = 2\gamma_{lv} \tag{3.8}$$

To obtain an equation for the spreading coefficient, *S*, one must take the difference between W_{ad} and W_{co} thus:

$$S = W_{ad} - W_{co} = \gamma_{sv} - \gamma_{sl} - \gamma_{lv} \tag{3.9}$$

From Equation (3.9) it can then be deduced that *S* is the determinant as to whether a drop of liquid would spread across the surface allowing it to become wet and provide a coating or determine whether the droplet will remain finite giving an equilibrium contact angle. Leading on from this, one can use certain boundary conditions to determine the condition required for spreading to occur. The first boundary condition is that $W_{ad} > W_{co}$ allowing the spreading coefficient S to become positive and the contact angle equates to 0° giving rise to spontaneous spreading over the surface producing a thin film of liquid. Alternatively, the second boundary condition is that $W_{ad} < W_{co}$ giving the spreading coefficient, S, to be negative leading on to the contact angle to be greater than 0. This indicates that the liquid would not spread across the surface and would produce a droplet allowing a finite contact angle to be achieved. From this, by equating Equation (3.1) and Equation (3.9) this would allow one, in terms of *S*, to determine the condition expression for spreading to occur spontaneously:

$$S = \gamma_{lv}(\cos\theta - 1) > 0 \tag{3.11}$$

3.4 - Surface Energy and Dispersive/Polar Characteristics

From Equation (3.1) it can be seen that the quantities γ_{lv} and θ can relatively be easily measured experimentally. Whereas γ_{sl} is a parameter which would require further work to determine. Throughout any wettability study it is known that the effect of adsorption of the measuring liquid on the solid surface should also be taken into account. Having said that, due to the negligible effect this phenomenon has in systems containing solid polymers many researchers choose to neglect it. In order to determine γ_{sl} further assumptions are required, with the interpretation of these assumptions

determining the direction of the methods for calculating the surface free energy of polymeric materials.

Fowkes [119] was a pioneer of approaching this subject with the idea of partitioning the surface free energy into individual components which assumes that interfacial interactions arising from the properties of the measuring liquid and surface layer determine the quantity γ^T. Fowkes originally stated that one can assume that the surface free energy of a solid is composed of a sum of individual components:

$$\gamma^T = \gamma_s{}^d + \gamma_s{}^p + \gamma_s{}^h + \gamma_s{}^i + \gamma_s{}^{ab} + \gamma_s{}^o \tag{3.12}$$

where $\gamma_s{}^d$, $\gamma_s{}^p$, $\gamma_s{}^h$, $\gamma_s{}^i$ and $\gamma_s{}^{ab}$ are the dispersive, polar, hydrogen, induction and acid-base components, respectively. Additionally, $\gamma_s{}^o$ denotes all other interactions that may be present in the system.

The Owens, Wendt, Rabel and Kaelble (OWRK)method [120] modified the Fowkes equation by assuming that all of the components on the right hand side of Equation (3.12), apart from $\gamma_s{}^d$, can be associated with and therefore incorporated in $\gamma_s{}^p$. Following on from this, they were then able to derive:

$$\gamma^T = \gamma_s + \gamma_l - 2\left(\gamma_s{}^d \gamma_l{}^d\right)^{0.5} - 2\left(\gamma_s{}^p \gamma_l{}^p\right)^{0.5} \tag{3.13}$$

From Equation (3.13) it can be seen that two unknown variables arise: $\gamma_s{}^d$ and $\gamma_l{}^p$. As a result of this Equation (3.13) can be deemed insufficient to determine the surface free energy of a polymer. Using two measuring liquids made it possible to calculate the surface free energy by combining Equation (3.1) and Equation (3.13) and adapting the resulting equation by transposing it to the general equation for a straight line. By implementing a sessile drop device with software such as SCA20 supplied by Dataphysics Instruments it is then possible to easily use the OWRK method for the software to calculate γ^T. This is done by the software producing a linear graph as shown in Figure 3.4 from the data inputted.

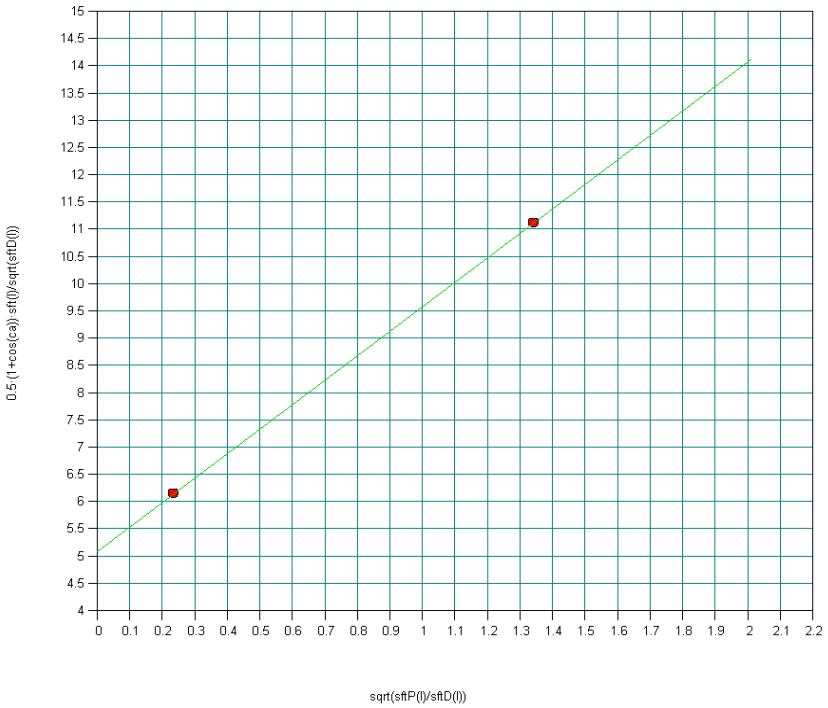

Figure 3.4 – Example linear regression plot for the SCA20 software to calculate γ^T.

In order to reduce errors the measuring liquids decided upon should be one with a dominant polar component and one dispersion liquid. As this method allows for the relative ease of derivation of components the OWRK technique is one of the most common used with water and diiodomethane being the most frequently used measuring liquids.

3.5 – Effects of Surface/System Parameters on the Contact Angle

Through research that has previously been carried out by others it is possible to utilize this knowledge to determine how the contact angle varies with regards to controllable parameters. Three of the main parameters that can have an effect on the contact angle of a system will be discussed here; with these being surface roughness, chemical composition and temperature.

3.5.1 – The Relationship Between Contact Angle and Surface Roughness

Throughout this chapter it has been assumed that an idyllic flat, homogenous, uniform solid surface has been used such that when the liquid comes into contact with the material a single contact angle is produced. In contrast, it can be seen that almost all surfaces have a defined roughness which would give rise to a number of contact angles that can be achievable. In order to counteract this, it is possible to use the contact angle hysteresis which has been discussed previously in Section 3.2.1.1. From extensive research over many years it has been found that the contact angle hysteresis of nearly all systems is principally a resulting factor that arises from surface roughness [121-125]. It is conveniently then possible for one to see that surface roughness is one of the most important factors

with regards to the contact angle due to the fact that the roughness of a surface has direct influence over the angle that can be produced between a liquid and a solid.

As it has been realized that the roughness of a surface can directly affect the size of the contact angle it has been determined that it is possible to visualize the roughness of a surface as a series of grooves. To simplify systems there has been two main types of grooves derived known as radial and circular grooves in which it is possible to characterize the roughness of a surface using both of these variations. This has led to the determination of two roughness parameters being the Wenzel type [126], D_R, and the Cassie-Baxter type [127], F_R. For laser irradiated surfaces it is usual to see that wetting occurs radially giving rise to a radial contact angle, θ_{rad}, which has been found to be related to the theoretical contact angle, θ_{th}, as given by

$$cos\theta_{rad} = D_R(1-F_R)cos\theta_{th} - F_R \tag{3.14}$$

In addition to this, from the workings of Neumann and Good it was found that when F_R equates to zero it is possible to deduce a model which is similar to that of heterogeneous solid surfaces that accounts for any surface irregularities present and can be expressed using Wenzel's equation [128,129]:

$$r_a\left(\gamma_{sv} - \gamma^T\right) = \gamma_{lv}\cos\theta_w \tag{3.15}$$

with r_a being the roughness factor which can be determined by calculating the ratio of real and apparent surface areas and θ_w is the characteristic contact angle for the wetting of the rough surface. By rearranging Equation (3.15) γ_{sl} can be defined as

$$\gamma^T = \gamma_{sv} - \left(\frac{\gamma_{lv}\cos\theta_w}{r_a}\right) \tag{3.16}$$

From Equation (3.16) one can see that γ^T is inversely proportional to the roughness factor, r_a, indicating that if r_a is small the surface would be rough allowing γ^T to become small. Therefore, this would result in the contact angle of the solid-liquid system to be increased allowing the material to become more hydrophobic. However, it should be noted here this approach taken by Wenzel can only be effective at the position of the wetting triple line [123].

It has also been seen that a mixed-state wetting regime could arise in certain systems [92,102,130,131]. That is, there is a combination of Wenzel and Cassie-Baxter wetting regimes present over the solid-liquid interface. For instance, it has been shown that it is possible for a hydrophilic material to give rise to this mixed-state as a result of the surface roughness and topography [102]. Due to the possibility of the mixed-state wetting regime arising on rough surfaces one can then extrapolate that this could give rise to an unexpected rise in contact angle which would not necessarily coincide with current theory which states that for an increase in roughness for a hydrophilic material, θ should decrease.

3.5.2 – The Relationship Between Contact Angle and Chemical Composition

It has been seen that the chemical composition of the surface of a material can allow the contact angle to be somewhat influenced by either allowing it to become more hydrophilic or hydrophobic. This is due to the fact that the surface energy of a material can be modified by varying the chemical composition at the surface. It has been widely reported that the oxygen content of surfaces can be manipulated in order to produce the desired wettability characteristics on the surfaces of various materials [26,29,49,56,71,83,132]. For instance, it has been found that by increasing the surface oxygen content on MgO-PSZ, by CO_2 laser treatment in air, the contact angle for glycerol incident on the surface was dramatically reduced [88]. Similarly, it was determined by Lawrence and Li [88] that the O_2 content within the surfaces of PE and PMMA could be greatly increased by using excimer laser beam surface modification. This has seen to leadsto an increase in the polar component of the surface energy, allowing for the variation in the wettability characteristics of the polymeric materials used.

Even though there has been extensive research into using air and O_2 as the ambient processing gas it does not seem that the use of other processing gases has been widely researched with respect to polymeric biomaterials and their wettability characteristics. However, a comparative study using air, oxygen and helium has been carried out to laser modify polystyrene surfaces for biological applications [29]. Through the workings carried out by Pfleging *et al.* [29] it was determined that for laser irradiation wavelengths of 248 nm only a small variation of contact angle (10 to 20°) could be achieved and was seen to be mainly due to the modification of surface topography. Alternatively, it was found in the same research that wavelengths of 193 nm allowed the wettability of the polystyrene surfaces to be controlled using parameters such as fluence, processing gas and applied pulse number. Additionally, it has also been reported that is possible to use photolyzed hydrazine to vary the surface chemical composition of PTFE giving rise to stronger adhesion for metal layers [82]. From this it can then be seen that it would be advantageous to carry out experimentation to attempt and determine the optimum processing gas for each laser that is to be employed to modify the surface characteristics of the numerous polymeric biomaterials.

One other major aspect that is required to be taken into account when analysing wettability and the material surface chemistry composition is that of functional groups. It has been discussed by a number of researchers [4,33,133,134] that functional groups do tend to have a large influence on the wettability of materials. Pimanpang *et al.* [134] found that an increase in polar functionalities (C=O and –OH) on SiLK surfaces treated with H_2SO_4 solution could be attributed to the observed decrease in advancing and receding contact angles. Furthermore, it has been stated by O'Connell *et al.* [133] and Kim *et al.* [135] that functional groups could have a considerable influence on hydrophobic recovery.

3.5.3 – The Relationship Between Contact Angle and Temperature

As one can well imagine, one of the main parameters of a system that can be effectively controlled is the temperature of both the ambient atmosphere and the liquid. Over many years there has been

extensive research into how the variations in temperature can affect the contact angle produced by a liquid that is incident on a surface. From this research it has been realized that for temperatures between 20 and 80 °C there is a negligible effect on the contact angle produced [88]. Therefore, it can be noted that for any intended application which operates outside of this temperature range, the resulting affect on θ must be taken into account.

4
Cell Adhesion, Bioactivity and Testing of Polymeric Biomaterials

This chapter a comprehensive review of the literature pertaining to the biological evaluation of materials, discusses bonding and shows the distinct potential link between wettability and biofunctionality. In addition, in vitro techniques are discussed in terms of the relationship between bioactivity and wettability characteristics.

4.1 – Introduction

Within the biomaterials industry it is crucial that the bioactivity of the materials employed is sufficient in order to ensure that the failure rate of the implants is kept to a minimum. This can be done by ensuring that, through extensive testing methods, a biomaterial incites adequate cell adhesion and proliferation to allow for the biological environment to accept the biofunctional material. It is essential for implants to be accepted and integrated into the biological environment as quickly as possible as increased integration time would give rise to the possibility of common clinical problems such as loss of tissue in the vicinity of the implant or the implant becoming loose allowing for discomfort or pain to the patient [136]. As a result of this, in order to achieve the best possible results from a polymeric biomaterial a range of skills are required that span over multiple disciplines. As such, throughout the research of many over this multi-disciplinary subject it has been realized that both the bulk and surface properties of all biomaterials hold the ability to influence the degree of *in vivo* bioactivity. From this, one can then deduce that there appears to be a direct link between the characteristic wettability of a biomaterial and the level of bioactivity that a material possesses. This has allowed many to research this area in the common aim of determining how the properties of a biomaterial can affect the bioactivity. Van Oss *et al* [95] investigated into how van der Waals forces and hydrogen bonds affect the adhesion of proteins to low energy polymeric surfaces. This publication highlights many aspects of adhesion and indicates that the term ‘hydrophobic interactions’, which was used at the time for explaining wettability, was ambiguous and introduced the term ‘interfacial forces’. In addition, the work carried out by Xu *et al* [137]showed that by varying the contact angle of LDPE, using glow discharge plasma, the stronger adhesion forces for numerous proteins was optimized for contact angles between 60 to 65°. The results from this research also allowed Xu *et al.* [137] to conclude that by increasing the contact time from 0 to 50 s the adhesion force considerably increased independent of the LDPE surface wettability. Following on, it is to be concluded whether the surface topography and/or surface chemistry of a polymeric biomaterial is the driver to manipulate the wettability and bioactivity characteristics. Much work has already been carried out for ceramics and metals such as the research underataken by Wirth *et al.* [138] which indicated that NiTi surface roughness only appeared to influence cell proliferation only whereas the surface chemistry gave rise to the manipulation of cell adhesion.

This chapter will introduce bonding, cell adhesion and will also discuss how the wettability of a material can be utilized to determine the bioactivity characteristics. There are many factors in which it is possible for a medical implant to fail such that it is necessary for these to also be considered. In addition to this, various methods of analysis will be discussed which are commonly used throughout the biomaterials industry to determine the quality of the bio-implant materials. It can be seen that these analytical techniques, which can be employed prior to the use of biomaterials, allows for one to attempt and foresee whether or not a biomaterial is suitable for the required task.

4.2 – Bonding of Liquids and Solids

For sufficient bonding to take place it is necessary that the wettability of the solid surface is required to be sufficient along with the fact that the liquid's surface tension should not be excessively high. To ensure efficient wetting and bonding it is required that the surface of the solid be free from coarse irregularities and dirt giving rise to the need of a sufficiently clean work space. In contrast, it should be noted here that it has been seen that various coatings, which can be applied to the surface prior to bonding, are held more firmly by rougher surfaces. In addition it should also be noted here that during the bonding process between the liquid and solid the composition of the liquid is of major importance due to the fact that this factor determines the coefficient of thermal expansion and the surface tension.

There are numerous mechanisms that can take place to create the bond between the liquid and solid materials. In a generalized sense these mechanisms can be categorized into three basic groups; these being physical, mechanical and chemical bonding. It can be seen, within chemical bonding especially, that a number of various theories are available for the reasoning behind the three categories. Through experimentation; however, it has been determined that it is possible for a combination of these mechanisms to take place to give rise to the bonding and is dependent on the materials that are used [88]. Therefore, it can be seen that by modifying materials to strive to enhance these mechanisms, this may hopefully give rise to a stronger more durable bond.

4.2.1 – Physical Bonding

This specific type of bonding arises when two perfectly flat surfaces become incident such that they are brought together to atomic interaction distances allowing local atomic rearrangement to take place resulting in adhesion taking place. It has been seen that a typical example of physical bonding arises from van der Waals bonding [139] in which the resultant work of adhesion is the energy difference between the two specific surface energies. From the work of adhesion it is possible to deduce a characteristic theoretical breaking stress which has been found to be several orders of magnitude less than the actual value [88]. As a result of this, it has been realized that this type of bonding can be utilized as a selection guideline for materials to determine if they will bond to produce sufficient adhesion [139].

4.2.2 – Mechanical Bonding

Mechanical bonding occurs through the attachment of rough surfaces such that an interlocking microstructure is formed in order to give tensile strength and frictional strengthening. In order to enhance the mechanical bonding process it is possible to roughen the substrate using various techniques that have been mentioned previously. All the techniques mentioned in sections 2.3 and 2.4 have varying effectiveness which is dependent on the required application, materials used for that application and the optimum application in which they can be utilized. Following on from this, it is possible to see that chemical interactions between the liquid and solid can give rise to mechanical bonding. It should also be noted here that it is possible to increase the surface area of a mechanically roughened surface to induce an enhancement of physical bonding.

4.2.3 – Chemical Bonding

There has been extensive research into the numerous mechanisms that can take place during the chemical bonding process. Through this research it has been found that during the bonding of two dissimilar materials a chemical bond is produced at an interface when there is a balance of bond energies, along with a continuous electronic structure. In addition to this, it has been seen that this arises when a thermodynamically stable equilibrium is reached at the interface and arises from chemical reactions which take place on the surface of the material. It should be noted here that a chemical bond constitutes an electronic structure and a balance of bond energies that arise across the interface for each main type of bonding: ionic, covalent and metallic bonding.

4.2.3.1 – Ionic Bonding [140]

Ionic bonding consists of electron donor (metallic) atoms transferring one or more electrons to an electron acceptor (non-metallic) atom. This gives rise to a cation and an anion to be produced which are both highly attracted to each other through electrostatic and Coulomb effects. From this high state of attraction between the two atoms it can then be seen that the ionic bond is formed due to this phenomenon.

One well known structure that arises from ionic bonding is that of crystalline structures in which the many ions within the solid are arranged in such a way as to become surrounded by as many anions as possible. This is done to attempt and reduce the overall energy within the system by reducing the very strong repulsion forces that arise between the cations.

4.2.3.2 – Covalent Bonding [140]

It has been seen that those materials which have atoms with four valence electrons have the capability of both donating and receiving electrons and as such are not able to produce the strong ionic bonds. To counteract this, these atoms can produce covalent bonding in which the two bonding atoms donate an electron to form a shared pair between the atoms.

Carbon atoms produce covalent bonds with each atom having four nearest neighbours in which a bond is shared with each. This gives rise to a very stable structure and extremely strong materials such as diamond can be produced indicating that covalent bonding can produce bonds as strong as those produced by ionic bonding.

4.2.3.3 – Metallic Bonding [140]

Metallic bonding is another strong bond that can form; however, it should be noted here that this specific type of bonding is the least understood compared to the other variations. It is known, as metal atoms are strong electron donors, that they cannot bond via either ionic or covalent bonding. Furthermore, it has also been realized that metals are very strong and also have high melting temperatures indicating that there has to be relatively strong bonds that hold the atoms together. The widely accepted model in which this type of bonding can be visualized is that the atoms are positioned in an orderly, repeating pattern with the valence electrons being allowed to move freely between the atoms.

4.3 – Cell Adhesion

There are various types of biological molecules that allow for adhesion between cell and the extracellular environment to take place. The four main categories that cell adhesion molecules fall into are cadherins, selectins, immunoglobulins and integrins [136]. These molecules essentially function as flexible cell membrane receptors as they allow for the possibility of both mechanical and biochemical signals to be transmitted and allows for those signals to be transmitted across the membrane bidirectionally. It can then be seen that this signalling gives rise to numerous processes such as cellular migration, apoptosis, gene expression and differentiation. It should also be noted here that for normal cellular function to take place around a bio-implant implant it is necessary to have multiple cell adhesion molecules operating to produce the required bond.

4.3.1 – Cadherins

This category of cell adhesion molecule has the main function of ensuring that solid tissue is organized and also ensures that the tissue's integrity is optimized. As such, they are specialized in maintaining stable adhesive interactions by giving rise to the possibility of forming long lasting, almost permanent bonds. It is possible for cadherins to fail in their task due to the fact that mutations can occur giving rise to the possibility of tissue disorder and cellular dedifferentiation and, on some occasions, could even give rise to malignancy. Cadherin adhesion has been found to be highly dependant on calcium as it is calcium ions that allow for rigid cadherin structures. The presence of calcium ions also allow conformational changes required for adhesion to take place and aids by giving the necessary resistance to proteolysis.

4.3.2 – Selectins

Selectins can be seen to be very dissimilar in comparison to cadherin molecules due to the fact that they give rise to short-lived, temporary bonding. The process of selectin adhesion can occur under flow and is dependant on divalent calcium ions. Selectins are known to possess five domains, these being three extracellular, one transmembrane and one intracellular or cytoplasmic. In addition to this, it should be noted here that it has been realized that selectins have the ability to bond with carbohydrate-containing liquids and integrin ligands.

4.3.3 – Immunoglobulins

There are numerous various molecules that fall under the immunoglobulins that can be found to aid in cell adhesion within the biological environment. Due to the numerous types of these molecules it can be seen that this family of cell adhesion molecules can assist in various types of adhesion. For example, they have been found to aid in platelet-endothelial cell adhesion, neural cell-matrix adhesion and vascular cell-matrix adhesion. Immunoglobulins have been found to possess the ability to carry out both homotypic and heterotypic bonding to integrin and extracellular matrix ligands.

4.3.4 – Integrins

It has been found that the family of integrin cell adhesion molecules is one of the main, most important families with regards to cell adhesion. As a result, it has been seen that extensive research has been carried out within this area of cell adhesion. Through the research that has been carried out it has been determined that integrin molecules play vital roles in numerous processes that can give rise to the bonding of two materials and it can be argued that integrin molecules are the principal cell adhesion receptors for numerous proteins such as fibronectin and collagen. Following on from this, it has also been seen that it is possible for cells to incorporate more than one singular type of integrin receptor molecule which allows for the signals across the membrane to be differentially regulated. It has also been observed that integrins can operate as mechanotransducers between a cell and the close proximity surrounding area of the biological environment.

4.4 – The Role of Wettability in Biomaterials Science

The role of wettability in biomaterials science has been one of the most interesting subject areas in biomaterials surface science for a number of years now and has allowed many to endeavour to determine the complex links between surface wetting and bioactivity. A number of theories have been put forward in order to explain this phenomenon in which they usually fall into two basic categories. The first attempts to correlate the surface energy with the bioactive properties whilst the second involves water solvent properties near the surface in which a correlation between the contact angle and bioactivity is strived for. It should be noted; however, that in both of these categories arises a fundamental factor in which the surface energy/wetting is related somewhat to the biological response [141]. Many researchers have taken various approaches as to ascertain quantitative reasoning to bioactivity such as van Oss *et al* [142] by utilizing the ‘equation of state’ approach to calculate

interfacial tensions from previously measured contact angles in order to attempt and predict cell adhesion. Such approaches have been found to fall short for determining a quantitative theory regarding the bioactivity of a material; however, through research it is hoped that one day the role of wettability can be manipulated and used to allow one to predict quantitatively how a material can operate within a biological environment. Spijker *et al* [143]produced a very useful review paper which took into account flow conditions, surface wettability and how these factors could manipulate blood compatibility of biomaterials. This concise report on current blood-contacting devices allowed them to highlight that both thrombosis and high shear stress platelet deposition were two severe setbacks with regards to the application of these devices. In addition, they also concluded that devices used for vena cava filters and blood bags give rise to undesirable side effects which mainly incorporate coagulation. From these conclusions it can then allow one to see that these problems arise due to insufficient surface properties as the materials have been chosen due to the bulk properties. In order to counteract this Spijker *et al* [143] suggest that these surfaces be modified in order to withstand the shear conditions and associated mass transport.

4.4.1 – Biomaterial Interfaces

One of the major critical factors that arises from biomaterials surface science is that of surface sensitivity due to the fact that only the uppermost atomic layers are in direct physiochemical contact with the surrounding biological environment [4,141]. As a result of this it is then possible for one to deduce that only a few molecular layers of a material determines the bioactivity of that specific material. It has been realized that chemical reaction events such as hydrogen bonding, ion exchanging and acid-base reactions transpire within atomic distances. In addition to this, it has also been determined that longer-range hydrophobic forces have the ability to act over distances up to 10nm and can be found to be accountable for such processes as non-specific adsorption, surface-induced water structuring and adhesion within this 10 nm distance. It is then possible to come to the conclusion that any interaction carried out between the biological environment and a material will take place within a small, narrow region which has been named the interface. Following on from this, it can then be seen that the bioactivity of a material is determined by both the surface chemistry and surface topography of the material within the uppermost few nanometres.

4.4.2 – Tensiometry

Tensiometry is the term given to the broad range of processes that can be utilized as wetting techniques in order to determine the surface energy of a system. One of the most common tensiometric methods available, and which has already been discussed, is that of the contact angle arising between a liquid incident on a solid surface. The role of tensiometry within the biomaterials industry can be seen to be one of major importance as this allows analytical techniques to be performed in the attempt to link surface sensitivity to the bioactivity of a material. When considering tensiometry it is necessary to realize that these various methods encompass three major factors. The first factor to be taken into account is that the wetting measurements that can be achieved are sensitive to only approximately the upper 0.5 nm of the material's surface [144,145]. As a result, it is possible

for one to see that the methods used to characterize this phenomenon are some of the most surface-sensitive techniques currently available to biomaterials scientists. Secondly, experimental tensiometric methods allows for the fundamental energy at a specific interface to be determined which has been found to be one of the major causes for processes such as adsorption and adhesion to take place. This second factor can be seen to be of specific interest to biomaterial scientists as this would then allow an analytical approach to link the interface energies to such processes as protein adsorption and cell adhesion. The third factor that can be considered is that it is possible to carry out specific wetting measurement experiments in conjunction with using proteinaceous saline solutions which have been found to be of importance and relevance to many biomedical applications.

4.4.3 – Interfacial Biophysics

From physiochemical research studies of biomaterial interfaces it has been determined that the energies arising at the interfaces for a given system are the most important, primary determinants with regards to the bioactivity of a material. Within colloidal science it has been seen that a theory has arose which allows the interactions at small distances to be quantified and that it can be applied to biomaterial applications. This theory is named the Derjaguim Landau Verwey Overbek (DLVO) theory and allows one to see the relationship between particle (cell) distance from the surface, repulsive (electrostatic) and attractive (typically van der Waals) interaction energies [4]. This theory can be visualized as seen in the graph shown in Figure 4.1.

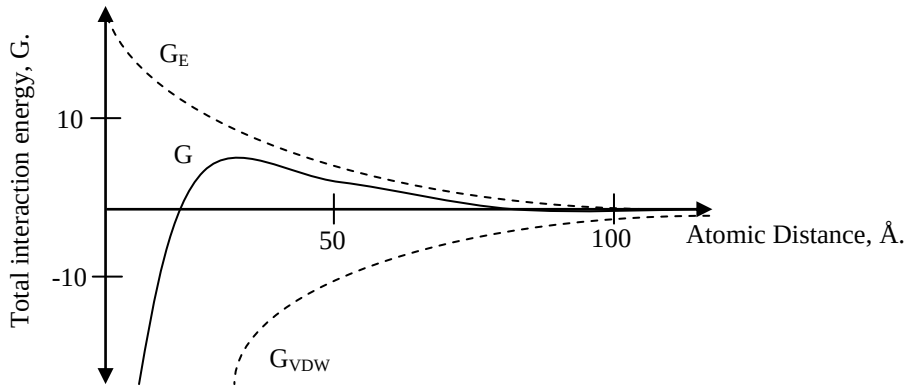

Figure 4.1 – Example graph showing the interaction energies between a particle (cell) approaching a solid.

From Figure 4.1 it can be seen that *G*, the total interaction energy incorporated within the system is made up of the attractive van der Waals forces ,G_{VDW}, and repulsive electrostatic forces, G_E. It is also possible to see that two minimums are acheiveable in which the first arises at approximately <5 Å and the second arising when the distance is approximately 100 Å. Following on from this an energy barrier arises around 40 Å in which the total interaction energy, *G*, can be determined to be

$$G = G_E + G_{VDW} \tag{4.1}$$

where G_E is the electrostatic interaction between a particle and a solid substrate. It should also be noted here that G_{VDW} can be determined using

$$G_{VDW} = -Ha/(6D) \tag{4.2}$$

Equation (4.2) characterizes the van der Waals interaction that arises between a particle with a radius, *a*, and a distance, *D*, to a flat solid substrace. With *H* being the Hamaker constant.

The foundation in which the DLVO theory is based upon is that the attractive van der Waals potentials and the repulsive electrostatic forces that arise within a given system can be summed up by addition. The way in which these various interaction potentials can arise within the system can be seen to be relatively complex; however, when a macroscopic approach is taken to the system a qualitative prediction can usually be easily achieved. If the system was to be viewed from a physicochemical angle, the kinetics in which the adhesion takes place can be simply described as long range interactions [119] and short range interactions [95]. These two different types of interactions are also commonly known as dispersive and polar forces respectively. It is thought that the dispersive forces arise from the second occurring minimum but only requires a minimum amount of energy to remove the particle from the surface. On the other hand the short range polar forces between a cell and a solid surface can only arise with distances of less than 20 Å in which more energy is required to remove the particles from the surface in comparison to the long distance dispersive forces.

The DLVO theory has been widely accepted and used throughout the biomaterials industry whilst carrying out research into this field. From the literature, one can see that this theory is applicable to a wide variety of applications. For instance, it was observed by Botero *et al.* [146] that their results into the investigation of surface chemistry and biosorption of *Rhodococcus opacus* was supported and verified by the DLVO and X-DLVO (extended DLVO) theories. It should be noted here that the X-DLVO theory was developed by van Oss [147] by incorporating the Lewis acid-base interactions. Both these theories have allowed for the investigation into the net interaction between inert surfaces and bacterial cells such as through the work carried out by Sushko and Shluger [148] who used the DLVO theory to explain the mechanism arising from the interactions between DNA and polymer surfaces.

4.4.4 – Thermodyamics in Biomaterials Science

Since the 18th century many scientists have been researching and devising theories/relationships within the wide subject area of thermodynamics. From these investigations it has been realized that surface thermodynamics is a very useful tool in order to model the biological response of numerous materials. This is due to the fact that surface thermodynamics offers a dynamic way to efficiently deal with multicomponent systems. As previously discussed, it has been proven through scientific investigation that the wettability of a material is a relatively important and crucial determinant as to whether cell adhesion will take place. From this, it has been seen that the surface free energy of a material, along with the characteristic resulting contact angle evaluated with a liquid, can be directly related to the determination of bioactivity and cell adhesion. It has also been discussed previously that small values of θ (<30°) correspond to the hydrophilic effect in which high surface energies can be determined. These hydrophilic surfaces have been seen to offer a better potential for cell adhesion to

occur in comparison to those materials that exhibit the hydrophobic effect in which give a θ more than 90° and usually have considerably lower surface free energies.

It has been widely observed and is now accepted that poor cell spreading on hydrophobic materials and good cell spreading on those materials exhibiting hydrophilic phenomenon can arise in both the absence and presence of pre-absorbed serum proteins [4]. Furthermore, it has also been seen that through researching into wettability gradient surfaces protein adsorption is more likely to occur with hydrophobic materials in comparison to those that are hydrophilic. From this one can then deduce that the exchange of a pre-absorbed protein by another protein would be more likely to occur on a hydrophilic material, adsorption-induced conformational variations occur greater on hydrophobic materials and that cell adhesion reaches an optimum on those materials exhibiting mild hydrophilic tendencies with θ around 60°.

Through thermodynamical reasoning it is possible to determine the interfacial free energy of adhesion, ΔF_{adh}, from the process of adhesion and spreading of a liquid incident on a solid substrate as

$$\Delta F_{adh} = \gamma_{cs} - \gamma_{cl} - \gamma_{sl} \tag{4.3}$$

where, γ_{cs} is the cell-solid interfacial free energy, γ_{cl} is the cell-liquid interfacial free energy and γ_{sl} is the solid-liquid interfacial free energy. By applying the two limiting boundary conditions it is possible for one to see that for $\Delta F_{adh}<0$ adhesion and spreading is likely to occur due to the fact that this is favorable energetically. By taking into account the other boundary condition, $\Delta F_{adh}>0$, then it can be seen that adhesion and spreading is least likely to occur due to this not being favorable when taking into account the interfacial free energies. By researching into parameters such as the interfacial free energy of adhesion and substrate surface free energy (or wettability) it was found by Stewart *et al* [149] that a graphical relationship can be devised using these parameters, as shown in Figure 4.2.

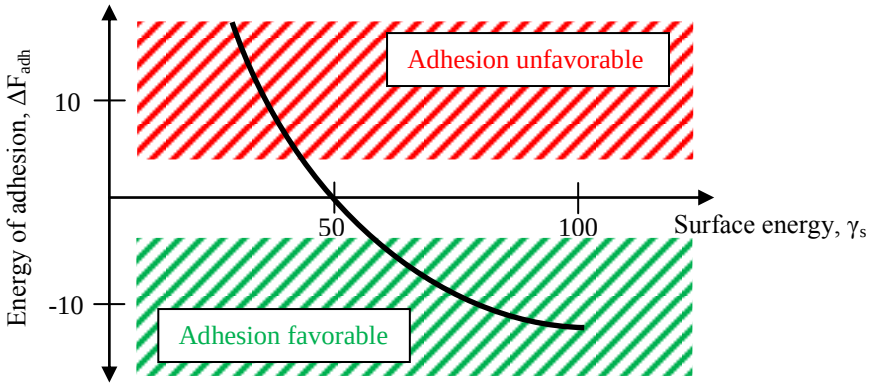

Figure 4.2 – An example graph indicating the relationship between the interfacial energy of adhesion and the substrate surface energy.

From the work of Stewart *et al* [149] it was found that hydrophobic materials with $\gamma_s<40$ ergcm^{-2} do not give rise to the adhesion of fibroblasts. It should also be noted that it has been discovered that exceptionally hydrophilic materials do not give rise to adhesion [4].

4.5 – Failure Mechanisms of Polymeric Biomaterials

When considering materials for use in biological environments it is critical to understand the possible failure mechanisms that can arise. By researching and analysing into these failure mechanisms it is then possible to design biomaterials to function appropriately with some certainty as to the integrity of the material used. Obviously, one of the most important failure mechanisms that can occur with a biomaterial is that cell adhesion does not take place rendering the material used as bio-incompatible. Even though most biological environments appear to be relatively good environments for cell growth due to the neutral pH and modest temperatures it has been realized that specialized mechanisms have been produced over time by the human body in the attempt to rid the body of foreign objects [150]. Within this section some of the main failure mechanisms, both mechanical, chemical and biochemical linked to polymeric biomaterials will be discussed.

4.5.1 – Elastic Behaviour and Brittle Fracture [140]

From the work carried out by Hooke in 1678 it was found that most solids behave in an elastic manner and if a load great enough was applied then an elastic limit would be reached eradicating the elastic manner of the material. This phenomenon is also known as Hooke's Law and indicates that a material under the influence of a tensile force would be extended in the direction of that force. The length of this resultant extension was found to be proportional to the load that was applied to the material. This also allows one to see that almost all solids exhibit elastic behaviour if any applied external forces do not exceed the specific elastic limit for the corresponding material. One can also see that the amount of extension achieved in this way varies somewhat with the geometry of the sample. In order to counteract this, normalization can be applied such that a normalized load (force/area), also known as stress , σ, and a normalized deformation (change in length/original length), also known as strain , ε, can be determined. These normalized parameters can be applied to two main situations; these being tension/compression and shear. With the tension/compression area being perpendicular to the direction of applied force (tensile stress) and the extension being parallel to the original length (tensile strain). For shear the applied force can be seen to be parallel to the shear area (shear stress, τ) and the resultant extension is perpendicular to the original length (shear strain, γ). Following on from this a materials elastic constant can be determined for tension/compression and shear forces with these being the tensile (Young's) modulus, E, and the shear modulus, G, respective of tension/compression and shear forces. These material dependant constants can be determined with

$$E = \frac{\sigma}{\varepsilon} \tag{4.4}$$

and

$$G = \frac{\tau}{\gamma} \tag{4.5}$$

E and *G* can be seen to be crucial constants which can be utilized to determine some of the inherent properties of a given material. This is due to the fact that they allow a direct macroscopic insight into the strengths of the interatomic bonds incorporated within the corresponding material. Though, it should be noted that *E* and *G* can be used to characterize the stiffness of an isotropic material; however, for materials such as many polymers which are anisotropic then more than two elastic constants are required in order to determine a relationship between the stress and strain parameters.

In reality it has been realized that the elastic behaviour of a material is usually not constant over time due to the fact that microscopic defects will begin to rapidly grow if the material is under constant tensile and/or shear stress. These micro-defects will then overwhelm the material, causing it to suddenly fail by a mechanism known as brittle fracture. For many materials a graph of stress as a function of strain will produce a linear relationship until brittle fracture occurs at which this point on the graph is referred to as the fracture stress. Brittle fracture is exhibited by various types of materials including some polymers such as polymethylmethacrylate and unmodified polyvinyl chloride (PVC). It should also be noted here that brittle fracture occurrence is highly dependent on the number and size of the defects originally incorporated within the material.

4.5.2 – Plastic Deformation and Fatigue [140]

It has been found that for various materials ranging over metals, alloys and polymers plastic deformation occurs after a specific stress level is reached; however, plastic deformation can be seen to only occur between this stress level and the fracture stress point of the material. Once plastic deformation is achieved the elastic behaviour of the material ceases and the strains produced are somewhat greater than what can be observed during the elastic region. Plastic deformation is an irreversible process which arises due to whole arrays of atoms being manipulated by the applied force such that they are relocated within the crystal structure. This large scale displacement of atoms without complete failure is generally only achievable in those materials which incorporate metallic bonds; therefore, polymers cannot achieve plastic deformation as long-distance manipulation of arrays of atoms is not possible with ionic and convolutedly bonded materials.

Across many industries it has been seen that almost all materials suffer from fatigue which can be defined as structural failure as a resultant of repetitive cyclic stresses that are usually considerably less than the maximum yield tensile stress. The fatigue strength of a material is dependent on a number of parameters such as environment, temperature, corrosion, deterioration and cycle rates. As fatigue occurs with almost all materials it can then be deduced that this is a major factor which needs to be taken into account when considering biological applications for materials. This is due to the fact that one would require a biomaterial that has a long lifespan when taking into account the fatigue properties of that material.

4.5.3 – Degradation of Polymers in Biological Environments

Many materials that are subjected to biological environments suffer from the harsh environments leading to either rapid or incremental breakdown of those materials [150]. This is known as

biodegradation and can be defined as the chemical breakdown of a material by the incidence of living organisms giving rise to a modification of the physical properties of that material [151,152]. Polymers like all materials used for biomaterial implants are subjected to environments in which degradation can take place both physical and chemical or, in some instance, both physical and chemical degradation can occur. For example one of the main degradation process to occur with polymers can be seen from using gamma radiation for sterilization of UHMW polyethylene. This technique of sterilization gives rise to the production of free radicals within the material and can react with oxygen to produce reaction products which are highly undesirable for bioactivity conditions. Following on from this, chain oxidation and scission can occur which would lead to the polymer losing strength and potentially increasing the probability of brittle fracture occurring. Upon the analysis of polymeric implants using explant analysis or metabolite evaluation it has been found that chemical degradation generally is an occurrence as a result of numerous processes that incorporate either hydrolysis or oxidation.

4.5.4 – Calcification of Biomaterials

A number of biomaterial implants have been found to be affected by calcification (or mineralization) in which calcium compounds (usually calcium phosphate also known as apatite) are deposited onto the biomaterial in the biological environment [153]. In most cases these deposits have had devastating effects causing the bioimplant to fail. It should be noted here; however, that in some cases biomaterials are produced and used to give rise to calcification as this is required in such fields as dentistry applications. Calcification has been seen to occur with many various materials, which have been used as biological implants, especially for those materials used for applications incorporating the circulatory system and prosthetics.

There are two main classifications of pathological calcification that has arisen through studies of this failure mechanism of biomaterials and tissue; these are dystrophic and metastatic. The dystrophic calcification occurs within those biomaterials/tissues that are damaged and give rise to calcium salts to be deposited onto them. Alternatively, metastatic calcification occurs with the deposition of salts on the biomaterial/tissues that have unstable mineral metabolisms. From this, it can be seen that for biological implants one of the main concerns considering calcification is that of dead tissue as the cells and extracellular matrix of these tissues have been found to be the sites in which this failure mechanism occurs the most. It should also be noted that calcification can occur in two localities; these are intrinsic and extrinsic calcification. With intrinsic calcification being this mechanism occurring deep within the tissue and extrinsic being the calcification at the interface surface in which the attached cells and proteins are associated and affected.

4.6 – Methods of Testing Biomaterials

As it is crucial to achieve the best possible material for specific areas of the body for biological implants to enhance and sustain cell adhesion and proliferation it can be seen that the testing of biomaterials is a very important factor that should be considered prior to any material being implemented within a biological environment. As a result of this, numerous experimental tests have

been derived and utilized in order to analyse how a material will function within a specific environment. For biological implants there are two main areas of testing that can be seen; these being the bioactivity with regards to cell adhesion etc and the mechanical strength of the material. Both of these factors are of major importance due to the fact that without high bioactivity and an overall high mechanical strength then the biomaterial in the biological environment would fail causing potential pain for the patient and potentially causing more biological problems than necessary such as infections. By using experimental testing prior to the implantation one can then determine the risks involved with the procedure and also determine whether materials are feasible for use as biomaterials. Hereafter, in this section, various testing techniques will be discussed for both the biological and mechanical testing of polymers for use as biomaterials.

4.6.1 – *In Vitro* Assessment

In vitro testing of biomaterials is one of the most common ways in which biological functionality and cytotoxicity can be determined without causing harm to humans or animals. It has been seen that when researching new materials and techniques for biomaterials this method of testing is extensively utilized.

There are three main types of primary cell culture assays that are used under this method of biological assessment to determine the bioactivity of a material; these are direct contact, agar diffusion and elution (also known as extract dilution). Direct contact allows one to mimic physiological conditions whilst allowing for standardizing the amount of test material. Also, this method allows for target cell contact with the proposed biomaterial. Even so, disadvantages that this method poses are that cellular trauma can occur if the biomaterial sample moves during testing and cellular trauma is also possible with those materials that possess high densities. It has also been seen with this type of assay that the cell population can be highly decreased if highly soluble toxicants are present. Agar diffusion assays allow for an improved concentration gradient of present toxicants in addition to the possibility of allowing one to have the ability to assess the bioactivity of one side of the sample material. Having said that, it should be noted here that agar diffusion assays require flat surfaces to function efficiently and there is a risk of thermal shock when the agar overlay is being prepared. Alternatively, elution assays give rise to the possibility of separating extraction from the biological testing and is flexible with this method allowing one a wider variation in choice for extraction conditions and solvents. One of the main disadvantages that has been seen with elution assays is that additional time and steps are required in comparison to the other two alternative assays.

In most cases it is seen that *in vitro* assessment is carried out prior to *in vivo* assessment due to the fact that *in vitro* assessment allows one to gain a preliminary understanding of how a material will react within a biological environment. In some instances; however, i*n vitro* methods have been criticized for not giving a full picture of how materials will act in an environment which is relatively difficult to mimic. For example, it has been realized in some cases that *in vitro* assays do not incorporate cells that possess sufficient metabolic activity and would give results for toxicity that would not necessarily be observed within an *in vivo* assessment.

4.6.1.1 – Bone-Like Apatite Layers

Simulated body fluid (SBF) is a metastable calcium phosphate solution with an ion concentration approximately equivalent to that of human blood plasma. It can be seen throughout the literature that SBF can be implemented as a screening technique to predict and assess the bioactivity and osseointegration potential of materials [154]. This is owed to the fact that the bioactivity of almost all orthopaedic biomaterials has a strong relationship with the ability of that material to promote the formation of bone-like carbonite apatite crystals [62,155,156]. What is more, this apatite layer associates specific bone proteins which are crucial for any form of bone reconstruction [157]. Under healthy normal conditions, body fluid is known to usually be already supersaturated with respect to apatite and, upon nucleation of the apatite, the layer can grow through the consumption of calcium and phosphate ions that are present in the body fluid.

In vitro experimentation with SBF is usually carried out by soaking the material in question in SBF over a period of time at a constant temperature of 37°C in order to form an apatite layer on the surface. Afterwards, by analysing the surface one can then determine the possible suitability of that material for use as an implant and predict how that material will perform when bonding to bone. For example, by using some form of surface chemistry analysis, such as EDX or XPS, surface functionalities can be identified prior to immersion in the SBF. This can be seen to be of some importance as some hydroxyl groups can induce apatite nucleation in addition to calcium and phosphorous being vital to the adhesion of osteoblast cells as discussed by Song *et al* [62]. Through the work of Uchida *et al* [158] it has been identified that in some cases the extent of nucleation of apatite on the biomaterial surface is directly dependant on the functional groups present. That is, some functional components are released from the surface into the body fluid giving rise to an increase in ionic activity product which can allow for accelerated apatite formation.

On the other hand, it should also be noted that, like many *in vitro* experiments, employing SBF does not fully reproduce the *in vivo* environment for bone formation and may produce misleading results. But, as stated by Roach [154], *in vitro* techniques using SBF allows for a potential rapid screening of materials in the endeavour of development and optimization of biomaterials. Furthermore, these initial *in vitro* experiments can be used as preliminary studies prior to carrying out experimentation *in vivo*.

4.6.1.2 – Cytotoxicity

Cytotoxicity or cell death is usually evaluated by the quantification of plasma membrane damage. This is due to the fact that upon damage of the plasma membrane lactate dehydrogenase (LDH), a stable enzyme present in all cell types, is rapidly released into the cell culture medium. As a result of this, LDH is the most common and widely used marker in cytotoxicity studies. Thus it can be seen throughout the literature that due to the significance of cytotoxicity in determining the cell response of biomaterials a number of studies have been carried out using various materials [4,159-161]. There are a number of different *in vitro* cytotoxicity tests that can be carried out and are usually separated into two categories: direct methods, in which the cells are in direct contact with the testing solution, and indirect methods, where the cell culture medium is extracted prior to being analysed [162]. What is

more, Cytotoxicity kits are readily available "off-the shelf" and carrying out this study would allow one to determine the quality of the cells produced. It could also be used to determine if a specific biomaterial surface gives rise to better quality cell growth and proliferation in terms of cytotoxicity.

4.6.1.3 – Alkaline Leukocyte Phosphatase

Alkaline leukocyte phosphatase (ALP) activity is involved in bone formation and has been shown that ALP is significant in the development of skeletal calcification [163]. Also, ALP has been shown to be of major importance when detecting chronic myeloid leukemia owed to the fact that ALP activity typically decreases in patients who have contracted the disease [164]. With regards to bone formation, it is believed that ALP acts at the focal site of bone creation by eradicating inorganic pyrophosphate which is known to potentially inhibit calcification [163]. As a result of this, experimentation has been carried out previously to detect the ALP activity in order to assess the biofunctionality of biomaterials [4]. Like cytotoxicity, ALP kits are readily available 'off-the shelf' in a number of varieties and for a complete *in vitro* study of bioactivity ALP should be accounted for to ascertain how the ALP activity is modulated by the biomaterial in question.

4.6.1.4 – Protein Adsorption

It is well known and accepted that protein adsorption is the first event to occur following implantation prior to cell growth and proliferation [137]. Furthermore, cell behavior in terms of cell growth and proliferation is highly dependent on the properties of this protein layer [59]. Owed to the importance attributed to protein adsorption for osteoblast cell growth numerous studies have been carried out using different substrates to ascertain the protein adsorption response [4,137,165-167]. The protein thicknesses that arise are usually at most around 10 Å [4] and as a result of this, ellipsometry is the main technique to determine the layer thickness. Ellipsometry is therefore widely used for metals and ceramics; however, as most polymers possess a refractive index close to that of the protein layer, ellipsometry cannot be carried out making it very difficult to obtain results [167].

4.6.2 – *In Vivo* Assessment

In vivo assessment in comparison with *in vitro* is considerably more expensive and is usually carried out towards the latter stages of research into a biomaterial and is usually carried out following extensive *in vitro* testing. The reasoning for [154] this is due to the fact that in most cases *in vivo* relies on placing the proposed biomaterial into an animal in the aim to model the environment that would be observed within the human body. Also, one of the ultimate aims for *in vivo* testing is to ensure that the material/device would perform as expected allowing one to determine if the material would potentially present any significant harm to the patient [168,169]. Leading from this, it can be seen that a major factor with regards to these techniques is the selection of the animal to utilize. When selecting the animal the animal model in regards to the human application must be taken into account as this will have an impact on the results that will be obtained. For instance sheep are commonly used for the testing and evaluation of heart valves due to size constraints and the tendency to calcify tissue components of the biomedical devices. This would allow one to attempt and use an environment in

which the most sensitive model is available; however, it can still be argued in some instances that the environments used are not sensitive enough to determine whether a material would be accepted within the human body. *In vivo* assessment allows for various compatibility issues to be determined with some of these being sensitization, irritation, genotoxicity, hemacompatiblity, biodegradation and immune responses.

PART 2 – METHODOLOGY

5
Experimental Technique

The experimental procedures undertaken for laser processing, analysis of processed samples and biological testing are presented in this Chapter. For laser processing IR and UV lasers were used. For analysis of processed samples a sessile drop device, SEM and WLI were employed. Biological testing was carried out by seeding normal human osteoblast cells onto the samples and then observing. Further, SBF response, cytotoxicity and ALP activity was determined for each sample. Any procedures that differed from those within this chapter will be discussed along with the analysis.

5.1 – Nylon 6,6 Material

The nylon 6,6 (T_m: 255°, ρ: 1.3 gcm^{-3}) was sourced in 100 mm^2 sheets with a thickness of 5 mm (Goodfellow Cambridge, Ltd). To obtain a conveniently sized sample for experimentation the as-received nylon sheet was cut into 20 mm diameter discs using a 1 kW continuous wave (cw) CO_2 laser (Everlase S48; Coherent, Ltd). No discernible heat affected zone (HAZ) was observed under optical microscopic examination.

5.2 – Laser Processing Procedures

As four separate experiments were required for the laser processing, each is described seperately in sections 5.2.1, 5.2.2, 5.2.3 and 5.2.4. The lasers employed were a cw CO_2 laser marker (10 W; Synrad, Inc.), a 248 nm KrF excimer laser (LPX 200i; Lambda Physik, Inc.) and a cw 100 W CO_2 laser (DLC; Spectron, Ltd). The Synrad 10 W CO_2 cw laser marker was used for surface patterning, the Spectron 100 W CO_2 cw laser was used for the whole area irradiative processing and the Lambda Physik KrF laser was implemented for both patterning and large area irradiative processing of the nylon 6,6 samples.

5.2.1 – CO_2 Laser-Induced Patterning

In order to generate the required marking pattern with the 10 W CO_2 laser system (see Figure 5.1), Synrad Winmark software version 2.1.0, build 3468 was used. The software was capable of using images saved as .dxf files which can be produced by using CAD programs such as, in this case, Licom AutoCaM. The nylon 6,6 samples were placed into the laser system onto a stage in which they were held in place using a bracket with a 20.5 mm diameter hole cut into the centre of the bracket. The surface of the sample was set to be 250 mm away from the output facet of the laser system to obtain focus and the system employed a galvanometer scanner to scan the 95 μm spot size beam directly across the stationary target material. It should be noted that the target material and laser system was

held in a laser safety cabinet in which the ambient gas was air and an extraction system was used to remove any fumes produced during laser processing.

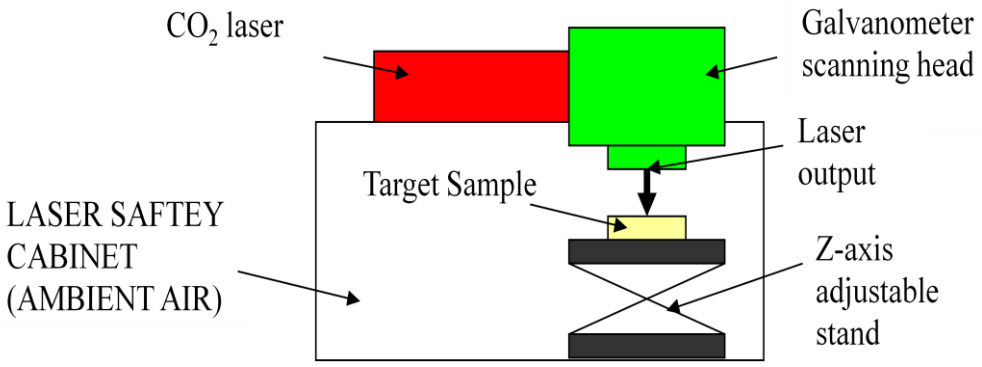

Figure 5.1 – Schematic diagram showing the experimental setup for the CO_2 laser-induced patterning and CO_2 laser whole area irradiative processing.

There were four patterns induced onto the surfaces of the nylon 6,6 samples; were trenches with 50 μm spacing (CT50), hatch with 50 μm spacing (CH50), trenches with 100 μm spacing (CT50) and hatch with 100 μm spacing (CH100). In addition, an as-received control sample was used (A1). For each of the irradiated patterns the laser power was set to 70% (7 W) operating at 600 mms^{-1}.

5.2.2 – CO_2 Laser Whole Area Irradiative Processing

A cw 100 W CO_2 laser (DLC; Spectron, Ltd) was used to scan a 5mm diameter beam across the target sample with one pass in order to irradiate the test area with an irradiance of 510 Wcm^2. By using a galvanometer as shown in Figure 5.1, scanning speeds of 150, 100, 75, 50, 25 and 20 mms^{-1} were employed to irradiate six samples with effective fluences of 16.84 (samples CWA17), 25.51 (sample CWA26), 34.18 (sample CWA34), 51.02 (sample CWA51), 102.04 (sample CWA102) and 127.55 (sample CWA128) Jcm^{-2}, respectively. As with the laser-induced patterning experimentation the samples were held in place on a z-variable stage with the whole experiment being carried out in a laser safety cabinet with the ambient gas being air.

5.2.3 – KrF Excimer Laser-Induced Patterning

For the patterned experiments (see Figure 5.2) the repetition rate was kept constant at 25 Hz, with a number of 10 pulses per site and used Aerotech CNC programming to induce the required pattern. A constant laser energy of 80±7 mJ was used with the attenuator set to 0.3 (30%) giving a measured energy at the target sample of 23.67±2.5 mJ, resulting in a fluence of 858±91 mJ/cm^2. In order to induce the intended pattern a projection imaging system was implemented with a focusing lens of x10 demagnification. The patterns induced using this technique were 50 μm trench (ET50), 100 μm trench (ET100), 50 μm hatch (EH50) and 100 μm (EH100). Two non-contact masks were used for both dimensioned patterns which included a brass mask with six 1 mm diameter holes spaced by 2 mm,

centre to centre, for the 100 μm dimensions and a SS316 foil (Laser Micromachining Ltd., UK) with five 0.5 mm diameter holes spaced by 1.5 mm, 'centre to centre', for the 50 μm dimensions (see Figure 5.3). To keep the constant 10 pulses per site it should also be noted here that scanning velocities of 0.125 mms^{-1} and 0.25 mms^{-1} were used for the 50 μm and 100 μm dimensioned patterns, respectively.

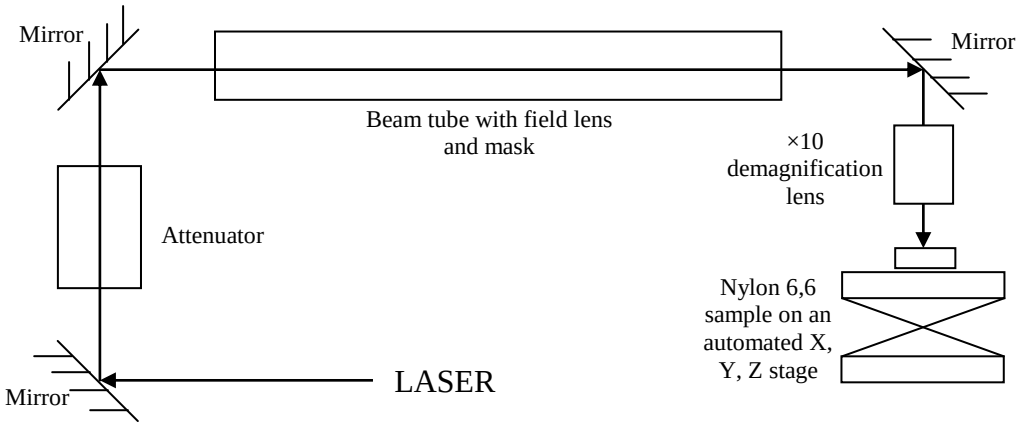

Figure 5.2 – Schematic diagram showing the experimental setup for the KrF excimer laser-induced patterning.

No processing gases were used throughout the experimentation and all laser processing was carried out in an enclosure in which the ambient gas was air. Also, for all laser processing no homogonizer was implemented meaning that the raw beam was used which would have given rise to energy spikes pulse to pulse, having some possible effect on the incident laser fluence and laser material processing

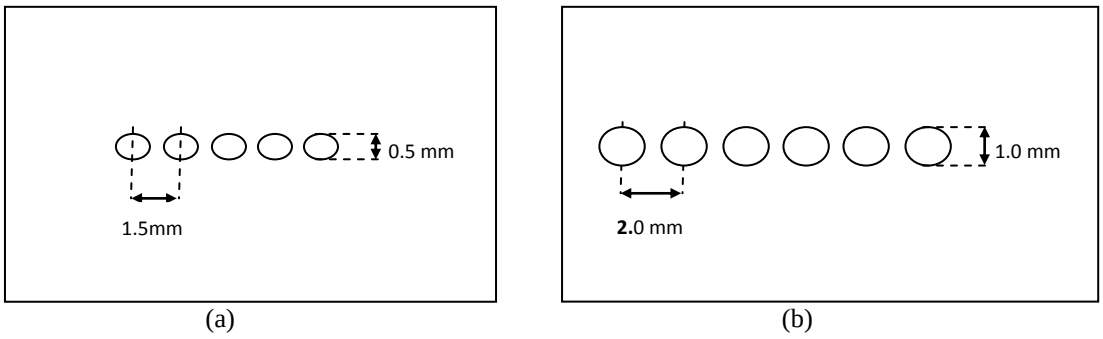

Figure 5.3 – Diagram showing the two projection masks used for (a) 50 μm and (b) 100 μm dimensioned trenches. With a ×10 demagnification lens, 0.5 mm and 1.0 mm diameter holes were required respectively for the 50 and 100 μm dimensioned trenches.

.

5.2.4 –KrF Excimer Laser Whole Area Irradiative Processing

For the whole area processing with an excimer laser (see Figure 5.4) the raw 23 × 12 mm^2 beam was used to irradiate a large section of each sample at a time. In order to hold the sample normal to the beam a bracket on the optical train was used. For the large area processing experiments 6 samples

where studied; these being 100 pulses at 100 mJ (EWA100), 100 pulses at 150 mJ (EWA150), 100 pulses at 200 mJ (EWA200), 100 pulses at 250 mJ (EWA250), 500 pulses at 250 mJ (EWA250_500) and 1000 pulses at 250 mJ (EWA250_1000). This gave fluences of 36±3, 54±5, 72±8 and 91±10 mJ/cm2, respectively for the different energies used. Throughout the whole area excimer experiments the repetition rate was kept constant at 25 Hz and Aerotech CNC programming ensured that the correct number of pulses was applied to each sample.

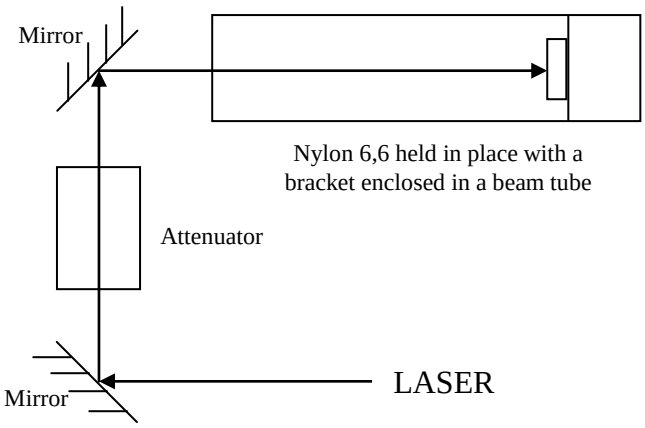

Figure 5.4 – Schematic diagram showing the experimental setup for the KrF excimer laser whole area irradiative processing.

5.3 – Topography, Wettability Characteristics and Surface Chemistry Analysis

After laser irradiation the nylon 6,6 samples were analysed using a number of techniques. The surface profiles were determined using a white light interferometer (WLI) (NewView 500; Zygo, Ltd) with MetroPro and TalyMap Gold Software. The WLI was set-up using a ×10 Mirau lens with a zoom of ×0.5 and working distance of 7.6 mm. This system also allowed Sa and Ra roughness parameters to be determined for each sample.

In accordance with the procedure detailed by Rance [108] the samples were ultrasonically cleaned in isoproponal (Fisher Scientific Ltd.) for 3 minutes at room temperature before using a sessile drop device to determine various wettability characteristics. This was to allow for a relatively clean surface prior to any θ measurements being taken. To ensure that the sample surfaces were dry a specimen dryer (Metaserv, Ltd.) was employed to blow ambient air across the samples. A sessile drop device (OCA20; Dataphysics Instruments, GmbH) was used with relevant software (SCA20; Dataphysics Intrsuments, GmbH) to allow the recent advancing and receding θ for triply distilled water and the recent advancing angle for diiodomethane to be determined for each sample. From the measured advancing and receding θ the hysteresis for the system was established. Thereafter the advancing θ for the two liquids were used by the software to draw an OWRK plot to determine the surface energy of the samples. For the two reference liquids the SCA20 software used the Ström *et al* technique (triply distilled water – SFT(total:72.80), SFT(D:21.80), SFT(P:51.00); diiodomethane – SFT(total:50.80),

SFT(D:50.80), SFT(P:0.00)) to calculate the surface energy of the material. It should be noted here that ten θ, using two droplets in each instance, were recorded to achieve a mean θ for each liquid and surface.

All samples were analysed using x-ray photoelectron spectroscopy (XPS). This allowed any surface modifications in terms of surface oxygen content due to the laser irradiation to be revealed. XPS measurements were performed on a photoelectron spectrometer (Axis Ultra DLD; Kratos Analytical Ltd., UK) employing monochromatic aluminium k-alpha radiation source, operating at 120 W power and an associated photon energy of 1486.6 eV. To test the reproducability of the surface, two sections of each sample were analysed; the analysis area on each sample was 700×300 microns. The spectrometer was run in its Hybrid mode and spectra were acquired at pass energies of 20 eV (for the high resolution scans) and 160 eV for the survey scans. All data was analysed through CasaXPS (v2.3.14) analysis software using sensitivity factors supplied by the instrument manufacturer.

5.4 – Simulated Body Fluid Procedure

SBF is a liquid which has inorganic ion concentrations equivalent to those of human extracellular fluid (human blood plasma). SBF can be used to evaluate the formation of apatite on bioactive materials *in vitro*. It can also be used as a coating to enhance the characteristic bioactivity of materials. SBF is a metastable solution containing calcium and phosphate ions already supersaturated with respect to the apatite. The SBF was prepared by using a magnetic stirrer hotplate (RCT Basic; IKA, GmbH) keeping the solution at a constant temperature of 36.5°C. 500 ml of distilled water was put into an autoclaved 1000 ml beaker and stirred until the constant temperature of 36.5°C was reached. At this time the chemicals given in Table 2 were added in order until the sodium sulphate (No 9) had been added.

Table 5.1 – Amounts and order of reagents to prepare 1000 ml SBF

Order	Reagent	Amount
		1000 ml
1	Distilled water	750 ml
2	Sodium Cholride (NaCl)	7.996 g
3	Sodium Bicarbonate ($NaHCO_3$)	0.350 g
4	Potassium Chloride (KCl)	0.224 g
5	Potassium Phosphate Dibasic ($K_2HPO_4{\cdot}3H_20$)	0.228 g
6	Magnesium Chloride Hexahydrate ($MgCl_2{\cdot}6H_20$)	0.305 g
7	Hydrogen Chloride (~0.1 M in H_2O) (HCl)	40 ml
8	Calcium Chloride ($CaCl_2$)	0.278 g
9	Sodium Sulphate (Na_2SO_4)	0.071 g
10	Tris(hydroxymethyl)aminomethane $(CH_2OH)_3CNH_2$	6.057 g
11	Hydrogen Chloride (~0.1 M in H_2O) (HCl)	Adjustment of pH

Once the sodium sulphate (No 9 in Table 2) had been added the Tris(hydroxymethyl) aminomethane (No 10 in Table 2) was supplemented into the solution less than a gram at a time in order to avoid

local increase of pH. Finally, in order to adjust the pH value to 7.4, hydrogen chloride (No 11 in Table 2) was added and the beaker was then filled to 1000 ml using distilled water.

Prior to using the SBF all of the samples and apparatus to be used were autoclaved if not already sourced in sterile packaging. The samples were then placed into sterile 30 ml glass containers , immersed in 30 ml of SBF and placed into an incubator to keep the temperature constant at 37°C for 7 days.

5.5 – Scanning Electron Microscopy (SEM), Energy-Dispersive X-Ray Spectroscopy (EDX) and Optical Microscopy Analysis of SBF Immersed Samples

Prior to being immersed in the SBF the nylon 6,6 samples were weighed using a balance (S-403; Denver Instrument, GmbH) with a readability of 0.001 g. Once the 14 days had elapsed the samples were removed from the SBF, rinsed lightly with distilled water and allowed to air dry in a clean room. Once fully dry the samples were weighed and the difference in weight before and after being immersed in the SBF was determined. Following this the samples were gold coated and analysed using optical microscopy and SEM. Furthermore, the samples were analysed using EDX in order to identify elements present after the immersion in SBF.

5.6 – *In Vitro* Experimentation

Prior to any biological testing being carried out the samples were autoclaved (D-Series Bench-Top Autoclave; Systec, GmbH) to ensure that all samples were sterilized. For all biological work undertaken, unless stated, a biological safety cabinet (BSC) (Microflow Class II ABS Cabinet; BioQuell UK, Ltd) was used to create a safe working environment and to provide a clean, sterile environment to manipulate the cells used.

Normal human osteoblast cells (Clonetics CC-2538; Lonza, Inc.) were initially cultured in a T75 (75 ml) flask by suspending the cells in 19 ml culture medium comprising of 90% eagle minimum essential medium (Sigma-Aldrich, Ltd., UK) and 10% foetal bovine serum (FBS) (Sigma-Aldrich Ltd., UK). The flask was then placed in an incubator and left for 24 hrs. After 24 hrs the cells were assessed and the spent media was aspirated before dispensing 15 ml of fresh media and returning the flask to the incubator for three days.

The period of three days allowed the cells to become confluent in the flask providing enough cells for seeding onto the samples. The cells were detached from the flask using 5 ml Trypisn-EDTA (Sigma-Aldrich Ltd., UK) whilst placed in the incubator for seven minutes. Once all cells had become detached 10 ml culture medium was added to neutralize the Trypsin. In order to aspirate the supernatant the cell culture was centrifuged (U-320R; Boeco, GmbH) for five minutes at 200 g. To ensure the cells were ready for seeding they were resuspended in 10 ml of culture medium and

dispensed between the samples in the 6-well plates. This equated to 0.55 ml (2×10^4 cells/ml) for each sample. The well plates were placed in the incubator were one was removed after 24 hrs and two other plates after four days. A well plate from 24 hrs and four days were prepared for the SEM as will be discussed later and other plate removed after four days was prepared for counting using an improved neubauer hemacytometer (Fisher Scientific Ltd., UK) by mixing 10 µl of each cell suspension with 10 µl of trypan-blue (Sigma-Aldrich Ltd., UK).

5.7 – Scanning Electron Microscopy of *In Vitro* Samples

In order to view the attached cells using SEM it was necessary to undertake a procedure to produce a sample that was dehydrated ready for Au coating. The samples were initially rinsed with phosphate-buffered saline (PBS) (Sigma-Aldrich, UK) to remove any unattached cells and then adherent cells were fixed using 1.2% glutaraldehyde in water (Sigma-Aldrich, UK) at room temperature for one hour within the BSC. After an hour the glutaraldehyde solution was removed and the fixed cells were washed with PBS prior to carrying out a graded series of ethanol/distilled water mixtures of 50/50, 80/20, 90/10, 95/5, 98/2 and 100/0. Each sample was left in these mixtures for 10 min to ensure dehydration. Once this procedure was carried out, the samples were mounted and sputter coated with Au so that SEM micrographs could be obtained. In order to produce the best images possible each image was manipulated in terms of brightness, contrast and gamma by using ImagePro Version 5.0.0.39 for Windows XP/Professional software (Media Cybernetics Inc., USA).

5.8 – Cytotoxicity and Alkaline Leukocyte Phosphatase Activity (ALP)

Prior to any biological testing being carried out the samples were autoclaved (D-Series Bench-Top Autoclave; Systec, GmbH) to ensure that all samples were sterilized. For all biological work undertaken, unless stated, a biological safety cabinet (BSC) (Microflow Class II ABS Cabinet; BioQuell UK, Ltd) was used to create a safe working environment and to provide a clean, sterile environment to manipulate the cells used.

Normal human osteoblast cells (Clonetics CC-2538; Lonza, Inc.) were initially cultured in a T75 (75 ml) flask by suspending the cells in 19 ml culture medium comprising of 90% eagle minimum essential medium (Sigma-Aldrich, UK) and 10% foetal bovine serum (FBS) (Sigma-Aldrich, UK). The flask was then placed in an incubator and left for 24 hrs. After 24 hrs the cells were assessed and the spent media was aspirated before dispensing 15 ml of fresh media and returning the flask to the incubator for three days.

The period of three days allowed the cells to become confluent in the flask providing enough cells for seeding onto the samples. The cells were detached from the flask using 5 ml Trypisn-EDTA (Sigma-Aldrich Ltd., UK) whilst placed in the incubator for seven minutes. Once all cells had become detached 10 ml culture medium was added to neutralize the Trypsin. In order to aspirate the supernatant the cell culture was centrifuged (U-320R; Boeco, GmbH) for five minutes at 200 g. To

ensure the cells were ready for seeding they were resuspended in 10 ml of culture medium and dispensed between the eighteen samples in the 6-well plates. This equated to 0.55 ml (2×10^4 cells/ml) for each sample. Two 6-well plates were prepared. The first plate was analysed using SEM after 24 hrs which required the samples to be initially rinsed with phosphate-buffered saline (PBS) (Sigma-Aldrich, UK) to remove any unattached cells. Then, adherent cells were fixed using 1.2% glutaraldehyde in water (Sigma-Aldrich Ltd., UK) at room temperature for one hour within the BSC. After an hour the glutaraldehyde solution was removed and the fixed cells were washed with PBS prior to carrying out a graded series of ethanol/distilled water mixtures of 50/50, 80/20, 90/10, 95/5, 98/2 and 100/0. Each sample was left in these mixtures for 10 minutes to ensure dehydration. Once this procedure was carried out the samples were mounted and sputter coated with Au so that SEM micrographs could be obtained. In order to produce the best images possible each image was manipulated in terms of brightness, contrast and gamma by using ImagePro Version 5.0.0.39 for Windows XP/Professional software (Media Cybernetics Inc., USA). The second plate was kept incubated for two days by which time the media for each sample was removed to assess both the cytotoxicity and ALP levels.

A number of assay kits are readily available "off the shelf" in order to assess the cytotoxicity and ALP activity for a variety of cell types. In order to determine the cytotoxicity and ALP activity of the seeded osteoblast cells in the second plate after two days of incubation an LDH-cytotoxicity assay kit II (313-500; Biovision, Inc.) and a Sensolyte FDP Alkaline Phosphatase Assay Kit (71109; Anaspec, Inc.) were used, respectively. In order to measure the cytotoxicity level for each of the samples a number of controls were setup; background control which had 100 µl per well of culture medium without cells, low control which had 100 µl per well of culture medium with cells, test substance which had 100 µl per well of culture medium from the nylon 6,6 samples and high control which had 100 µl per well of culture medium with cells in addition to 10 µl of cell lysis solution. Each of these wells were performed in duplicate, had 100 µl of LDH reaction mix added to them and were incubated at room temperature for 30 min prior to measuring the absorbance with a 96-well plate reader. The absorbance was measured with a 450 nm (440 to 490 nm) filter and used a reference wavelength of 650 nm. Using the controls that had been set it was possible to ascertain the percentage cytotoxicity by using

$$cytotoxicity\ (\%) = \frac{(Test\ sample - Low\ control)}{(High\ control - Low\ control)} \times 100 \qquad (5.1)$$

ALP activity was determined by setting up three controls; negative control which had 50 µl per well of unused culture medium, substrate control which contained 50 µl per well of 1X lysis buffer and the test substrate which had 50 µl per well of the culture media from the nylon 6,6 samples. In order to measure the ALP activity 50 µl of FDP reaction was added to each well, mixed and incubated at room temperature for 30 minutes. After this time the 96-well plate was placed into a spectrophotometer and the fluorescence intensity was measured at Ex/Em= 485±20 nm/528±20 nm. One should note that for both cytotoxicity and ALP activity the background/substrate control was taken away from all readings to account for background levels.

5.9 – Statistical Analysis

All statistical analysis was carried out using SPSS 16.0.2 for Windows software (SPSS Inc., USA) in order to analyse the data obtained using one-way ANOVA to obtain F-ratios and significance levels, p. In addition to ANOVA analysis post hoc multiple comparison tests in the form of Scheffe's range tests were performed in order to determine statistic significance between groups in which results are reported at a mean difference significance level of $p<0.05$.

PART 3 – Polymeric Laser-Induced Surface Modification and Wettability Characteristics

6
CO_2 Laser Patterning and Whole Area Irradiative Processing of Nylon 6,6

This chapter presents and details the results obtained from laser surface patterning and whole area irradiative processing of nylon 6,6 using a CO_2 laser. The modification of topography, wettability characteristics and O_2 content are discussed and a potential driving force for the determination of the ϑ is considered.

6.1 – Introduction

Laser-induced surface treatment offers the ability to vary only the physiochemical surface properties with considerably more control and accuracy in comparison to the other possible techniques. As a result of surface treatment one can imagine that this would have a large effect upon the wettability characteristics of the material. This can be seen through the modulation of surface properties such as surface roughness, γ^P, γ^T, and surface oxygen content which are factors known to potentially have, to some extent, dominance in determining the characteristic wettability.

On account of the means by which CO_2 lasers can modify a number of surface properties whilst keeping the bulk properties in tact, this chapter details how the surface topography, surface oxygen content and wettability characteristics of nylon 6,6 was modified by using CO_2 laser-induced patterning and whole area irradiative processing. The experimental procedures undertaken and meanings for the sample I.D. referred to for this work can be found in Chapter 5.

6.2 – Effects of CO_2 Laser Processing on Topography

This section discusses the variations in surface topography as result of the two CO_2 laser surface modification techniques implemented; namely CO_2 laser-induced patterning and CO_2 laser whole area irradiative processing.

6.2.1 – CO_2 Laser-Induced Patterning

Previous work has already identified that the CO_2 laser-material interaction is that of a thermolytical nature that gives rise to melting and resolidification as the laser beam passes over the target material [103,104]. As a result of this, scanning a predetermined pattern across the nylon 6,6 surfaces gave rise to a significant variation in topography when compared to the as-received sample (AR). This becomes more apparent when comparing the as-received sample (see Figure 6.1) with the laser patterned

samples in which the continuous axonometric 3-D images profiles can be seen in Figure 6.2 and profile extractions in Figure 6.3

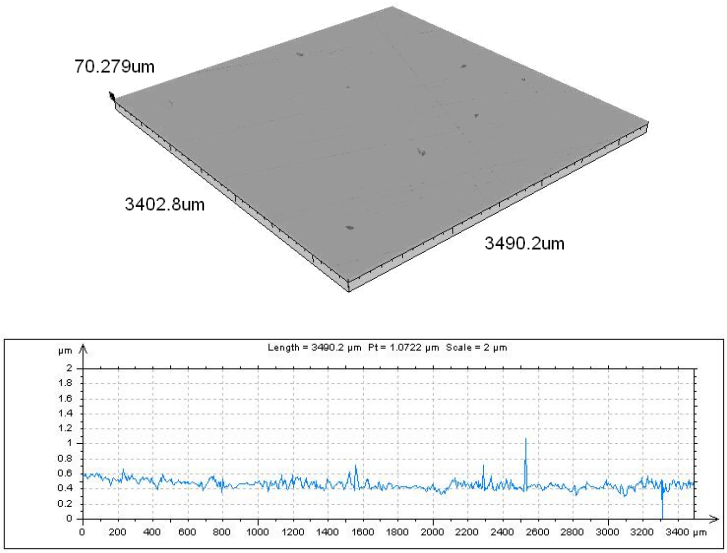

Figure 6.1 – Continuous axonometric 3-D image and profile extraction for the as-received sample (AR).

From Figures 6.1, 6.2 and 6.3 it can be deduced that the CO_2 laser-induced patterned samples had considerably rougher surfaces with the largest peak heights being of the order of 2 µm (see Figure 6.3) in contrast to the as-received sample (see Figure 6.1) which had peaks heights of up to 0.2 µm. On account of the increase in peak heights over the CO_2 laser-patterned samples the surface roughness (see Table 6.1) increased considerably with the largest Sa of 0.4 µm being achieved with the 50 µm hatch sample (CH50) and largest Ra of 0.2 µm for the 100 µm trench sample (CT100). It is given in Table 6.1 that the patterned samples with scan dimensions of 50 µm (samples CT50 and CH50) have larger Sa roughness values when compared to the samples patterned with 100 µm scan dimensions (samples CT100 and CH100). This can be attributed to the fact that the 50 µm scan dimensions irradiated more of the sample giving rise to an increase of mass being melted and re-solidified. Also, it can be seen from the Table 6.1 that the roughness for the hatch patterns had decreased in comparison to the trench patterns. This can be explained by the laser re-melting sections of the nylon 6,6 surface owed to the scanning process of the system. By re-melting these sections the material could then have re-solified into a smoother surface topography.

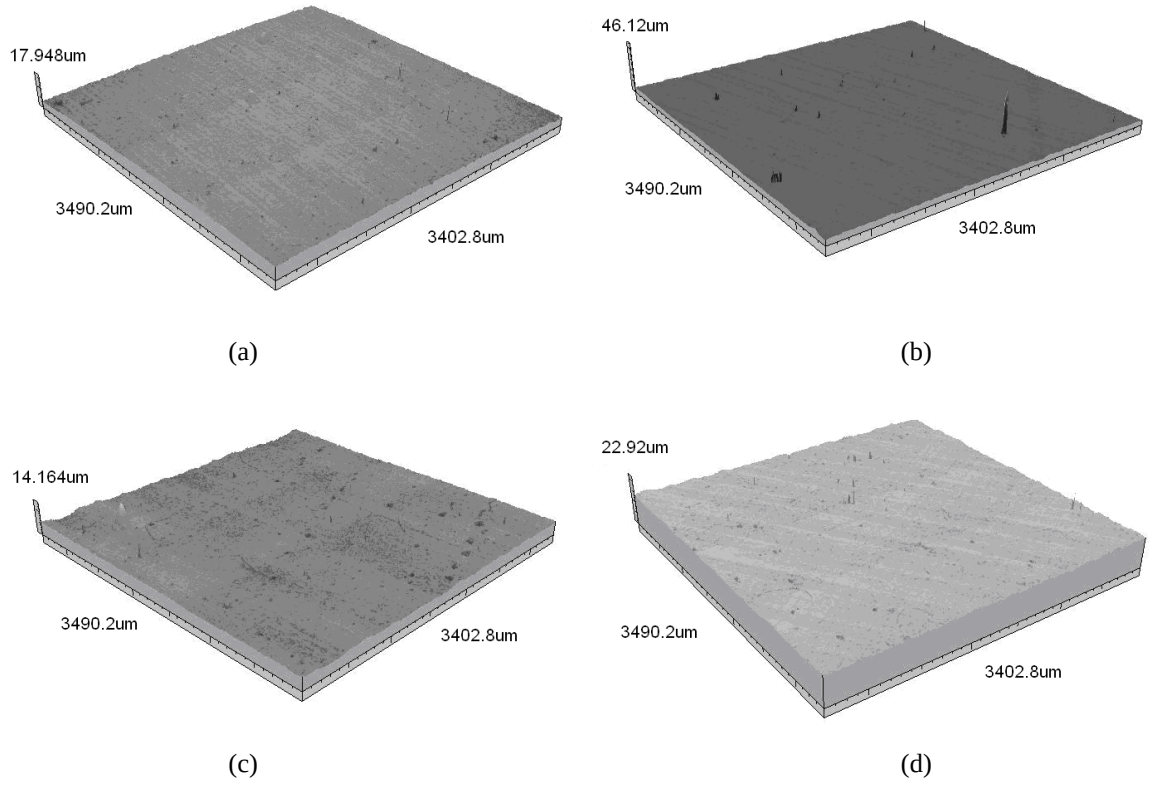

Figure 6.2 – Continuous axonometric 3-D images for (a) CT50, (b) CT100, (d) CH50 and (d) CH100.

Table 6.1 –The surface roughness values for each of the CO_2 laser-induced patterned nylon 6,6 samples in relation to the as-received sample.

Sample I.D.	Sa (µm)	Ra (µm)
AR	0.126	0.029
CT50	0.636	0.148
CT100	0.297	0.185
CH50	0.423	0.103
CH100	0.326	0.155

The profile extractions shown in Figure 6.3 indicate that for the most part, a high level of periodicity arose in the topography of the laser patterned samples as a result of the scanned pattern. In contrast, it is evident that from Figure 6.3 that the 50 µm patterns (CT50 and CH50) had the least periodicity, which can be attributed to the fact that the beam spot size was 95 µm and consequently allowed the scans to overlap and thus eliminate the natural periodicity of the original scanned pattern. This could also allow one to explain the surface Sa roughness increase as seen in Table 6.1 as the scanned 50 µm dimensioned patterns (samples CT50 and CH50) had up to a three times larger Sa value compared to the 100 µm scan dimensioned nylon 6,6 samples (samples CT100 and CH100). That is on account of significantly more melting and re-solidifcation taking place, on account of the overlapping, a rougher surface could have resulted. Another point of interest which is shown in Figure 6.3 is that sharp steep gradients arise on account of the CO_2 laser-induced patterning of the nylon 6,6 samples. This along

with the periodicity of the peaks could have a distinct impact on the wettability characteristics, which will be further discussed in Section 6.3.

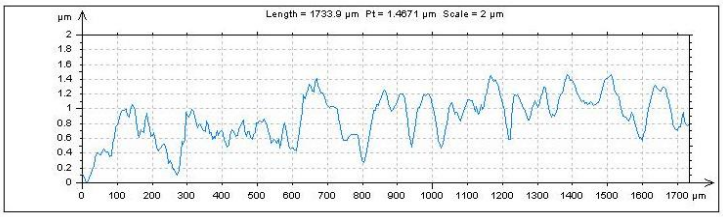

(a)

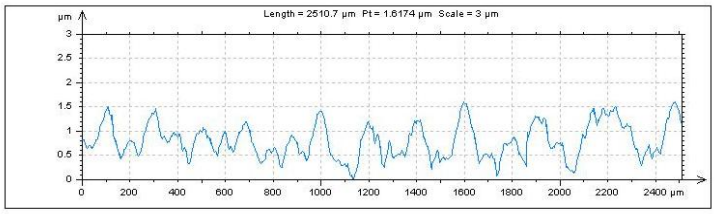

(b)

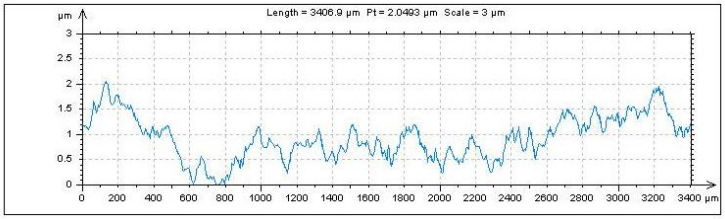

(c)

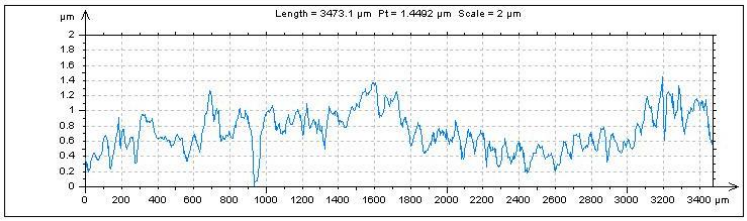

(d)

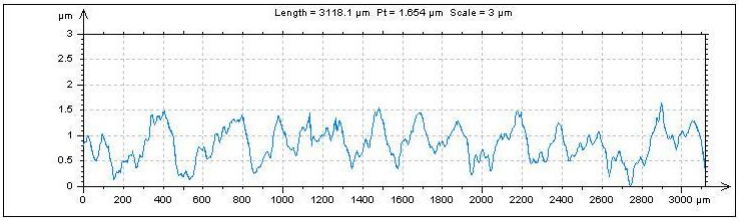

(e)

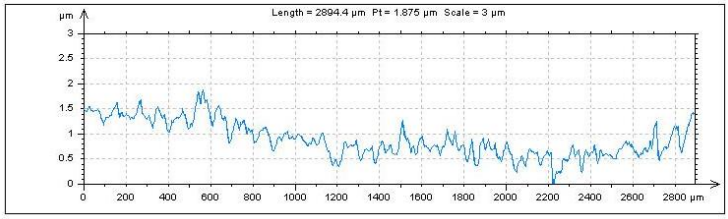

(f)

Figure 6.3 – Profile extractions for (a) CT50, (b) CT100, (c) CH50 x-axis, (d) CH50 y-axis, (e) CH100 x-axis and (f) CT100.

6.2.2 – CO_2 Laser Whole Area Irradiative Processing

It can be seen from Figure 6.4 and Figure 6.5 that the CO_2 whole area irradiative processing of the nylon 6,6 gave rise to a significantly modified surface, especially with those samples which had been irradiated with large fluences (samples CWA102 and CWA128). This can be accounted for by more melting taking place arising from the significantly larger temperature rise owed to the large irradiances incident on the nylon 6,6 surfaces.

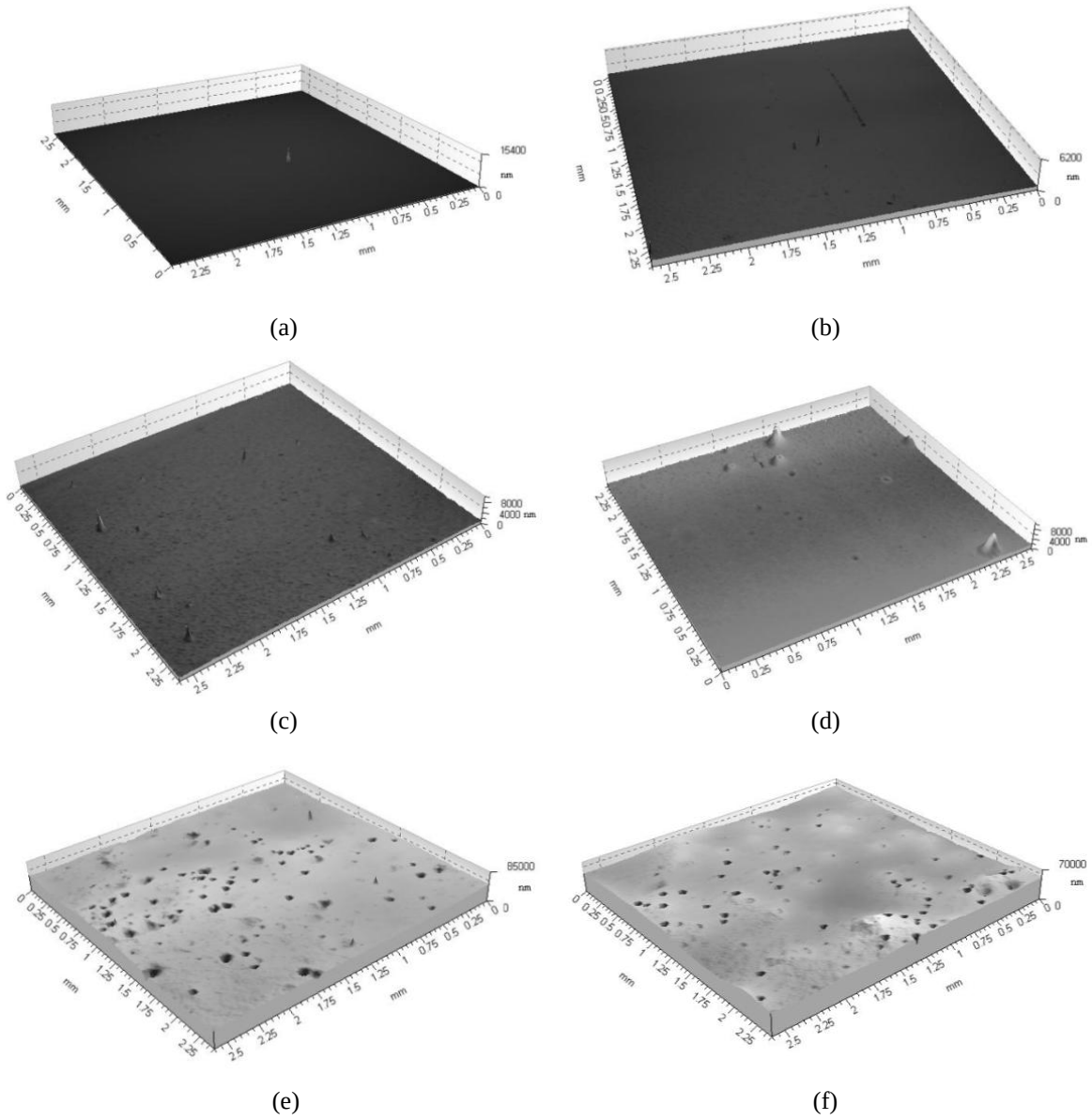

Figure 6.4 – Continuous axonometric images of samples (a) CWA17, (b) CWA26, (c) CWA34, (d) CWA51, (e) CWA102 and (f) CWA128.

Figure 6.4 also shows that there was further evidence of considerable melting on account of one being able to identify craters left from evolved gases breaking at the surface. This is especially apparent for sample CWA102 and sample CWA128 which had larger incident fluences (see Figure 6.4(e) and

Figure 6.4(f)). Secondly the extent of melting can be further identified through the profile extractions (see Figure 65) which show that peak heights of 10 to 15 µm was achieved for those samples with incident fluences of 102 and 128 Jcm^{-2} (samples CWA102 and CWA128). It should also be noted here that as the fluence used for samples CWA17 (see Figure 6.4(a) and Figure 6.5(a)) and CWA26 (see Figure 6.4(b) and Figure 6.5(b)) appeared experimentally to be close to that of the threshold, qualitatively there did not appear to be significant difference between the topographies observed for them and that of the as-received sample (see Figure 6.1).

As given in Table 6.2, for all samples with the exception of whole area samples CWA17, CWA26 and CWA34 there was a significant increase in the surface roughness in comparison to the as-received sample (AR) which had a roughness of Sa, 0.1µm, and Ra, 0.03 µm. It should be noted that as a result of the fluences being close to that of the threshold which were used for samples CWA17, CWA26 and CWA34 the surface roughness results obtained for these samples can be seen to be equivalent to that of the as-received sample (AR). On the other hand, it can be seen that the largest surface roughness arises from samples CWA102 and CWA128 with Sa of 4 and 3 µm, respectively.

Table 6.2 – The surface roughness values for each of the CO_2 laser whole area irradiative processed samples in relation to the as-received sample (AR)

Sample I.D.	Sa (µm)	Ra (µm)
AR	0.126	0.029
CWA17	0.111	0.060
CWA26	0.100	0.158
CWA34	0.101	0.092
CWA51	0.341	0.139
CWA102	4.356	1.236
CWA128	3.201	1.335

(a)

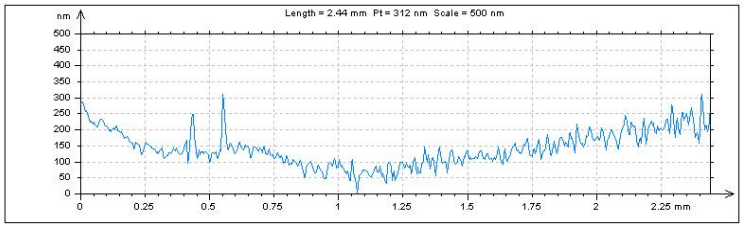

(b)

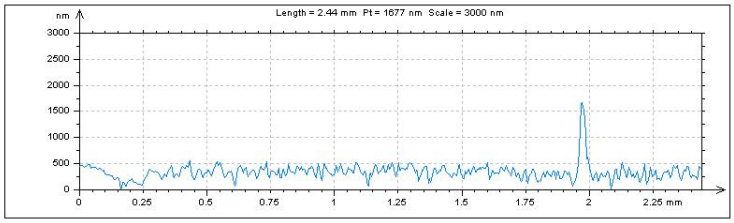

(c)

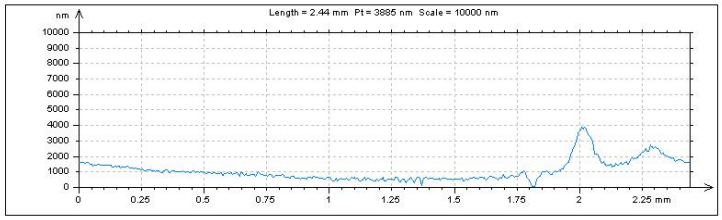

(d)

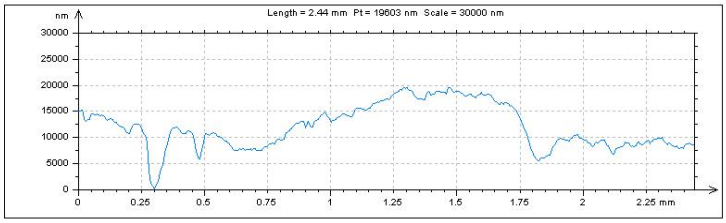

(e)

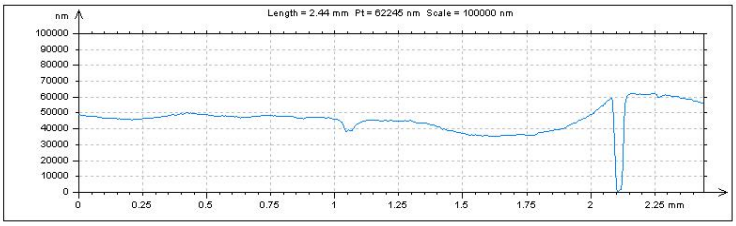

(f)

Figure 6.5 – Profile extractions for samples (a) CWA17, (b) CWA26, (c) CWA34, (d) CWA51, (e) CWA102 and (f) CWA128.

6.2.3 – Comparison Between CO_2 Laser-Induced Patterning and CO_2 Laser Whole Area Irradiative Processing

From Section 6.2.1 and Section 6.2.2 it is evident that a CO_2 laser can be employed to modify significantly the surface topography of nylon 6,6 if the laser-material interaction threshold in terms of fluence is exceeded. The CO_2 whole area irradiated processed samples at large fluencies (sample CWA102 and sample CWA28) gave rise to an order of magnitude increase in Sa and surface topographies arising from the surface treatment differed significantly when compared to the CO_2 laser-induced nylon 6,6 samples. It was found that the topographies of the CO_2 laser-induced patterned were somewhat periodic with steep, sharp gradients when considering the peak heights; whereas, the CO_2 laser whole area irradiative processed samples gave rise to a more cratered surface. This was on account of more melting taking place which in turn gave rise to evolved gases being able to break to the surface (see Figures 6.2, 6.3, 6.4 and 6.5). As a result of this, the maximum peak heights achieved for the CO_2 laser whole area processed were found to be considerably larger by up to 13 μm but were less densely situated when compared to the CO_2 laser patterned samples which had maximum peaks heights of approximately 2 to 3 μm and were more periodic (see Figure 6.3 and Figure 6.5).

For the CO_2 whole area irradiative processed samples it was found that in terms of surface topography the first three samples (samples CWA17, CWA26 and CWA34) gave rise to negligible modifications when compared to the as-received sample (AR) while all of the CO_2 laser-induced patterning gave rise to a noteworthy variation in the surface topography of the nylon 6,6. This can be on account of samples CWA17, CWA26 and CWA34 having been irradiated with fluences below or around the threshold fluence. On account of this, one can then deduce that all other samples gave rise to significant modifications in the surface topography as the fluences used to irradiate the other samples were considerably higher. As such, one can reasonably state that above the threshold, both CO_2 whole area processing and laser-patterning gave rise to considerable modifications in terms of topography of the nylon 6,6 samples.

6.3 – Effects of CO_2 Laser Processing on Wettability Characteristics

On account of the notable variations in surface topography owed to both the CO_2 laser-induced patterning and CO_2 whole area irradiative processing it is possible to imagine that these topographies along with other surface parameter variations could have an impact on the wettability characteristics of nylon 6,6. This section discusses the results obtained for the wettability characteristics of the CO_2 laser-induced patterned and CO_2 whole area irradiative processed nylon 6,6 samples.

6.3.1 – CO_2 Laser-Induced Patterning

Table 6.3 gives a summary of the results obtained for each of the nylon 6,6 samples including surface roughness, γ^T, surface oxygen content and θ. Current theory states that for a hydrophilic material such as nylon 6,6 an increase in roughness and surface oxygen content should bring about a reduction in θ

[4]. But, Table 6.3 shows that this is not the case for the CO_2 laser-induced patterned samples as θ had increased by up to 10° even though a maximum increase in Sa was determined to be around 0.5 μm when compared to the as-received sample (AR). As hypothesized previously [103,104], this phenomenon can be explained by the existence of a mixed-state wetting regime [102,130,131,170] which will be further discussed later in section 6.3.3. This mixed-state wetting regime can also account for the observed reduction in apparent γ^P and apparent γ^T with γ^P reducing by up to 8 mJm^{-2} and γ^T reducing by up to 7 mJm^{-2} when compared to the as-received sample (AR) which had γ^P and γ^T values of 17.69 and 47.34 mJm^{-2}, respectively. Having said that, it should be noted that the transition to a mixed-state wetting regime, in this instance, is not definite but is a likely explanation for the observed increase in θ. As a result of this, it can be seen that this area of wettability would benefit from further study in order to ascertain the presence of a mixed-state wetting regime.

Table 6.3 – Results summary for all samples showing roughness parameters, surface oxygen content and wettability characteristics following CO_2 laser processing of nylon 6,6.

Sample ID	Sa (μm)	Ra (μm)	Polar Component, γ^P (mJm^{-2})	Dispersive Component, γ^D (mJm^{-2})	Total Surface Energy, γ^T (mJm^{-2})	Surface Oxygen Content (%at.)	Contact Angle (°)
AR	0.126	0.029	17.69	29.66	47.34	13.26	56.4±1.2
CO_2 Laser-Induced Patterned Samples							
CT50	0.636	0.148	12.24	28.63	40.87	14.33	66.0±4.0
CT100	0.297	0.185	16.86	29.83	46.69	14.05	57.5±2.4
CH50	0.423	0.103	10.93	31.64	42.58	14.99	65.8±2.9
CH100	0.326	0.155	13.63	30.37	44.00	14.84	62.2±2.3
CO_2 Whole Area Irradiative Processed Samples							
CWA17	0.111	0.060	18.36	28.75	47.11	13.56	55.8±2.7
CWA26	0.100	0.158	19.67	28.35	48.02	13.86	54.6±3.5
CWA34	0.101	0.092	14.89	38.55	53.43	14.34	56.4±3.5
CWA51	0.341	0.139	10.66	38.59	49.26	15.45	64.1±2.2
CWA102	4.356	1.236	28.49	23.82	52.31	16.77	46.6±4.7
CWA128	3.201	1.335	31.98	22.78	54.76	18.93	43.0±3.7

Figure 6.6 shows that θ had to some extent an inverse function of both γ^P and γ^T in which θ reduced on account of an increase in γ^P and γ^T. This is highly significant as even though θ has, in general, increased upon an increase in surface roughness (see Figure 6.7), γ^P and γ^T must still play an important role in determining the wettability of laser surface modified nylon 6,6. In terms of surface roughness, Figure 6.7 shows the correlation observed between θ and the surface roughness parameters Ra and Sa. It can be seen from Figure 6.7(a) that θ did not appear to have any correlation between Ra; however, Figure 6.7(b) suggests that an increase in Sa gives rise to an increase in θ up to 0.4 μm where θ seems to plateu. This could be important as it may indicate a transition in wetting regimes on account of how the liquid droplet sits in equilibrium on the rough periodic laser-modified nylon 6,6 surface.

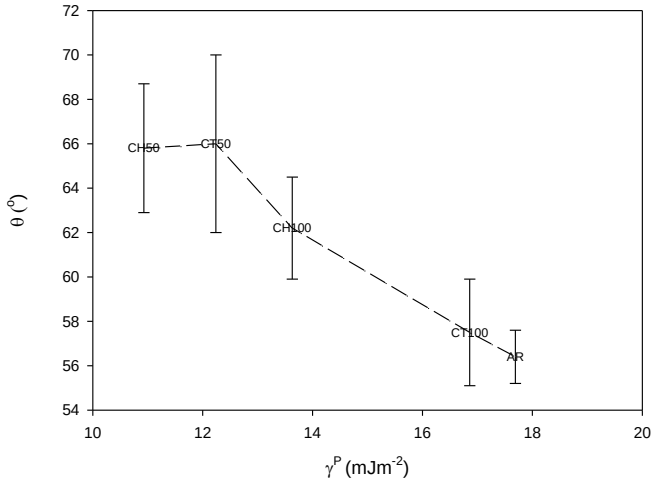

(a)

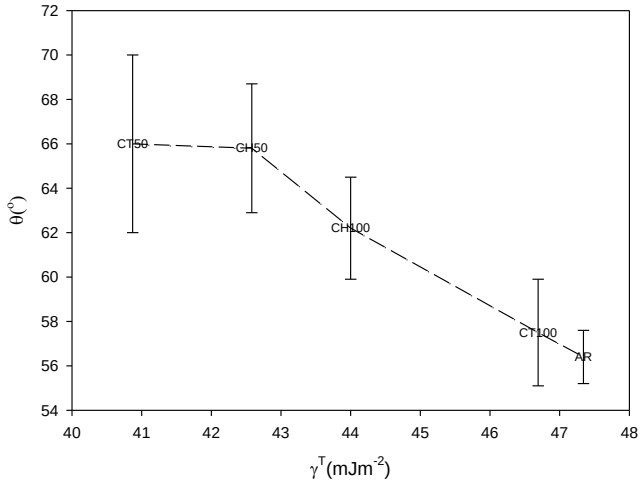

(b)

Figure 6.6 – Graphs showing the correlation between θ and (a) γ^P and (b) γ^T.

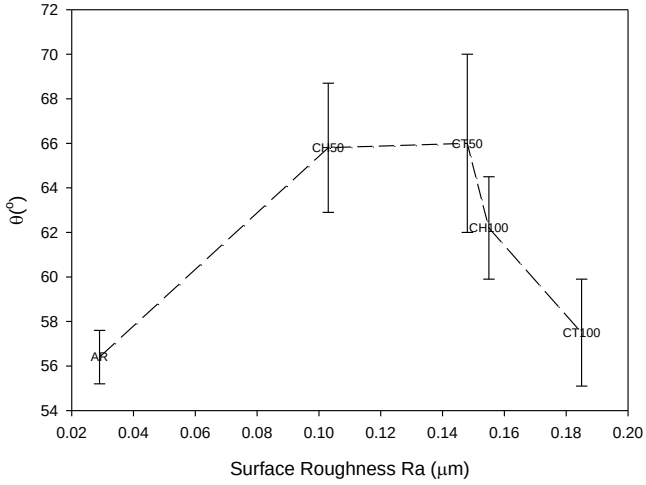

(a)

Figure 6.7 continued overleaf

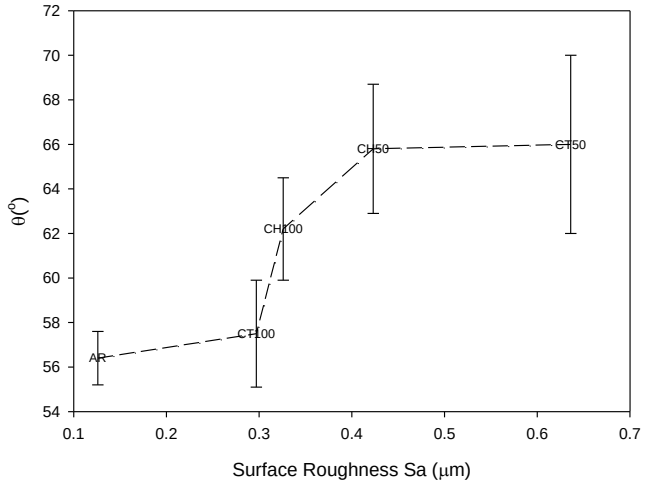

(b)

Figure 6.7 – Graphs showing the correlation between θ and (a) Ra and (b) Sa.

6.3.2 – CO_2 Laser Whole Area Irradiative Processing

The CO_2 whole area irradiative processed samples appear to correspond with current theory such that the reduction in θ arises from the surface roughness, γ^P and γ^T increasing. Furthermore, From Table 6.3 it is possible to deduce that θ for sample CWA51 increases in comparison to the as-received sample (AR). This could be on account of the presence of a mixed-state wetting regime as mentioned earlier in section 6.3.1, even though the surface roughness increased, apparent γ^P decreased and surface oxygen content increased. From Table 6.3 , in comparison to the as-received sample (AR) the largest decrease of 13° in θ was found to arise from sample CWA128 which had the largest incident fluence of 128 Jcm^{-2}

Also, it has been observed that there appears to be an inverse correlation between γ^P, γ^T and θ. In order to confirm what was observed from the results given in Table 6.3, Figure 6.8 shows graphically that following CO_2 laser whole area irradiative processing θ was an inverse function of γ^P and, to some extent and inverse function of γ^T. Following on, further confirmation that these samples corresponded to current theory was determined by Figure 6.9 which shows that with the exception of sample CWA51 the CO_2 laser whole area irradiative processed samples gave rise to a θ with an inverse function correlation with the surface roughness parameters Ra and Sa.

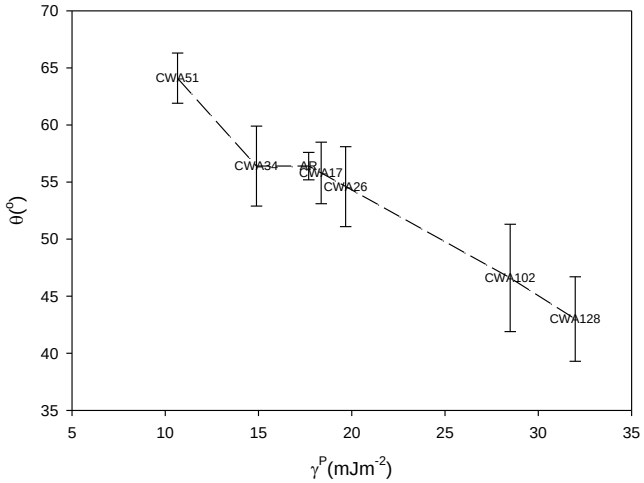

(a)

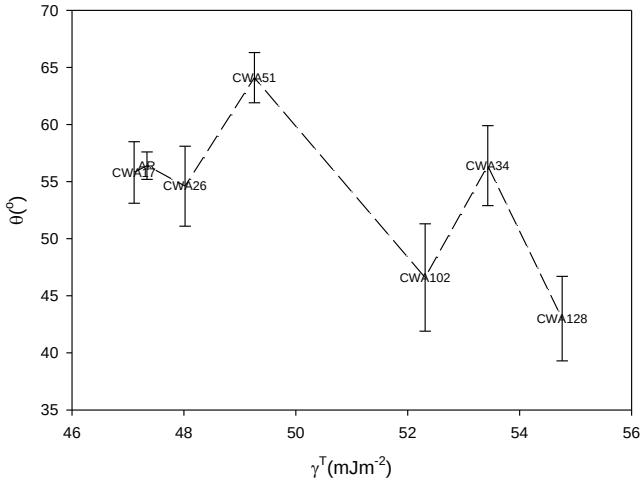

(b)

Figure 6.8 – Graphs showing the correlation between θ and (a) γ^P and (b) γ^T.

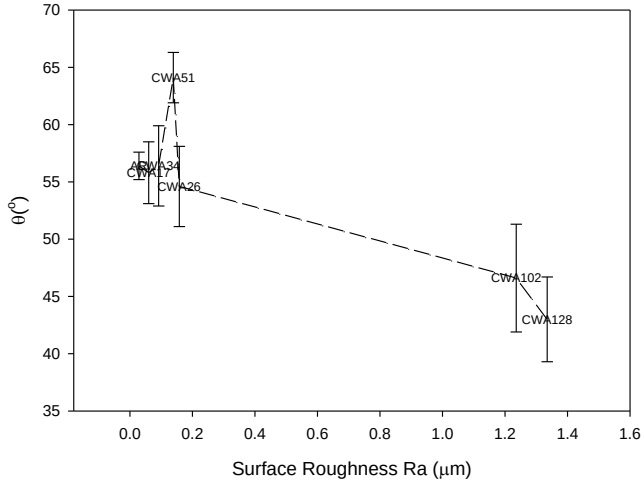

(a)

Figure 6.9 continued overleaf

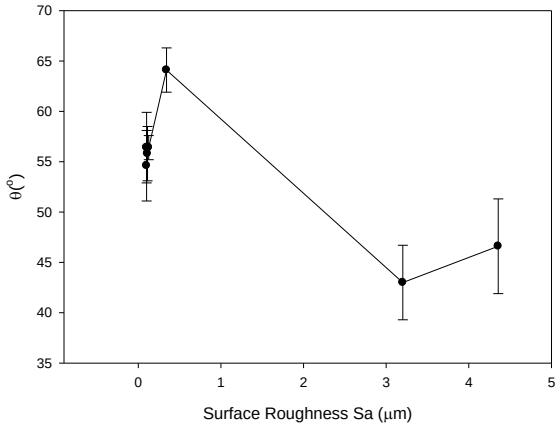

(b)

Figure 6.9 – Graphs showing the correlation between θ and (a) Ra and (b) Sa.

6.3.3 – Comparison Between CO_2 Laser-Induced Patterning and CO_2 Laser Whole Area Irradiative Processing

Owed to the fact that the CO_2 laser-induced patterned samples induced a more hydrophobic response and a more hydrophilic response was observed for the whole area irradiated patterns it is possible to deduce that surface oxygen content may not be the main driving force for wettability as the oxygen content increased in all instances by up to 2 %at. for the patterned samples and up to 5 %at. for the whole area irradiated samples. This is owed to the thermolytical interaction between the nylon 6,6 material and the CO_2 laser light that gives rise to melting of the nylon surface allowing oxidation to take place.

Upon analysing the CO_2 laser-induced patterned surfaces it was found that the γ^T and γ^P had decreased by up to 7 mJm^{-2} and the surface roughness had considerably increased. It was found that γ^P and γ^T for the samples studied were both a decreasing function of the θ, which correlates with current theory; however, current theory states that θ for a hydrophilic surface should decrease upon increasing surface roughness which has not been seen throughout this experimentation. As discussed by Jung and Bhushan [101] there are two regimes in which a material can wet: the Cassie-Baxter and Wenzel regimes. The Wenzel regime, shown in Figure 6.10, allows the whole sample to be wetted such that the droplet is in complete contact with the surface. It is believed that the Wenzel wetting regime was present on the CO_2 laser whole area irradiative processed samples on account of the small θ observed. In contrast, the alternative wetting regime which gives rise to large θ of over 90° is that of the Cassie-Baxter regime, shown in Figure 6.11, which allows the droplet to rest upon the roughened surface peaks forming air gaps between the droplet and the surface.

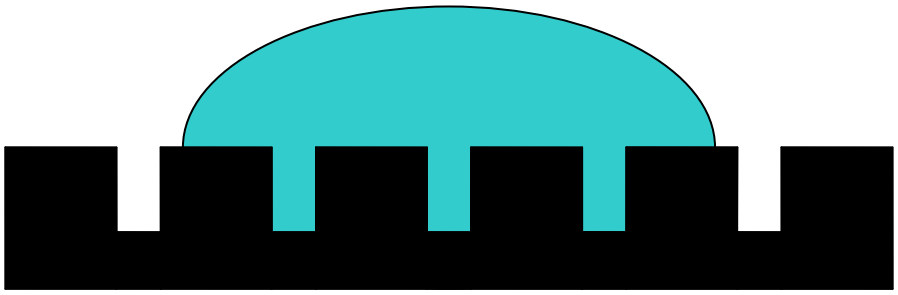

Figure 6.10 – Schematic diagram showing a droplet of water on a patterned surface giving rise to the Wenzel wetting regime.

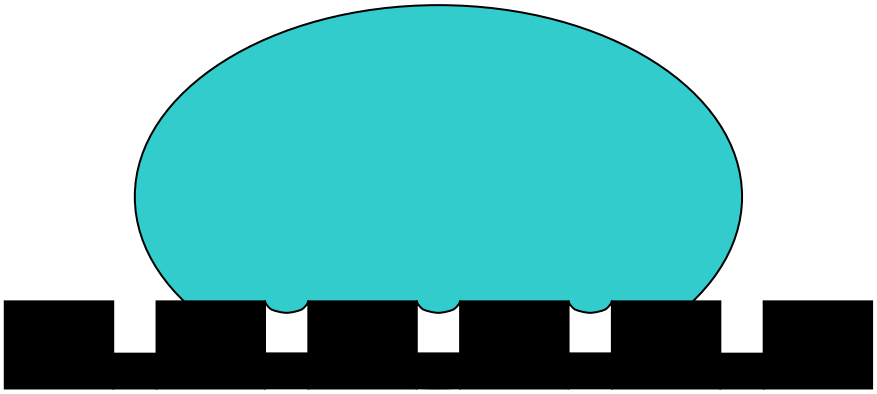

Figure 6.11 – Schematic diagram showing a droplet of water on a patterned surface giving rise to the Cassie-Baxter wetting regime.

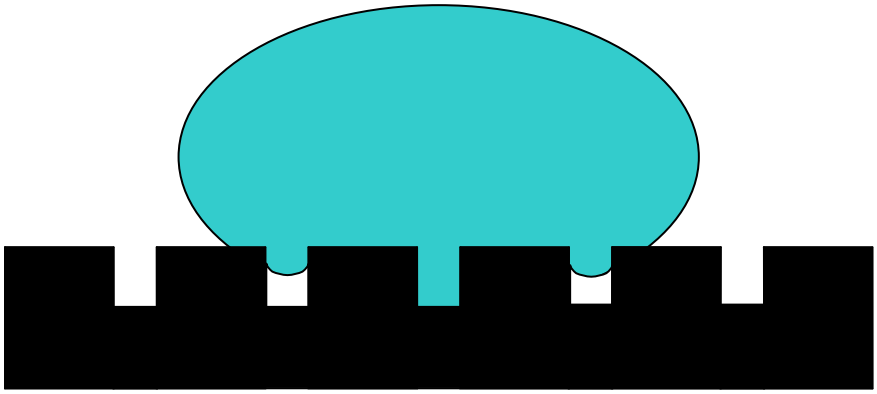

Figure 6.12 – Schematic diagrams showing the possible intermediate mixed-state wetting regime.

It is proposed here that a change from the Wenzel regime to a mixed-state wetting regime (see Figure 6.12) was the likely reason for the observed increase in θ for the CO_2 laser-induced patterned nylon 6,6 in accordance with work carried out by others [102,130,131,170]. That is, the liquid, when in contact with the sample surface, gives rise to a mixture of Wenzel and Cassie-Baxter regimes. So, the surface roughness along with the induced pattern yields a water droplet which is held in an intermediate state such that both wetting regimes coexist .This can be an explanation as to how an

increase in θ and reduction in apparent γ^P was observed for the laser patterned samples and still be hydrophilic. Therefore, it has been seen in this instance that the topographical surface pattern appears to be the main driver for the manipulation of the wettability characteristics. What is more, following whole area irradiative processing an increase in surface roughness, increase in γ^P and γ^T gave rise to a reduction in θ. This further suggests that the induced patterns had a large impact on the wetting regime.

To determine if the surface energy components or surface roughness appeared to be the dominant factor in determining θ graphs were drawn as seen in Figure 6.13 and 6.14, respectively, using the data obtained given in Table 3. One can see from Figure 6.10 that θ was an inverse function of both γ^P and γ^T when collating the results for the CO_2 laser-induced patterned samples and CO_2 laser whole area irradiative processed samples. This allows one to identify that all samples corresponded to the theory that an increase in surface energy components gives rise to a reduction in θ even though an increase in θ was observed for the CO_2 laser-induced patterned nylon 6,6 samples.

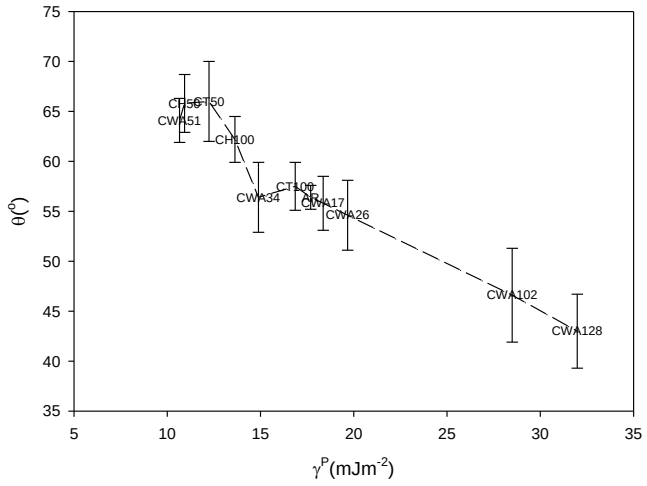

(a)

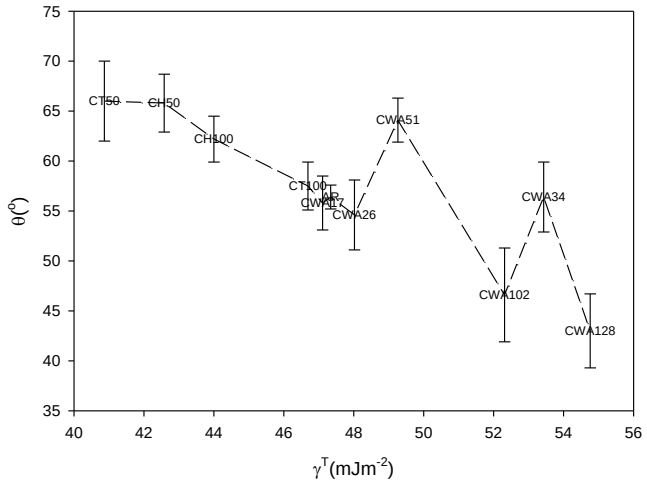

(b)

Figure 6.13 – Graphs showing the correlation between θ and (a) γ^P and (b) γ^T.

Figure 6.14 shows that there did not seem to be any specific correlation between θ and the surface roughness parameters. This is on account of the samples with Ra and Sa values slightly higher than the as-received sample (AR), between 0 and 1 μm, giving rise to an increase in θ of up to 15°. This can be primarily seen to be on account of the CO_2 laser-induced patterned samples in which a mixed-state wetting regime occurred to give an increase in θ even though a reduction in surface energy components and an increase in surface roughness was observed.

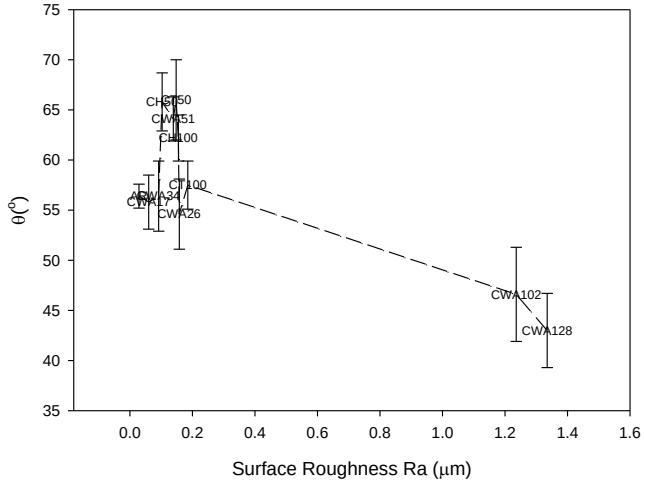

(a)

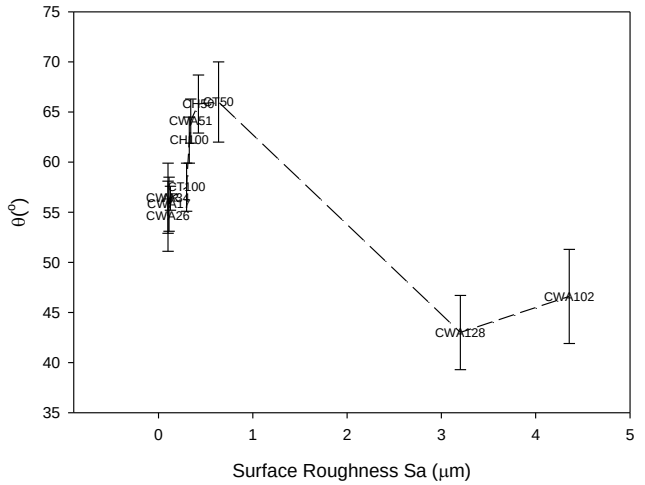

(b)

Figure 6.14 – Graphs showing the correlation between θ and (a) Ra and (b) Sa.

7
KrF Excimer Laser Patterning and Whole Area Irradiative Processing of Nylon 6,6

This chapter presents and discusses the results obtained for the modification of surface topography and wettaibility characteristics of nylon 6,6 after patterning and large area irradiative processing with a KrF excimer laser.

7.1 – Introduction

Two of the main advantages offered by excimer laser surface treatment are that of accuracy and precision. This is on account of the fact that these lasers allow as small as a few nanometers of material to be removed upon every incident pulse. As such, excimer lasers offer the opportunity of inducing varying levels of topography depending on how the laser is employed. For instance, periodic patterns can be induced using a focused beam whereas a more random pattern can be employed using a larger, more divergent, laser beam.

The fact that excimer lasers offer an efficient means of precise μm surface modification for nylon 6,6, this chapter gives an account of the results obtained with regards to surface topography and wettability characterstics upon KrF excimer laser surface patterning and whole area irradiative processing of nylon 6,6.

7.2 – Effects of KrF Excimer Laser Processing on Topography

This section discusses how KrF excimer laser surface treatment *via* KrF excimer laser-induced patterning and whole area irradiative processing modified the surface of nylon 6,6 compared to the as-received material. The experimental technique can be found in Chapter 5.

7.2.1 – KrF Excimer Laser-Induced Patterning

It can be seen in Figure 7.1 that the topography of the nylon 6,6 had been modified significantly through excimer laser patterning when compared to the as-received sample (see Figure 6.1). For the 50 μm dimensioned patterns (see Figure 7.1(a) and Figure 7.1(c)) trench depths of around 1 μm was obtained from the employed laser processing parameters. These constant laser processing parameters also gave rise to trench depths of roughly 4 to 5 μm for the 100 μm dimensioned patterned samples (see Figure 7.1(b) and Figure 7.1(d)). What is more, on account of the accuracy and precision of the excimer laser system implemented, the trenches produced in the nylon 6,6 materials which can be

seen in Figure 7.1 were highly periodic. This periodicity was also confirmed upon obtaining the profile extractions as shown in Figure 7.1.

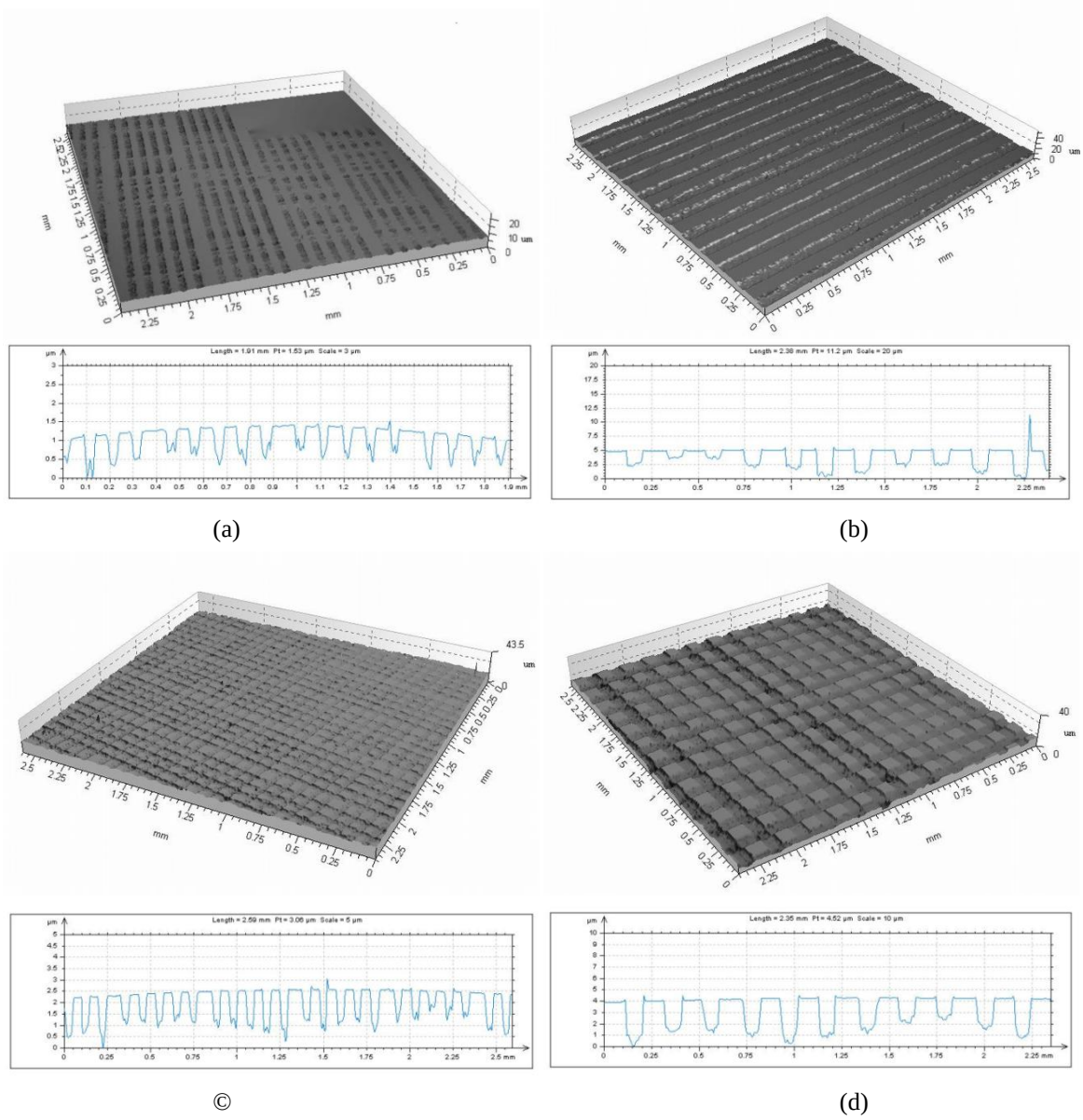

Figure 7.1 – Continuous axonometric 3-D images and profile extractions for the KrF excimer laser patterned samples (a) ET50, (b) CT100, (c) EH50 and (d) H10.

Table 7.1 gives the surface roughness values for each of the KrF excimer laser-induced patterned samples and shows that the surface roughness had dramatically increased for the excimer laser patterned samples with the largest increases being seen for the 100 µm dimensioned patterns which had an Sa of approximately 1.5 µm. This can be seen to be on account of the fact that the 100 µm dimensioned patterned samples gave rise to deeper trenches in comparison to the 50 µm dimensioned samples.

Table 7.1 – The surface roughness values for each of the KrF laser-induced patterned samples in relation to the as-received sample (AR)

Sample I.D.	Sa (µm)	Ra (µm)
AR	0.126	0.029
ET50	0.281	0.312
ET100	1.320	0.679
EH50	0.739	0.548
EH100	1.530	1.032

7.2.2 – KrF Excimer Laser Whole Area Irradiative Processing

Through WLI it was found that the KrF excimer laser whole area irradiative processed samples (see Figure 7.2) appeared to have a similar topography to that of the as-received sample (see Figure 6.1). This can be attributed to the fact that the whole sample was irradiated meaning that any ablation taking place would remove a somewhat uniform layer from the surface of the nylon 6,6. On the other hand, especially for the samples with low incident fluences, it may be possible that the material did not ablate on account of the threshold fluence not being achieved.

Table 7.2 – The surface roughness values for each of the KrF whole area irradiative processed samples in relation to the as-received sample (AR)

Sample I.D.	Sa (µm)	Ra (µm)
AR	0.126	0.029
EWA100	0.119	0.029
EWA150	0.092	0.039
EWA200	0.108	0.030
EWA250	0.107	0.031
EWA250_500	0.164	0.039
EWA250_1000	0.198	0.036

With regards to surface roughness the whole area irradiated samples had roughnesses equivalent to that of the as-received sample (AR) which had an Sa of 0.126 µm and an Ra of 0.029 µm (see Table 7.2). This can be accounted for by the observation through the WLI which showed a negligible effect on the surface topography for these samples. This further confirms that the fluences implemented for these samples was not sufficient to elicit an ablative response from the nylon 6,6 samples. Having said that, it may still have been possible for surface chemistry changes to occur and will be further discussed in section 7.3. This is on account of the fact that directly after the irradiation of the samples using the KrF excimer laser, the samples were warm to the touch, with the warmest sample being WA250_1000 which had 1000 pulses and the highest fluence of 91 $mJcm^{-2}$.

7.2.3 – Comparison Between KrF Excimer Laser-Induced Patterning, KrF Excimer Whole Area Irradiative Processing

It has been observed that KrF excimer laser-induced patterning can significantly modify the topography of nylon 6,6 insofar as the roughness had increased and distinct periodic patterns had been induced into the material surface. In contrast, the KrF excimer whole area irradiative processed samples gave rise to a negligible variation in surface parameters when compared to the as-received sample such that the Sa remained around 0.1 to 0.2 µm and Ra around 0.03 µm.

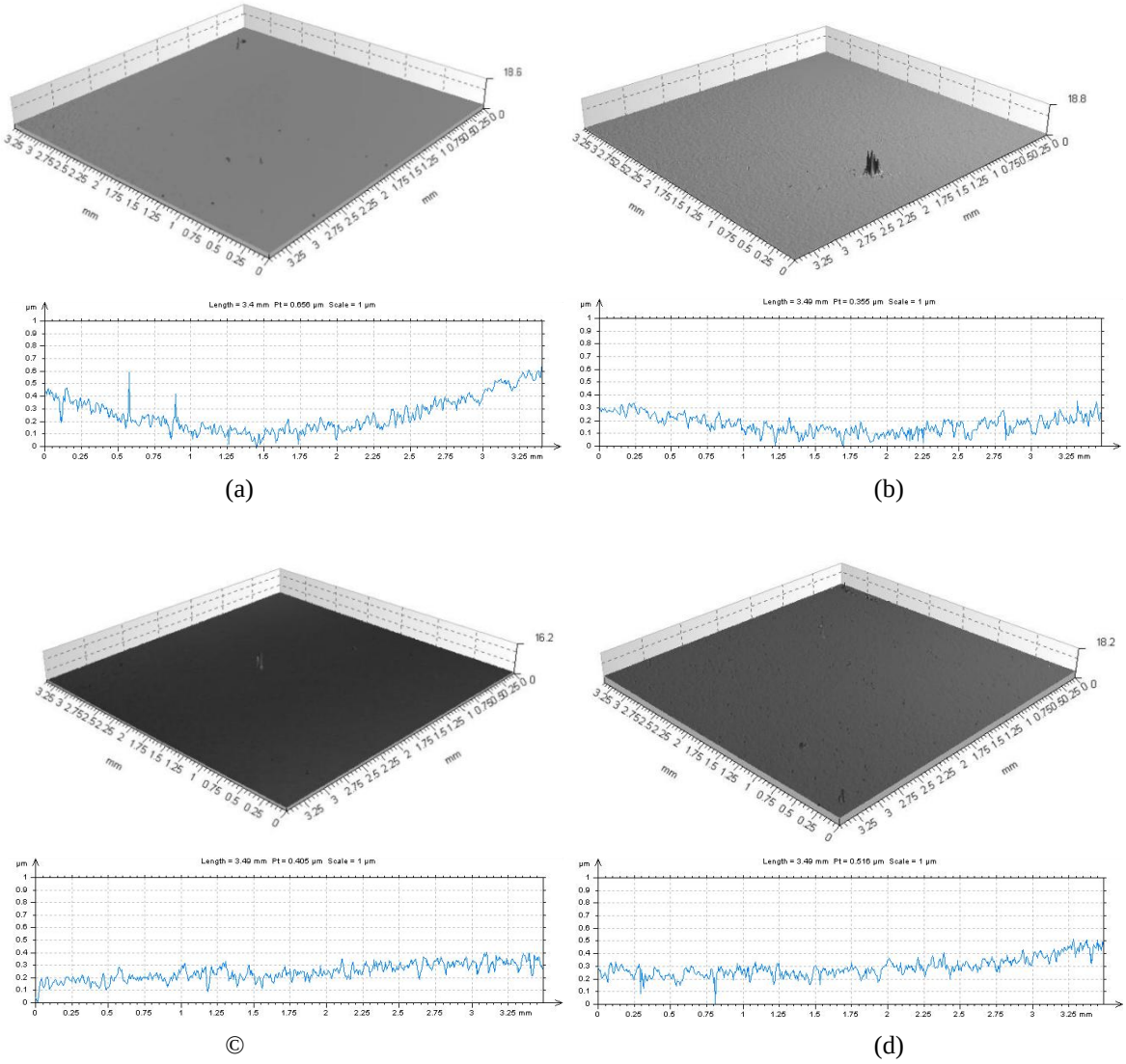

(a) (b)

© (d)

Figure 7.2 continued overleaf

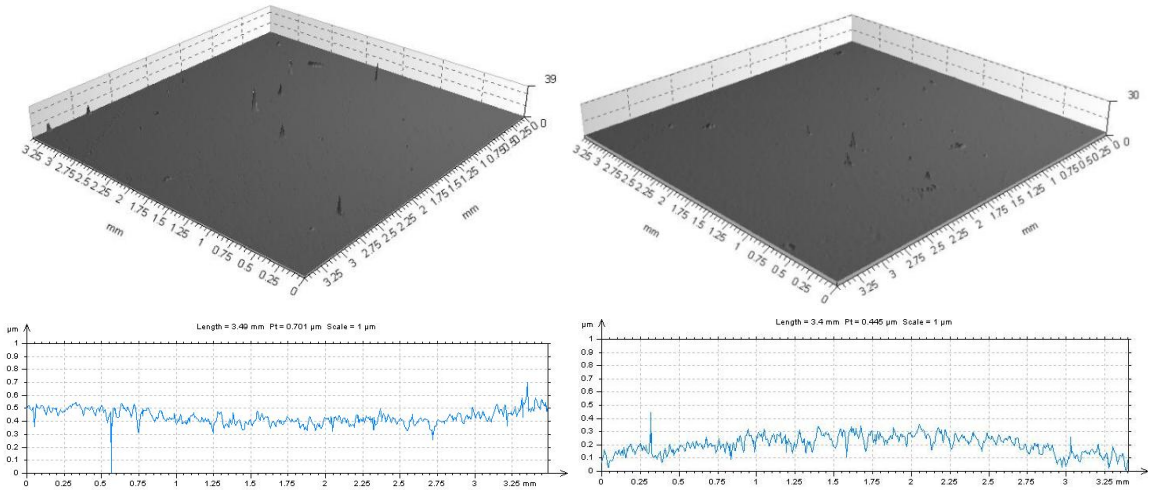

(e) (f)

Figure 7.2 – Continuous axonometric 3-D images and profile extractions for (a) EWA100, (b) EWA150, (c) EWA200, (d) EWA250, (e) EWA250_500 and (f) EWA250_1000.

7.3 – Effects of KrF Excimer Laser Processing on Wettability Characteristics

In this section the wettability characteristics are described and discussed for both the KrF excimer laser-induced patterning and KrF excimer whole area irradiative processing of nylon 6,6 in relation to the as-received sample.

7.3.1 – KrF Excimer Laser-Induced Patterning

Table 7.3 gives a summary of the surface parameters and wettability characteristics for each of the samples studied. It can be seen that on account of the KrF excimer laser-induced patterning of the nylon 6,6 samples θ increased by up to 24° in comparison to the as-received sample (AR) which had a θ of 56.4±1.2°. This does not appear to corroborate with current theory as an increase in surface roughness for a hydrophilic material should bring about a reduction in the θ, as previously discussed in Chapter 6. This increase in θ arising from the excimer patterned samples can be accounted for by the reduction in apparent polar component, γ^P, and apparent total surface free energy, γ^T, which is modified by the liquids equilibrium state. That is, the wetting regime has changed on account of the surface topography. As discussed in Chapter 6 there is a likelihood that this transition in wetting regime is a mixed-state wetting regime in which both Wenzel and Cassie-Baxter regimes form along the liquid-surface interface [92,102,130,131]. It should also be noted here that Table 7.3 confirms that as a result of the KrF excimer laser-material oxidation of the surface was observed, allowing the surface oxygen content to increase by at most 1.6 %at. The largest increase in surface oxygen content was found to be from the hatch patterned samples (EH50 and EH100) owed to the fact that more material was ablated inducing more surface oxidation.

From Figure 7.3 it can be seen that θ was an inverse function of γ^P and γ^T which does agree with current theory for a hydrophilic material such as nylon 6,6. This suggests that even though there is a likely-hood of a mixed-state wetting regime is arising on the KrF excimer laser patterned samples γ^P and γ^T still play a distinct role in terms of the wettability of the nylon 6,6. It is also possible to ascertain from Figure 7.3(b) that similar values of γ^T give rise to equivalent values of θ. That is, with a γ^T of approximately 30 mJm^{-2}, a θ of between 75 and 80° could be expected.

Table 7.3 – Results summary for all samples showing roughness parameters, surface oxygen content and wettability characteristics for KrF processed nylon 6,6.

Sample ID	Sa (μm)	Ra (μm)	Polar Component, γ^P (mJm^{-2})	Dispersive Component, γ^D (mJm^{-2})	Total Surface Free Energy, γ^T (mJm^{-2})	Surface Oxygen Content (%at.)	Contact Angle (°)
AR	0.126	0.029	17.69	29.66	47.34	13.26	56.4±1.2
Laser-Induced Patterned Samples							
ET50	0.281	0.312	15.48	28.74	44.22	13.87	60.6±3.0
ET100	1.320	0.679	6.52	23.54	30.06	13.53	80.8±5.2
EH50	0.739	0.548	12.94	17.24	30.17	14.15	75.1±3.9
EH100	1.530	1.032	17.06	13.55	30.61	14.83	73.0±3.7
Whole Area Irradiative Processed Samples							
EWA100	0.119	0.029	21.72	27.08	48.79	13.11	52.8±1.1
EWA150	0.092	0.039	25.98	24.76	50.74	13.03	49.1±4.7
EWA200	0.108	0.030	25.26	25.86	51.12	13.28	48.9±2.6
EWA250	0.107	0.031	22.37	28.66	51.03	13.24	50.3±1.5
EWA250_500	0.164	0.039	33.31	21.40	54.71	15.32	42.9±1.6
EWA250_1000	0.198	0.036	37.56	20.89	58.46	18.36	37.6±3.2

Figure 7.4 shows the correlation arising between θ and the surface roughness parameters Ra and Sa. For the KrF excimer laser-induced patterned samples it can be seen that θ is an increasing function of both Ra and Sa with the exception of the last data point which was for sample EH100 which had an Ra of 1.032 μm, an Sa of 1.530 μm and a resulting θ of 73±3.7°. This could suggest that an increase in the surface roughness could give rise to an increase in θ until a certain point at which θ remains constant or begins to decrease by which time would then start to correspond with current theory insofar as an increase in surface roughness gives rise to a more hydrophilic response. Furthermore, this could suggest that over the different rough periodic surfaces a transition in wetting regime could have taken place and would explain the decrease in θ for the roughest sample (sample EH100).

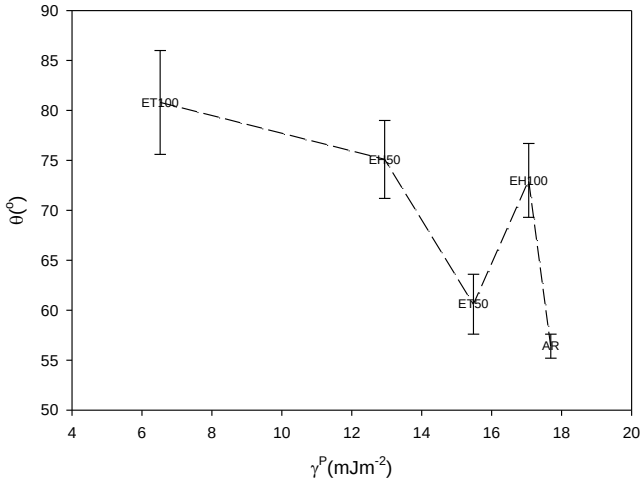

(a)

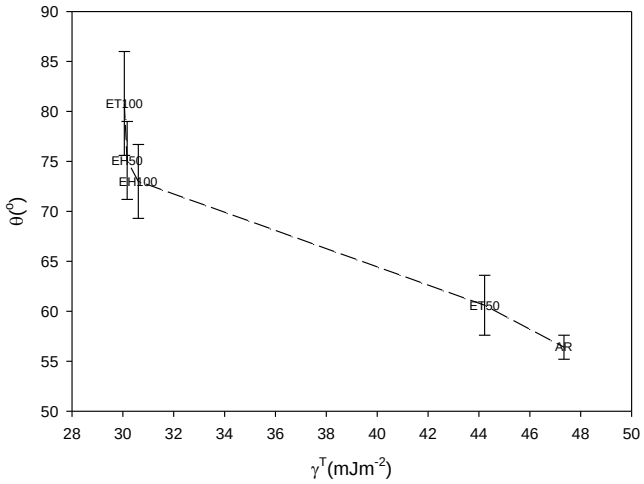

(b)

Figure 7.3 – Graphs showing the correlation between θ and (a) γ^P and (b) γ^T.

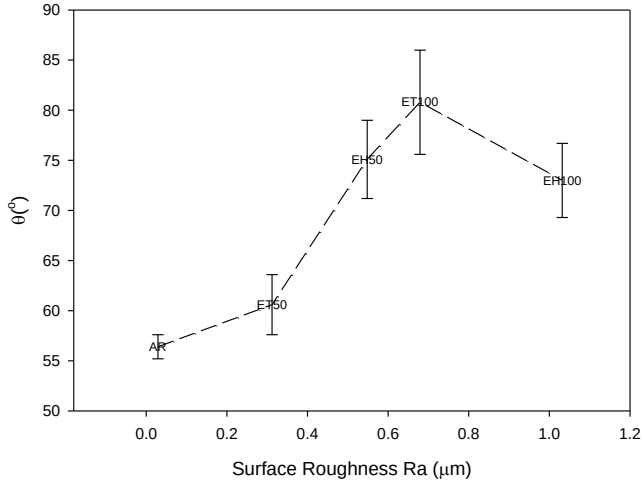

(a)

Figure 7.4 continued overleaf

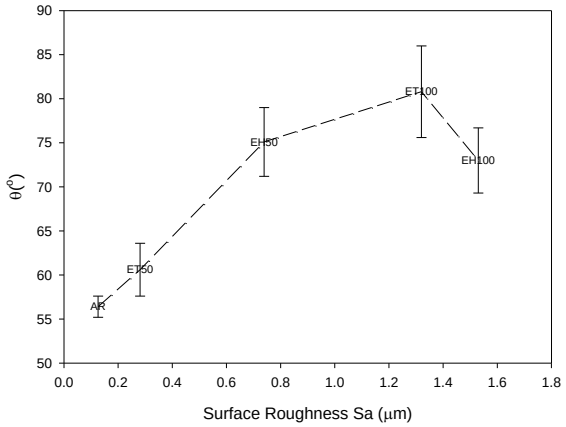

(b)

Figure 7.4 – Graphs showing the correlation between θ and (a) Ra and (b) Sa.

7.3.2 – KrF Excimer Laser Whole Area Irradiative Processing

From Table 7.3 it can be seen that the KrF excimer laser whole area irradiated samples gave rise to a decrease in θ of up to 20°. The largest decrease in θ was observed for samples WA250_500 and WA250_1000 which had the largest fluence of 91 mJm^{-2} and more pulses compared to the other samples. The reduction observed in θ can be attributed to the increase in γ^P and γ^T. In terms of surface oxygen content it was seen that there was an increase of up to 5 %at. which could have also given rise to the reduction in θ; however, as the surface oxygen content for all samples throughout this research have given rise to an increase in θ it is reasonable to state that surface oxygen content is not the main driving parameter to determine θ. Another factor which can be taken from Table 7.3 is that the surface roughness variation was negligible compared to the as-received sample (AR) which had an Ra of 0.029 μm and Sa of 0.126 μm it stands to reason that γ^P and γ^T has to be dominant in determining the wettability.

Figure 7.5 shows that θ over all KrF excimer laser processed samples was an inverse function of γ^P and γ^T with very good correlation. What is more it can be seen from Figure 7.5 that those samples which had equivalent γ^P or γ^T values gave rise to similar observed θ. For instance, for γ^P values of around 22 and 25 mJm^{-2}, θ was approximately 51 and 48° (see Figure 7.5(a)). Also, from Figure 7.5(b) it can be seen that samples with similar γ^T of around 51 mJm^{-2} gave rise to θ in the region of 50°.

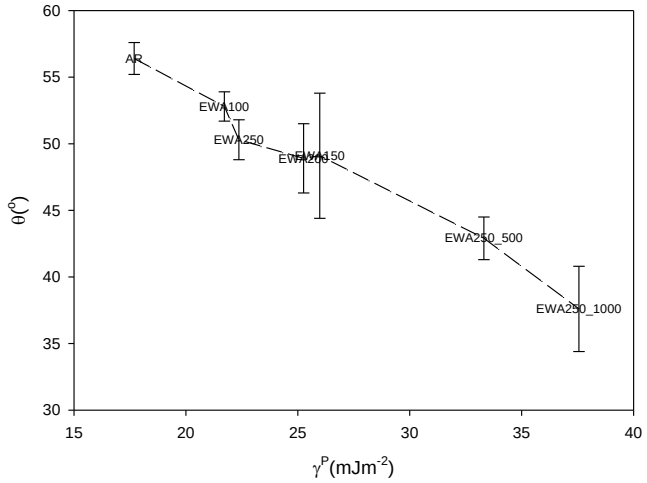

(a)

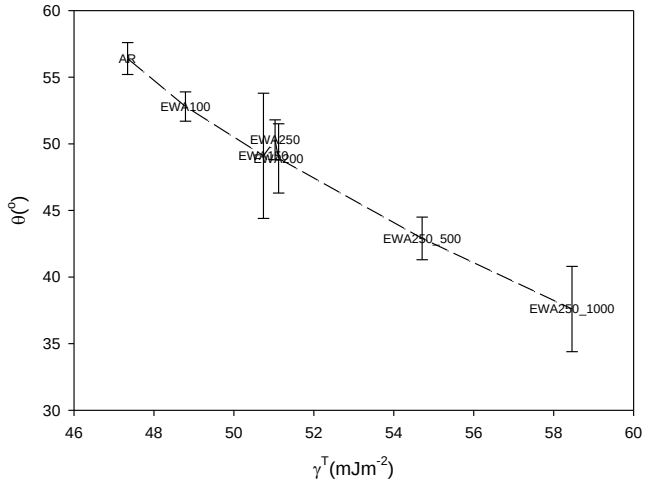

(b)

Figure 7.5 – Graphs showing the correlation between θ and (a) γ^P and (b) γ^T.

Figure 7.6 shows a reasonable inverse correlation between the surface roughness and θ when collating the results for all KrF excimer laser whole area irradiative processed samples. However, on account of the relatively small variations in Ra and Sa for these samples, a conclusive relationship between surface roughness and θ cannot be determined within this section.

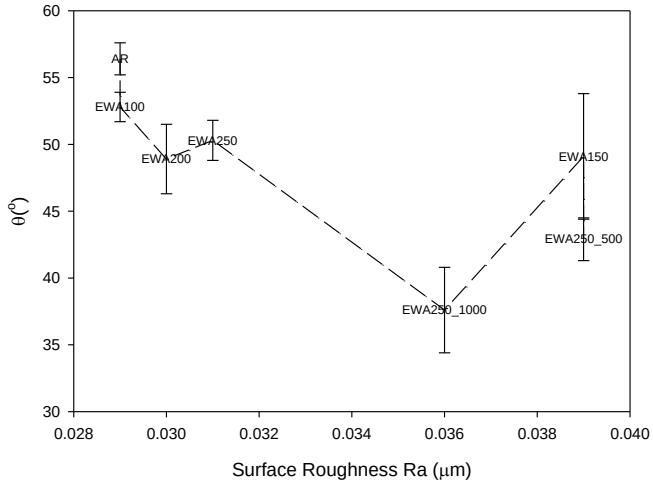

(a)

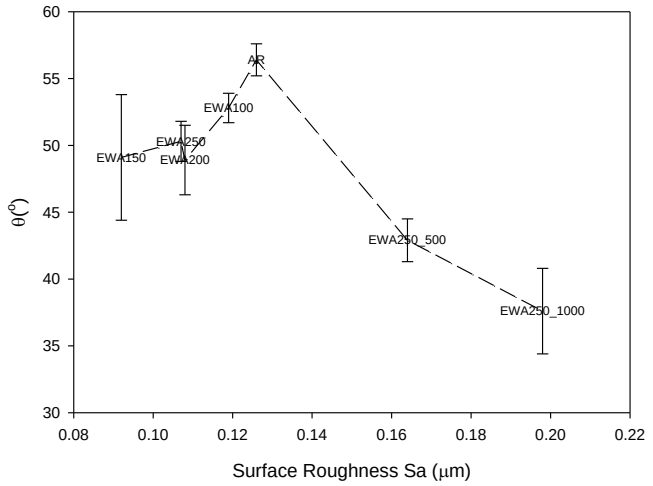

(b)

Figure 7.6 – Graphs showing the correlation between θ and (a) Ra and (b) Sa.

7.3.3 – Comparison Between KrF Excimer Laser-Induced Patterning and KrF Excimer Laser Whole Area Irradiative Processing

Table 7.3 allows one to identify that there was some significant differences between the as-received (AR), KrF excimer laser-induced patterned and KrF excimer laser whole area processed nylon 6,6 samples in terms of surface parameters and wettability characteristics. It was observed that for the KrF laser-induced patterned samples θ increased even though there was a significant increase in surface roughness. This increase in θ can be attributed to the reduction in γ^P and γ^T and the likelihood of a transition in wetting regime as discussed in Chapter 6. On the other hand, it was found that on account of an increase in γ^P and γ^T, θ decreased for the KrF excimer laser whole area irradiative processed nylon 6,6 samples. It was observed that for all KrF excimer laser processed samples the surface oxygen content increased by up to 5 %at. when compared to the as-received sample (AR). This increase in surface oxygen content indicates that this may have given rise to the observed

reduction in θ for the laser whole area processed samples. Still, this is does not seem to be the case as a reduction in θ was not observed for the KrF excimer laser-induced patterned samples. This suggests that a significant variation in surface topography of the nylon 6,6 may bring about the change in wettability regime; whereas when there is no significant variation in topography it is possible that a variation in wettability is brought about by other parameters such as γ^P and γ^T. In addition, even though there was a change in wetting regime for the KrF excimer laser-induced patterned samples to account for the increase of Sa and Ra, it was still found that θ remained strongly linked to variations in γ^P and γ^T.

In terms of collating the γ^P and γ^T results for the entire KrF excimer laser processed samples and the effects thereof on θ, Figure 7.7 shows that there was a strong inverse function correlation between θ and the surface energy parameters regardless of the processing technique used. This indicates that γ^P and γ^T could be the main driving parameters determining the wettability of the nylon 6,6 samples in this instance. As a result it may be possible to use these parameters as indicators of how nylon 6,6 will wet as long as the results are repeatable. Having said that, as discussed in Section 7.3.2, similar values of γ^P and γ^T give rise to equivalent θ suggesting that this process is repeatable.

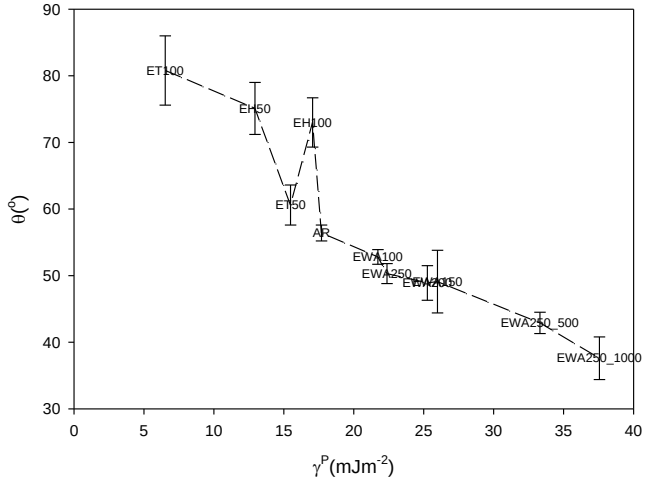

(a)

Figure 7.7 continued overleaf

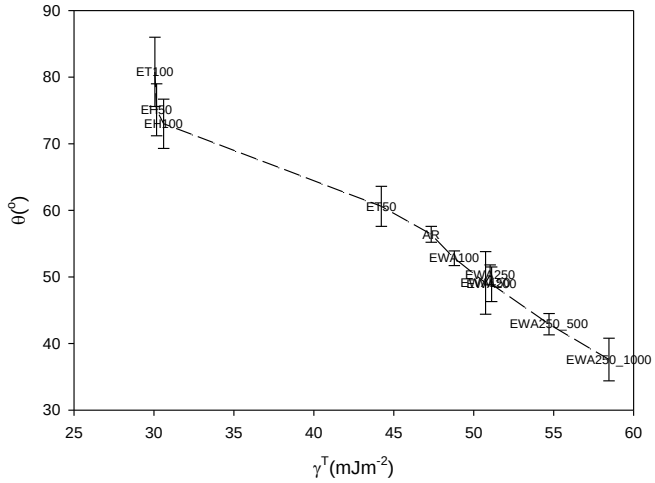

(b)

Figure 7.7 – Graphs showing the correlation between θ and (a) γ^P and (b) γ^T.

Another parameter which is known to have a significant impact on the wettability characteristics of a material is that of surface roughness. Figure 7.8 shows that upon collating the results for the KrF excimer laser processed samples in terms of Ra and Sa and the effects thereof on θ, there does not appear to be a good correlation between the parameters. This is likely on account of the fact that the periodic surface roughness brought about by the KrF excimer laser-induced patterning has given rise to a transition in wetting regime and gives rise to the current theory not being followed by those samples exhibiting a mixed-state wetting regime.

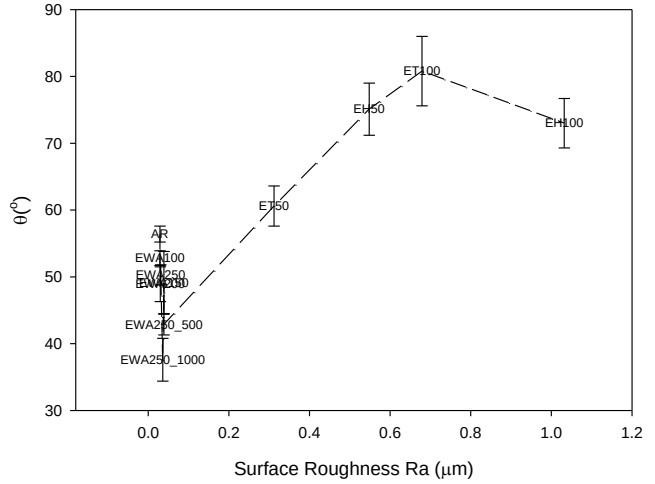

(a)

Figure 7.8 continued overleaf

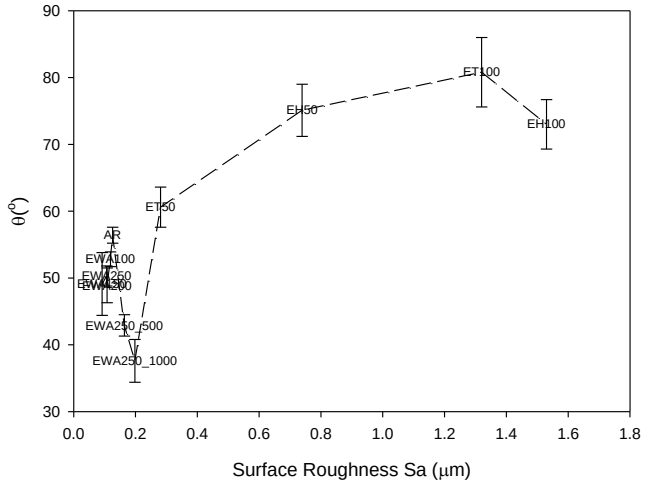

(b)

Figure 7.8 – Graphs showing the correlation between θ and (a) Ra and (b) Sa.

8
A Comparative Study Between CO_2 and F_2 Excimer Laser Patterning of Nylon 6,6

From Chapter 6 and Chapter 7 it was identified that surface roughness, γ^P and γ^T had a significant impact upon ϑ. As a result of this more evidence is required to ascertain the main driving parameters determining the wettability of nylon 6,6 following laser surface treatment. As such, this chapter details a study into using CO_2 and F_2 excimer lasers for patterning nylon 6,6 in relation to manual roughening.

8.1 – Introduction

Variations in micro and nano-structured topographies have been seen to have a major influence on θ angle that arises from the processing [171,172]. In addition, it has also been observed that in some instances the surface chemistry dominates the wettability characteristics of a material, such as through the work of Kietzig et al. [173]. Through Chapter 6 and Chapter 7 it has been seen that the surface roughness on account of the laser surface modification has played a major part in the possible arising wetting regime taking place on the nylon 6,6 samples. As a result it has been seen that surface roughness, γ^P and γ^T all, to some extent, effect the wettability of nylon 6,6.

On account of the surface roughness, γ^P and γ^T all having some impact on the wettability of nylon 6,6 more evidence is required to determine if a dominant parameter for each of laser surface treatment techniques can be identified. As a result, this chapter details the way in which CO_2 lasers and F_2 lasers can modify the surface topography and wettability characteristics of nylon 6,6 in relation to manually roughening. What is more, an excimer F_2 laser has been employed to identify any variations in wavelengths in terms of modification of the wettability characteristics.

8.2 – Additional Experimental Procedures

As this chapter required additional experimental procedures to those given in Chapter 5, this section will detail any extra methodology. For the analytical method regarding WLI, θ measurements and analsysis of surface oxygen content see Chapter 5.

8.2.1 – CO_2 Laser System

In order to generate the required marking pattern, software (Winmark software 2.1.0.3468; Synrad Inc.) specific to the laser was used. In addition, the software was capable of using images saved as .dxf files which can be produced by using CAD programs such as, in this case, Licom AutoCaM. The sample material was held in the system with a bracket on a variable z-axis stage and was positioned at the focal length, which was 250 mm from the laser aperture to the sample surface. The 10.6 μm

wavelength cw 10 W CO_2 laser system (Synrad Inc., USA), with a spot size of 100 μm, used a galvanometer scanner to scan the beam directly across the target material in conjunction with the pattern produced on the Synrad software. It should be noted here that the target material and laser system were held in a laser safety cabinet in which the ambient gas was air. Additionally, an extraction system was used to remove any fumes produced during laser processing.

8.2.2 – F_2 Excimer Laser System

The F_2 excimer laser system (LPF 202; Lambda Physik Inc.) operated at a wavelength of 157 nm. The max pulse energy was 35 mJ and a pulse duration of 11 ns at 26 kV charging voltage. Samples were irradiated using a projection etching system with the lateral position of the samples being controlled using computerized stages with typically one micron resolution. The beam delivery system consisted of a 2 meter long stainless steel beam tube between the laser and sample chamber which was evacuated to expel absorbing oxygen species. Experiments were carried out at pressure of around 2×10^{-3} mbar.

In order to achieve the required trench dimensions an aperture projection mask was produced using SS316 foil (Laser Micromachining, Ltd.). The mask was 30×30 mm^2 and consisted of an array of five apertures with a diameter of 0.5 mm in a straight line spaced by 1mm centre to centre. This allowed 50 μm wide trenches to be etched, spaced by 50 μm upon using a demagnification of 10.

8.2.3 – Laser Irradiation Procedures

Trenches were produced using the Synrad CO_2 laser system with a spacing of 50 μm between each trench by scanning the laser beam across the nylon 6,6 samples. Two samples were produced; one using a power of 50% (5 W) with a velocity of 1000 mms^{-1} and the second using a power of 80% (8 W) with the same velocity (sample C10 and C9, respectively). With powers of 5 and 8 W used and a spot size of 100 μm the corresponding irradiances used for these experiments was 6.4 and 10.2 kWcm^{-2}, respectively.

The F_2 excimer laser system was used to produce two areas of etched trenches by traversing the stage and keeping the beam stationary. The first of these being to achieve an etch depth of approximately 1 μm (sample F3) and the second giving a depth of approximately 10 μm (sample F4). In order to achieve these depths each site required 1,000 and 10,000 pulses, respectively. The etch depth per pulse was determined to be approximately 1 nm per pulse. By knowing this it was possible to determine the traverse velocities, v_t, with

$$v_t = \frac{DR}{N} \tag{8.1}$$

where D is the diameter of one of the apertures in the mask, R is the repetition rate (which was 20 Hz) and N is the number of pulses. From Equation (8.1) it was determined that for 1 and 10 μm deep

trenches velocities of 0.01 and 0.001 mms^{-1} were to be used, respectively. It should be noted that the when carrying out the experiments using the F_2 laser a constant fluence of 40 $mJcm^{-2}$ was used. For comparison between the laser irradiated samples an as-received reference sample (N6) was also studied. This allowed any deviations from the original as-received characteristics to be identified after the laser processing had taken place.

8.2.4 – Mechanical Roughening Procedure

For further verification of laser-induced θ modification two samples were roughened manually using DA-F P220 emery paper. One sample was roughened using a zig-zag motion traversing from the top to the bottom of the sample (sample R1). The second sample (sample R2) was roughened by carrying out the same technique as the first sample, with the addition of rotating the sample through 90° and repeating the roughening method with the emery paper.

8.3 – Effects of CO_2 and F_2 Laser Processing on Surface Topography

This section discusses the results obtained in terms of surface topography for the CO_2 laser-induced patterning, F_2 excimer laser-induced patterning and mechanical roughening of the nylon 6,6 samples.

8.3.1 – CO_2 Laser-Induced Patterning

Figure 8.1 and Figure 8.2 show continuous axonometric 3-D images and profile extractions (perpendicular to the grooves) for the CO_2 laser-induced patterned samples. From these Figures it was identified that the maximum peak heights observed for C10 and C9 were 2 and 3 μm respectively, which is considerably larger than that of the as-received reference sample (AR) which can be seen in Figure 6.1. Even though the effect the CO_2 laser beam had on the surface topography can be seen more prominently in Figures 8.1 and 8.2, by taking a profile extraction (see Figures 8.1 and 8.2) of the surfaces perpendicular to the direction of the grooves, it can be seen that there was only slight periodicity to the surface induced pattern. This is due to the fact that the CO_2 laser spot size was larger than the intended surface pattern and the scanned beam overlapped during processing inherently eradicating the natural periodicity of the induced pattern.

The surface roughness parameters, Sa and Ra, were determined for each of the surfaces, all of which are given in Table 5. The Sa roughness values for the 5 W CO_2 laser irradiated nylon surface was found to be 0.262 μm, whereas the higher power of 8 W gave rise to a slightly rougher surface with an Sa value of 0.358 μm. Even so, it can be seen that the CO_2 laser-induced patterns gave rise to a considerable increase in the surface roughness when compared to the as-received sample (AR) which had an Ra of 0.126 μm and an Sa of 0.029 μm.

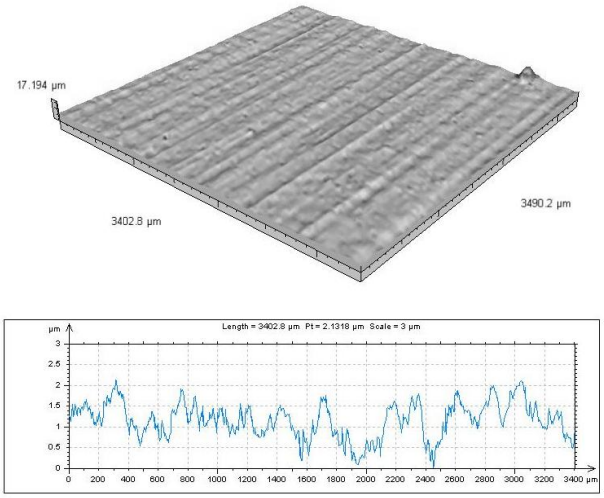

Figure 8.1 – Continuous axonometric 3-D image and profile extraction for CO_2 laser irradiated nylon 6,6 at 5 W (6.4 kWcm^{-2}), 1000 mms^{-1} (Sample C10).

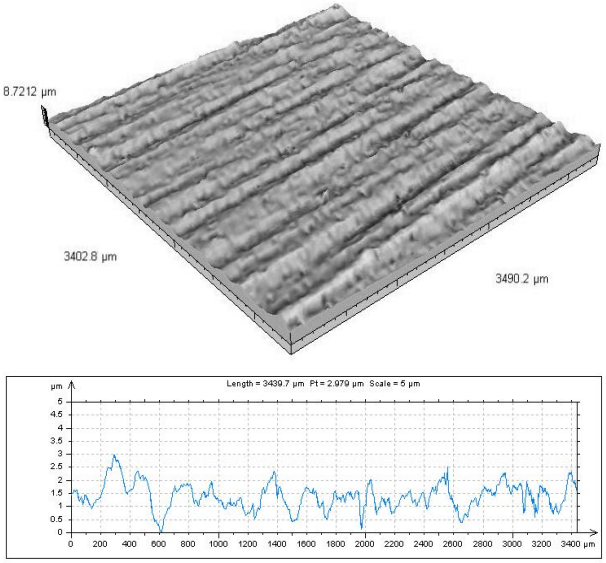

Figure 8.2 – Continuous axonometric 3-D image and profile extraction for CO_2 laser irradiated nylon 6,6 at 8 W (10.2 kWcm^{-2}), 1000 mms^{-1} (Sample C9).

Table 8.1 – A summary of the results for the seven samples along with θ and hysteresis with triply distilled water following CO_2 and F_2 laser processing.

Sample ID	Sa (μm)	Ra (μm)	γ^P (mJm^{-2})	γ^D (mJm^{-2})	γ^T (mJm^{-2})	Surface Oxygen Content (% at.)	Contact Angle (°)
AR	0.126	0.029	17.69	29.66	47.34	13.26	56.4±1.2
CO_2 Laser-Induced Patterning							
C10	0.262	0.346	20.75	27.38	48.13	14.60	53.9±3.2
C9	0.358	0.256	24.27	23.90	48.17	14.90	52.4±2.9
F_2 Excimer Laser-Induced Patterning							
F3	0.248	0.253	9.78	37.19	46.98	10.80	66.7±4.1
F4	2.647	2.947	8.46	28.44	36.90	10.30	72.9±4.3
Mechanical Roughening							
R1	3.104	2.368	22.57	34.86	57.43	13.20	44.0±2.3
R2	3.735	3.055	24.68	36.85	61.53	13.21	38.4±1.5

8.3.2 – F_2 Excimer Laser-Induced Patterning

Figure 8.3 and Figure 8.4 show the continuous axonometric 3-D images for the F_2 excimer laser-induced patterned nylon 6,6 samples for different pulse numbers per site. From these Figures it was determined that the F_2 laser could significantly modify the surface topography of the nylon 6,6 samples when compared to the as-received sample (AR). It was found that for sample F3 (see figure 8.3) trench depths of 1 μm were achieved with a highly periodic pattern induced into the material surface. In addition, Figure 8.4 confirmed that sample F4 had 10 μm deep trench which were also highly periodic.

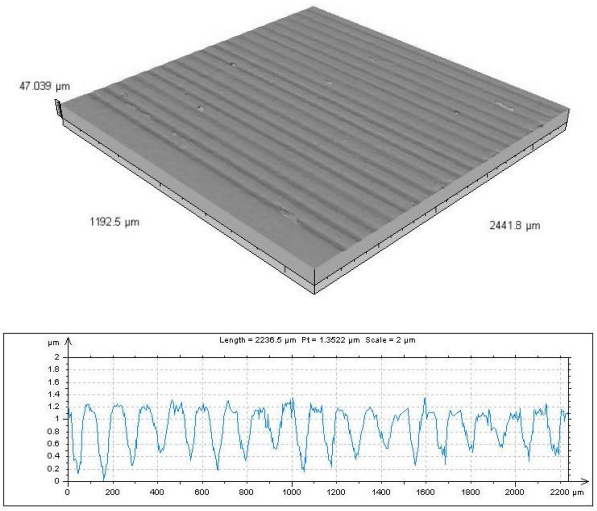

Figure 8.3 – Continuous axonometric 3-D image and profile extraction for F_2 excimer laser irradiated nylon 6,6 at 40 $mJcm^{-2}$ and 1,000 pulses per site (Sample F3).

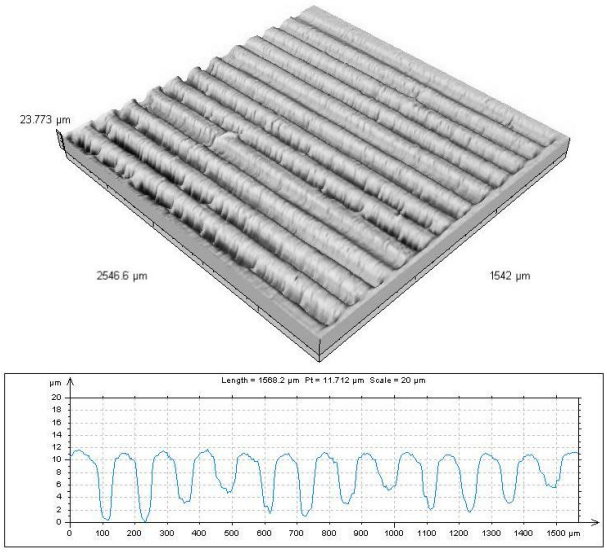

Figure 8.4 – Continuous axonometric 3-D image and profile extraction for F_2 excimer laser irradiated nylon 6,6 at 40 mJcm^{-2} and 10,000 pulses per site (Sample F4).

Table 8.1 shows that on account of the noteworthy surface modifications attributed to the F_2 laser-induced patterns the surface roughness was considerably higher than the as-received sample (AR). For instance, Sa for sample F3 and F4 was found to be 0.248 and 2.647 µm, respectively. It would be significant to note here that sample F4 had a considerably greater Sa compared to sample F3 due to the depth of the trenches being an order of magnitude large for sample F4.

8.3.3 – Mechanical Roughening

To elucidate and clarify how the laser induced patterns effected changes in θ, two samples were mechanically roughened using emery paper, of which the continuous axonometric 3-D images can be seen in Figure 8.5 and Figure 8.6. It can be seen that visually the roughness of the nylon 6,6 samples have been considerably increased when compared to the as-received sample (see Figure 6.1). This finding can be seen to be of significance as even though there was a considerable increase in surface roughness the manually roughened samples (see Figure 8.5 and Figure 8.6) gave an indication that no periodic pattern was induced on the surface of the nylon 6,6 samples.

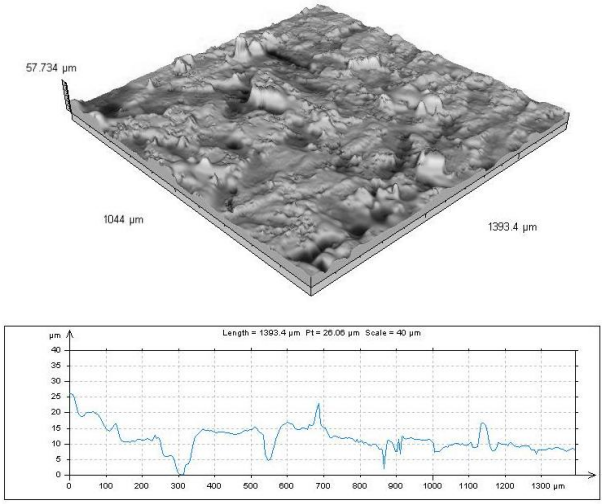

Figure 8.5 – Continuous axonometric and profile extraction of the first emery paper roughened sample (Sample R1).

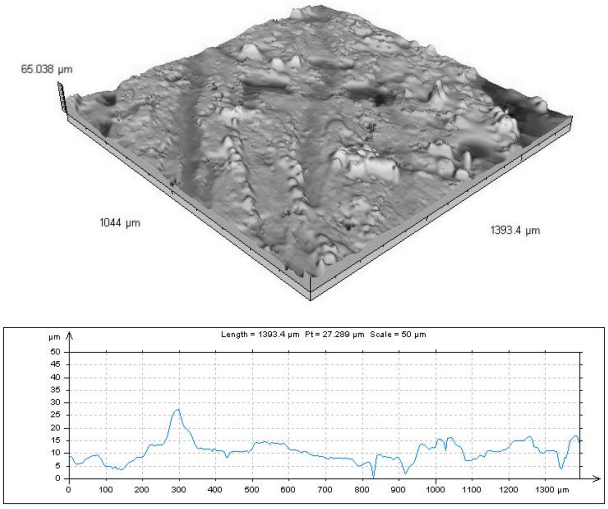

Figure 8.6 – Continuous axonometric and profile extraction of the second emery paper roughened sample (Sample R2).

The surface roughness of the mechanically roughened samples was determined as given in Table 8.1. It can be seen from the data given in Table 8.1 that the mechanically roughened samples gave rise to, at most, a two order of magnitude increase in roughness compared to the as-received sample. That is, the Ra increased by up to 3.1 µm and the Sa by up to 3.7 µm in comparison to the as-received sample (AR) which had an Ra and Sa of 0.029 and 0.126 µm, respectively.

8.3.4 – Comparison Between CO_2 Laser-Induced Patterning, F_2 Laser-Induced Patterning and Mechanical Roughening

For all of the laser surface patterned samples it can be seen from Table 8.1 that the surface roughness has been increased considerably in comparison to the as-received reference sample (AR). That is, the Ra and Sa increased by up to 2.9 and 2.6 μm, respectively. The largest roughness values were produced using the F_2 excimer laser (samples F3 and F4) which can be owed to the fact that deeper trenches were induced compared with the features arising from using the CO_2 laser marker (samples C10 and C9).

It is known that the CO_2 laser couples into the material via resonant coupling which gives rise to bond vibrations allowing the temperature to rise and melt the material. Upon cooling the molten material re-solidifies and a protrusion away from the surface becomes evident on the surface. This is contrasted with the F_2 excimer laser as it ablates the nylon 6,6 allowing the required pattern to be etched into the material. As a result the F_2 excimer laser system offers a major advantage over the CO_2 in the fact that it ablates approximately 1nm per pulse, with the fluence used in this instance, allowing the user to be more precise and accurate with the surface topography they require. However, the amount of time it takes to pump the F_2 vacuum system to operating pressure and the amount of time it takes to produce a number of few μm deep trenches is considerably greater than the CO_2 laser system employed in this study. What is more, the etched trenches using the F_2 excimer laser shown in Figure 8.3 and Figure 8.4 were considerably more defined than the CO_2 laser-induced patterned samples (see Figure 8.1 and Figure 8.2). This can also be attributed to the resulting differences in laser-material interaction between the CO_2 and F_2 excimer lasers.

8.4 – Effects of CO_2 and F_2 Laser-Induced Patterning on Wettability Characteristics

This section details and discusses the wettability characteristics of the nylon 6,6 samples which had undergone CO_2 laser-induced patterning, F_2 excimer laser-induced patterning and mechanical roughnening.

8.4.1 – CO_2 Laser-Induced Patterning

As given in Table 8.1, following CO_2 laser-induced patterning the γ^T had slightly reduced due to a change in γ^P and γ^D. It can be seen that the apparent γ^P increases by up to 4.12 mJm^{-2} for the rougher sample (sample C9), whereas the γ^D was reduced at most by 12.22 mJm^{-2}. As it is γ^P of the surface energy that plays the major role in determining the θ it can be seen that these results also do not correspond with existing theory. For instance, Lawrence and Li [75] stated that a laser-induced increase in the γ^P, along with an increase in O_2 content and increase in surface roughness, would give rise to a reduction in the θ. However, a significant rise in surface roughness and γ^P has led to an increase in the observed θ by up to 5°. Having said that, it has been seen that the apparent γ^T reduces

for the CO_2 laser-induced patterned nylon 6,6 surfaces and this could correspond with current theory as it has previously been observed that θ is inversely proportional to γ^T [103].

In order to explain the increase in γ^P, increase in surface roughness and resulting increase in θ it is possible to deduce that a mixed-state wetting regime may occur as discussed in Chapter 6. On account of a mixed-state wetting regime in which both Wenzel and Cassie-Baxter regimes are present along the liquid-surface interface it would be possible for one to identify that γ^P could become modulated, effectively becoming an apparent γ^P. However, even if this is the case it may still be possible for an apparent γ^P to play some distinct role in the determination of the wettability of CO_2 laser-induced patterned nylon 6,6. This mixed-state wetting regime would also allow one to see how a rougher hydrophilic surface could give rise to slightly larger θ when compared to the as-received sample (AR).

With regards to the surface oxygen content it can be seen from Table 8.1 that on account of surface oxidation arising through the melting and re-solidification of the CO_2 laser processing the surface oxygen content had increased by up to 1.5 %at. when compared to the as-received sample (AR) which had an initial oxygen content of 13.26 %at. It could be argued that the surface oxygen content could have an impact on the wettability of nylon 6,6; however, on account of what has been observed in Chapter 6 and Chapter 7 it is highly unlikely that the surface oxygen content is the main driving force parameter for the wettability observed from the nylon 6,6.

8.4.2 – F_2 Excimer Laser-Induced Patterning

Subsequent to F_2 excimer laser-induced patterning of nylon 6,6, γ^T and γ^P had considerably reduced with γ^P reducing by up to 10 mJm^{-2} (See Table 8.1). It is highly likely that the rise in θ of up to 25° can be attributed to the significant reduction of the apparent γ^T resulting from an intermediate mixed-state wetting regime arising from the rough periodic topographical pattern induced onto the nylon 6,6 samples. This mixed-state wetting regime as discussed in Chapter 6 was also hypothesized by Lee and Kwon who also observed an increase in θ for patterned topographies on a hydrophilic surface [102].

Table 8.1 also shows that the surface oxygen content of the nylon 6,6 samples following the F_2 excimer laser-induced patterning had reduced up to 1.6 %at. in comparison to the as-received sample (AR). An explanation for this is that as the F_2 excimer laser system was under vacuum, there would have been a considerable reduction in ambient air and as a result the surface would not oxidize and could potentially lose O_2 content during the laser ablation process.

8.4.3 – Mechanical Roughening

As a result of the mechanical roughening of the samples it can be seen from Table 8.1 that an increase in γ^P and roughness has given rise to a significant reduction in θ by at least 10°, which agrees with Lawrence and Li [75]; that is, the apparent polar component increased by up to 4.53 mJm^{-2} and a considerable increase in surface roughness of up to 100 times that of the as-received reference sample was observed for samples R1 and R2. Also, as given in Table 8.1 the surface O_2 content for the

manually roughened samples was somewhat unchanged in comparison to the as-received reference sample, highlighting that the surface roughness, surface energy and topographical pattern have more of an impact on the wettability characteristics of nylon 6,6.

8.4.4 – Comparison Between CO_2 Laser-Induced Patterning, F_2 Laser-Induced Patterning and Mechanical Roughening

Both of the laser systems affected differently the nylon 6,6 samples with regards to wettability and surface energy parameters. The CO_2 laser-induced patterns had been seen to be capable of producing θ slightly larger in comparison to the as-received reference sample (AR). It can also be seen from Table 8.1 that θ for each laser patterned sample increased with the F_2 excimer laser patterned samples giving the largest change with a θ of 72.92° for the roughest sample (sample F4). This does not concur with current theory as θ should decrease with increasing surface roughness for initially hydrophilic materials which have a θ less than 90° prior to any modifications taking place [4,88]. In this instance, as a result of the CO_2 laser-induced patterning the surface oxygen content increased by up to 1.5 % at. and the apparent polar component also increased by up to 4.12 mJm^{-2}. This also does not agree with current theory as an increase in apparent polar component and surface oxygen content should give rise to a reduction in θ. In contrast, for the F_2 excimer laser patterned samples the apparent polar component and surface oxygen content decreased by up to 11.69 mJm^{-2} and 1.6 %at., respectively. It has been proposed here that the increase in θ resulting from the laser modifications is due to the patterned topographies, such that they give rise to an intermediate mixed-state wetting regime in which both Wenzel and Cassie-Baxter regimes arise. This allows one to see how the laser-induced patterend samples would give a larger θ in comparison to the as-received sample.

To aid in clarification, manually roughened samples were analysed which showed that for a non-periodic rough surface the apparent polar component increased by 5 mJm^{-2} and surface O_2 content remained somewhat unchanged giving rise to a reduction in θ. Significantly, this shows that the surface pattern dominates the wettability characteristics for the laser induced patterned nylon 6,6 samples.

Another significant aspect to note is that of the correlation between γ^P, γ^T and θ as, in previous Chapters, the surface energy parameters have been found to have a correlative impact on determining the wetting nature of nylon 6,6. Figure 8.7 shows that θ was an inverse function for all samples within this work regardless of the surface processing technique used. This furthers the likelihood that γ^P and γ^T have an important role to play in determining the wettability of nylon 6,6 irrespective of which surface modification is employed. That is, an increase in γ^P and γ^T gives rise to a reduction in θ.

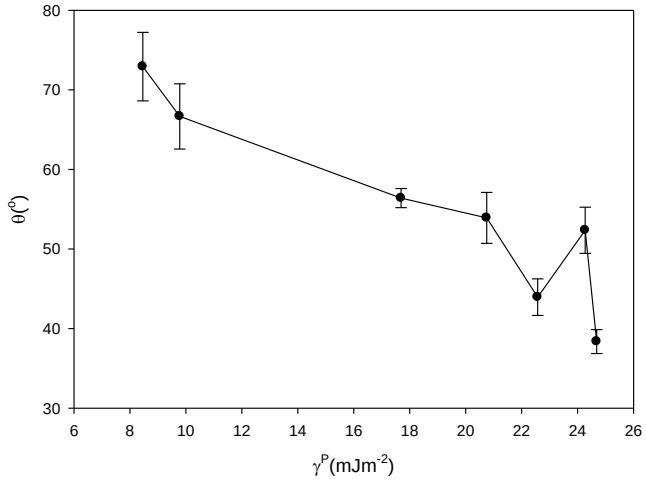

(a)

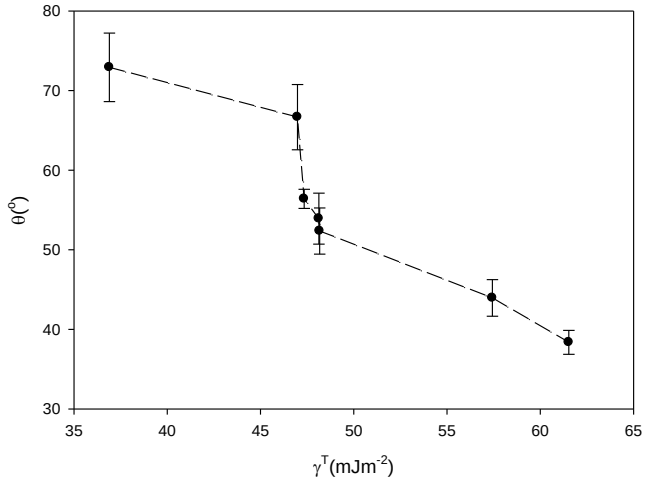

(b)

Figure 8.7 – Graphs showing the correlation between θ and (a) γ^P and (b) γ^T.

9
The Possible Effects of Atmospheric Conditions on the Wettability Characteristics of CO_2 Laser Patterned Nylon 6,6

Over time it is known that polymer surfaces can degrade on account of water absorption and hydrophobic recovery. This Chapter details a long term study into the wettability characteristics of laser-induced patterned nylon 6,6. Also, this Chapter discusses atmospheric conditions and the potential impact they can have on the measured ϑ.

9.1 – Introduction

A number of various long term studies have been carried out investigating the effect of different parameters on the wettability of a material over a set amount of time [36,40,133,174]. In addition to long term studies it has also been observed that the differing atmospheric pressure and differing environments can have a major effect on the wettability of a material as seen by Li *et al* [175], Hansen *et al* [176] and Siemons *et al* [177].

Although CO_2 lasers have been shown to be capable of modifying the wettability of polymeric materials, it is known that the wettability modifications of these materials can vary over time. But at the same time, ambient atmospheric parameters will affect θ and must therefore be accounted for as a control variable in any long-term study of wettability. This can be seen to be crucial from a commercial point of view as this would indicate that a shelf-life has to be established. As a result, a unique study has been undertaken by analysing how the wettability varies over time and how atmospheric parameters effect θ of four CO_2 laser patterned nylon 6,6 samples with differing topographical patterns and one as-received sample.

9.2 – Additional Experimental Procedures

As this chapter required additional experimental procedures to those given in Chapter 5 on account of this work being a long term study, this section will detail any extra methodology.

9.2.1 – Contact Angle Measurements and X-Ray Photoelectron Spectroscopy (XPS) Analysis

The samples were ultrasonically cleaned in isoproponal (Fisher Scientific Ltd.) for 3 minutes at room temperature before using a sessile drop device to determine various wettability characteristics, in accordance with the procedure detailed by Rance [108]. This was to allow for a relatively clean surface prior to any θ measurements being taken. A sessile drop device (OCA20; Dataphysics

Instruments, GmbH) was used in conjunction with specific software (SCA20; Dataphysics Instruments, GmbH) so that the recent advancing and receding θfor triply distilled water and the recent advancing angle for diodomethane could be determined for each sample. This was repeated every two weeks throughout the 30 week period. By achieving the advancing and receding θ the hysteresis for the system was determined. This was done by using the 'needle in' method to accurately add or remove liquid to give the advancing and receding liquid-solid-vapour line, respectively. In addition, by knowing the advancing θ for the two liquids it was possible to use the software to draw a OWRK plot to determine the surface energy of the samples. For the two reference liquids the SCA20 software used the Ström *et al.* technique to calculate the surface energy of the material. It should be noted here that 10 θ, using 2 droplets, in each instance was recorded to achieve a mean θ for each liquid-surface interface. Atmospheric data was recorded using a portable weather station (Meteo Clock Evolution Advance SM1840; Lexibook, S.A.).

Each sample was also analysed before and after the study by using X-ray photoelectron spectroscopy (XPS) to allow any surface modifications in terms of chemical composition due to the laser patterning to be revealed. Also, XPS was used to identify any changes within the surface chemical composition that may have come about over the experimental period. Further details of the XPS experimental procedure are described in [1].

9.3 – Effect of Time on the Topography of CO_2 Laser-Induced Patterned Nylon 6,6

Over time it is believed that it may be possible for the surface topographies to degrade. That is, on account of water absorption by polymeric materials dimensional changes can occur on account of swelling [36,40]. In particular with nylons, it has been seen that the presence of amide groups in the polyamide backbone gives rise to water absorption being favorable [36]. As such, it was necessary to analyse the samples using WLI before and after the experimental period to assess whether any changes had occurred during this time.

Figure 9.1 shows the continuous axonometric and profile extraction for the as-received sample at weeks 0 and 30. It can be seen from Figure 9.1 that, in terms of peak heights and surface features, the as-received surface topography did not vary over the 30 week period. This is confirmed with the profile extraction shown in Figure 9.1 with the peak heights observed to be, at most, 0.5 μm after 30 weeks. This is also confirmed by the roughness parameters, shown in Table 9.1, in that the Sa and Ra did not change over the allotted time for the as-received sample.

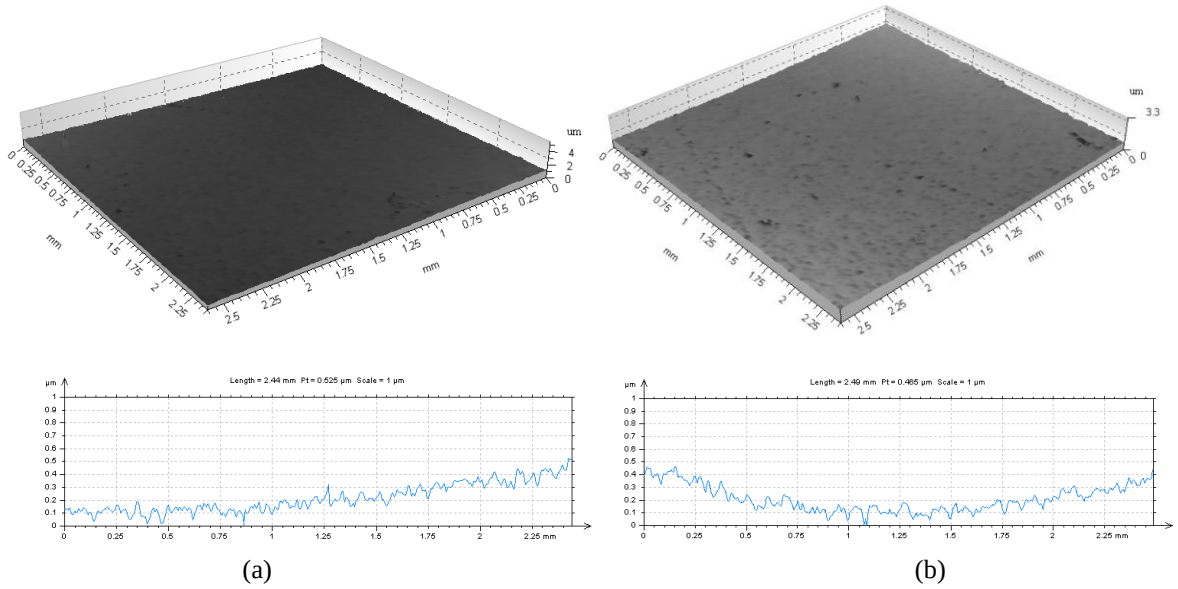

(a) (b)

Figure 9.1 – Continuous axonometric 3-D images and profile extractions for the as-received sample (AR) – (a) week 0 and (b) week 30.

Table 9.1 – Surface roughness values for Ra and Sa before and after the long term experiment for each sample.

	Week 0			Week 30		
Sample	Ra (μm)	Sa (μm)	θ (°)	Ra (μm)	Sa (μm)	θ (°)
AR	0.028	0.111	56.4±1.2	0.032	0.100	65.3±2.1
CT50	0.238	0.537	66.0±4.0	0.213	0.312	69.2±1.8
CT100	0.305	0.375	57.5±2.4	0.235	0.297	71.8±3.2
CH50	0.200	0.408	65.8±2.9	0.212	0.385	69.6±2.7
CH100	0.202	0.285	62.2±2.3	0.274	0.323	76.0±3.4

In order to identify any variations in surface topography over the 30 week experimentation period for the laser patterned samples WLI analysis was employed. The results for the laser patterned samples are detailed in Table 9.1 and Figures 9.2 to 9.5.

Through WLI analysis for the 50 μm trench pattern (sample CT50) shown in Figure 9.2 it was seen that in terms of surface topography there was no significant difference between week 0 and week 30. This coincides with what was observed for the as-received sample (AR) shown in Figure 9.1. By means of the CO_2 laser patterning of the 50 μm trench pattern (sample CT50) it can be seen through the profile extraction shown in Figure 9.2 that there does appear to be some slight periodicity to the pattern induced; however, less periodicity can be identified after the 30 week experiment. With regards to maximum peak heights for the 50 μm trench pattern it can be seen in Figure 32 that they remained around 2 μm over the 30 week testing period. From Table 9.1 it can be seen that Ra remained equivalently constant after 30 weeks with the Ra for week 0 being 0.238 μm and week 30 being 0.213 μm. For Sa it was found that this value decreased over time with the sample surface

giving an Sa of 0.537 and 0.312 for week 0 and week 30, respectively. This could be on account of degradation of the surface topography over time. For instance, this can be attributed to water absorption as discussed by Monson *et al* [40] the nylon 6,6 could have swelled giving rise to a surface dimensional change.

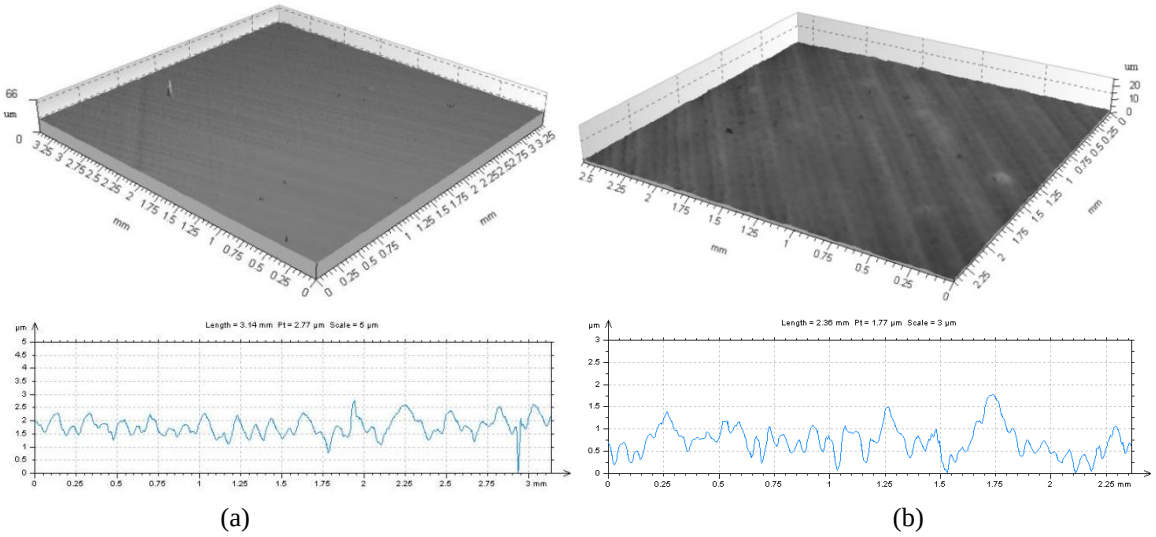

(a) (b)

Figure 9.2 – Continuous axonometric 3-D images and profile extractions for the 50 µm trench pattern (A3) – (a) week 0 and (b) week 30.

Figure 9.3 shows the continuous axonometric 3-D image and profile extraction for the laser induced 100 µm trench pattern (sample CT100) before and after 30 weeks. Firstly, it can be seen that in comparison to the 50 µm trench pattern (see Figure 9.2) the 100 µm trench pattern (see Figure 9.3) has a more defined periodic pattern. This is owed to the fact that the beam spot size used was 95 µm giving rise to overlap of the pattern during processing ultimately eradicating the intended periodicity of the 50 µm trench pattern.

Similar to the topography observed for the 50 µm trench pattern (see Figure 9.2), it was found that the 100 µm trench pattern periodicity (see Figure 9.3) did appear to deteriorate after the 30 week study. Furthermore, it can be seen from Figure 9.3 that the 100 µm trench pattern gave rise to peak heights of around 2 µm which, coinciding with the as-received sample, did not vary substantially over the 30 week experimentation period. However, slight differences in Sa and Ra was observed between week 0 and week 30. For example, taking Sa into consideration, the roughness decreased from 0.375 µm to 0.297 µm and could be attributed to natural degradation of the surface over the 30 week period.

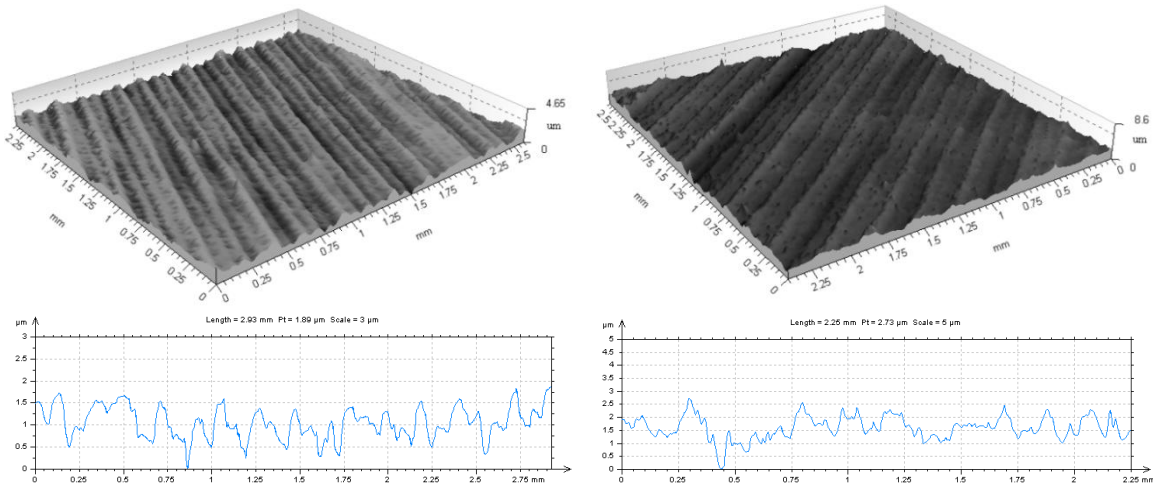

(a) (b)

Figure 9.3 – Continuous axonometric 3-D images and profile extractions for the 100 µm trench pattern (B1) – (a) week 0 and (b) week 30.

Figure 9.4 shows the continuous axonometric 3-D image and profile extractions for the 50 µm hatch patterned sample (CH50). From this it can be seen that peak heights between 1 and 2 µm were achieved during the laser patterning of the 50 µm hatch samples. Another factor to note between Figure 9.4(a) and Figure 9.4(b) is the difference in profile topography. For instance, at week 0 the gradients of the resulting peaks, owed to laser patterning, is somewhat greater than those observed after the 30 week period. This could also be a result of surface degradation. Even though there appeared to be a difference in surface topography, the results given in Table 9.1 show that the Ra remains somewhat constant over the 30 week period; whereas the Sa roughness was seen to decrease by 0.023 µm over the time allotted to study the samples.

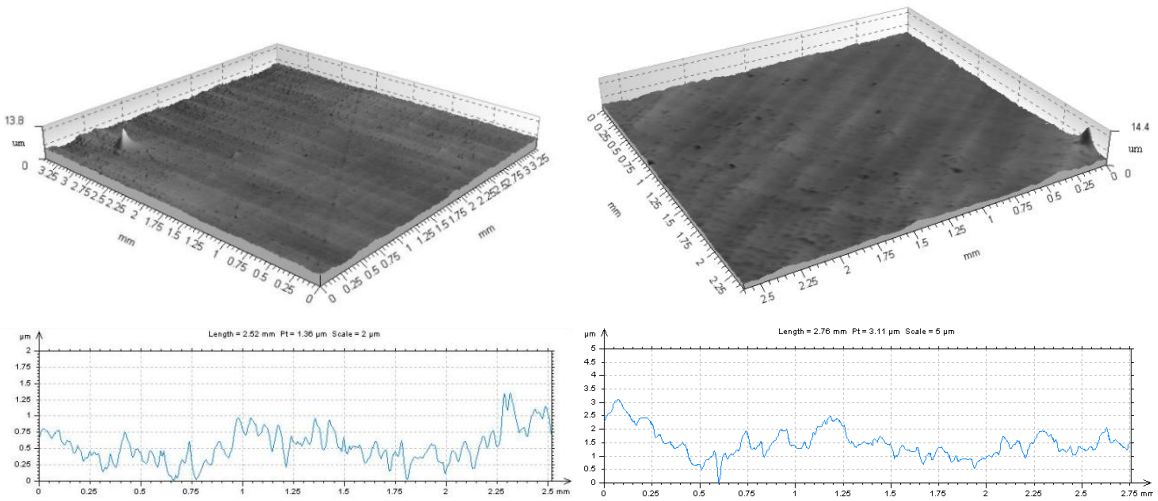

(a) (b)

Figure 9.4 – Continuous axonometric 3-D images and profile extractions for the 50 µm hatch pattern (B2) – (a) week 0 and (b) week 30.

Over the 30 week long experiment it was observed, for the CO_2 laser-induced patterned 100 µm hatch sample (see Figure 9.5) that the peak heights also remained equivalent between 1 and 2 µm. Additionally, in terms of surface topography Figure 9.5 shows that, similarly to the 50 µm hatch sample (see Figure 9.4), there was larger gradients for the peaks at week 0 than that of week 30. Again, this could be due to the natural degradation of the sample surface over time.

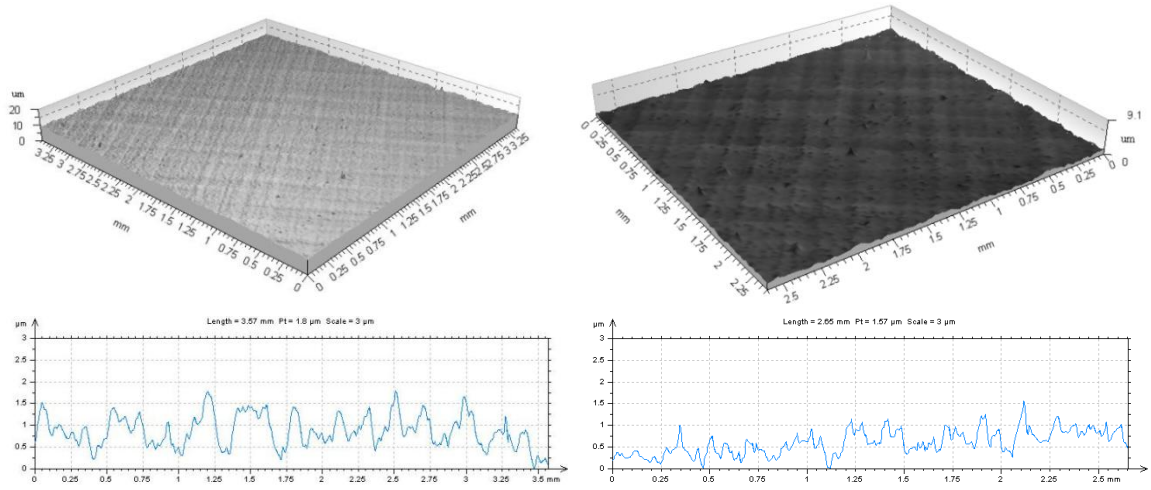

(a) (b)

Figure 9.5 – Continuous axonometric 3-D images and profile extractions for 100 µm hatch pattern (B3) – (a) week 0 and (b) week 30.

On the whole it can be seen that there is significant differences in terms of topography when comparing the as-received sample (AR) and CO_2 laser-induced patterned samples (CT50, CT100, CH50 and CH100). In addition, it was also observed that there appeared to be a significant difference in topography in terms of profile between the laser patterned samples at week 0 and week 30. That is, the peak heights do not appear to be as sharp as was seen during WLI analysis at week 0. This is highlighted throughout the profile extractions shown in Figures 9.2 to 9.5.

9.4 – Wettability and Surface Chemistry

The recently advancing θ for water on the samples was recorded each fortnight over the 30 week experimental period. The results for each sample are given in the graphs shown in Figure 9.6 and Figure 9.7. Figure 9.6 shows the variation in θ for the trench patterns (CT50 and CT100) in comparison to the as-received sample (AR), over the 30 weeks. Similarly, Figure 9.7 shows the trend in θ for the hatch patterns (CH50 and CH100) also in comparison to the as-received sample (AR). In general, it can be seen that all samples, with the exception of the 50 µm trench pattern, display some form of hydrophobic recovery insofar as θ for these samples increases by up to 10°. This coincides with what has been observed previously through the work of O'Connell *et al.* [133]. As already stated, the results for the 50 µm trench pattern (see Figure 9.6) do not initially follow the same trend as the other samples due to a reduction in θ in the first 4 to 5 weeks. Having said that, it can be seen that

after this 4/5 week period that the results for this sample do correlate to the trend which can be identified through the other samples given in Figure 9.6 and Figure 9.7.

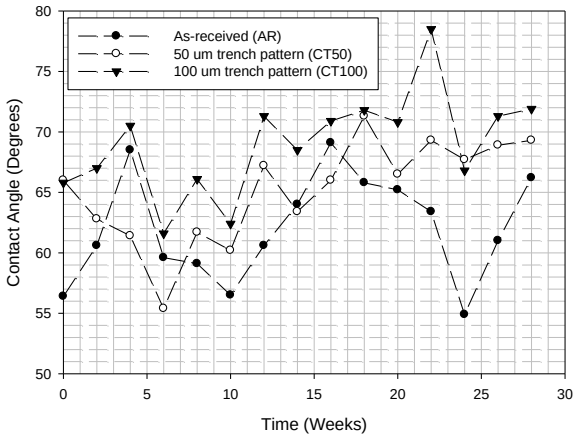

Figure 9.6 – Variation of θ for samples AR, CT50 and CT100 over 30 weeks.

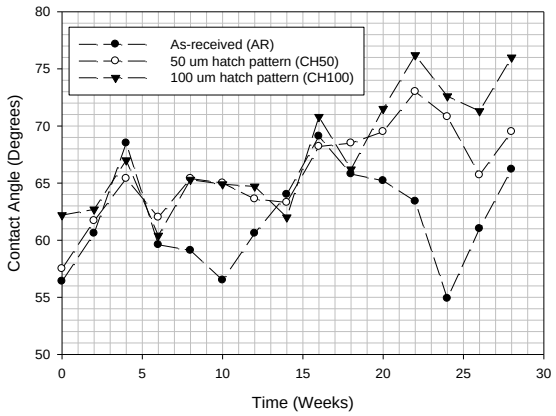

Figure 9.7 – Variation of θ for samples AR, CH50 and CH100 over 30 weeks laser patterned samples.

Most work [133,135,174] focuses on the variation of θ over 28 days and does not consider any long term effects post-28 days. This could be of some significance as it can be seen through Figure 9.6 and Figure 9.7 that θ dramatically decreases for all samples after the 4 week hydrophobic recovery period. After this time it can be seen that in general each of the samples tended to correlate with one another in terms of hydrophobic loss/recovery. The only difference between each of the samples can be seen through the actual recorded value of θ. For instance, apart from weeks 4, 6, 14 and 16 all laser patterned samples (CT50, CT100, CH50 and CH100) gave rise to less hydrophilic θ in comparison to the as-received sample.

There are a number of possible mechanisms which can be linked to hydrophobic loss/recovery and how the wettability of surfaces vary over time. Two of these, as discussed by Kim *et al.* [135] are reorientation of polar or nonpolar groups and condensation of the surface hydroxyl groups. Another

possible mechanism is that of surface degradation which has been observed for the laser patterned samples (CT50, CT100, CH50 and CH100). It is also reasonable to say that it is even likely that a number of mechanisms may contribute to the resulting θ.

As the samples, over the 30 weeks, were stored in ambient air it was also necessary to carry out XPS analysis to identify if the surface oxygen content had varied between weeks 0 and 30. The results of the XPS analysis can be seen in Table 9.2.

Table 9.2 – XPS data for surface oxygen content for each sample at week 0 and 30.

	Week 0		Week 30	
Sample	Surface Oxygen Content (% At.)	θ (°)	Surface Oxygen Content (% at.)	θ (°)
AR	13.26	56.4±1.2	17.38	65.3±2.1
CT50	14.33	66.0±4.0	21.56	69.2±1.8
CT100	14.05	57.5±2.4	15.61	71.8±3.2
CH50	15.21	65.8±2.9	15.88	69.6±2.7
CH100	12.99	62.2±2.3	13.97	76.0±3.4

As it would be expected, from Table 9.2 it was found that the surface oxygen content for each of the samples had increased by up to 7.3 %at. This can be attributed to surface oxidation owed to the storage conditions in which the samples were kept in ambient air. It has previously been highlighted by Hao and Lawrence [4] that as a general rule an increase in surface oxygen content should give rise to a reduction in θ. This has not been seen in this instance; however, this could indicate that either another factor is dominant or that a combination of parameters gave rise to the observed θ.

Table 9.3 gives the results of the main parameters believed to effect θ; these are Ra, Sa, γ^P and γ^T. On the whole it can be seen that following 30 weeks the surface roughness does not appear to have a definitive effect on θ as in some instances (such as with samples AR and CT100) θ increases with a negligible variation in Ra or Sa. On the other hand, it was observed that for sample CT50 the Sa value decreased by up to 0.3 μm even though an increase in θ was determined following the 30 week storage period. Table 9.3 also shows that the surface energy components had a significant impact upon θ insofar as a decrease in γ^P and γ^T elicited a significant increase in θ. This further suggests that even though a possible transition in wetting regime is taking place to give an increased θ compared to the as-received sample (AR), as discussed in Chapter 6, γ^P and γ^T still play a distinct role in determining the wettability of nylon 6,6.

Table 9.3 – Results summary for all CO_2 laser-induced patterned nylon 6,6 samples on week 0 and week 30.

	Week 0					Week 30				
Sample I.D.	Ra (µm)	Sa (µm)	γ^P (mJm^{-2})	γ^T (mJm^{-2})	θ (°)	Ra (µm)	Sa (µm)	γ^P (mJm^{-2})	γ^T (mJm^{-2})	θ (°)
AR	0.029	0.126	17.69	47.34	56.4±1.2	0.032	0.100	12.44	40.44	66.3±2.1
CT50	0.148	0.636	12.24	40.87	66.0±4.0	0.213	0.312	9.96	39.37	69.3±1.8
CT100	0.185	0.297	16.86	46.69	57.5±2.4	0.235	0.297	8.59	38.07	71.9±2.1
CH50	0.103	0.423	10.93	42.58	65.8±2.9	0.212	0.385	8.97	40.58	69.5±1.8
CH100	0.155	0.326	13.63	44.0	62.2±2.3	0.274	0.323	5.19	38.95	76.0±2.3

To further determine the correlation between the surface energy parameters and θ it was necessary to account for the results obtained at week 30. Figure 9.8 shows that at 30 weeks θ still had a good inverse correlation with γ^P and γ^T, with the strongest correlation being given with γ^P (see Figure 9.8(a)). This shows that this inverse function correlation exists as was seen at week 0, which was discussed in Chapter 6 and that the nylon 6,6 material appears to fit with current theory in that a reduction in γ^P and γ^T gives rise to an increase in θ.

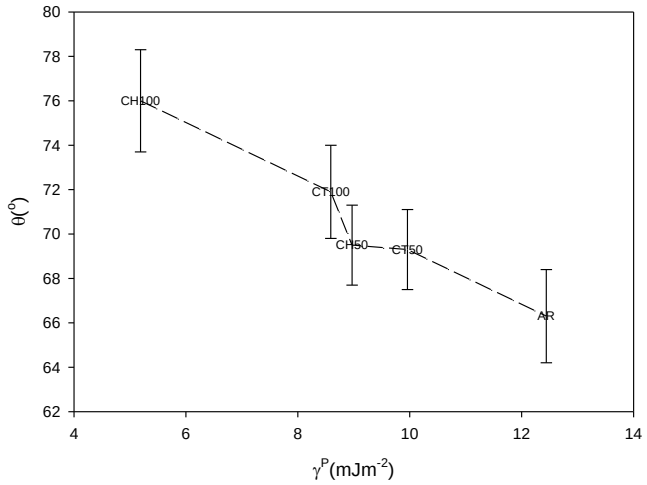

(a)

Figure 9.8 continued overleaf

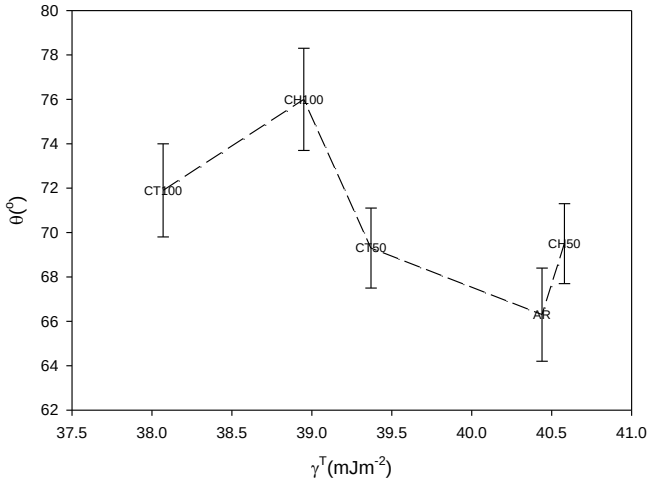

(b)

Figure 9.8 – Graphs showing the correlation between θ and (a) γ^P and (b) γ^T after storage of 30 weeks.

9.5 – Atmospheric Parameters

In addition to determining θ every two weeks, atmospheric pressure was recorded to identify if changes in pressure would have an impact on the observed θ. Figures 9.9 and 9.10 show graphs of the variation in mean θ and atmospheric pressure over the 30 weeks In general it can be seen that a slight trend arises from Figures 9.9 and 9.10 such that, on a whole, the θ appears to increase with a significant increase in atmospheric pressure.

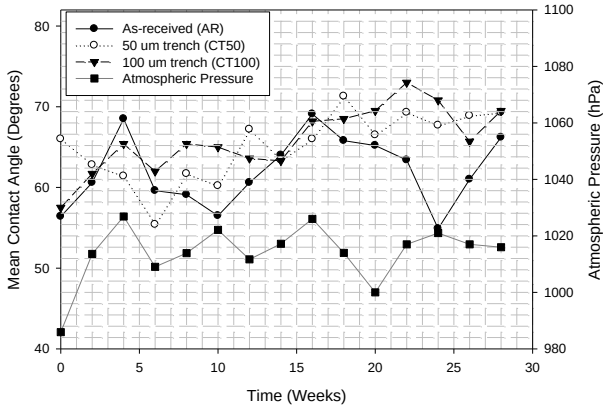

Figure 9.9 – Variation in mean θ for samples AR, CT50, CT100 and atmospheric pressure over 30 weeks.

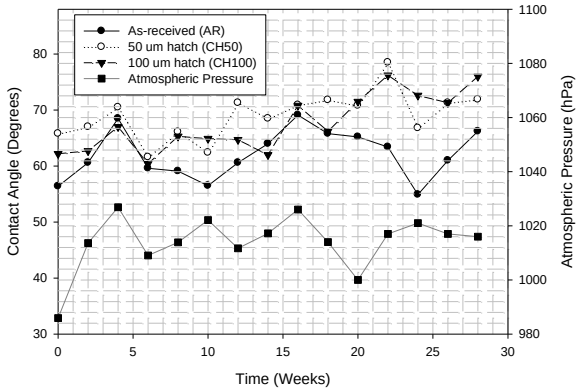

Figure 9.10 – Variation in mean θ for samples AR, CH50, CH100 and atmospheric pressure over 30 weeks.

In order to further determine whether this is of any significance, graphs of change in mean θ, ΔCA and change in atmospheric pressure, ΔP, for each of the samples over the 30 week period were drawn. These can be seen in Figure 9.11. The graphs depicted in Figure 9.11 further highlight the possible correlative trend between the observed θ and atmospheric pressure. That is, it can be seen that an increase in θ arises when a significant increase in pressure occurs. Furthermore, from the results shown in Figures 9.9, 9.10 and 9.11 significant decreases in the ambient air pressure leads to a noteworthy reduction in the measured θ. However, it should be noted that this data alone does not give conclusive results as to the pressure being the dominant factor. This is due to the fact that in some instances θ does not follow this trend. For example, at week 12 θ for the as-received (see Figure 9.11(a)), the 50 μm trench (see Figure 40(b)) and 100 μm trench (see Figure 9.11(c)) samples gave a relatively large increase in θ regardless of the reduction of up to 10 hPa in barometric air pressure.

Through laser patterning of two 50 and 100 μm patterns, namely trench and hatch, it was determined that peak heights of up to 3 μm could be achieved with Ra and Sa values of up to 0.305 and 0.408 μm, respectively. This is significantly higher when in comparison with the as-received sample (AR) which was found to have peak heights of up to 0.2 μm with Ra and Sa values of 0.028 and 0.111 μm, respectively. The long term study has identified that after 30 weeks each of the samples studied had become less hydrophilic, with θ increasing by up to 10°. However, over the 30 week period it was observed that θ was erratic, increasing and decreasing rather than converging to a constant value. In terms of topography, surface roughness for the laser patterned samples decreased, in general, over the 30 week period; whereas the roughness of the as-received sample remained constant. It was also found that the surface oxygen content had increased through oxidation owed to the storage of the samples in ambient air. It is likely that these may not be the main driving force owed to the difference in surface roughness between the as-received and laser patterned samples.

It is evident through the results obtained that atmospheric pressure may be a main driving force for the observed θ. That is, θ in general increases with significant increases of atmospheric pressure. Having said that, in some weeks throughout the 30 week period this was not conclusive and allows one to identify that this requires more research in order to determine whether or not atmospheric pressure

plays a role in determining θ. On the other hand strong evidence has showed that γ^P and γ^T has a significant impact on θ insofar as a reduction in these surface energy parameters has brought about a significant increase in θ when comparing the CO_2 laser-induced patterned samples to the as-received and when comparing all samples over the 30 week storage period.

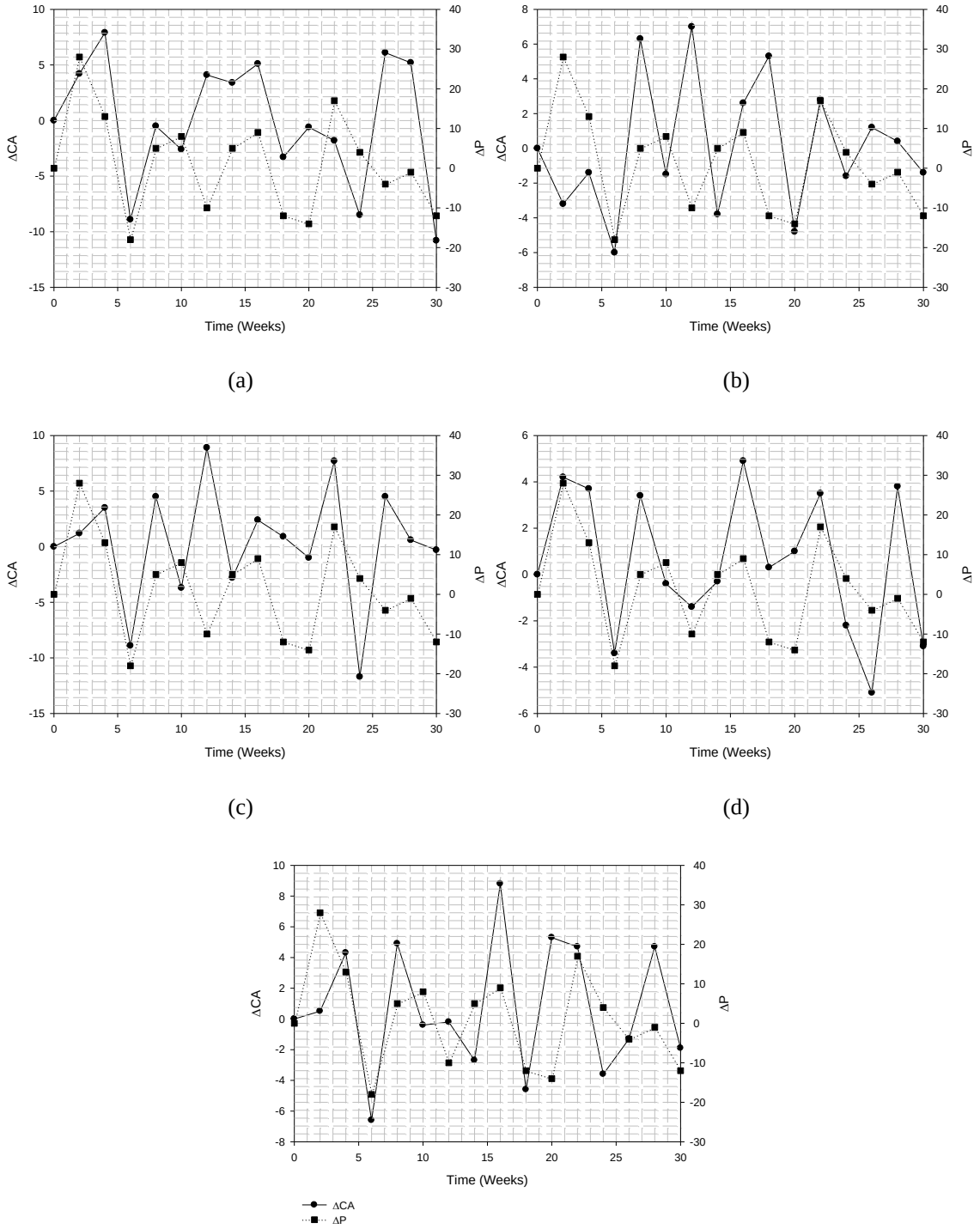

Figure 9.11 – Change in θ, ΔCA, and change in pressure, ΔP, over 30 weeks for (a) AR (b) CT50 (c) CT100 (d) CH50 and (e) CH100.

10
Identifying Generic Parameters that Determine the Wetting Nature of Nylon 6,6

Since a number of surface parameters have been reported to have an impact on the wettability nature of maeterials, it is necessary to examine and determine any generic parameters that have arisen through Chapter 6 to Chapter 9. This Chapter discusses the possible generic parameters which play a dominant role in the wettability characteristics of nylon 6,6.

10.1 – Introduction

From the experimental evidence presented in Chapters 6 to 9 it has been seen that a number of parameters can have a large effect upon the wettaiblity of nylon 6,6. In order to determine if one parameter is more dominant over others it is necessary to consider the results on the whole by collating the results obtained for each processing technique.

On account of collating the results obtained for the different surface processed nylon 6,6 samples, this Chapter details and discusses the main surface parameters and their influence on θ.

10.2 – CO_2 and KrF Excimer Laser-Induced Patterning

Throughout this work it has been observed that CO_2, KrF excimer and F_2 excimer laser-induced patterning of nylon 6,6 inherently gives rise to a significant increase in θ. As discussed in Chapter 6 this could be seen to be on account of the likelihood of a mixed-state wetting regime taking place along the liquid-surface interface. This is due to the fact that the periodic laser-induced surface would have given rise to a liquid droplet in an equilibrium state that cannot be explained through the Wenzel and Cassie-Baxter wetting regimes.

Current theory has not been corroborated with, in terms of the laser-induced patterning of nylon 6,6, insofar as the increase in Sa and Ra have not given rise to a reduction in θ. However, it has been seen that surface energy parameters may have a significant impact on the wetting nature of nylon 6,6 even if a wetting transition has taken place. Figure 10.1 and 10.2 show the relationship between θ and γ^P and γ^T, respectively. From these graphs it is possible to identify that by collating all results for the patterning of nylon θ was a strong inverse function in correlation with γ^P and γ^T. On account of this, it is reasonable to say that for the patterned nylon 6,6 samples γ^P and γ^T were a dominant parameters for determining the wettability. This is also further confirmed by the long term study carried out in Chapter 9 in which surface roughness did not vary over the 30 week experimental period; whereas γ^P and γ^T reduced in order to give an increase in θ.

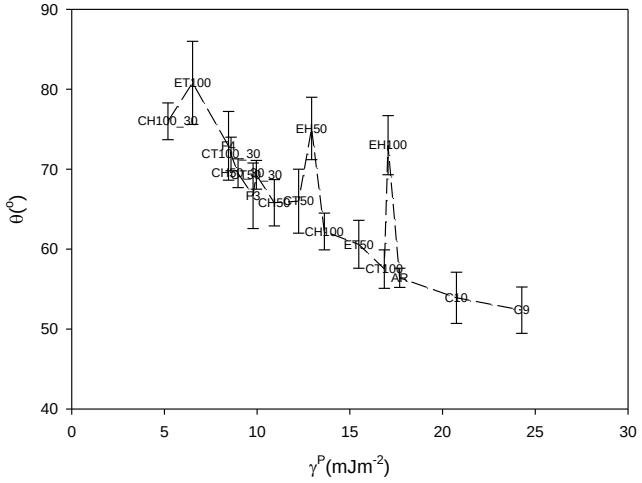

Figure 10.1 – Graph showing the correlation between θ and γ^P.

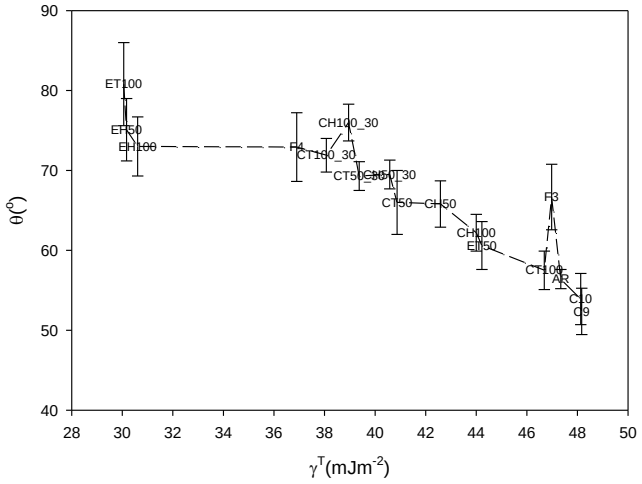

Figure 10.2 – Graph showing the correlation between θ and γ^T.

Surface roughness is another surface parameter which could have a significant impact upon the way in which a material wets. However, from Figure 10.3 it can be seen that the surface roughness in terms of Ra and Sa did not seem to have a dominant role in determining θ for the laser-induced patterned nylon 6,6 samples. This is due to θ being slightly erratic as the surface roughness increased.

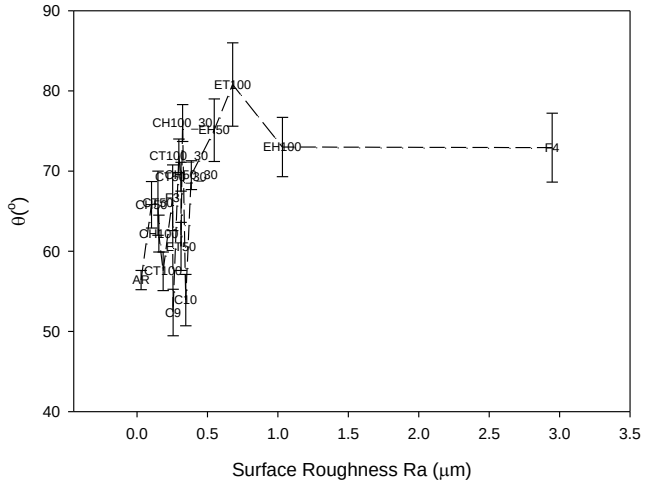

(a)

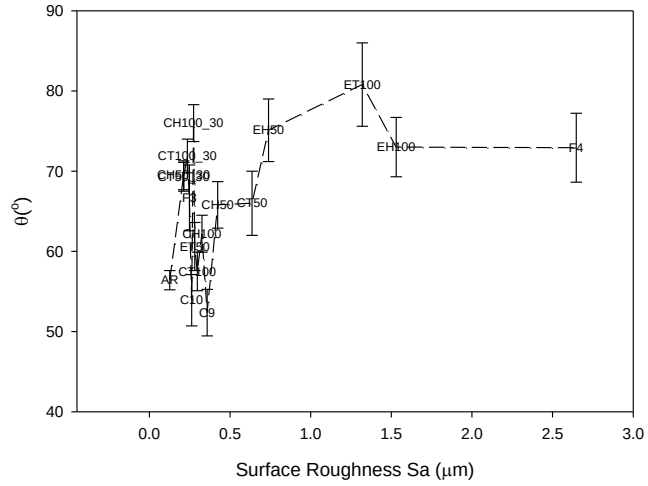

(b)

Figure 10.3 – Graphs showing the correlation between θ, (a) Ra and (b) Sa.

10.3 – CO_2 and KrF Excimer Laser Whole Area Irradiative Processing

The work (see Chapter 6 and Chapter 7) involving CO_2 and KrF excimer laser whole area irradiative processing has shown that the wettability characteristics of nylon 6,6 did tend to correspond with current theory in that θ decreased on account of an increase in surface roughness, increase in γ^P, increase in γ^T and increase in surface oxygen content. From Figure 10.4 it was found upon collating the results for all laser whole area irradiative processed nylon 6,6 samples that there was a strong inverse relationship between θ and γ^P. In addition to this, it can also be seen from Figure 10.5 that γ^T showed a similar correlation with θ. This further suggests that the surface energy parameters are the most dominant parameter in giving rise to θ. What is more, Figure 10.4 and Figure 10.5 indicate that it may be possible to use γ^P and γ^T to predict θ on account of the fact that they show that the results are reproducible as samples which had similar values of either γ^P and γ^T give rise to equivalent θ.

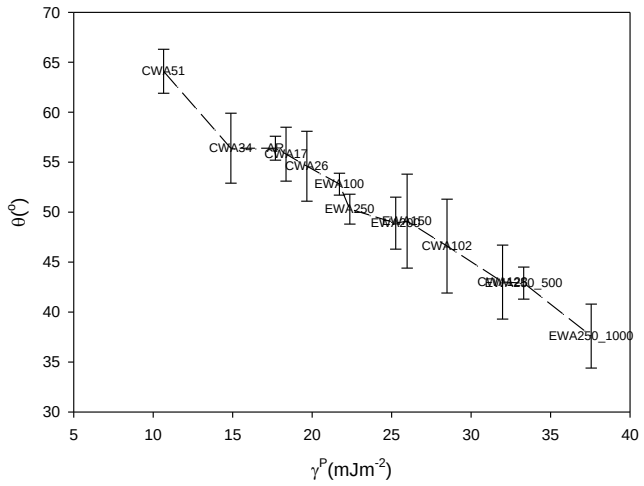

Figure 10.4 – Graph showing the correlation between θ and γ^P.

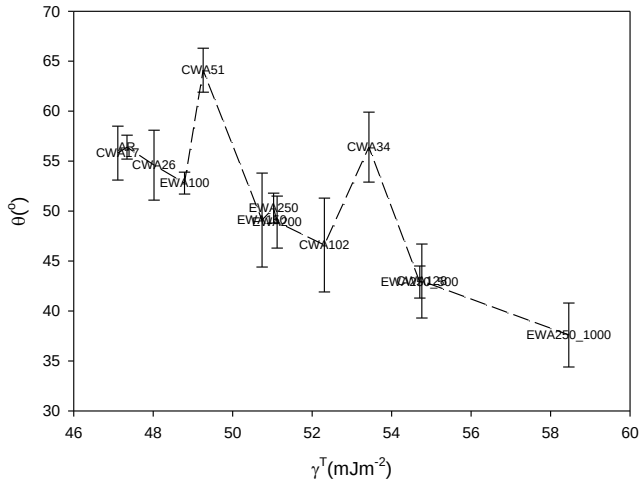

Figure 10.5 – Graph showing the correlation between θ and γ^T.

As surface roughness had increased, it appeared that Sa and Ra may have a significant impact upon θ; however, it can be seen from Figure 10.6 that the surface roughness did not tend to have any particular correlation with θ. This is highly noteworthy as it allows one to further deduce that from the results of the laser whole area processed nylon 6,6 samples γ^P and γ^T were the most dominant parameter in determining θ.

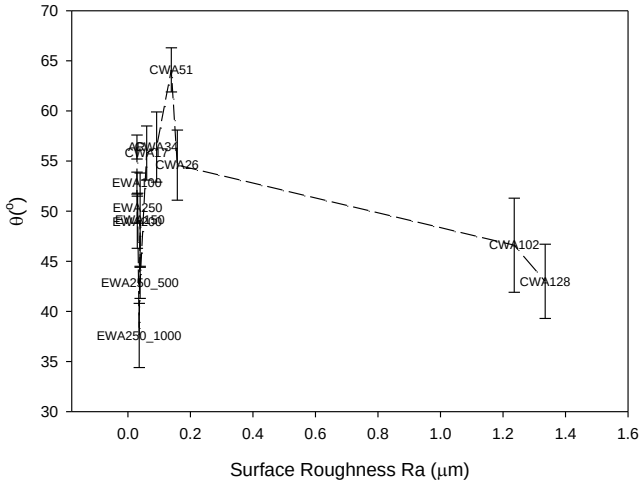

(a)

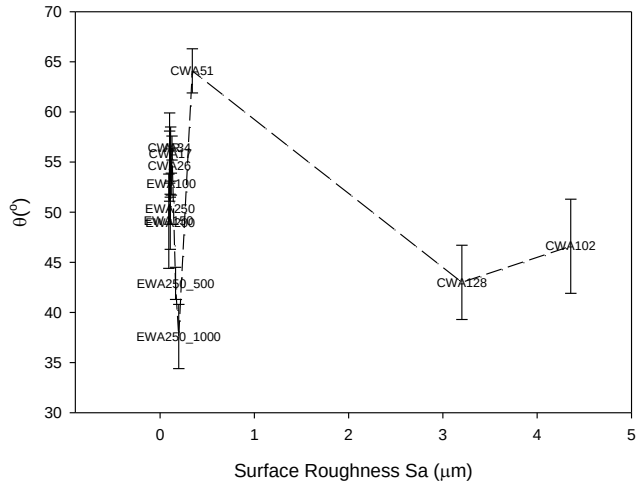

(b)

Figure 10.6 – Graphs showing the correlation between θ, (a) Ra and (b) Sa.

10.4 – Comparisons Between Laser-Induced Patterning and Laser Whole Area Irradiative Processing

By taking into account all results that have been obtained throughout Chapters 6 to 9 it was possible to ascertain the effect of all surface parameters studied on θ. For all CO_2 and KrF excimer laser CO_2 and KrF excimer laser-induced patterning of nylon 6,6 the surface oxygen content had increased which can be attributed to oxidation of the surface during the laser processing. It is reasonable to conclude from the results obtained in Chapters 6 to 9 that surface oxygen content in this instance was not a main driving parameter which accounts for the measured θ. This is owed to variations in θ between the laser-induced patterned and laser whole area irradiative processed samples.

When compared to one another it was found that all laser-induced surface patterning elicited an increase in θ; whereas the laser whole area irraditative processing of the nylon 6,6 gave rise to a more hydrophilic surface in which θ decreased. As discussed in Chapter 6, in order to explain the increase in θ for the laser-induced patterned samples a mixed-state wetting regime is proposed in which both Cassie-Baxter and Wenzel regimes occur along the interface once the droplet is in equilibrium. Thus mixed-state wetting regime is believed to arise from the rough periodic patterns induced by the laser processing, allowing one to infer that the periodic topographical patterns have a dominant role in the determination of θ. Having said that, upon collating the results from all studied samples it is possible to see from Figure 10.6 that γ^P is highly correlated with θ, such that an increase in γ^P gives rise to a reduction in θ regardless of the topography or surface modification technique implemented. In addition to this, Figure 10.7 shows that θ was also an inverse function of γ^T in a similar manner to that seen with γ^P. This is highly significant as this shows that the surface energy parameters are one of the most dominant parameters in determining the wetting nature of nylon 6,6.

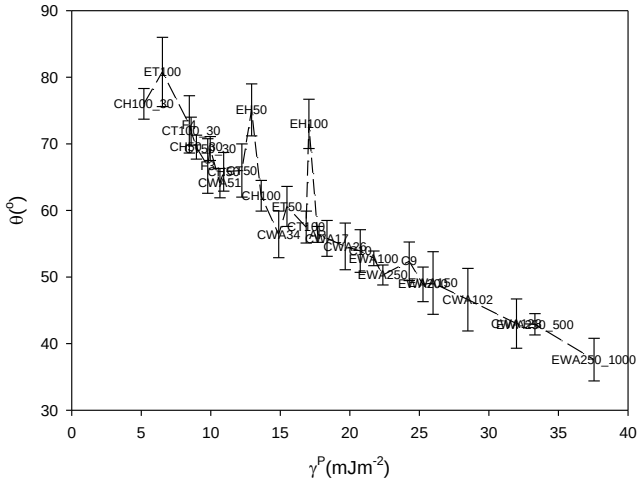

Figure 10.6 – Graph showing the correlation between θ and γ^P.

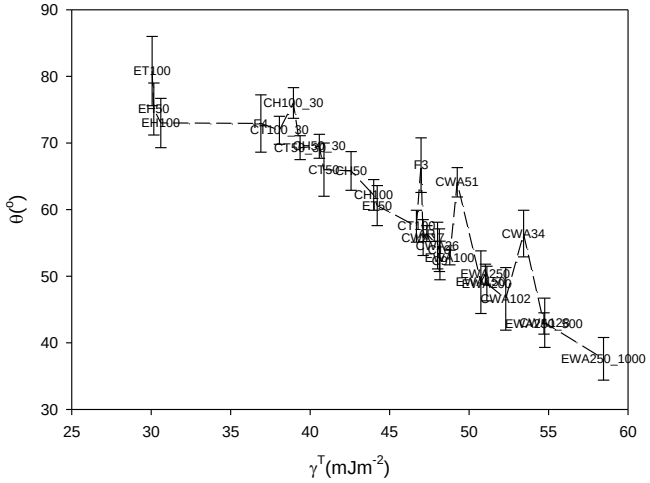

Figure 10.7 – Graph showing the correlation between θ and γ^T.

In order to confirm that the surface energy parameters were the most dominant in terms of the wettability characteristics of nylon 6,6, Figure 10.8 shows that surface roughness in regards to Ra and Sa did not have a good correlation with θ. This could be on account of these results include both laser-induced patterning and laser whole area irradiative processing results in which a transition in wetting regime has been proposed to account for the differences in measured θ. As a result of this, it can be said that from the evidence presented here the surface energy parameters; namely γ^P and γ^T are the central factor which govern the wetting nature of nylon 6,6, irrespective of the surface modification used or arising wetting regime.

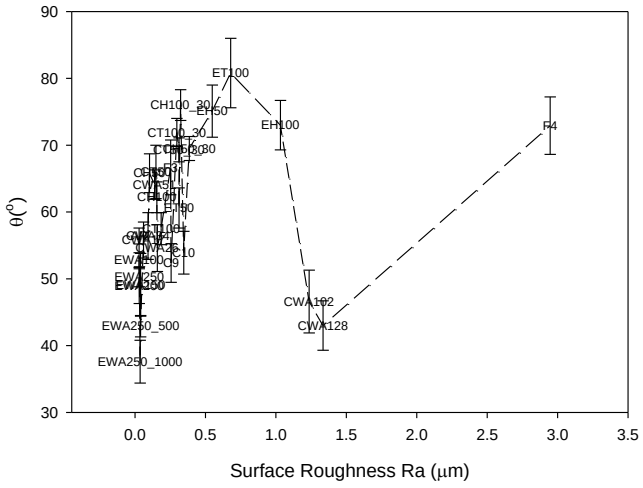

(a)

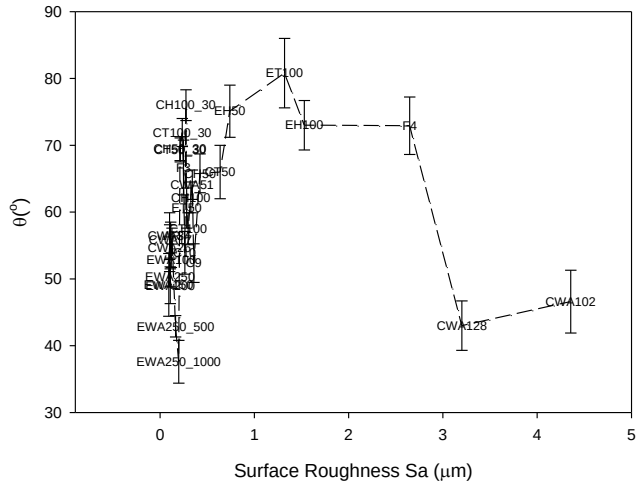

(b)

Figure 10.8 – Graphs showing the correlation between θ, (a) Ra and (b) Sa.

PART 4 – Bioactivity of Laser Processed Nylon 6,6

11
The Effects of CO_2 Laser Processing on the Bioactivity of Nylon 6,6 with Reference to Wettability

This chapter gives an account of the biological analysis of CO_2 laser-induced patterned and CO_2 laser whole area irradiative processed nylon 6,6. This has been carried out by immersion of as-received and CO_2 laser surface treated samples in SBF, seeding samples with normal human osteoblast cells and determining cytotoxicity and alkaline leukocyte phosphatase (ALP) levels.

11.1 – Introduction

It has been realized that the surface properties of polyermic materials in many situations, are not sufficient with regards to bioactivity, leading to clinical failure of the *in vivo* [4,138,178,179] which causes unnecessary discomfort to the patient and potentially the need for extra surgery. This situation conveys the necessity of changing the surface properties of the polymer giving rise to a more improved biological response in terms of cell adhesion and proliferation.

In vitro testing of biomaterials is one of the most common ways in which biological functionality and cytotoxicity can be determined without causing harm to humans or animals. It has been seen that when researching new materials and techniques for biomaterials this method of testing is extensively utilized [27,64,138,179]. Following on, this Chapter details a comparative study between CO_2 laser-induced patterning and CO_2 laser whole are irradiative processing of nylon 6,6 and the effects thereof on SBF response, normal human osteoblast response, cytotoxicity and ALP levels.

11.2 – Effects of CO_2 Laser Processing on Apatite-Layer Response

This section describes how CO_2 laser-induced patterning and CO_2 laser whole area irradiative processing of nylon 6,6 modulated the formation of an apatite layer upon being immersed in SBF for 14 days. A more detailed explanation of the experimentation carried out can be found in Chapter 5.

11.2.1 – CO_2 Laser-Induced Patterning

From Figure 11.1 it was observed that only a very small amount of sediment was present on the as-received sample (see Figure 11.1(a)) in comparison to the other samples which had undergone CO_2 laser-induced patterning (see Figures 11.1(b) to (e)). It is also apparent from Figure 11.1(b) and

11.1(e) that the sediment preferentially forms around craters formed due to evolved gases breaking at the surface during the melting taking place following the CO_2 laser processing. This highlights that it may be possible to construct a polymeric surface which allows selective apatite formation giving rise to selective positioning for the growth of osteoblast cells.

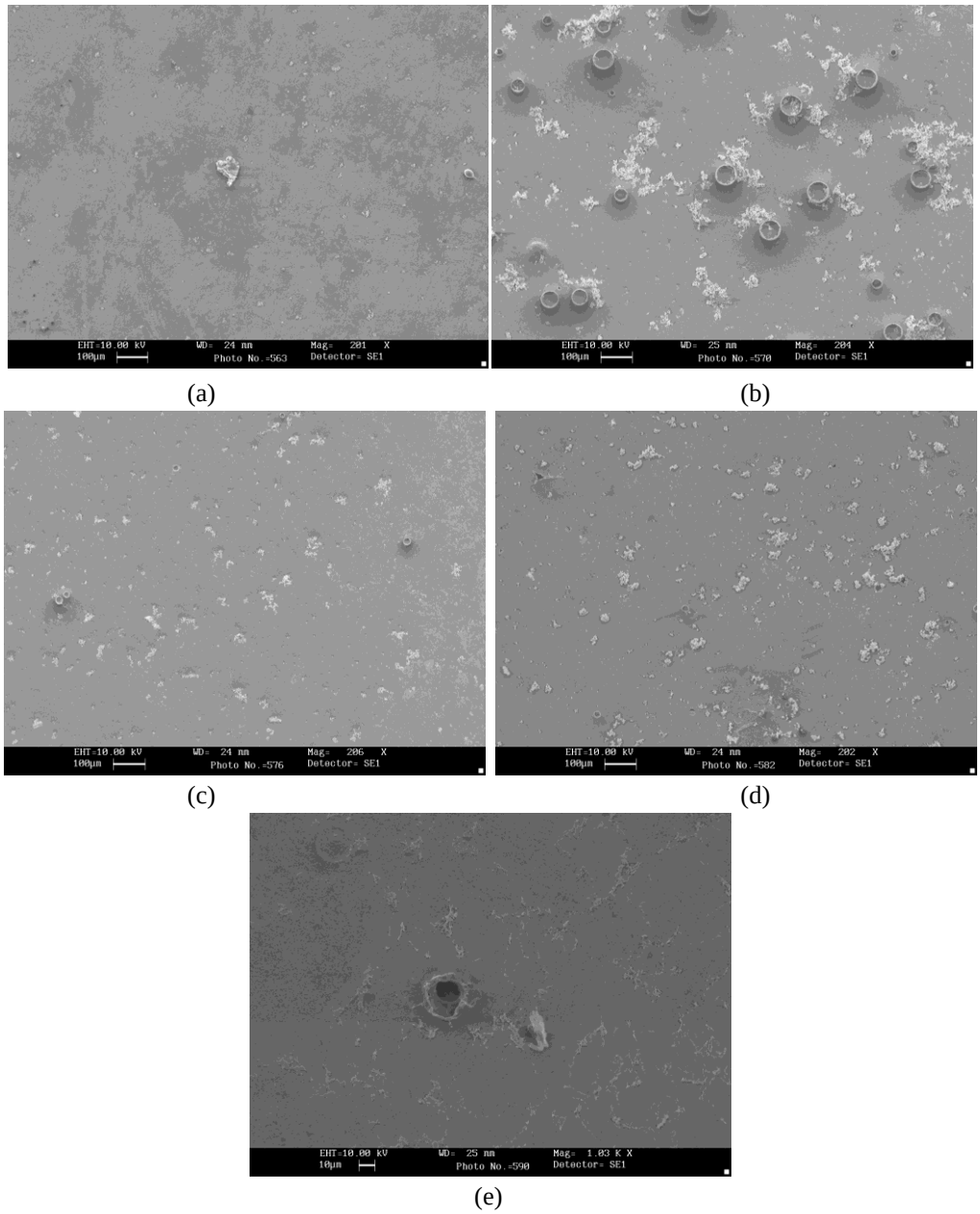

Figure 11.1 – SEM micrographs for (a) AR, (b) CT50, (c) CT100, (d) CH50 and (e) CH100 after immersion in SBF for 14 days.

It is also significant to note that following immersion in SBF for 14 days each of the CO_2 laser-induced samples and as-received sample (AR) gave rise to an increase in mass which can be attributed to the formation of the sediment which was identified in Figure 11.1. Figure 11.2 shows that the CO_2 laser-induced patterned nylon 6,6 samples (CT50, CT100, CH50 and CH100) gave rise to a larger

increase mass when compared to the as-received sample (AR) by up to 0.015 g. Furthermore, Figure 11.2 shows that the increase in mass for all of the CO_2 laser-induced patterned samples was around 0.026 g which suggests that in terms of apatite response there was no difference between any of the CO_2 laser-induced patterned nylon 6,6 samples.

The increase in sediment formation could be attributed to a number of surface parameters such as surface energy components, θ, surface roughness or surface oxygen content. As such, this will further be discussed in Section 11.2.4.

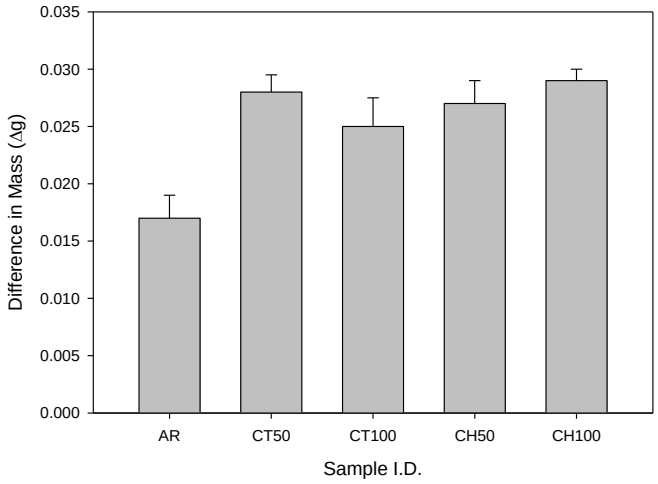

Figure 11.2 – Graph showing the mass increase for the CO_2 laser-induced patterned nylon 6,6 samples following 14 days immersion in SBF.

11.2.2 – CO_2 Laser Whole Area Irradiative Processing

Figure 11.3 shows the SEM micrographs for the CO_2 laser whole area processed samples, allowing one to see that more sediment adhered to the surface when compared to the as-received sample (see Figure 11.1(a)). When comparing the CO_2 laser whole area irradiative processed samples on their own it can be seen from Figure 11.3(e) and Figure 11.3(f) that the samples irradiated with the largest fluences of 102 and 128 Jcm^{-2} (CWA102 and CWA128) appeared to give rise to the largest cover density of sediment across the surface. It can also be seen that in some instances, especially as can be seen in Figure 11.3(f), that the apatite layer formed around the craters that arose from the laser processing.

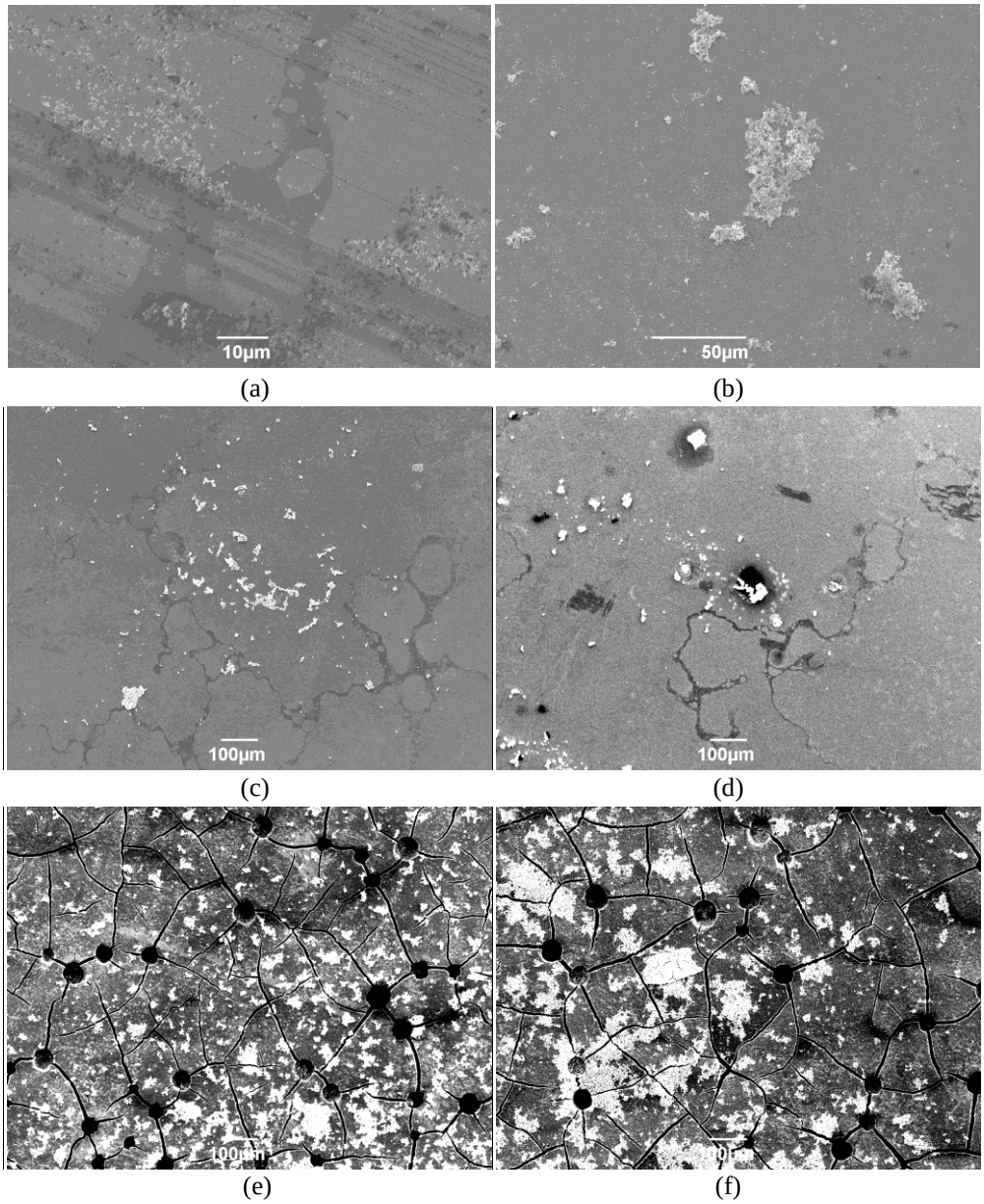

Figure 11.3 – SEM micrographs showing the SBF apatite formation on the whole area CO_2 laser processed samples (a) CWA17, (b) CWA26, (c) CWA34, (d) CWA51, (e) CWA102 and (f) CWA128.

Figure 11.4 gives a histogram of the difference in mass for the CO_2 laser whole area irradiative processed samples and confirms that on account of more sediment formation on the CO_2 laser whole area irradiative processed samples the increase in mass was considerably larger when compared to the as-received sample (AR). The increase in mass for the CO_2 laser whole area irradiative processed samples had increased by at most 0.05 g with the as-received sample giving an increase in mass of only 0.018 g. Another factor which cen be taken from Figure 11.4 is that the increase in mass steadily increases from sample CWA17 to sample CWA51which gave the largest increase in mass of 0.05 g in comparison to the other CO_2 laser whole area irradiative processed samples. This could be noteworthy as it suggests that an operating window to give the most optimum apatite response is possible owed to the fact that larger fluences that 51 Jcm^{-2} (sample CWA102 and CWA128) gave the lowest increase in mass of 0.03 and 0.025 g, respectively.

As discussed in Chapter 6, the CO_2 laser whole area irradiative processing had distinct effects on the surface and wettability characteristics of the nylon 6,6. As such, it is reasonable to say that these surface modifications could have given rise to the increase in sediment formed when compared to the as-received sample. As a result of this, the surface and wettability characteristics and their effects on the apatite-layer response will be further discussed in Section 11.2.4.

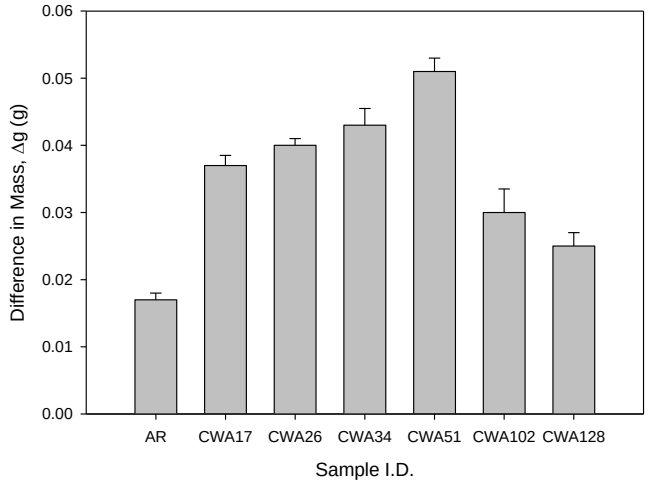

Figure 11.4 – Graph showing the mass increase for the CO_2 laser whole area irradiative processed samples following 14 days immersiond in SBF.

11.2.3 – Comparison Between CO_2 Laser-Induced Patterning and CO_2 Laser Whole Area Irradiative Processing

It has been confirmed from Figure 11.1 and Figure 11.3 that apatite sediment, following immersion of the samples in SBF for 14 days, formed on all of the nylon 6,6 samples studied. Visually, it can also be seen that more sediment had formed upon the CO_2 laser whole area irradiative processed samples, especially with those samples high fluences of 102 and 128 Jcm^{-2}. What is more, with those samples which had craters formed as a result of the evolved gases arising from the CO_2 laser processing, the sediment appeared to be preferentially forming around them. This is a very interesting result as it suggests that both of the CO_2 laser processing techniques could be implemented for processing nylon 6,6 samples for selective osteoblast cell growth.

From Figure 11.5(a) it can be seen that the CO_2 whole area irradiative processed nylon 6,6 samples gave rise to a more enhanced apatite layer response insofar as there was more sediment present following 14 days of immersion in SBF which inherently gave rise to a significant increase in mass. With regards to the CO_2 laser-induced patterned samples it was found that there was an equivalent mass increase for all samples of around 0.03 g. In contrast, the CO_2 laser whole area irradiative processed samples gave a more modulated response in that the difference in mass increased steadily up to 0.05 g as a result of larger incident fluences until 51 mJm^{-2}, beyond which the increase in mass

became less which was similar to that of the CO_2 laser-induced patterned samples. On account of the larger increase in mass for most of the CO_2 laser whole area irradiative processed samples it is reasonable to say that the compared to the as-received sample (AR) and the CO_2 laser-induced patterned samples, the CO_2 laser whole area irradiative processed samples could give rise to a more enhanced osteoblast cell response, allowing for a more sufficient surface for osteoblast cell growth and proliferation. In addition to this, it is possible to deduce from Figure 11.5(a) that there appeared to be a potential threshold fluence between 51 and 102 Jcm^{-2} beyond which the apatite layer response is less enhanced compared to the other CO_2 laser whole area irradiative processed samples.

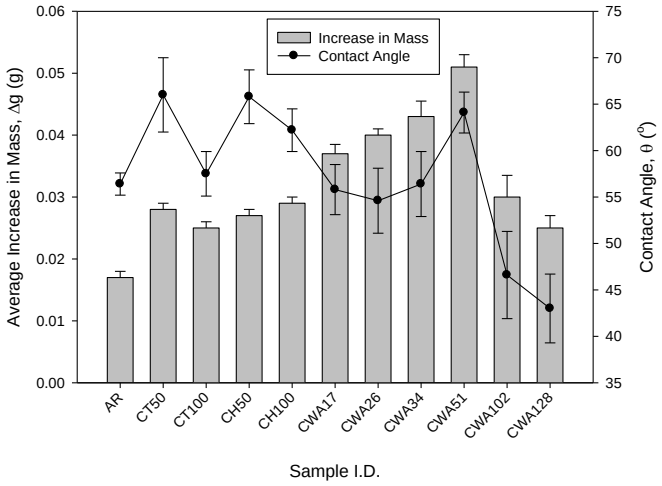

(a)

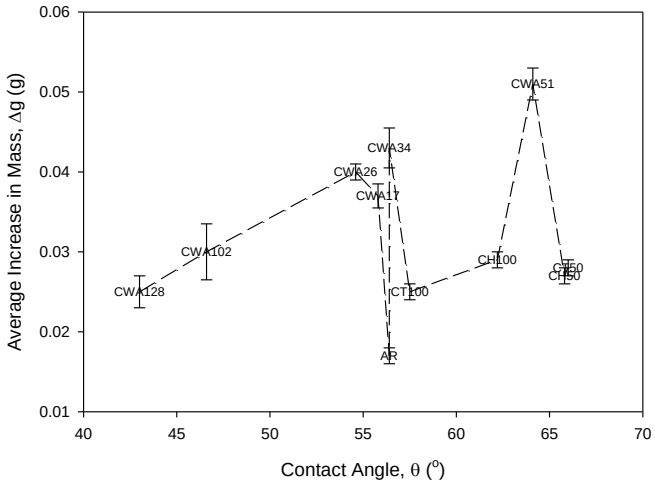

(b)

Figure 11.5 – (a) Histogram showing the difference in mass before and after immersion in SBF for all CO_2 laser processed samples in relation to θ, (b) Graph showing the relationship between Δg and θ.

*(In terms of increase in mass – One-Way ANOVA showed an overall significance with F = 117.706 and p = 0.000. Scheffe's range test showed that there was statistical difference between AR and all other samples and between the patterned and whole area processed samples. However, no statistical difference was found between those samples with equivalent mass increases*p<0.5).*

In order to determine if adequate elements were present in the formed apatite crystals XPS was carried out for the as-received sample and the entire CO_2 laser processed samples. Figure 11.6 shows the surface elemental data for the as-received sample (AR) and a typical CO_2 laser surface modified spectra, indicating that phosphorous and calcium was present on the surface of the nylon 6,6 samples, following the formation of the apatite crystals. This is of importance due to phosphorous and calcium having to be present in order for an apatite to form which would inherently increase the bioactivity of the material. The sediments analysed also incorporated sodium, magnesium and chlorine which had all been present in the SBF and indicates that these elements would also make up some of the apatite layer formed.

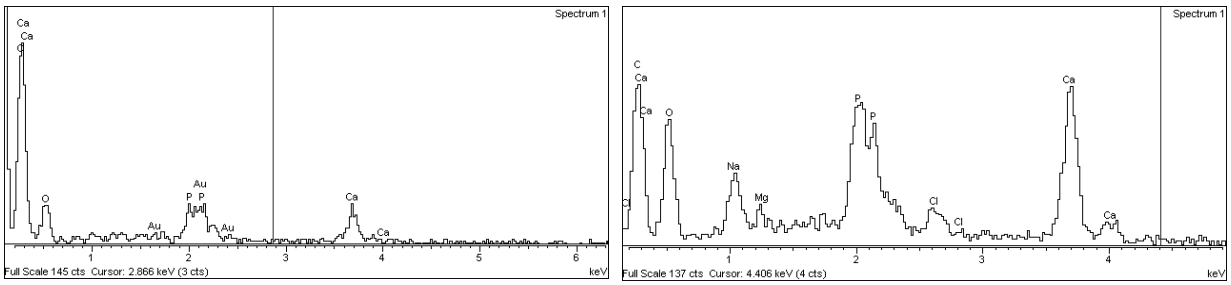

(a) (b)

Figure 11.6 - EDX spectra of (a) the as-received sample (AR) and (b) a typical CO_2 laser surface modified sample following immersion in SBF after 14 days.

11.2.4 – Wettability Characteristics and Surface Parameters

Figure 11.5(a) shows a histogram of the increase in mass for each sample in relation to θ. In terms of θ it can be said that for all of the CO_2 laser-induced patterned nylon 6,6 samples there did not appear to be any correlation between the sediment formation and θ. This could be owed to the transition in wetting regime, as discussed in Chapter 6, playing a significant role in the apatite response of the nylon 6,6 samples. On the other hand, the CO_2 laser whole area laser irradiative processed samples shown in Figure 11.5(a) correspond somewhat to the variation in θ. Since, for those samples with incident fluences between 17 and 51 Jcm^{-2} (CWA17, CWA26, CWA34 and CWA51) an increase in θ gave rise to an increase in mass. Beyond the fluence of 51 Jcm^{-2} it was found that upon a decrease in θ the increase in mass became considerably less for sample CWA102 and CWA128. This could be accounted for by the nylon 6,6 becoming too hydrophilic or too toxic which shall be further discussed in Section 11.5. This relationship between θ and increase in mass can be further seen in Figure 11.5(b) if one was to neglect those data points from the as-received sample and CO_2 laser-induced patterned samples (data points between 55 and 67° with Δg values of between 0.01 and 0.03 g). By neglecting these data points one can see that for the CO_2 laser whole area irradiative processed samples gave a positive correlation in which an increase in θ gives a linear increase in Δg. By taking into account those data points plotted for the as-received sample and CO_2 laser-induced patterned samples it can be seen from Figure 11.5(a) that for the entire CO_2 laser processed samples there was not a correlation between θ and increase in mass. This indicates that on account of the different surface processing

techniques there are different driving parameters for the apatite response of the nylon 6,6 material irrespective of the fact that the same wavelength was implemented to carry out both of the surface processing in this instance.

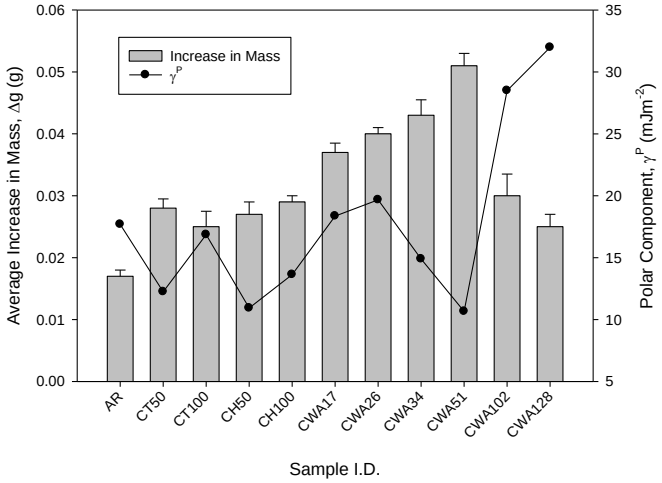

(a)

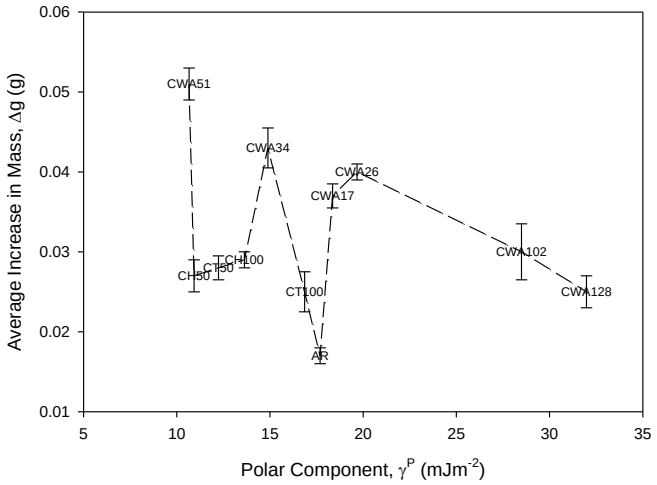

(b)

Figure 11.7 – (a) Histogram showing the increase in mass, Δg, in relation to γ^P for all CO_2 laser processed samples, (b) Graph showing the relationship between γ^P and Δg for all CO_2 laser processed nylon 6,6 samples following 14 days immersion in SBF.

From Figure 11.7(a) one can see that there was no correlation between the increases in mass for the CO_2 laser-induced patterned samples and γ^P which can be attributed to the differences in wetting regime as discussed in Chapter 6 playing a role in the apatite response of the nylon 6,6 samples. With regards to the CO_2 laser whole area irradiative processed samples it can be seen that for these samples there was a correlation between the observed increase in mass and variation in γ^P. Since, Δg increased upon a reduction in γ^P and can be further confirmed using Figure 11.7(b) if the as-received and CO_2 laser-induced patterned sample data points were neglected (data points of γ^P between 10 and 20 mJm^{-2} with Δg values of below 0.03 g). Upon neglecting these data points it is possible to ascertain that for

the CO_2 laser whole area irradiative processed samples the increase in mass was a reducing linear function of the measured γ^P. Then, by taking into account the other data points it can be seen that there is no correlation between the CO_2 laser processed samples on a whole on account of the different processing techniques exhibiting different apatite responses. What is more, as discussed previously with regards to θ, this none correlation between γ^P and the increase in mass for the entire CO_2 laser processed samples indicates that the emphasis of apatite response may be on surface processing technique rather than the laser wavelength used.

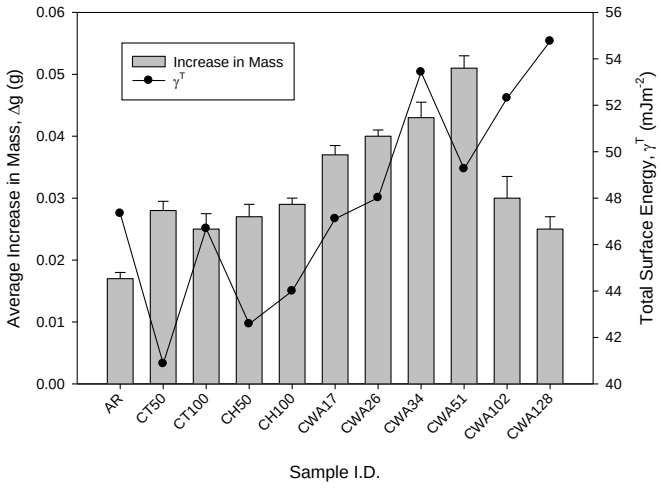

(a)

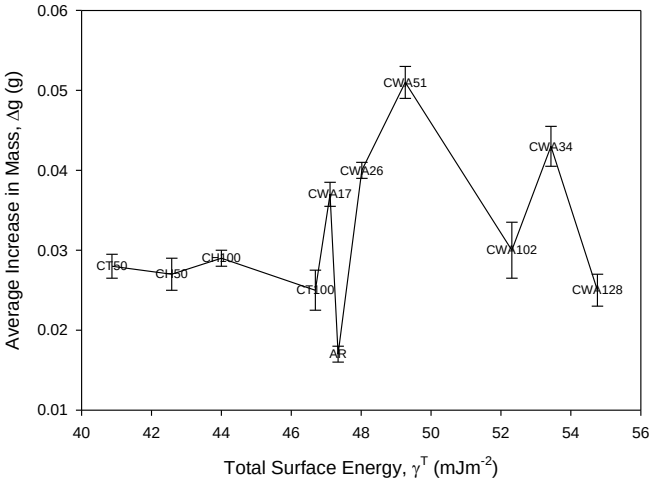

(b)

Figure 11.8 – (a) Histogram showing the increase in mass, Δg, in relation to γ^T for all CO_2 laser processed samples, (b) Graph showing the relationship between γ^T and Δg for all CO_2 laser processed nylon 6,6 samples following 14 days immersion in SBF.

Figure 11.8(a) shows that in terms of the increase in mass for the entire CO_2 laser processed samples there was no correlation between γ^T and Δg. This is on account of the CO_2 laser-induced patterned samples giving equivalent increases in mass even though a variation in γ^T was observed. Also, the none correlation can be accounted for by the fact that the CO_2 laser whole area irradiative processed

samples did not follow the trend set out by γ^T in that an increase in γ^T upon an increase in incident fluence did not elicit a similar response from Δg as was seen in terms of θ and γ^P. With this in mind, it can be stated that for the CO_2 laser processed samples γ^T may not a dominating parameter in terms of apatite response.

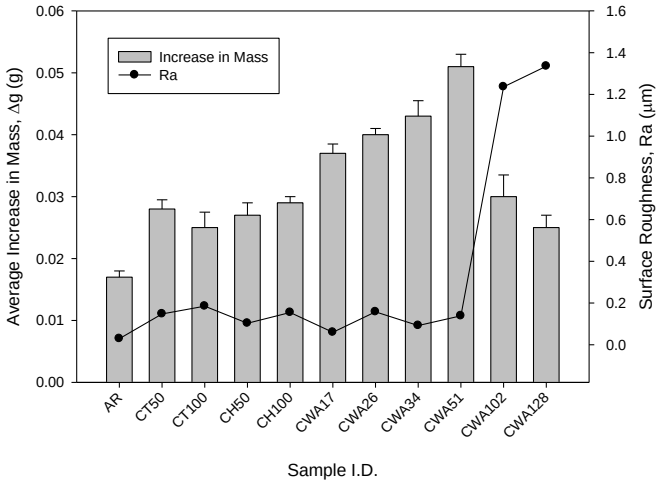

(a)

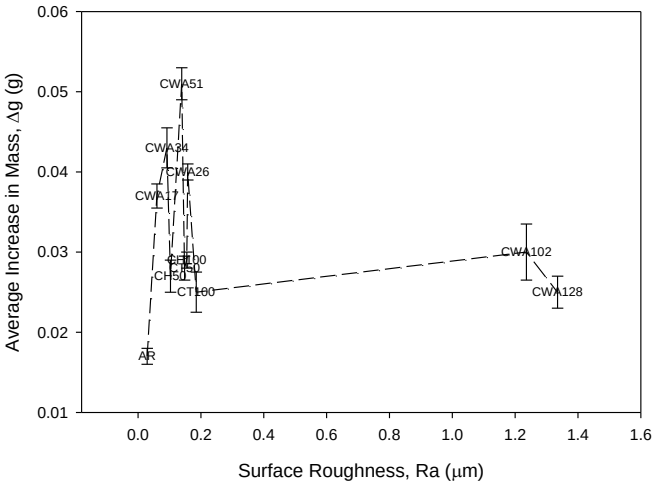

(b)

Figure 11.9 – (a) Histogram showing the increase in mass, Δg, in relation to surface roughness, Ra, for all CO_2 laser processed samples, (b) Graph showing the relationship between Ra and Δg for all CO_2 laser processed nylon 6,6 samples following 14 days immersion in SBF.

Figure 11.9(a) indicates that there was no correlation between the measured increases in mass for the entire CO_2 laser processed samples and the surface roughness in terms of Ra. This is on account that Δg was modulated between the different processing techniques even though the Ra values were similar for all samples with the exception of sample CWA102 and sample CWA128 which were an order of magnitude rougher owed to considerably larger incident fluences being used. The fact that no trend could be found between Ra and Δg is further confirmed through Figure 11.10(b) which shows no correlation between these two parameters for either the CO_2 laser-induced patterned and CO_2 laser

whole area irradiative processed nylon 6,6 samples. What is more, a similar none correlation was observed between Sa and Δg as shown in Figure 11.10(a) and Figure 11.10(b) in that similar values of Sa gave rise to large different measured Δg. Bearing this in mind, from Figure 11.10 and Figure 11.11 it can be said that in terms of apatite response the surface roughness was not a determining factor.

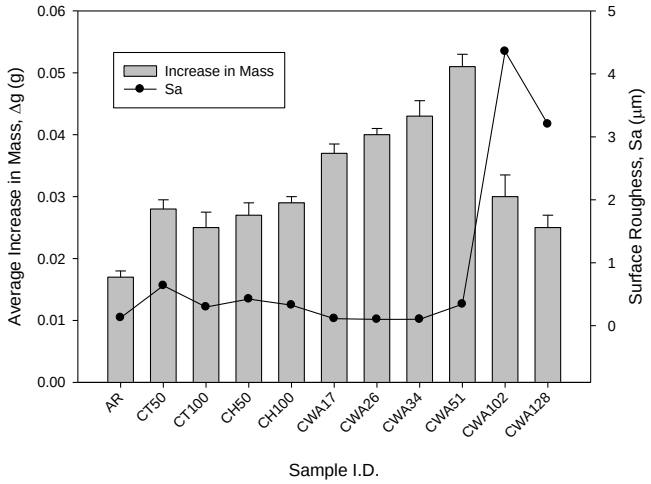

(a)

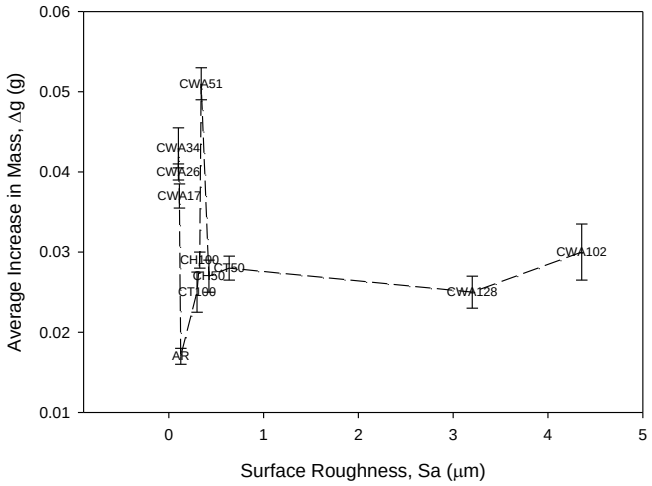

(b)

Figure 11.10 – (a) Histogram showing the increase in mass, Δg, in relation to surface roughness, Sa, for all CO_2 laser processed samples, (b) Graph showing the relationship between Sa and Δg for all CO_2 laser processed nylon 6,6 samples following 14 days immersion in SBF.

Figure 11.11(a) gives the relationship between the surface oxygen content and the measured Δg for the entire CO_2 laser processed samples and shows that like for all of the other surface parameters and wettability characteristics, the CO_2 laser-induced patterned samples did not correlate to any trend with the rise in surface oxygen content. As discussed previously this could be on account of the different wetting regime present which was shown in Chapter 6. Also, in terms of the CO_2 laser whole area irradiative processed samples, Figure 11.11(a) allows one to see that for samples CWA17, CWA26, CWA34 and CWA51 there is a strong correlation between an increase in surface oxygen content and

an increase in Δg. Furthermore, with fluences larger than 51 Jcm^{-2} (sample CWA102 and sample CWA128) it was found that Δg reduced on account of the increase in surface oxygen content. However, this may not be directly related to surface oxygen content as the reduced apatite response for sample CWA102 and sample CWA128 could be accounted for by the nylon 6,6 becoming too hydrophilic or too toxic which will be further discussed in Section 11.5. The trend for the surface oxygen content and Δg for the CO_2 laser whole area irradiative processed samples can be further identified by Figure 11.11(b) if one was to disregard the CO_2 laser-induced patterned data points (data points with a surface oxygen content between 14 and 15 %at. and Δg between 0.025 and 0.03 g). By just taking into account the data points for the as-received sample and CO_2 laser whole area irradiative processed samples it can be seen that Δg increases to a maximum around 15.5 %at beyond which Δg begins to reduce.

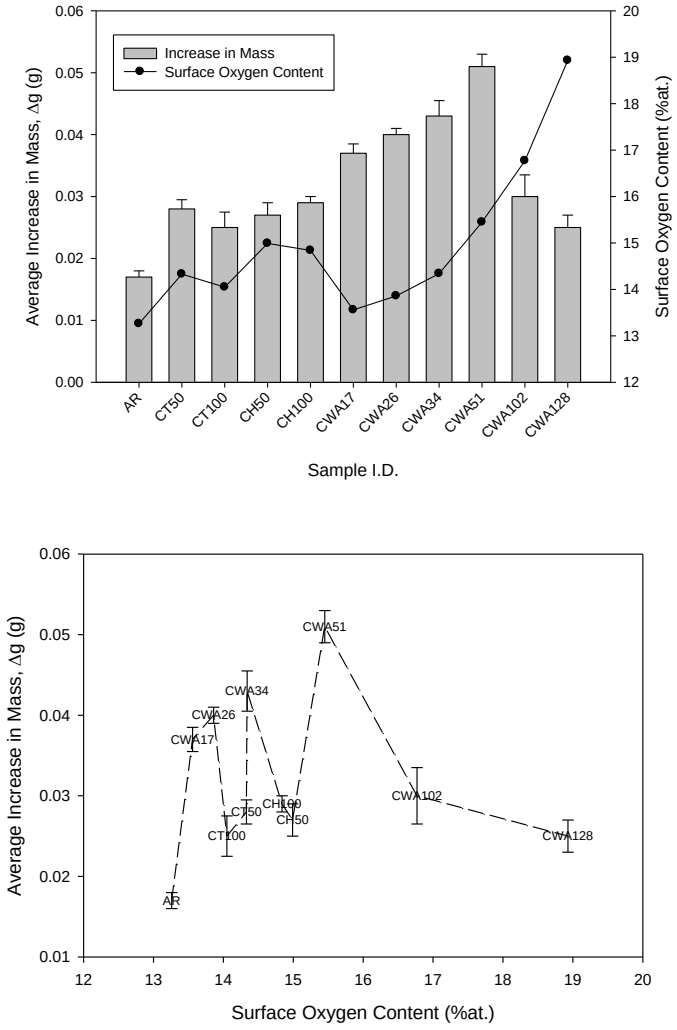

Figure 11.11 – (a) Histogram showing the increase in mass, Δg, in relation to surface oxygen content for all CO_2 laser processed samples, (b) Graph showing the relationship between surface oxygen content and Δg for all CO_2 laser processed nylon 6,6 samples following 14 days immersion in SBF.

11.3 – Effect of CO_2 Laser Processing on Osteoblast Cell Response: 24 Hrs

This Section discusses the results obtained following seeding normal human osteoblast cells onto CO_2 laser-induced patterned and CO_2 laser whole area irradiative processed nylon 6,6 samples after 24 hrs of incubation. The methodology of which can be found in Chapter 5.

11.3.1 – CO_2 Laser-Induced Patterning

It can be seen in Figure 11.12 and Figure 11.13 that for all samples the osteoblast cells have to some extent adhered to the differing surfaces. That is, the cells have firstly attached, adhered and have begun to spread across the surfaces. The extent to which this phenomenon has taken place appears to be dependent on the laser processing owed to the larger areas of cell coverage after 24 hrs of incubation time. In terms of cell morphology it can be seen that following 24 hrs of incubation the osteoblast cells on both the as-received (see Figure 11.12) and the CO_2 laser-induced patterned nylon 6,6 samples (see Figure 11.13) are bipolar in nature apart from the 100 µm trench samples (see Figure 11.13(b) which was at a more advanced stage of cell growth. This suggests that after 24 hrs of cell adhesion and growth there is no difference in terms of cell signaling. What is more, Figure 11.13 highlights that the CO_2 laser-induced patterned nylon 6,6 samples did not give rise to any directionality owed to the fact that the cells appear to be growing in random directions.

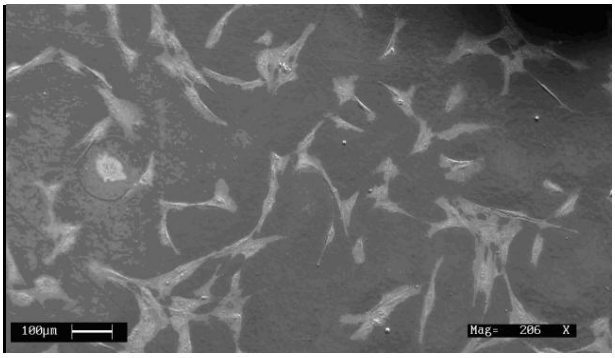

Figure 11.12 – SEM micrograph of Au coated samples 24 hrs post seeding for the as-received sample (AR).

In order to quantify the cover density as shown in Figure 11.14 was measured. This histogram allows one to see that the CO_2 laser-induced patterned samples gave rise to a more enhanced biological response with the largest cover density of around 40% being found to be due to of the trench patterned samples (CT50 and CT100). From Figure 11.14 it allows one to see that the CO_2 laser-induced patterned nylon 6,6 samples gave rise to a more advanced cell proliferation when compared to the as-received sample (AR). This further backs the results obtained for the apatite-layer response as discussed in Section 11.2.1.

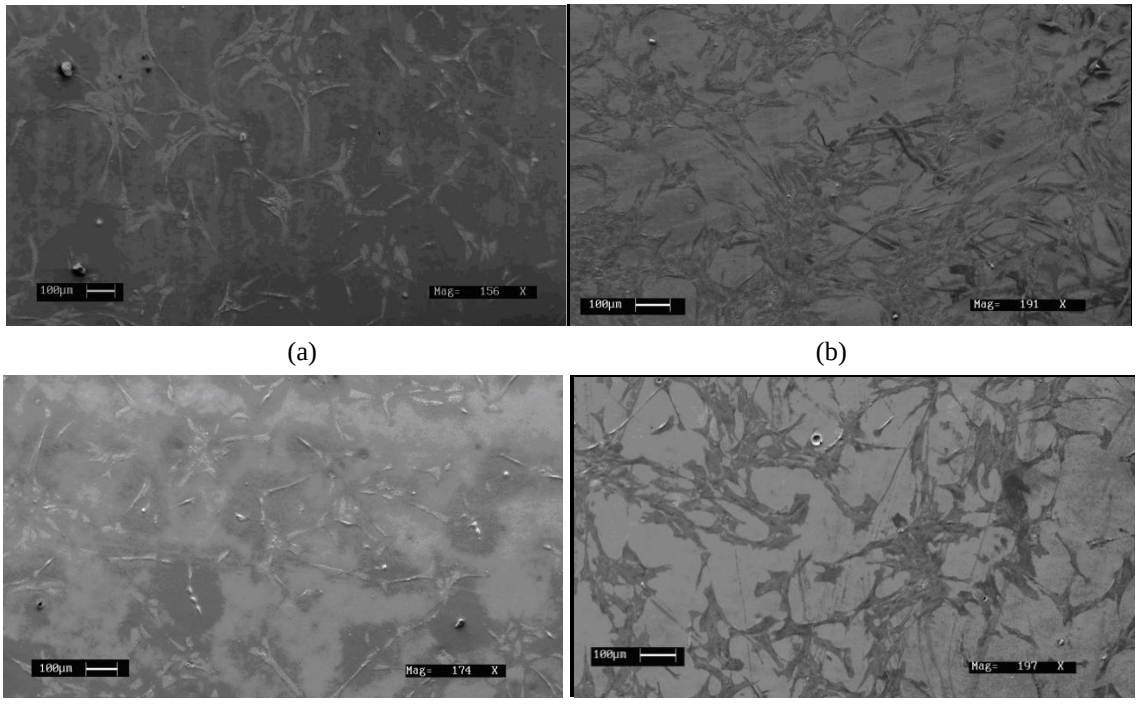

Figure 11.13 – SEM micrographs of Au coated samples 24 hrs post seeding for the CO_2 laser-patterned samples (a) CT50, (b) CT100, (c) CH50 and (d) CH100.

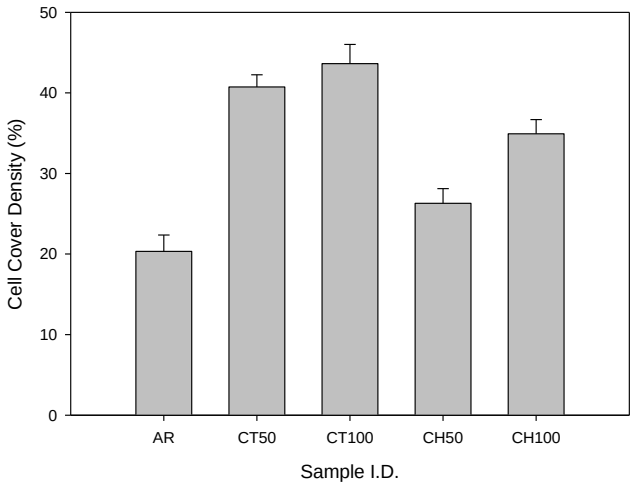

Figure 11.14 – Histogram showing the cell cover density for the CO_2 laser-induced patterned nylon 6,6 samples following 24 hrs of incubation.

11.3.2 – CO_2 Whole Area Irradiative Processing

Figure 11.15 shows that after 24 hrs of incubation the osteoblast cells had begun to adhere and proliferate across the nylon 6,6 surface following CO_2 whole area irradiative processing. Similar to the as-received sample (see Figure 11.12(a)) the morphology of the cells shown in Figure 11.15 was equivalent to that observed such that in general they were bipolar in nature. On the other hand, in

addition to bipolar shapes, those cells shown in Figure 11.15(b) and 11.15(c) also indicate a clumped cell morphology. This indicates that the different fluences used for the CO_2 whole area irradiative processing lead to modulation in cell signaling as this would account for the observed modification in cell differentiation.It should also be noted that those samples irradiated with high fluences of 102 and 128 Jcm^{-2} (CWA102 and CWA128) appeared to achieve a less osteoblast cell response owed to the fact that the cells had covered less area of the samples studied.

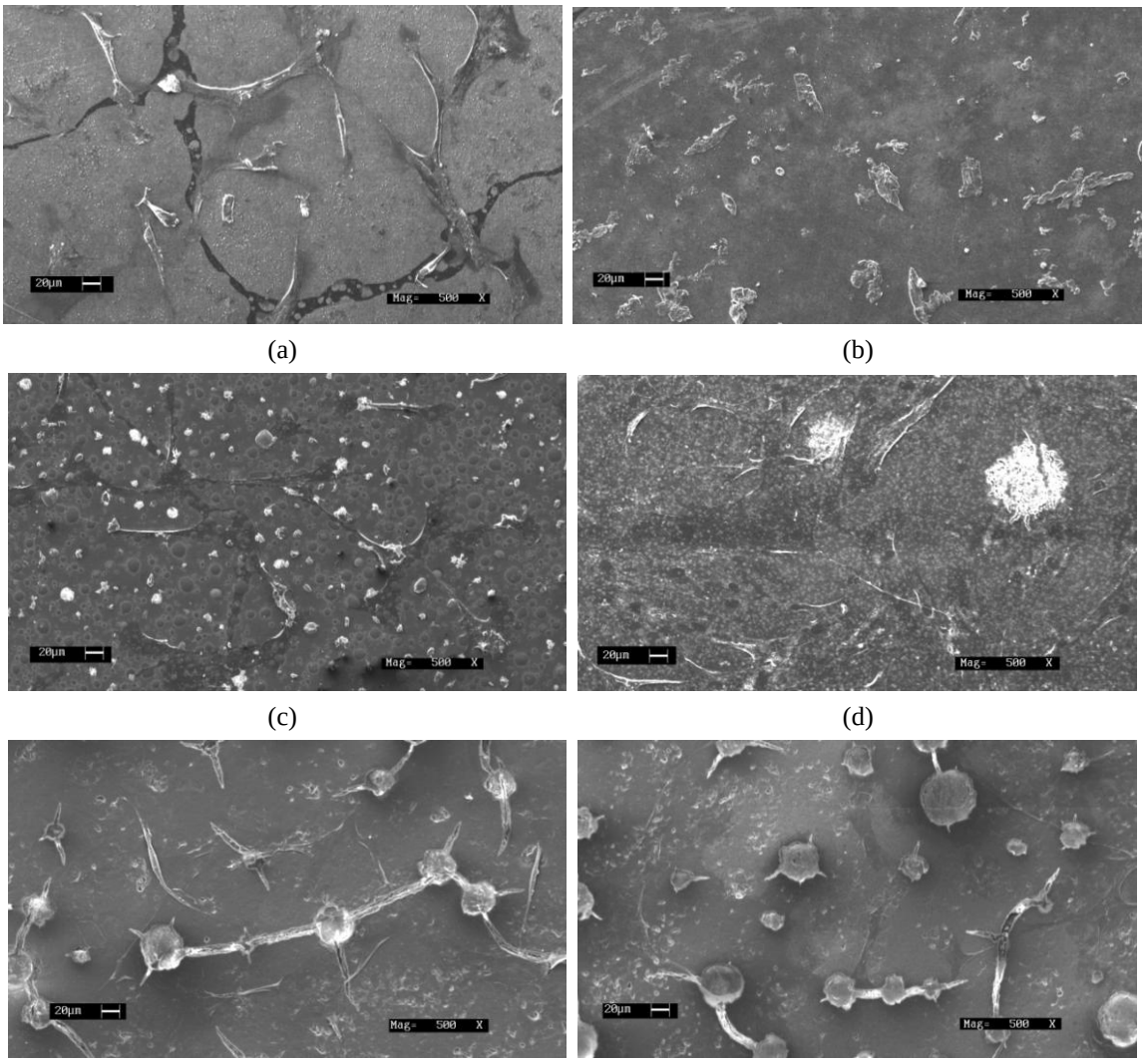

Figure 11.15 – SEM micrographs of Au coated samples 24 hrs post seeding for the CO_2 laser whole area irradiated samples (a) CWA17, (b) CWA26, (c) CWA34, (d) CWA51, (e) CWA102 and (d) CWA128.

The histogram shown in Figure 11.16 shows the cell cover density for each of the CO_2 laser whole area irradiative processed samples in relation to the as-received sample (AR). The largest cell cover density was found to be around 30% which was given by samples CWA34 and CWA51. In contrast it can be seen from Figure 11.16 that samples CWA17 and CWA26 gave a cell cover density of around 20%, which was equivalent to that of the as-received sample (AR). Also, from Figure 11.16 the cover densities determined for samples CWA102 and CWA128 were considerably lower of less than 10% compared to the as-received sample (AR). The equivalent cell cover densities achieved for samples

CWA17 and CWA26 and be explained by the fact that the fluences of 17 and 26 Jcm^{-2} were found experimentally to be close to the threshold fluence for the nylon 6,6 material. As such, as discussed in Chapter 6 this allowed for a negligible effect on the surface parameters, on account of similar results being obtained. For samples CWA102 and CWA128 it was found through wettability characteristic analysis that the surface had become more hydrophilic shown in Chapter 6 and could suggest that by making the nylon 6,6 surface too hydrophilic, osteoblast cell response has been hindered.

Another aspect that should be taken into consideration is that samples CWA102 and CWA128 were irradiated with high fluences (102 and 128 Jcm^{-2}) and as such 'over-melting' would likely have occurred, allowing toxic elements to form at the surface. Toxicity of the nylon 6,6 surfaces on account of the CO_2 laser processing will be further discussed in Section 11.5.

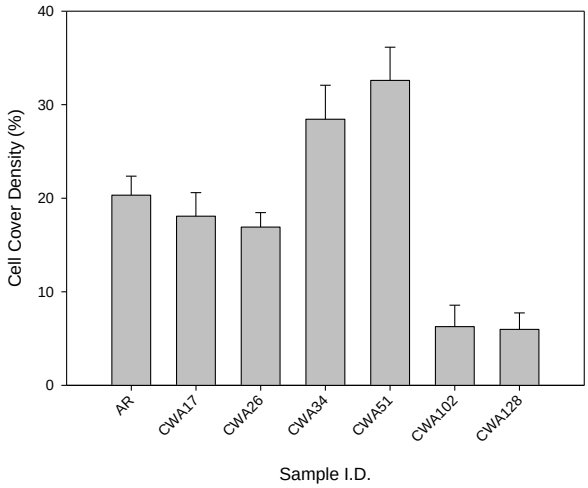

Figure 11.16 – Histogram showing the cell cover density for the CO_2 laser whole area irradiative processed nylon 6,6 samples following 24 hrs of incubation.

11.3.3 – Comparison Between CO_2 Laser-Induced Patterning and CO_2 Laser Whole Area Irradiative Processing

The micrographs shown in Figure 1.13 and Figure 11.15 allows one to identify that the CO_2 laser treatment of samples does not appear to give rise to directionality in terms of cell growth and proliferation. In fact the cells seem to be growing in random directions in conjunction with the CO_2 laser processed surfaces. In terms of cell morphology, the micrographs in Figure 11.13 and 11.15 show that most of the samples gave rise to bipolar shapes, apart from the CT100 sample (see Figure 11.13(b)) which was at a more advanced stage of the cell growth process. This could indicate that the growth process on the nylon 6,6 samples begins with a bipolar morphology and progresses to a more radial morphology as the incubated time progresses. In respect of proliferation, it appeared that samples CWA102 (see Figure 11.15(e) and Figure 11.16) and CWA128 (see Figure 11.15(f) and Figure11.16) gave rise to less proliferation in contrast to both the as-received sample (AR) and the other CO_2 laser surface treated samples. Furthermore, the cells appeared to be more concentrated in

and around the craters and cracks arising from the CO_2 laser processing. This may be owed to the possibility of more surface oxygen content or a higher surface roughness being present in these areas giving rise to promoting better cell adhesion.

In order to quantify how the osteoblast cells reacted to the different surface topographies the cell cover density was measured for each of the samples. A histogram showing the cell cover densities can be seen in Figure 11.17. The histogram shows that the cell cover density after 24 hrs was larger for all laser irradiated samples in comparison with the as-received (AR) sample apart from samples CWA17, CWA26, CWA102 and CWA128. The largest cell cover density of 38% was achieved with sample CT100, whilst 17% was observed for the as-received (AR) sample. Samples CWA102 and CWA128 samples gave the lowest cell cover densities of 6 and 9%, respectively in comparison to the other surfaces and can be owed to the samples becoming too hydrophilic or becoming too cytotoxic as a result of the laser processing. As a direct result of the cell cover density results shown in Figure 11.17 one can deduce that on the whole, the CO_2 laser surface modification gave rise to an increase in proliferation, speeding up the cell growth process as a result of allowing the material to enhance osteoblast cell response by changing the surface characteristics.

11.3.4 – Wettability Characteristics and Surface Parameters

With regards to the osteoblast cell response in relation to θ, it can be seen from Figure 11.17(a) that the CO_2 laser-induced patterned nylon 6,6 samples did not give rise to values of θ which could be correlated with the observed osteoblast cell response. Yet, from Figure 11.17(a) it can be seen that θ could play a role in determining the osteoblast cell response of the CO_2 laser whole area irradiative processed nylon 6,6. This is on account of the cell cover density increasing as θ increases over samples CWA17, CWA26, CWA34 and CWA51 whereas samples CWA102 and CWA128, which gave rise to reductions in θ gave rise to a hindered cell response with considerably lower cell cover densities. Also, with Samples CWA17 and CWA26 giving rise to similar θ to that of the as-received (AR) sample on account of the fluences being close to that of the threshold for nylon 6,6 the cell cover density can be seen to be equivalent for these three samples at approximately 20%. As a direct result of this, it appears that the processing at low fluences has had a negligible effect on cell response in comparison to the as-received sample (AR). It is worth remarking here that one of the main differences between the CO_2 laser-induced patterned and CO_2 laser whole area irradiative processed nylon 6,6 samples is that a difference in wetting regime has been proposed to explain the difference in wettability characteristics observed which has been discussed in Chapter 6. As a result, this transition in wetting regime for the CO_2 laser-induced patterned samples may have had a large impact on the osteoblast cell response of the nylon 6,6 samples. For instance, if the cell media was to have formed air gaps between some of the solid-liquid interface then the cells would not have been able to come into contact with the whole of the nylon 6,6 surfaces and could have lead to a hindered cell response.

The trend shown in Figure 11.17(a) for the CO_2 laser whole area irradiative processed nylon 6,6 and θ can be further confirmed using Figure 11.17(b). For instance, if one was to disregard the CO_2 laser-induced patterned sample data points in Figure 11.17(b) then it is possible to determine that the cell

cover density had a linear relationship with θ for the CO_2 laser whole area processed samples. This coincides with what was observed in Section 11.2.4 in that the osteoblast cell response to the CO_2 laser whole area irradiative processed samples became more enhanced upon an increase in θ compared to the as-received sample. Furthermore, by taking into account all data points in Figure 11.17(b) it can be seen that the CO_2 laser-induced patterned samples do not follow the same trend as the CO_2 laser whole area irradiative processed samples. In fact, by using Figure 11.7(a) and Figure 11.7(b) it can be ascertained that the cell cover density for the CO_2 laser-induced patterned samples had no correlation with θ which can be explained by the transition in wetting regimes on account of the laser-induced surface patterns.

Figure 11.18(a) shows a histogram allowing one to see the cell cover density in relation to γ^P for all CO_2 laser processed samples. From Figure 11.18(a) it can be seen that the cell cover density increased as a result of a decrease in γ^P for the CO_2 laser whole area irradiative processed samples. Also, it is significant to note here those samples which gave results that do not correspond to this trend are those results determined for the CO_2 laser-induced patterned nylon 6,6 samples. The transition in wetting regime could be accountable for these erroneous data points as discussed earlier. Similar to what was seen in Section 11.2.4, the linear relationship between the cell cover density and γ^P was further confirmed through Figure 11.18(a) if one was to disregard those data points arising from the CO_2 laser-induced patterning. This is owed to the fact that the proposed transition in wetting regime would have had a large impact upon the osteoblast cell response to the nylon 6,6 samples insofar as the mixed-state wetting regime did not allow the trends observed for the CO_2 laser whole area irradiative processed samples to be mimicked by the CO_2 laser-induced patterned samples.

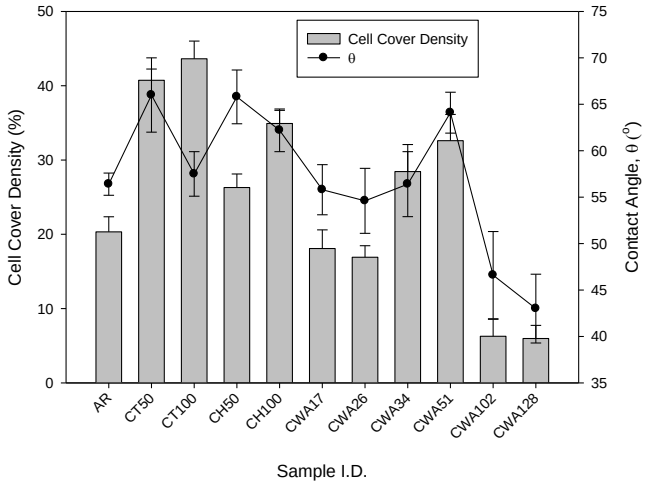

(a)

Figure 11.17 continued overleaf

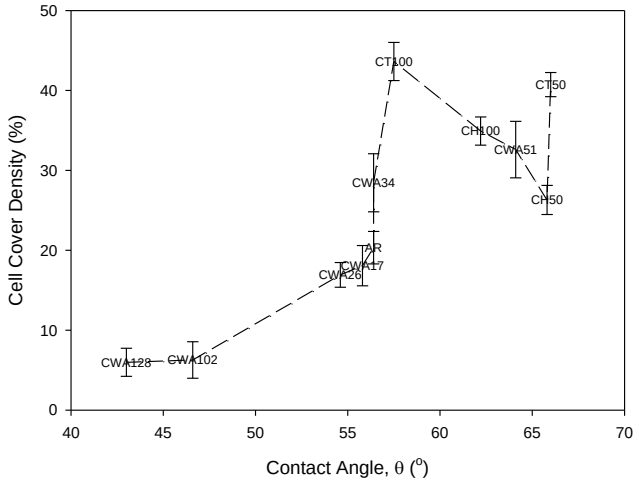

(b)

Figure 11.17 – (a) Histogram showing the cover densities for each of the seeded CO_2 laser processed nylon 6,6 samples after 24 hrs with relation to θ, (b) Graph showing the relationship between θ and cell cover density for all CO_2 laser processed samples.

*(In terms of cell cover density One-Way ANOVA showed an overall significance with F = 26.437 and p = 0.000. Scheffe's range test showed that there was significant statistical difference between AR and all samples apart from CWA17 and CWA26. Also, there was statistical difference between all samples apart from CT50 and CT100, CH100 and CWA51, CWA17 and CWA26, CWA102 and CWA128*p<0.05).*

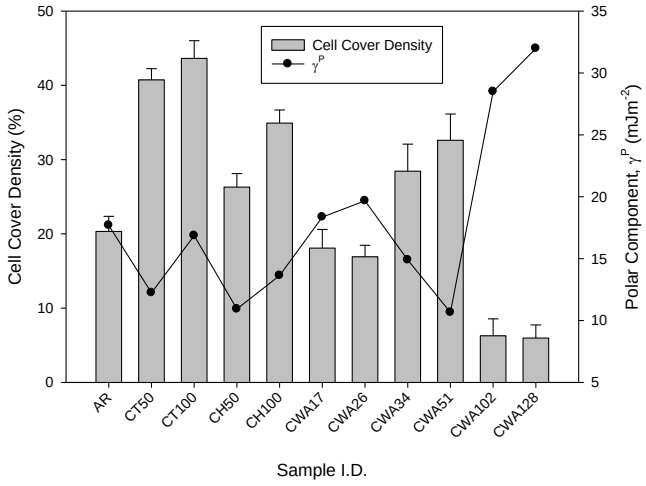

(a)

Figure 11.18 continued overleaf

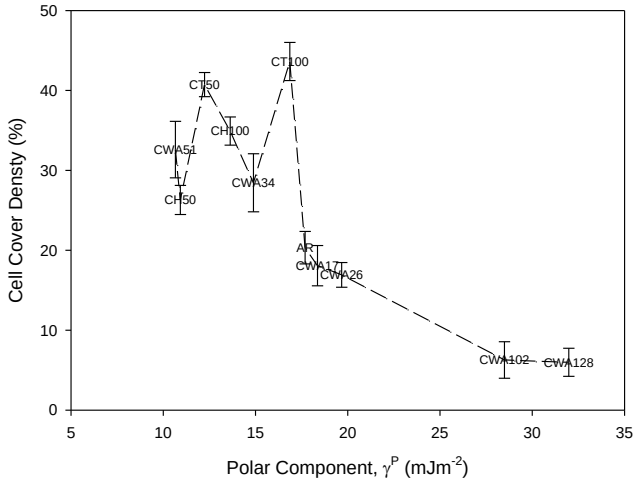

(b)

Figure 11.18 – (a) Histogram showing the increase in cell cover density in relation to γ^P for all CO_2 laser processed samples, (b) graph showing the relationship between γ^P and cell cover density.

Figure 11.19(a) gives the histogram for the cell cover density in relation to γ^T showing that there was no particular correlation between the measured cell cover density and γ^T for any of the CO_2 laser processed samples. Furthermore, Figure 11.19(b) confirms that there was no correlation for either the CO_2 laser-induced patterned and CO_2 laser whole area irradiative processed samples as the cell cover density was erratic when correlated with γ^T. This result also concurs with what was observed in Section 11.2.4 in that the results obtained indicate that γ^T was not a dominant parameter in determining the osteoblast cell response to the nylon 6,6 samples.

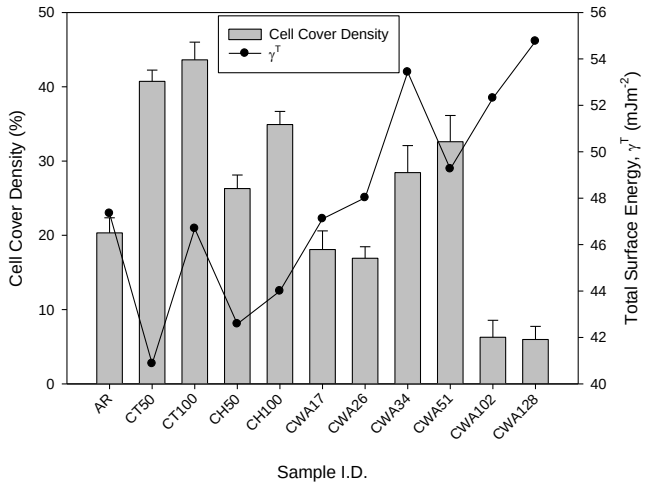

(a)

Figure 11.19 continued overleaf

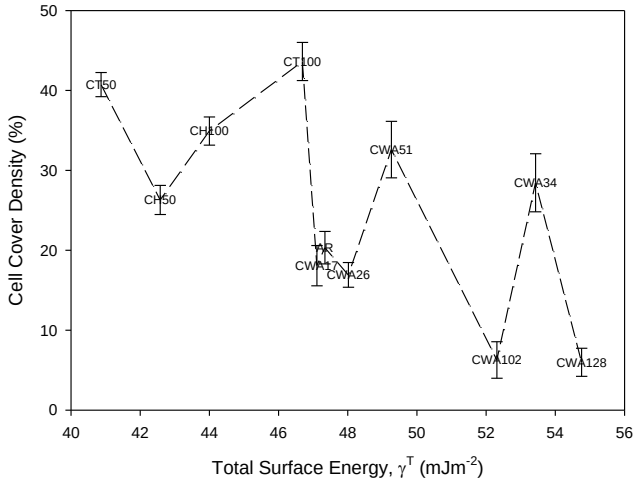

(b)

Figure 11.19 – (a) Histogram showing the increase in cell cover density in relation to γ^P for all CO_2 laser processed samples, (b) graph showing the relationship between γ^P and cell cover density.

It is also evident from Figure 11.20 and 11.21 that there was no correlative relationship between the cell cover densities observed and the surface roughness Ra and Sa for the CO_2 laser processed nylon 6,6 samples. The none correlative trend in this instance can be seen to be on account of similar values of Ra (see Figure 11.20(a) and Sa (see Figure 11.21(b)) giving rise to a large variation in cell cover density. In addition to this, Figure 11.20(b) and Figure 11.21(b) show that the cell cover density was erratic in terms of surface roughness. This indicates that the surface roughness did not appear to be a dominant surface characteristic to determine the osteoblast cell response to the nylon 6,6 surfaces.

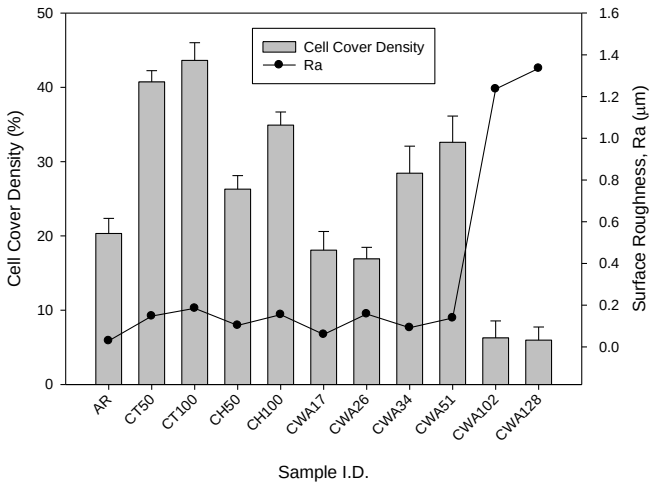

(a)

Figure 11.20 continued overleaf

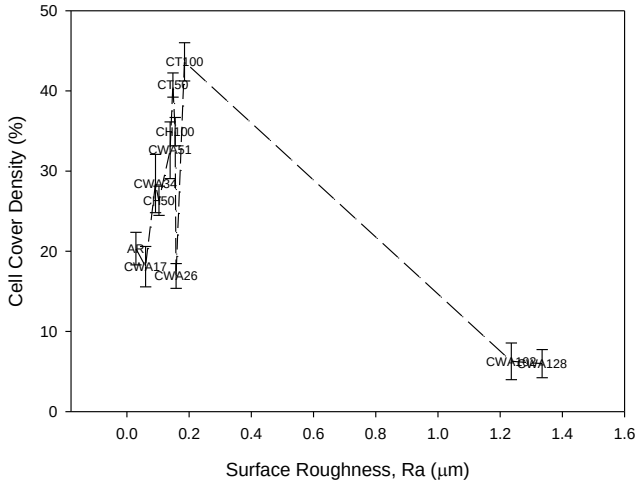

(b)

Figure 11.20 – (a) Histogram showing the cell cover density in relation to Ra for all CO_2 laser processed samples, (b) graph showing the relationship between Ra and cell cover density.

In terms of the surface oxygen content, it can be seen from Figure 11.22(a) that the CO_2 laser-induced patterned samples did not show any trend in terms of measured cell cover density and the surface oxygen content of each of the nylon 6,6 samples. On the other hand, Figure 11.22(a) shows that in general an increase in surface oxygen content for the CO_2 laser whole area irradiative processed samples gave rise to an increase in cell cover density until the incident fluence of 51 Jcm^{-2} was passed. After 51 Jcm^{-2} it was determined that even though an increase in surface oxygen content had been brought about, a reduction in the cell cover density was observed. It is possible for one to realize that this may not be a direct result of the increase in surface oxygen and could be attributed to the nylon 6,6 becoming too hydrophilic or too toxic on account of the high fluences used, which will be discussed in more detail in Section 11.5.

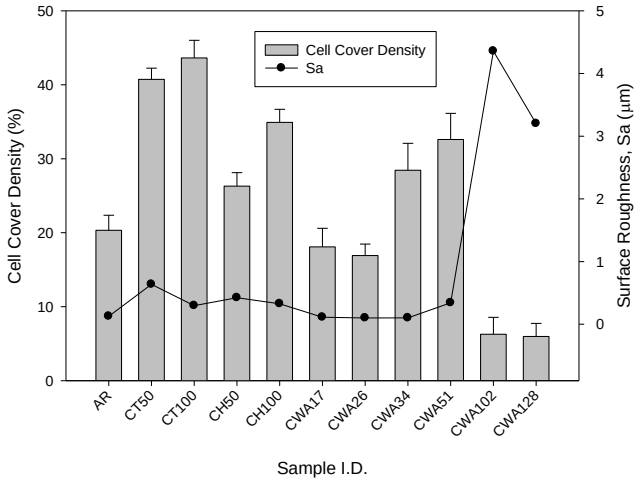

(a)

Figure 11.21 continued overleaf

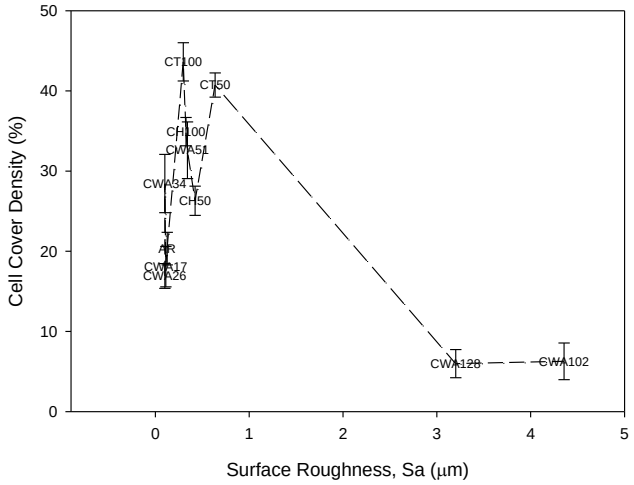

(b)

Figure 11.21 – (a) Histogram showing the cell cover density in relation to Sa for all CO_2 laser processed samples, (b) graph showing the relationship between Sa and cell cover density.

In Section 11.2.4 it was seen that there was a maximum level of surface oxygen content for enhanced bioacitivty, arising from correlating the osteoblast cell response to the surface oxygen content. Figure 11.22(b) shows that for the entire CO_2 laser processed samples there was no correlation between the surface oxygen content and cell cover density which can be accounted for by the CO_2 laser-induced samples not following any trend owed to the transition in wetting regime. Having said that, for the CO_2 laser whole area irradiative processed samples, shown in Figure 11.22(b), it can be seen that the cell cover density has a maximum peak between 15 and 16 %at. before reducing on account of an increase in surface oxygen content. It is worthwhile noting here that even though the trend shown in Figure 11.22(b) is not as conclusive as the trend shown in Figure 11.11(b) the same correlation within 11.22(b) is still within the margin of error for the CO_2 laser whole area irradiative processed samples.

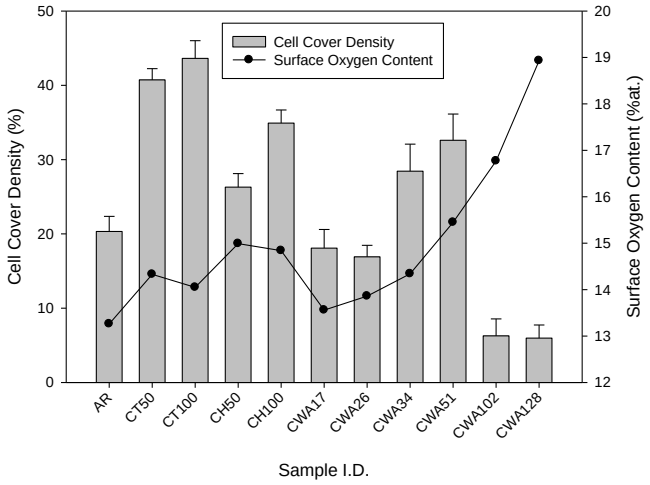

(a)

Figure 11.22 continued overleaf

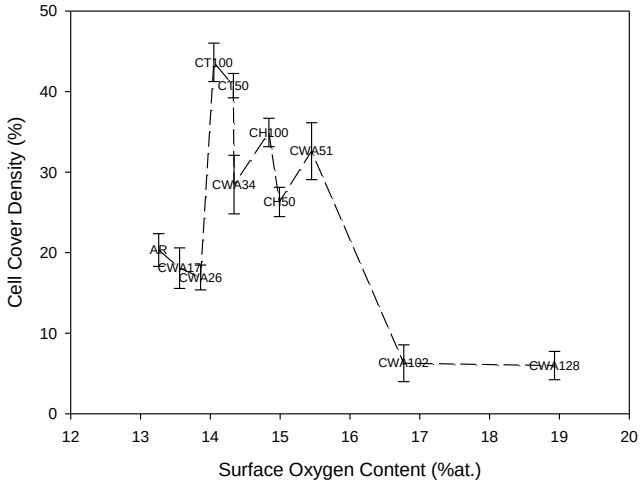

(b)

Figure 11.22 – (a) Histogram showing the cell cover density in relation to surface oxygen content for all CO_2 laser processed samples, (b) graph showing the relationship between surface oxygen content and cell cover density.

11.4 – Effects of CO_2 Laser Processing on Osteoblast Cell Response: 4 Days

Following the 24 hr study of the seeded osteoblast cells another well plate was kept in incubation for a further 72 hrs. This Section discusses the results obtained for the CO_2 laser-induced patterned and CO_2 whole area irradiative processed samples after seeding with normal human osteoblast cells and incubating for 4 days. The experimental technique can be found in Chapter 5.

11.4.1 – CO_2 Laser-Induced Patterning

From Section 11.3 it was observed that following 24 hrs of incubation the cells had attached and begun to spread across the as-received (AR) and CO_2 laser-induced patterned samples. As such it was necessary to analyse the seeded osteoblast cells on samples which had been incubated for longer than 24 hrs to assess the long term osteoblast cell response to the samples. After 4 days of incubation Figure 11.23 and Figure 11.24 show that the cells had grown and proliferated across almost the whole surface of both the as-received sample (see Figure 11.23) and the CO_2 laser-induced patterned samples (see Figure 11.24).

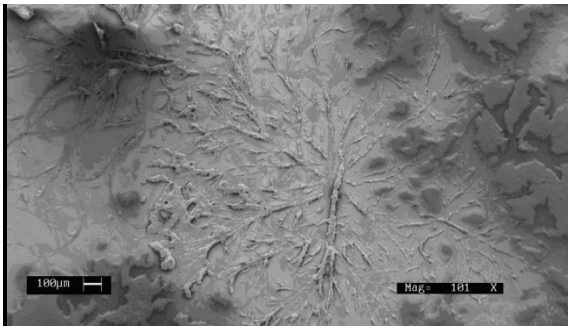

Figure 11.23 – SEM micrograph of Au coated sample after 4 days incubation for sample AR.

Another factor which can be taken from Figure 11.23 and 11.24 is that the cell morphologies appeared to differ between samples; for instance, it was found that the as-received sample (see Figure 11.13) gave rise to a more coral-like morphology. The 50 µm trench (CT50) patterned sample (see Figure 11.24(a)) shows that the cell morphology was more clumped, spindle-like and was growing in a radial nature. The 100 µm trench patterned (CT100) sample (see Figure 11.24(b)) was seen to produce a clumped radial cell morphology. Also, it was seen that the two hatch patterns (CH50 and CH100) (see Figure 11.24(c) and Figure 11.24(d)) had cell morphologies which where clumped radial with the 50 µm trench pattern (see Figure 11.24(d)) appearing to be more coral-like. This suggests that the different nylon 6,6 surfaces could have given rise to modulation in cell signaling and reveals that this effect occurs following the initial stages of cell adhesion as shown in Section 11.3 after 24 hrs of incubation. With this in mind, it is possible for one to see that by having the ability to modulate cell signaling this type of surface treatment has the potential to be implemented for applications within regenerative medicine.

Figure 11.25 confirms that the cell cover densities for the as-received sample (AR) and CO_2 laser-induced patterned nylon 6,6 samples were tending towards 100%. As such, in terms of cell cover density it was not possible to decipher whether or not the CO_2 laser-induced patterned samples gave rise to a more enhanced osteoblast cell response when compared with the as-received sample. However, a cell count as shown in Figure 11.26 after the 4 day incubation period provided the opportunity to determine that the CO_2 laser-induced patterned nylon 6,6 samples had given rise to a higher cell count with up to 60,000 cells/ml when compared to the as-received sample (AR) which had a cell count of approximately 38,000 cells/ml. This allows one to ascertain that even after 4 days incubation period with cover densities tending towards 100%, the CO_2 laser-induced patterned nylon 6,6 samples still gave rise to enhanced cell response in terms of cell growth.

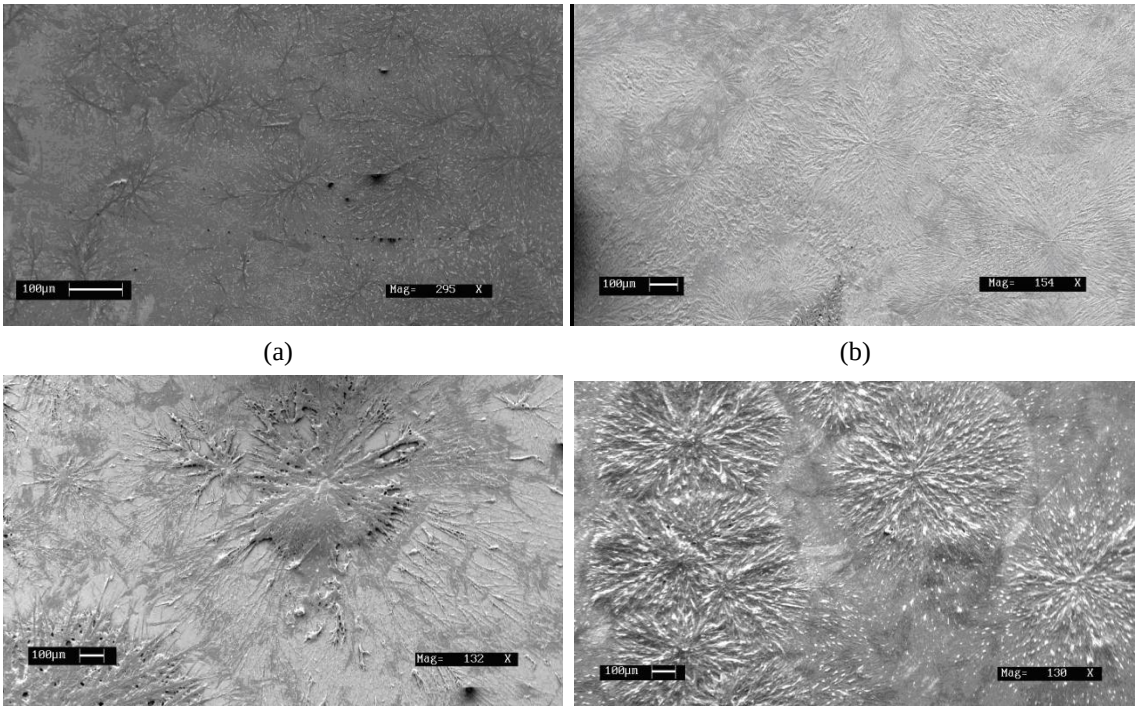

Figure 11.24 – SEM micrographs of Au coated samples after 4 days incubation for CO_2 laser-patterned samples (a) CT50 (b) CT100 (c) CH50 and (d) CH100.

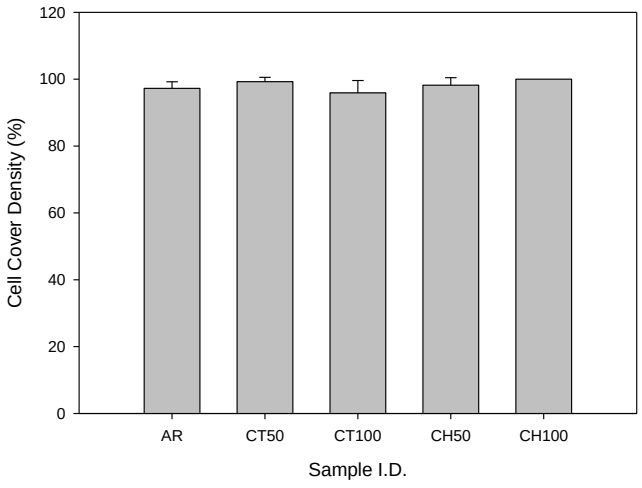

Figure 11.25 – Histogram showing the cell cover density for the CO_2 laser-induced patterned nylon 6,6 samples following 4 days incubation.

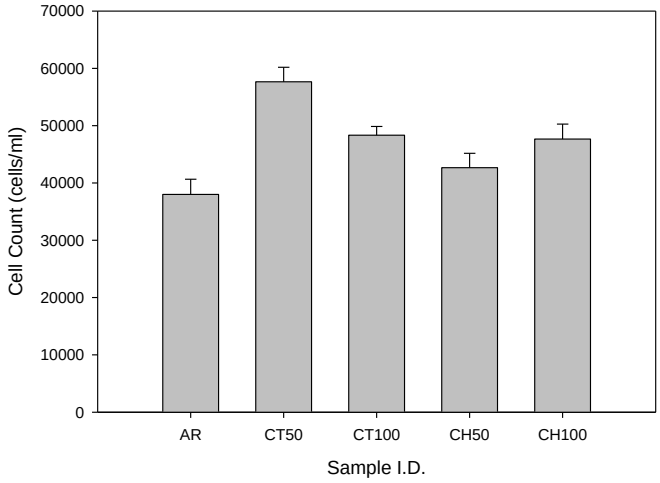

Figure 11.26 – Histogram showing the cell count for the CO_2 laser-induced patterned nylon 6,6 samples following 4 days of incubation.

11.4.2 – CO_2 Laser Whole Area Irradiative Processing

The 24 hr incubation period discussed in Section 11.3 showed a distinct variation in osteoblast cell response on account of the CO_2 laser whole area irradiative processing. After 4 days of incubation there still was a variation between some of the samples. From Figure 11.27 it is evident that the cells had rapidly begun to proliferate over the 4 day incubation period such that for all of the samples the cell cover density was tending towards 100% apart from samples CWA102 and CWA128 (see Figure 11.27(e) and Figure 11.27(f), respectively).

In terms of cell morphology for the CO_2 laser whole area irradiative processed samples (see Figure 11.27) the morphologies where somewhat different. CWA17 (see Figure 11.27(a)) gave rise to a clumped morphology which was slightly spindle-like. Whereas samples CWA26, CWA34 and CWA51 (see Figures 11.27(b), (c) and (d) respectively) gave rise to spindle-like morphologies with larger filopodia as the incident fluence increased. Finally, samples CWA102 and CWA128 (see Figure 11.27(e) and Figure 11.27(f), respectively) gave rise to morphologies that were similar to that observed after 24 hrs in that the cells were bipolar in nature. The observation of cell differentiation for the CO_2 laser whole area irradiative processed samples allows one to identify that there is a likelihood of variations in cell signaling taking place on account of the different surface parameters which have been induced by the CO_2 laser processing. This identifies that CO_2 laser whole area irradiative processing of nylon 6,6 has potential to be applied to regenerative medicine applications. In addition to this, it should be noted that it was again seen that the cell growth appeared to be more preferential to the craters and cracks which formed during processing indicating that this has a potential to be used for applications which may require selective osteoblast cell growth.

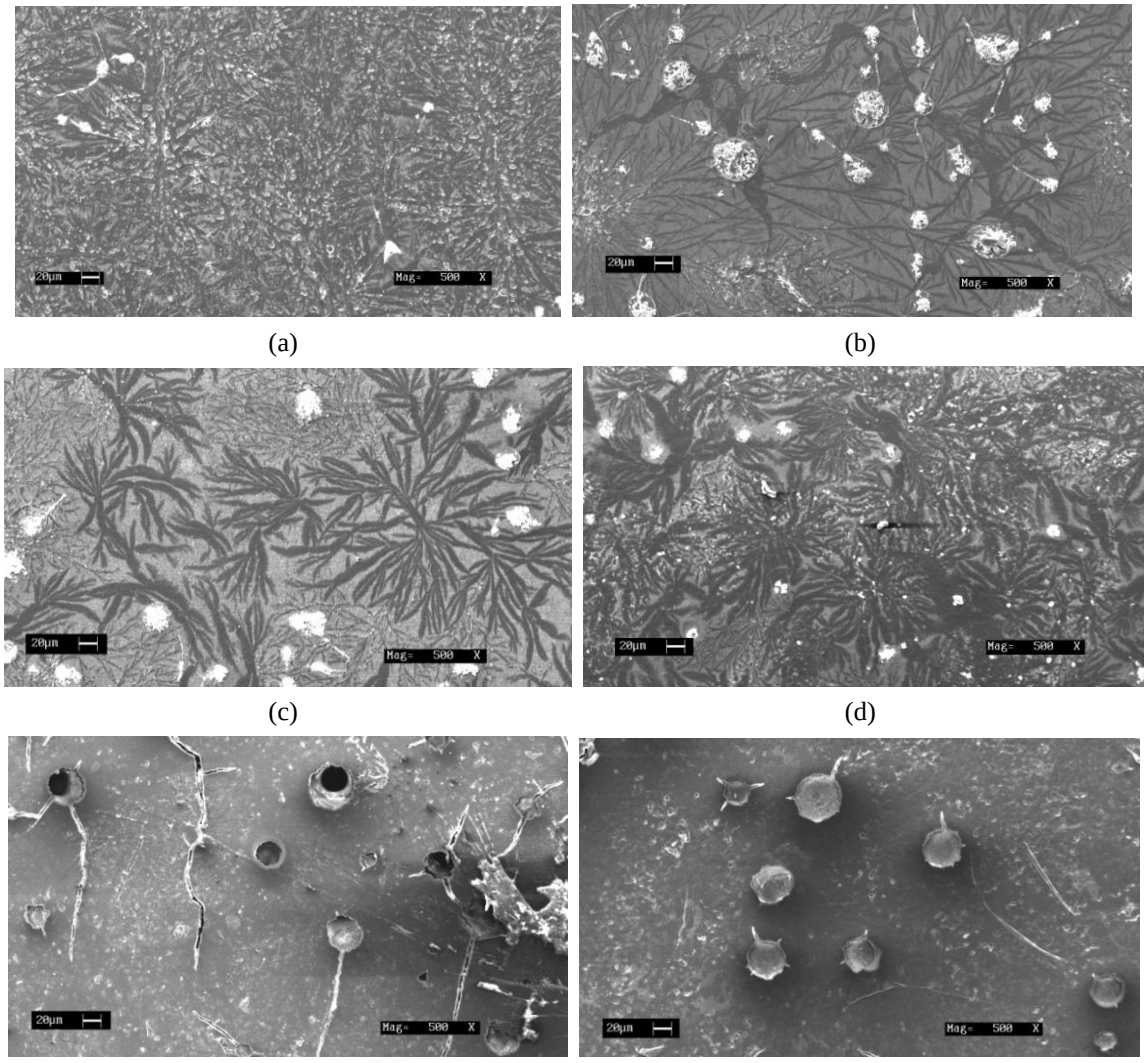

Figure 11.27 – SEM micrographs of Au coated samples after 4 days incubation for CO_2 laser whole area irradiated samples (a) CWA17, (b) CWA26, (c) CWA34, (d) CWA51, (e) CWA102 and (d) CWA128.

Figure 11.28 shows a histogram showing the cover densities of the entire CO_2 laser whole area irradiative processed samples in relation to the as-received sample (AR). From this histogram it can be confirmed that the cell cover densities for all of the samples were tending towards 100% with the exception of samples CWA102 and CWA128 which had cover densities of around 65% and 55%, respectively. This along with the analysis given in Section 11.3 shows that these two CO_2 laser modified surfaces gave rise to a hindered osteoblast cell response slowing down the cell growth and proliferation. As suggested previously, this may be because of the nylon 6,6 surfaces for samples CWA102 and CWA128 being too hydrophilic or too toxic on account of toxic elements leaching into the cell media. This will be further discussed in Section 11.5.

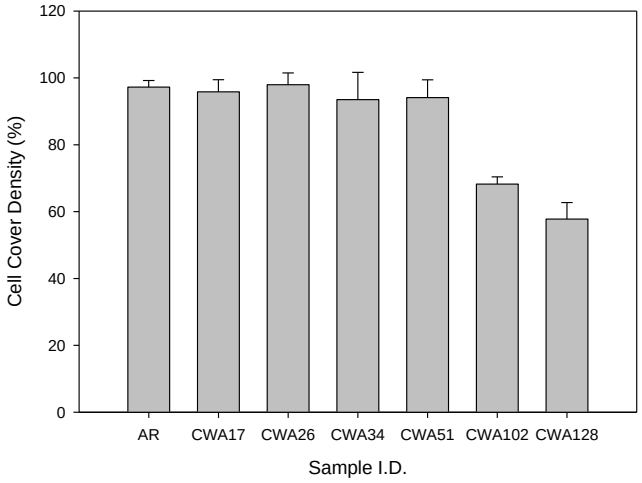

Figure 11.28 – Histogram showing the cell cover density for the CO_2 laser whole area irradiative processed nylon 6,6 samples following 4 days of incubation.

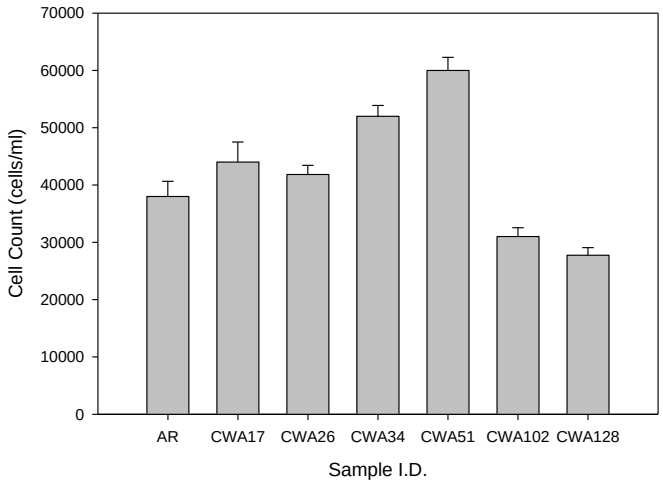

Figure 11.29 – Histogram showing the cell count for the CO_2 laser whole area irradiative processed nylon 6,6 samples following 4 days of incubation.

Figure 11.29 shows that with an increase of fluence between the region of 17 and 51 Jcm^{-2} for the CO_2 laser whole area irradiative samples the cell count gradually began to increase from 40,000 cells/ml for sample CWA17 to 60,000 cells/ml for sample CWA51. Fluences that were used beyond this region (CWA102 and CWA128) gave rise to a reduction in the cell count such that the CO_2 laser whole area irradiative processing of these nylon 6,6 samples made them inherently less bioactive. This coincides with the effects the fluence had on other bioactive properties such as apatite layer response (see Section11.2) and cell cover density (see Section 11.3). With this in mind, the results together allow one to see that a threshold fluence is highly likely for this specific type of CO_2 laser processing.

11.4.3 – Comparison Between CO_2 Laser-Induced Patterning and CO_2 Laser Whole Area Irradiative Processing

From Figure 11.30 it is evident that for each sample the cover density was approximately tending towards 100% apart from CWA102 and CWA128 – so no statistical significance to be obtained from the plotted data for the samples with similar cell cover densities. It should be noted here; however, that there was statistical difference between all samples and CWA102 and CWA128. This also implies that, with the exception of sample CWA102 and sample CWA128, the seeded osteoblast cells over 4 days had covered all the surfaces of each sample regardless of how the surface was treated. Having said that, it should be noted that for the 100 μm hatch (CH100) patterned sample each image used to calculate the cover density gave 100% covered resulting in the error being 0, as shown in Figure 11.26. Also, CWA102 and CWA128 gave rise to cover densities of 76 and 58%, respectively and as a result there could be some correlation between how the nylon 6,6 was treated prior to seeding and how the osteoblast cells react to the samples *in vitro*. The reasoning for the reduced cover densities for samples CWA102 and CWA128 in comparison to the other samples could be that the resulting θ may not give rise to sufficient cell adhesion and proliferation. In addition, as a result of the laser processing, considerably more melting was observed for these samples and may have left them more toxic which would ultimately hinder osteoblast cell growth.

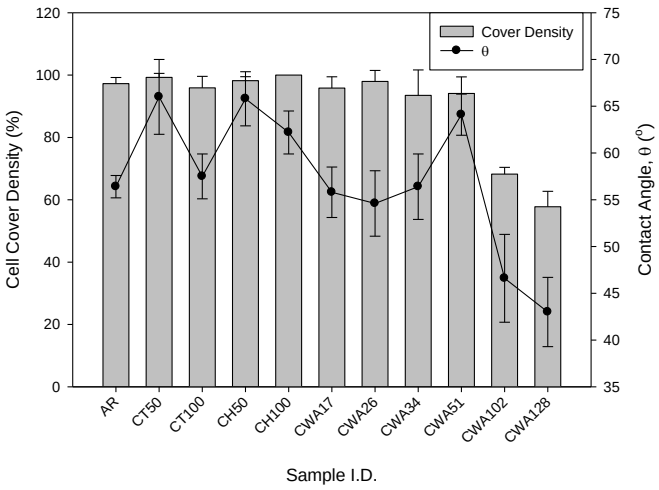

*Figure 11.30 – Cover density for each of the CO_2 laser processed nylon 6,6 samples 4 days after incubation. (One-Way ANOVA showed that there was not an overall significance with F = 38.338 and p = 0.002. Scheffe's range test showed that there was statistical difference between AR, CT50, CT100, CH50, CH100, CWA17, CWA26, CWA34, CWA51 and CWA102, CWA128. However, there was no statistical difference between those samples close to 100% and no difference between CWA102 and CWA128*p<0.05).*

A graph of cell count for each CO_2 laser processed sample can be seen in Figure 11.31(a), which indicates that there was a higher cell count after 4 days incubation for all samples, apart from samples CWA102 and sample CWA128, in comparison to the as-received sample (AR). It has been seen throughout this study that most of the nylon 6,6 surfaces which have been treated with the CO_2 laser

beam gave rise to improved cell adhesion, proliferation and as such promotes a better interface for mitosis to take place. For those samples which did not show an enhanced osteoblast cell response, namely samples CWA102 and CWA128, cytotoxicity and hydrophilic nature are two possible explanations for the hindered cell growth. The explanation of which will be discussed in Chapter 5.

11.4.4 – Wettability Characteristics and Surface Parameters

Similar to what has been seen previously in Section 11.3 and 11.4, it is clear from Figure 11.27(a) that there was no correlation between the cell count and θ for the CO_2 laser-induced patterned nylon 6,6 samples which can be accounted for by the transition in wetting regime as discussed in Chapter 6, Section 11.3 and Section 11.4. In addition, Figure 11.27(a) does show that there was a strong correlation between the osteoblast cell response and θ. That is, for the CO_2 laser whole area irradiative processed samples an increase in cell count was determined for an increase in θ. This can be further confirmed using Figure 11.27(b) which shows that when only taking into account the data points for the CO_2 laser whole area irradiative processed samples a linear correlation can be seen. In contrast, by taking into account the data points for both the CO_2 laser-induced patterned and CO_2 laser whole area irradiative processed samples the correlation is not as strong on account of the CO_2 laser-induced patterned samples not following the same trend. As a result, this suggests that it is the surface processing technique regardless of the CO_2 wavelength that determines the osteoblast cell response of the nylon 6,6 samples. It should be further noted here that this evidence corresponds with what was observed for the 24 hr incubation analysis as discussed in Section 11.2 and Section 11.3.

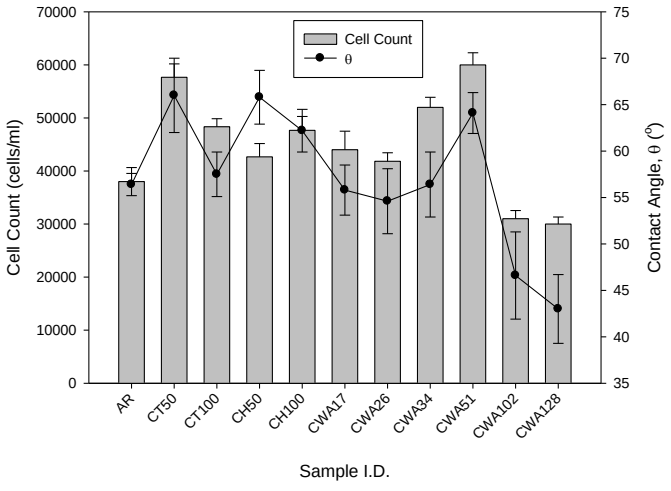

(a)

Figure 11.31 continued overleaf

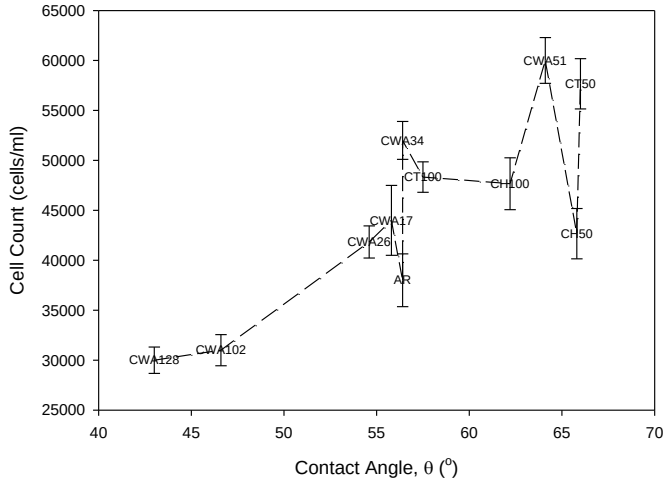

(b)

Figure 11.31 – (a) Histogram showing the cover count for each of the seeded CO_2 laser processed nylon 6,6 samples after 24 hrs in relation to θ, (b) graph showing the relationship between θ and cell count for all CO_2 laser processed samples.

*(In terms of cell count, One-Way ANOVA showed that there was not an overall significance with F = 64.248 and p = 0.003. Scheffe's range test showed that there was statistical difference between AR, CT50, CT100, CH100, CWA34, CWA51 and CWA128. However, there was no statistical difference between the other samples which had similar cell counts*p<0.05).*

Figure 11.32(a) shows the cell count for all of the CO_2 laser processed samples in relation to γ^P allowing one to see that there does not appear to be a trend in regards to the CO_2 laser-induced patterned samples and γ^P. In contrast, the CO_2 laser whole area irradiative processed samples had a good correlation with γ^P insofar as the cell count steadily decreased over each of the samples upon an increase in γ^P. This can be corroborated by Figure 11.32(b) which shows that the cell count was a strong reducing function of γ^P and that the data points for the CO_2 laser whole area irradiative processed samples take away from this correlation as they do not appear to fit the same trend. This further supports what has been determined within Section 11.2.4 and Section 11.3.4.

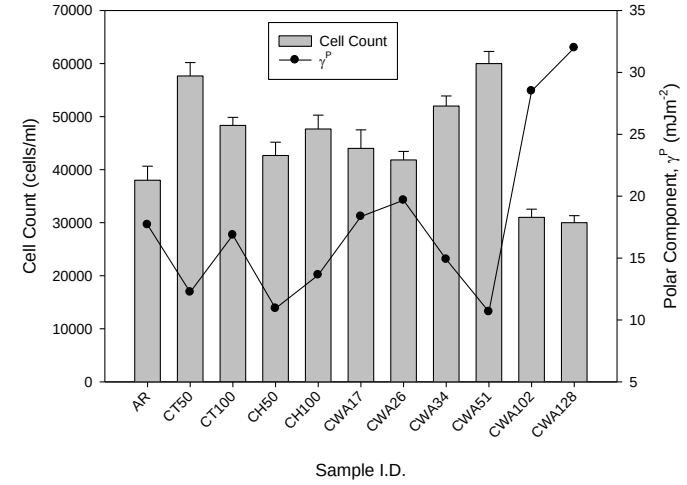

(a)

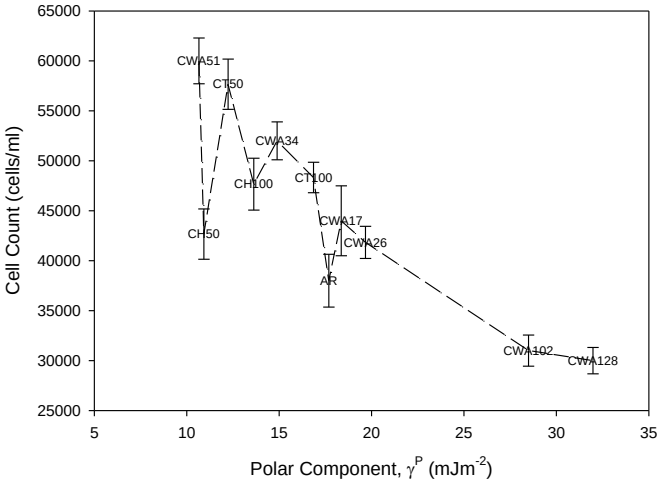

(b)

Figure 11.32 – (a) Histogram showing the increase in cell count in relation to γ^P for all CO_2 laser processed samples, (b) graph showing the relationship between γ^P and cell count.

Figure 11.33(a) shows that the cell count for both the CO_2 laser-induced patterned and CO_2 laser whole area irradiative processed nylon 6,6 samples did not have any distinct correlation in terms of cell count and γ^T. This is also reaffirmed by Figure 11.33(b) which shows no strong trend between the two parameters. Again, this further supports what has been observed previously in Section 11.2.4 and Section 11.3.4 in that γ^T does not appear to be a dominating parameter when it comes to determining the osteoblast cell response to the nylon 6,6 samples; in fact from the results obtained it is evident that one can reasonably say that θ and γ^P have a stronger correlation with the bioactive characteristics of the CO_2 laser processed nylon 6,6 samples.

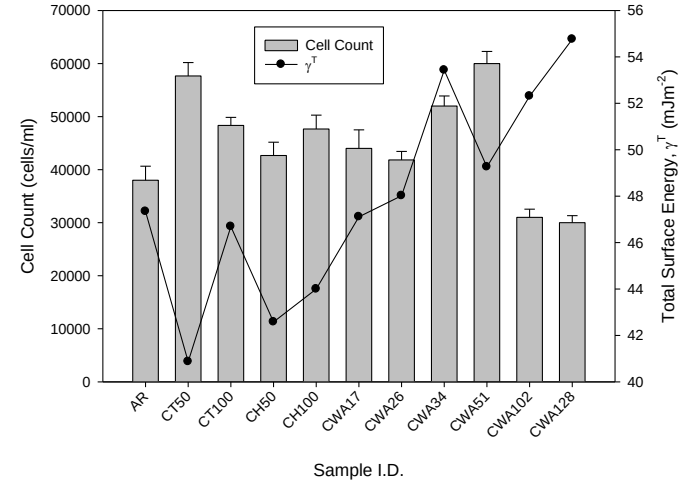

(a)

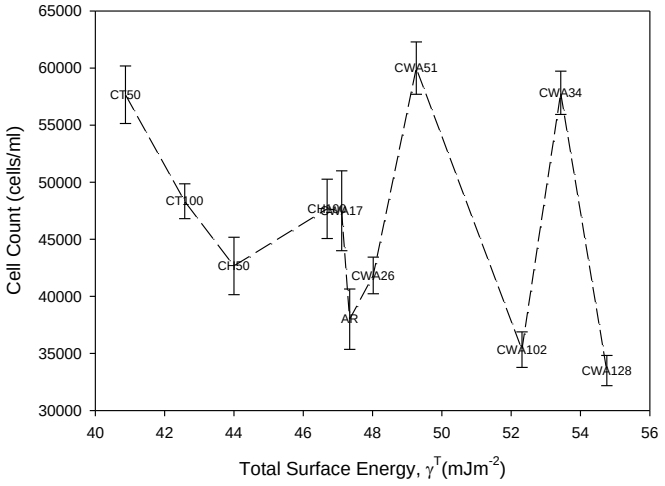

(b)

Figure 11.33 – (a) Histogram showing the increase in cell count in relation to γ^T for all CO_2 laser processed samples, (b) graph showing the relationship between γ^T and cell count.

Figure 11.34(a) and Figure 11.35(a) show that there was not any distinct correlation between the cell count, Ra (see Figure 11.34(a)) and Sa (see Figure 11.35(a)). This is owed to the fact that similar values of Ra (see Figure 11.34(a)) and Sa (see Figure 11.35(a)) gave rise to considerable variation in cell count for the entire CO_2 laser processed samples. This is further confirmed through Figure 11.34(b) and Figure 11.35(b) which shows explicitly that similar roughness values give rise to a large differentiation in cell count. This also corroborates with the results discussed in Section 11.2.4 and Section 11.3.4 which indicates that surface roughness, like γ^T, is not a dominating parameter in the osteoblast cell response to nylon 6,6. Having said that, through the work carried out by Nebe [180] surface roughness is reported to have a large influence on cell signaling. Throughout this Chapter evidence of cell signaling has been apparent by the observation of different cell morphologies (see Figures 11.10, 11.11 and 11.13). As a result of this it is possible to say that even though no discernible correlation between the cell count and roughness could be determined in this instance surface

roughness could still play a significant role in cell differentiation. Furthermore, owed to the significant modification in surface roughness on account of both the CO_2 laser-induced patterning and CO_2 laser whole area irradiative processing, these techniques could be applied to regenerative medicine.

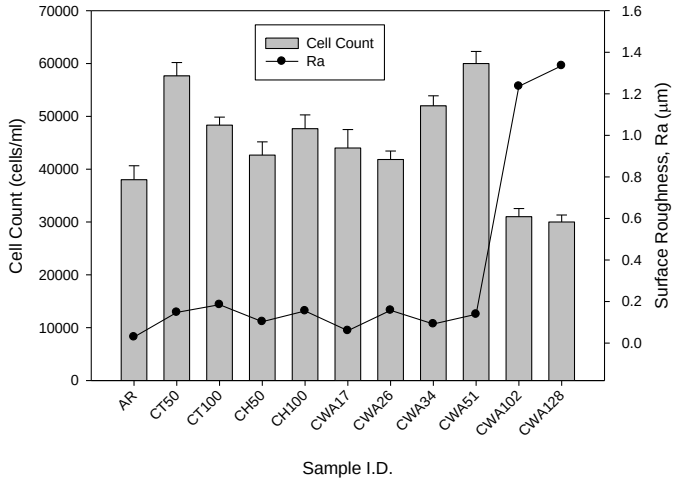

(a)

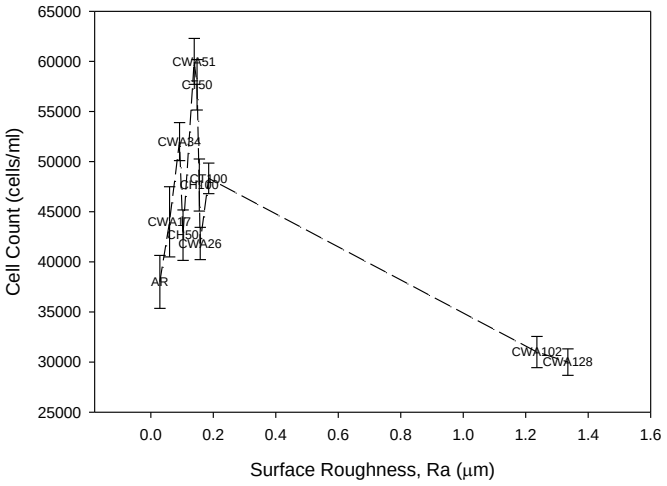

(b)

Figure 11.34 – (a) Histogram showing the increase in cell count in relation to Ra for all CO_2 laser processed samples, (b) graph showing the relationship between Ra and cell count.

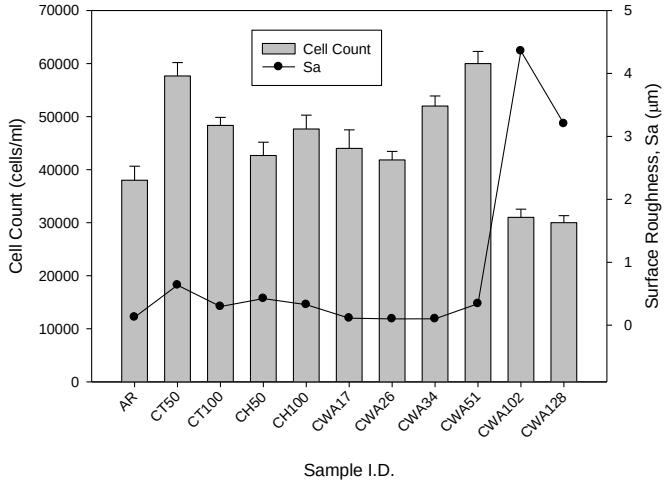

(a)

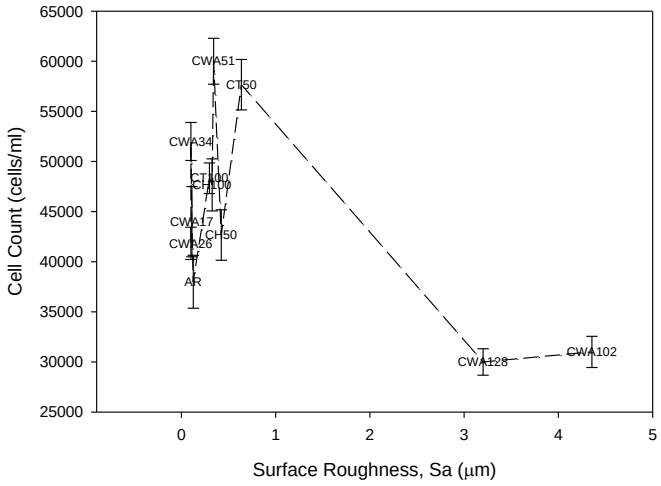

(b)

Figure 11.35 – (a) Histogram showing the increase in cell count in relation to Sa for all CO_2 laser processed samples, (b) graph showing the relationship between Sa and cell count.

Figure 11.36(a) is a histogram showing the cell count for the entire CO_2 laser processed samples in relation to the surface oxygen content for each sample. From this histogram one can see that, like in Section 11.2.4 and Section 11.3.4, the surface oxygen content does not have any correlation with the cell count for the CO_2 laser-induced patterned samples. Conversely, it can be seen from Figure 11.36(a) that the cell count for the CO_2 laser whole area irradiative processed samples increased on account of an increase in surface oxygen content up to sample CWA51 which had an incident fluence of 51 Jcm^{-2}. For those samples which had higher incident fluences (sample CWA102 and sample CWA128) it can be seen from Figure 11.36(a) that the cell count had dramatically been reduced in comparison to the as-received sample (AR). By disregarding the data points for the CO_2 laser-induced patterned samples in Figure 11.36(b) it can be further validated that there was a maximum surface oxygen content threshold beyond which the samples did not give rise to a sufficient bioactive surface in terms of osteoblast cell response. It should be noted here that the reduction in osteoblast cell

response to sample CWA102 and sample CWA128, which has been discussed through this Section, Section 11.2.4 and 11.3.4, may not necessarily be on account of an increase in surface oxygen content but may be due to the fact that the samples had become too hydrophilic or too toxic on account of the large incident fluences used. As such, this is further discussed in Section 11.5.

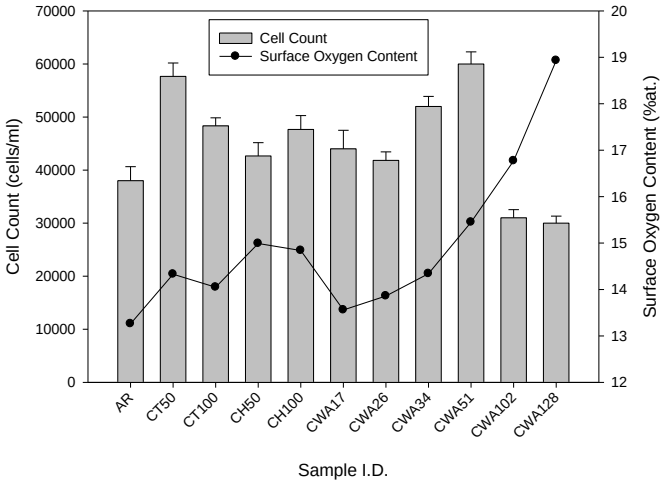

(a)

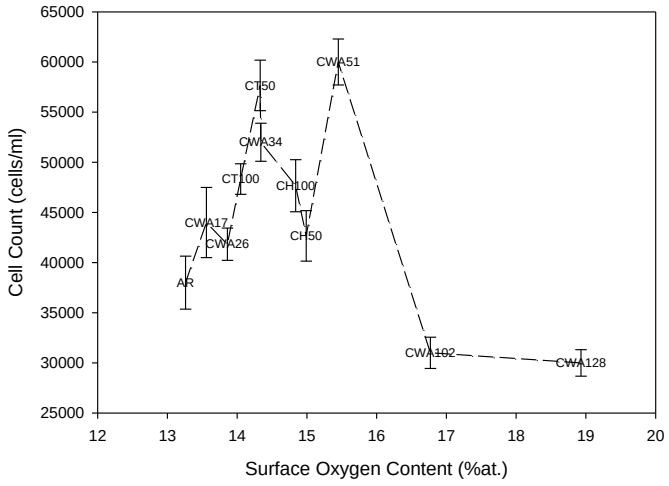

(b)

Figure 11.36 – (a) Histogram showing the increase in cell count in relation to surface oxygen content for all CO_2 laser processed samples, (b) graph showing the relationship between surface oxygen content and cell count.

11.5 – Effects of CO_2 Laser Processing on Cytotoxicity and Alkaline Leukocyte Phosphatase (ALP) Levels

To ascertain the viability of the seeded osteoblast cells cytotoxicity and ALP levels were determined for all of the samples following 2 days of incubation. This section discusses and compares the results obtained in relation to wettability. The full experimental technique can be found in Chapter 5.

11.5.1 – CO_2 Laser-Induced Patterning

Figure 11.37 shows that both the CO_2 laser-induced patterned and as-received samples gave rise to a higher cytotoxicity when compared to the low control (LC); however, it should be noted that all CO_2 laser-induced patterned samples had cytotoxicity levels equivalent to that of the as-received sample (AR) with an absorbance of around 0.005. Even so, sample CT100 can be seen to have the lowest cytotoxicity which could be the explanation as to why this sample gave rise to more prominent cell growth after 24 hrs (see Section 11.3).

Leading on, it can be extrapolated that laser surface modification may also have an influence on ALP levels which is significant to osteoblast cell growth. Figure 11.38 shows the ALP activity levels for the CO_2 laser-induced patterned nylon 6,6 samples and allows one to see that all samples, including the as-received sample (AR), gave rise to significantly higher levels of ALP compared to the negative control (NC). Furthermore, the CO_2 laser-induced patterned samples all had slightly higher ALP levels compared to that of the as-received sample (AR) which had an RFU value of around 22. This evidence further implies that a more preferential cell response would arise due to these slightly higher levels of ALP for the CO_2 laser-induced patterned samples.

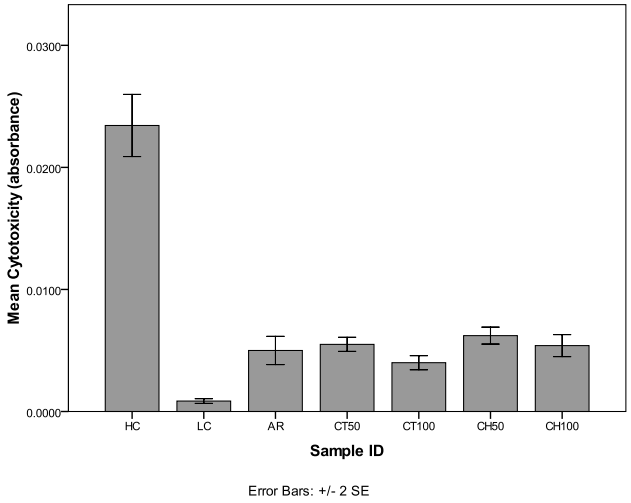

*Figure 11.37 – Histogram showing the cytotoxicity of the nylon 6,6 samples following CO_2 laser patterning. (One-Way ANOVA showed an overall significance with F=155.148 and p=0.000. Scheffe's tests showed that there was statistical difference between HC, LC and the other samples. Whereas there was no difference between the laser treated samples and AR. *p<0.5).*

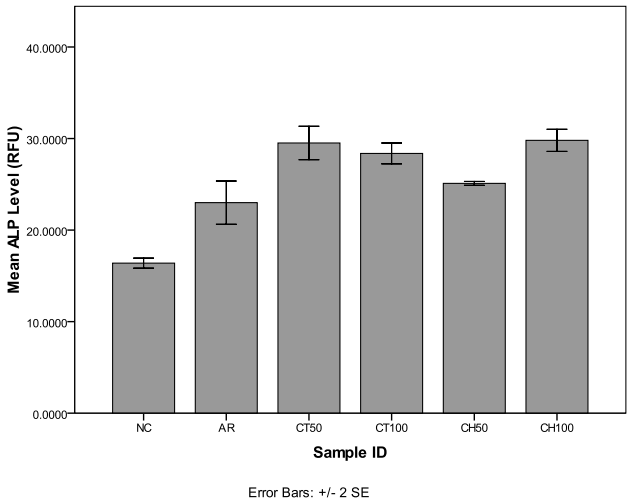

*Figure 11.38 – Histogram showing the ALP levels for each of the CO_2 laser patterned samples. (One-Way ANOVA showed an overall significance with F=99.935 and p=0.000. Scheffe's tests showed that there was statistical difference between all samples but AR:CT50:CT100 and CT50:CT100:CH100*p<0.5).*

11.5.2 – CO_2 Laser Whole Area Irradiative Processing

Figure 11.39 shows that the cytotoxicity level for both the as-received and the CO_2 laser whole area irradiative processed samples was significantly higher than that of the low control (LC). Also, samples CWA17, CWA26, CWA34 and CWA51 all had cytotoxicity levels equivalent to that of the as-received sample (AR). Significantly, it can be seen from Figure 11.39 that for higher fluences sample CWA102 and sample CWA128 gave rise to a considerable increase in cytotoxicity with an absorbance of around 0.018 being measured compared to 0.005 for the other test samples. This can be attributed to the fact that at the higher fluences further melting could cause the surface of the nylon 6,6 to become more toxic which would hinder cell growth compared to the other samples. That is, upon considerable heating and melting of the nylon 6,6 it is known that toxic substances such as CO and HCN can evolve [181]. These evolved toxic substances could have been present on the surface on account of the rapid heating and cooling, trapping these substances until they leached out into the cell media. This would have had a considerable deleterious effect on the osteoblast cell growth as it has been shown that CO and HCN affect cell growth and proliferation [182]. On account of this, it is reasonable to assume that a rise in toxicity for samples CWA102 and CWA128 rather than the samples becoming too hydrophilic gave rise to the hindered cell response which was discussed previously in Sections 11.2, 11.3 and 11.4. Additionally, this further suggests that there may be a threshold as to how much incident fluence can be used before cell growth is hindered. From Figure 11.39 this threshold is indicated to be between 50 and 100 Jcm^{-2} for nylon 6,6 using a 10.6 μm CO_2 laser.

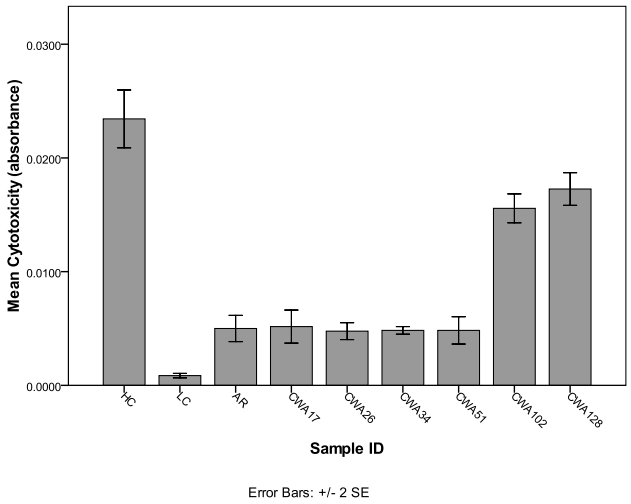

*Figure 11.39 – Histogram showing the cytotoxicity absorbance for the CO_2 whole area irradiated samples. (One-Way ANOVA showed an overall significance with F=134.226 and p=0.000. Scheffe's tests showed that there was statistical difference between all samples apart from AR:CWA17:CWA26:CWA34:CWA51 and CWA102:CWA128*p<0.5).*

It is clear from Figure 11.40 that for both the as-received sample (AR) and most of the CO_2 laser whole area irradiative processed samples the resulting ALP levels identified was significantly larger when compared to the negative control (NC). Compared to the as-received sample (AR) for the CO_2 laser whole area irradiative processed samples apart from CWA102 and CWA128 the ALP levels had increased by up to 15 RFU with the largest increase being given by sample CWA34. The results shown in Figure 11.40 suggest that specifically for the CO_2 laser whole area irradiative processing the ALP activity mirrors the cytotoxicity (see Figure 11.39). Due to the entire CO_2 laser whole area irradiative processed samples having an equivalent ALP Level of around 30 RFU. The decrease in ALP seen primarily through samples CWA102 and CWA128 could be attributed to the observed high cytotoxicity levels which can be explained through the material becoming more toxic through over-melting as discussed previously in this Section.

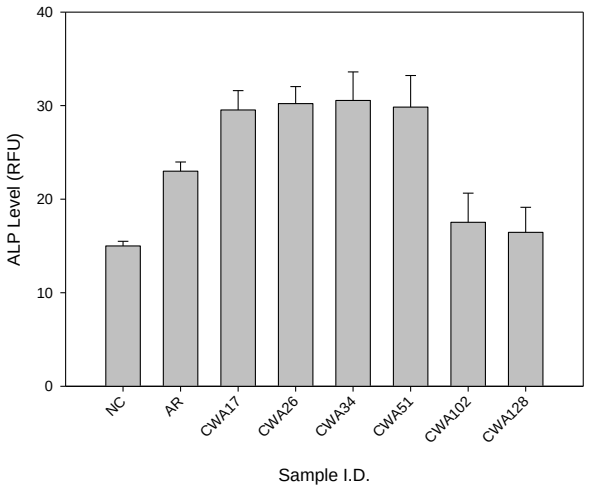

Figure 11.40 – Histogram showing the mean ALP levels for each of the CO_2 laser whole area irradiated samples.

*(One-Way ANOVA showed an overall significance with F=30.623 and p=0.002. Scheffe's tests showed that there was statistical difference between NC and all samples except CWA102 and CWA128. There was no statistical difference between the other samples*p<0.5).*

11.5.3 – Comparison Between CO_2 Laser-Induced Patterning and CO_2 Laser Whole Area Irradiative Processing

It has been seen that both the CO_2 laser-induced patterned and CO_2 laser whole area irradiative processed nylon 6,6 samples to some extent each had an effect on the cytotoxicity and ALP levels. From Figure 11.41(a) it can be seen that all CO_2 laser treated samples apart from samples CT100, CWA102 and CWA128 had the same cytotoxicity rating of around 18% compared to the as-received sample (AR). Whereas sample CT100 gave rise to a lower cytotoxicity of approximately 15% and samples CWA102 and CWA128 had the highest cytotoxicity level of around 53%. It would be significant to add here that cytotoxicity values of 18% and above which have been determined for most samples in this instance could have a large clinical relevance insofar as they appear to be high levels, even for the as-received sample. However, throughout this research it has been seen that the osteoblast cells still adhere and proliferate to some extent over both the as-received sample and all laser surface treated samples. Prior to *in vivo* applications, further *in vitro* experimentation should be carried out by repeating studies to confirm results obtained and to assess the response from other less robust cell types, such as fibroblast cells, to identify whether they can withstand the cytotoxicty levels.

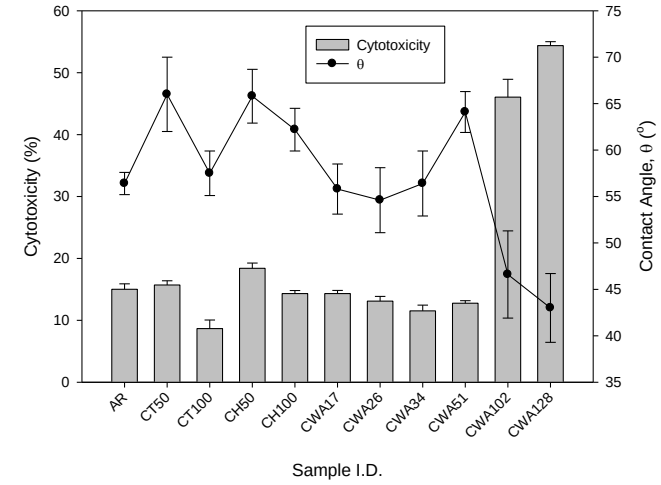

(a)

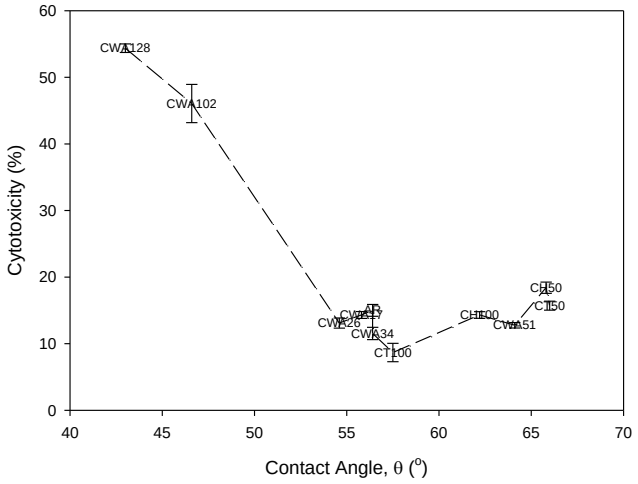

(b)

Figure 11.41 – (a) Histogram showing the cytotoxicity in relation to θ for all CO_2 laser processed samples, (b) graph showing the relationship between θ and cytotoxicity.

.

As one can seen from Figure 11.42(a), in comparison to the as-received sample (AR), the ALP level had increased for all of the CO_2 laser processed nylon 6,6 samples with the exception of sample CWA102 and CWA128 which had ALP levels of around 17 and 16 RFU, respectively. This can be attributed to the increase in cytotoxicity for these samples as shown in Figure 11.41(a) which would have hindered the ALP level. As all of the other CO_2 laser processed samples had increased ALP levels in comparison to the as-received sample (AR) this would explain the observed enhanced bioactivity in terms of cell cover density and cell count which was determined in Section 11.3 and Section 11.4. Furthermore, it can be seen from Figure 11.42(a) that the entire CO_2 laser processed samples, with the exception of sample CWA102 and CWA128, had equivalent levels of ALP. Again, this can be accounted for by the levels of cytotoxicity being equivalent, as can be seen in Figure 11.41(a).

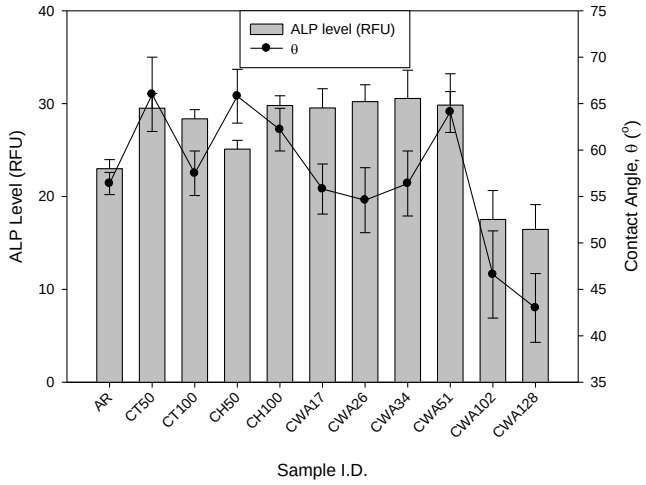

(a)

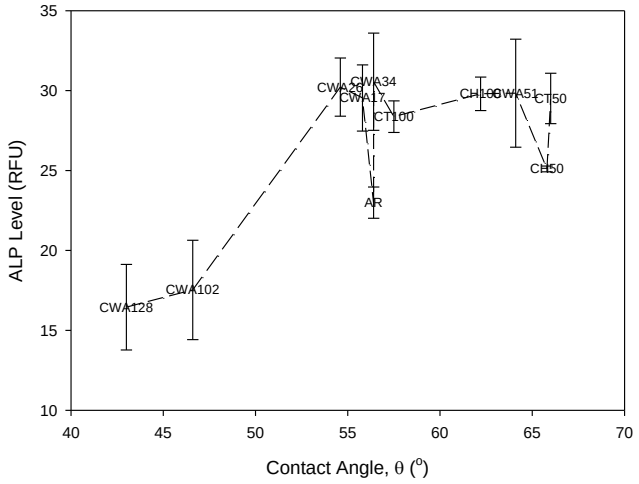

(b)

Figure 11.42 – (a) Histogram showing the ALP level in relation to θ for all CO_2 laser processed samples, (b) graph showing the relationship between θ and ALP level.

11.5.4 – Wettability Characteristics and Surface Parameters

11.5.4.1 - Cytotoxicity

From Figure 11.41(a), in terms of θ, it can be seen that the entire CO_2 laser surface processed samples with θ between 55 and 65° gave cytotoxicity levels equivalent to that as-received sample (AR). The two samples which had θ below this range; namely CWA102 and CWA128, were found to have considerably larger cytotoxicity levels which can be attributed to the samples becoming more toxic as discussed in Section 11.5.2. With this in mind, it is possible to deduce that below a certain threshold fluence (between 51 and 102 Jcm^{-2}), the surface parameters and wettability characteristics as described in Section 11.3.4 and Section 11.4.4 are more dominant in that θ, γ^P and surface oxygen content all have a strong link to forge the osteoblast cell response to the nylon 6,6 samples. Above this

threshold fluence it can be then said that, on account of the toxicity of the nylon 6,6 samples considerably increasing, the cytotoxicity dominates the bioactivity of the nylon 6,6 hindering the osteoblast cell growth and proliferation.

Figure 11.41(b) indicates that there could be a possible correlative trend between the cytotoxicity and θ for the CO_2 laser processed samples. This is due to the fact that the cytotoxicity starts high at around 55% for low θ of between 40 and 45°, then begins to decrease upon an increase in θ. The correlation shown in Figure 11.41(b) suggests that θ could hold the potential to be used to predict whether CO_2 laser processed nylon 6,6 will provide a sufficient surface for osteoblast cell growth. Furthermore, even though it has been proposed that the cytotoxicity dominates for larger fluences, it can still be seen that θ could still play a distinct role in predicting the osteoblast cell response to the CO_2 laser modified nylon 6,6, especially for the CO_2 laser whole area irradiative processed samples, as the combination of surface roughness and surface chemistry which gives rise to the toxicity could have contributed to the observed θ.

Figure 11.43(a) allows one to see that for all of the CO_2 laser processed samples there was not a clear correlative relationship between γ^P and the cytotoxicity for each of the nylon 6,6 samples. This is on account of the cytotoxicity levels staying constant around 15% for γ^P between 10 and 20 mJm^{-2}. Having said that, from Figure 11.43(b) it is shown that by putting the cytotoxicity levels in order of γ^P for the entire CO_2 laser processed samples the cytotoxicity remains between 10 and 20% until γ^P increased beyond 20 mJm^{-2} at which point the cytotoxicity rose suddenly to 50% around 30 mJm^{-2}. As a result, Figure 11.43(b) shows an inverse relationship of what was observed with θ (see Figure 11.41(b)) and can be explained by the strong relationship between θ and γ^P discussed in Chapter 6 and Chapter 10. With this relationship in mind, it is possible to see that θ or γ^P has the potential to predict the cytotoxic nature of the CO_2 laser processed samples even though for those samples with large fluences (CWA102 and CWA128) the cytotoxicity dominates the osteoblast cell response. As discussed previously, this is on account of θ and γ^P arising from the surface parameters which made the nylon 6,6 samples too toxic to elicit an enhanced osteoblast cell response.

Figure 11.44(a) shows that γ^T did not have any distinct connection with the measured cytotoxicity for the CO_2 laser processed samples. This is on account of the cytotoxicity remaining constant even though a large variation in γ^T was measured. Furthermore, this can also be seen in Figure 11.44(b) in that the cytotoxicity does not follow any particular trend on account of an increase in γ^T. These results given in Figure 11.44(a) and Figure 11.44(b) correspond with the other osteoblast cell responses studied in Sections 11.2.4, 11.3.4 and 11.4.4 in that γ^T, unlike θ and γ^P, does not play a role in the determination of the biofunctionality of CO_2 laser surface treated nylon 6,6 in terms of osteoblast cell response and apatite layer formation.

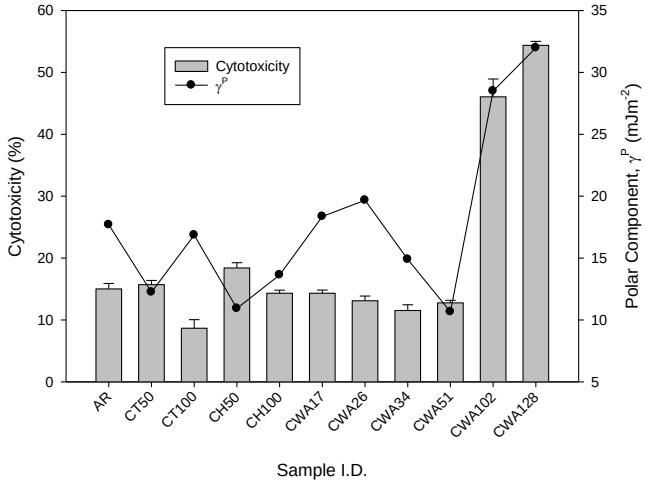

(a)

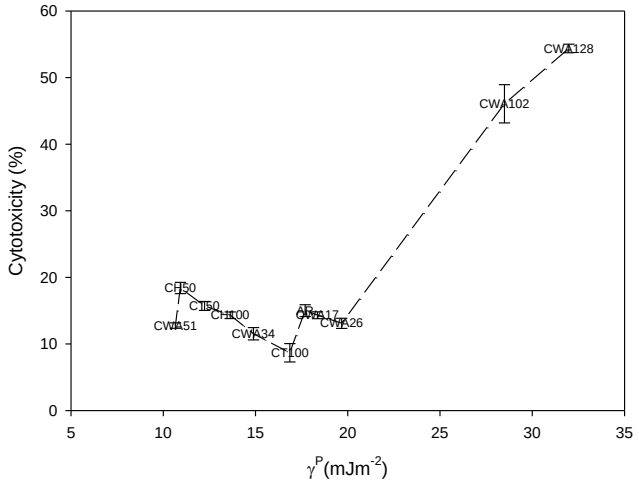

(b)

Figure 11.43 – (a) Histogram showing the cytotoxicity in relation to γ^P for all CO_2 laser processed samples, (b) Graph showing the relationship between γ^P and cytotoxicity.

In terms of surface roughness, Figure 11.45(a) shows that there could have been a relationship between Ra and the cytotoxicity of the CO_2 laser processed samples. For instance it can be seen from Figure 11.45(a) that similar values of between 0 and 0.2 µm for Ra correlated with a constant cytotoxicity of 15%. Also, upon a large increase in Ra of up to 1.3 µm the cytotoxicity followed suit by trebling to around 50%. It should also be noted here that Figure 11.45(b) further implies this trend. This can be seen to be of some significance as other osteoblast cell responses such as cell cover density (see Section 11.3.4) and cell count (see Section 11.4.4) did not have a correlation with Ra. Having said that it may be possible to use Ra to indirectly determine the cytotoxicity of nylon 6,6 having undergone CO_2 laser whole area processing as a large increase in surface roughness suggests that significant melting has taken place which would lead to more evolved gases and an increase in toxicity, as discussed in Section 11.5.2. Even so, by comparing Figures 11.41(b), 11.43(b) and 11.45(b) one can ascertain that the correlation with cytotoxicity is stronger for θ and γ^P indicating that

Ra may not be the optimum parameter to use in order to predict the cytotoxicity of the CO_2 laser processed nylon 6,6 samples.

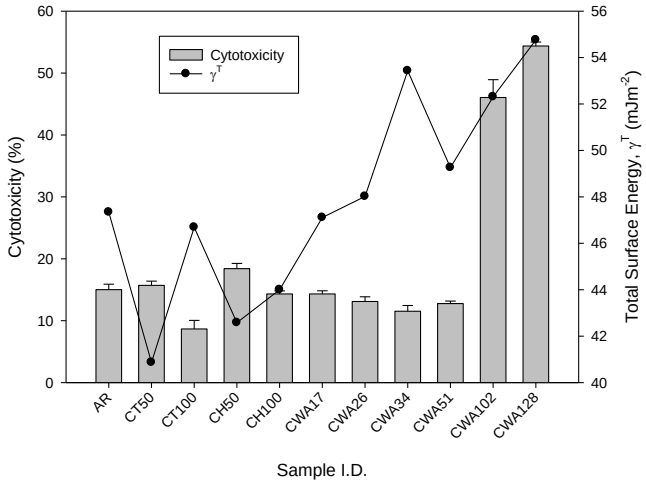

(a)

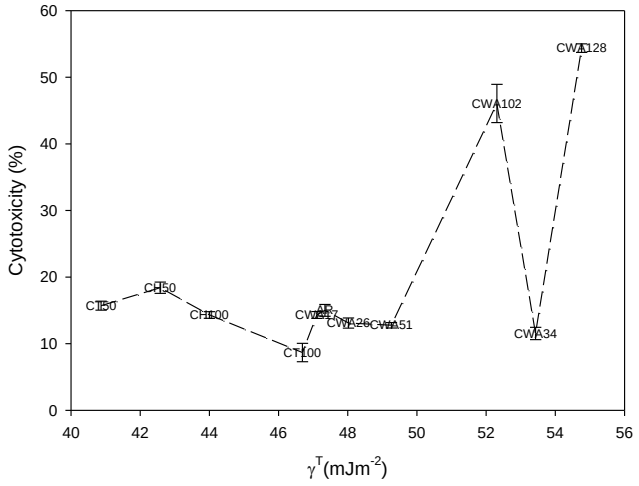

(b)

Figure 11.44 – (a) Histogram showing the cytotoxicity in relation to γ^T for all CO_2 laser processed samples, (b) graph showing the relationship between γ^T and cytotoxicity.

Analogous to Ra (see Figure 11.45), Sa shown in Figure 11.46(a) also seemed to have a correlative trend with the measured cytotoxicity insofar as low similar values between 0 and 1 μm for Sa corresponded with the lowest constant values of 15% cytotoxicity which was found for almost all of the samples. A significant increase in Sa can also be seen in Figure 11.46(a) to follow a trend in that the cytotoxicity significantly increases which can be further confirmed using Figure 11.46(b). As with Ra (see Figure 11.45) it is possible to deduce that the surface roughness may hold a possible correlation with cytotoxicity and that both Ra and Sa could possibly be used to predict how osteoblast cell will react in terms of toxicity. However, as discussed previously for Ra, the surface roughness does not have as strong a correlation as was found for θ and γ^P in terms of osteoblast cell response (also see Section 11.3.4 and Section 11.4.4) indicating that surface roughness may not be the best

parameter to implement in predicting the osteoblast cell biofunctionality of CO_2 laser processed nylon 6,6.

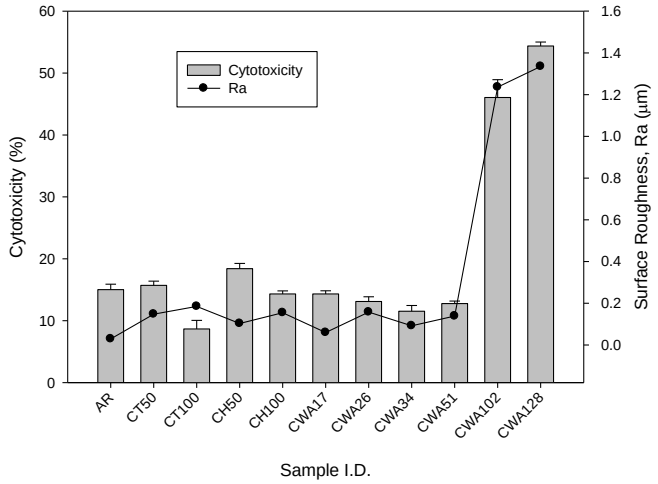

(a)

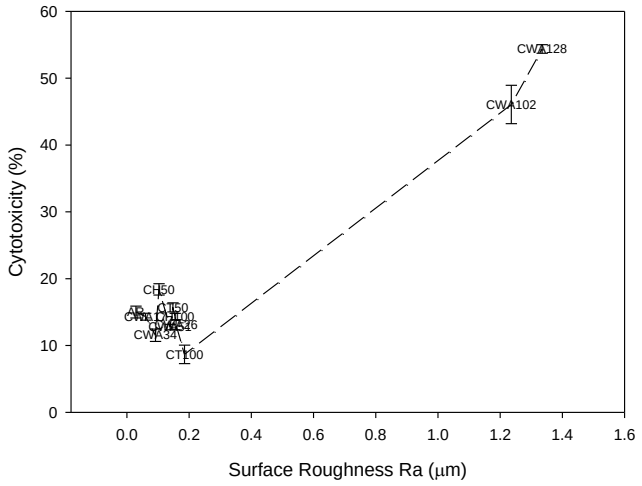

(b)

Figure 11.45 – (a) Histogram showing the cytotoxicity in relation to Ra for all CO_2 laser processed samples, (b) graph showing the relationship between Ra and cytotoxicity.

The surface oxygen content, as shown in Figure 11.47(a), had a relatively strong correlation with the cytotoxicity level measured for the CO_2 laser processed nylon 6,6 samples, which can also be confirmed from Figure 11.47(b). As such, from the histogram (see Figure 11.47(a)) and trend graph (see Figure 11.47(b)) it can be seen that the cytotoxicity levels for between 13 and 16 %at. surface oxygen content remained constant at around 15%. By increasing the surface oxygen content beyond 16 %at. the cytotoxicity was found to increase significantly. These results shown in Figure 11.47 allow one to see that the surface oxygen content, like θ (see Figure 11.41) and γ^P (see Figure 11.43), could be used to indirectly determine the cytotoxic nature of CO_2 laser whole area irradiative processed nylon 6,6. This is on account of the fact that upon melting and re-solidification, from the laser-material interaction, oxidation takes place giving rise to an increase in surface oxygen content.

However, by melting the nylon 6,6 with large fluences in addition to more surface oxidation occurring, it is necessary to note that more evolved toxic gases would become present, as discussed in Section 11.5.2. These toxic substances would then increase the toxicity of the nylon 6,6 even though an increase in surface oxygen content is apparent. Following on, this would explain the increase in surface oxygen content and cytotoxicity with those samples with considerably large fluences (CWA102 and CWA128).

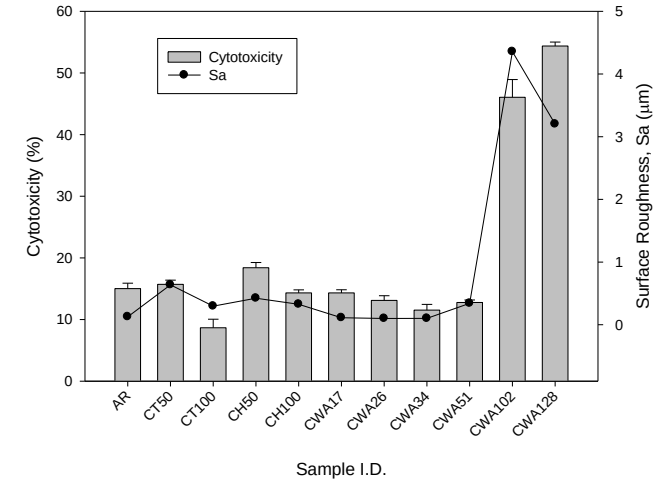

(a)

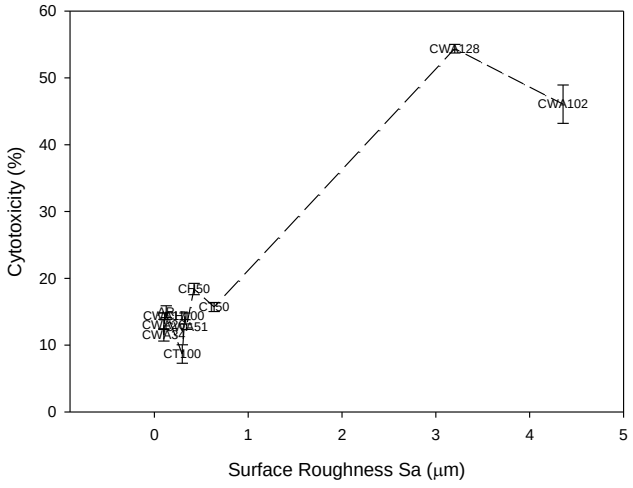

(b)

Figure 11.46 – (a) Histogram showing the cytotoxicity in relation to Sa for all CO_2 laser processed samples, (b) graph showing the relationship between Sa and cytotoxicity.

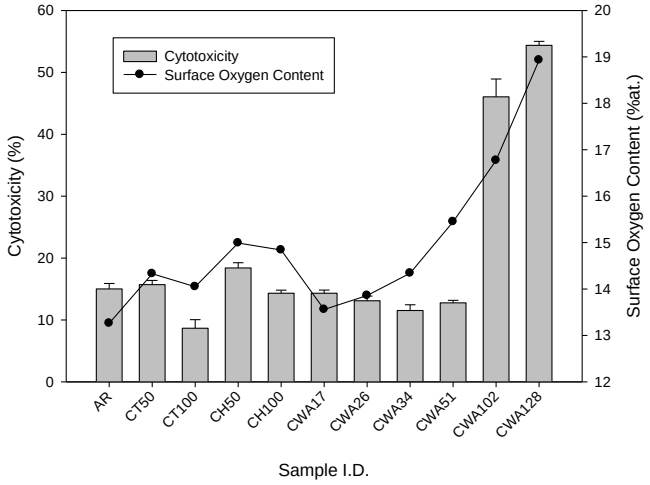

(a)

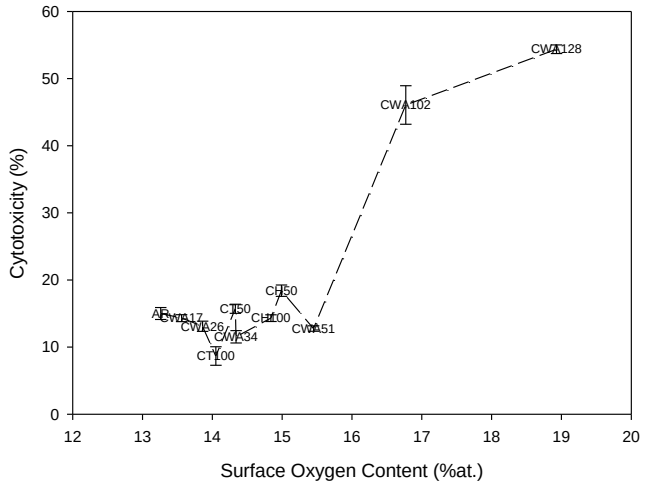

(b)

Figure 11.47 – (a) Histogram showing the cytotoxicity in relation to surface oxygen content for all CO_2 laser processed samples, (b) graph showing the relationship between surface oxygen content and cytotoxicity.

11.5.4.1 – Alkaline Leukocyte Phosphatase (ALP) Levels

From Figure 11.42 it can be seen that on the whole the relationship between ALP level and θ mirrored what was observed with the cytotoxicity (see Figure 11.41(a)). That is, the ALP level remained somewhat constant around 30 RFU for those CO_2 laser processed samples with θ between 55 and 65°, then suddenly decreasing as θ decreased. As seen with the cytotoxicity, sample CWA102 and sample CWA128, which had θ of less than 50° could highlight a possible threshold by which one can predict the osteoblast cell response. In reality however it would be more reasonable to believe that in this case the hindrance of the osteoblast cell response was more likely to be on account of an increase in cytotoxicity as seen in Figure 11.41(a) which can be attributed to an increase in toxicity following the CO_2 laser processing with high fluences (102 and 128 Jcm^{-2}), as discussed in Section 11.5.2. Having said that, like with the cytotoxicity as shown in Figure 11.41(a), θ still appears to be an attractive

means of predicting the bioactive nature of nylon 6,6 owed to the fact that the combination of surface roughness and surface chemistry modifications, arising from the CO_2 laser processing, which contribute to the increase in toxicity would have given rise to the observed θ.

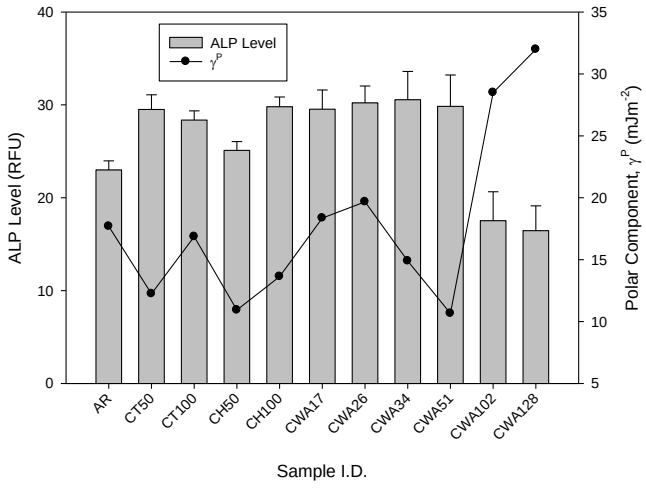

(a)

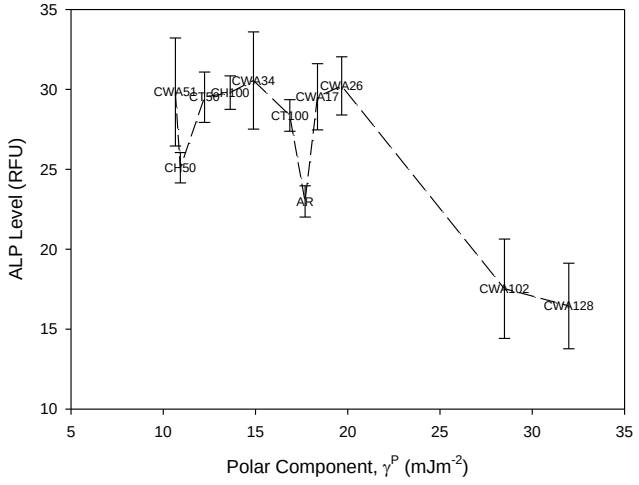

(b)

Figure 11.48 – (a) Histogram showing the ALP level in relation to γ^P for all CO_2 laser processed samples, (b) graph showing the relationship between γ^P and ALP level.

Figure 11.48(a) and Figure 11.48(b) show that the relationship between the ALP level and γ^P was the inverse of the relationship observed between the cytotoxicity and γ^P (see Figure 11.43). Initial γ^P values between 10 and 20 mJm^{-2} correlated with the constant ALP level in the region of 25 to 30 RFU. For larger values of γ^P, beyond 20 mJm^{-2}, it can be seen from Figure 11.48(b) that the ALP level reduced considerably. On account of this, γ^P could be used to predict the ALP levels for CO_2 laser processed samples even though an increase in cytotoxicity is proposed to be the main driving force in the reduction of the ALP level for sample CWA102 and sample CWA128. This is explained by the surface parameters giving rise to the toxic nylon 6,6 surface, as discussed in Section 11.5.2, potentially playing a role in determining the value of γ^P.

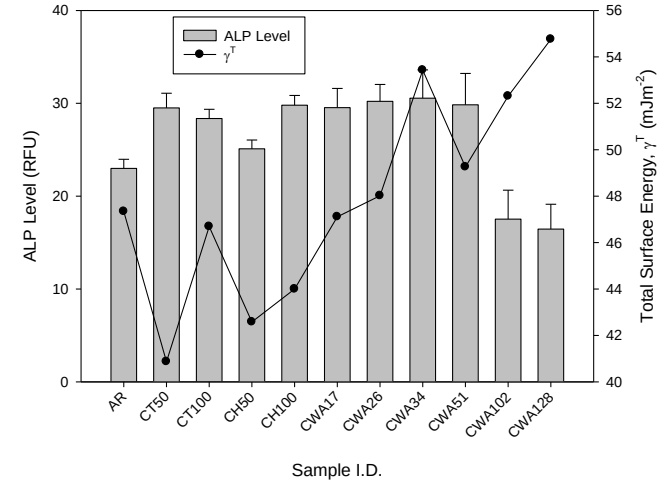

(a)

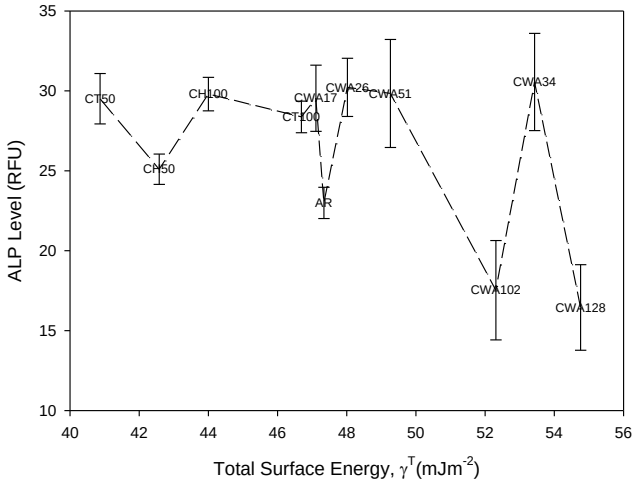

(b)

Figure 11.49 – (a) Histogram showing the ALP level in relation to γ^T for all CO_2 laser processed samples, (b) graph showing the relationship between γ^T and ALP level.

It can be seen using Figure 11.49(a) and Figure 11.49(b) that γ^T did not have a correlation with the measured ALP level of the CO_2 laser processed samples. This is owed to the fact that Figure 11.49(b) shows that for increasing values of γ^T the ALP level did not follow any particular trend. This further corroborates with what has been observed in Sections 11.3.4, 11.4.4 and 11.5.4.1 in that γ^T does not play a major role in determining the osteoblast cell response to the CO_2 laser processed samples.

Figure 11.50(a) allows one to see that surface roughness may have had a trend linked with the ALP levels for the CO_2 laser processed samples, such that for Ra values between 0 and 0.2 µm the ALP levels generally were around 30 RFU. With those samples which had large Ra values of up to 1.4 µm (CWA102 and CWA128) the ALP level was seen to decrease considerably which can be attributed to the cytotoxicity level being very high for these samples as discussed in Section 11.5.4.1. From this one can extrapolate that by using Ra it may be possible to predict the ALP level, especially for those

samples which had undergone CO_2 laser whole area irradiative processing, on account of a significant increase in incident fluence gave rise to a large Ra through melting. As discussed in Section 11.5.2, through the melting and re-solidification of the nylon 6,6 using the incident CO_2 laser beam, toxic substances were likely to be present on the surface giving rise to the high cytotoxicity rating and low ALP levels for samples CWA102 and sample CWA128. With this in mind, as the surface became rougher through excessive melting, Ra could be used to indirectly predict whether a CO_2 laser whole area irradiative processed sample would give rise to an enhanced osteoblast cell response. Having said that, like the cytotoxicity discussed in Section 11.5.4.1, θ (see Figure 11.42) and γ^P (see Figure 11.48) seem to be a more attractive means of predicting bioactivity on account of them having stronger correlations with cell cover density (see Section 11.3), cell count (see Section 11.4), cytotoxicity (see section 11.5.4.1) and ALP level.

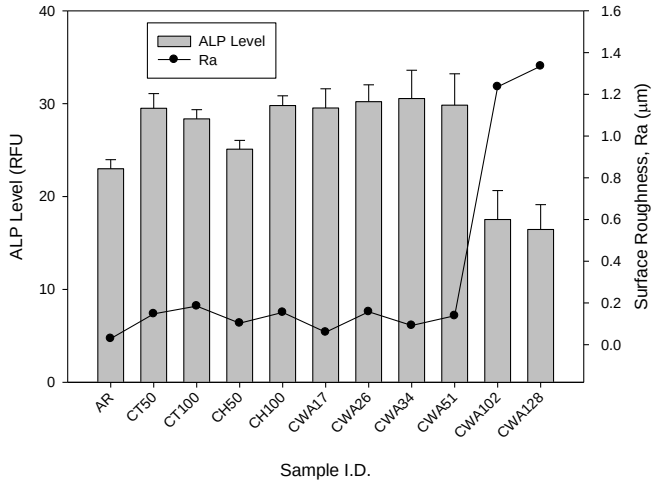

(a)

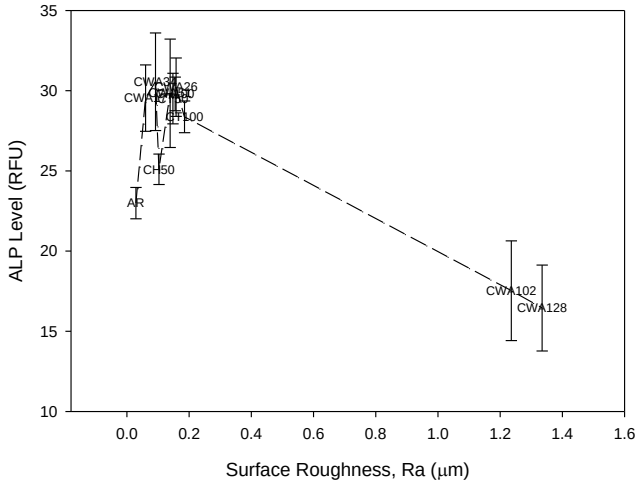

(b)

Figure 11.50 – (a) Histogram showing the ALP level in relation to Ra for all CO_2 laser processed samples, (b) graph showing the relationship between Ra and ALP level.

A similar trend as seen with Ra (see Figure 11.50(a)) was found between Sa and the ALP level as shown in Figure 11.51(a) in that small similar values of Sa around 0.5 µm appeared to correlate with similar values of ALP levels of approximately 30 RFU. A significant increase in Sa for sample CWA102 and sample CWA128 can also be seen to follow a similar trend to that seen for Ra (see Figure 11.50(a) such that the ALP level decreased for these samples. Figure 11.51(b) further shows this trend by ordering the ALP levels for each sample in terms of Sa. As discussed previously for Ra, an explanation for the observed reduction in ALP level upon an increase in Sa is that the surface roughness had increased *via* considerable melting, which in turn increases the toxicity (see Section 11.5.2) allowing the samples to become less bioactive. What is more, the results shown in Figure 11.51 give further evidence that for large increases in surface roughness the Ra and Sa could be used to indirectly predict what will happen to the cytotoxicity and ALP levels of CO_2 laser processed nylon 6,6 samples.

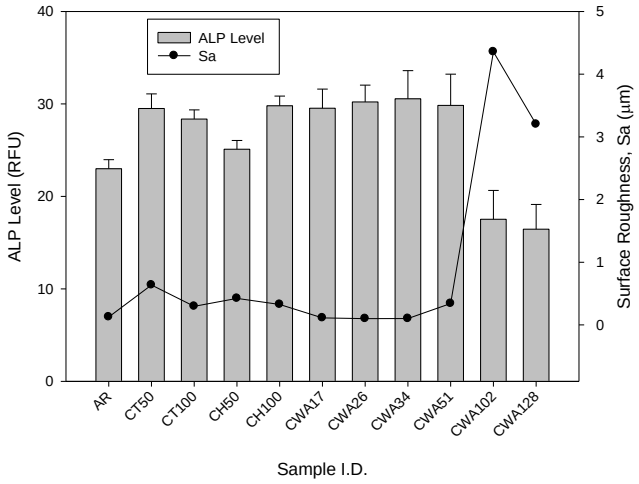

(a)

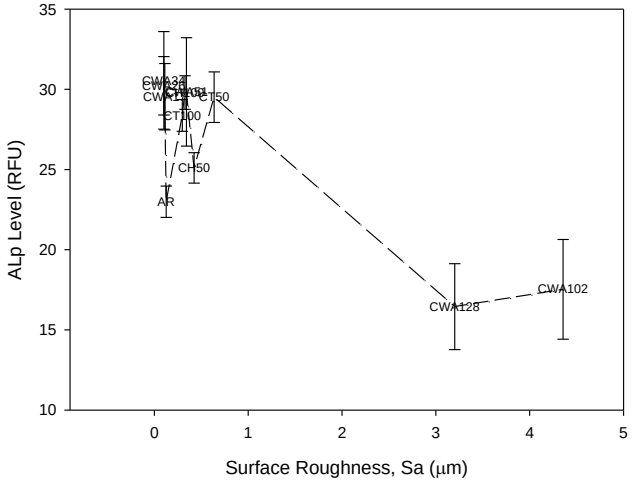

(b)

Figure 11.51 – (a) Histogram showing the ALP level in relation to Sa for all CO_2 laser processed samples, (b) graph showing the relationship between Sa and ALP level.

As shown in Figure 11.52(a) and Figure 11.52(b) there was less correlation between the surface oxygen content and ALP level than was seen with the surface oxygen content and cytotoxicity (see Section 11.5.4.1). That is, using Figure 11.52(b) it can be seen that 13 to 16 %at. surface oxygen content values gave rise to ALP levels between 22 and 30 RFU. Having said that, it was found that for surface oxygen contents greater than 16 %at. the ALP level reduced considerably by approximately half of the maximum ALP level achieved (30 RFU). This again shows that large fluences had a large impact upon the osteoblast cell response to the nylon 6,6 samples such that on account of an increase in cytotoxicity, as discussed in Section 11.5.2, the ALP level inherently decreased and the samples became less enhanced in terms of osteoblast cell response. What is more, on account of the link between the increase in surface oxidation and the increase in toxic substances resulting from excessive melting, which was discussed in Section 11.5.4.1, surface oxygen could potentially be used as a predictive precursor of the osteoblast cell response to the CO_2 laser processed nylon 6,6 samples in terms of cytotoxicity and ALP levels.

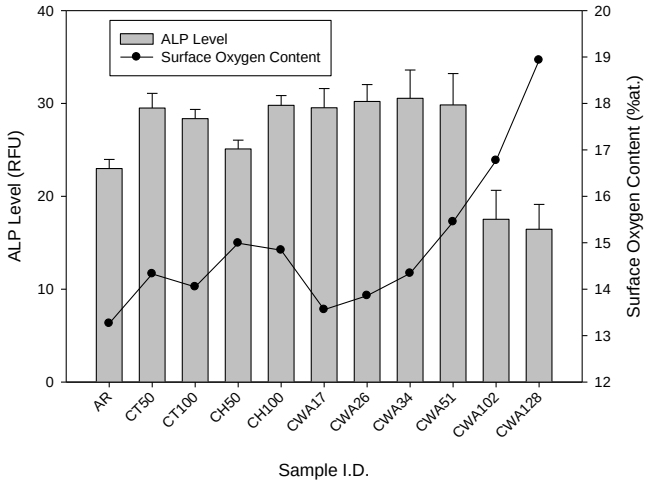

(a)

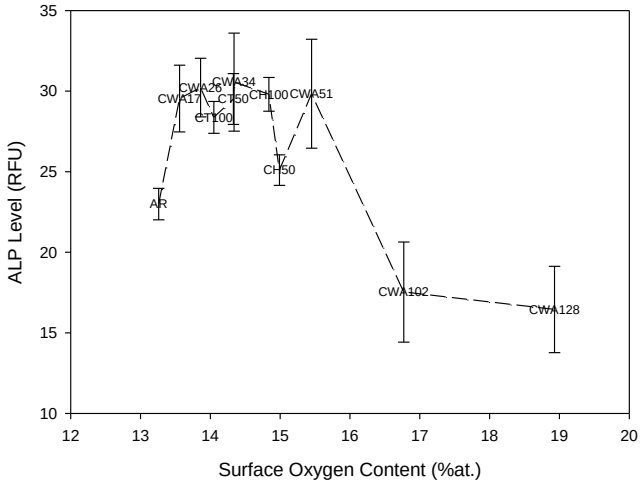

(b)

Figure 11.52 – (a) Histogram showing the ALP level in relation to surface oxygen content for all CO_2 laser processed samples, (b) graph showing the relationship between surface oxygen content and ALP level.

11.6 – Effects of Laser-Induced Cytotoxicity on Osteoblast Cell Response and Alkaline Leukocyte Phosphatase (ALP) Level

Figure 11.53(a) shows a histogram of the cytotoxicity in relation to the cell count and ALP level allowing one to see that the ALP level to a certain extent follows the inverse trend as the cytotoxicity. For instance, samples CH50, CWA102 and CWA128 all have increased cytotoxicity levels in comparison to the other samples and as such gives rise to a reduction in the ALP level as discussed in Section 11.5.4.2. On the other hand, it can be seen from Figure 11.53(a) that the cell count does not correspond with the cytotoxicity for the CO_2 laser-induced patterned samples and the CO_2 laser whole area irradiative samples with the exception of sample CWA102 and CWA128. This indicates that below a threshold fluence of between 51 and 102 Jcm^{-2} the cytotoxicity does not appear to dominate the osteoblast cell response. With this in mind, it is evident from the results shown in Figure 11.53(a) and the results presented in Sections 11.3.4, 11.4.4 and 11.5.4 that θ, γ^P and the surface oxygen content played a major role in the bioactivity of the CO_2 laser whole area irradiative processed nylon 6,6 for those samples which had incident fluences of 51 Jcm^{-2} or less. Above the fluence of 51 Jcm^{-2} it is reasonable to say that, as discussed in Section 11.5.2, the nylon 6,6 became excessively toxic, giving rise to a less enhanced osteoblast cell response. This is a highly significant result as it allows one to deduce that the surface parameters and wettability characteristics play a role in the osteoblast cell response to the nylon 6,6 until the toxicity becomes too great, at which time, the cytotoxicity and consequently dominates hindering osteoblast cell response.

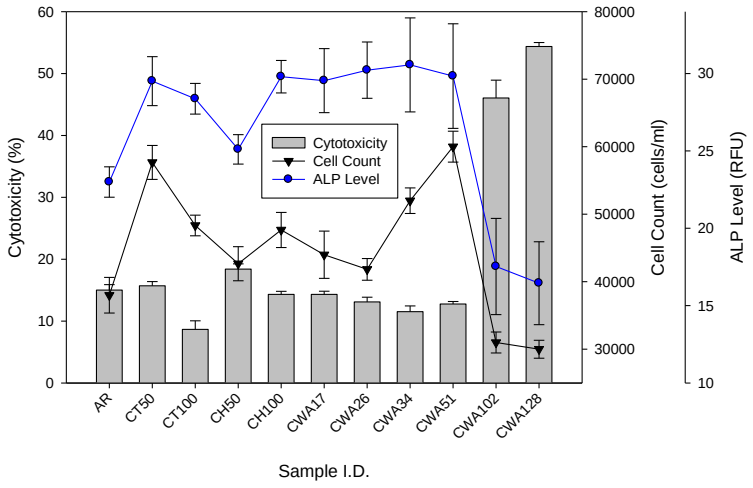

(a)

Figure 11.53 continued overleaf

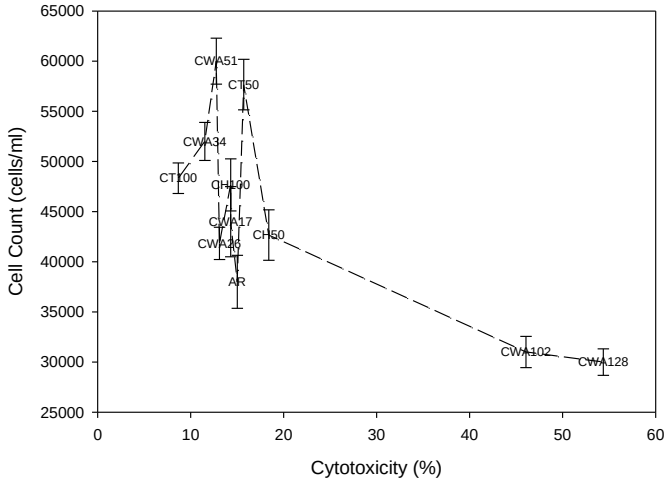

(b)

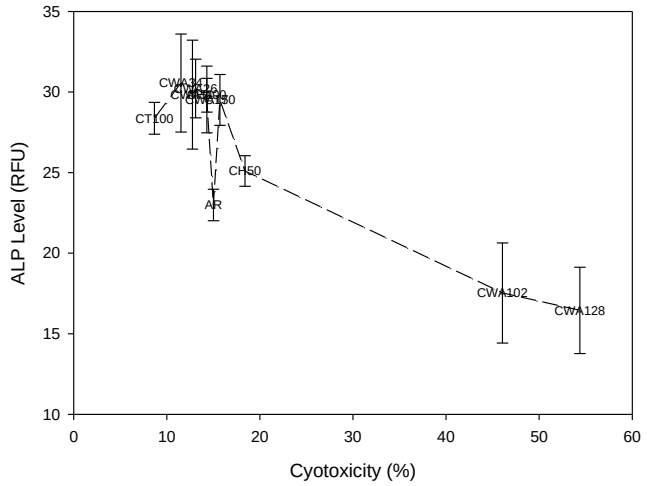

(c)

Figure 11.53 – (a) Histogram showing the cytotoxicity in relation to cell count and ALP for all CO_2 laser processed samples, (b) graph showing the relationship between cell count and cytotoxicity and (c) graph showing the relationship between ALP level and cytotoxicity.

Figure 11.53(b) further confirms that the cell count did not follow a trend in terms of cytotoxicity, with those samples which had cytotoxicity levels between 10 and 20 %at. can be seen to have had large variations in cell count, between 40,000 and 60,000 cells/ml. In contrast, Figure 11.53(c) further highlights that the ALP level for the CO_2 laser processed samples was a decreasing function of cytotoxicity. Throughout Section 11.3 and Section 11.4 it has been seen that for most of the CO_2 laser whole area processed nylon 6,6 samples the osteoblast cell response was enhanced in comparison to the as-received sample, indicating that the ALP level was sufficient to promote osteoblast cell adhesion and proliferation. It should also be noted here that even though the CO_2 laser-induced patterned samples did not appear to follow any trend with regards to surface parameters and wettability characteristics, the samples did follow the measured cytotoxicity and ALP levels apart

from sample CT100 (see Figure 11.53(a)). This is significant because of the CO_2 laser-induced patterning only irradiating certain sections of the nylon 6,6, whilst leaving other un-irradiated sections in order to generate the patterns. This would allow both laser irradiated and un-irradiated nylon 6,6 to come into contact with the seeded cells. As such, in the un-irradiated sections the cell will act as they would do on an as-received sample. This along with the change in wetting regime discussed in Chapter 6 is likely to have a major effect on the osteoblast cells and can account for those samples not following the trends exhibited by the CO_2 laser whole area irradiative processed nylon 6,6 samples.

12
The Effects of KrF Excimer Laser Processing on the Bioactivity of Nylon 6,6 with Reference to Wettability

In this chapter the results obtained from the biological testing of nylon 6,6 samples which had undergone KrF excimer laser-induced patterning and KrF excimer laser whole area irradiative processing are presented and discussed. This includes SBF response, normal human osteoblast response, cytotoxicity analysis and ALP activity analysis.

12.1 – Introduction

With respect to a biomaterial, various materials such as metals, ceramics and polymers have been used for biomedical implants [4,27,154,183]; however, for polymers it has been identified that they are not bioactive materials owed to insufficient surface properties [4,52]. On account of this many have endeavoured to vary the surface properties of polymers in order to modify the surface characteristics to achieve an enhanced cell response [27,30,103,132,184]. Laser surface treatment offers numerous advantages such as it can be accurate, precise and non-contact allowing one to see that this can be a relatively clean process. This can be seen as an ideal opportunity for the biomedical industry in that a clean process would require considerably less post processing.

On account of the fact that excimer lasers offer a unique, repeatable means of modifying the surface of nylon 6,6 as seen in Chapter 7, this Chapter discusses the results achieved by using KrF excimer laser processing of nylon 6,6 to modulate apatite layer response, osteoblast cell response, cytotoxicity levels and ALP activity. The techniques used to obtain the results can be found in Chapter 5.

12.2 – Effects of KrF Excimer Laser Processing of Nylon 6,6 on Apatite Layer Response

This section details the results obtained on the formation of an apatite layer response resulting from KrF excimer laser processing of nylon 6,6 which has been immersed in SBF for 14 days. The experimental technique can be found in Chapter 5.

12.2.1 – KrF Excimer Laser-Induced Patterning

Following the immersion in SBF for 14 days it was seen that for each of the KrF excimer laser-induced patterned samples sediment had formed on the surfaces of the nylon 6,6 samples (see Figure

12.1). Also, there appears to be more sediment on the KrF excimer laser-induced patterned samples (see Figure 12.1) in comparison to the as-received sample (see Figure 11.1(a)) indicating that the KrF excimer laser-induced patterned samples could employed for a more enhanced osteoblast cell response. Furthermore, it can be seen from the SEM micrographs in Figure 12.1 that the sediment in the most part was formed in the trenches formed by the excimer laser beam further indicating that this may give rise to cell growth directionality. From the results shown in Figure 12.1 the initial tests using SBF highlighted the potential for using excimer laser processing of nylon 6,6 for enhanced osteoblast cell response and that the UV laser modified surfaces, in this instance, could give rise to more efficient cell adhesion and proliferation.

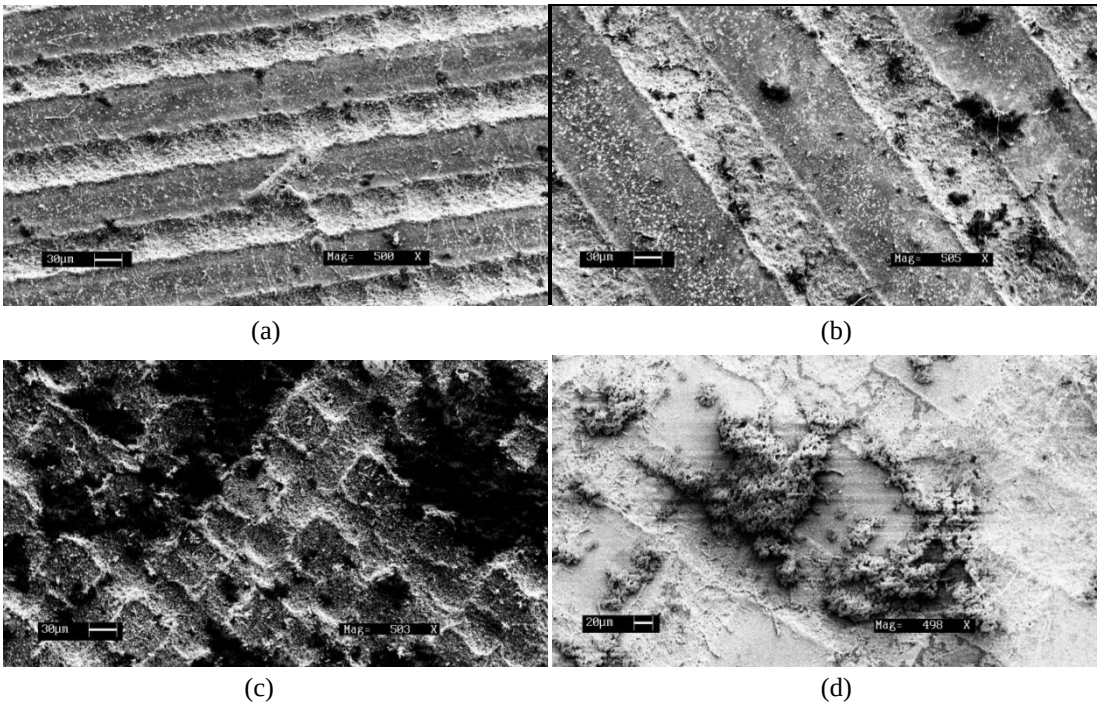

Figure 12.1 –SEM micrographs for (a) ET50, (b) ET100, (c) EH50 and (d) EH100 after immersion in SBF for 14 days.

Figure 12.2 shows a histogram giving Δg for all of the KrF excimer laser-induced patterned nylon 6,6 samples in comparison to the as-received sample (AR). From this Histogram on can see that on the most part Δg had increased for all of the KrF excimer laser-induced patterned samples with the largest Δg of approximately 0.032 g being achieved with the 50 µm trench sample (ET50). Comparing the KrF excimer laser-induced patterned samples, the two samples which gave the smallest Δg of around 0.2 g were that of the hatch patterned samples (EH50 and EH100). Even so, it can be seen from Figure 12.2 that these samples gave Δg slightly higher than the as-received sample (AR) which had a Δg in the region of 0.017 g. A possible explanation for the hatch patterned samples (EH50 and EH100) giving such a low response in terms of the apatite formation compared to the trench patterned samples (ET50 and ET100) is that of a likely change in wetting regime as discussed in Chapter 7. That is, for the hatch patterned samples if a mixed-state wetting regime was dominant then this would reduce the adhesion characteristics of certain areas of the nylon 6,6 samples. However, in those areas

were the Wenzel regime is more distinct then the apatite could have formed more preferentially on these regions giving rise to the slight increase in Δg observed when compared to the as-received sample (AR).

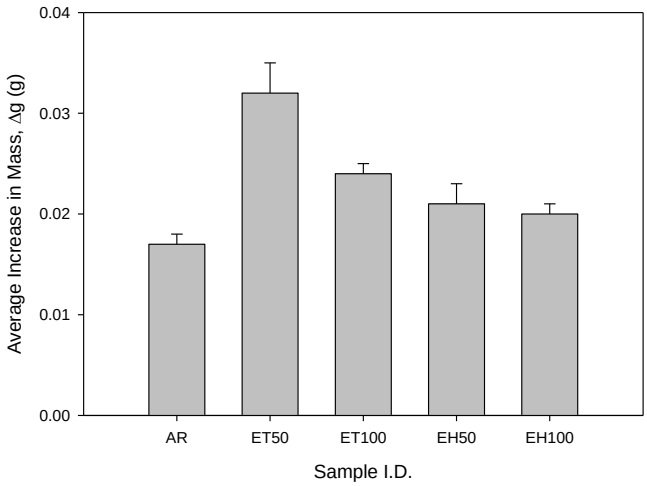

Figure 12.2 – Histogram showing Δg for the KrF excimer laser-induced patterned nylon 6,6 samples following 14 days immersed in SBF.

12.2.2 – KrF Excimer Laser Whole Area Irradiative Processing

It can be seen from Figure 12.3 that following 14 days of immersion in SBF each of the KrF excimer laser whole area irradiative processed samples promoted the adhesion of apatite sediment. In addition to this, when compared to the as-received sample (see Figure 11.3(a)) the KrF excimer laser whole area irradiative processed samples gave rise to considerably more sediment to form on the nylon 6,6 surface. Furthermore, Figure 12.3 identifies that those samples with the largest amount of incident pulses (EWA250_500 and EWA250_1000) gave rise to significantly more sediment compared to any of the other KrF excimer laser whole area irradtiative processed and as-received samples.

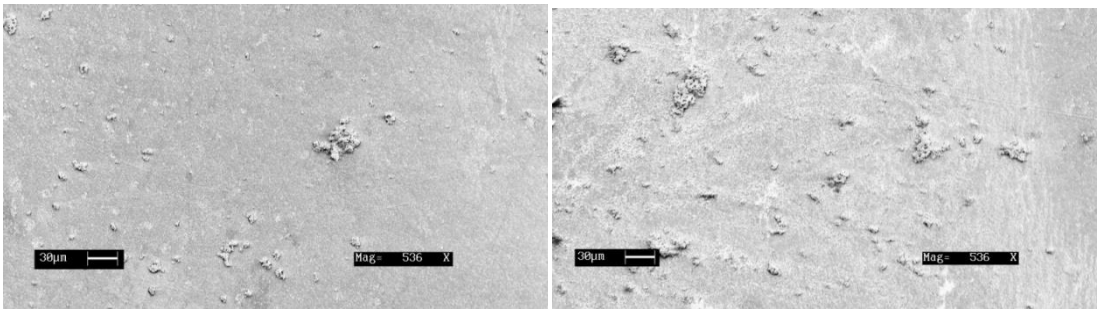

(a) (b)

Figure 12.3 continued overleaf

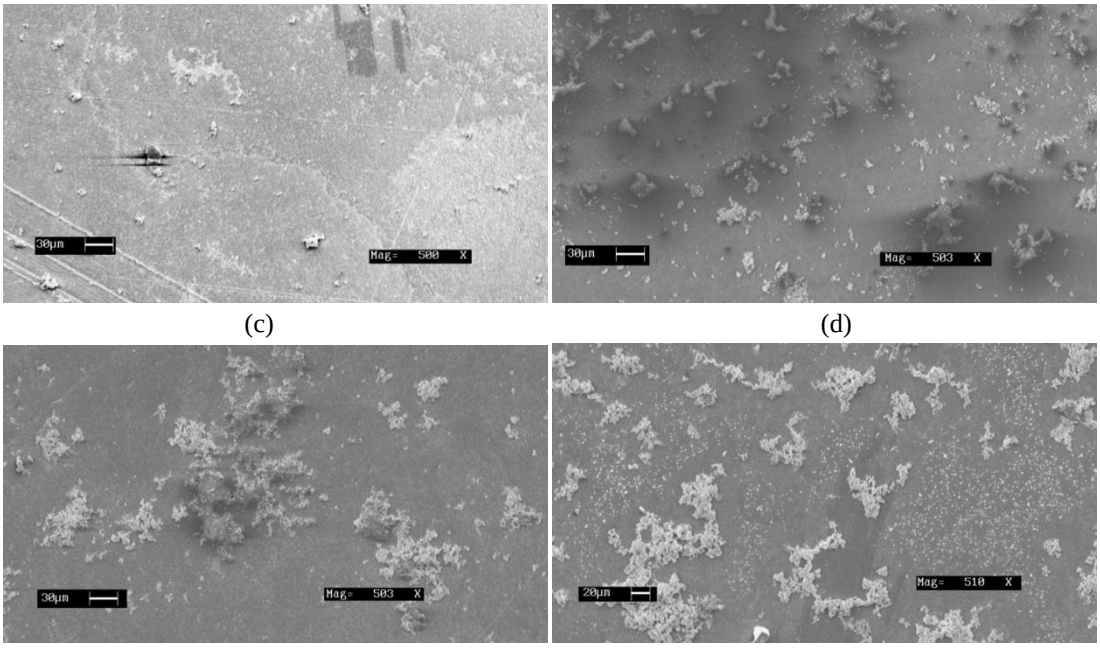

Figure 12.3 – SEM micrograph of all samples (a) EWA100 (b) EWA150, (c) EWA200, (d) EWA250, (e) EWA250_500 and (f) EWA250_1000 immersed in SBF after 14 days.

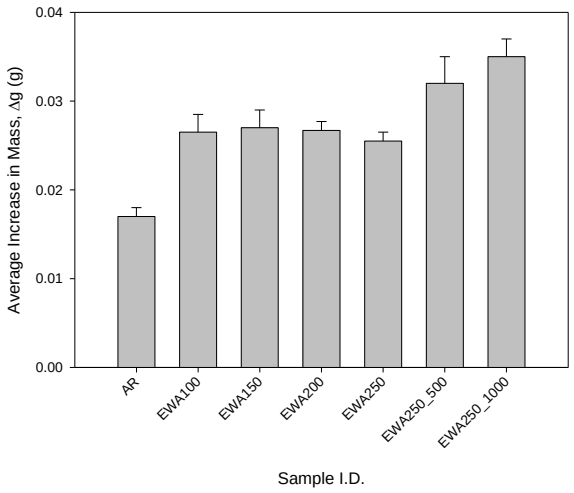

Figure 12.4 – Histogram showing Δg for the KrF excimer laser whole area irradiative processed nylon 6,6 samples following 14 days immersion in SBF.

It was further confirmed from Figure 12.4 that the KrF excimer laser whole area irradiative processed nylon 6,6 samples gave rise to an increase in apatite sediment formation compared to the as-received sample (AR): due to the entire KrF excimer laser whole area irradiative processed samples giving a Δg of at least 0.025 g in comparison to the as-received sample (AR) in which Δg was determined to be 0.017 g. The two largest increases of Δg were obtained by samples EWA250_500 and EWA250_1000 with 0.033 and 0.035 g, respectively. This indicates that more incident pulses on the nylon 6,6 gives rise to a surface which promotes better apatite sediment formation. What is more,

Figure 12.4 allows one to see that for samples EWA100, EWA150, EWA200 and EWA250 Δg remained somewhat unchanged at around 0.027 g and may be accounted for by the similar surface parameters and wettability characteristics which were determined in Chapter 7. Further consideration into this will be discussed in Section 12.2.4. Even though for the majority of the KrF excimer laser whole area irradiative samples Δg remained constant, results shown in Figure 12.3 and Figure 12.4 suggest that compared to the as-received sample, KrF excimer laser whole area irradiative processing of nylon 6,6 could be implemented to significantly increase the bioactivity in terms of osteoblast cell response.

12.2.3 – Comparison Between KrF Excimer Laser-Induced Pattering and KrF Excimer Laser Whole Area Irradiative Processing

Figure 12.5(a) shows that each of the KrF excimer laser processed samples gave rise to an increase in Δg compared to the as-received sample (AR) which confirms that more sediment had formed on the KrF excimer laser surface treated nylon 6,6 samples. The largest observed Δg compared to the as-received sample (AR) and other KrF excimer laser processed samples was found to be obtained for sample EWA250_1000. This could be attributed to the fact that this sample received 1000 incident pulses which was considerably more than any of the other KrF excimer laser processed samples which had either 10, 100 or 500 incident pulses. The smallest increase when taking into consideration the KrF excimer laser processed samples was found to be given for samples ET100, EH50 and CH100 with a mass difference of around 0.02 g. This could be significant as with the exception of sample ET50, all of the KrF excimer laser-induced patterned nylon 6,6 samples gave rise to a less enhanced apatite response compared to the KrF excimer laser whole area irradiative processed nylon 6,6 samples. This could be on account of the dominant wetting regime as discussed in Section 12.2.1.

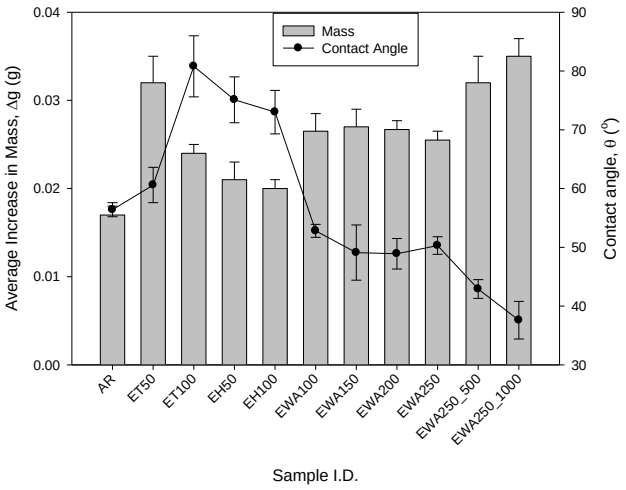

(a)

Figure 12.5 continued overleaf

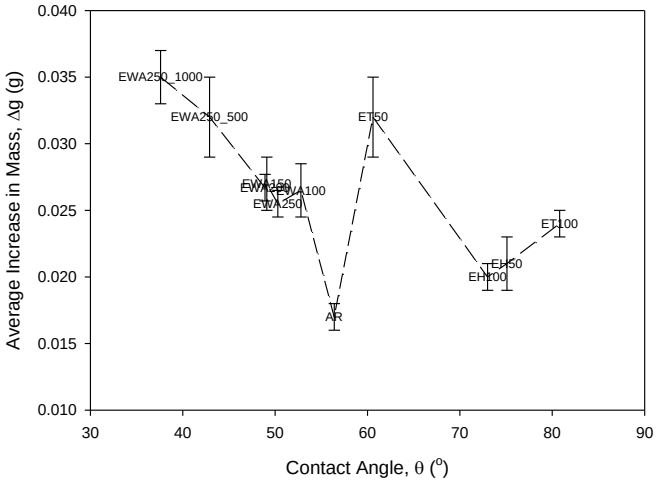

(b)

Figure 12.5 – (a) Histogram showing Δg in relation to θ for all KrF excimer laser processed samples and (b) graph showing the relationship between θ and Δg following immersion in SBF for 14 days.
*(In terms of weight, One-Way ANOVA showed an overall significance with F = 32.626 and p = 0.000. Scheffe's range test showed that there was statistical difference between each sample apart from AR;EH50;EH100, ET50;EWA100;EWA150;EWA200;EWA250_500;EWA250_1000 and ET100;EWA200;EWA250*p<0.5).*

Following on from all of the results obtained, as shown in Figures 12.1, 12.3 and 12.5(a), it has been indicated that the surface modifications arising from the implemented KrF excimer laser surface treatments gave rise to an enhanced apatite formation. As a screening method this shows that osteoblast cell response could be more preferential on the KrF excimer laser processed nylon 6,6 samples due to the enhanced ability for those nylon 6,6 samples to promote the formation pf apatite.

In order to further confirm the possible potential of these surfaces being able to promote sufficient osteoblast cell growth, EDX analysis was carried out on the sediment formed. Figure 12.6 gives the typical EDX spectra for the as-received sample (AR) and a typical KrF excimer laser processed sample showing that there was a presence of phosphorous and calcium in the sediment of each of the samples. This is highly important owed to the fact that the ability of a material to form phosphorous and calcium sediment on the surface allows for a more enhanced osteoblast cell growth. It should also be noted here that other elements that were discovered through employing EDX can be explained by the fact that these elements were present in the SBF during the experimentation.

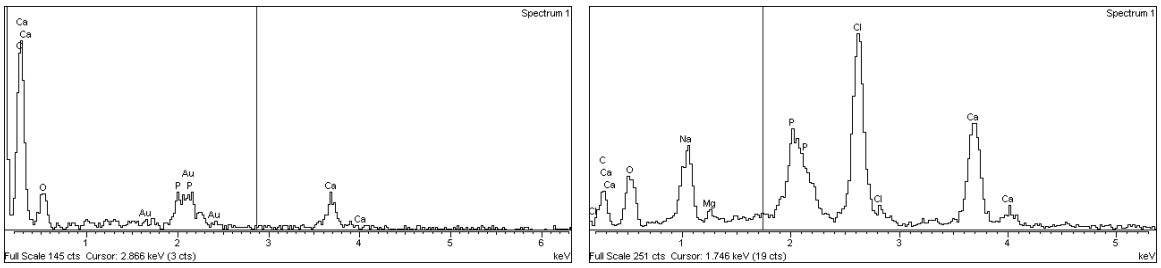

(a) (b)

Figure 12.6 – EDX results for (a) as-received sample (AR) and (b) a typical EDX spectra for the KrF excimer laser processed samples (sample H100) following immersion in SBF after 14 days.

12.2.4 – Wettability Characteristics and Surface Parameters

From Figure 12.5(a) it can be seen that there may be two different relationships between the two different KrF laser processing techniques and θ. For the KrF excimer laser-induced patterned nylon 6,6 samples, with the exception of sample ET50, that Δg decreases upon a reduction in θ. In direct contrast, the KrF excimer laser whole area irradiative processed samples gave an increased apatite response with Δg increasing on a reduction in θ. These different apatite responses can be further identified through Figure 12.5(b) which allows one to see that the KrF excimer laser whole area irradiative processed samples reduced in Δg linearly with a decreasing θ. Whereas, the KrF excimer laser-induced patterned samples, with the exception of sample ET50, gave a linear increase in Δg with an increase in θ. It is highly likely that the transition in wetting regimes for the KrF excimer laser-induced patterned samples, as discussed in Chapter 7, could be attributed to the non-correlative result given with sample ET50 and can be used as a possible explanation as to why the results for the two different KrF excimer laser processing techniques did not correlate. This is on account of the mixed-state wetting regime and the presence of as-received nylon 6,6 material between the KrF laser-induced patterns having a significant impact upon the adhesion characteristics.

Figure 12.7(a) shows that for the KrF excimer laser-induced patterned samples Δg decreased upon a decrease in γ^P, with the exception of sample ET50 which did not appear to follow this trend. This can be accounted for by the transition in wetting regime as discussed in Chapter 7 such that a mixed-state wetting regime was likely to have a significant impact upon the apatite response to the nylon 6,6. For the KrF excimer laser whole area irradiative processed samples, from Figure 12.7(a) the opposite was seen to occur in that an increase in γ^P brought about a increase in Δg. The relationships between Δg and γ^P for the two KrF excimer laser processing techniques are further accentuated using Figure 12.7(a) as this graph shows the linear relationship for each of the different laser processing methods. That is, for the KrF laser-induced patterned samples, with the exception of sample ET50, Δg decreased in a linear relationship with regards to an increase in γ^P. Furthermore, for the entire KrF excimer laser whole area irradiative processed nylon 6,6 samples Δg increased with an increase in γ^P. The KrF excimer laser whole area irradiative processed samples can be seen to correspond with the fact that for a hydrophilic material such as nylon 6,6 an increase in γ^P allows the material to become more hydrophilic which increases the adhesion characteristics. One can then deduce from this that an increase in adhesion characteristics would inherently bring about an increase in Δg. The difference in

relationships between Δg and γ^P for the two different KrF excimer laser processes could be explained by the transition in wetting regime giving rise a large variation in results. This is further evidenced by the results obtained with sample ET50 which did not appear to follow either trend. It should also be noted here that the relationships identified using Figure 12.7 were the inverse of what was observed between Δg and θ (see Figure 12.5) and can be attributed to the relationship between θ and γ^P, as determined in Chapter 10. As a result of this, the observed strong relationship between θ and γ^P is further evidenced by the strong trend they both have with Δg.

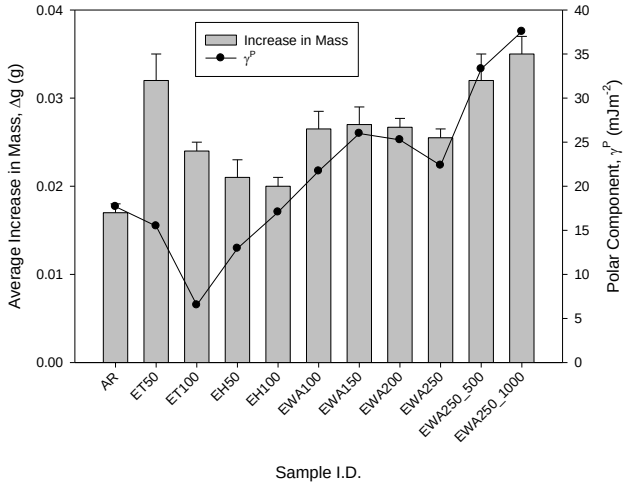

(a)

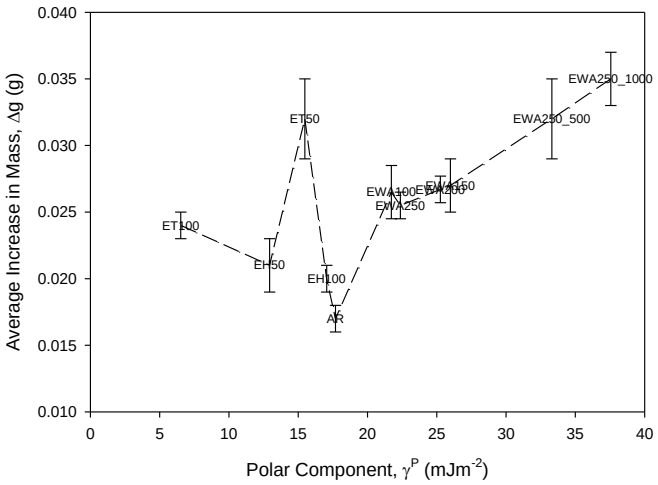

(b)

Figure 12.7 – (a) Histogram showing Δg in relation to γ^P for all KrF excimer laser processed samples and (b) graph showing the relationship between γ^P and Δg following immersion on SBF after 14 days.

One can see from Figure 12.8(a) that with regards to the KrF laser-induced patterned nylon 6,6 samples, there did not appear to be any distinct correlation between γ^T and Δg. On the other hand, Figure 12.8(b) also attests that there may have been a correlation between γ^T and Δg in that an increase in γ^T gave rise to an increase in Δg. These relationships can be further identified in Figure 12.8(b) which shows that the KrF excimer laser-induced patterned samples did not have a correlative

trend with Δg, whereas, for the KrF excimer laser whole area irradiative processed samples there appeared to be a correlative trend between Δg and γ^T showing an increase in Δg was potentially brought about by an increase in γ^T. This further suggests that for the KrF excimer laser whole area irradiative processed nylon 6,6 samples an increase in hydrophilic properties gave rise to increased adhesion characteristics which enhanced the promotion of apatite response. In contrast, as no relationship was identified between γ^T and Δg for the KrF excimer laser-induced patterned samples, it should be further proposed that a likely change in wetting regime as discussed in Chapter 10 appeared to be the likely explanation as to the observed difference in trends for each of the KrF excimer laser processing techniques.

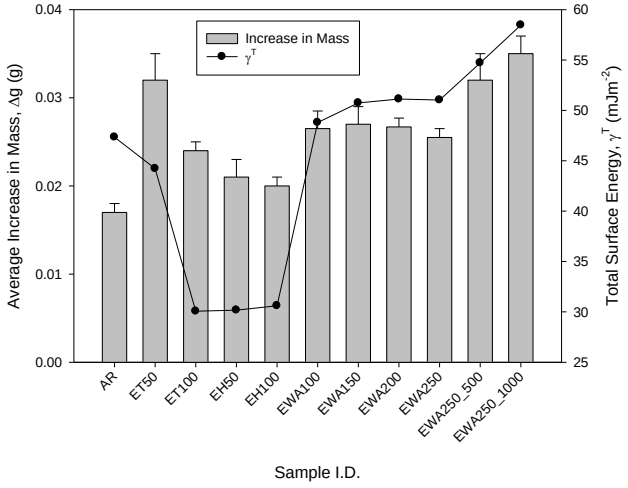

(a)

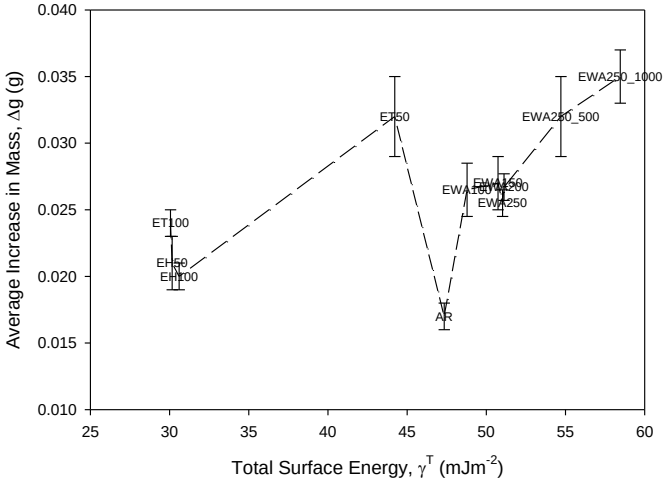

(b)

Figure 12.8 – (a) Histogram showing Δg in relation to γ^T for all KrF excimer laser processed samples and (b) graph showing the relationship between γ^T and Δg following immersion in SBF after 14 days.

Figure 12.9(a) shows Δg in relation Ra for the entire KrF excimer laser processed nylon 6,6 samples. For the KrF excimer laser-induced patterned samples Δg could have had a trend with Ra in that an increase in Ra appeared to elicit a decrease in Δg. Conversely, it can be seen from Figure 12.9(a) that

the KrF excimer laser whole area irradiative processed samples did not give rise to a relationship between Ra and Δg on account of similar values of Ra determined for observed variations in Δg. This is further identified in Figure 12.9(b) which shows no correlative trend for the KrF excimer laser whole area irradiative processed samples and a potential decreasing linear function for the KrF excimer laser-induced patterned nylon 6,6 samples. With another observed difference in relationships between Δg and surface parameter for the two different KrF excimer laser processing methods then it is further highlighted that the likely transition in wetting regimes have a large impact upon apatite formation. Also, for the KrF excimer laser-induced patterned samples, even though θ (see Figure 12.5) or surface energy (see Figure 12.7 and Figure 12.8) did not appear to have a correlation with Δg, Ra could be the driving parameter for these samples in that an increase in Ra decreases Δg further indicating a distinct difference between the KrF excimer laser-induced patterned and KrF excimer laser whole area irradiative processed samples.

Figure 12.10(a) and Figure 12.10(b) allow one to see that Sa seemed to have an impact on Δg similar to that observed for Ra (see Figure 12.9) for all KrF excimer laser processed nylon 6,6 samples. That is, on account of similar Sa values and variations in Δg, there did not appear to be any correlative trend between Sa and Δg for the KrF excimer laser whole area irradiative processed samples. Also, it can be seen from Figure 12.10(a) and Figure 12.10(b) that for the KrF excimer laser-induced patterned samples Δg potentially could have been a linear reducing function of Sa further suggesting that surface roughness played a distinct role in the formation of apatite for these samples alone. These results further add to the evidence that, in terms of apatite response, the change in wetting regime which was likely to occur for the KrF excimer laser-induced patterned samples had a large impact upon the enhancement of apatite formation and as a result different surface parameters have more influence when compared to the KrF excimer laser whole area irradiative processed samples.

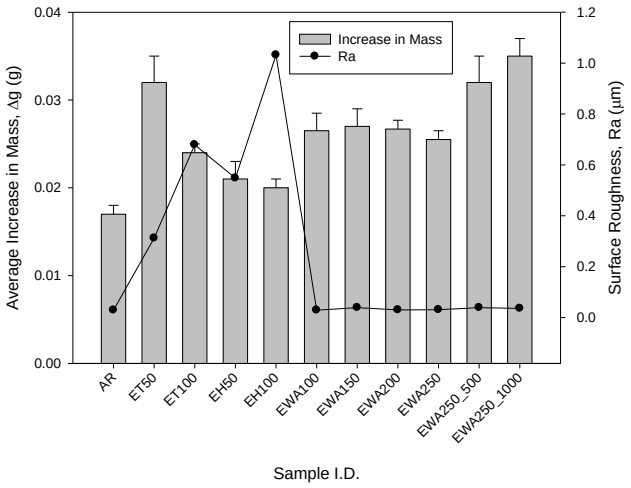

(a)

Figure 12.9 continued overleaf

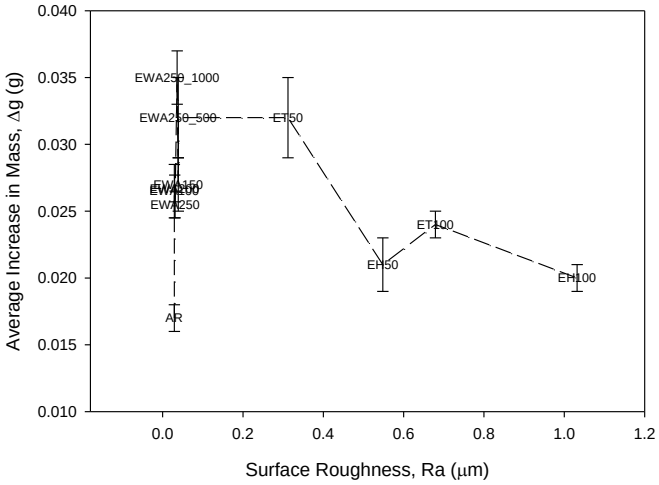

(b)

Figure 12.9 – (a) Histogram showing Δg in relation to Ra for all KrF excimer laser processed samples and (b) graph showing the relationship between Ra and Δg following immersion in SBF after 14 days.

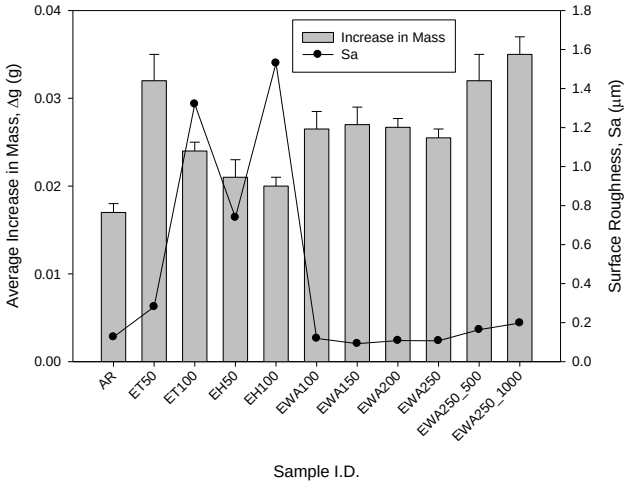

(a)

Figure 12.10 continued overleaf

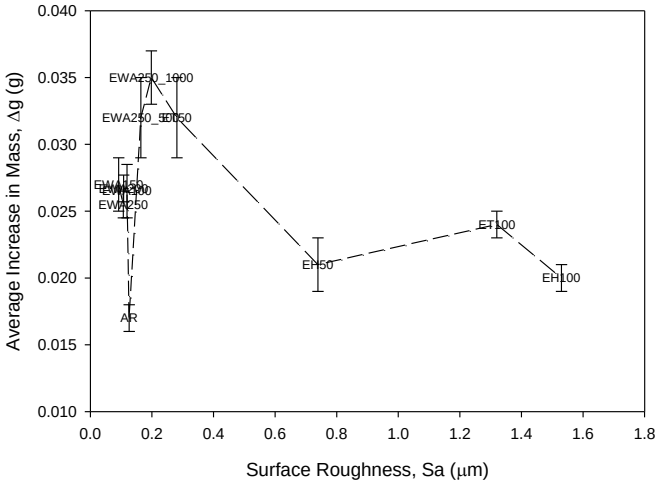

(b)

Figure 12.10 – (a) Histogram showing Δg in relation to Sa for all KrF excimer laser processed samples and (b) graph showing the relationship between Sa and Δg following immersion in SBF for 14 days.

As seen in Figure 12.11(a), there did not appear to be a clear relationship between the surface oxygen content and Δg for the KrF excimer laser-induced patterned nylon 6,6 samples. It can also be seen from Figure 12.11(a) that there could have been a correlation between the surface oxygen content and Δg for the KrF excimer laser whole area irradiative processed samples. This is on account of similar values of 13 %at. surface oxygen content giving rise to similar values of Δg of around 0.027 g and then Δg increasing upon an increase in surface oxygen content. These relationships can be further identified using Figure 12.11(b); however, it can also be seen that there was no conclusive relationship between the surface oxygen content and Δg for the KrF excimer laser whole area irradiative processed samples even though the results shown in Figure 12.11 suggest that one may be possible. As a result of this it has been seen that for the KrF excimer laser-induced patterned samples the surface roughness appeared to be a dominating factor in terms of apatite response. In contrast, θ, γ^P and potentially the surface oxygen content appear to be the dominant parameters to determine apatite formation for the KrF excimer laser whole area irradiative processed samples. With this in mind it one can deduce the two different KrF excimer laser processes of nylon 6,6 elicit variable responses in terms of apatite formation suggesting that the dominant wetting regime may play a big role in the adhesion characteristics of apatite.

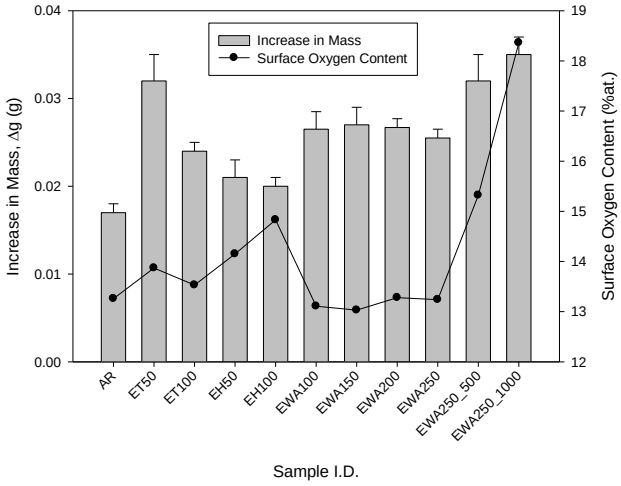

(a)

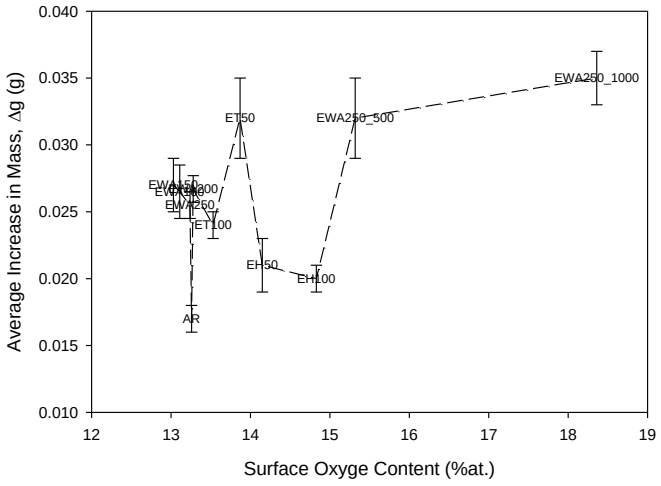

(b)

Figure 12.11 – (a) Histogram showing Δg in relation to surface oxygen content for all KrF excimer laser processed samples and (b) graph showing the relationship between surface oxygen content and Δg following immersion in SBF after 14 days.

12.3 – Effects of KrF Excimer Laser Processing of Nylon 6,6 on Osteoblast Cell Response: 24 Hrs

This Section discusses the results obtained for the KrF excimer laser processed nylon 6,6 samples which had been seeded with normal human osteoblast cells and incubated for 24 hrs. The methodology can be found in Chapter 5.

12.3.1 – KrF Excimer Laser-Induced Patterning

After 24 hrs incubation time for the osteoblast cell seeded samples it can be seen from the SEM micrographs shown in Figure 12.12 that the cells had begun to adhere and proliferate across each of the KrF excimer laser-induced patterned nylon 6,6 samples. Similar to the as-received sample (see Figure 11.10) the KrF excimer laser-induced patterned samples gave rise to osteoblast cells with a bipolar cell morpohology. In addition to this, one major difference between the cell growth on the as-received sample (see Figure 11.10) and the KrF excimer laser-induced patterned samples is that the excimer patterned nylon 6,6 samples gave rise to some form of directionality; that is, the cells appear to be preferentially growing along the grooves formed by the excimer laser. This could have been induced by the surface roughness and surface oxygen content being higher (see Table 7.3) in the grooves produced allowing for preferential cell growth.

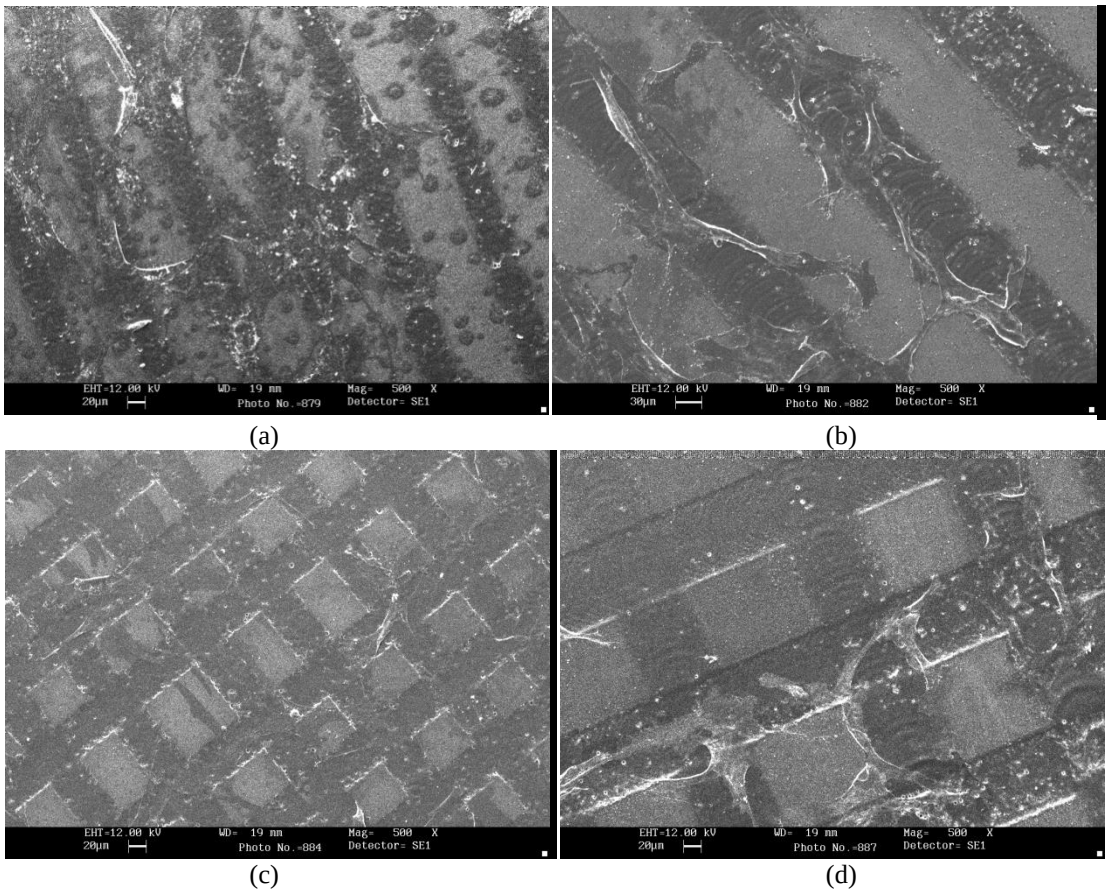

Figure 12.12 – SEM micrographs of the KrF excimer laser-induced patterned samples (a) ET50, (b) ET100, (c) EH50 and (d) EH100 after 24 hrs incubation.

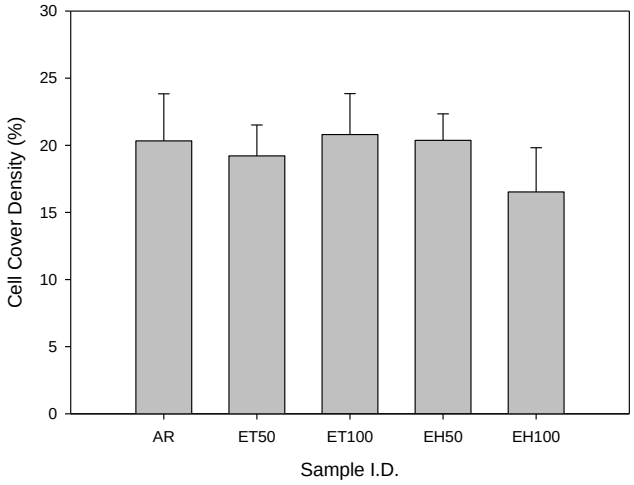

Figure 12.13 – Histogram showing the cell cover density for the KrF excimer laser-induced patterned nylon 6,6 samples following 24 hrs incubation.

Figure 12.13 allows one to see that in terms of cell cover density, following 24 hrs of incubation, the KrF excimer laser-induced patterned nylon 6,6 samples gave rise to a cell cover density equiqvalent to that observed with the as-received sample (AR). That is, all of the KrF excimer laser-induced patterned samples gave a cell cover density of around 20% suggesting that the nylon 6,6 surfaces had not given rise to a more enhanced osteoblast cell response following KrF excimer laser patterning. This result coincides with what was observed with the apatite response in Section 12.2.1 in that most of the KrF excimer-laser induced patterned nylon 6,6 samples had a Δg similar or slightly higher than that of the as-received sample (AR).

12.3.2 – KrF Excimer Laser Whole Area Irradiative Processing

Figure 12.14 shows the SEM micrographs for the KrF excimer laser whole area irradiative processed nylon 6,6 samples after 24 hrs incubation. From this it can be seen that the KrF excimer whole area irradiative processed samples gave rise to variations in cell morphology in comparison to the as-received sample (see Figure 11.10) in that, the cells shown in Figure 12.14 appeared to be more clumped radial. This could be attributed to the fact that the combination of differing wettability characteristics and surface oxygen content could have contributed to cell differentiation. As a result, one can deduce that by modulating cell differentiation through varying wettability characteristics and surface oxygen content would have a large potential for using laser surface treated polymeric materials within regenerative medicine.

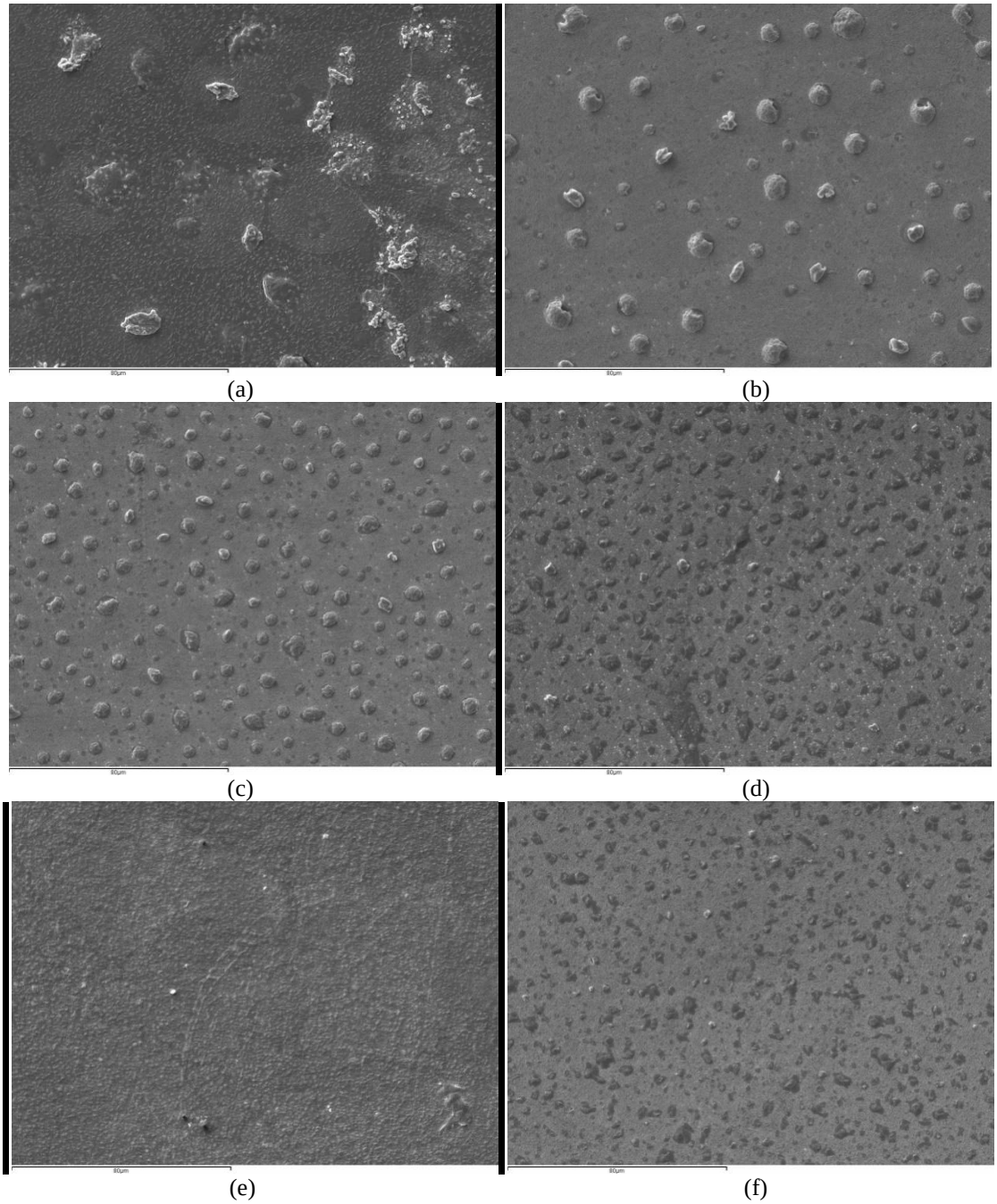

Figure 12.14 – SEM micrographs of the KrF excimer laser whole area irradiated samples (a) EWA100, (b) EWA150, (c) EWA200, (d) EWA250, (e) EWA250_500 and (f) EWA250_1000 after 24 hrs incubation .

It is apparent from Figure 12.15 that all of the KrF excimer laser whole area irradiative processed samples gave rise to larger cell cover densities when compared to the as-received sample (AR) with the exception of sample EWA250_500 and sample EWA250_1000. The largest cover density of 25% was obtained with samples EWA100, EWA150, EWA250 and EWA250 which was 5% more than what was observed for the as-received sample (AR). It should be noted here that the results shown in Figure 12.15 do not appear to correspond with those result given in Section 12.2.2 for the apatite layer response. Since, sample EWA250_500 and sample EWA250_1000 being found to have the largest Δg following 14 days of immersion in SBF. However, it may be possible that the reduction in osteoblast

cell response (see Figure 12.15) for these two samples could be attributed to the samples becoming too hydrophilic (see Table 7.3) in which the modified nylon 6,6 surfaces are not sufficient to promote an enhanced osteoblast cell response.

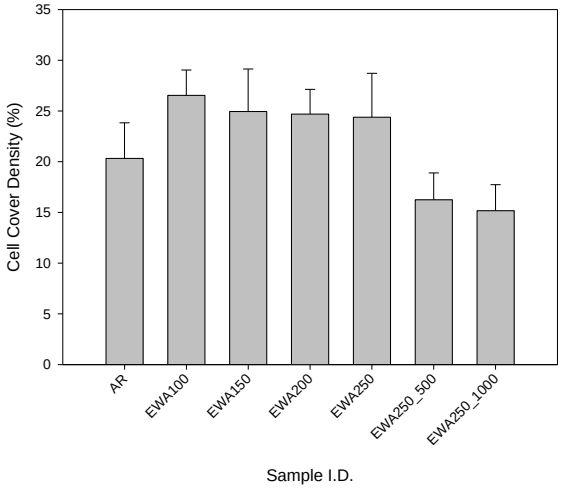

Figure 12.15 – Histogram showing the cell cover density for the KrF excimer laser whole area irradiative processed nylon 6,6 samples following 24 hrs incubation.

12.3.3 – Comparison Between KrF Excimer Laser-Induced Pattering and KrF Excimer Laser Whole Area Irradiative Processing

Figure 12.16(a) shows a histogram of the cover density for each of the KrF excimer laser processed samples seeded with normal human osteoblast cells after 24 hrs incubation. It can be seen that the KrF excimer laser-induced patterned samples had a cover density of around 20% which was seen to be equivalent to that seen for the as-received sample (AR). It was also seen that samples WA250_500 and WA250_1000 gave rise to slightly less cover densities of around 17 and 19%, respectively, whereas the largest cover density of 25% was obtained for the other KrF excimer laser whole area irradiative processed samples. Figure 12.16(a) also allows one to see that through different excimer laser processes the osteoblast cell response on the nylon 6,6 surfaces, in terms of cell cover density, can be significantly modulated, indicating that KrF excimer laser processing is an attractive means for enhancing and hindering cell growth dependant on the intended application.

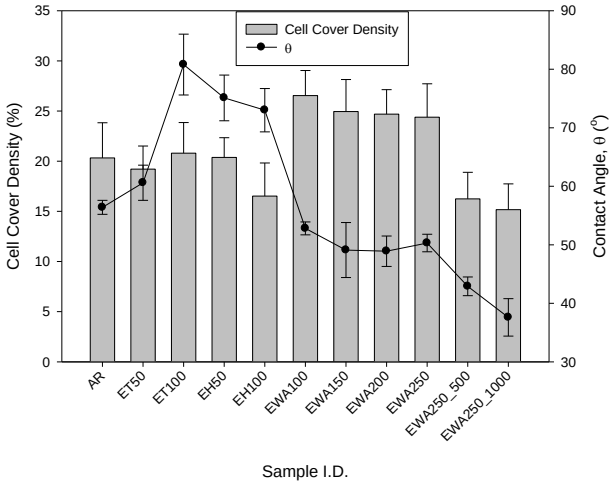

(a)

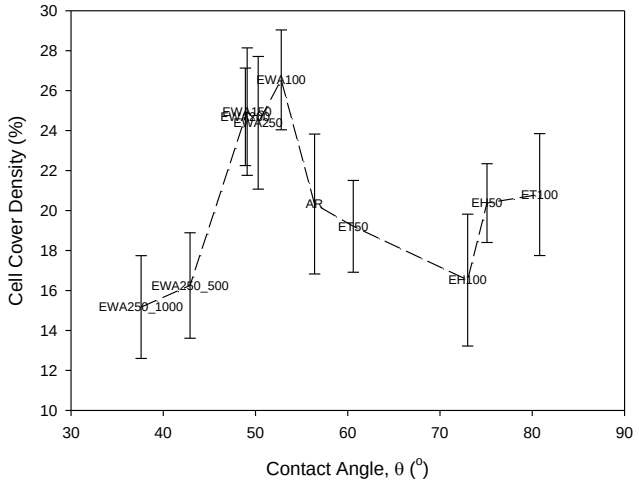

(b)

*Figure 12.16 – (a) Histogram showing the cell cover density in relation to θ for all KrF excimer laser processed samples and (b) graph showing the relationship between θ and cell cover density after 24 hrs incubation. (In terms of cell cover density, One-Way ANOVA showed an overall significance with F=6.607 and p=0.000. Scheffe's range test showed that there was statistical difference between H100 and WA250; WA250, WA250_500 and WA250_1000*p<0.5).*

12.3.4 – Wettability Characteristics and Surface Parameters

By taking into account the effects of θ on the osteoblast cell response following 24 hrs incubation, it can be seen that the data plotted in Figure 12.16(a) and Figure 12.16(b) suggest a possible threshold window for θ between 47 and 53° which gave rise to an enhanced osteoblast cell response in terms of cell cover density. On the other hand, this also indicates that above or below this θ threshold window the osteoblast cell response would inherently be hindered slowing the cell proliferation and reducing the cell cover density. The proposed θ threshold window for the cell cover density can be further identified in Figure 12.16(b) such that for sample EWA250_500 and sample EWA250_1000 with the

lowest θ of around 40° the cell cover density had reduced to around 15%. Also, for the KrF excimer laser-induced patterned samples which gave rise to the largest θ of approximately 70 to 80° it can be seen from Figure 12.16(b) that the cell cover density reduced to around 18%. These two reductions in cell cover densities are significant when compared to the other samples with θ between 47 and 53° because these samples gave rise to the largest cell cover densities of 25% or more allowing one to extrapolate that a θ threshold window is possible.

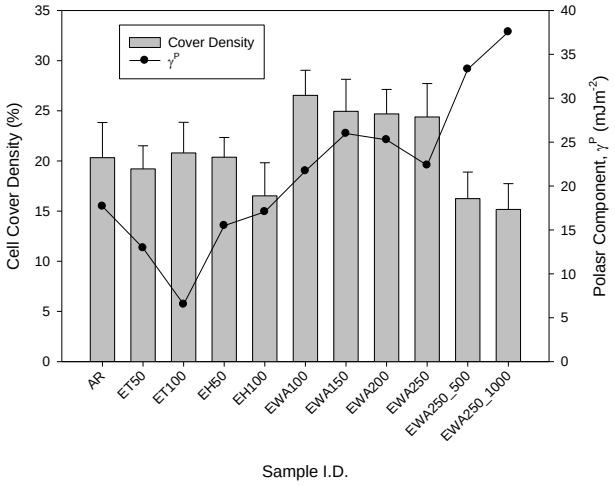

(a)

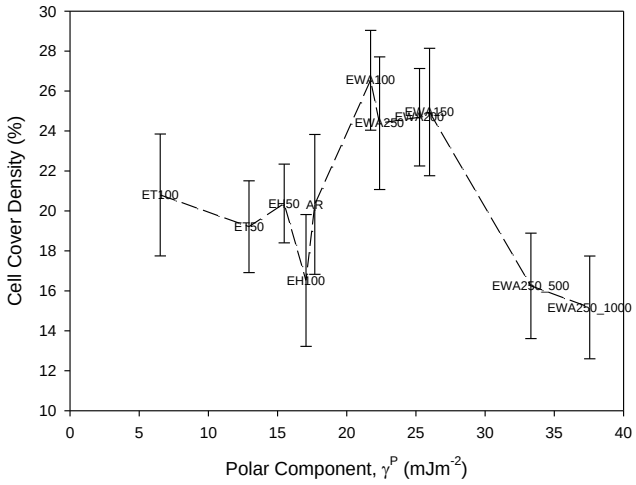

(b)

Figure 12.17 – (a) Histogram showing the cell cover density in relation to γ^P for all KrF excimer laser processed sample and (b) graph showing the relationship between γ^P and cell cover density after 24hrs incubation.

The likelihood of this threshold window is further confirmed using Figure 12.17(a) and Figure 12.17(b) which shows that there could be a γ^P threshold window (see Figure 12.15(a)) of 17 to 25 mJm^{-2} which would give rise to an enhanced osteoblast cell response in terms of cell cover density. It should also be noted here that the results shown in Figure 12.17 are mostly the inverse to what was observed with θ (see Figure 12.16) which can be attributed to the relationship between γ^P and θ, as

determined in Chapter 10. From this the inverse relationship for the two parameters with the cell cover density further attests to the relationship between θ and γ^P.

In addition to what was observed for θ (see Figure 12.16) and γ^P (see Figure 12.17), γ^T threshold window (see Figure 12.18(a) and Figure 12.18(b)) of 47 to 53 mJm^{-2} in which osteoblast cell growth is enhanced with regards to cell cover density. However, it should be said that Figure 12.18(b) suggests that even though a threshold window could be possible the KrF excimer laser-induced patterned nylon 6,6 samples did not conclusively follow the trend in that those samples with γ^T of around 30 mJm^{-2} gave rise to a variation of cell cover densities ranging between 16 and 21%. This could be accounted for by the likelihood of a mixed-state wetting regime arising on these samples, as discussed in Chapter 7, which is likely to have a large impact upon how the osteoblast cells react to the patterned nylon 6,6 surface. As a result, Figures 12.16, 12.17 and 12.18 point towards a dominance such that the wettability characteristics in terms of θ, γ^P and γ^T for the KrF excimer laser processed nylon 6,6 samples could be implemented to predict the bioactive nature of the modified surfaces. Having said that, one should be mindful of the possibility that the KrF excimer laser-induced patterned samples could have given results for the cell cover density which were misleading on account of the fact that the mixed-state wetting regime could play a distinct role in the osteoblast cell response to the nylon 6,6.

Figure 12.19(a) shows a histogram of the cell cover density in relation to Ra, allowing one to see that, especially for the KrF excimer laser whole area irradiative processed samples, Ra did not appear to have any clear correlation with the measured cell cover density. This is attributed to the fact that for the KrF excimer laser whole area irradiative processed samples Ra remained somewhat constant at around 0.05 μm even though a modulation in the cell cover density was determined. This is further attested to by Figure 12.19(b) which shows the KrF excimer laser whole area irradiative processed samples giving large variations in cell cover density for equivalent Ra. In contrast, it can be seen from Figure 12.19(b) that the KrF excimer laser-induced patterned nylon 6,6 samples appeared to have to some extent a trend with the cell cover density in that the cell cover density decreased upon an increase in Ra. This corresponds with what was observed inSection 12.2 and suggests that Ra could potentially be a driving force for the KrF excimer laser-induced patterned nylon 6,6 samples and that this parameter could be implemented to determine the osteoblast cell response to KrF excimer laser-induced patterned nylon 6,6.

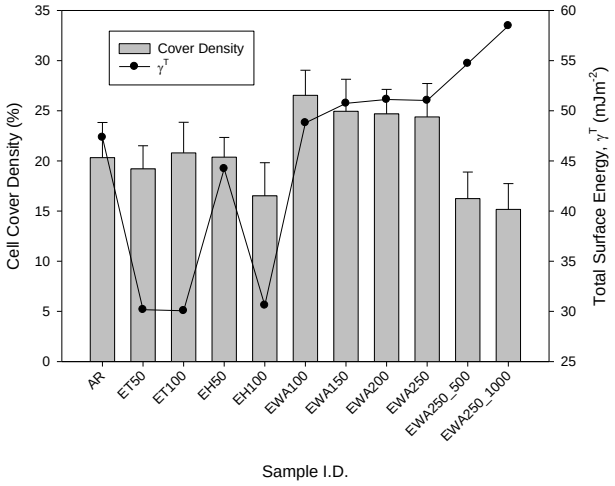

(a)

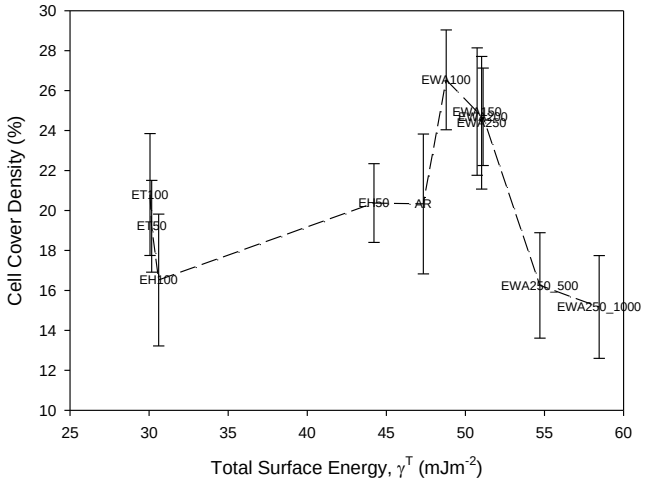

(b)

Figure 12.18 – (a) Histogram showing the cell cover density in relation to γ^T for all KrF excimer laser processed samples and (b) graph showing the relationship between γ^T and cell cover density after 24 hrs incubation.

Figure 12.20(a) allows one to identify that Sa for the KrF excimer laser whole area irradiative processed samples did not have any particular correlative trend with the observed cell cover density. This is owed to the fact that all of the KrF excimer laser whole area irradiative processed nylon 6,6 samples had Sa values of between 0.1 and 0.2 µm, giving a modulated response in terms of cell cover density. Figure 12.20(b) further shows that there did not appear to be any trend between Sa and the cell cover density, whereas the KrF excimer laser-induced patterned samples appeared to be a decreasing function of Sa which was also observed for Ra (see Figure 12.19(b)) and in section 12.2. With this in mind, it is possible to deduce that the surface roughness shows potential to be used as an indicator of osteoblast cell response to the KrF excimer laser-induced patterned nylon 6,6. In addition to this, the relationship identified between the apatite response (See Section 12.2), cell cover density (see Figure 12.19 and Figure 12.20) and surface roughness could further suggest that the wetting

regime is playing a big part in the osteoblast cell response This is on account of the KrF excimer laser-induced patterning giving rise to a roughness from a periodic topography which gives rise to the transition in wetting regime.

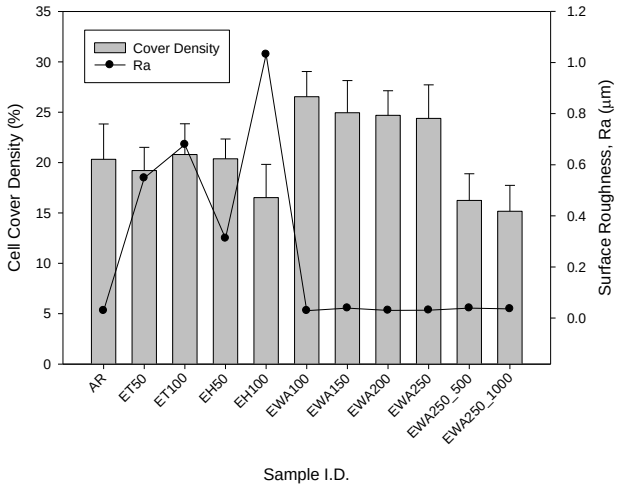

(a)

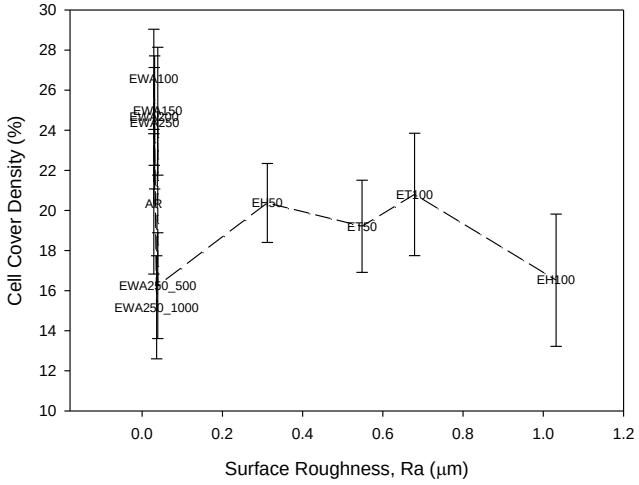

(b)

Figure 12.19 – (a) Histogram showing the cell cover density in relation to Ra for all KrF excimer laser processed samples and (b) graph showing the relationship between Ra and cell cover density after 24 hrs incubation.

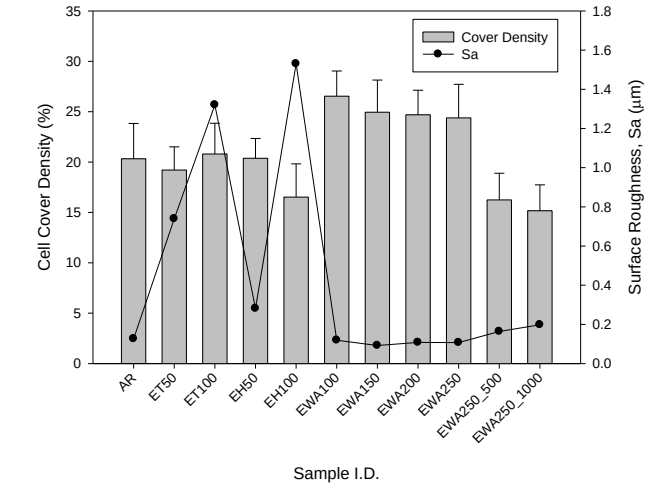

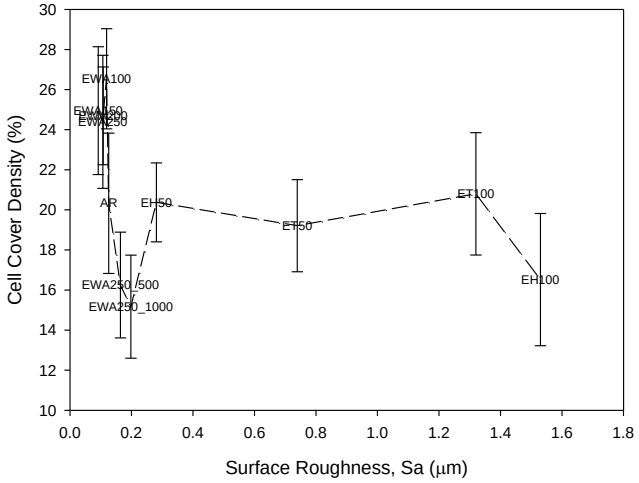

(b)

Figure 12.20 – (a) Histogram showing the cell cover density in relation to Sa for all KrF excimer laser processed samples and (b) graph showing the relationship between Sa and cell cover density after 24 hrs incubation.

Figure 12.21(a) and Figure 12.21(b) allow one to see that the cell cover density for the KrF laser processed samples after 24 hrs of incubation could be a decreasing function of the surface oxygen content such that the lowest cell cover densities of around 17% were achieved when the surface oxygen content had increased up to 18%. With this in mind, along with the other surface parameters and wettability characteristics of the nylon 6,6 samples studied it is possible to deduce that no one parameter stands out as the most dominant in determining the bioactive nature. As such, this further contributes to the thinking that more than one surface parameter will contribute to the biofunctionality of the KrF excimer laser processed nylon 6,6 samples. Also, it can be seen that the relationship between cell cover density surface oxygen content does not correspond with what was observed in Section 12.2. Still, it is possible that the cell cover density being a reducing function of surface energy content indicates that the toxicity of the samples may be increasing in accordance with what was

discussed in Section 11.5. On account of this, cytotoxicity and its effects on osteoblast cell response will be further discussed in Section 12.5.

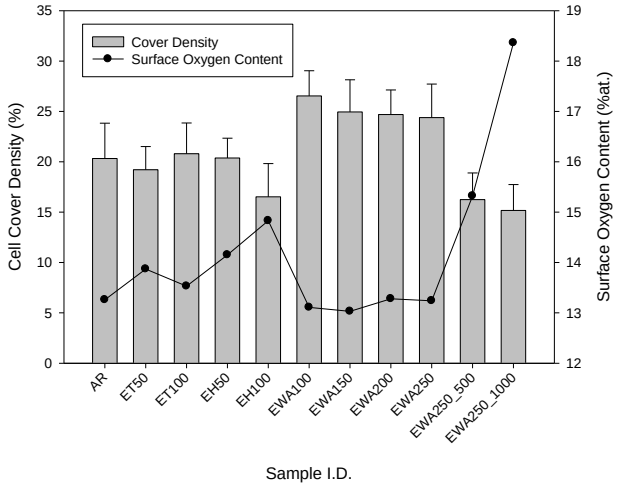

(a)

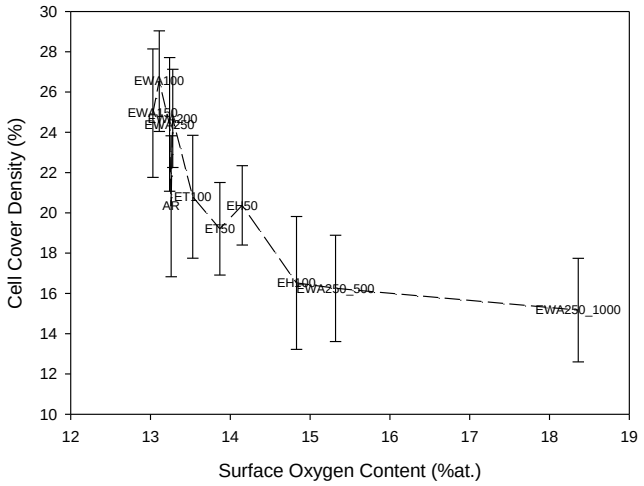

(b)

Figure 12.21 – (a) Histogram showing the cell cover density in relation to surface oxygen content for all KrF excimer laser processed samples and (b) graph showing the relationship between surface oxygen content and cell cover density after 24 hrs incubation.

12.4 – Effects of KrF Excimer Laser Processing of Nylon 6,6 on Osteoblast Cell Response: Four Days

This Section discusses the results obtained for those KrF excimer laser processed samples that had been seeded with normal human osteoblast cells incubated for 4 days. The full experimental technique can be found in Chapter 5.

12.4.1 – KrF Laser-Induced Patterning

With four days of incubation elapsed, Figure 12.22 shows that the cell growth was at an advanced stage for the KrF excimer laser-induced patterned nylon 6,6 samples compared to what was observed following 24 hrs incubation time (see Figure 12.12). From Figure 11.23 it can be seen that the cell morphology for the as-received sample was radial and coral-like which differed from the KrF excimer laser-induced patterned samples (see Figure 12.22) which gave a more clumped like morphology. It can also be identified using Figure 12.22 that there appeared to be more directionality for the KrF excimer laser-induced patterned samples compared to the as-received sample (see Figure 12.22 and Figure 11.23, respectively). As discussed following 24 hrs incubation, this could potentially be due to the grooves being rougher and having more oxygen content giving rise to more preferential cell growth in these areas.

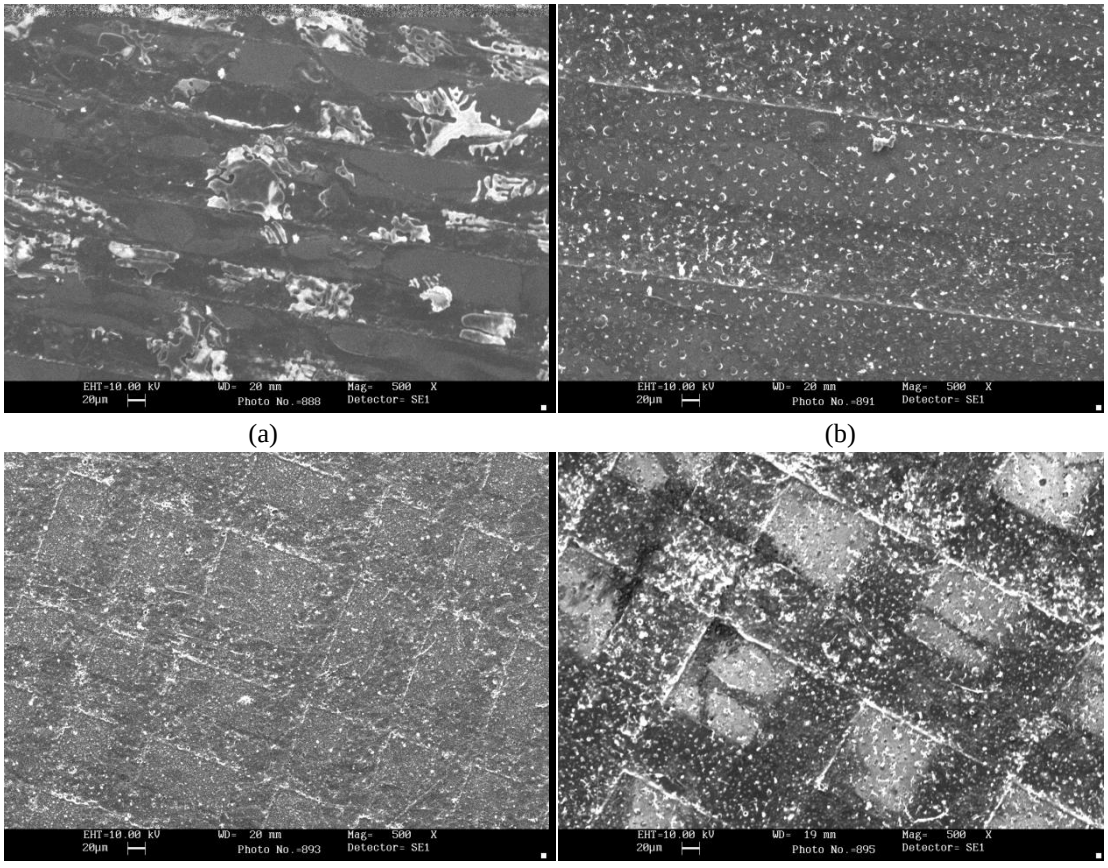

Figure 12.22 – SEM micrographs of the KrF excimer laser-induced patterned nylon 6,6 samples following four days incubation.

It can be seen from Figure 12.23 that the KrF excimer laser-induced patterning of the nylon 6,6 samples gave rise to cover densities of just under 100% which was equivalent to that observed with the as-received sample (AR). To confirm that the bioactivity had not changed for the KrF excimer laser-induced patterned samples compared to the as-received sample (AR) after four days of incubation cell count was also taken into account. Figure 12.24 allows one to realize that the cell

count was also equivalent to that of the as-received sample which was around 40,000 cells/ml. By knowing this in addition to the results obtained in Section 12.3.1, it is possible to see that the KrF excimer laser-induced patterned nylon 6,6 samples did not give rise to an enhanced osteoblast cell response when compared to the as-received sample (AR). Having said that, the KrF excimer laser-induced patterned nylon 6,6 samples did not hinder cell response either and as such can be seen to give an equivalent response to that seen with the as-received sample. In fact, the only difference which could be ascertained between the as-received sample and the KrF excimer laser-induced patterned samples was that of the cell morphology which can be attributed to surface parameter variations on account of the laser-material interaction.

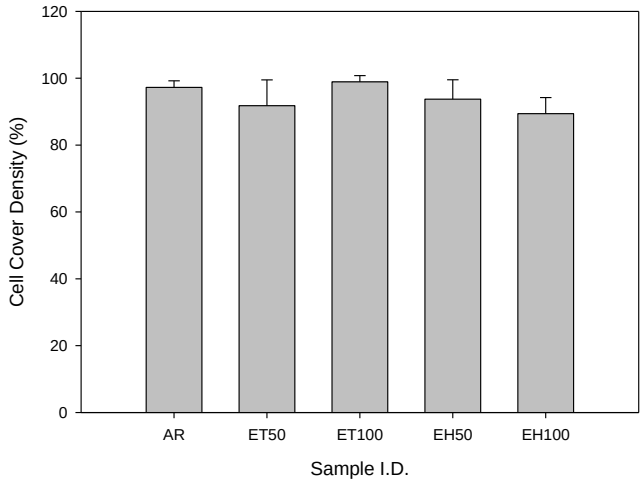

Figure 12.23 – Histogram showing the cell cover density for the KrF excimer laser-induced patterned nylon 6,6 samples following four days incubation.

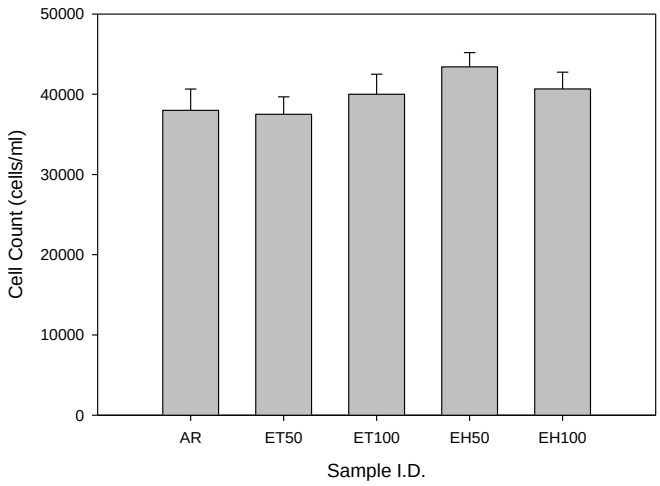

Figure 12.24 – Histogram showing the cell count for the KrF excimer laser-induced patterned nylon 6,6 samples following four days incubation.

12.4.2 – KrF Excimer Laser Whole Area Irradiative Processing

Figure 12.25 shows the SEM micrographs for the KrF excimer laser whole area irradiative processed nylon 6,6 samples following four days incubation. As one can see the osteoblast cells were at an advanced stage of cell growth following four days of incubation. Furthermore, it can be seen that the morphologies appear to have varied somewhat. Sample EWA100 (see Figure 12.25(a)) gave rise to a more clumped like whereas the other samples (see Figure 12.25(b) to Figure 12.25(f)) gave rise to a more radial cell morphology. This, along with the cell differentiation observed using Figure 12.25 further suggests that the variation in surface properties as a result of the laser treatment has a significant impact upon cell signalling and could be seen as an attractive means for potential use within regenerative medicine.

Figure 12.26 shows that the cell cover density for all of the KrF excimer laser whole area irradiative processed samples tended towards 100% after 4 days of incubation. However, it can be said that the lowest cell cover density was determined for sample EWA250_1000 which had a cell cover density of around 83%. This could be significant as it suggests that a considerably more hydrophilic surface such as that exhibited by EWA250_1000 (see Section 7.3) compared to the as-received sample (AR) gives rise to a less enhanced osteoblast cell response to the nylon 6,6 surface.

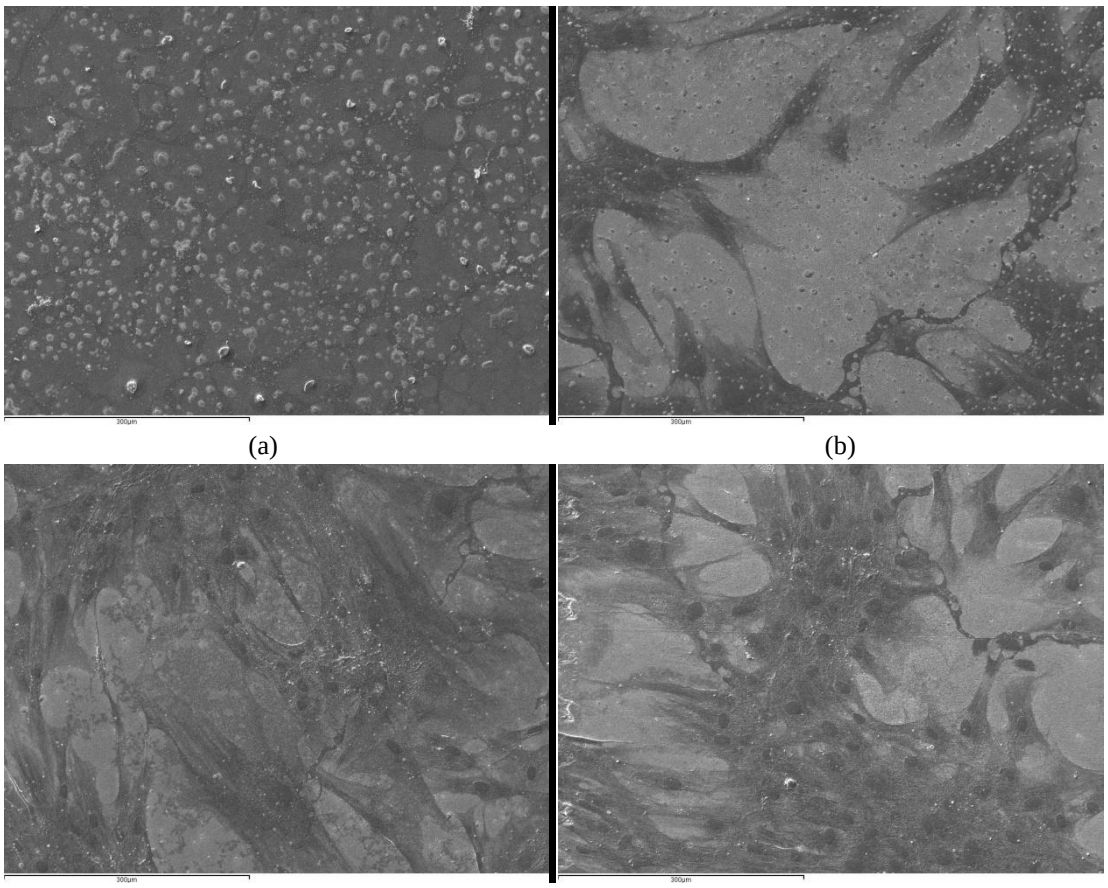

(a) (b)

(c) (d)

Figure 12.25 continued overleaf

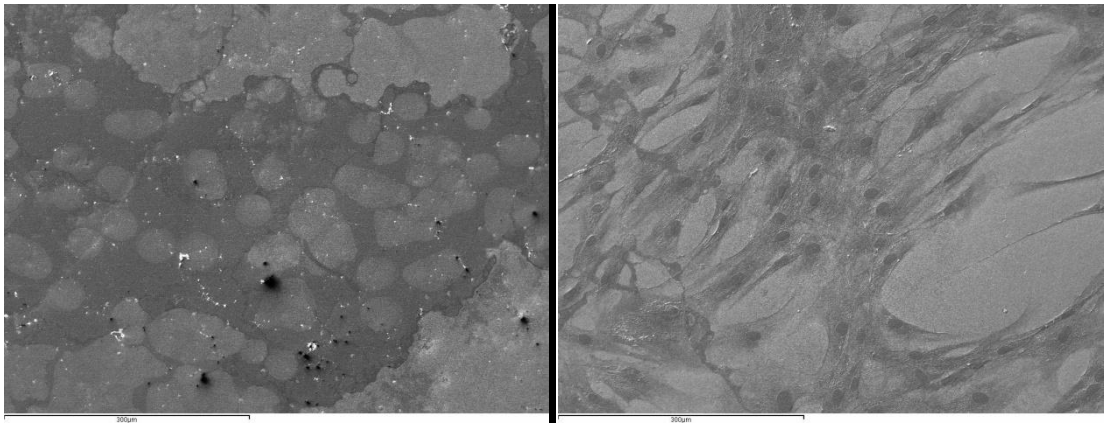

(e) (f)

Figure 12.25 – SEM micrographs of KrF excimer laser whole area irradiative processed samples (a) EWA100, (b) EWA150, (c) EWA200, (d) EWA250, (e) EWA250_500 and (f) EWA250_1000 following four days incubation

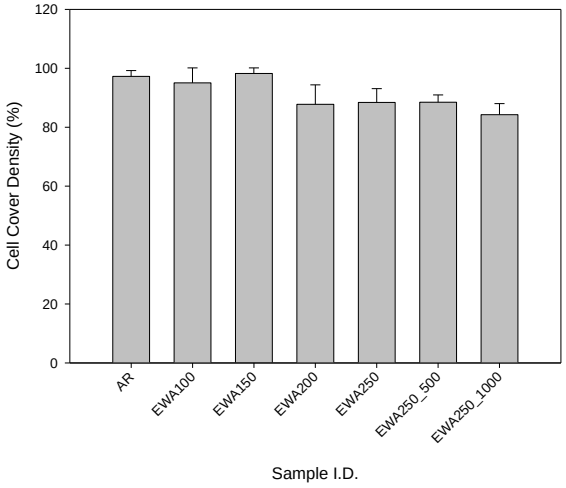

Figure 12.26 – Histogram showing the cell cover density for the KrF excimer laser whole area irradiative processed nylon 6,6 samples following four days incubation.

To further confirm the effects of the KrF excimer laser whole area irradiative processing on the osteoblast cell response after four days a cell count was undertaken. Figure 12.27 shows that most of the KrF excimer laser whole area irradiative processed samples gave rise to a larger cell count of around 47,000 cells/ml when compared to the as-received sample (AR) which had a cell count of just less than 40,000 cells/ml. By comparing the KrF excimer laser whole area irradiative processed samples alone it was found that upon an increasing fluence and incident pulse numbers, the cell count reduced considerably to the point where sample EWA250_500 and sample EWA250_1000 had a cell count around 33,000 cells/ml which was less than that of the as-received sample (AR). This can allow one to see that these samples have hindered the osteoblast cell resonse in comparison to the as-received sample (AR). Again, an explanation as to the observed reduction in enhanced osteoblast cell response can be accounted for by the nylon 6,6 surfaces becoming too hydrophilic, as discussed in Section 7.3.

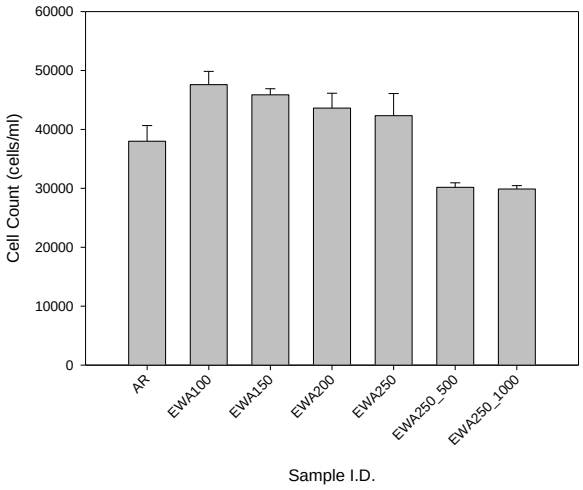

Figure 12.27 – Histogram showing the cell count for the KrF excimer laser whole area irradiative processed nylon 6,6 samples following four days incubation.

12.4.3 – Comparison Between KrF Excimer Laser-Induced Pattering and KrF Excimer Laser

In order to quantify the proliferation, the cover density for each of the KrF excimer laser processed samples was determined (see Figure 12.28). This shows that for all samples the cover density was tending towards 100%; however, it can be seen that a slight reduction in cover density was determined for samples EWA200, EWA250, EWA250_500 and EWA250_1000. This slight reduction in cover density could be attributed to a more hydrophilic nature brought about by the increase in fluences and incident pulse numbers. On the other hand, another explanation could be the rise in toxicity for the nylon 6,6 samples upon the KrF excimer laser surface treatment which would have been similar to that proposed in Chapter 11. This will be further discussed in Section 12.5.

To further ascertain how the osteoblast cells reacted to each of the KrF excimer laser processed samples a cell count was also taken after 4 days incubation. Figure 12.29(a) shows that the largest cell count was achieved for sample EWA100 and sample EWA150 with cell counts tending to 50,000 cells/ml. This is highly significant as it allows one to see that only sample EWA100 and EWA150 gave rise to a more enhanced osteoblast cell response to the nylon 6,6 surface compared to all other nylon 6,6 samples studied. The smallest cell counts were found for sample EWA250_500 and sample EWA250_1000 with cell counts of around 30000 cells/ml being determined, which was less that the as-received sample (AR). As a ersult of the data presented in Figure 12.29(a) it is further highlighted that KrF excimer laser processing of nylon 6,6 can be implemented to modulate osteoblast cell response after 4 days of incubation.

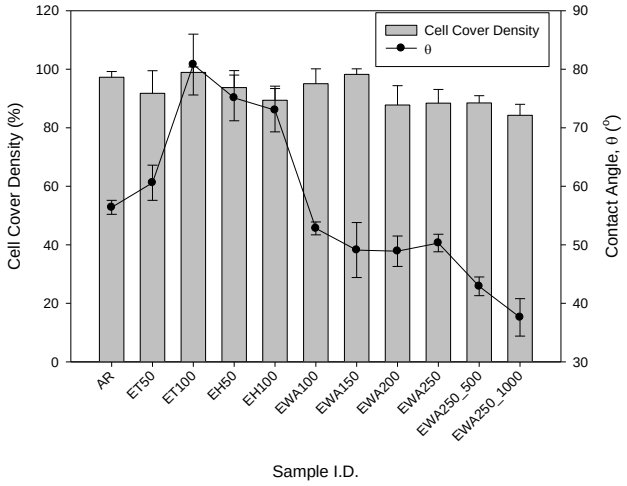

Figure 12.28 – Histogram showing the cell cover density in relation to θ for all KrF excimer laser processed samples following four days incubation.

*(One-Way ANOVA showed that there was no over significance with F=3.266 and p=0.010. Scheffe's range test showed that there was no statistical difference between the samples on account of each result being too similar*p<0.5).*

12.4.4 – Wettability Characteristics and Surface Parameters

Figure 12.29(a) shows that for the KrF excimer laser-induced patterned samples there did not appear to be any correlative relationship between the cell count and θ. This can be further accounted for by the transition in wetting regime which is likely to have had effect on the osteoblast cell response. On the contrary, it can be seen from Figure 12.29(a) that the KrF excimer laser whole area irradiative processed samples could to some extent have had a correlation between the cell count and θ. Since, the cell count appears to have reduced on account of a drop in θ. The trends observed in Figure 12.29(a) can be supported by the graph shown in Figure 12.29(b) which allows one to see the trend for the KrF excimer laser whole area irradiative processed samples. Also, for the KrF excimer laser-induced patterned samples it is possible to further ascertain that the samples do not follow any particular correlative trend. This does not coincide with what was observed in Section 12.2 and 12.3 in that no conclusive link between cell count and θ for the KrF excimer laser-induced patterned nylon 6,6 samples indicating that a mixed-state wetting regime could be giving rise to large variations in results in terms of osteoblast cell response.

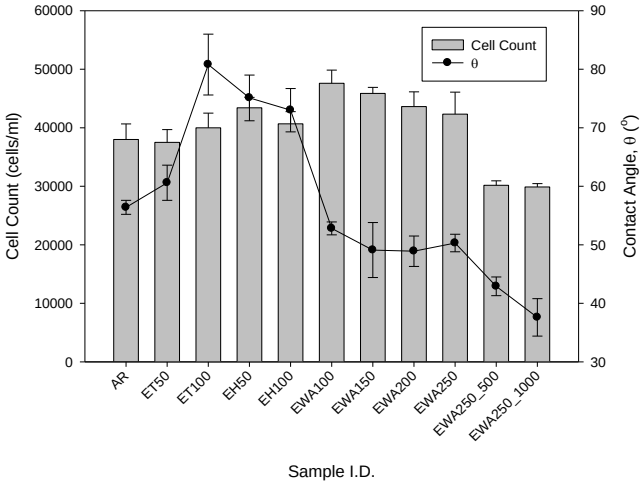

(a)

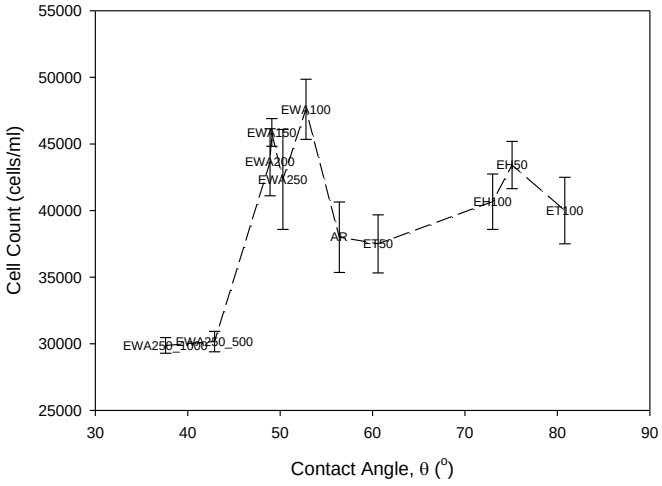

(b)

*Figure 12.29 – (a) Histogram showing the cell count in relation to θ for all KrF excimer laser processed samples and (b) graph showing the relationship between θ and cell count following four days incubation. (One-Way ANOVA showed an overall significance with F=54.196 and p=0.000. Scheffe's range test showed that there was statistical difference between all samples apart from AR; ET50; ET100 and EH100, EWA100; EWA150; EWA200 and EWA250, EH50; EWA150; EWA200 and EWA250, EWA250_500 and EWA250_1000*p<0.5).*

It can be seen from Figure 12.30(a) that there did not appear to be any correlation between γ^P and the cell count for the KrF excimer laser-induced patterned nylon 6,6 samples. In general, for the KrF excimer laser whole area irradiative processed samples Figure 12.30(a) shows that there could have been a slight correlative trend in that the cell count reduced on account of an increase in γ^P. This can be further identified in Figure 12.30(b) showing no distinct correlation for the KrF excimer laser-induced patterned samples and a slight decreasing function trend for the KrF excimer laser whole area irradiative processed samples. The cell count being a decreasing function of γ^P can be seen to coincide with what was observed in Section 12.2 and Section 12.3, which gave evidence of increasing γ^P

giving rise to less enhanced osteoblast cell response. In addition to this, the data presented in Figure 12.30 to some extent is the inverse of that seen for θ and again supports what has been observed in Section 12.2 and Section 12.3. Furthermore, this further supports the relationship between θ and γ^P as determined in Chapter 10.

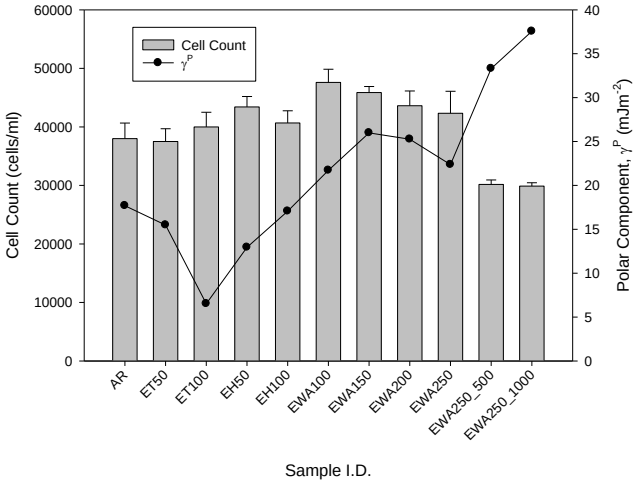

(a)

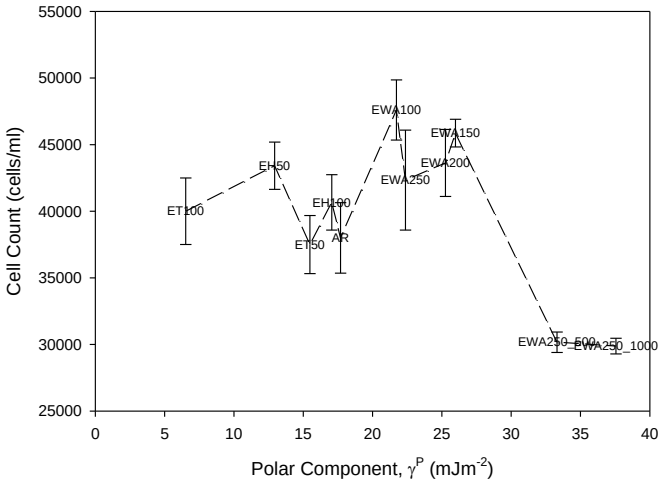

(b)

Figure 12.30 – (a) Histogram showing the cell count in relation to γ^P for all KrF excimer laser processed samples and (b) graph showing the relationship between γ^P and cell count following four days incubation.

Figure 12.31(a) shows that upon a significant reduction in γ^T for the KrF excimer laser-induced patterned samples the cell count increased slightly by up to 5,000 cells/ml compared to the as-received sample (AR). Similarly, for the KrF excimer laser whole area irradiative processed samples it was found that the cell count decreased dramatically on account of an increase in γ^T. These similar trends can also be identified through Figure 12.31(b). It has been suggested throughout Section 12.2 and Section 12.3 that there could potentially be an operating threshold window for θ, γ^P and γ^T in order for KrF excimer laser processed nylon 6,6 to give an enhanced osteoblast cell response. However, Figures 12.29, 12.30 and 12.31 do not conclusively follow this trend and suggest that the

two different KrF excimer laser processing techniques do not correlate to the same trend when it comes down to the osteoblast cell response. On account of this, by comparing the two KrF excimer laser processing techniques it can be seen that the worst and best osteoblast cell responses came from the KrF excimer laser whole area irradiative processed nylon 6,6 samples indicating that this method would potentially be the most optimum technique for the modulation of osteoblast cell adhesion and proliferation.

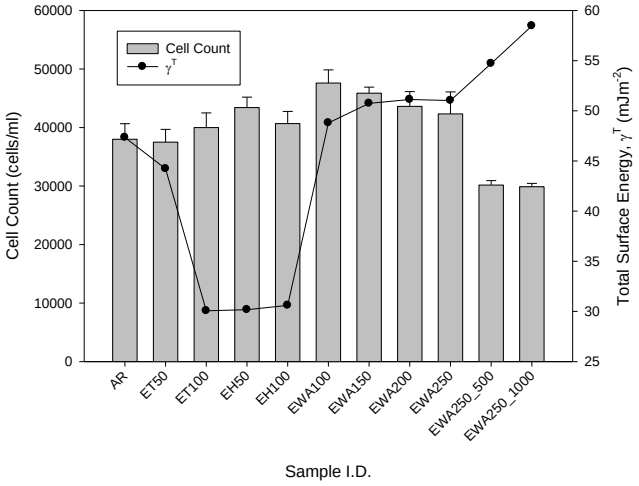

(a)

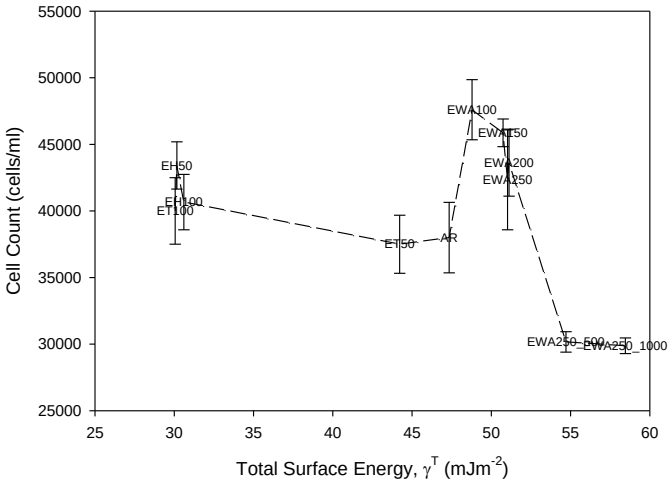

(b)

Figure 12.31 – (a) Histogram showing the cell count in relation to γ^T for all KrF excimer laser processed samples and (b) graph showing the relationship between γ^T and cell count following four days incubation.

From Figure 12.32(a) one can see that the cell count could not have been modulated by the Ra for the KrF excimer laser whole area irradiative processed nylon 6,6 samples on account of the fact that the Ra for all of these samples is around 0.05 µm. This corresponds with what has been observed in Section 12.2 and Section 12.3 which identifies that Ra is not a dominant parameter in determining the osteoblast cell response to the KrF excimer laser whole area irradiative processed samples. The same cannot necessarily be said for the KrF excimer laser-induced patterned samples as Figure 12.32(b)

further highlights that the cell count could have been an increasing function of Ra. This suggests that in contrast to what was reported in Section 12.3, the increase in Ra for the KrF excimer laser-induced patterned samples appeared to be a positive influence for osteoblast cell response in terms of cell count. Again this could be due to the mixed-state wetting regime giving rise to results which do not correspond to any particular trend which implies that predicting the bioactive nature of the KrF excimer laser patterned nylon 6,6 would be very difficult to carry out.

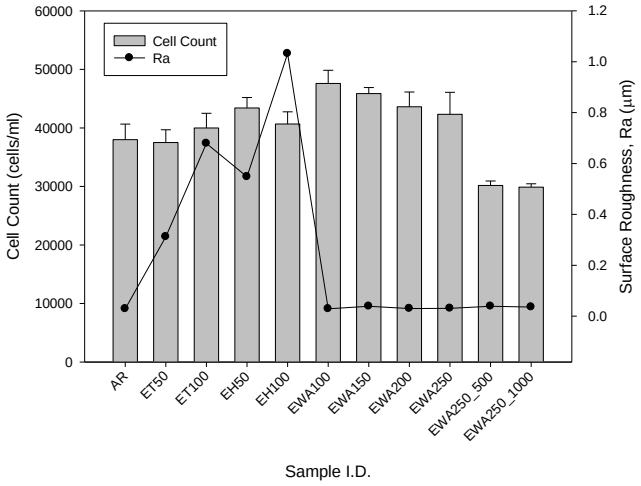

(a)

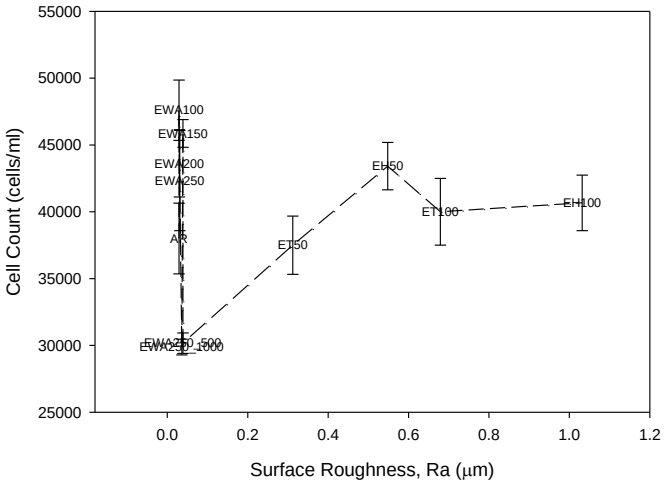

(b)

Figure 12.32 – (a) Histogram showing the cell count in relation to Ra for all KrF excimer laser processed samples and (b) graph showing the relationship between Ra and cell count following four days incubation.

In terms of Sa Figure 12.33(a) and 12.33(b) show that the Sa for the KrF excimer laser whole area irradiative processed nylon 6,6 samples had a negligible effect upon the osteoblast cell response in terms of cell count. This is due to the fact that the cell count was modulated and Sa stay somewhat constant at around 0.1 μm. Conversely, similar to what was observed with Ra (see Figure 12.32), Figure 12.33 allows one to see that the cell count for the KrF excimer laser-induced patterned samples was a slight increasing function of Sa which also does not correspond with Section 12.3. These results

show that for the KrF excimer laser-induced patterned samples an increase in surface roughness appears to have a positive influence on osteoblast cell count but not on cell cover density (see Section 12.3). This could be accounted for by the transition in wetting regimes across the patterned nylon 6,6 surfaces which would have large effects on the osteoblast cell response. Having said that, if the trends shown here and in Section 12.3 were to hold true then surface roughness could be implemented as a tool to aid in predicting the osteoblast cell response to nylon 6,6.

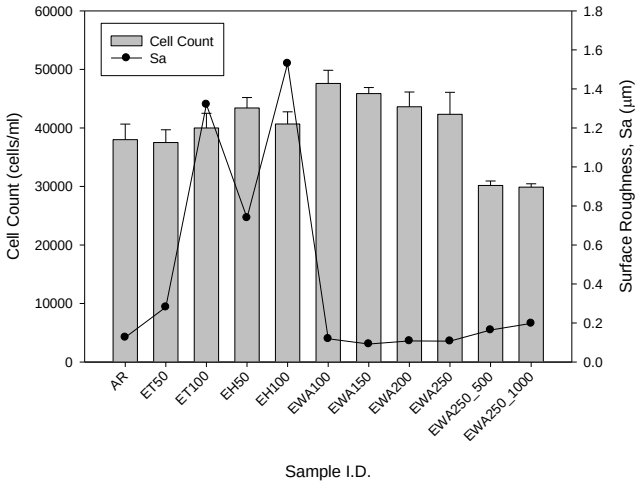

(a)

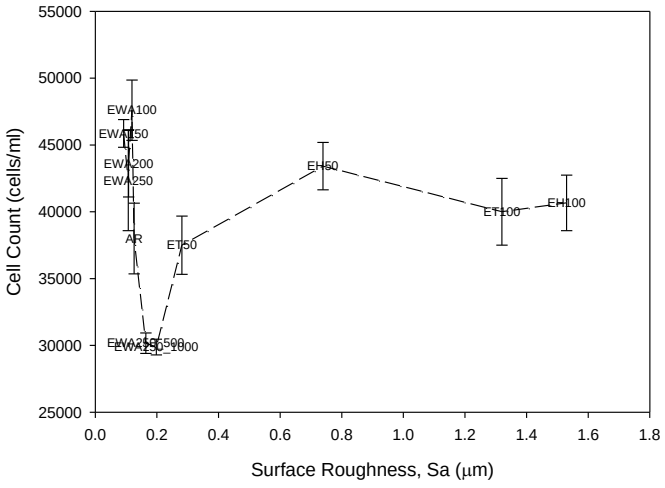

(b)

Figure 12.33 – (a) Histogram showing the cell count in relation to Sa for all KrF excimer laser processed samples and (b) graph showing the relationship between Sa and cell count following four days incubation.

Figure 12.34(a) and Figure 12.34(b) allow one to see that for all of the KrF excimer laser processed nylon 6,6 samples the cell count appeared to have a strong correlation with surface oxygen content in that an increase in surface oxygen content brought about a reduction in the cell count. This does not necessarily mean that an increase in the surface oxygen content hinders cell response but could be used as an indirect indicator of how a KrF excimer laser processed nylon 6,6 will perform when in contact with osteoblast cells. This is on account of the nylon 6,6 potentially becoming excessively

toxic as discussed in Chapter 11 through melting of the nylon 6,6 surface giving rise to toxic substances which would hinder cell growth. Even though these substances may be present it is likely that surface oxidation would have taken place which would explain the increase in surface oxygen content and reduction in cell count for the KrF excimer laser processed samples. As such cytotoxicity will be further discussed in Section 12.5.

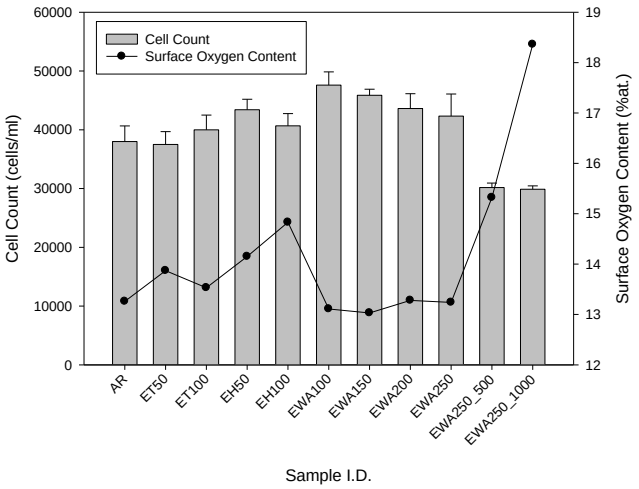

(a)

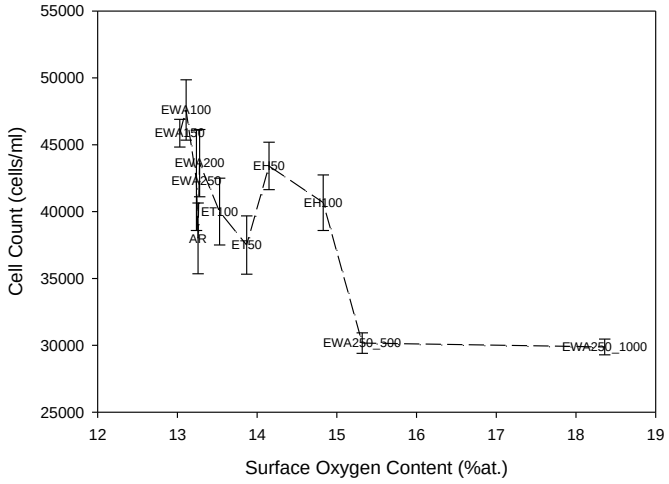

(b)

Figure 12.34 – (a) Histogram showing the cell count in relation to surface oxygen content for all KrF excimer laser processed samples and (b) graph showing the relationship between surface oxygen content and cell count following 4 days incubation.

12.5 – Effects of KrF Excimer Laser Processing of Nylon 6,6 on Cytotoxicity and Alkaline Leukocyte Phosphatase (ALP) Activities

This Section discusses the results obtained on the osteoblast cell cytotoxicity and ALP levels for the KrF excimer laser processed nylon 6,6 samples after two days of incubation. The experimental technique can be found in Chapter 5.

12.5.1 – KrF Excimer Laser-Induced Patterning

Figure 12.35 allows one to identify that the osteoblast cell cytotoxicity was affected by the KrF excimer laser-induced patterning of the nylon 6,6 samples such that for all of the KrF excimer laser-induced patterned samples the cytotoxicity absorbance reading had increased by at least 0.002 in comparison to the as-received sample (AR) which had a cytotoxicity absorbance reading of around 0.003. The largest increase in cytotoxicity absorbance was determined for the 50 µm dimensioned patterned samples (ET50 and EH50) with approximately 0.005. The slight increase in cytotoxicity for the KrF excimer laser-induced patterned nylon 6,6 samples can be attributed to the samples becoming more toxic as discussed in Section 11.5. Furthermore, it can be seen from Figure 12.35 that even though slight increases in cytotoxicity was observed, the osteoblast cell response determined in Section 12.3 and Section 12.4 remained somewhat unchanged indicating that the osteoblast cell was not necessarily affected by the small variations in cytotoxicity.

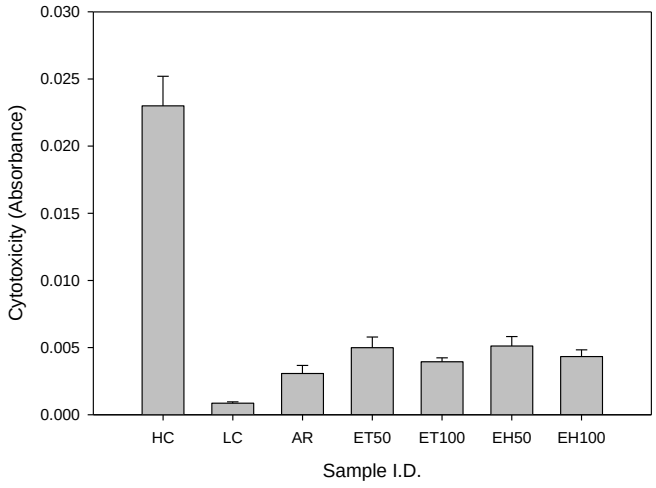

Figure 12.35 – Histogram showing the cytotoxicity level for each of the KrF excimer laser-induced patterned nylon 6,6 samples after two days incubation.

As a result of the increase in cytotoxicity for all of the KrF excimer laser-induced patterned samples it can be seen that the ALP levels (see Figure 12.36) had all reduced by up to 10 RFU compared to the as-received sample (AR). Leading on from this, even though both the cytotoxicity and ALP levels were modulated for the KrF excimer laser-induced patterned samples the osteoblast cell response as discussed in Section 12.3 and Section 12.4 did not show a significant variation in comparison to the

as-received sample (AR). Therefore, it is reasonable to say that the observed increase in cytotoxicity (see Figure 12.35) and reduction in ALP levels (see Figure 12.36) for the KrF excimer laser-induced patterned samples in comparison to the as-received sample (AR) was not enough to significantly modulate the osteoblast cell response.

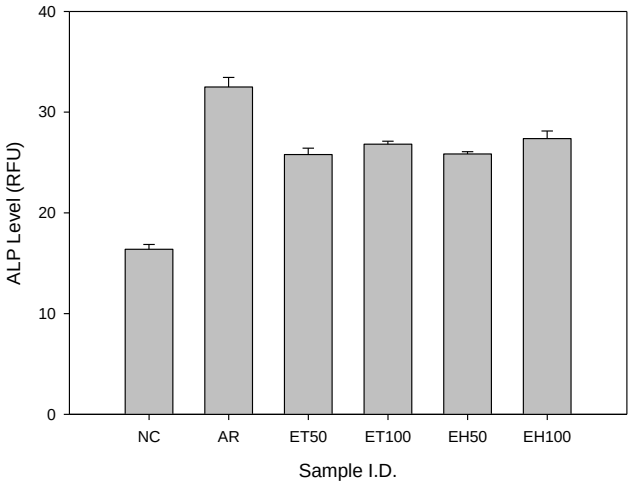

Figure 12.36 – Histogram showing the ALP level for each of the KrF excimer laser-induced patterned nylon 6,6 samples after two days incubation.

12.5.2 – KrF Excimer Laser Whole Area Irradiative Processing

Figure 12.37 shows that the cytotoxicity of the KrF excimer laser whole area irradiative processed samples increased on account of an increase in fluence and increase in incident pulse number. Furthermore, it is possible to ascertain that sample EWA100 and EWA150 had equivalent cytotoxicity absorbance levels of 0.003 compared to the as-received sample (AR). The largest cytotoxicity absorbance level of 0.007 was determined for sample EWA250_1000 which had the largest fluence and more incident pulses suggesting that the increase in fluence and incident pulse numbers were making the nylon 6,6 surfaces more toxic. This further corresponds to what was stated in Section 11.5 in that above a certain laser-material interaction time the nylon 6,6 becomes too toxic inherently hindering the osteoblast cell response in terms of adhesion and proliferation. Leading on, the increase in cytotoxicity for the KrF excimer laser whole area irradiative processed nylon 6,6 samples is likely to be an explanation as to the observed osteoblast cell response as discussed in Section 12.3 and Section 12.4.

On account of the modulation of cytotoxicity absorbance levels as seen in Figure 12.37, it can be seen in Figure 12.38 that the ALP levels mirrored the cytotoxicity levels. For instance, sample EWA250_1000 gave the largest value of cytotoxicity and as a result gave rise to the lowest ALP level of about 17 RFU. Like with the cytotoxicity level, it is possible to see that both the ALP and cytotoxicity levels can be used to explain the observed osteoblast cell response as discussed in Section 12.3 and Section 12.4, such that a high level of ALP and low level of cytotoxicity gave rise to an enhanced osteoblast cell response.

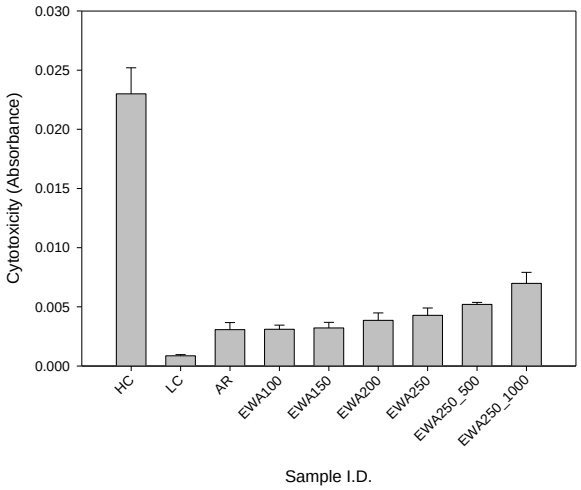

Figure 12.37 – Histogram showing the cytotoxicity level for each of the KrF excimer laser whole area irradiative processed nylon 6,6 samples after two days incubation.

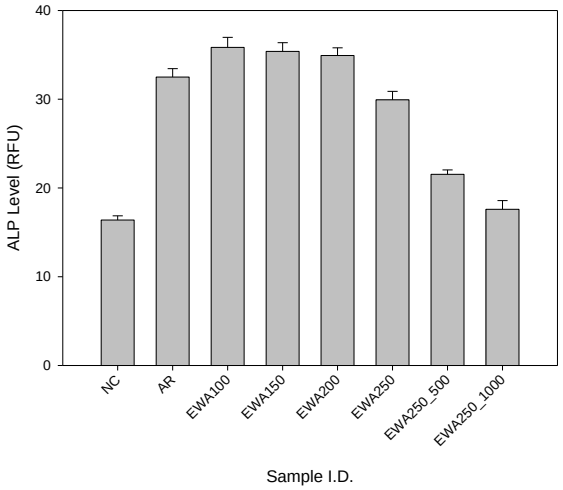

Figure 12.38 – Histogram showing the ALP level for each of the KrF excimer laser whole area irradiative processed nylon 6,6 samples after two days incubation.

2.5.3 – Comparison Between KrF Excimer Laser-Induced Pattering and KrF Excimer Laser

From Figure 12.39(a) one can see that the use of different KrF excimer laser processing techniques has allowed for the modulation of the cytotoxicity for the osteoblast cells. In terms of the KrF excimer laser–induced patterned nylon 6,6 samples it can be seen that the cytotoxicity increased by up to 18% for the 50 µm dimension patterned samples (ET50 and EH50) in comparison to the as-received sample (AR), which could be attributed to the fact that there was less as-received area between the KrF excimer laser-induced trenches in comparison to the 100 µm dimension patterned samples (ET100 and EH100). A different trend was observed for the KrF excimer laser whole area irradiative processed samples in that the largest increase in cytotoxicity for all samples with around 27% was

determined to be brought about by sample EWA250_1000 which had 1000 incident pulses and a fluence of approximately 90 mJcm^{-2}. It can also be ascertained from Figure 12.39(a) that the KrF excimer laser whole area irradiative processed samples gave rise to a trend in that an increase of fluence and incident number of pulses gave rise to an increase in cytotoxicity.

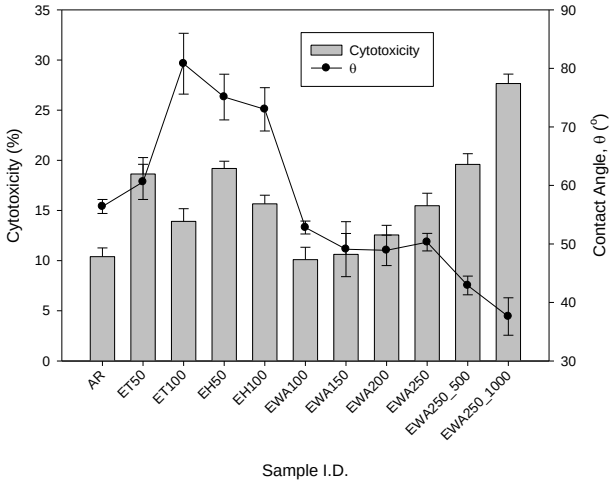

(a)

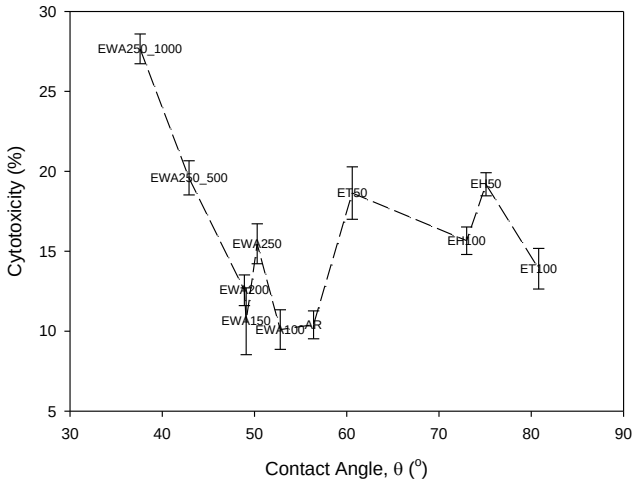

(b)

*Figure 12.39 – (a) Histogram showing the cytotoxicity in relation to θ for all KrF excimer laser processed samples and (b) graph showing the relationship between θ and cytotoxicity after two days incubation. (In terms of cytotoxicity, One-Way ANOVA showed an overall significance with F = 51.798 and p = 0.000. Scheffe's range test showed that there was statistical significance between all samples apart from AR; EWA100; EWA150 and EWA200, ET50; EH50 and EWA250_500, ET100; EH100; EWA200 and EWA250*p<0.5).*

From Figure 12.40(a) it can be seen that on account of the KrF excimer laser patterning of the nylon 6,6 samples the ALP levels all decreased slightly in comparison to the as-received sample (AR). Having said that, the KrF excimer laser whole area irradiative processed samples gave rise to a more modulate ALP level in that by increasing the fluence and incident pulse number, the ALP level

progressively decreased which can be attributed to the increase in cytotoxicity as seen in Figure 12.39 which hindered the ALP level.

Even though it has been observed that the cytotoxicity was manipulated by the KrF excimer laser surface treatment insofar as the cytotoxicity levels had increased on the most part. Through the assessment of the osteoblast cells after 24 hrs it was seen that the samples gave rise to an enhanced osteoblast cell response such that the cells had adhered and begun to proliferate across the samples. This finding suggests that the osteoblast cells had an enhanced response on account of the KrF excimer laser surface treatment, even though the cytotoxicity levels had increased when compared with the as-received sample. Also, even though both the cytotoxicity and ALP levels had been modulated with the differing excimer laser surface treatment, the study of the osteoblast cells did not appear to have shown that these modulating levels had not been able to completely stop osteoblast cell growth altogether. This can be explained by the fact that osteoblast cells are a robust cell type and as such may be able to still grow and proliferate even though cytotoxicity levels have increased and ALP levels have decreased.

12.5.4 – Wettability Characteristics and Surface Parameters

Figure 12.39(a) shows the cytotoxicity levels for each sample in relation to θ. From this it can be seen that a significant reduction of around 20° in θ compared to the as-received sample (AR) gave rise to the largest increase in cytotoxicity of approximately 30% for the KrF excimer laser whole area irradiative processed samples. This could be highly significant in terms of searching for a threshold parameter to predict how osteoblast cells will react when in a biological environment as this suggests that, for the KrF laser whole area irradiative processed samples, a large increase in cytotoxicity occurred with $\theta<50°$. In fact, the largest reduction in θ was observed for sample EWA250_1000 which had a θ of 37.6° and a cytotoxicity level of 28%. Another factor that may have contributed to this increase in cytotoxicity is that the fluence implemented in this instance was 90 $mJcm^{-2}$ and 1000 pulses were used. This could potentially have given rise to noteworthy surface modifications in terms of surface chemistry allowing the sample to become more toxic which has previously been discussed in Section 11.5, inherently allowing for the increase in cell death. In addition to this, it should be noted that most of the KrF excimer laser processed samples gave rise to an increase in cytotoxicity when compared to the as-received sample (AR). The least increase in cytotoxicity is attributed to the sample EWA100 and sample EWA150 which can be explained by the fact that the fluences used in this instance may not have been high enough to modify either the surface chemistry or surface topography of the nylon 6,6 samples. As a result of this, one observes that the cytotoxicity levels for these samples are equivalent to the as-received sample (AR) which had a cytotoxicity of around 10%. The trend for the KrF excimer laser whole area irradiative processed samples can also be identified using Figure 12.39(b) showing that the cytotoxicity appeared to have a strong correlation with θ in that the cytotoxicity was a decreasing function of θ. This trend corresponds with what was observed throughout Section 12.3 and Section 12.4 which identified that the osteoblast cell response was hindered with θ less than 50°.

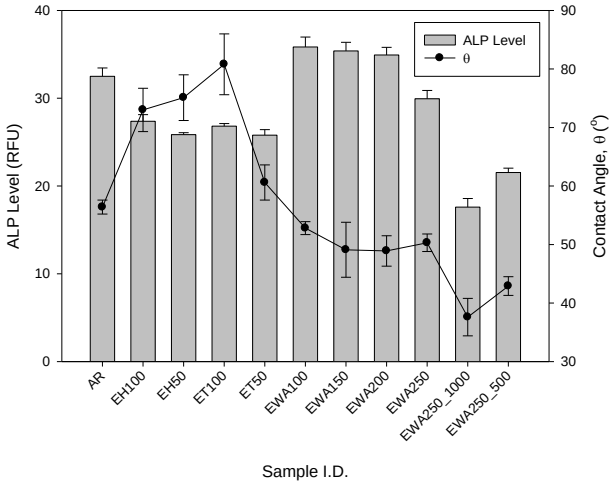

(a)

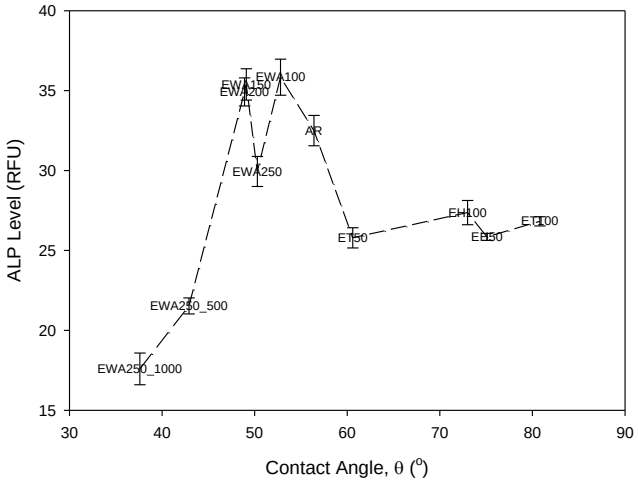

(b)

*Figure 12.40 – (a) Histogram showing the ALP level in relation to θ for all KrF excimer laser processed samples and (b) graph showing the relationship between θ and ALP level after two days incubation. (In terms of ALP, One-Way ANOVA showed an overall significance with F = 194.367 and p = 0.001. Scheffe's range test showed that there was statistical difference between all samples apart from AR; EWA100; EWA150 and EWA200, ET50; ET100;EH50;EH100 and EWA250*p<0.5).*

Figure 12.39(a) and Figure 12.39(b) also show that for the KrF excimer laser-induced patterned nylon 6,6 samples there did not appear to be any correlation with what was observed for the KrF excimer laser whole area irradiative processed samples. This can be attributed to the likely transition in wetting regime, discussed in Chapter 10, having a large impact on varying the results obtained. However, by taking the entire KrF excimer laser processed samples into account, Figure 12.39(b) allows one to see that there appeared to be an optimum window of θ for the nylon 6,6 between 47 and 55° which elicited a reduction in cytotoxicity. This also corresponds with what has been observed in Section 12.3 and Section 12.4. Nevertheless, owing to some erratic results not following any trend for the KrF excimer laser-induced patterned samples throughout this Chapter, it is necessary for one to

realize that these results may not be reliable. Nevertheless, it cannot be ignored that the results on a whole point towards an optimum parameter window for the nylon 6,6 material in terms of osteoblast cell response.

With the modulation of the cytotoxicity levels being observed it is possible for one to deduce that the KrF excimer laser surface treatments would have a similar effect on the ALP levels. Figure 12.40(a) shows a histogram of the ALP levels in relation to θ. It was found from Figure 12.40(a) that sample EWA250_1000 gave rise to the lowest ALP level of 16 RFU which can be attributed to the increase in cytotoxicity and a decrease in θ. In general all of the KrF excimer laser whole area irradiative processed samples, apart from samples EWA100, EWA150 and EWA200, lead to a reduction in ALP as a result of the increase in cytotoxicity levels. In terms of θ, from Figure 12.40(b) it can be seen that there appears to be a threshold window of between 47 and 55° for nylon 6,6 which gives rise to an increased ALP level of between 33 and 40 RFU. That is, any θ below or above this threshold results in a hindered ALP response. This gives further evidence to the optimum parameter window proposed earlier for the cytotoxicity (see Figure 12.39).

Figure 11.41(a) shows that in general, for the KrF excimer laser whole area irradiative processed nylon 6,6 samples, the cytotoxicity increased steadily upon an increase in γ^P. In contrast, a correlative trend between the cytotoxicity and γ^P for the KrF excimer laser-induced patterned samples was not readily discernible from Figure 11.41(a). Having said that, Figure 11.41(b) does show that the cytotoxicity for all of the KrF excimer laser processed samples could have had a trend with γ^P such that between γ^P values of 17 and 26 mJm^{-2} the nylon 6,6 gave rise to less cytotoxicity and to some extent a more enhanced cell response (see Section 12.3 and Section 12.4). It can also be seen from Figure 12.39(b) and Figure 12.41(b) that the correlation between the cytotoxicity, θ and γ^P were the inverse of one another further highlighting the link between θ and γ^P as determined in Chapter 10.

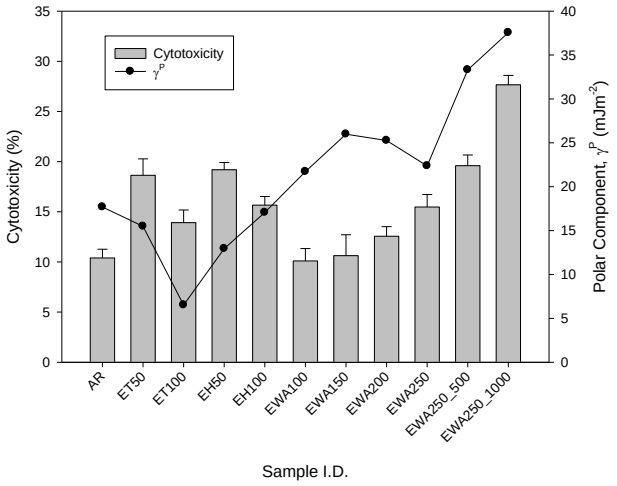

(a)

Figure 12.41 continued overleaf

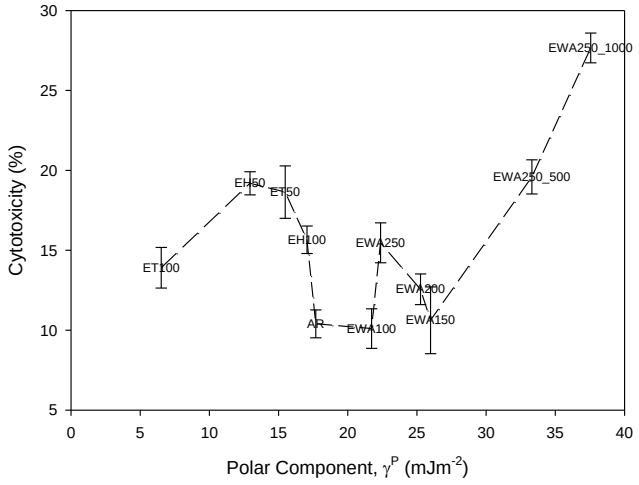

(b)

Figure 12.41 – (a) Histogram showing the cytotoxicity density in relation to γ^P for all KrF excimer laser processed samples and (b) graph showing the relationship between γ^P and cytotoxicity after two days incubation.

It can be ascertained from Figure 12.42(a) that, with regards to the KrF excimer laser whole area irradiative processed samples, the cytotoxicity increased steadily from 10 to 27% upon a rise in γ^T. On the other hand, the cytotoxicity and γ^T exhibited by the KrF excimer laser-induced patterned samples did not appear to have any particular correlative trend. These relationships can be further identified using Figure 12.42(b) and by combining the data points together for both KrF excimer laser processing techniques an operating threshold window can be potentially identified. That is, by taking into account all samples Figure 12.42(b) shows that the lowest cytotoxicity levels of around 10% were obtained with γ^T between 47 and 52 mJm^{-2}. Even though the transition in wetting regime may have been affecting the osteoblast cell response it is further evidenced in Figure 12.42(b) that an operating threshold window for the surface energy could be used to predict the osteoblast cell response to KrF excimer laser processed nylon 6,6.

Figure 12.43(a) and Figure 12.43(b) shows that Ra did not have any correlative trend with cytotoxicity for the KrF excimer laser whole area irradiative processed nylon 6,6 samples. This is on account of the cytotoxicity being highly modulated for these samples with the Ra remaining somewhat constant at around 0.05 μm. In contrast, it can be seen from Figure 12.43(b) that the cytotoxicity may have had some correlation with Ra for the KrF excimer laser-induced patterned samples such that the cytotoxicity reduced slightly upon an increase in Ra. Still, if one was to compare the cytotoxicity (see Figure 12.43), the apatite response (see Figure 12.9), the cell cover density (see Figure 12.19) and the cell count (see Figure 12.32) in terms of Ra it can be seen that the osteoblast cell response gave differing trends allowing one to identify that Ra may not be a useful parameter to determine the osteoblast cell response to KrF excimer laser-induced patterned nylon 6,6. This can accounted for by the transition in wetting regime which would have affected the results obtained for the different bioactive parameters. With this in mind, it is necessary for one to realize that

it may not be possible to predict the bioactivity of KrF excimer laser-induced patterned nylon 6,6 owed to the non-conformity of the results on the whole.

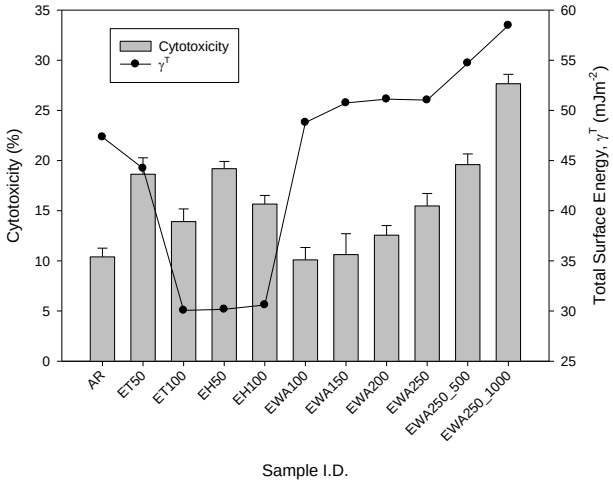

(a)

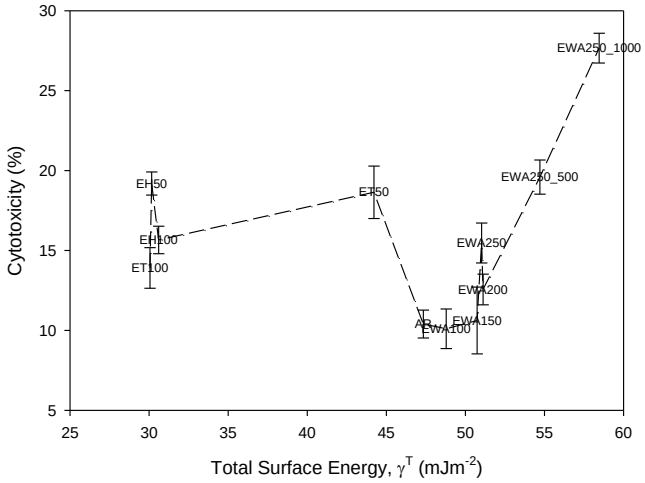

(b)

Figure 12.42 – (a) Histogram showing the cytotoxicity in relation to γ^T for all KrF excimer laser processed samples and (b) graph showing the relationship between γ^T and cytotoxicity after two days incubation.

Figure 12.44(a) and Figure 12.44(b) also show that for the KrF excimer laser whole area irradiative processed samples the Sa parameter of each of the samples did not have any distinct correlative relationship with the cytotoxicity. This is due to the Sa being similar, around 0.1 µm, for these samples when compared with the cytotoxicity levels which were found to be highly modulated. On the other hand, like with Ra (see Figure 12.43) the cytotoxicity appeared to be a slight decreasing function of Sa. However, by comparing the cytotoxicity (see Figure 12.44), the apatite response (see Figure 12.10), the cell cover density (see Figure 12.20) and the cell count (see Figure 12.33) in terms of the relationship with Sa it can be seen that the trend of an increase in Sa lead to an enhanced osteoblast cell response was not always followed. This further highlights the fact that the results for the KrF excimer laser-induced patterned nylon 6,6 samples in some instances gave rise to erratic

results which can be attributed to the transition in wetting regime playing a major role in giving erroneous results.

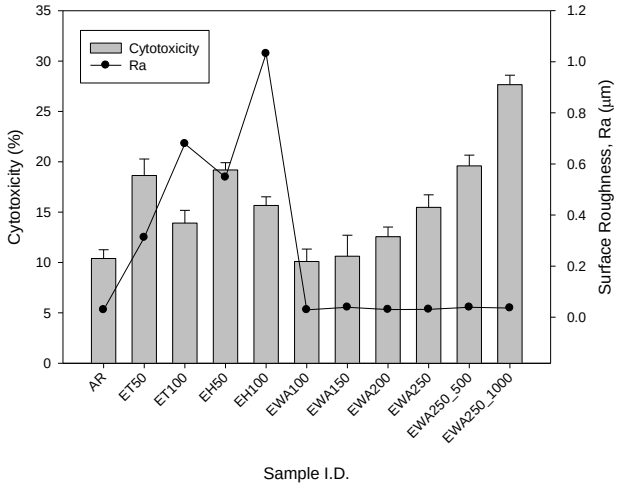

(a)

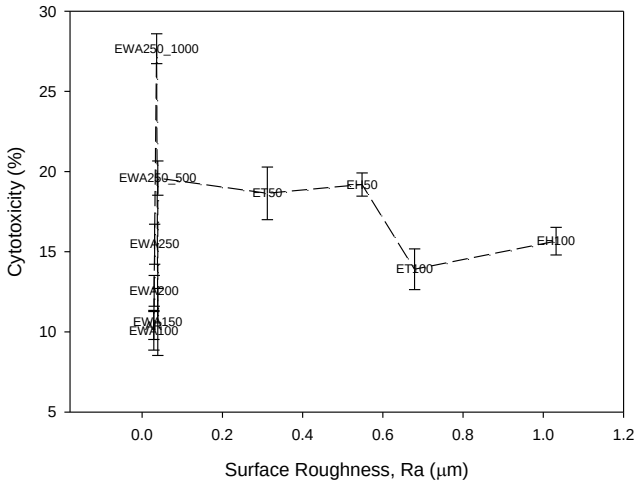

(b)

Figure 12.43 – (a) Histogram showing the cytotoxicity in relation to Ra for all KrF excimer laser processed samples and (b) graph showing the relationship between Ra and cytotoxicity after two days incubation.

In terms of surface oxygen content, it can be seen from Figure 12.45(a) that for the KrF excimer laser-induced patterned nylon 6,6 samples the cytotoxicity did not appear to have a correlation with the surface oxygen content. This is on account of the surface oxygen content increasing for these samples and the cytotoxicity not showing a correlative response. For the KrF excimer laser whole area irradiative processed samples there was a correlative trend in that the cytotoxicity steadily increased with an increase in surface oxygen content. Even though Figure 12.45(a) did not allow one to observe a correlative trend between the cytotoxicity and surface oxygen content for the KrF excimer laser-induced patterned samples, Figure 12.45(b) shows that when collating all of the results together the cytotoxicity increased on an increase in surface oxygen content. This does not necessarily account directly for the increase in cytotoxicity as those samples with larger fluences and incident pulse

numbers could have given rise to an increase in surface toxicity, as previously discussed in Section 11.5. By taking this into account, one can realize that oxidation will also take place during the laser processing even though there is a likelihood of toxic substances becoming present on the surface of the nylon 6,6 surfaces. If these substances were to be present then the cytotoxicity would then be seen to dominate the osteoblast cell response after a certain incident fluence and laser-material interaction time. As a result of this, the surface oxygen content could be implemented to indirectly determine the cytotoxicity and osteoblast cell response to the KrF excimer laser processed nylon 6,6. It should also be noted here that those results shown in Figure 12.45 correspond to what was observed for the cell cover density (see Figure 12.21) and the cell count (see Figure 12.34) which further gives evidence to the potential use of the surface oxygen content to indirectly predict the osteoblast cell response to KrF excimer laser processed nylon 6,6.

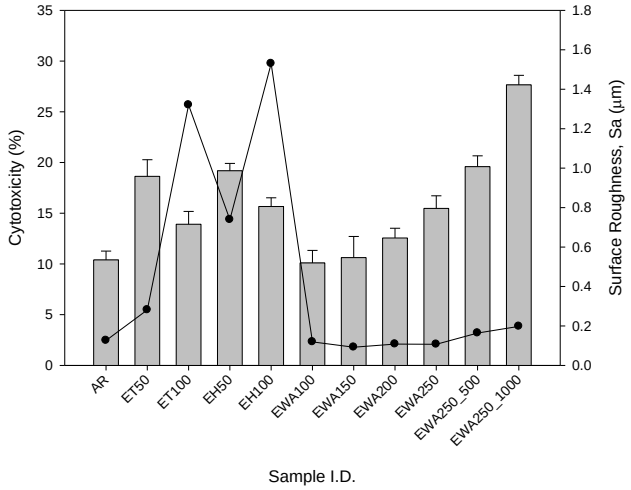

(a)

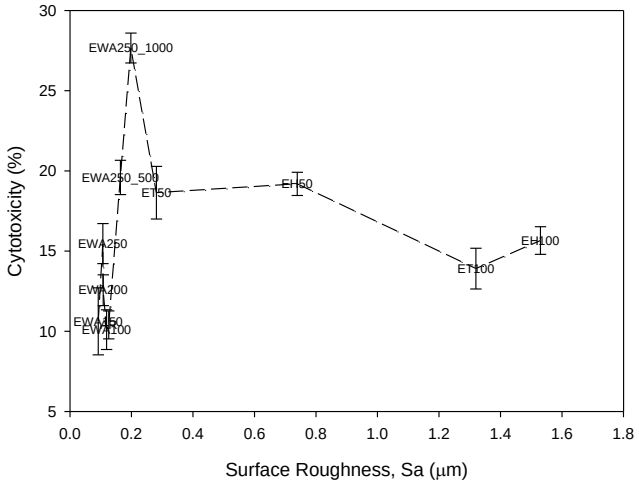

(b)

Figure 12.44 – (a) Histogram showing the cytotoxicity in relation to Sa for all KrF excimer laser processed samples and (b) graph showing the relationship between Sa and cytotoxicity after two days incubation.

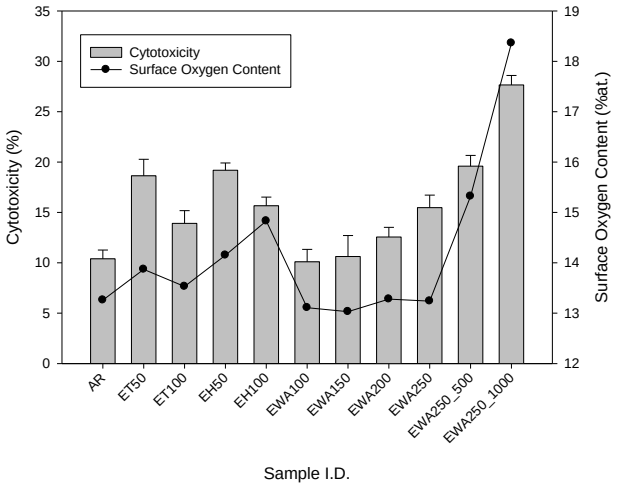

(a)

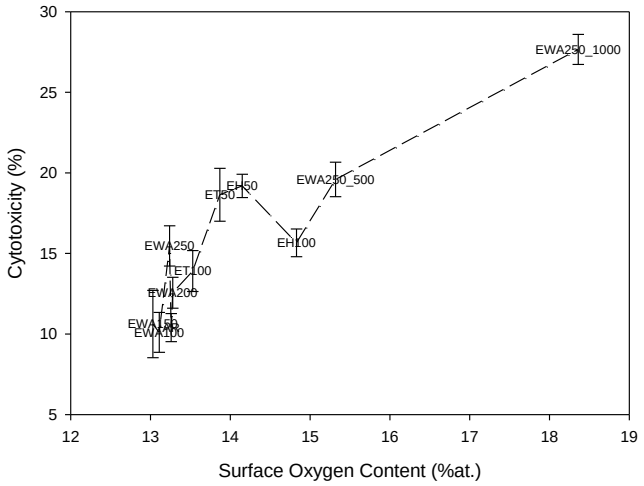

(b)

Figure 12.45 – (a) Histogram showing the cytotoxicity in relation to surface oxygen content for all KrF excimer laser processed samples and (b) graph showing the relationship between surface oxygen content and cytotoxicity after two days incubation.

The relationship between the ALP level and θ was determined to be the inverse of what was observed between the cytotoxicity and θ owed to the account that the cytotoxicity and ALP levels are closely linked. From Figure 12.46(a) and Figure 12.46(b) it can be seen that in terms of the relationship between ALP levels and γ^P, this was no different. This is owed to the account that Figure 12.46(b) shows a similar threshold operating window for γ^P between 17 and 27 mJm^{-2} which gave rise to the largest increase in ALP levels of approximately 35 RFU. Also, Figure 12.46(a) and Figure 12.46(b) show that for the largest increases in γ^P gave rise to the lowest ALP levels further indicating that a more hydrophilic material compared to the as-received sample lead to a less enhanced osteoblast cell response. This can be accounted for by the rough, toxic surface giving rise to a more hydrophilic surface, an increase in cytotoxicity which resulted in a hindered ALP level and a hindered osteoblast cell response.

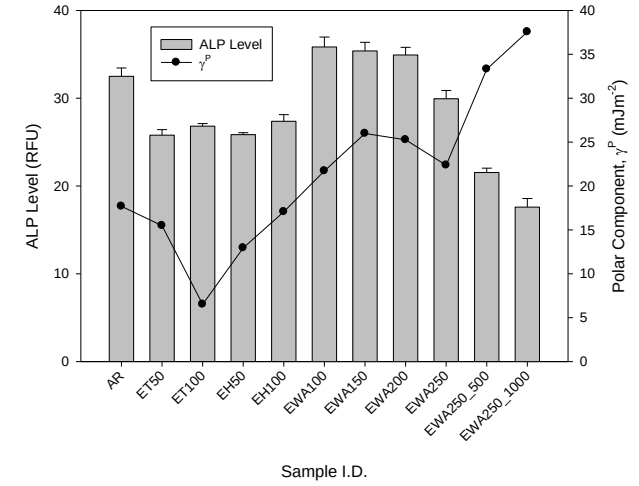

(a)

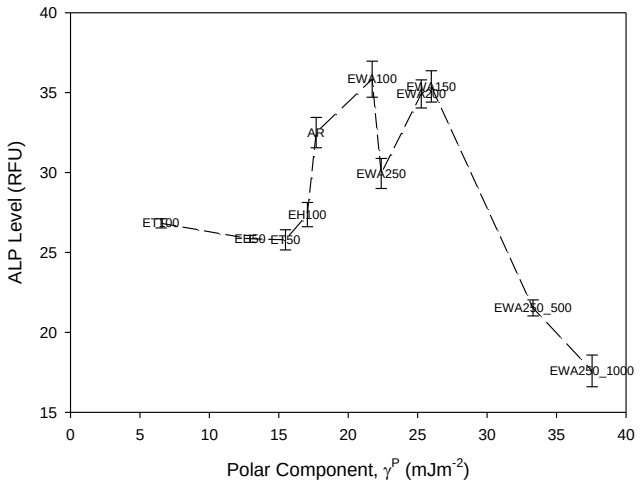

(b)

Figure 12.46 – (a) Histogram showing the ALP level in relation to γ^P for all KrF excimer laser processed samples and (b) graph showing the relationship between γ^P and ALP level after two days incubation.

Figure 12.47(a) and Figure 12.47(b) allow one to see that like with γ^P the ALP level also showed the inverse for γ^T as to what was observed with the cytotoxicity and γ^T (see Figure 12.42). In addition to this, the ALP levels shown in Figure 12.47(b) give further evidence of an operating threshold window for γ^T of between 47 and 53 mJm^{-2} which elicited the highest ALP levels and enhanced osteoblast cell response (see Section 12.3 and Section 12.4). Furthermore, Figure 12.47(a) and Figure 12.47(b) further indicate that an increase in γ^T, with the nylon 6,6 becoming more hydrophilic, gave rise to a less enhanced osteoblast cell response. As discussed previously for γ^P, this can be explained by the surface parameters giving rise to a more hydrophilic toxic surface leading to hindered osteoblast cell growth.

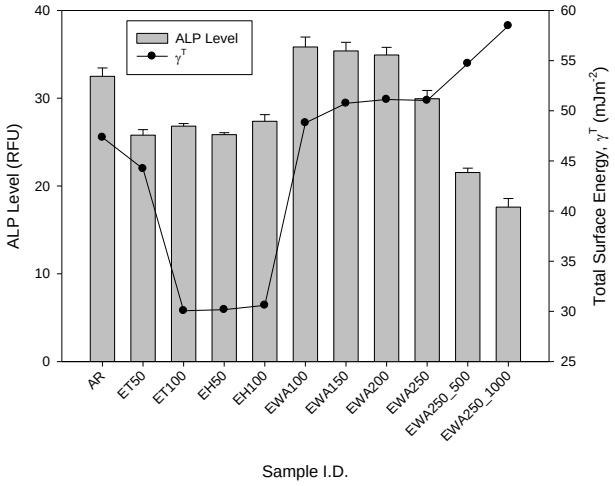

(a)

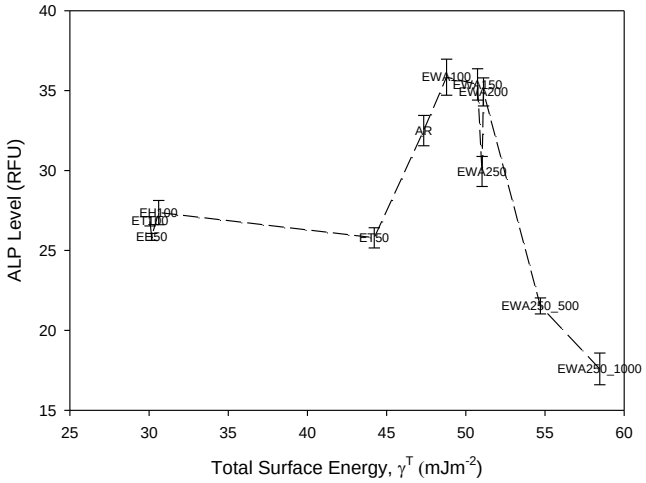

(b)

Figure 12.47 – (a) Histogram showing the ALP level in relation to γ^T for all KrF excimer laser processed samples and (b) graph showing the relationship between γ^T and ALP level after two days incubation.

It is further evidenced by Figure 12.48(a) that Ra for the KrF excimer laser whole area irradiative processed nylon 6,6 did not have a correlative trend with the observed osteoblast cell response. This is on account of similar values of 0.05 µm for Ra giving a somewhat modulated ALP level which mirrored the cytotoxicity levels. The trend can also be determined using Figure 12.48(b) which shows the modulated ALP level around 0.05 µm. Another factor which can be taken from Figure 12.48(b) is that the ALP level for the KrF excimer laser-induced patterned samples remained almost constant at around 25 RFU regardless of the large variations in Ra. This further attests to the likelihood that the surface roughness cannot be easily implemented to predict the osteoblast cell response to the KrF excimer laser-induced patterned nylon 6,6.

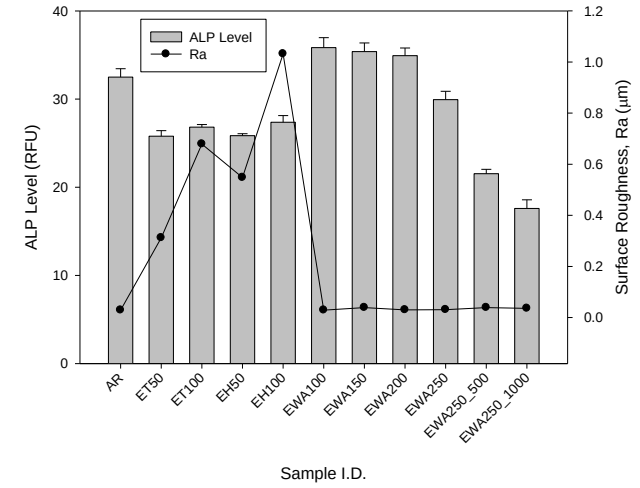

(a)

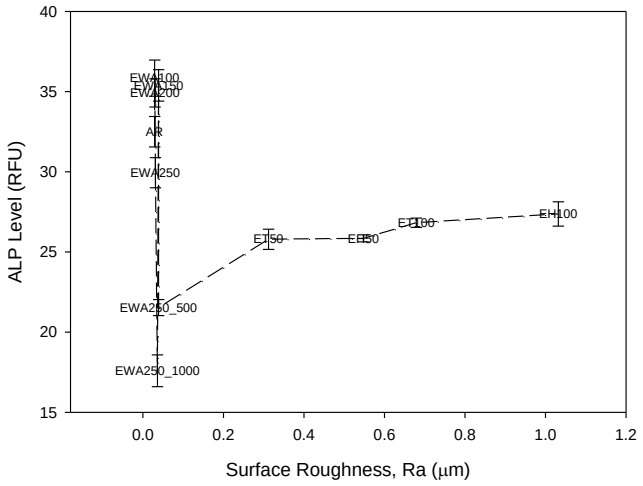

(b)

Figure 12.48 – (a) Histogram showing the ALP level in relation to Ra for all KrF excimer laser processed samples and (b) graph showing the relationship between Ra and ALP level after two days incubation.

One can see from Figure 12.49(a) that a similar result to that for Ra (see Figure 12.48) was observed for the relationship between ALP levels and Sa for the KrF excimer laser processed nylon 6,6 samples. For the KrF excimer laser whole area irradiative processed samples it can be seen from Figure 12.49(a) and Figure 12.49(b) that even though there were large variations in the ALP levels, the Sa did not vary significantly. This allows one to further realize that the surface roughness did not play a dominant role in the osteoblast cell response. Also, Figure 12.49(b) shows that the ALP levels for the KrF excimer laser-induced patterned samples remained constant regardless of the large variations in Sa. With this in mind, along with the other surface roughness results discussed in Sections 12.2, 12.3 and 12.4 there is not a conclusive trend between surface roughness and osteoblast response suggesting that in some instances it can be used to predict the osteoblast cell response to nylon 6,6. Realistically, however, one can deduce that, owed to the transition in wetting regime, the KrF excimer laser-induced patterned nylon 6,6 samples gave rise to some results which were highly

unpredictable indicating that surface roughness may not be able to be implemented as a predictive tool.

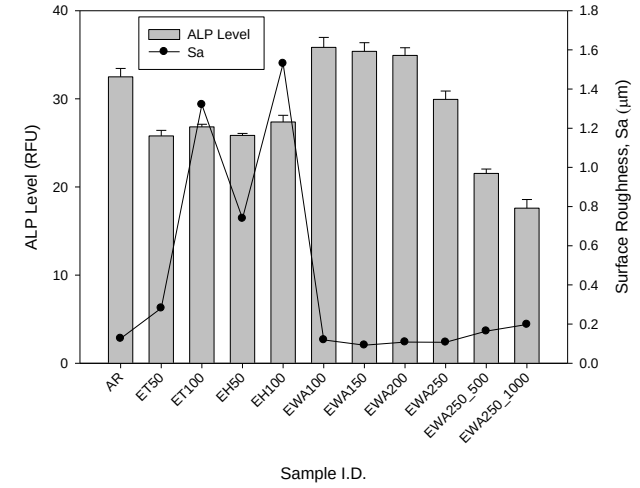

(a)

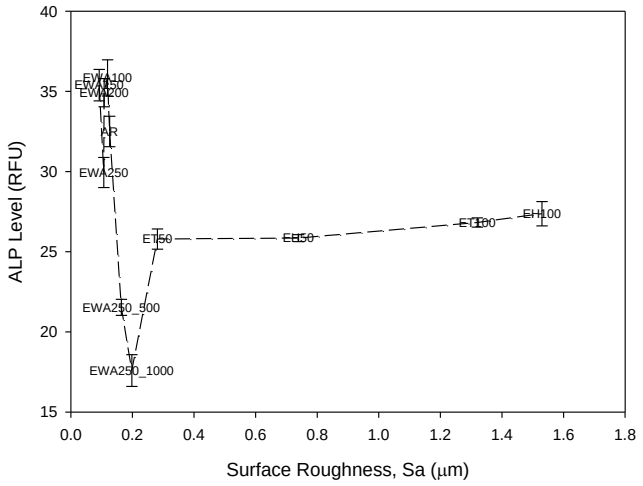

(b)

Figure 12.49 – (a) Histogram showing the ALP level in relation to Sa for all KrF excimer laser processed samples and (b) graph showing the relationship between Sa and ALP level after two days incubation.

Figure 12.50(a) shows that there may not have been any distinctive correlative trend between the ALP level and the surface oxygen content for the KrF excimer laser-induced patterned samples owed to the fact that there was no considerable variation in ALP level, even though surface oxygen content increased compared to the as-received sample (AR). In contrast, the KrF excimer laser whole area irradiative processed nylon 6,6 samples can be seen from Figure 12.50(a) that the ALP level reduced upon a significant increase in surface oxygen content. What is more, upon collating the entire results for the KrF excimer laser processed samples, Figure 12.50(b) shows that upon an increase in surface oxygen content a decrease in ALP level was elicited. This further suggests that the surface oxygen content can be used to predict the ALP level and osteoblast cell response for nylon 6,6. Having said that, as discussed previously it is highly likely that this trend arises from oxidation of the nylon 6,6

surface taking place whilst the toxicity of the surface increased leading on to a reduced enhanced osteoblast cell response.

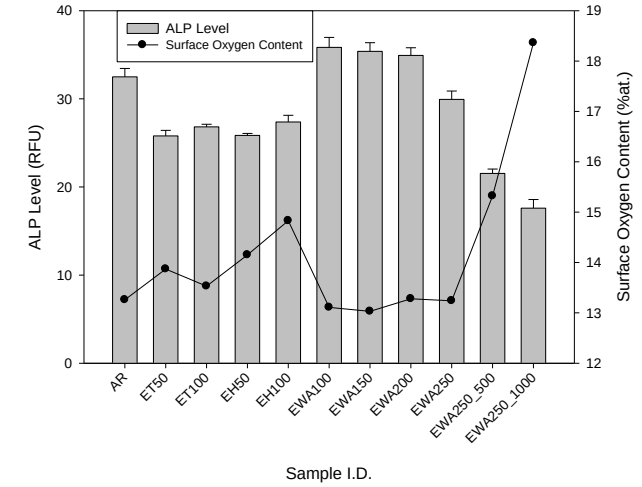

(a)

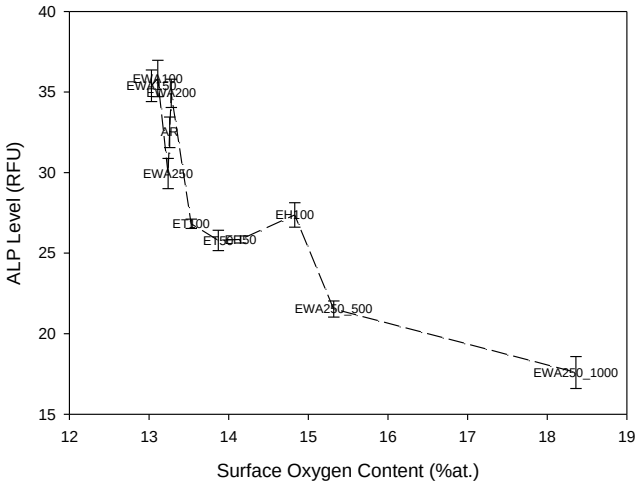

(b)

Figure 12.50 – (a) Histogram showing the ALP level in relation to surface oxygen content for all KrF excimer laser processed samples and (b) graph showing the relationship between surface oxygen content and ALP level after two days incubation.

12.6 – Effects of KrF Laser-Induced Cytotoxicity on Osteoblast Cell Response and Alkaline Leukocyte Phosphatase (ALP) Levels

It has been seen in Sections 12.3, 12.4 and 12.5 that the KrF laser surface treatment implemented has given rise to a modulation in osteoblast cell response in terms of cell cover density (see Section 12.3), cell count (see Section 12.4), cytotoxicity (see Section 12.5) and ALP levels (see Section 12.5). Even so, it has been seen throughout this Chapter that, at some point, the cytotoxicity appeared to dominate the osteoblast cell response in that a large increase in cytotoxicity, especially for sample

EWA250_500 and sample EWA250_1000, hindered the osteoblast cell response. Figure 12.51(a) shows a histogram of the cytotoxicity for each of the KrF excimer laser processed samples in relation to the cell count and ALP level. In both instances it can be seen from Figure 12.51(a) that, in general, the cell count and ALP level reduces on account of an increase in cytotoxicity. In fact, that highest ALP levels and cell counts were determined for those samples with the lowest cytotoxicity (Sample EWA100 and sample EWA150); however, it can be seen that these samples had equivalent cytotoxicity levels to the as-received sample (AR) of around 10% and the cell count can be seen to be significantly low. This is important to note as this indicates that even though the cytotoxicity is low for sample EWA100 and EWA150, other surface parameters will also have an effect on the osteoblast for those samples which have an incident fluence and pulse number below a certain threshold. Above this threshold the cytotoxicity will dominate, ultimately hindering the osteoblast cell growth.

Figure 12.51(b) allows one to see that even though a number of parameters could have played a role in the osteoblast cell response at low fluences and low incident pulse numbers, the cytotoxicity still appeared to play some role in the measured cell count. That is, the cell count reduced on account of an increase in cytotoxicity further suggesting that the KrF laser-induced cytotoxicity played a significant role in the osteoblast cell response to the nylon 6,6 samples.

In a similar means, the ALP level can be seen in Figure 12.51(b) to be a decreasing function of the cytotoxicity for the KrF excimer laser processed samples. This is a highly important result along with what was observed in Figure 12.51(b) as it allows one to deduce that two common parameters in cytotoxicity and ALP level have been identified which links the osteoblast cell response to a certain extent for both the KrF excimer laser-induced patterned and KrF excimer laser whole area irradiative processed nylon 6,6. On account of this, it can be seen that even though different wetting regimes can explain the difference in trends between the osteoblast cell response and surface parameters, the laser-induced cytotoxicity and resulting ALP levels have the major potential in being able to be implemented to predict the osteoblast cell response to KrF excimer laser processed nylon 6,6.

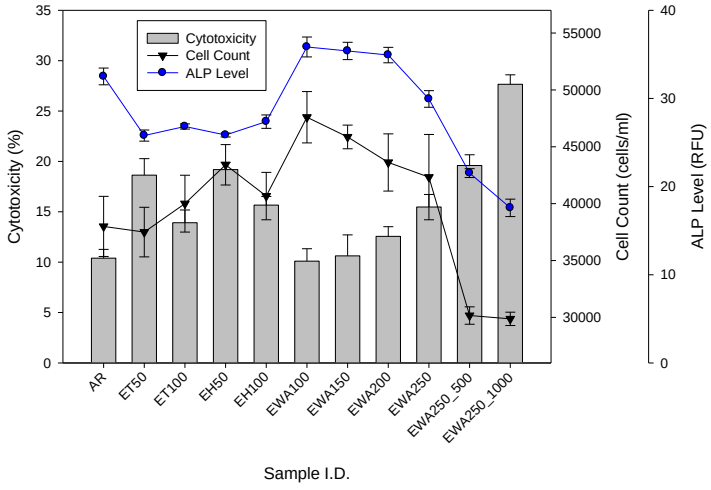

(a)

Figure 12.51 continued overleaf

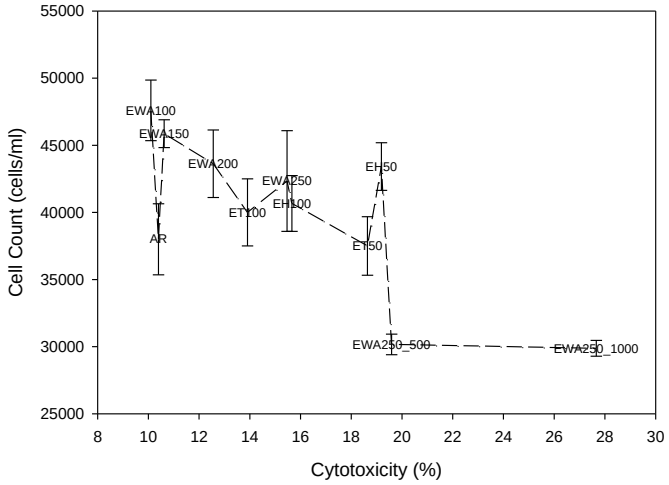

(b)

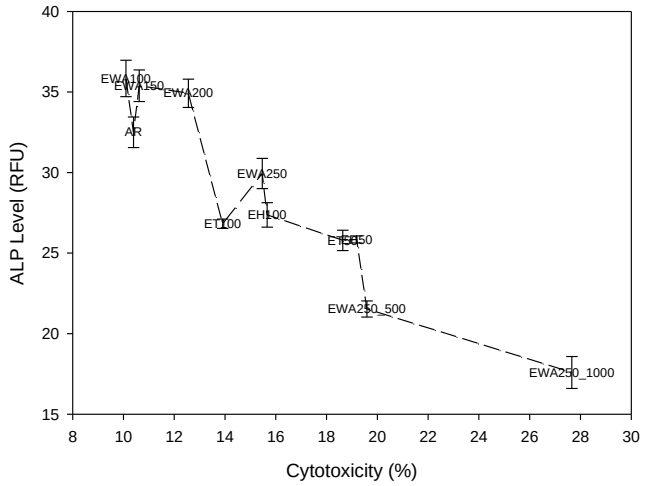

(c)

Figure 12.51 – (a) Histogram showing the cytotoxicity in relation to cell count and ALP level for all KrF excimer laser processed samples, (b) graph showing the relationship between cell count and cytotoxicity and (c) graph showing the relationship between ALP level and cytotoxicity.

13
Identifying Generic Wettability Characteristics to Determine the Osteoblast Cell Response to Nylon 6,6

In previous Chapters CO_2 and KrF excimer laser processing has been found to have modified significantly the surface parameters and wettability characteristics of the nylon 6,6 samples. As a result of this one can expect that these surface modifications will have a large impact upon the osteoblast cell response to the nylon 6,6. This Chapter discusses possible generic parameters which will dominate and determine the biofunctionality of the nylon 6,6 following laser surface treatment.

13.1 – Introduction

A number of different surface parameters have been seen to hold the potential of driving the bioactive nature of materials [4]. It has been seen throughout Chapter 6 to 10 that both CO_2 and excimer lasers have the ability to modify significantly the surface parameters and wettability characteristics of nylon 6,6. In addition to this, in Chapter 11 and Chapter 12 it was shown that the osteoblast cell response to the nylon 6,6 samples could be modulated as a result of the surface modifications brought about by the different laser processing techniques.

Because the modulation of surface parameters, wettability characteristics and osteoblast cell response can be brought about by the different laser processing techniques it is necessary to collate the results in order to determine if there are any generic parameters which can be used to manipulate the surface of the nylon 6,6 material in order to enhance osteoblast cell response.

13.2 – CO_2 and KrF Excimer Laser-Induced Patterning

This section discusses and details the results obtained for the laser-induced patterned nylon 6,6 in order to determine if any correlative trends could be identified between the wettability characteristics apatite response and osteoblast cell response.

13.2.1 – Apatite Response

Upon first appearances the results shown in Figure 13.1(a) seem to suggest that there may not have been a strong correlation between apatite formation and θ for the laser-induced patterned nylon 6,6 samples. Yet, Figure 13.1(b) allows one to see that there may have been some correlation as between θ of 57 to 65° Δg was at a maximum of around 0.03 g, implying that an optimum θ threshold window could be applied to CO_2 and KrF excimer laser-induced patterned nylon 6,6. Even though a threshold window is indicated in Figure 13.1(a), it is also worthwhile noting that some samples such as EH50

and ET100, do not appear to totally follow this trend as they displayed a θ value considerably larger than the proposed threshold window with Δg increasing. This could be attributed to the fact that the mixed-state wetting regime, as discussed in Chapter 10, gave rise to different apatite response which did not follow any particular relationship with θ.

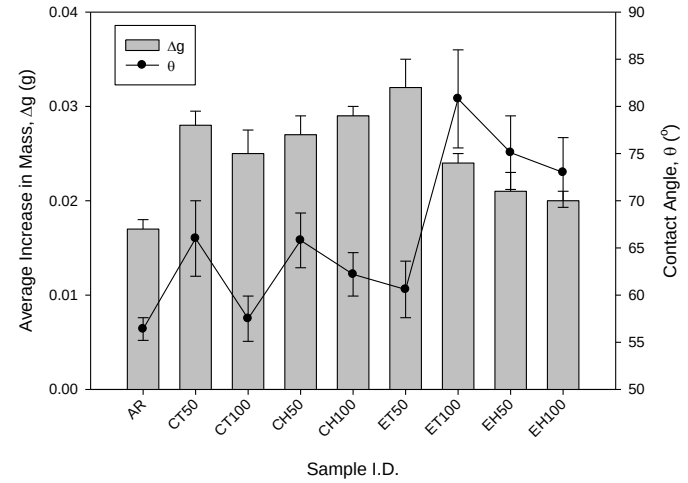

(a)

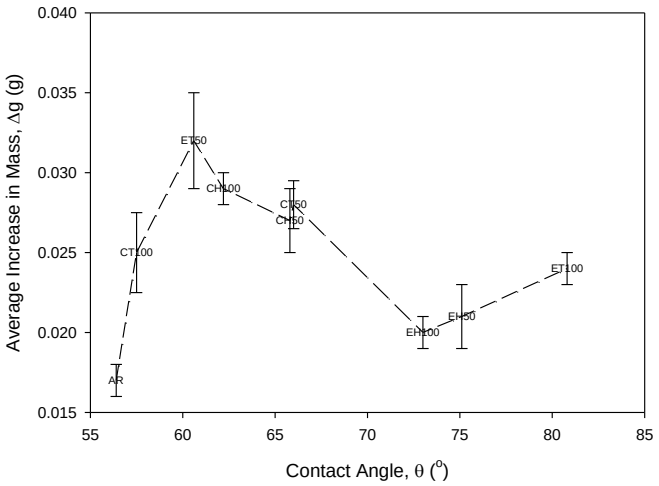

(b)

Figure 13.1 – (a) Histogram showing Δg in relation to θ and (b) graph showing the relationship between Δg and θ for the entire CO_2 and KrF excimer laser-induced patterned nylon 6,6 samples following 14 days immersion in SBF.

Throughout Chapter 11 and Chapter 12 it was seen that in most cases the results for γ^P exhibited an inverse relationship with bioactivity when compared to θ on account of the relationship determined between θ and γ^P in Chapter 10. This has not been seen for the laser-induced patterned samples and apatite response, as Figures 13.2(a), 13.2(b) and 13.2(c) show, since there did not appear to be any conclusive relationship between surface energy and apatite formation. However, even though it is not conclusive, it can be extrapolated from Figure 13.2(b) that there may have been a threshold window for γ^P between 12 and 14 mJm^{-2} in which an enhanced apatite response could have occurred. In

contrast, due to some erratic results shown in Figure 13.2(c) it is reasonable to say that γ^T was not a determinant parameter in the bioactive nature of the laser-induced pattern nylon 6,6 samples in terms of apatite response and formation. Furthermore, as the relationship in terms of γ^P is not conclusive and does not correlate with being the inverse of what was observed with θ, the surface energy does not appear to be useful in predicting apatite response. Once again, this could be attributed the mixed-state wetting regime as discussed in Chapter 10.

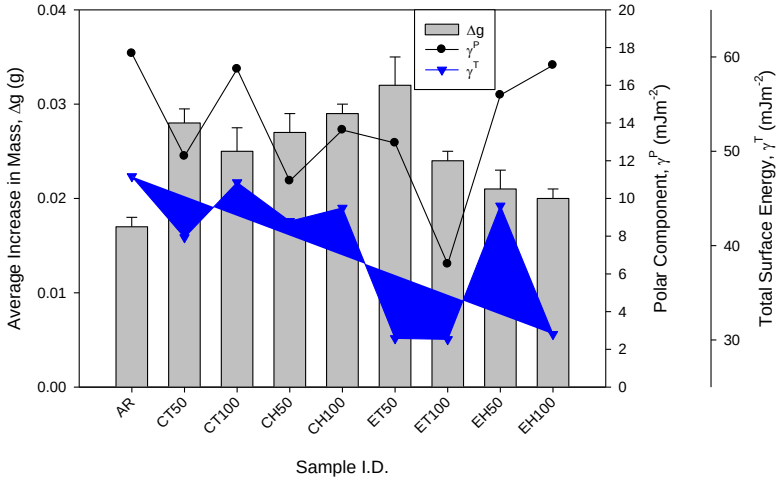

(a)

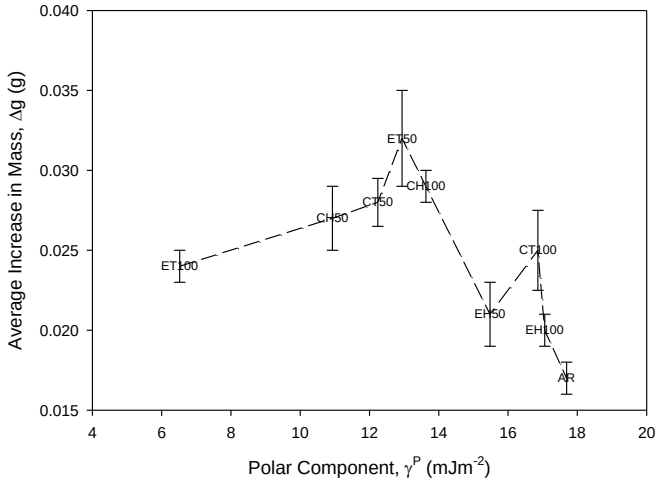

(b)

Figure 13.2 continued overleaf

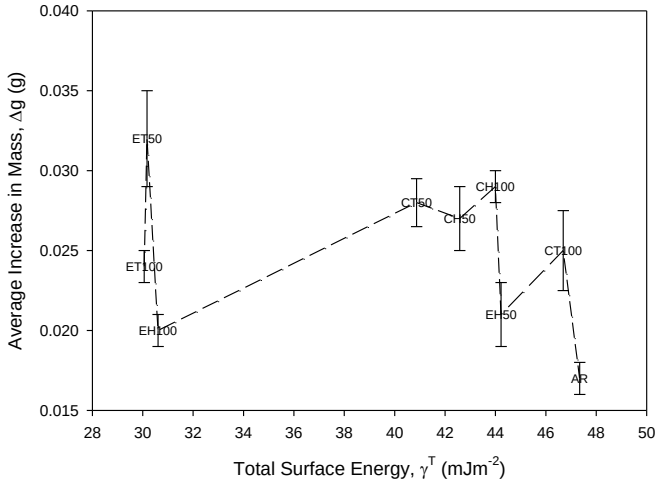

(c)

Figure 13.2 – (a) Histogram showing Δg in relation to γ^P and γ^T, (b) graph showing the relationship between Δg and γ^P and (c) graph showing the relationship between Δg and γ^T for the entire CO_2 and KrF excimer laser-induced patterned nylon 6,6 samples following 14 days immersion in SBF.

Figure 13.3 allows one to discern the relationship between Δg and the surface roughness parameters Ra and Sa. In terms of Ra, Figure 13.3(a) and Figure 13.3(b) show that there was no correlative relationship with the apatite response as the resulting Δg was erratic upon an increase Ra. On the other hand, Figure 13.3(c) indicates that there was a maximum threshold window for Sa of between 0.5 and 0.9 μm which lead to a maximum increase in Δg. This can be seen to be of some importance as Ra may not be the ideal roughness parameter to implement as this only gives the arithmetic average deviation of the surface in a single straight section of the sample, whereas the Sa parameter is the arithmetic average deviation over the whole plane of the surface. As a result, Sa can be seen to be of more significance as it includes the whole of the laser-induced patterned sample which incorporates periodic laser treated and as-received areas and would not depend on where the reading was taken aswith Ra. Another point to consider is that Sa could be used to potentially predict the apatite response of laser-induced nylon 6,6. This further attests that the surface roughness is significant in this instance, as the periodic surface patterns with increased roughness gave rise to a likely mixed-state wetting regime (see Chapter 6), which appeared to have a great effect on the apatite response to the nylon 6,6.

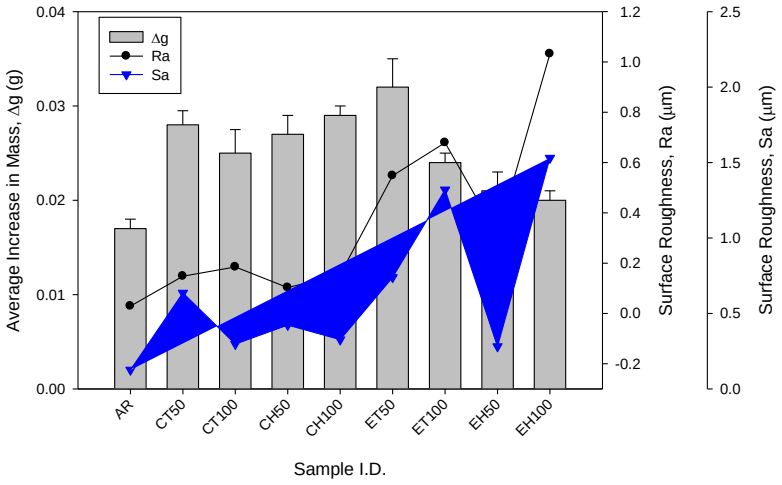

(a)

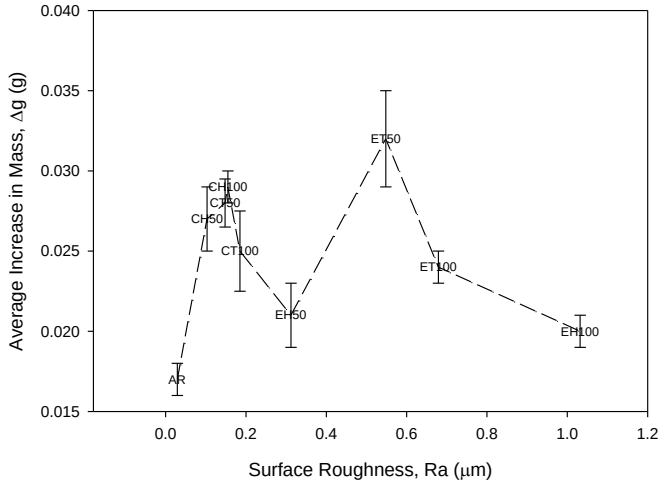

(b)

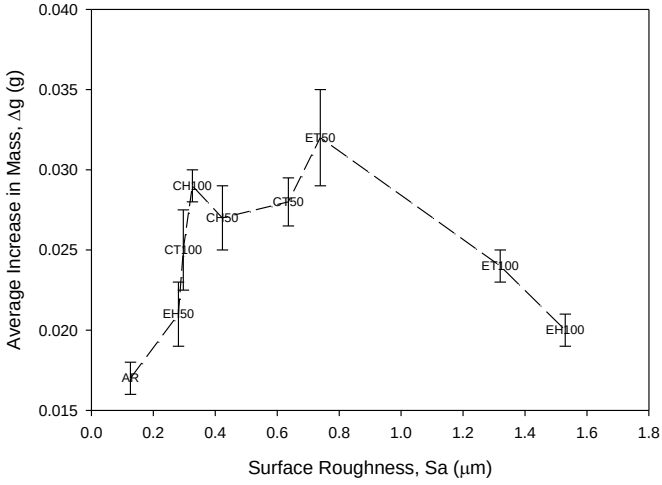

(c)

Figure 13.3 – (a) Histogram showing Δg in relation to Ra and Sa, (b) graph showing the relationship between Δg and Ra and (c) graph showing the relationship between Δg and Sa for the entire CO_2 and KrF excimer laser-induced patterned nylon 6,6 samples following 14 days immersion in SBF.

In terms of surface oxygen content, Figure 13.4(a) and Figure 13.4(b) show that for the CO_2 and KrF excimer laser-induced patterned samples there did not appear to be any correlative trend between Δg and surface oxygen content. However, by neglecting the KrF excimer laser-induced patterned samples in Figure 13.4(b) it can be seen that the CO_2 laser-induced patterned had a somewhat linear relationship with Δg. This suggests that the different laser-material interaction for the two different wavelengths had various impacts upon the surface oxygen content which in turn had a variation in the results for apatite formation. As a result of this one can deduce that the surface oxygen content alone would not be able to be used as a predictive tool for laser-induced nylon 6,6 and the ability to form apatite on account of this modulated response determined for the two different lasers.

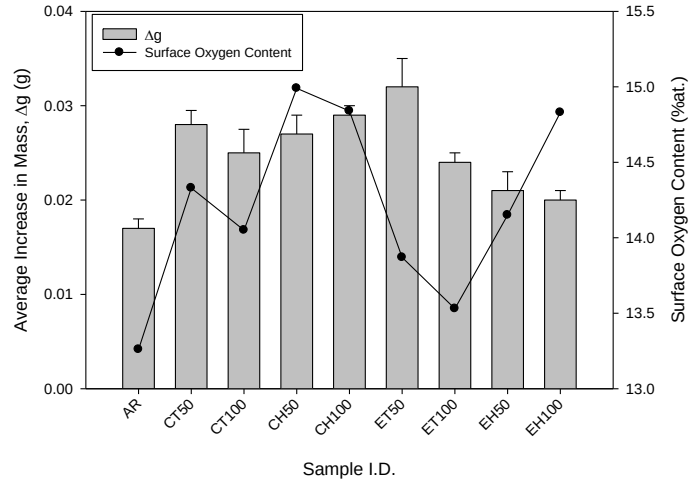

(a)

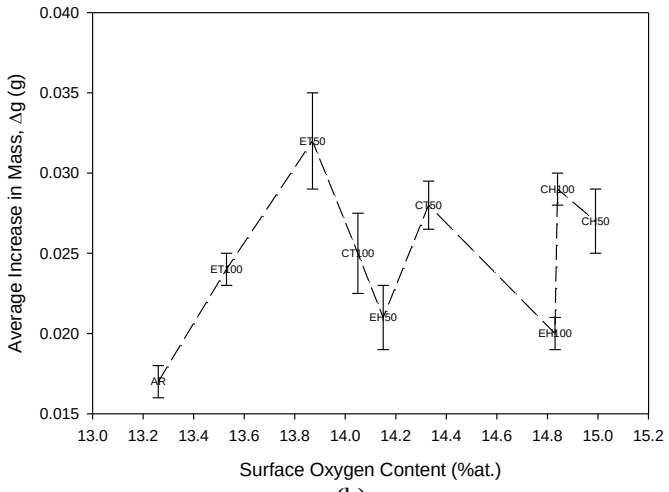

(b)

Figure 13.4 – (a) Histogram showing Δg in relation to surface oxygen content and (b) graph showing the relationship between Δg and surface oxygen content for the entire CO_2 and KrF excimer laser-induced patterned nylon 6,6 samples following 14 days immersion in SBF.

With regards to the apatite formation it has been seen that only θ and Sa appeared to have a conclusive relationship with Δg insofar as threshold operating windows for each were evidenced in Figure 13.1 and Figure 13.3, respectively. This is significant as this further attests to the fact that a

mixed-state wetting regime, as discussed in Chapter 10, arises for these samples because the laser-induced periodic pattern gives rise to an increase in Sa and results in a modification in θ which then leads on to the modulation of apatite formation.

13.2.2 – Cell Cover Density and Cell Count

In Figure 13.5(a) it is clear that the cell cover density and cell count for each of the laser-induced patterned nylon 6,6 samples did not correspond to any correlative trend with the modulated θ. This is further evidenced by Figure 13.5(b) which shows that the cell cover density and cell count varied significantly upon an increase in θ when comparing all results together. Even so, by taking into account the KrF excimer laser-induced patterned results it can be seen from Figure 13.5(b) that both the cell cover density and cell count remain somewhat constant even though an increase in θ was observed. In contrast, the CO_2 laser-induced patterned samples can be seen to have had no correlation when being taken into account separately. This highlights a possible difference between the two wavelengths implemented as the CO_2 laser-induced patterns gave rise to a more modulated osteoblast cell response when compared to the KrF excimer laser-induced patterned samples, in terms of cell cover density and cell count.

Similar to that seen with θ (see Figure 13.5), Figure 13.6(a) shows that in terms of cell cover density and cell count, γ^P and γ^T did not have a correlative relationship for the laser-induced patterned samples. Furthermore, Figure 13.6(b) and Figure 13.6(c) also show that there was no relationship between surface energy, cell cover density and cell count; however, Figure 13.6(b) does show to some extent an inverse trend to what was observed with θ (see Figure 13.5(b)). This further attests to the relationship determined between θ and γ^P, as discussed in Chapter 10. It can also be seen from Figure 13.6(b) that, even though the CO_2 laser-induced patterned samples showed considerable variation upon an increase in γ^P, the KrF excimer laser-induced patterned samples had a somewhat constant cell count and cell cover density. As a result, this supplements the likelihood of a different osteoblast cell response been elicited on account of the two dissimilar laser wavelengths employed. In addition, Figure 13.6(c) allows one to see that γ^T did not have a correlative trend with the osteoblast cell response for the laser-induced patterned nylon 6,6 samples, allowing one to deduce that the surface energy and its components did not have a strong link with the bioactivity of the samples. This could be attributed to the mixed-state wetting regime, discussed in Chapter 10, in that it would have affected the contact made between the material surface and the cell culture media.

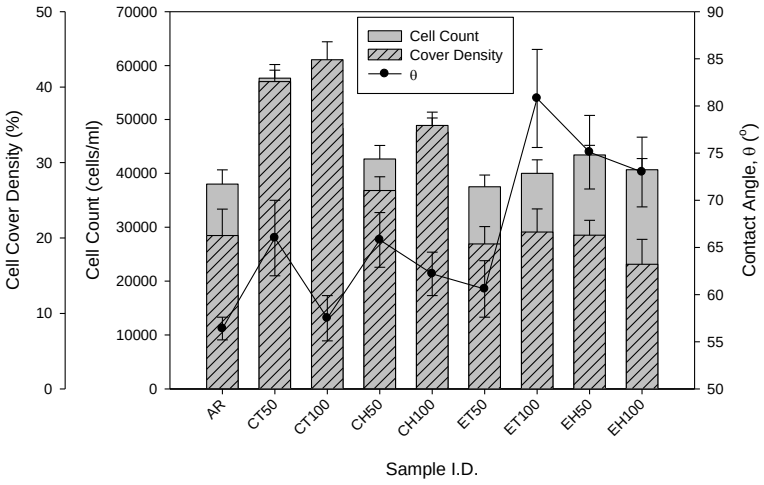

(a)

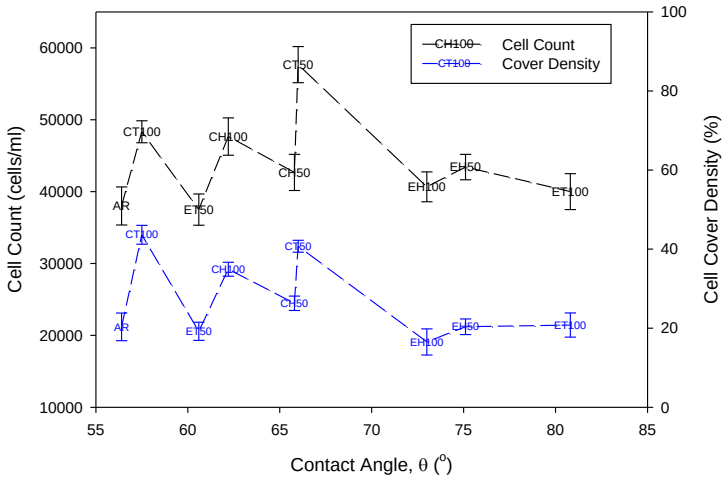

(b)

Figure 13.5 – (a) Histogram showing cell cover density and cell count in relation to θ and (b) graph showing the relationship between cell count, cell cover density and θ for the entire CO_2 and KrF excimer laser-induced patterned nylon 6,6 samples following 14 days immersion in SBF.

From Figure 13.7(a) it is not possible to conclusively determine if there was any correlation between Ra, Sa, the cell cover density and cell count. However, Figure 13.7(b) suggests that there may have been some correlation between Ra and the osteoblast cell response. That is, when taking all laser-induced patterned samples into account, a maximum threshold operating window between 0.1 and 0.2 µm is indicated. But, it can be seen that the KrF laser-induced patterned samples gave rise to a somewhat constant osteoblast cell response when compared to the CO_2 laser-induced patterned samples. With this in mind, it is possible to deduce that it may be the case that two different trends for the two different employed wavelengths were being exhibited. For instance the CO_2 laser-induced patterned samples gave rise to a large increase in cell count and cell cover density on an increase in Ra; whereas the cell count and cell cover density remained constant at around 40,000 cells/ml and 20%, respectively, for the KrF laser-induced patterned samples. Leading on, this could also be attributed to the resulting topographies brought about by using the different laser types such that the

CO_2 laser with its relatively larger spot size gave a slight periodic pattern, with small areas of as-received material between the induced patterns (see Chapter 6). In direct contrast, the KrF excimer laser allowed for a more precise processing technique, giving a considerably more periodic patterned topography with a lot more as-received areas between the etched patterns (see Chapter 7). As a result, this was likely to have a large impact upon the wettability characteristics and subsequent osteoblast cell growth and proliferation.

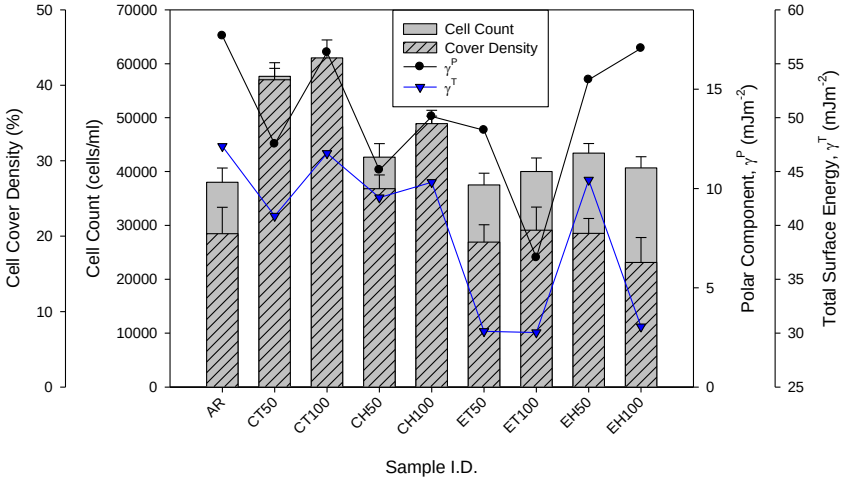

(a)

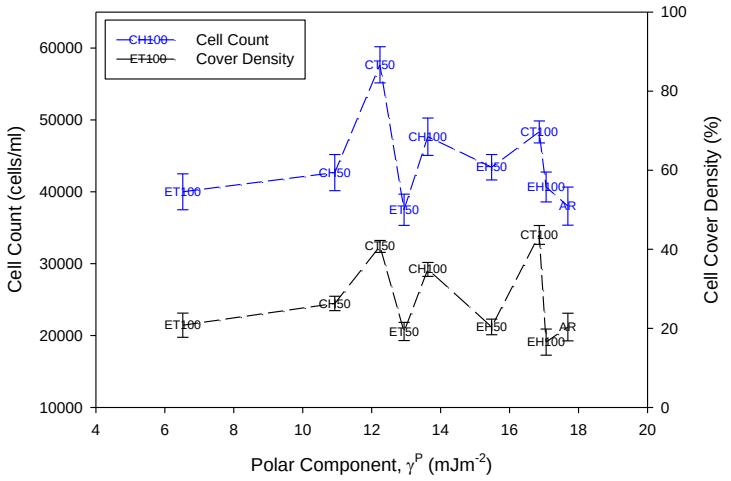

(b)

Figure 13.6 continued overleaf

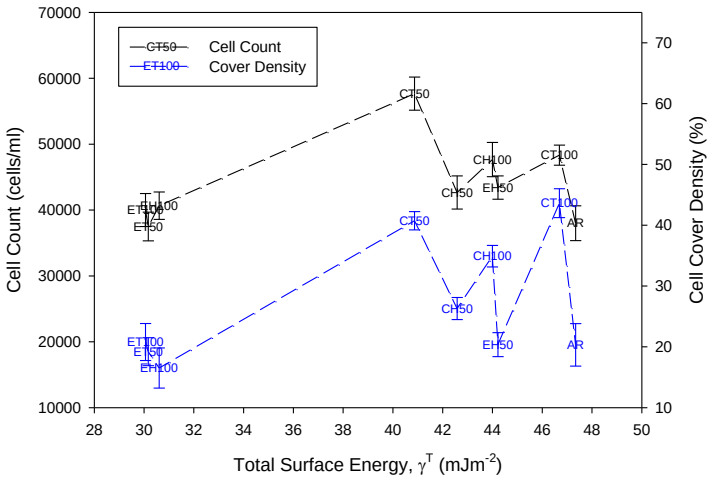

(c)

Figure 13.6 – (a) Histogram showing cell cover density and cell count in relation to γ^P and γ^T, (b) graph showing the relationship between cell count, cell cover density and γ^P and (c) graph showing the relationship between cell count, cell cover density and γ^T for the entire CO_2 and KrF excimer laser-induced patterned nylon 6,6 samples following 14 days immersion in SBF.

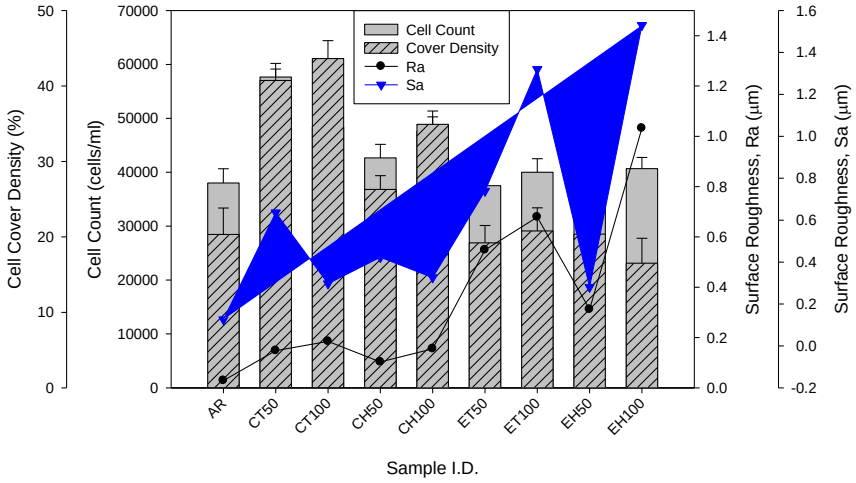

(a)

Figure 13.7 continued overleaf

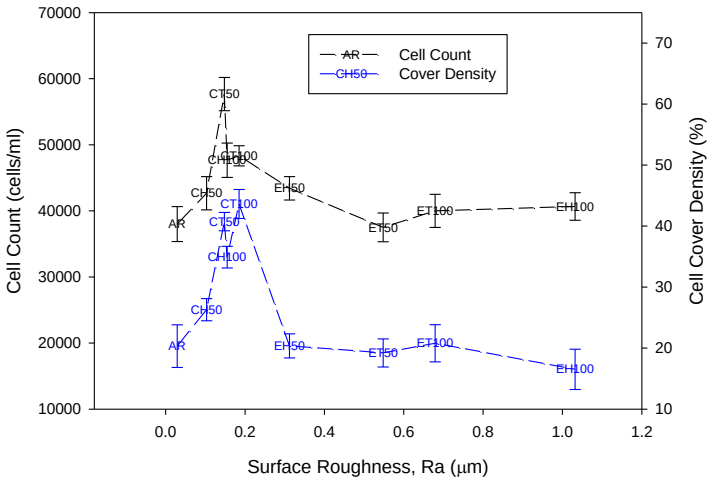

(b)

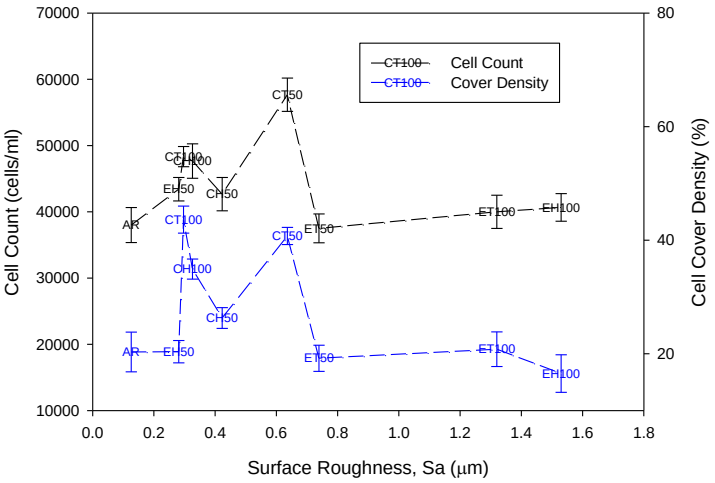

(c)

Figure 13.7 – (a) Histogram showing cell cover density and cell count in relation to Ra and Sa, (b) graph showing the relationship between cell count, cell cover density and Ra and (c) graph showing the relationship between cell count, cell cover density and Sa for the entire CO_2 and KrF excimer laser-induced patterned nylon 6,6 samples following 14 days immersion in SBF.

Figure 13.8(a) and Figure 13.8(b) show that there was no distinct correlative relationship between the surface oxygen content and osteoblast cell response in terms of cell cover density and cell count. Having said that, from Figure 13.8(b) it can be seen that by taking into account the processing techniques separately, a trend can be observed. For the KrF excimer laser-induced patterned samples the cell count and cell cover density remained constant at around 40,000 cells/ml and 20%, respectively. On the other hand, Figure 13.8(b) shows that the increase in surface oxygen content ultimately elicited a less enhanced response for the CO_2 laser-induced patterned nylon 6,6 samples. This can be accounted for the fact that there were more areas of as-received material for the KrF excimer laser-induced patterned samples which would have counteracted any potential enhancement in osteoblast cell response. Leading on from this, as the CO_2 laser spot size was larger than most of

the intended patterns (see Chapter 6) there would have been less areas of as-received material. One can deduce that owed to this, a rise in toxicity, which was discussed in Section 11.5, could have given rise to the hindered enhancement of the osteoblast cell response, even though an increase in surface oxygen content was observed.

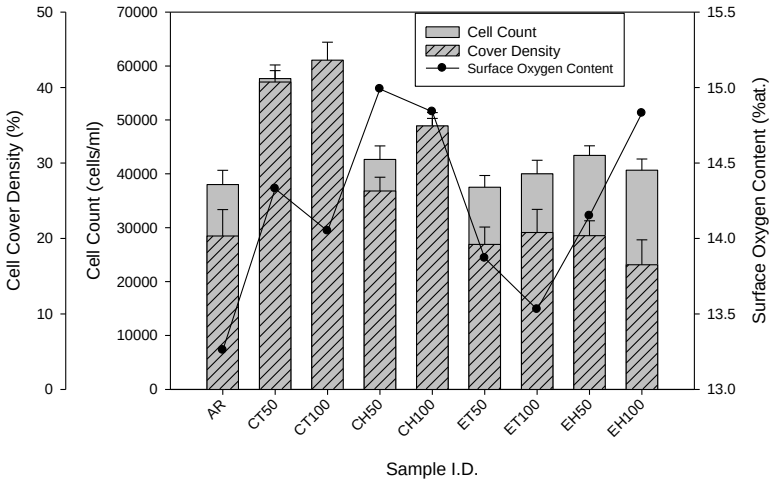

(a)

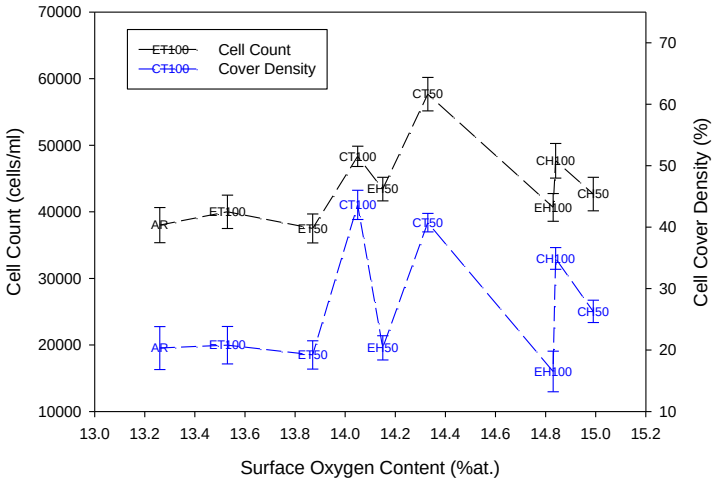

(b)

Figure 13.8 – (a) Histogram showing cell cover density and cell count in relation to surface oxygen content and (b) graph showing the relationship between cell count, cell cover density and surface oxygen content for the entire CO_2 and KrF excimer laser-induced patterned nylon 6,6 samples following 14 days immersion in SBF.

It has been seen that there are a number of results, Figures 13.5, 13.6, 13.7 and 13.8, which do not correlate to any particular trend and can be attributed to the mixed-state wetting regime arising from the laser-induced topographies (see Chapter 10). Another aspect of interest is that in most cases it has been observed that each of the employed lasers have given rise to results which exhibit their own different trends with the osteoblast cell response. This is highly significant as it suggests that there may be a difference between the wavelengths employed to surface pattern nylon 6,6 in order to modulate osteoblast cell growth and proliferation.

13.2.4 – Cytotoxicity and Alkaline Leukocyte Phosphatase (ALP) Levels

It has been seen throughout Chapter 11 and Chapter 12 that the cytotoxicity and ALP levels for all laser processed samples had to some extent an impact upon the observed osteoblast cell response. Figure 13.9(a) shows a histogram of the cytotoxicity and ALP levels for all of the laser-induced patterned samples in relation to θ. Upon first reflection of Figure 13.9(a) it appeared that there was no distinct relationship between the cytotoxicity, ALP level and θ. However, from Figure 13.9(b) it can be seen that the ALP level appeared to be a decreasing function of θ until a minimum ALP level was achieved with the KrF excimer laser-induced samples. With regards to the cytotoxicity, Figure 13.9(b) shows that there did not appear to be any correlative trend between cytotoxicity and θ. In addition to this, it can be seen that most of the CO_2 laser-induced patterned samples (CH100, CT50 and CH50) gave rise to somewhat erroneous results for the ALP level. On account of this and the observed erratic results for the cytotoxicity, it is possible to maintain that this could be accounted for by the change in wetting regime, as discussed in Chapter 6 and Chapter 10, which was surely to have some impact upon the osteoblast cell response. Furthermore, as these nylon 6,6 samples were patterned, there were areas of as-received sample in-between the laser-induced patterns which would have also had a large effect on osteoblast cell growth and proliferation. As a result of this, it is highly likely that this would then lead to a variation in cytotoxicity and ALP levels which has been identified by Figure 13.9.

Similar to θ (see Figure 13.9), Figure 13.10(a) shows the variation in cytotoxicity and ALP levels in relation to γ^P and γ^T. From this it can be seen that there did not appear to be any correlative trends that stood out between these parameters. Yet, Figure 13.10(b) allows one to see that the graphs drawn for γ^P were the inverse of that determined for θ (See Figure 13.9(b)) which gives further evidence as to the relationship between θ and γ^P which was found in Chapters 6, 7 and 10. It could be loosely stated that the ALP level was, to a certain extent, an increasing function of γ^P; however, erratic results for ALP levels and especially for the cytotoxicity suggest that γ^P and θ may not be able to be implemented to predict the osteoblast cell response to nylon 6,6 in terms of the ALP level and cytotoxicity of osteoblast cells. Furthermore, Figure 13.10(c) shows that there was a similar relationship with γ^T and with some of the results not following the trend it can be reasonably said that surface energy as a whole cannot be implemented to predict how osteoblast cell are going to react upon when seeded onto laser-induced patterned nylon 6,6. This further attests to the likely transition in wetting regime and large areas of as-received material between the laser-induced patterned samples being a large factor in the arising erroneous results.

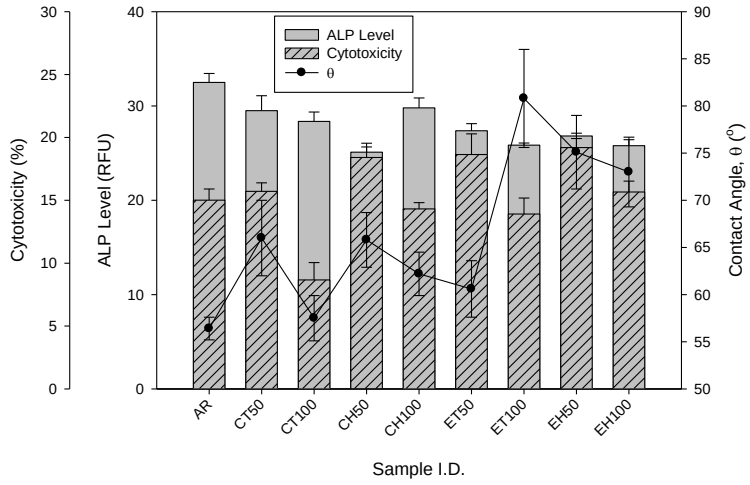

(a)

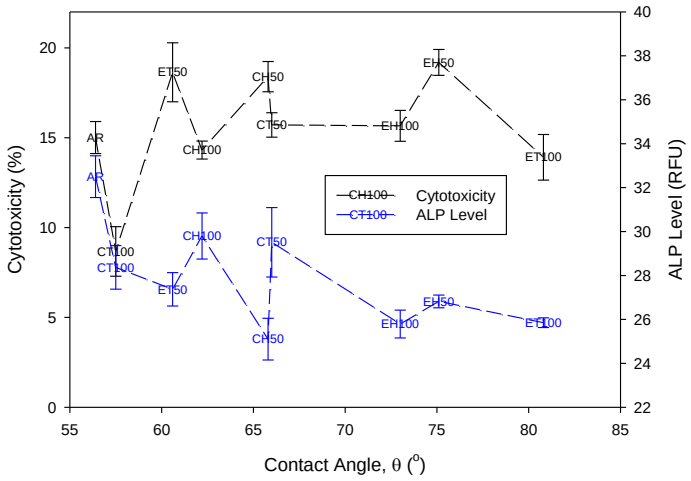

(b)

Figure 13.9 – (a) Histogram showing cytotoxicity and ALP level in relation to θ and (b) graph showing the relationship between cytotoxicity, ALP level and θ for the entire CO_2 and KrF excimer laser-induced patterned nylon 6,6 samples following 14 days immersion in SBF.

It can be seen from Figure 13.11(a), 13.11(b) and 13.11(c) that the ALP level for the laser-induced patterned samples was, on the most part, a decreasing function of Ra and Sa. This could further suggest that the wetting regime is playing a big role in the osteoblast cell response as it is the topography of the laser-induced patterned nylon 6,6 which is proposed to have given rise to a transition in wetting regime (see Chapter 6 and Chapter 10). On the other hand, it can be seen from these Figures that the cytotoxicity measured for the samples did not appear to have any correlative trend with the surface roughness. It can also be said for those results for the ALP level that there are some erroneous results such as sample CH50 not following the trend in terms of Ra (see Figure 13.11(b). As a result of this, it can be seen that the relationships between surface roughness, ALP levels and cytotoxicity is not conclusive in terms of having the ability to predict the osteoblast cell response. Again this could be attributed to the transition in wetting regime and the fact that there were

areas of as-received material in-between the laser-induced patterns which was likely to have an effect on the bioactivity of nylon 6,6 in terms of osteoblast cell growth.

From Figure 13.12(a) and Figure 13.12(b) it can be seen that there did not appear to be any correlative relationship between the surface oxygen content, ALP levels and cytotoxicity. This can be accounted for by the likely transition in wetting regime and areas of as-received material in-between the laser-induced patterned samples having a significant impact on the bioactivity of the nylon 6,6 samples leading to erroneous results.

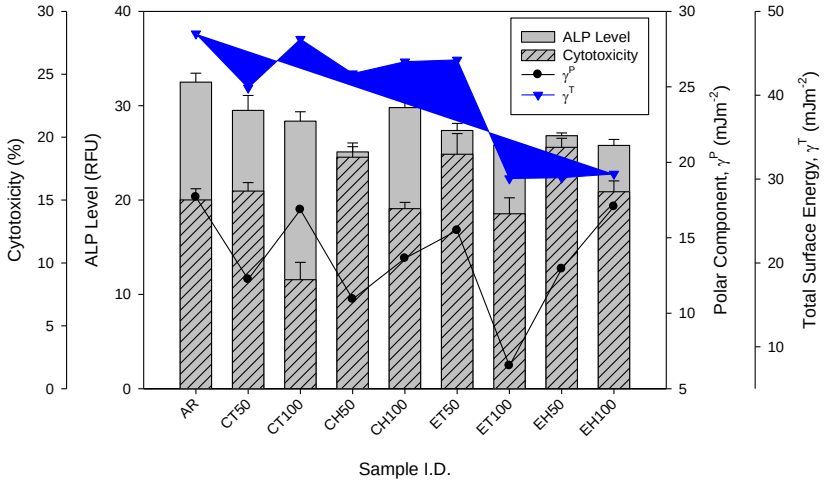

(a)

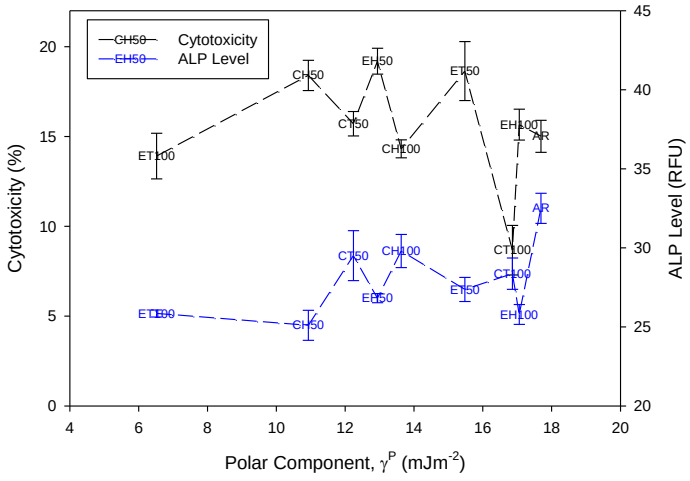

(b)

Figure 13.10 continued overleaf

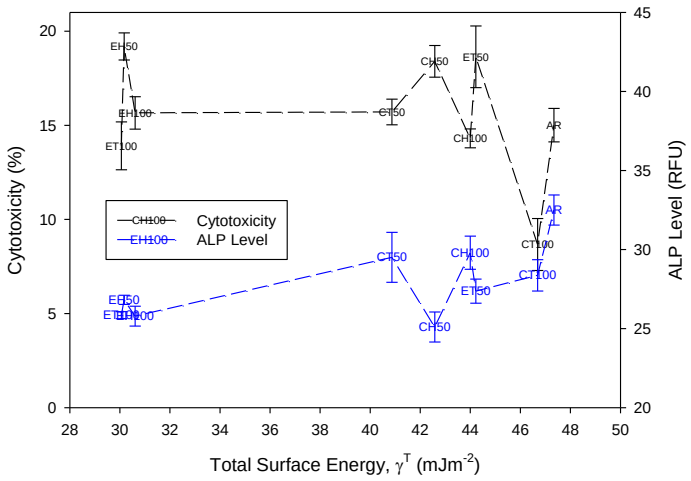

(c)

Figure 13.10 – (a) Histogram showing cytotoxicity and ALP level in relation to γ^P and γ^T, (b) graph showing the relationship between cytotoxicity, ALP level and γ^P and (c) graph showing the relationship between cytotoxicity, ALP level and γ^T for the entire CO_2 and KrF excimer laser-induced patterned nylon 6,6 samples following 14 days immersion in SBF.

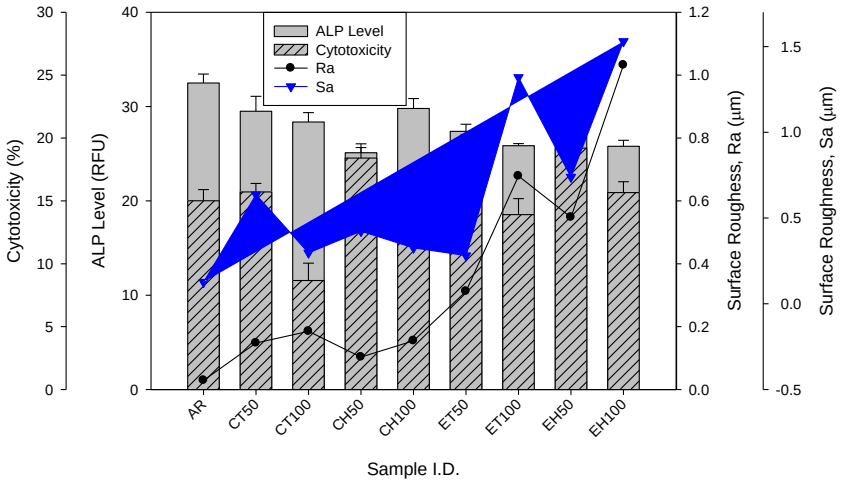

(a)

Figure 13.11 continued overleaf

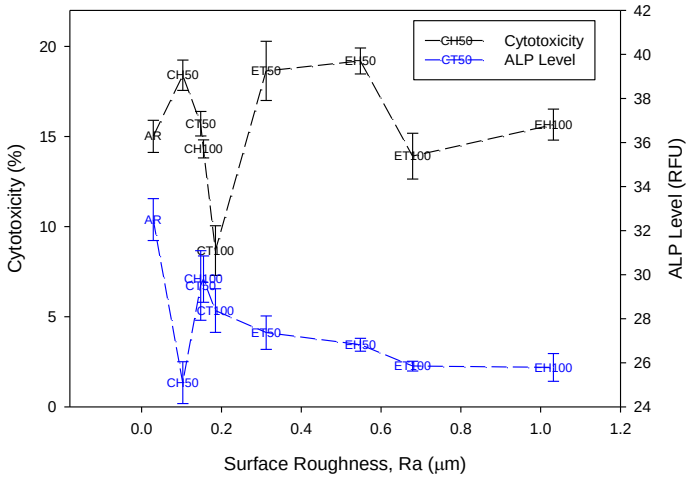

(b)

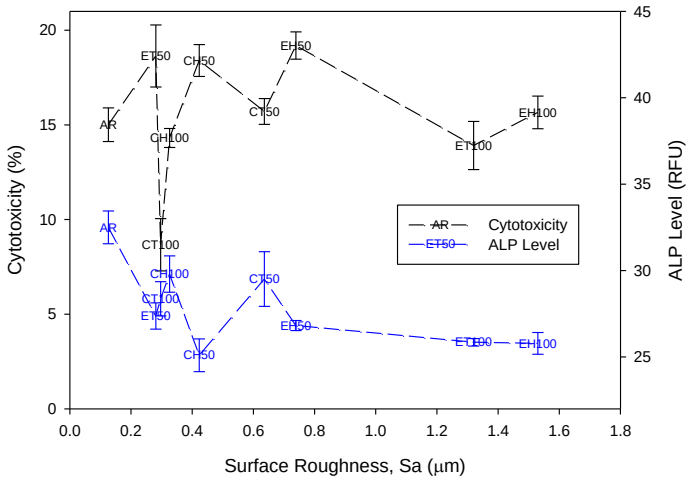

(c)

Figure 13.11 – (a) Histogram showing cytotoxicity and ALP level in relation to Ra and Sa, (b) graph showing the relationship between cytotoxicity, ALP level and Ra and (c) graph showing the relationship between cytotoxicity, ALP level and Sa for the entire CO_2 and KrF excimer laser-induced patterned nylon 6,6 samples following 14 days immersion in SBF.

For all of the laser-induced patterned samples it has been seen that many of the samples do not appear to follow any particular trend in terms of wettability characteristics and other surface parameters. It has been proposed that a combination of the likely mixed-state wetting regime and areas of as-received material on the laser-induced patterned samples have given rise to erroneous results which do not fit with any correlative trend, allowing the prediction of the biofunctionality, in terms of osteoblast cells, of laser-induced patterned nylon 6,6 to be very difficult to make. Having said that, in some instances, it was found that separately the CO_2 and KrF excimer laser-induced samples appeared to follow their own separate trend and could indicate a major difference between using the two different lasers for laser surface patterning to enhance osteoblast cell response. In addition to this, ALP levels were also found to have a strong relationship with most of the samples in terms of surface

roughness (see Figure 13.11) and could potentially be used to predict the osteoblast cell response to the nylon 6,6 samples.

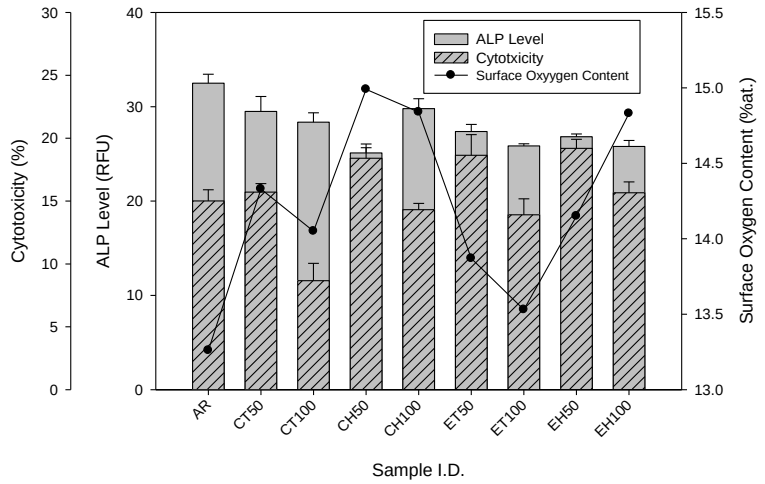

(a)

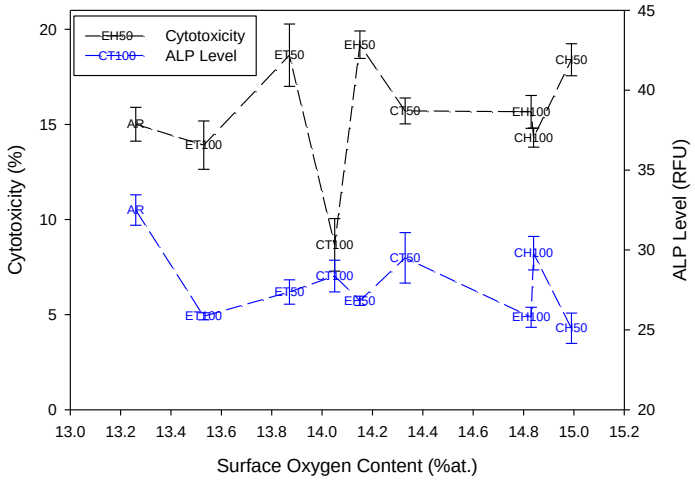

(b)

Figure 13.12 – (a) Histogram showing cytotoxicity and ALP level in relation surface oxygen content and (b) graph showing the relationship between cytotoxicity, ALP level and surface oxygen content for the entire CO_2 and KrF excimer laser-induced patterned nylon 6,6 samples following 14 days immersion in SBF.

13.3 – CO_2 and KrF Excimer Laser Whole Area Irradiative Processing

This Section details and discusses the results obtained for the laser whole area irradiative processed nylon 6,6 samples. Also, correlative trends between the wettability characteristics, apatite response and osteoblast cell response are considered.

13.3.1 – Apatite Response

It can be seen from Figure 13.13(a) that there were two very different trends with regards to Δg and θ for the CO_2 and KrF excimer laser whole area irradiative processed samples. Since, for the CO_2 laser whole area irradiative processed samples Δg appeared to decrease upon an increase in θ; whereas an increase in Δg was observed for a decrease in θ. These trends can be seen more explicitly in Figure 13.13(b), which shows that the KrF excimer laser whole area irradiative processed samples gave rise to a reducing function of θ in terms of Δg. In addition to this, Figure 13.13(b) allows one to see that a very different response was observed for the CO_2 laser whole area irradiative processed samples in that Δg was an increasing function of θ. With these two trends in mind is it possible to deduce that this suggests that in terms of apatite response, there are different relationships for each of the laser type employed when determining a correlation with θ. This suggests that there could be a likely λ dependency upon the observed relationship between Δg and the laser-modified θ.

Figure 13.14(a) allows one to observe that the trend between Δg and γ^P was somewhat similar to that observed with θ (see Figure 13.13). That is, for the CO_2 laser whole area irradiative processed nylon 6,6 samples Δg decreased upon an increase in γ^P. In contrast, Δg increased with increasing γ^P for the KrF excimer laser whole area irradiative processed samples. A similar trend for γ^T can also be observed for the KrF excimer laser whole area irradiative processed samples in that an increase in γ^T appeared to bring about an increase in Δg. For the CO_2 laser whole area irradiative processed samples, however, there did not appear to be any distinct trend between Δg and γ^T.

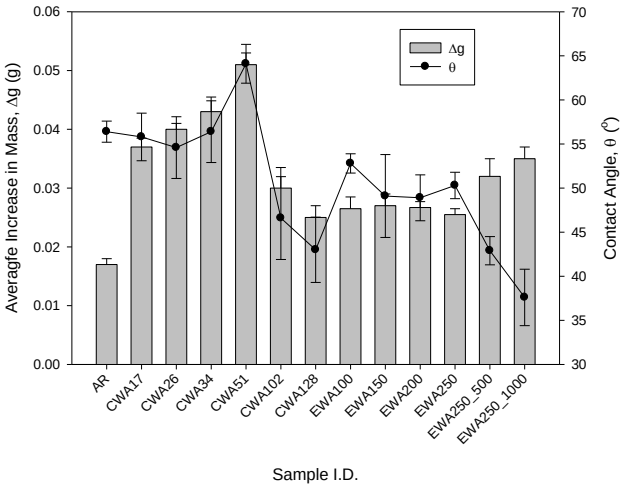

(a)

Figure 13.13 continued overleaf

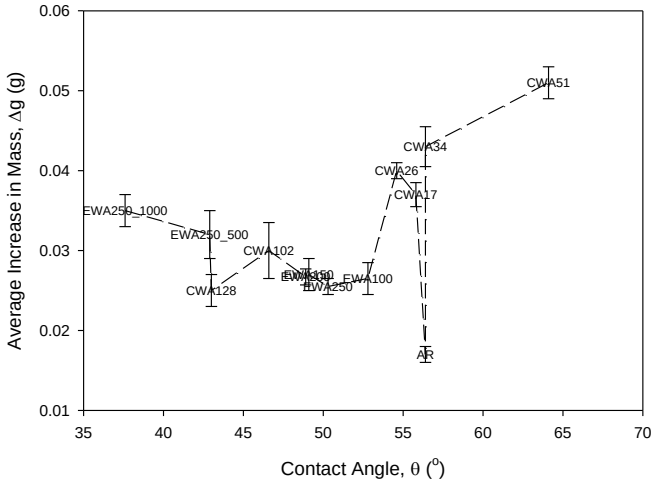

(b)

Figure 13.13 – (a) Histogram showing Δg in relation to θ and (b) graph showing the relationship between Δg and θ for the entire CO_2 and KrF excimer laser whole area irradiative processed nylon 6,6 samples following 14 days immersion in SBF.

As for the relationship between γ^P and Δg, Figure 13.14(b) further shows the trends observed in Figure 13.14(a). Whereas the CO_2 laser whole area irradiative processed samples Δg was a decreasing function of γ^P, for the KrF excimer laser whole area irradiative processed samples Δg was found to be an increasing function of γ^P. This further gives evidence to the potential dependence on λ for the apatite response and also can be seen to be the inverse of what was observed with θ (see Figure 13.13) which promotes the relationship between γ^P and θ, as determined in Chapter 10.

Figure 13.14(c) also attests to the possible dependence on λ for the apatite response on account of the fact that there was no clear relationship between γ^T and Δg for the CO_2 laser whole area irradiative processed samples. However, for the KrF excimer laser whole area irradiative processed samples there was a somewhat linear relationship observed such that an increase in γ^T brought about an increase in Δg. The two different observed relationships allow one to see that it is likely that on account of the different λ implemented, there was wettability characteristics and surface parameters which appeared to be more dominant in one case of samples when compared to the other.

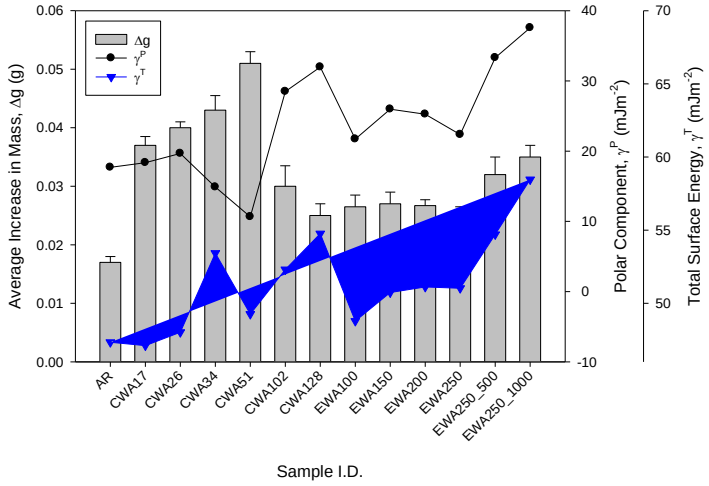

(a)

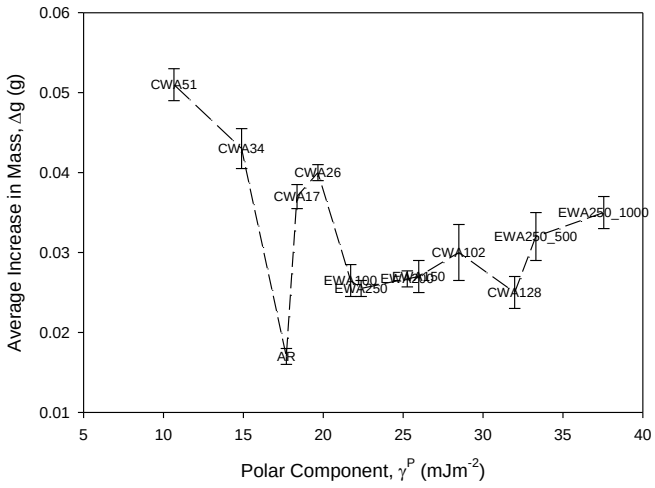

(b)

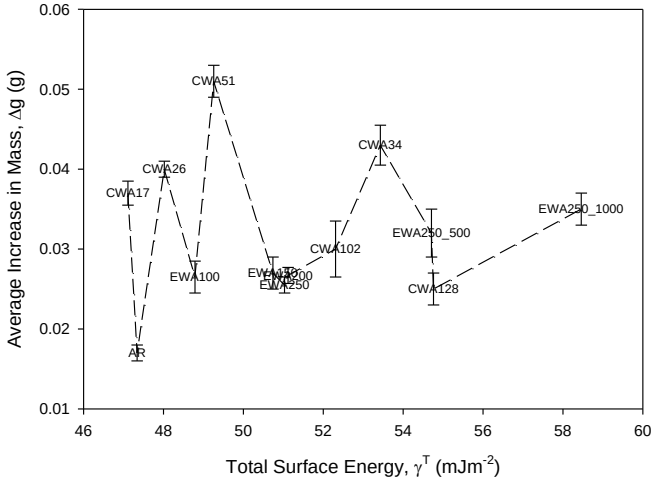

(c)

Figure 13.14 – (a) Histogram showing Δg in relation to γ^P and γ^T, (b) graph showing the relationship between Δg and γ^P and (c) graph showing the relationship between Δg and γ^T for the entire CO_2 and KrF excimer laser whole area irradiative processed nylon 6,6 samples following 14 days immersion in SBF.

Figure 13.15(a) shows that there did not appear to be any correlative trend between Ra, Sa and apatite response in terms of Δg. This is owed to the fact that, with the exception of sample CWA102 and CWA128, all samples gave rise to similar Ra and Sa values even though modulated Δg was determined for the samples. Yet, both Figure 13.15(b) and Figure 13.15(c) allow one to see that there may have been some correlation between Δg and the surface roughness in that the apatite response could reach an enhanced maximum before reducing on an increase in Ra and Sa. But, on account of very similar roughness values giving rise to a large variation in Δg, it is reasonable to say that this relationship may not hold true and would be very difficult to be implemented as a apatite response predictive tool. Nevertheless, it may still be possible, especially for the CO_2 laser whole area irradiative processed samples, to use large increases in Ra and Sa to indirectly predict the apatite response as considerable melting gave rise to large Sa and Ra values and increasing toxicity (see Section 11.5), reducing the bioactivity of nylon 6,6 samples.

It can be seen from Figure 13.16(a) that, on the whole, the laser whole area irradiative processed samples had a correlative trend between the arising surface oxygen content and Δg such that Δg increased with an increase in surface oxygen content. However, for the CO_2 laser whole area irradiative processing it was found that this trend did not fit with sample CWA102 and sample CWA128 which could be attributed to the likely surface chemical changes (see Section 11.5) having a detrimental effect on the apatite adhesion characteristics.

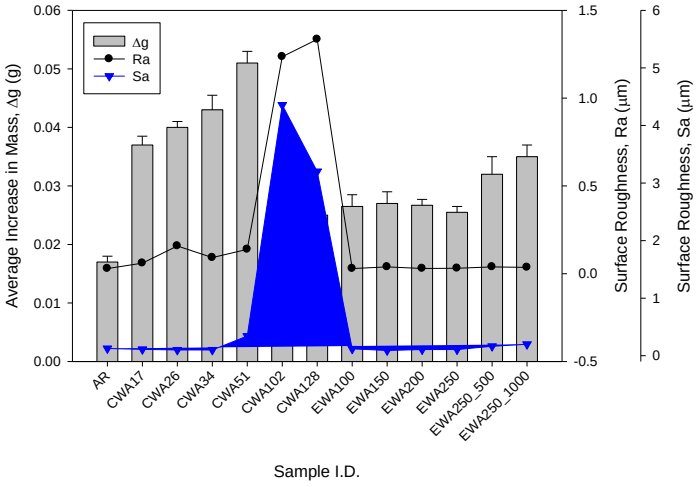

(a)

Figure 13.15 continued overleaf

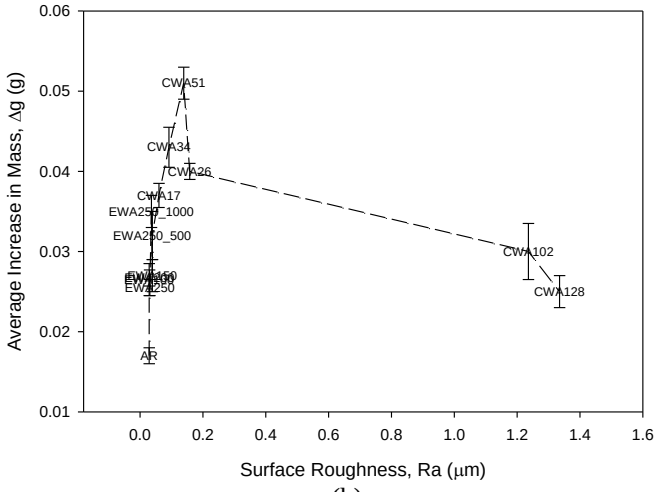

(b)

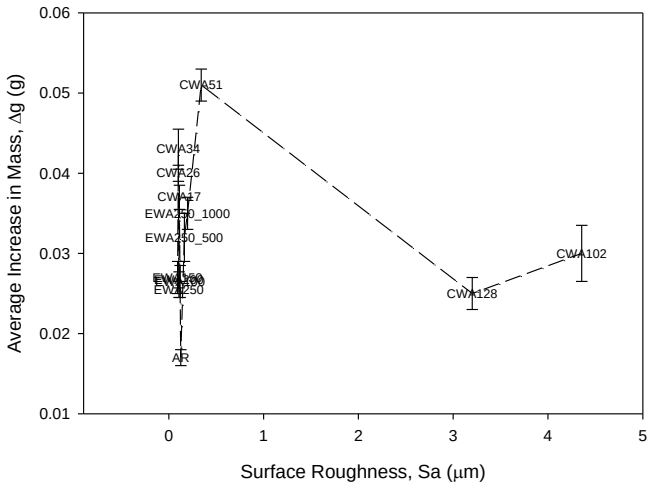

(c)

Figure 13.15 – (a) Histogram showing Δg in relation to Ra and Sa, (b) graph showing the relationship between Δg and Ra and (c) graph showing the relationship between Δg and Sa for the entire CO_2 and KrF excimer laser whole area irradiative processed nylon 6,6 samples following 14 days immersion in SBF.

The trend shown in Figure 13.16(a) can be further seen in Figure 13.16(b) which identifies that even though both laser types gave rise to a similar trend, there still is a distinct difference between the relationship between surface oxygen content and Δg. For instance, the CO_2 laser whole area irradiative processed samples gave a sharper rise in Δg upon an increase in surface oxygen content until a maximum was reached prior to Δg beginning to reduce. On the other hand, for the KrF excimer laser whole area irradiative processed samples it was found that the increase in Δg was somewhat more linear upon an increase in surface oxygen content. Also, a maximum optimum oxygen content was not observed for the KrF excimer laser whole area irradiative processed nylon 6,6 samples. This could be significant as it was observed that considerably more melting took place for the CO_2 laser processing which would likely have given rise to more chemical changes (see Section 11.5), which could have reduced the apatite response to the nylon 6,6. By taking this into account along with the

other relationships observed (see Figures 13.13, 13.14 and 13.15), one can deduce that it is likely that the apatite response is somewhat dependant on the λ employed. Furthermore, it has also been seen that a number of parameters such as θ, γ^P and surface oxygen content have the potential to be applied to aid in the prediction of how laser whole area irradiative processed nylon 6,6 will promote the adhesion of apatite upon immersion in SBF.

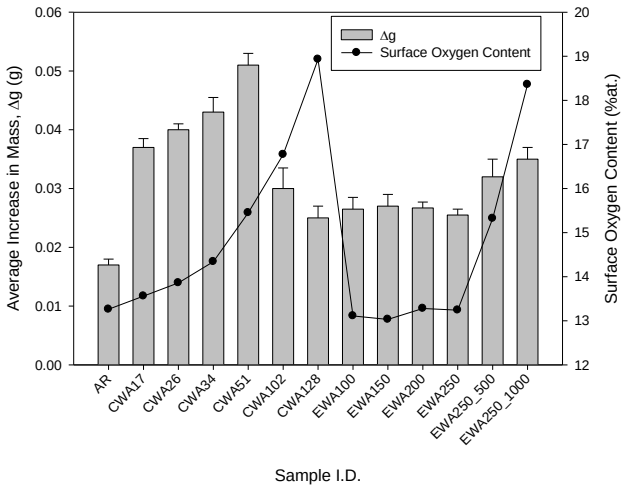

(a)

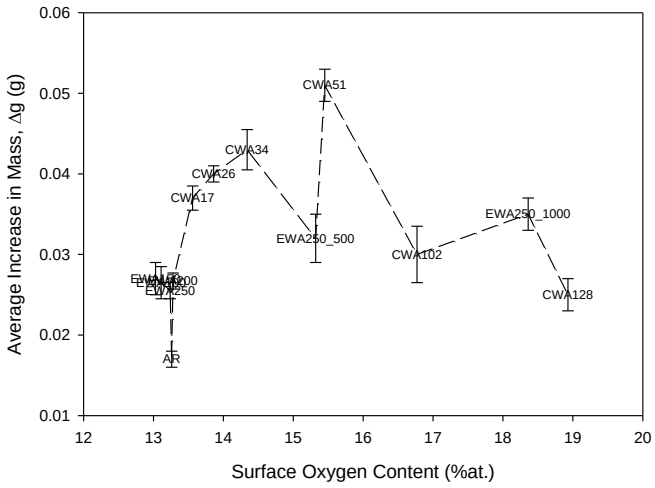

(b)

Figure 13.16 – (a) Histogram showing Δg in relation to surface oxygen content and (b) graph showing the relationship between Δg and surface oxygen content for the entire CO_2 and KrF excimer laser whole area irradiative processed nylon 6,6 samples following 14 days immersion in SBF.

13.3.2 – Cell Cover Density and Cell Count

From Figure 13.17(a) one can see the correlative trend between cell cover density, cell count and θ for the entire laser whole area irradiative processed nylon 6,6 samples. For both the CO_2 and KrF excimer laser it was found that the osteoblast cell response became more enhanced upon an increase in θ in that the cell count and cell cover density both increased as a result of an increase in θ. These trends

can be more explicitly seen in Figure 13.17(b) which shows that the cell count and cell cover density was an increasing function of θ. Having said that, for the cell cover density it can be recognized that there may have been a different relationship when comparing the laser types in that the CO_2 laser whole area irradiative processed samples gave a larger gradient with increasing θ. On the other hand, for the cell count it was determined that for all samples both types of laser whole area irradiative processed samples gave rise to a strong linear relationship. This suggests that the cell cover density could be a more linear relationship with θ as it could be argued that for sample CWA102 and CWA128, the cytotoxicity (see Section 11.5 and Section 11.6) could have been the most dominant leading to erroneous results with regards to the relationship between osteoblast cell response and wettability characteristics. From this it is possible to realize that for laser whole area irradiative processed nylon 6,6 there was a correlative trend between cell cover density, cell count and θ, regardless of the laser type implemented until the toxicity of the sample began to dominate.

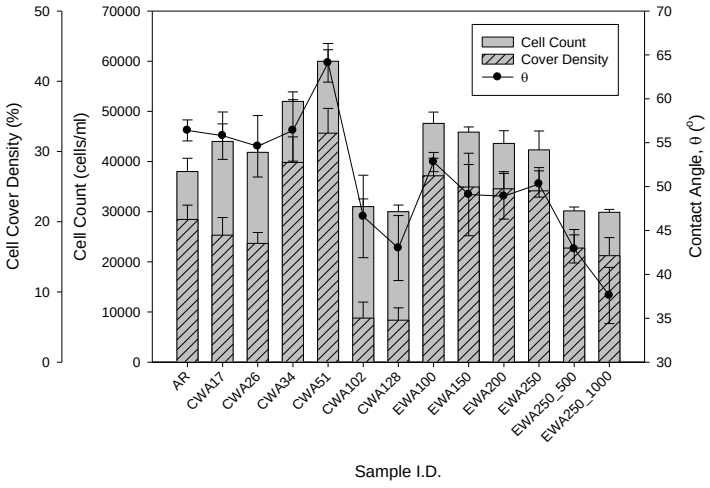

(a)

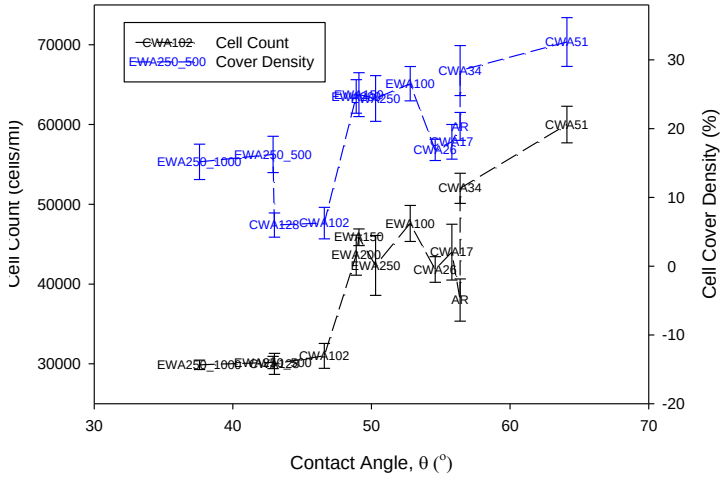

(b)

Figure 13.17 – (a) Histogram showing cell count and cell cover density in relation θ and (b) graph showing the relationship between cell count, cell cover density and θ for the entire CO_2 and KrF excimer laser whole area irradiative processed nylon 6,6 samples.

One can see from Figure 13.18(a) that γ^P had a correlative trend with the cell cover density and cell count insofar as the cell cover density and cell count reduced with an increase in γ^P. It can also be seen from Figure 13.18(a) and Figure 13.18(c) that there did not appear to be any trend between γ^T and the osteoblast cell response in terms of cell cover density and cell count. These trends can also be seen from Figure 13.18(b) and Figure 13.18(c). Figure 13.18(b) shows that the relationship observed between γ^P, cell cover density and cell count was to a certain extent the inverse of what was observed with θ which gives further evidence of the strong link between γ^P and θ, ascertained in Chapter 10. The cell cover density and cell count was seen to be a decreasing function of γ^P for the laser whole area irradiative processed samples with sample CWA102 and CAW128 not conclusively following the trend for cell cover density. As discussed earlier, for θ (see Figure 13.17) this could be accounted for by the toxicity of the samples, as discussed in Section 11.5, being the most dominant giving rise to some erroneous results for the relationships between osteoblast cell response and the modified wettability characteristics. Even so, the results determined for θ (see Figure 13.17) and γ^P (see Figure 13.18) indicate that these parameters could be used to predict the osteoblast cell response to laser whole area irradiative processed nylon 6,6 until the toxicity of the samples begins to dominate.

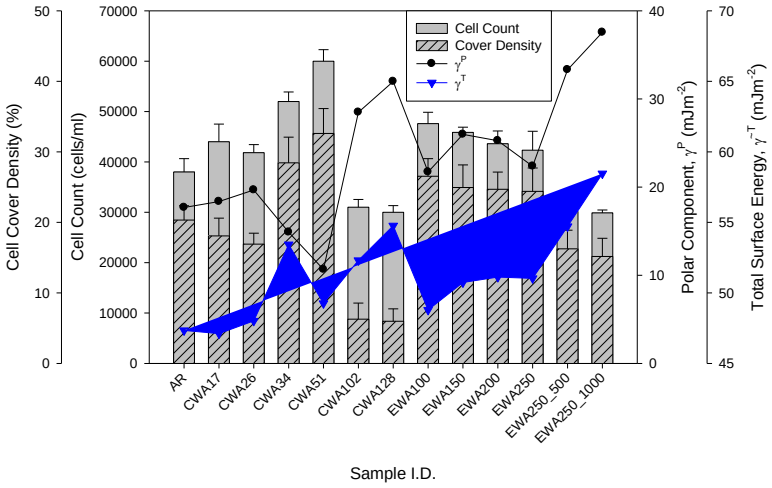

(a)

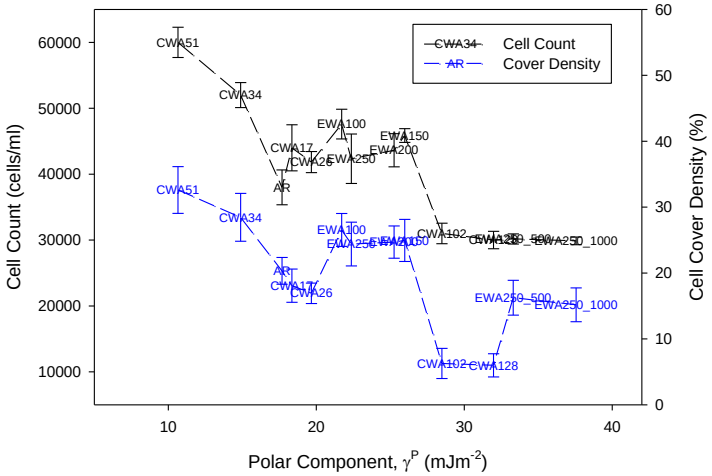

(b)

Figure 13.18 continued overleaf

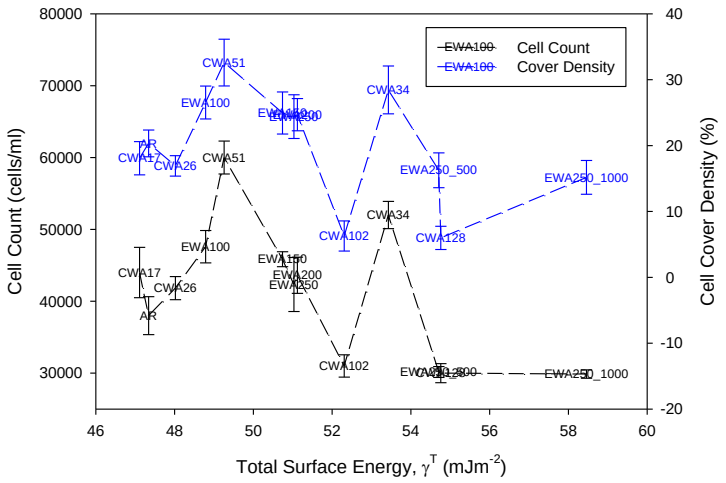

(c)

Figure 13.18 – (a) Histogram showing cell count and cell cover density in relation to γ^P and γ^T, (b) graph showing the relationship between cell count, cell cover density and γ^P and (c) graph showing the relationship between cell count, cell cover density and γ^T for the entire CO_2 and KrF excimer laser whole area irradiative processed nylon 6,6 samples.

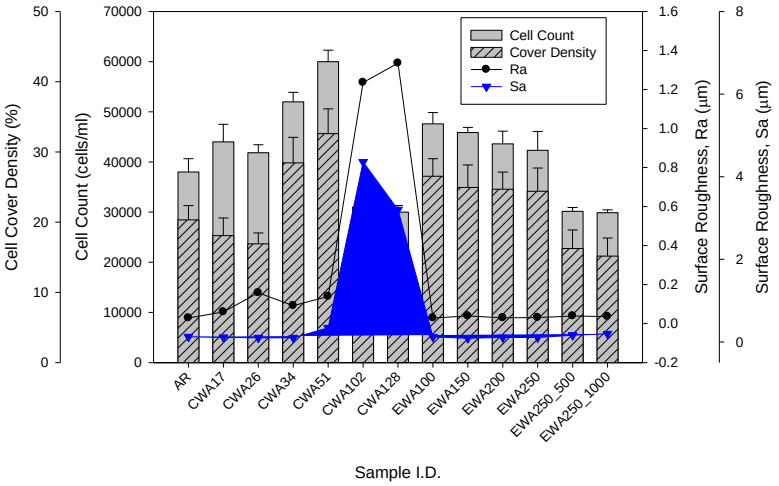

(a)

Figure 13.19 continued overleaf

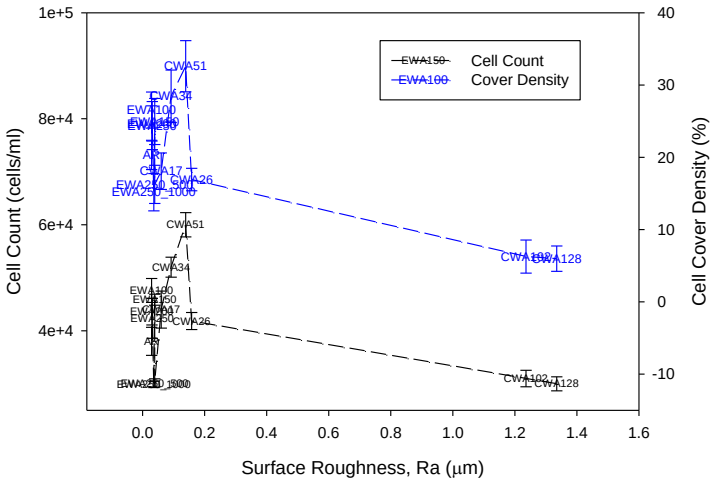

(b)

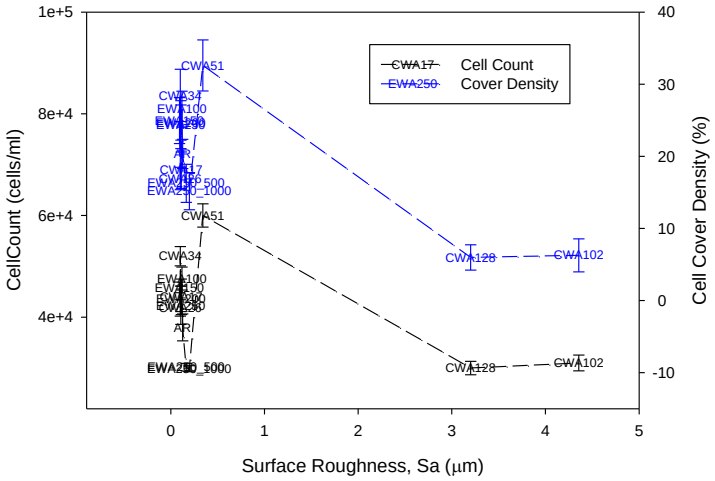

(c)

Figure 13.19 – (a) Histogram showing cell count and cell cover density in relation to Ra and Sa, (b) graph showing the relationship between cell count, cell cover density and Ra and (c) graph showing the relationship between cell count, cell cover density and Sa for the entire CO_2 and KrF excimer laser whole area irradiative processed nylon 6,6 samples.

From Figure 13.19(a) one can maintain that there did not seem to be any correlative trend between the osteoblast cell response and the surface roughness. This is due to the fact that samples with similar values of Ra and Sa gave rise to a significantly modulated osteoblast response with regards to cell count and cell cover density. The non-correlative trend can be further identified with Figure 13.19(b) and Figure 13.19(c); however, it could be argued that there may be a slight correlation similar to what was seen in Figure 13.15. This is owed to the results obtained for sample CWA102 and CWA128 and can be explained that the slight correlation is not true on account of the toxicity of the samples dominating the bioactive nature of the nylon 6,6 samples. As a result, it may be possible to use the surface roughness to indirectly predict the bioactive nature of CO_2 laser whole area irradiative processed nylon 6,6. This is due to the fact that the melting which gives rise to the toxicity also gave rise to the significant increase in Sa and Ra. Apart from this, it is reasonable to say that the surface

roughness, Ra and Sa, cannot be implemented to readily predict the osteoblast cell response to the laser whole area irradiative processed nylon 6,6.

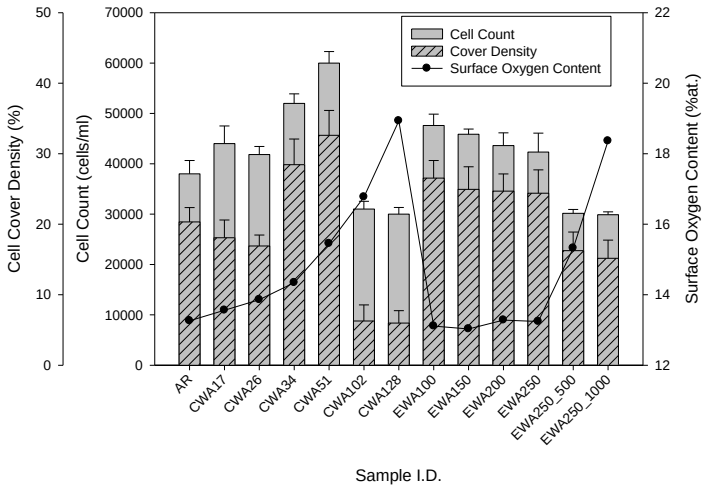

(a)

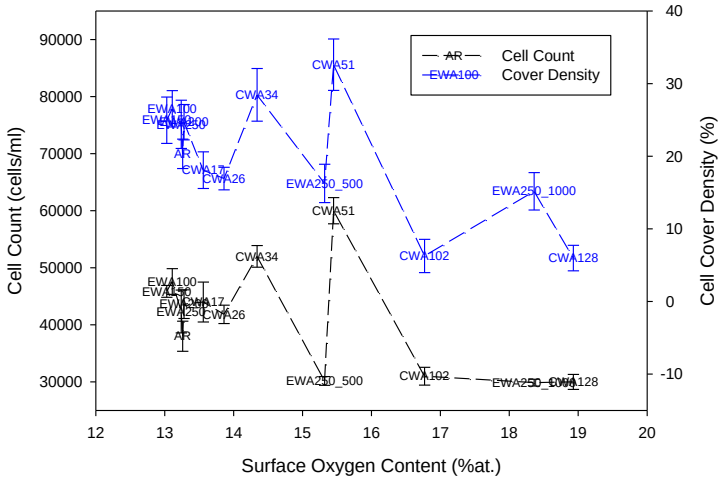

(b)

Figure 13.20 – (a) Histogram showing cell count and cell cover density in relation to surface oxygen content and (b) graph showing the relationship between cell count, cell cover density and surface oxygen content for the entire CO_2 and KrF excimer laser whole area irradiative processed nylon 6,6 samples.

Figure 13.20(a) allows one to see that there appeared to be a difference in correlative trends between the surface oxygen content of the CO_2 and KrF excimer laser whole area irradiative processed samples and the osteoblast cell response, which identifies another potential parameter which indicates λ dependency on the osteoblast cell response. For the CO_2 laser whole area irradiative processed samples the cell cover density and cell count increased upon an increase in surface oxygen content until a certain point around 16 %at. at which the cell cover density and cell count began to decrease. Conversely, the trend exhibited by the KrF excimer laser whole area irradiative processed samples was one by which the cell count and cell cover density steadily decreased upon an increase in surface oxygen content. These trends can be further identified with Figure 13.20(b) which shows a potential optimum threshold window for the CO_2 laser whole area irradiative processed samples of between

14.5 and 16 %at in which the most enhanced osteoblast cell response was observed. In addition, for the KrF excimer laser whole area irradiative processed samples, the cell cover density and cell count can be seen to be a steady decreasing function of the surface oxygen content. It should be noted here that it is highly likely that the increase in surface oxygen content of the samples did not directly have a detrimental effect on the osteoblast cell response. As discussed in Section 11.5, the melting and re-solidification of the nylon 6,6 is likely to have given rise to toxic substances which can be attributed to the hindrance of osteoblast cell growth. Even though this may be the case, it is evident that the surface oxygen content could potentially be used as an indirect predictive tool to estimate how osteoblast cells will react to the laser whole area irradiative processing of nylon 6,6. This is due to the surface oxygen content increasing with more melting and re-solidification taking place in addition to the toxicity of the samples also increasing.

13.3.3 – Cytotoxicity and Alkaline Leukocyte Phosphatase (ALP) Levels

It can be determined from Figure 13.21(a) that for most of the laser whole area irradiative processed samples, the cytotoxicity decreased and the ALP increased on account of an increasing θ. This is also shown in Figure 13.21(b) in that the cytotoxicity was a decreasing function of θ and the ALP level was an increasing function of θ. However, it can also be seen from Figure 13.21(a) that sample CWA102 and sample CWA128 do not correspond with the observed trend and can be attributed to the fact that the toxicity of the samples, as discussed in Section 11.5 and Section 12.5, played a more dominating role in the osteoblast cell response. What is more, the correlation that was observed in Figure 13.21 corroborates with what was observed in Figure 13.17 in that an increase in θ gave rise to a more enhanced osteoblast cell response to the laser whole area irradiative processed nylon 6,6 samples.

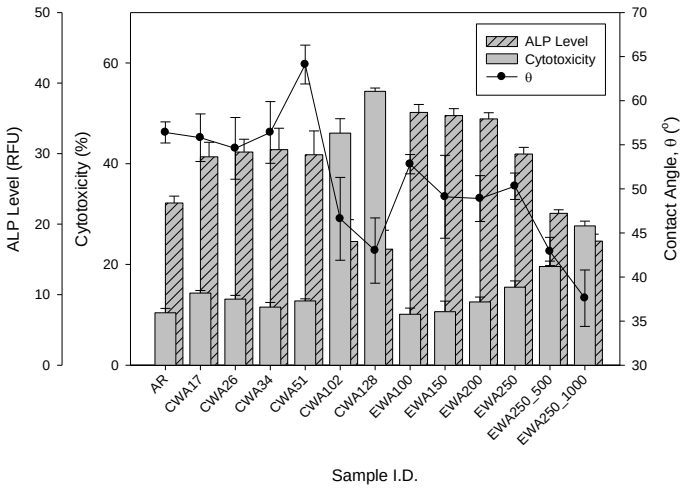

(a)

Figure 13.21 continued overleaf

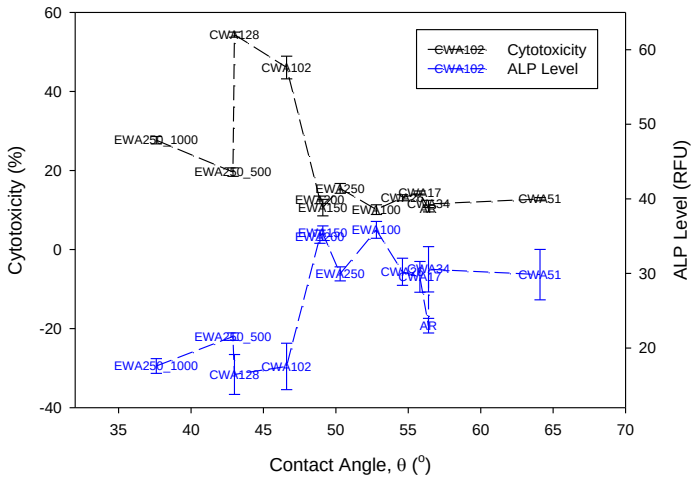

(b)

Figure 13.21 – (a) Histogram showing cytotoxicity and ALP level in relation to θ and (b) graph showing the relationship between cytotoxicity, ALP Level and θ for the entire CO_2 and KrF excimer laser whole area irradiative processed nylon 6,6 samples.

Figure 13.22(a) shows that for almost the entire laser whole area irradiative processed samples, the cytotoxicity increased and ALP level decreased on account of an increase in γ^P and γ^T. This is further shown in Figure 13.22(b) and 13.22(c) for γ^P and γ^T, respectively. Figure 13.22(b) shows that the relationship between the cytotoxicity, ALP level and γ^P was the inverse of that seen with θ (see Figure 13.21) and allows for further evidence of the strong relationship between γ^P and θ as was determined in Chapter 10. It can also be seen that the relationship between the cytotoxicity, ALP level and γ^P is somewhat a strong correlation regardless of the λ employed.

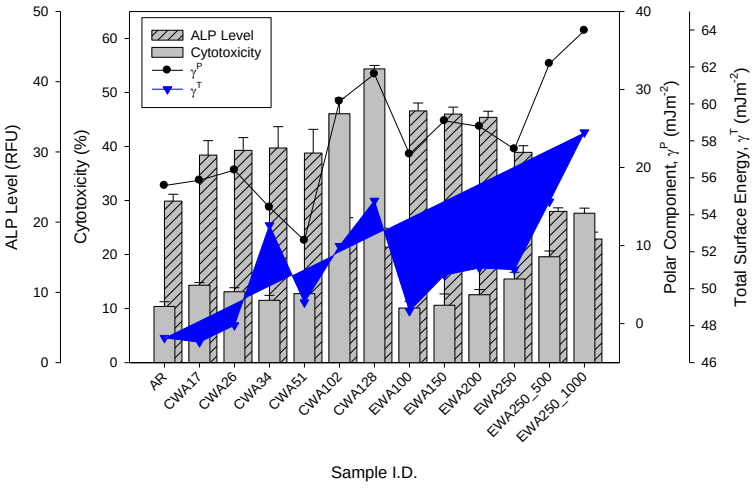

(a)

Figure 13.22 continued overleaf

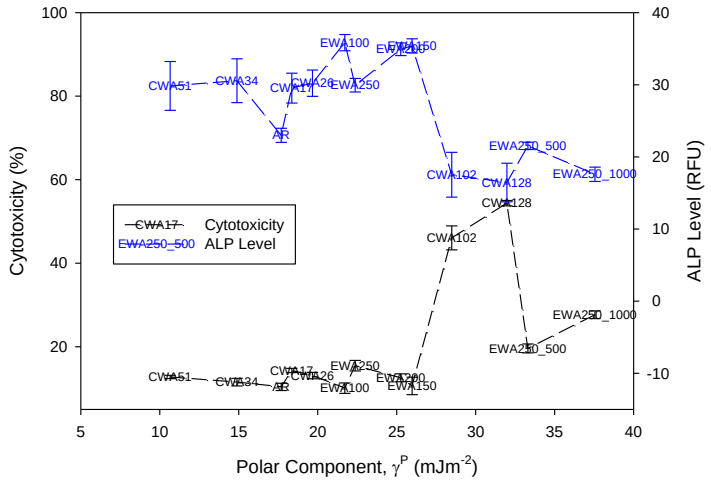

(b)

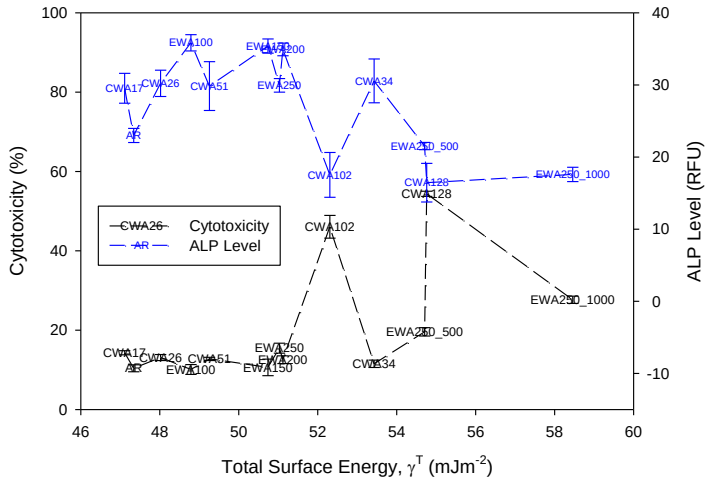

(c)

Figure 13.22 – (a) Histogram showing cytotoxicity and ALP level in relation to γ^P and γ^T, (b) graph showing the relationship between cytotoxicity, ALP Level and γ^P and (c) graph showing the relationship between cytotoxicity, ALP level and γ^T for the entire CO_2 and KrF excimer laser whole area irradiative processed nylon 6,6 samples.

Another correlation that can be seen in Figure 13.22(c) confirms the correlative relationship between cytotoxicity, ALP level and γ^T which was observed initially with Figure 13.22(a). It should also be further noted here that sample CWA102 and sample CWA128 did not follow the trend shown by the other samples in terms of cytotoxicity, ALP level, γ^P and γ^T and can be owed to the fact that the sample toxicity, discussed in Chapter 11.5 and Chapter 12.5, is the most dominant parameter and hindered the osteoblast cell growth. As a result of this, it can be said with reason that both θ and the surface energy of laser whole area irradiative processed nylon 6,6 can potentially be implemented to predict how osteoblast cells will react *in vitro*, unless the toxicity becomes more dominant. This implies that there is a threshold surface toxicity for the laser whole area irradiative processed nylon 6,6 samples, below which the wettability characteristics of θ, γ^P and γ^T appear to dominate showing to

some extent very strong correlative trends with the observed osteoblast cell response in terms of cell cover density (see Section 13.3.2), cell count (see Section 13.3.2), cytotoxicity and ALP level. Above this toxicity threshold for the laser whole area irradiative processed samples the toxicity seems to have become the most dominant parameter and hindered the osteoblast cell response and inherently ceasing the trends observed between osteoblast cell growth and the wettability characteristics.

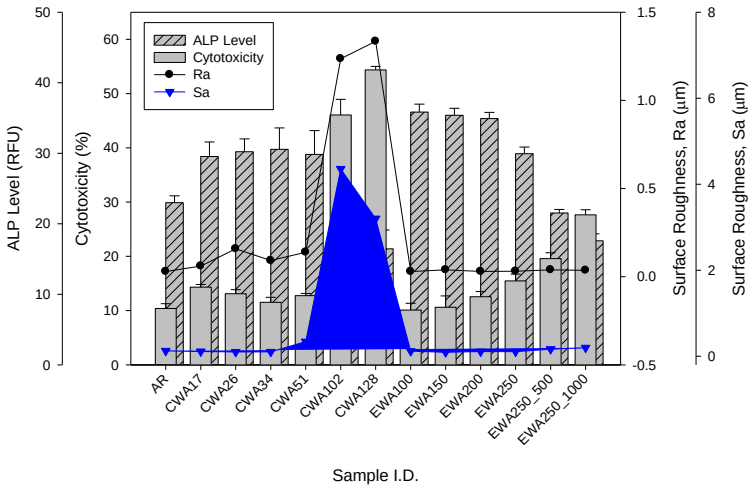

(a)

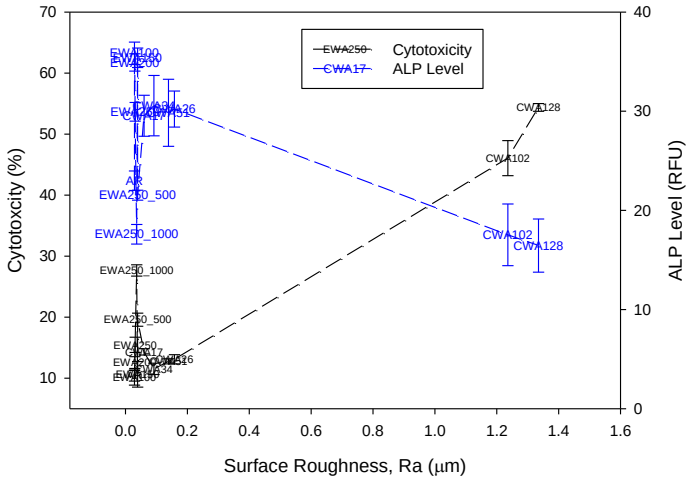

(b)

Figure 13.23 continued overleaf

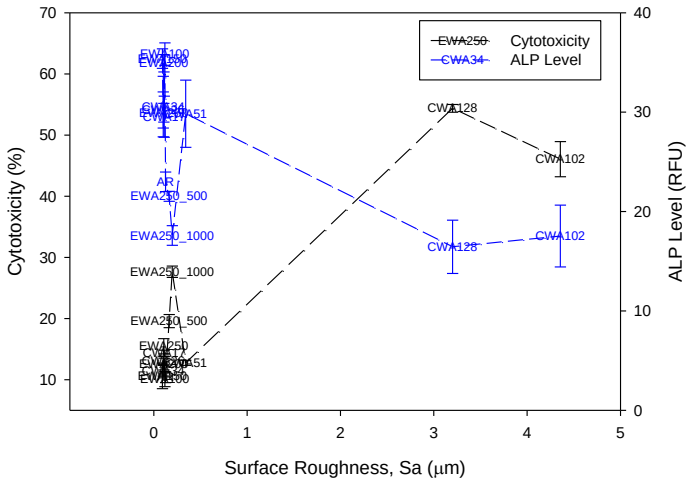

Figure 13.23 – (a) Histogram showing cytotoxicity and ALP level in relation to Ra and Sa, (b) graph showing the relationship between cytotoxicity, ALP Level and Ra and (c) graph showing the relationship between cytotoxicity, ALP level and Sa for the entire CO_2 and KrF excimer laser whole area irradiative processed nylon 6,6 samples.

Figures 13.23(a), 13.23(b) and 13.23(c) allow one to see that the surface roughness in terms of Ra and Sa did not appear to have any distinct correlative trend with the cytotoxicity and ALP levels. This is attributed to the fact that the cytotoxicity and ALP levels were highly modulated even though similar roughness values were observed for most of the laser whole area irradiative processed nylon 6,6 samples. Having said that, like what was observed with the apatite response (see Section 13.3.1), cell cover density (see Section 13.3.2) and cell count (see Section 13.3.2) the large increase in Sa and Ra for the CO_2 laser whole area irradiative processed samples (CWA102 and CWA128) could be indicative of the fact that the osteoblast cell count could be hindered. This is owed to the fact that considerable melting, leading to the surface becoming more toxic, would give rise to a larger surface roughness. But, it is more likely that other parameters such as θ and γ^P could potentially be used as a bioactivity indicator for laser whole area irradiative processed nylon 6,6 on account of their stronger correlative trends with the osteoblast cell response.

In Figure 13.24(a) it can be seen that the cytotoxicity and ALP levels for the KrF excimer laser whole area irradiative processed samples gave rise to a steady increase in cytotoxicity and steady decrease in ALP levels upon an increase in surface oxygen content. A slightly different trend was observed for the CO_2 laser whole area irradiative processed samples in that the cytotoxicity and ALP levels remained somewhat constant until the last two samples (CWA102 and CWA128) which gave rise to a large increase in surface oxygen content, a large increase in cytotoxicity and a reduction in the ALP level. By plotting the cytotoxicity and ALP levels in order of the surface oxygen content for the laser whole area irradiative processed samples as shown in Figure 13.24(b) it can be seen that there was a slight correlative trend between the surface oxygen content, the cytotoxicity and ALP level. That is, the cytotoxicity was an increasing function of surface oxygen content; whereas the ALP level was a

reducing function of the surface oxygen content. This corresponds with what was observed with the cell count and cell cover density (see Section 13.3.2) as an increase in surface oxygen content appeared to give rise to a hindered osteoblast cell response. Having said that, sample CWA102 and CWA128 do not necessarily tend to correspond with the observed correlative trend and could be accounted for by the increase in surface toxicity (see Section 11.5) dominating the osteoblast cell response and removing any possible correlation which may have been seen with the wettability characteristics and surface parameters. As a result of this, as seen with the cell count and cell cover density (see Section 13.3.2), the cytotoxicity and ALP level for the laser whole area irradiative processed nylon 6,6 could be indirectly predicted for osteoblast cells as long as the toxicity of the nylon 6,6 does not increase above a certain threshold which seems to have occurred in the case of sample CWA102 and CWA128.

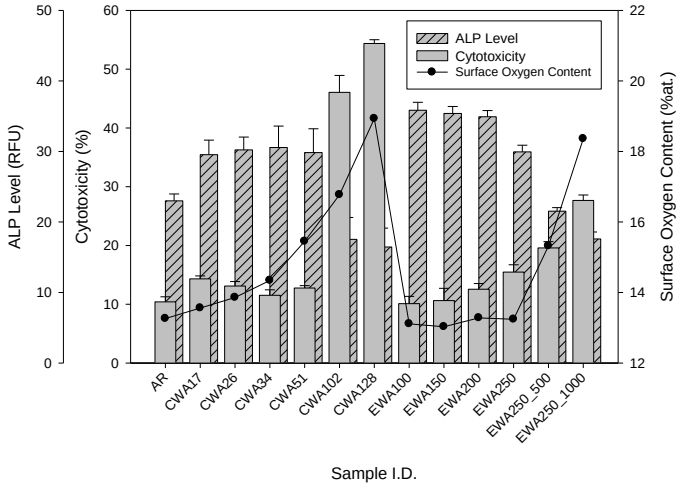

(a)

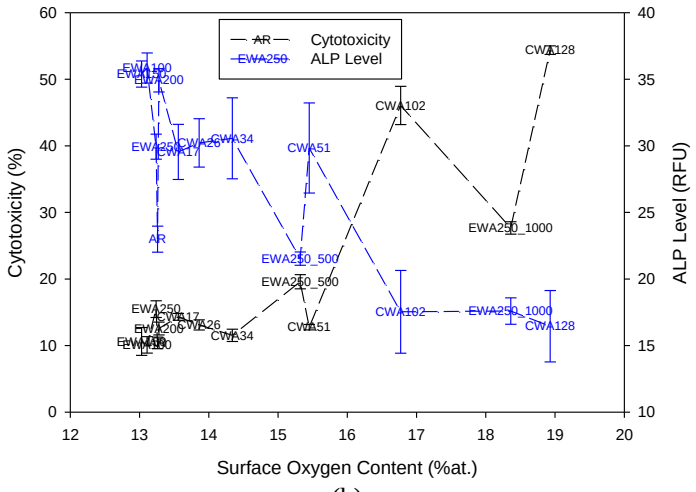

(b)

Figure 13.24 – (a) Histogram showing cytotoxicity and ALP level in relation to surface oxygen content and (b) graph showing the relationship between cytotoxicity, ALP Level and surface oxygen content for the entire CO_2 and KrF excimer laser whole area irradiative processed nylon 6,6 samples.

One aspect that can be taken into account for the laser whole area irradiative processed nylon 6,6 samples is that of the fluence. For the KrF excimer laser whole area irradiative processing the fluences was considerably smaller in comparison to the CO_2 laser whole area irradiative processing. Even so, it was seen on both occasions that the different lasers gave rise to modifications in wettability and bioactivity, which can be attributed to the different optical absorption characteristics exhibited by the nylon 6,6.

Figure 13.5 shows the modulation of the cell cover density for each of the laser whole area irradiative processed samples in that for both the CO_2 (see Figure 13.25(a)) and KrF excimer (see Figure13.25(b)) laser whole area irradiative processed samples the cell cover density increased as a function of fluence to a maximum threshold. Figure 13.25(a) allows one to see that the cell cover density increases as the fluence increases until between 51 and 100 Jcm^{-2} in which the cell cover density decreased considerably. This attests to a maximum threshold fluence in terms of optimum cell cover density. Similarly, Figure 13.25(b) shows that the cell cover density increased on account of fluence for the KrF excimer laser whole area irradiative processing until an increased number of incident pulses was implemented. This suggests that there is also a maximum threshold for fluence as the increased incident pulses increased the interaction time between the KrF excimer laser and the nylon 6,6 samples.

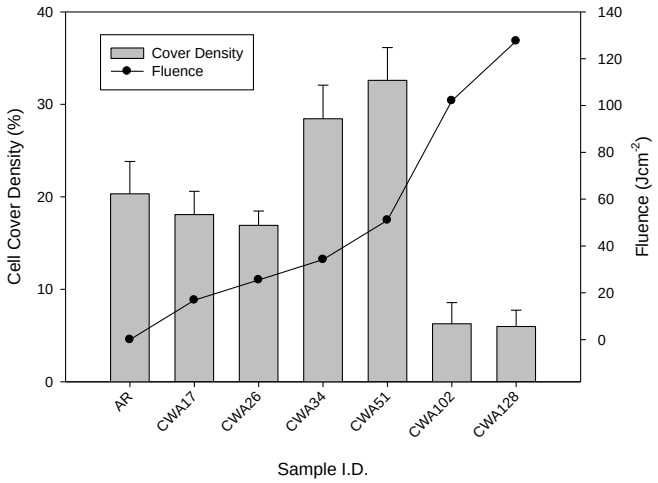

(a)

Figure 13.25 continued overleaf

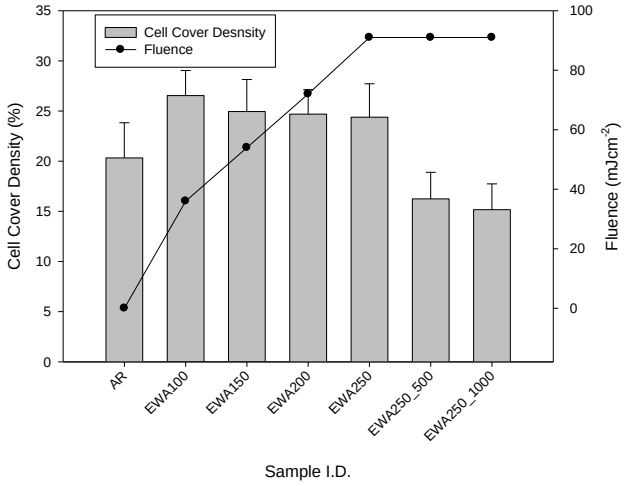

(b)

Figure 13.25 – Histograms showing the cell cover density in relation to incident fluence for (a) CO_2 laser whole area irradiative processed nylon 6,6 samples and (b) KrF excimer laser whole area irradiative processed nylon 6,6 samples.

The other parameters which give evidence to the bioactive nature of the nylon 6,6 samples; namely cell count (see Figure 13.26), cytotoxicity (see Figure 13.27) and ALP level (see Figure 13.28) also give strong evidence of a potential threshold for the CO_2 and KrF excimer laser whole area irradiative processed nylon 6,6 samples. Figure 13.26(a) shows that the cell count for the CO_2 laser whole area irradiative processed samples increased as the fluence increased until the fluence of 51 Jcm^{-2} was surpassed in which a reduction in cell count was observed highlighting a reduction of the osteoblast cell response to the nylon 6,6 samples. Figure 13.26(b) allows one to see that the cell count had increased initially with relatively low fluences of less than 60 $mJcm^{-2}$. Beyond this limit, however, the cell count decreased with the lowest cell counts of around 32,000 cells/ml being determined for the highest fluence of 91 $mJcm^{-2}$ and highest incident pulse number of 1000 pulses.

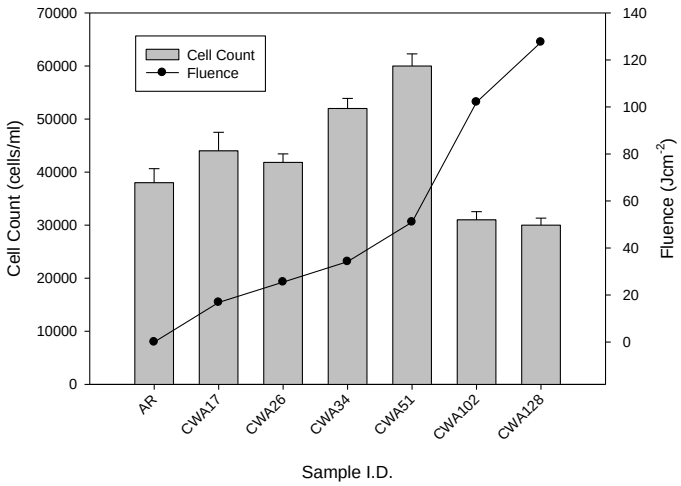

(a)

Figure 13.26 continued overleaf

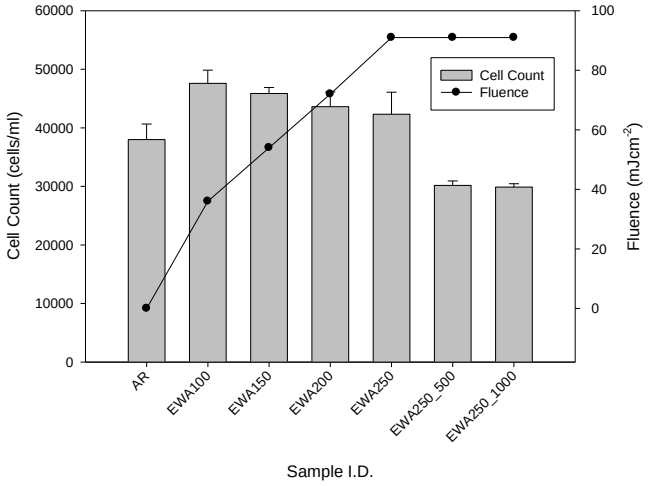

(b)

Figure 13.26 – Histograms showing the cell count in relation to incident fluence for (a) CO_2 laser whole area irradiative processed nylon 6,6 samples and (b) KrF excimer laser whole area irradiative processed nylon 6,6 samples.

The observed cell count as shown in Figure 13.26 can be explained by the increase in cytotoxicity (see Figure 13.27) which rises upon an increase in fluence (see Figure 13.27) and pulse number (see Figure 13.27(b)). To further give evidence of the threshold fluence and incident pulse number for both laser whole area irradiative processing techniques Figure 13.28 shows the ALP level for each sample in relation to the fluence. Figure 13.28(a) allows one to identify that the ALP level had increased upon a rise in fluence until a fluence of 34 Jcm^{-2} was reached, after which the ALP level began to decrease upon an increase in fluence. Similarly, Figure 13.28(b) shows that the an initial increase in fluence at 100 pulses for the KrF excimer laser whole area irradiative processed samples gave rise to an increase in ALP level but once the fluence reached around 70 $mJcm^{-2}$ and the incident pulse number was increased the ALP level began to fall.

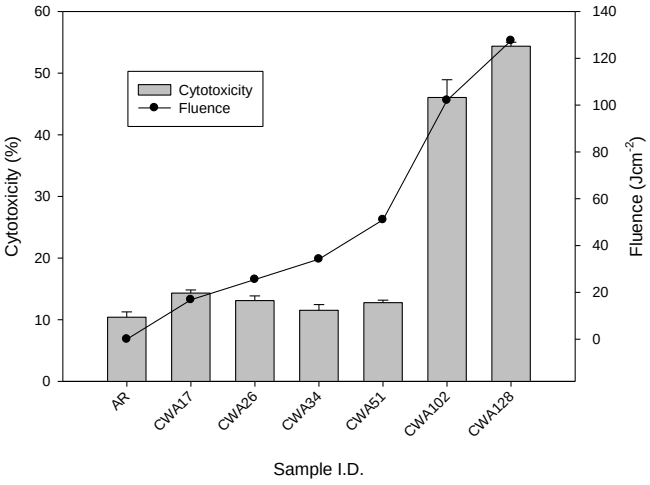

(a)

Figure 13.27 continued overleaf

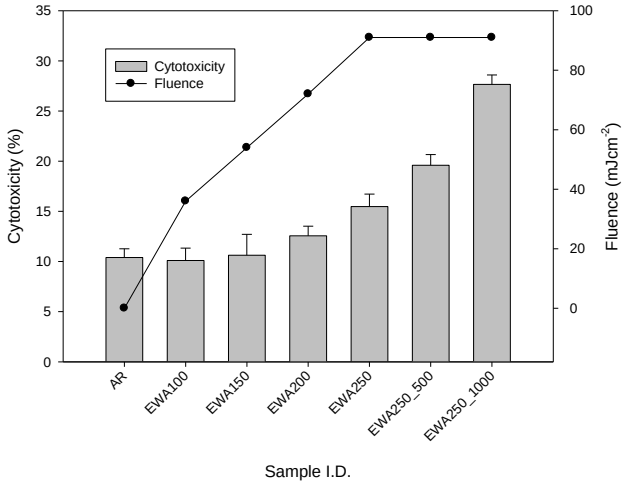

(b)

Figure 13.27 – Histograms showing the cytotoxicity in relation to incident fluence for (a) CO_2 laser whole area irradiative processed nylon 6,6 samples and (b) KrF excimer laser whole area irradiative processed nylon 6,6 samples.

It is evident from Figures 13.25, 13.26, 13.27 and 13.28 that for both of the laser systems a threshold fluence for each can be ascertained even though considerably different fluence values were implemented and even though the CO_2 laser was cw and the KrF excimer laser was pulsed. From the results obtained it can be seen that for the CO_2 laser whole area irradiative processing of the nylon 6,6 a threshold in the region of 60 to 95 Jcm^{-2} is the maximum which can be used to irradiate the nylon 6,6 samples before the samples hinder the osteoblast cell response. For the KrF excimer laser whole area irradiative processed samples a threshold in between 70 and 90 $mJcm^{-2}$ gives rise to a less enhanced bioactive nylon 6,6 sample. In addition to this, it can be seen that at the highest fluence of 90 $mJcm^{-2}$, incident pulse numbers of over 100 pulses gives rise to a nylon 6,6 surface which hinders the osteoblast cell growth to the point where the osteoblast cell response is worse than that of the as-received sample (AR).

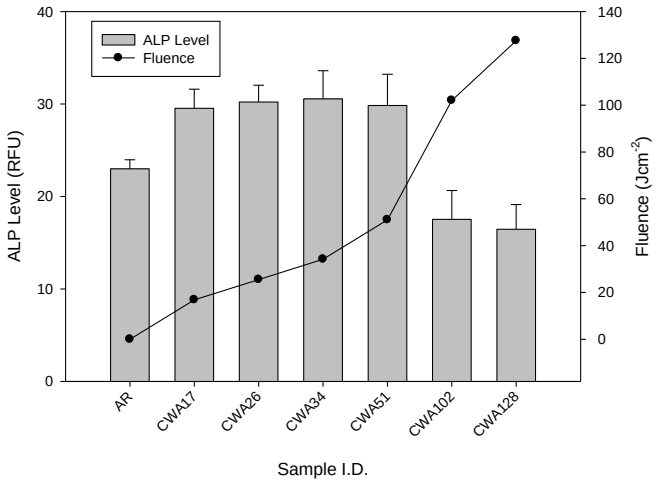

(a)

Figure 13.28 continued overleaf

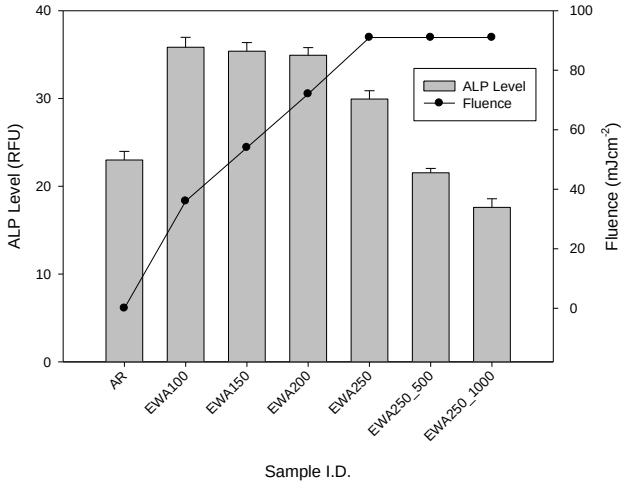

(b)

Figure 13.28 – Histograms showing the ALP level in relation to incident fluence for (a) CO_2 laser whole area irradiative processed nylon 6,6 samples and (b) KrF excimer laser whole area irradiative processed nylon 6,6 samples.

13.4 – Comparison Between Laser-Induced Patterning and Laser Whole Area Irradiative Processing

This section combines all results obtained for all samples for the apatite response, cell cover density, cell count, cytotoxicity and ALP Levels. As a result, these are discussed and compared in the attempt to find correlative trends between the different laser surface treatments.

13.4.1 – Apatite Response

It can be seen from Figure 13.29(a) that there did not appear to be an overall trend between the apatite formation in terms of Δg and θ. This can be further affirmed by Figure 13.29(b) which shows that each set of samples had their own specific trend. Δg for the CO_2 laser whole area irradiative processed samples was found to be an increasing function of θ; whereas, for the KrF excimer laser whole area irradiative processed samples, Δg was a decreasing function of θ. This suggests that with regards to apatite formation, Δg is somewhat λ dependant in the case of laser whole area irradiative processing. On the other hand, for the laser-induced patterned samples it was found that there was no distinct correlative trend which can be accounted for by the likely transition in wetting regime which was proposed in Chapters 6, 7 and 10.

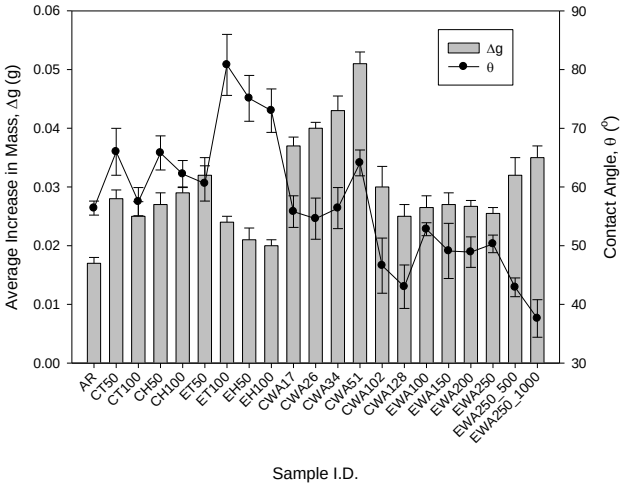

(a)

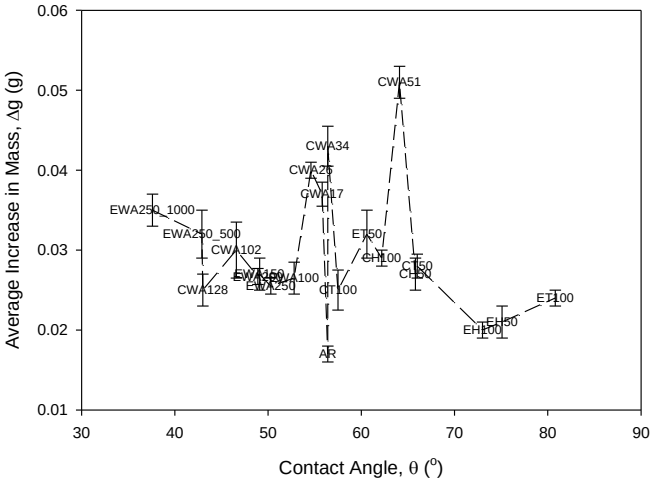

(b)

Figure 13.29 – (a) Histogram showing Δg in relation to θ and (b) graph showing the relationship between Δg and θ for all laser processed nylon 6,6 samples.

Similar to what was observed with θ (see Figure 13.29), Figure 13.30(a) allows one to see that there was no distinct overall relationship between the samples with regards to Δg, γ^P and γ^T. For γ^P, Figure 13.30(b) also shows that there was no correlative trend overall between the entire laser surface treated samples; however, it can be seen that different trends arise. First of all, it can be identified that the trends shown in Figure 13.30(b) were the inverse of what was observed for θ which gives evidence of the strong relationship between θ and γ^P, as was identified in Chapter 10. Leading on from this, for the CO_2 laser whole area irradiative processed samples it can be taken from Figure 13.30(b) that Δg was a decreasing function of γ^P. In a similar manner it can also be seen in Figure 13.30(b) that for the KrF excimer laser whole area irradiative processed samples Δg was an increasing function of γ^P. Another factor to be taken from Figure 13.30(b) is that for all the laser-induced patterned samples no distinct trend could be identified and could be a result of the transition in wetting regime giving erroneous results.

In terms of γ^T, it can be seen from Figure 12.30(c) that there definitely was no correlative trend for all of the samples. Furthermore, there was no distinct trend between Δg and γ^T for the CO_2 laser whole area irradiative processed and all laser-induced patterned samples when taking them into account individually. Yet, there was a slight trend between γ^T and Δg for the KrF excimer laser whole area irradiative processed samples in that Δg was, to a certain extent, an increasing function of γ^T. This further suggests that the dominant parameters to determine apatite adhesion could be dependent on the λ employed. As a result of this along with what was observed with θ (see Figure 13.29), by knowing the different trends for each of the laser surface treatment types it is possible to foresee that θ and surface energy could potentially be implemented as a predictive tool to estimate the apatite response of laser surface treated nylon 6,6 upon immersion in SBF.

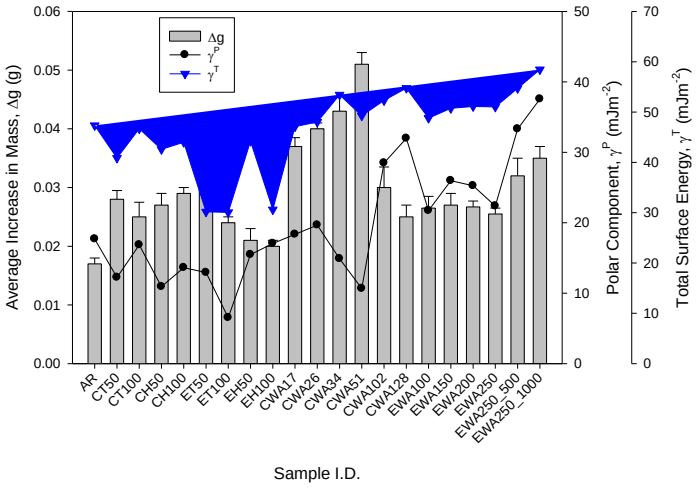

(a)

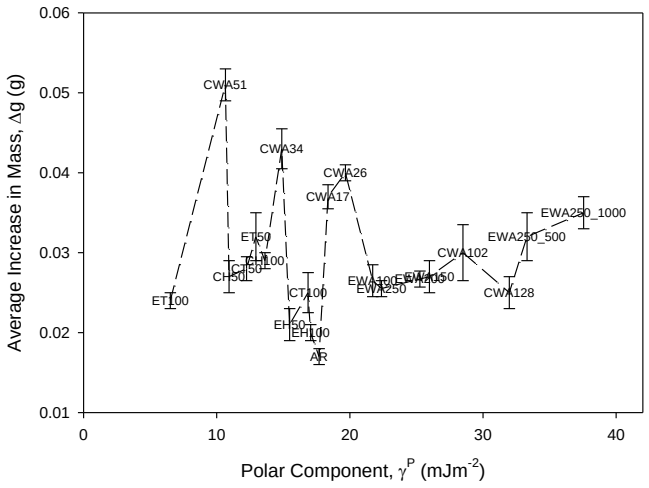

(b)

Figure 13.30 continued overleaf

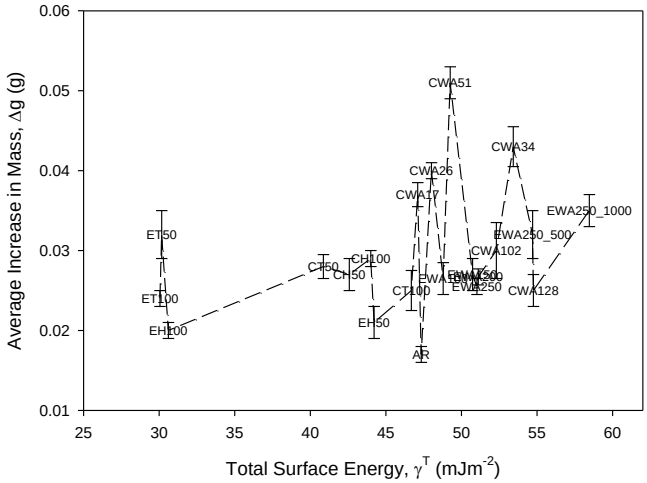

(c)

Figure 13.30 – (a) Histogram showing Δg in relation to γ^P and γ^T, (b) graph showing the relationship between Δg and γ^P and (c) graph showing the relationship between Δg and γ^T for all laser processed nylon 6,6 samples.

One can ascertain from Figure 13.31(a) that there did not appear to be an overall trend between Δg and surface roughness and can be further identified through Figure 13.31(b) and Figure 13.31(c). This is owed to the fact that similar Sa and Ra values gave rise to highly modulated Δg. It can be seen that even though the laser whole area irradiative processed samples did not give rise to a correlative trend, Figure 13.31(c) shows that for the laser-induced patterned samples Sa could be a dominant parameter (also see Section 13.2) which gave rise to an optimum threshold window giving the largest Δg. With this in mind, it could imply that the transition in wetting regime, as discussed in Chapter 10, which arose from the surface topography played a distinctive role in the adhesion characteristics with regards to apatite formation.

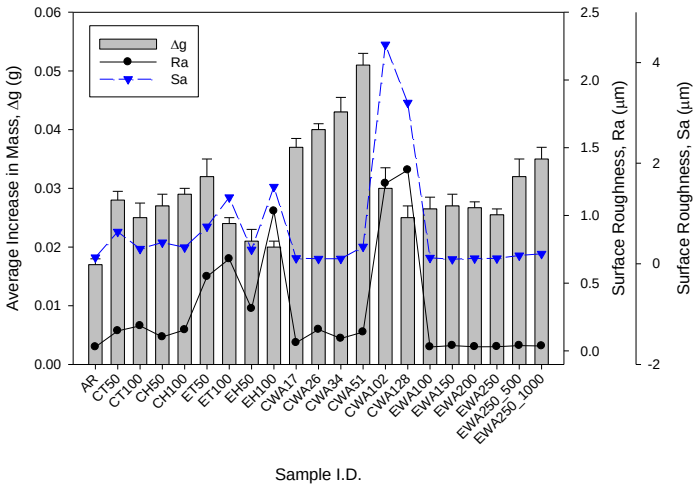

(a)

Figure 13.31 continued overleaf

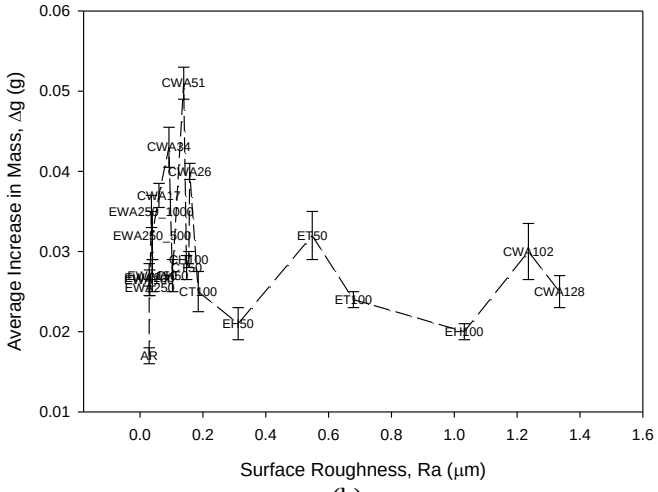

(b)

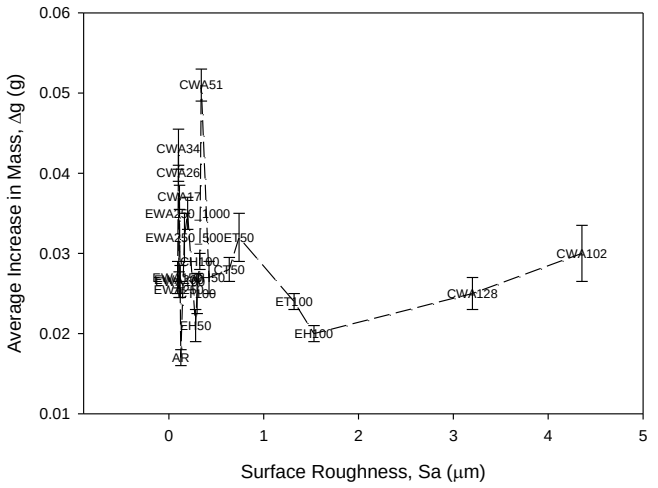

(c)

Figure 13.31 – (a) Histogram showing Δg in relation to Ra and Sa, (b) graph showing the relationship between Δg and Ra and (c) graph showing the relationship between Δg and Sa for all laser processed nylon 6,6 samples.

Figure 13.32(a) and Figure 13.32(b) show that there was no overall correlative trend between the surface oxygen content and Δg for the laser surface treated nylon 6,6; however, as discussed previously in Section 13.2.1 and 13.3.1 there was correlative trends between the individual processes. For instance, for the CO_2 laser whole area irradiative processed samples Δg increased to a maximum before decreasing with increasing surface oxygen content. This could be seen to on account of the surface oxygen content aiding the enhancement of the apatite response until the toxicity of the sample began to dominate (see Section 11.5). For the KrF excimer laser whole area irradiative processed samples Δg was found to be an increasing function of the surface oxygen content which could be due to the fact that the surface toxicity had not completely begun to dominate the apatite formation. Furthermore, it can be seen from Figure 13.32(b) that the laser-induced patterned samples did not give rise to any strong correlative relationship with Δg which can be attributed to the transition in wetting regime.

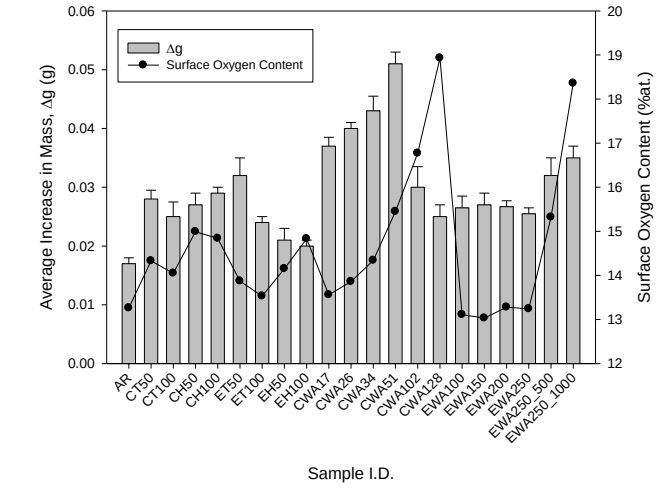

(a)

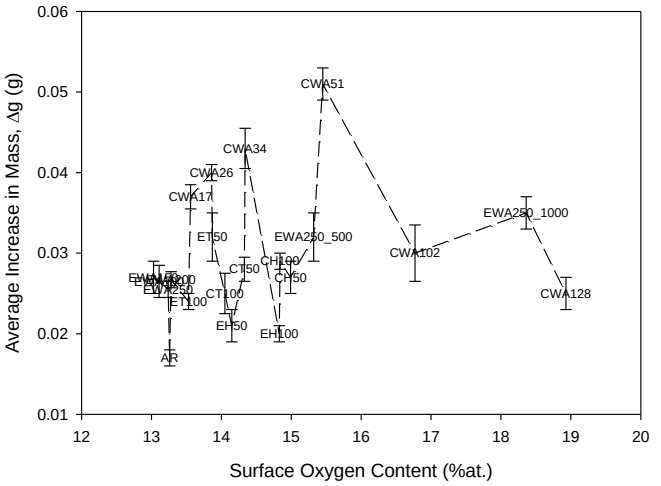

(b)

Figure 13.32 – (a) Histogram showing Δg in relation to surface oxygen content and (b) graph showing the relationship between Δg and surface oxygen content for all laser processed nylon 6,6 samples.

By taking into account all of the parameters it can be seen that for the laser whole area processed nylon 6,6 θ, surface energy and surface oxygen content have the potential to be implemented as an indicative tool to allow one to estimate the apatite response. On the other hand, owed to the likely transition in wetting proposed for the laser-induced patterned samples it has been determined that there does not appear to be a conclusive relationship between the wettability characteristics and apatite response. From this, it is possible to deduce that it may not be possible to determine with good reason how a laser-induced patterned nylon 6,6 material will act with regards to the formation of apatite.

13.4.2 – Cell Cover Density and Cell Count

Figure 13.33(a) allows one to see that overall the laser surface treated samples did not have a correlative trend between the cell cover density, cell count and θ. This is on account of the laser-induced patterned samples not correlating with the trend observed for the laser whole area irradiative processed samples which can be attributed to the transition in wetting regime (see Chapter 6) for the laser-induced patterned samples giving erroneous results. The trends identified can be further ascertain from Figure 13.33(b) which shows that for all laser whole area irradiative processed samples, with the exception of sample CWA102 and sample CWA128, the cell cover density and cell count were an increasing function of θ. It should be noted here that sample CWA102 and sample CWA128 did not follow the trend on account of the toxicity dominating (see Section 11.5).

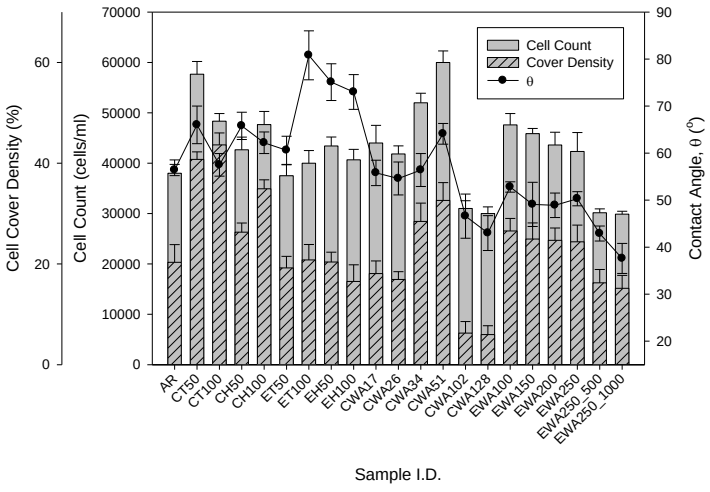

(a)

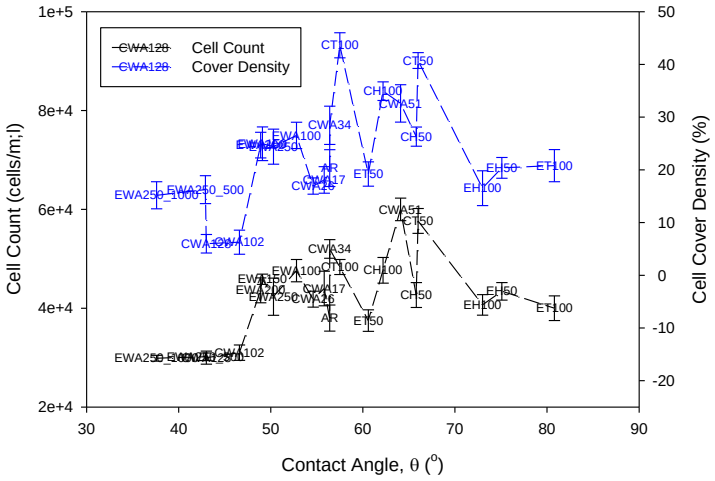

(b)

Figure 13.33 – (a) Histogram showing cell count and cell cover density in relation to θ and (b) graph showing the relationship between cell count, cell cover density and θ for all laser processed nylon 6,6 samples.

Figure 13.34(a) shows that there was no correlative relationship between γ^P, γ^T and osteoblast cell response for the laser surface treated nylon 6,6 samples when taken as a whole. Similar to θ (see Figure 13.33), this can be accounted for by the laser-induced patterned samples which gave rise to somewhat erroneous results on account of the likely transition in wetting regime. The relationship between cell cover density, cell count and γ^P for the entire laser whole area irradiative processed samples can be seen in Figure 13.34(b) in that the enhancement of osteoblast cell response was an increasing function of γ^P. However, sample CWA102 and sample CWA128 do not correspond with the trend identified and can be explained by the increase in surface toxicity (see Section11.5). Leading on, it can be seen from Figure 13.34(c) that for none of the samples there did not appear to be any correlative relationship between γ^T and the osteoblast cell response, indicating that γ^T was not a dominant parameter. Even though there was no overall trend observed for θ and γ^P it can still be said within reason that if a surface toxicity was low enough as to not dominate the osteoblast cell response, then it appears likely that θ and γ^P play an important role in determining the osteoblast cell response to the laser whole area irradiative processed nylon 6,6.

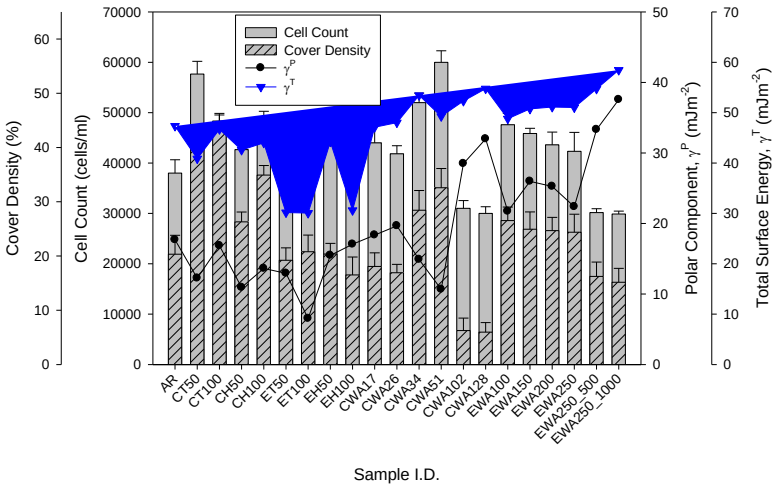

(a)

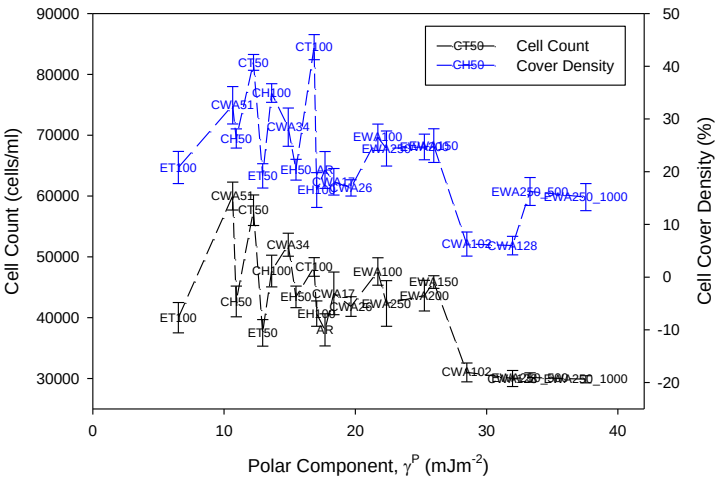

(b)

Figure 13.34 continued overleaf

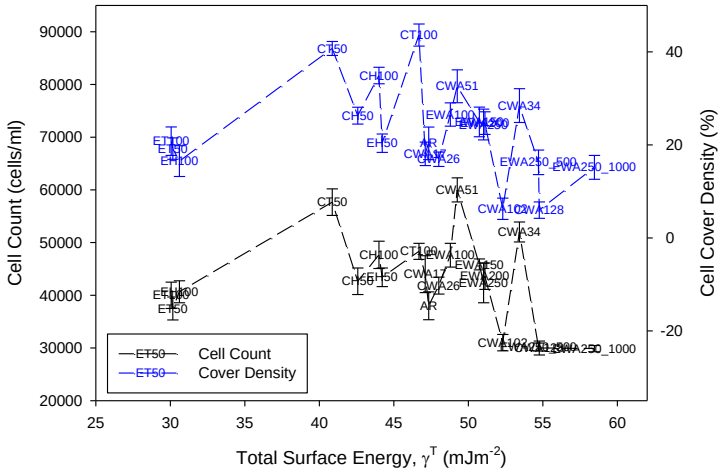

(c)

Figure 13.34 – (a) Histogram showing cell count and cell cover density in relation to γ^P and γ^T, (b) graph showing the relationship between cell count, cell cover density and γ^P and (c) graph showing the relationship between cell count, cell cover density and γ^T for all laser processed nylon 6,6 samples.

It can be seen from Figures 13.35(a), 13.35(b) and 13.35(c) that overall, the surface roughness in terms of Ra and Sa did not appear to have a distinct relationship with the osteoblast cell response with regards to cell cover density and cell count. Having said that, for those samples with the largest values of Sa and Ra (sample CWA102 and sample CWA128) the surface roughness could be indirectly indicative of the bioactive nature of the CO_2 laser whole area irradiative processed nylon 6,6 samples. This is due to the fact that the melting which gives rise to the proposed increase in toxicity (see Section 11.5) which dominated the osteoblast cell also gave rise to the significant increase in Ra and Sa.

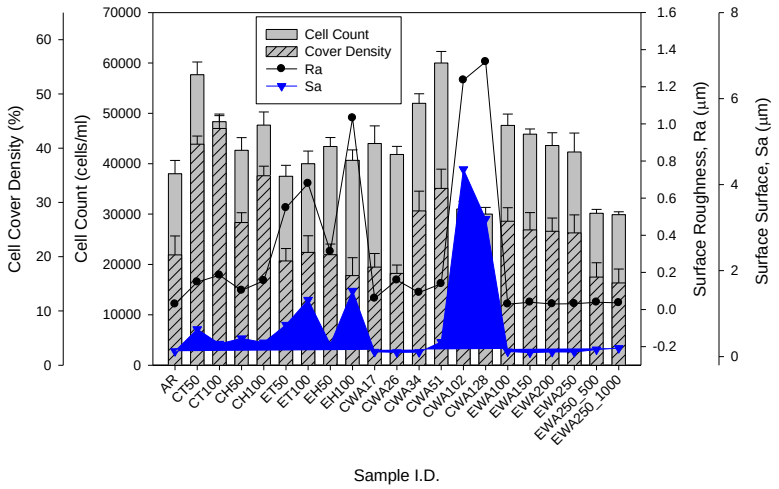

(a)

Figure 13.35 continued overleaf

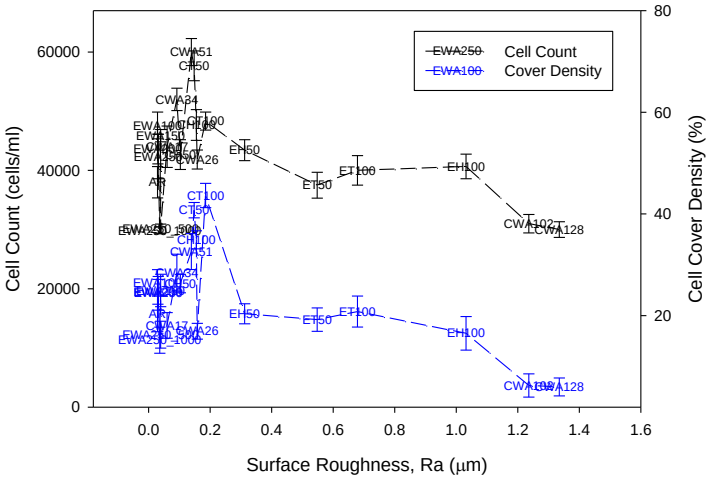

(b)

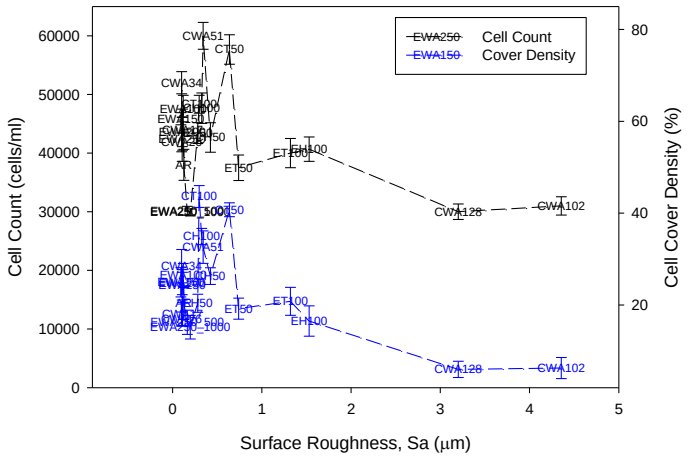

(c)

Figure 13.35 – (a) Histogram showing cell count and cell cover density in relation to Ra and Sa, (b) graph showing the relationship between cell count, cell cover density and Ra and (c) graph showing the relationship between cell count, cell cover density and Sa for all laser processed nylon 6,6 samples.

When taking into account all samples with respect to the relationship between the surface oxygen content and osteoblast cell response, it can be seen from Figure 13.36(a) and Figure 13.36(b) that there was no overall trend which could be implemented to predict the osteoblast cell response to the laser surface treated nylon 6,6. Having said that, as discussed in section 13.3.2, there was two different observed trends for the laser whole area irradiative processed samples which could potentially be used as an indirect method to estimate whether enhanced osteoblast cell response can be brought about by the nylon 6,6 samples. This is accounted for by the likelihood of the nylon 6,6 samples becoming more toxic upon more laser-induced melting even though the surface will also oxidize, giving rise to an increase in surface oxygen content.

In terms of cell cover density and cell count it has been seen that below a potential toxicity threshold θ and γ^P appear to dominate the bioactive nature of nylon 6,6 which has undergone laser whole area

irradiative processing regardless of the laser type used. With this in mind, one can extrapolate that θ and γ^P can be implemented to predict how osteoblast cells will react upon laser whole area irradiative processed nylon 6,6.

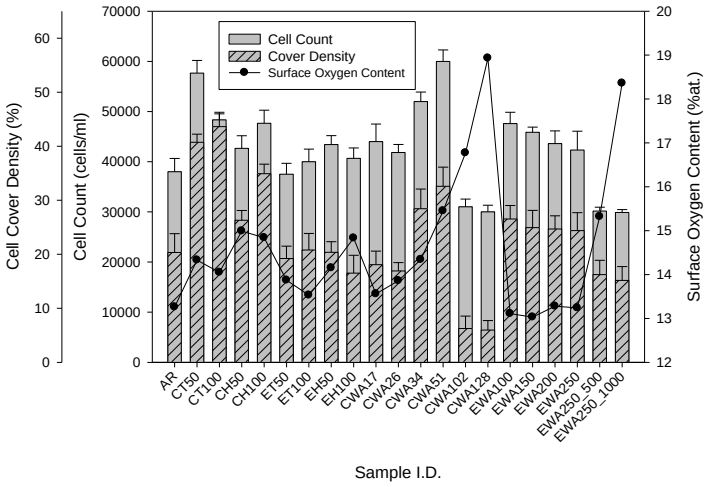

(a)

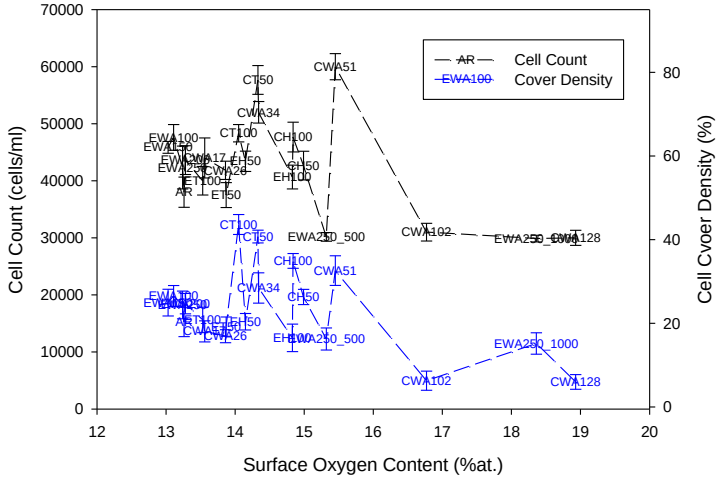

(b)

Figure 13.36 – (a) Histogram showing cell count and cell cover density in relation to surface oxygen content and (b) graph showing the relationship between cell count, cell cover density and surface oxygen content for all laser processed nylon 6,6 samples.

13.4.3 – Cytotoxicity and Alkaline Leukocyte Phosphatase (ALP) Levels

From Figure 13.37(a) it can be seen that the cytotoxicity decreases to a constant minimum and the ALP level increases to a constant maximum with an increase in θ. This can be seen more explicitly in Figure 13.37(b) which shows that the cytotoxicity was a decreasing function and the ALP level was an increasing function of θ until a minimum and maximum constant was achieved, respectively. It should also be noted here that sample CWA102 and sample CWA128 did not correspond with the observed trends which be explained through the toxicity of the sample being high enough to dominate

the osteoblast cell response. With this in mind, it can be extrapolated that it is likely that for those samples with around the region of the minimum cytotoxicity and maximum ALP levels the toxicity of the samples did not dominate, allowing for parameters such as θ and γ^P (see Section 13.4.2) to dominate the bioactive nature of the nylon 6,6, especially for those samples which had undergone laser whole area irradiative processing.

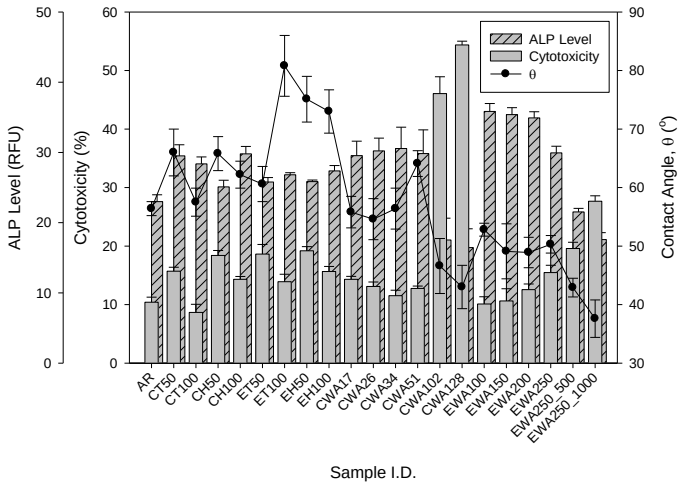

(a)

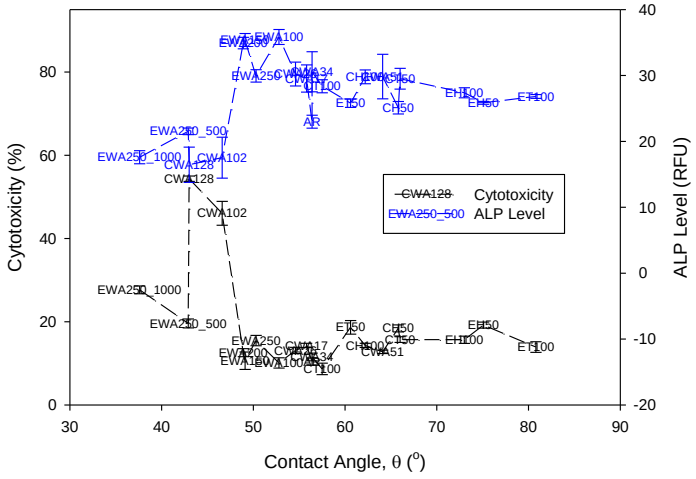

(b)

Figure 13.37 – (a) Histogram showing cytotoxicity and ALP level in relation to θ and (b) graph showing the relationship between cytotoxicity, ALP level and θ for all laser processed nylon 6,6 samples.

The inverse relationship of θ can be observed in Figure 13.38(a) and Figure 13.38(b) between the cytotoxicity, ALP levels and γ^P, further indicating the strong relationship between θ and γ^P which was identified in Chapter 10. Also, it can be seen from Figure 13.38(c) that the cytotoxicity and ALP level had a similar relationship with γ^T as was found with γ^P (see Figure 13.38(b)). Again, this indicates that the toxicity for the samples only appeared to dominate for sample CWA102 and sample CWA128 as these samples did not give results which fit with the correlative trend. With this in mind, it is implied that the surface toxicity of the sample played a major part in determining whether or not the wettability characteristics would be an integral driving force in terms of the osteoblast cell response.

It was found from Figures 13.39(a), 13.39(b) and 13.39(c) that the surface roughness with respect to Ra and Sa did not have a particular strong correlative relationship with the cytotoxicity or ALP level. On account of this, even though it may be possible to use large variations in Ra and Sa to predict the toxicity and bioactive nature of nylon 6,6 it is not likely that this would give rise to an accurate prediction. As such, it can reasonably said that there was no correlative relationship between the surface roughness and osteoblast cell response regardless of the evidence which has shown that the surface roughness may have given rise to variations in cell morphologies (see Chapter 11 and Chapter 12)

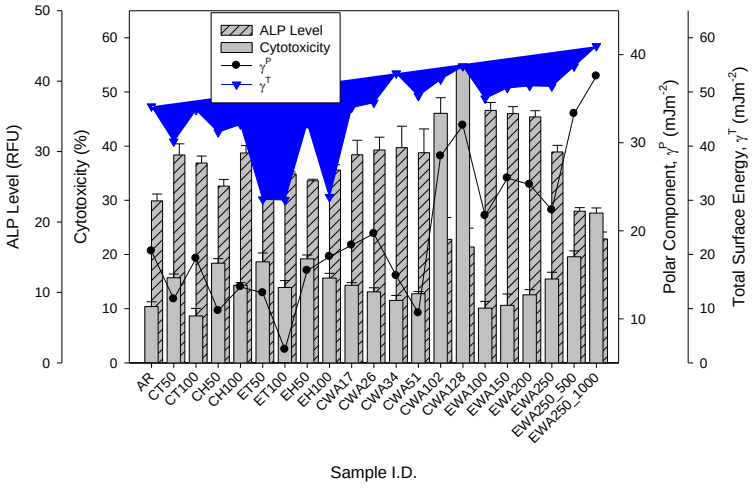

(a)

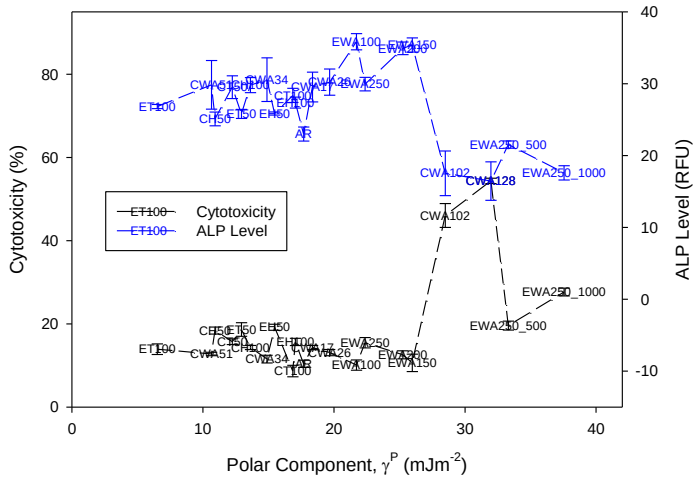

(b)

Figure 13.38 continued overleaf

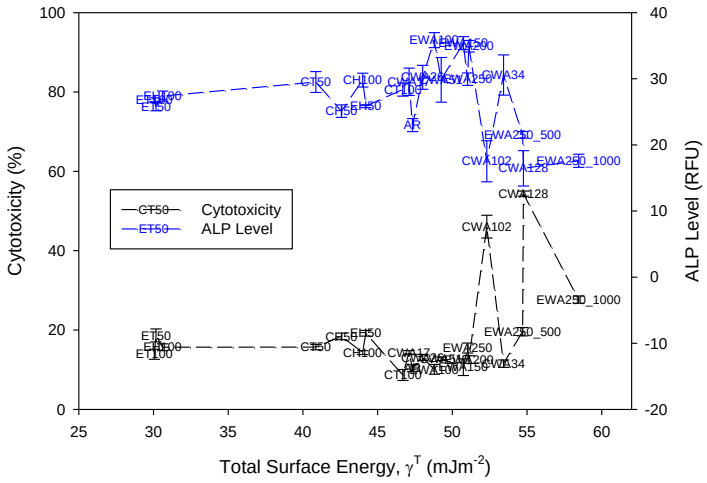

(c)

Figure 13.38 – (a) Histogram showing cytotoxicity and ALP level in relation to γ^P and γ^T, (b) graph showing the relationship between cytotoxicity, ALP level and γ^P and (c) graph showing the relationship between cytotoxicity, ALP level and γ^T for all laser processed nylon 6,6 samples.

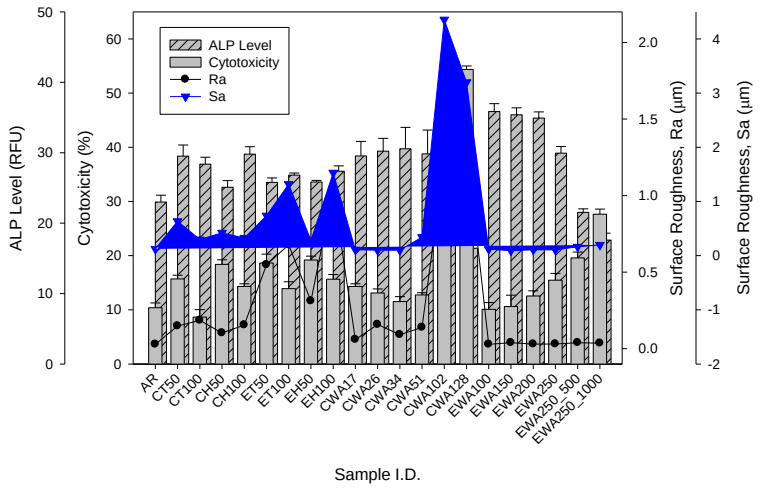

(a)

Figure 13.39 continued overleaf

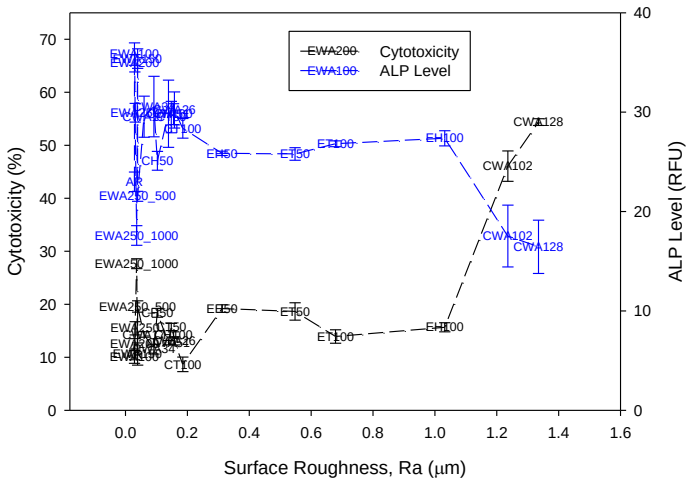

(b)

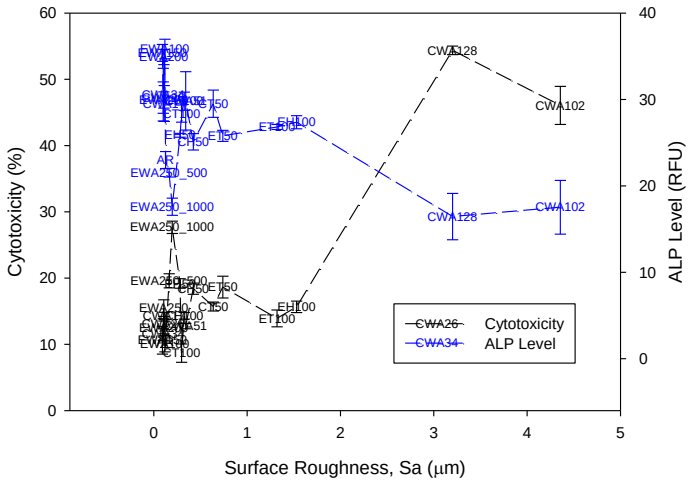

(c)

Figure 13.39 – (a) Histogram showing cytotoxicity and ALP level in relation to Ra and Sa, (b) graph showing the relationship between cytotoxicity, ALP level and Ra and (c) graph showing the relationship between cytotoxicity, ALP level and Sa for all laser processed nylon 6,6 samples.

From Figure 13.40(a) and 13.40(b) it can be realized that for all samples, except sample CWA102 and sample CWA128, the cytotoxicity was an increasing function and the ALP level was a decreasing function of surface oxygen content. It is highly likely the surface oxygen content did not bring about an increase in cytotoxicity but within reason can be seen to be an indirect indicator of the rise in surface toxicity which would have had a large detrimental effect on the osteoblast cell response. This indicates that there could be a surface oxygen content threshold above which the toxicity of the samples would have been too great, hindering cell response and stopping any correlative trend between the osteoblast cell response and wettability characteristics.

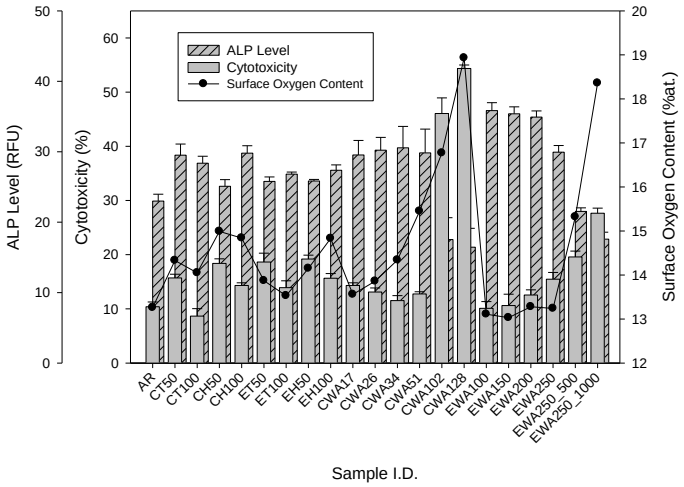

(a)

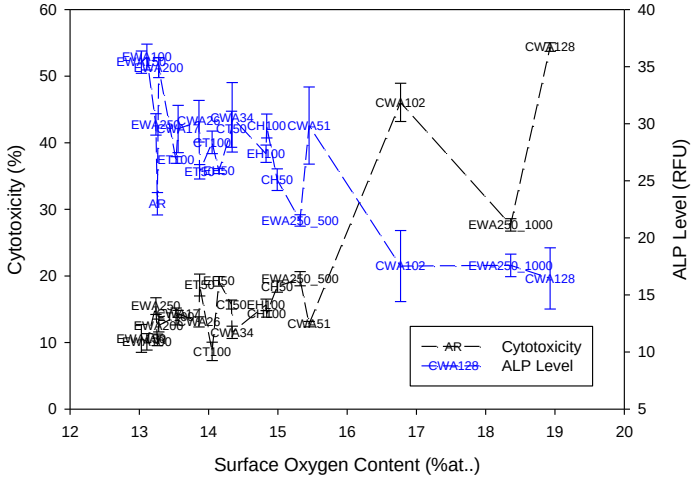

(b)

Figure 13.40 – (a) Histogram showing cytotoxicity and ALP level in relation to surface oxygen content and (b) graph showing the relationship between cytotoxicity, ALP level and surface oxygen content for all laser processed nylon 6,6 samples.

On account of the fact that the laser-induced patterning and laser whole area irradiative processing were very different insofar as the surface parameters and wettability characteristics were modified in different ways, there were no distinct correlations determined between the bioactive nature of the nylon 6,6 in terms of cell cover density and cell count. This suggests that it is highly likely that owed to the complexity of the osteoblast cell growth, a number of surface parameters would contribute to the osteoblast cell response to the nylon 6,6 samples. Having said that, it has been seen that there was a strong correlation for all samples with regards to the wettability characteristics, the cytotoxicity and ALP levels. This is significant as it implies that for low cytotoxicity levels and high ALP levels the proposed surface toxicity (see Section 11.5) does not dominate allowing the wettability characteristics such as θ and γ^P to have a distinct role in determining the bioactive nature of the nylon 6,6 samples, especially for those which had undergone laser whole area irradiative processing.

14
Generic Correlations Between Laser Processing Parameters and Wettability Characteristics of Nylon 6,6 and the Osteoblast Cell Response

Throughout this research a number of parameters have been shown to have the potential to be a driving force for both the wettability characteristics and subsequent osteoblast cell response. Furthermore, a number of correlative trends have been identified. This Chapter summarizes all of the results which have been detailed and discussed in Chapter 6 through to Chapter 13.

14.1 – Introduction

Owing to the complexity of wettability characteristics and osteoblast cell response it has been seen that a number of parameters can be seen to have the potential to affect the results observed. As a result of this it is necessary to take into account all those parameters which have been determined in Chapter 6 to Chapter 13, which have a correlative trend with the measured wettability and observed osteoblast cell response.

In order to concisely and efficiently carry out this task, this Chapter will summarize the results in stages using block diagrams to show the effects of the various laser-modified parameters on the wettability characteristics and resulting osteoblast cell response.

14.2 – Laser Surface Processing of Nylon 6,6

By implementing two different laser types, namely CO_2 and KrF excimer lasers, it has been determined and discussed within Chapters 6, 7, 8, 9 and 10 that both the surface topography and surface chemistry of nylon 6,6 can be greatly modified. The links which have been seen to arise between the laser process and surface modification of the nylon 6,6 can be seen in Figure 14.1. For instance, the CO_2 and KrF excimer laser-induced patterning gave rise to more periodic patterns compared to the laser whole area irradiative processed samples (see Chapter 6 and Chapter 7). Having said that, all of the laser processing techniques implemented, with the exception of the KrF excimer laser whole area irradiative processing, lead to a significant increase in Ra and Sa for the nylon 6,6 samples. The exception of the KrF excimer laser whole area irradiative process samples can be explained by the fact that most of the samples had an incident fluence below that of the threshold fluence (see Chapter 7). Then, for those samples with incident fluences just above the threshold only limited melting would have taken place due to the fluences being relatively small, especially when compared to the fluence used for the KrF excimer laser-induced patterning.

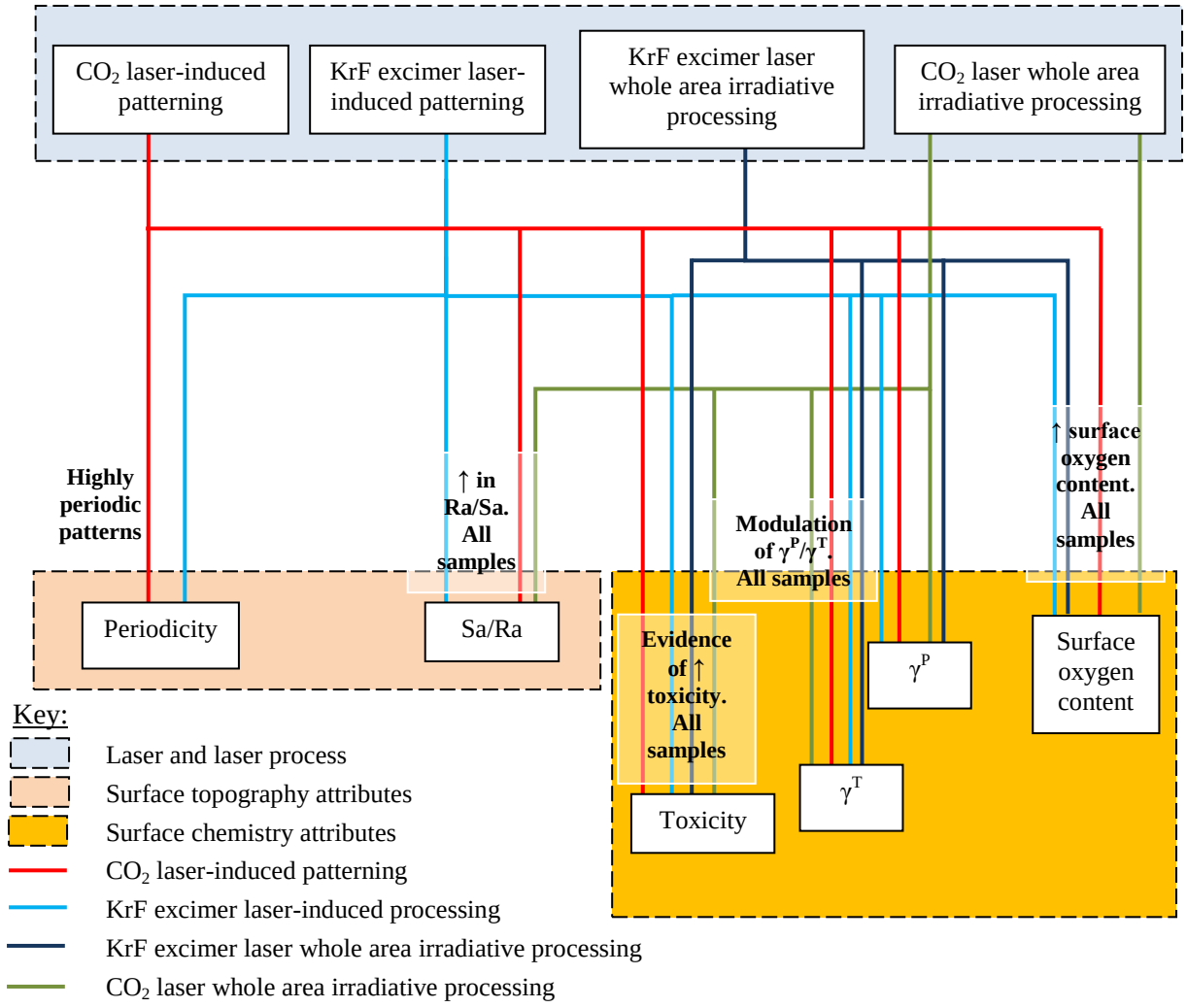

Figure 14.1 – Diagram showing the links between the observed variation in surface properties and laser parameters.

With regards to melting, it was found that considerably more melting took place for the CO_2 laser processing owed to the higher fluences and absorption characteristics of the nylon 6,6 which allowed one to see that the largest increase in Ra and Sa was determined for the CO_2 laser whole area irradiative processing (see Chapter 6). Because of the melting taking place for some of the CO_2 and KrF excimer laser processed nylon 6,6 samples it was also found that the surface oxygen increased as a result of oxidation taking place upon melting and re-solidification (see Chapter 6 and Chapter 7). Furthermore, through biological analysis (see Section 11.5) it has been proposed and is reasonable to say that upon laser surface treatment, the toxicity of the nylon 6,6 surfaces had augmented on account of evolved toxic gases becoming trapped into the rapidly re-solidified laser irradiated nylon 6,6.

As a result of the surface modifications that had taken place it was also seen that the surface energy, γ^T, and its components, namely γ^P, had been modulated to a great extent. This, along with the other surface modifications that had taken place gives further evidence as to the attractive means of using laser technology to manipulate both the surface topography and surface chemistry of nylon 6,6

simultaneously. What is more, it is highly likely that other polymeric materials could be modified in a similar manner and that laser technology could very well be applied to a number of applications which requires the surface modification of polymers.

14.3 – Laser Surface Processing of Nylon 6,6 and the Effects on Wettability Characteristics

With the effects on the surface topography and surface chemistry being observed it was further seen that these surface modifications had a large impact upon the wettability of the nylon 6,6. Leading on, Figure 14.2 allows one to see the further links between the laser-modified surface parameters and the wettability attributes observed. Predominantly determined throughout Chapters 6, 7 and 10, it was found that there was differing resulting θ for the two different processing techniques implemented; laser-induced patterning and laser whole area irradiative processing. That is, for the laser-induced patterned samples there was a significant increase in θ compared to the as-received sample which can be attributed to a mixed-state wetting regime arising from the rough periodic laser-induced pattern. On the other hand, for the laser whole area irradiative processed nylon 6,6 samples, the current theory for a hydrophilic material such as nylon 6,6 held as an increase in Ra and Sa gave rise to a reduction in θ. This is on account of the fact that the wetting regime was that of a Wenzel regime owed to the non-periodic roughness of the laser-modified nylon 6,6.

Through Chapter 6 to Chapter 10 it was also observed that there was a very strong relationship between θ, γ^P and γ^T. Since, θ was found to be a strong correlative decreasing function of both γ^P and γ^T which identified that the surface energy played a major role in the determination of the wettability of nylon 6,6. With this in mind, it is reasonable to say that this result allows one to realize that the wettability of laser-modified nylon 6,6 could be predicted by knowing the surface energy and its components. Furthermore, it can be deduced that the surface energy in terms of γ^P and γ^T could be estimated by knowing θ for a given laser surface treated nylon 6,6 sample. It should also be noted here that the surface oxygen content was not found to have a distinctive relationship with θ. Having said that, the toxicity of the sample as discussed in Section 11.5, could have been amplified on account of the laser surface treatment which could have lead to the toxicity playing some part in the wettability characteristics. However, it has been evidenced that γ^P and γ^T appeared to be the most dominant parameters when considering the wettability of the laser surface processed nylon 6,6.

As a result of the laser surface treatment and arising surface modifications it has been seen that the wettability characteristics of nylon 6,6 can be significantly modulated. Leading on form this, it has also been determined that a number of parameters, namely γ^P and γ^T, can be implemented to predict the wettability nature of laser surface treated nylon 6,6. With this in mind, it has been further evidenced that lasers offer an attractive means to surface treat nylon 6,6 in order to modulate the wettability characteristics.

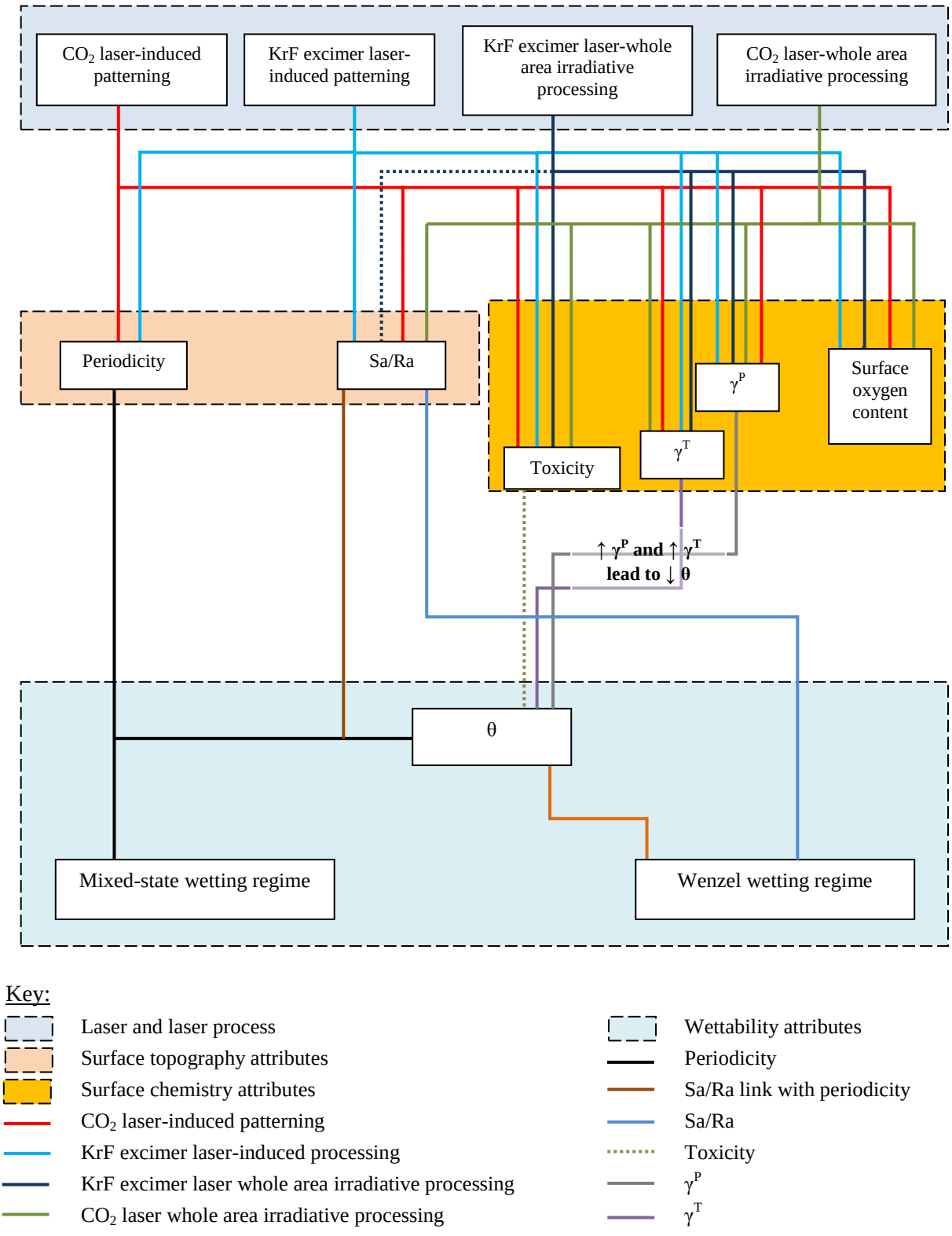

Figure 14.2 – Diagram showing the links between the surface parameters arising from the laser surface treatment and the observed modification in wettability.

14.4 – Laser Surface Processing of Nylon 6,6, the Effects on Wettability Characteristics and Subsequent Osteoblast Cell Response

In Section 14.3 and Section 14.4 it has been seen that the laser surface treatment of nylon 6,6 gave rise to significant variations in both the surface properties and wettability characteristics. Furthermore, links were determined between the arising surface modification and the wettability nature of the nylon 6,6 material. With regards to the cell response to nylon 6,6 in terms of apatite and osteoblast cell response, as shown in Figure 14.3, this was found to be no different as there was a number of links determined between the laser-induced surface modifications and the biofunctionality of the nylon 6,6 samples. For instance, in Chapter 11 and Chapter 12 it was found from SEM analysis that there was evidence in the variation of cell morphology which has been reported as a result of the differing surface roughness. On account of this, it can be said that the surface roughness, Ra and Sa, could have had a large impact upon the observed cell differentiation.

Figure 14.3 shows that there were links between the apatite response, θ, γ^P and to some extent γ^T; however, it was determined that different trends occurred for the different laser processes. For the CO_2 laser whole area irradiative processing it was seen that Δg was both an increasing function of θ and a decreasing function of γ^P (see Section 11.2 and Section 13.2.1). On the other hand, for the KrF excimer laser whole area irradiative processed samples, Δg was a decreasing function of θ and an increasing function of γ^P (see Section 12.2 and Section 13.2.1). It should also be noted here that the laser-induced patterned samples did not give rise to any distinct correlative trend with Δg, which can be attributed to the likely mixed-state wetting regime (see Chapter 6 and Chapter 10) giving rise to erroneous results. The difference in relationships between Δg and the modified surface parameters for laser whole area-irradiative processed samples could be accounted for by the different λ employed. This implies that in terms of the apatite response to laser whole area irradiative processed nylon 6,6, Δg could be easily modulated by implementing a specific laser type and process.

With regards to the osteoblast cell response, cell count and cell cover density were two parameters analyzed to assess the bioactive nature of the nylon 6,6 samples. It was found for all laser whole area irradiative processed samples that both the cell count and cell cover density were both increasing functions of θ and, owed to the strong inverse relationship between θ and γ^P, were both decreasing functions of γ^P. This implies that in terms of bioactivity there may be some surface parameters, such as this, which are independent of λ and some which rely on the absorption characteristics of nylon 6,6 giving rise to the variation in relationships for osteoblast cell response. The implied λ dependence is further evidenced when taking into account the effects of surface oxygen content on cell count and cell cover density (see Chapters 11, 12 and 13). That is, for the CO_2 laser whole area irradiative processed nylon 6,6 samples, the cell count and cell cover density increased to a maximum upon an increase in surface oxygen content before reducing rapidly. It has been proposed in Section 11.5 that this may be on account of a likely increase in toxicity even though an increase in surface oxygen content had been observed. In contrast, the KrF excimer laser whole area irradiative processed samples gave rise to a trend such that an increase in surface oxygen content elicited a decrease in cell count and cell cover density. It is possible that both the CO_2 ad KrF excimer laser irradiation gave rise

to an increased surface toxicity and as a result above a certain toxicity the osteoblast cell response was hindered. It should also be noted here that the laser-induced patterned nylon 6,6 samples did not appear to lead to any particular correlative trend between the modified surface parameters, cell count and cell cover density. This, as discussed in Chapters 11, 12 and 13, could be accounted for by erroneous results arising from the transition in wetting regimes.

The laser-induced cytotoxicity had a large effect on the ALP levels and subsequent osteoblast cell response. It has been reasonably proposed in Section 11.5 that the toxicity played a major role in the osteoblast cell response to those samples with large increases in cytotoxicity. This is a reasonable assertion these samples do not appear to correspond with the strong correlative relationships which have been identified between cytotoxicity, ALP levels and the laser-induced surface modification parameters. In Chapter 13 it was determined that θ, γ^P and γ^T all had very strong correlative relationships with both the cytotoxicity and the ALP levels which exhibited an inverse relationship to what was observed for the cytotoxicity. In terms of θ, the cytotoxicity reduced upon an increase in θ until a minimum constant was achieved; whereas the cytotoxicity remained constant at low γ^P and γ^T until a point at which the cytotoxicity began to increase. These results are noteworthy as they allow one to deduce that, with constant cytotoxicity levels, the cell count and cell cover density appeared to be modulated by the surface parameters and wettability characteristics. Then, upon the cytotoxicity increasing, on account of the increase in surface toxicity, the toxicity of nylon 6,6 began to dominate, neglecting the other surface parameters and wettability characteristics leading to the hindrance of osteoblast cell growth. It was also proposed in Chapters 11, 12 and 13 that the surface roughness and surface oxygen content could also be implemented indirectly to estimate the cytotoxicity and ALP levels, especially for the CO_2 laser whole area irradiative processed samples. This is due to the fact that the laser processing which gave rise to the melting and increase in surface toxicity also lead to an increased surface roughness and increase in surface oxygen content through oxidation.

It has been observed throughout this research that both CO_2 and excimer lasers offer a very convenient and efficient means of surface modifying nylon 6,6 both topographically and chemically. As a direct result of these modifications a number of surface parameters and wettability characteristics have been changed which in turn had, to some extent, a significant effect on the modulation of osteoblast cell growth. Furthermore, a number of parameters from the attributes studied have been found to have strong correlative links, allowing one to realize the potential of using these parameters to predict the wettability and osteoblast cell response to laser surface treated nylon 6,6.

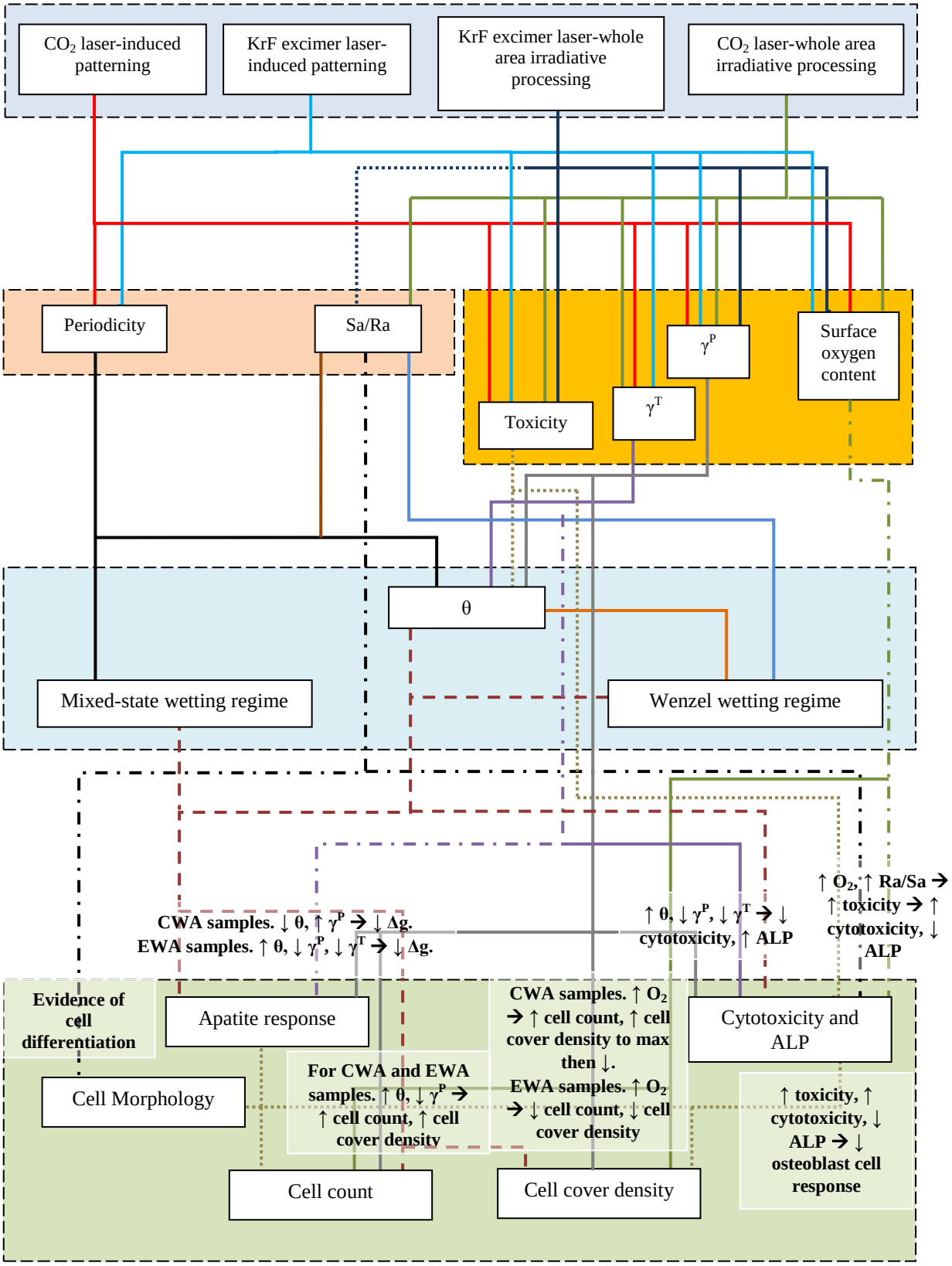

Figure 14.3 continued overleaf

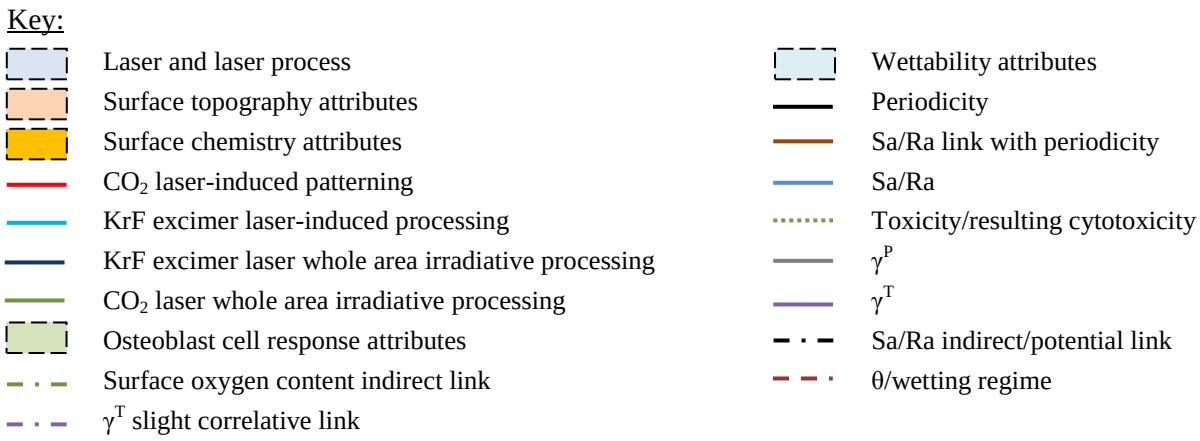

Figure 14.3 – Diagram showing the links between the wettability characteristics, surface parameters and osteoblast cell response attributes on account of laser surface treatment of nylon 6,6.

Conclusions

Throughout this research it has been further demonstrated that lasers offer an efficient and convenient means of surface modifying materials - in this case nylon 6,6, both chemically and topographically. As both CO_2 (IR) and KrF excimer (UV) lasers have been implemented to induce surface modifications it is necessary to initially understand the basic laser-material interactions; that is, how the CO_2 laser beam couples into the material *via* resonant coupling which gives rise to bond vibrations, allowing the temperature to rise and melt the material. Upon cooling the molten material re-solidifies and a protrusion away from the surface becomes evident on the surface. This is contrasted with the KrF excimer laser-material interaction, as it ablates the material allowing the required pattern to be etched into the material. As a result, the KrF excimer laser system offers a major advantage over the CO_2 insofar as they ablate 1 to 100 nm per pulse, allowing the user to be more precise and accurate with the surface topography they require.

Upon analysing the CO_2 laser induced patterned surfaces it was found that total surface energy, γ^T, and polar component, γ^P, had decreased by up to 7 mJm^{-2} and that the surface roughness had considerably increased. Through CO_2 laser-induced patterning of two 50 and 100 μm patterns (trench and hatch) it was determined that peak heights of up to 3 μm could be achieved with surface roughness, Ra and Sa, values of up to 0.305 and 0.408 μm, respectively. This is significantly higher compared to that of the as-received sample, which was found to have peak heights of up to 0.2 μm with Ra and Sa values of 0.028 and 0.111 μm, respectively. Also, it was found that γ^P and γ^T for the samples studied were both a decreasing function of θ, which correlates with current theory; however, current theory also states that θ for a hydrophilic surface should decrease upon increasing surface roughness which has not been seen throughout this experimentation. This can be attributed to an intermediate mixed Cassie-Baxter/Wenzel regime, in which both Wenzel and Cassie-Baxter regimes arise at the solid-liquid interface as a result of the formation of the water droplet on the various laser modified surface topographies. What is more, following CO_2 laser whole area irradiative processing an increase in surface roughness of up to 4.4 μm, increase in γ^P of up to 15 mJm^{-2} and increase in γ^T of up to 8 mJm^{-2} gave rise to a reduction in θ. This further suggests that the CO_2 laser-induced patterns on the nylon 6,6 samples had a large impact on the wetting regime. Another factor which has been taken in to account is that the surface oxygen content tended to increase by up to 2 %at. for the CO_2 patterned samples and up to 5 %at. for the CO_2 laser whole area irradiated samples. This is owed to the thermolytical interaction between the nylon 6,6 material and the CO_2 laser beam, bringing about melting of the nylon 6,6 surface allowing oxidation to take place. From the results obtained it was found that the γ^T and γ^P were the most dominating parameter in the modification of wettability which was a result of the mixed-state wetting regime owed to the surface topography produced from the different laser-induced patterns.

It has also been shown throughout this work that a KrF excimer laser can be used for two different types of KrF excimer laser surface treatment: surface patterning and whole area irradiative processing. These different types of KrF excimer laser surface treatment have been seen to be significantly different on account of topography and wettability modification of nylon 6,6. For the KrF excimer laser-induced patterned samples θ was found to have increased by up to 24° when compared to the as-received sample; whereas the KrF excimer laser whole area processed samples gave θ to either be equivalent to the as-received sample or have a θ less by up to 20°. The increase in θ for the KrF excimer laser-induced patterned samples can be explained through the decrease in apparent γ^P and γ^T owed to a change in wetting regime to a mixed-state in which both Wenzel and Cassie-Baxter regimes are present across the liquid-surface interface. This can be seen to arise from the likelihood of a change in the droplet equilibrium state as a result of the induced laser patterns. The decrease in θ for the KrF excimer laser whole area irradiative processed samples can be explained by an increase in γ^P and γ^T as the surface roughness modification was negligible compared to the as-received sample.

When comparing CO_2 and F_2 laser systems for the laser-induced patterning of nylon 6,6, the CO_2 laser was been seen to be capable of producing θ slightly larger in comparison to the as-received sample In this instance, as a result of the CO_2 laser-induced patterning the surface oxygen content increased by up to 1.5 %at. and γ^P also increased by up to 4.12 mJm^{-2}. This did not agree with current theory as an increase in γ^P and surface oxygen content should give rise to a reduction in θ. In contrast, for the F_2 excimer laser-induced patterned samples γ^P and surface oxygen content decreased by up to 11.69 mJm^{-2} and 1.6 %at., respectively. It was proposed here that the increase in θ resulting from the laser-induced modifications was again due to the laser-induced patterned topographies, such that they give rise to an intermediate mixed-state wetting regime in which both Wenzel and Cassie-Baxter regimes arise. This allows one to see how the CO_2 laser-induced patterned samples would give a larger θ in comparison to the as-received reference sample. To aid in clarification, manually roughened samples were analysed which showed that for a non-periodic rough surface the γ^P increased and surface oxygen content remained somewhat unchanged giving rise to a reduction in θ. Significantly, this shows that the laser-induced surface pattern dominated, to a certain extent, the wettability characteristics for the nylon 6,6 samples. Another factor to take into consideration when comparing these two lasers is that of processing time. On account of the short wavelength of the F_2 excimer laser all processing had to be carried out under vacuum. As a result of this, the amount of time it took to pump the F_2 vacuum system to operating pressure and the amount of time it took to produce a number of few μm deep trenches was considerably greater than the CO_2 laser system which was used in ambient air.

The long term study into the wettability of nylon 6,6 following CO_2 laser-induced patterning of nylon 6,6 has identified that after 30 weeks each of the samples studied had become less hydrophilic, with θ increasing by up to 10°. Over the 30 week period, however, it was observed that θ was erratic, increasing and decreasing rather than converging to a constant value. In terms of topography, surface roughness for the CO_2 laser-induced patterned samples decreased, in general, over the 30 week period; whereas the roughness of the as-received sample remained constant. It was also found that the surface oxygen content had increased through oxidation due to the storage of the samples in ambient

air. It is likely that these may not be the main driving force due to the difference in surface roughness between the as-received and laser patterned samples. It is evident from the results obtained that atmospheric pressure may be a main driving force for the observed θ. That is, θ in general increases with significant increases of atmospheric pressure and vice versa. Having said that, in some weeks throughout the 30 week period this was not conclusive. On the other hand a strong correlation was found between θ, γ^P and γ^T in that θ was a decreasing function of the surface energy which had been observed in previous experimentation. This gave further evidence of the strong correlative relationship between θ, γ^P and γ^T for nylon 6,6.

Throughout this research in terms of wettability characteristics, there was a common theme in which θ was observed to be a decreasing function of γ^P and γ^T indicating that the surface energy is a dominating parameter for the wettability of nylon 6,6. In addition to this, in some instances it can be seen that a change in wetting regime owed to the surface topography could possibly be the dominating factor giving rise to θ larger than expected for a hydrophilic material such as nylon 6,6. Following on, even when a change in wetting regime is likely it has still been observed that γ^P and γ^T still play a big role in the wettability of nylon 6,6.

Following immersion in SBF for 14 days it was observed that all CO_2 laser processed samples and KrF excimer laser processed samples gave rise to the formation of calcium and phosphorous containing sediment. An increase Δg of up to 0.015 and 0.024 g was observed for the CO_2 laser-induced patterned and whole area processed samples, respectively, when compared to the as-received sample which had a total increase Δg of 0.016 g. For the KrF excimer laser processed samples it was found that the largest increase in Δg was 0.035 g which was larger than both the as-received and CO_2 laser processed samples. The increase in the formation of sediment indicates that the laser surface treated samples enhanced apatite response potentially allowing for a surface that would enhance osteoblast cell adhesion and proliferation. Leading on from this, it was found that there were different correlative trends observed for the each of the laser processes between mainly θ and γ^P. For the CO_2 laser whole area irradiative processing it was seen that Δg was both an increasing function of θ and a decreasing function of γ^P; for the KrF excimer laser whole area irradiative processed samples, Δg was a decreasing function of θ and an increasing function of. Also, the laser-induced patterned samples did not give rise to any distinct correlative trend with Δg, which can be attributed to the likely mixed-state wetting regime giving rise to erroneous results. The difference in relationships between Δg and the modified surface parameters for laser whole area-irradiative processed samples can be accounted for by the different λ employed.

It has been seen that for most of the CO_2 laser surface treated nylon 6,6 samples, osteoblast cell response had been improved to become more efficient, allowing cell growth to become quicker. This has been seen through the fact that the cells had covered more area of the nylon 6,6 samples after 24 hrs and that the cell density count had increased after 4 days in comparison with the as-received sample; however, samples CWA102 and CWA128 did not appear to promote an enhanced osteoblast cell response resulting in the surfaces hindering cell adhesion and proliferation. This may be down to the fact that the surfaces became too hydrophilic or the whole area CO_2 laser processing at large

fluencies gave rise to a more toxic surface. Nevertheless, The results obtained imply that, in general, the laser surface treated nylon 6,6 gave rise to enhanced osteoblast cell response to the nylon 6,6. This response has been observed by instigating cell signalling which has been identified through variations in cell differentiation between each of the samples studied. It has also been observed that all samples incubated over 4 days apart from samples CWA102 and CWA128 gave rise to large cover densities of around 100% regardless of laser surface treatment. After 4 days the difference in cell morphology became more apparent, with the cell growth showing differing morphologies such as coral-like for the as-received (AR) sample and clumped radial growth for the 50 μm (H50) and 100 μm hatch (H100) patterned samples. This finding can be accounted for by the variation in surface energy and topography instigating cell signalling, which has a major influence on cell morphology. Also, it has been found that the KrF excimer laser surface treatment employed through this study has had a significant impact on cell response in terms of cell differentiation, cell cover density and cell count. After 24 hrs incubation it was seen that the osteoblast cells had begun to adhere and proliferate across the surface of each of the nylon 6,6 samples. Leading on, following 4 days of incubation it was found that all samples had given rise to an advanced stage of cell growth giving cell cover densities of around 100%.

By taking into account the cell count and cell cover densities after 24 hours it was seen that there was a distinct correlative trend between the osteoblast cell response, θ and γ^P for the laser whole area irradiative processed nylon 6,6 samples. That is, both the cell count and cell cover density were both increasing functions of θ and, owed to the strong inverse relationship between θ and γ^P, were both decreasing functions of γ^P. This implies that in terms of bioactivity there may be some surface parameters which are independent of λ and some which rely on the absorption characteristics of nylon 6,6 giving rise to the variation in relationships with regards to osteoblast cell response. The implied λ dependence is further evidenced when taking into account the effects of surface oxygen content on cell count and cell cover density. Since, for the CO_2 laser whole area irradiative processed nylon 6,6 samples, the cell count and cell cover density increased to a maximum upon an increase in surface oxygen content before reducing rapidly. It has been proposed that this may be on accountable with a likely increase in toxicity even though an increase in surface oxygen content had been observed. In contrast, the KrF excimer laser whole area irradiative processed samples gave rise to a trend such that an increase in surface oxygen content elicited a decrease in cell count and cell cover density. It is possible that both the CO_2 ad KrF excimer laser irradiation gave rise to an increased surface toxicity and as a result above a certain toxicity the osteoblast cell response was hindered. Furthermore, the laser-induced patterned nylon 6,6 samples did not appear to lead to any particular correlative trend between the modified surface parameters, cell count and cell cover density. This could be accounted for by erroneous results arising from the transition in wetting regimes.

It was found that after seeding with osteoblast cells all laser surface treated samples, with the exception of CWA102 and CWA128, gave rise to cell response better or equivalent to that achieved with the as-received samples (AR). This was on account of the cytotoxicity levels being relatively low and ALP levels being slightly higher by up to 15 RFU compared to the as-received sample. The more efficient cell response came from sample T100 which had the lowest cytotoxicity level of 8% when

compared with all other samples; whereas the least efficient response came from samples CWA102 and CWA128 which can be explained by the relatively large fluences over-melting the nylon 6,6 giving rise to an increase in cytotoxicity and potentially making the surface too hydrophilic. It was seen that most of the KrF excimer laser processed samples gave rise to an increase in cytotoxicity when compared to the as-received sample. The least increase in cytotoxicity is attributed to the KrF excimer laser whole area processed samples EWA100 and EWA150 which can be explained by the fact that the fluencies used in this instance may not have been high enough to modify either the surface chemistry or surface topography of the nylon 6,6 samples. With the modulation of the cytotoxicity levels being observed it was possible for one to deduce that the laser surface treatment would have an impact on ALP levels. In general all of the KrF excimer laser whole area irradiative processed samples, apart from samples EWA100, EWA150 and EWA200, lead to a reduction in ALP as a result of the increase in cytotoxicity levels. Even though the ALP and cytotoxicity levels appear to have been modulated with variations in surface parameters, the study of the osteoblast cells have shown that these modulated levels do not appear to have a significant impact on cell adhesion and proliferation. This may possibly be explained by osteoblast cells being a robust cell type and as such may be able to still grow and proliferate even though cytotoxicity levels have increased and ALP levels have decreased. Even so, it is likely that the increase in cytotoxicity for all laser processed samples when compared to the as-received sample is going to have a significant impact on cell response *in vivo*. Furthermore, it is likely that the increase in cytotoxicity for the laser processed samples indicated that this may have a detrimental effect on other cell types such as fibroblast and neuroblast cells, which are well known to be less robust as osteoblast cells. Nevertheless, it has been seen throughout this research that osteoblast cell response has been enhanced regardless of the increase in cytotoxicity levels. As a result of this, it could be argued that there appears to be a threshold cytotoxicity, beyond which the cell response is hindered and, even with the laser processing this threshold has only been surpassed by sample CWA102 and sample CWA128 giving rise to a hindered osteoblast cell response.

Upon correlating the modified surface parameters with the cytotoxicity and ALP Levels it was found that there was a very strong correlative relationship between cytotoxicity, θ, γ^P and γ^T, especially for the laser whole area irradiative processed samples. In terms of θ, the cytotoxicity reduced upon an increase in θ until a minimum constant was achieved; whereas the cytotoxicity remained constant at low γ^P and γ^T until a point at which the cytotoxicity began to increase. These results are noteworthy as they allow one to deduce that, with constant cytotoxicity levels, the cell count and cell cover density appeared to be modulated by the surface parameters and wettability characteristics. Then, upon the cytotoxicity increasing, on account of the increase in surface toxicity, the toxicity of nylon 6,6 began to dominate, neglecting the other surface parameters and wettability characteristics leading to the hindrance of osteoblast cell growth. It was also proposed that the surface roughness and surface oxygen content could also be implemented indirectly to estimate the cytotoxicity and ALP levels, especially for the CO_2 laser whole area irradiative processed samples. This is because the laser processing which gave rise to the melting and increase in surface toxicity also lead to an increased surface roughness and increase in surface oxygen content through oxidation. It should also be noted here that as a result of the relationship between cytotoxicity and ALP levels the relationships between

the ALP level, θ, γ^P and γ^T were determined to be the inverse to what was observed for the cytotoxicity relationships.

To conclude, it has been observed that both CO_2 and KrF excimer lasers offer a distinct means of surface treatment which can be applied to polymeric materials. These surface modifications are brought about by laser irradiation in terms of topographical and chemical changes without hindering the bulk properties. In terms of osteoblast cell response it was determined that the CO_2 laser-induced patterned samples, CO_2 whole area irradiative processed samples at low incident fluences and the KrF excimer laser whole area irradiative processed samples at low incident fluences and pulse numbers gave rise to the largest enhancements in bioactivity. However, on account of the erratic results obtained for the laser-induced patterned samples one can reasonably say that it is more likely that the laser whole area irradiative processing technique is a more attractive means on account of the fact that it has been evidenced here that these samples gave rise to more correlation in terms of osteoblast cell response and wettability characteristics. Owed to this, it would be more probable for the bio-implant industry to implement the laser whole area irradiative processing method due to the potential predictability of how the modified surface is going to act within a biological environment. Overall, it has been determined that the laser-induced modifications have given rise to enhanced osteoblast cell response which has seen osteoblast cell growth and proliferation to be improved when compared to the as-received sample. What is more, on account of the differing surface parameters giving rise to the modulation of cell morphologies across the nylon 6,6 surfaces and the fact a number of correlating attributes between the surface parameters and osteoblast cell response have been identified, one can deduce that laser surface treatment holds a large potential to be used within regenerative medicine.

Future Work Recommendations

Further Detailed Studies of Wettability Characteristics Modification

As it has been shown that a number of different parameters come into play when taking into account the wettability characteristics and bioactivity, the first major piece of work that is recommended is to ascertain any further possible links between wettability, bioactivity, functional groups and surface charge. Unfortunately, on account of time and limited access to equipment functional groups and surface charge have not been studied; however this does not detract from the results obtained and would only add a more in depth insight into the driving forces which determine both the wettability and bioactivity of polymers. Carrying out further future work in this subject field would allow one to make further inroads to identifying the complex link between surface parameters, wettability characteristics and the subsequent bioactivity of polymeric materials.

The second piece of work that is recommended in this area is to attempt and confirm the wettability regimes taking place across the solid-liquid interface, especially for the laser-induced patterned surfaces. That is, identify and confirm the presence of a mixed-state wetting regime in which both Wenzel and Cassie-Baxter regimes form. This work would be a major undertaking as it would potentially involve the use of specialist technology such as an elipsometric microscope. What is more, this would require one to study the effects of the same laser processing parameters on different polymeric materials to identify if the proposed mixed-state wetting regime occurs regardless of the material employed. It is worth noting here that confirming the presence of this phenomenon over the family of polymeric would be a major breakthrough in the scientific field of the wettability of polymeric materials.

Another large scientific undertaking would be to re-evaluate the effects of atmospheric conditions on the wettability of laser surface treatment over a long period of time. This would involve the need of isolating as many atmospheric parameters as possible in order to determine which, if any, have a conclusive role to play in the wettability characteristics over numerous weeks. As a result of what would be required to carry out such experimentation, this has unfortunately not been able to be carried out on account of limited time, limited access and limited funding.

Further Detailed Studies of in vitro Cell Response on Laser Modified Surfaces

Carrying out further SBF experiments using different SBF protocols would allow confirmation of the results obtained throughout this research. Leading on from this work one can also see that it would be advantageous to study how different cells, such as fibroblasts and stem cells respond to the laser surface treatment of polymeric biomaterials. What is more, by using cells that are relatively less robust compared to osteoblasts would allow one to identify whether these other cell types can potentially withstand the cytotoxicity levels which arise through the laser surface treatment. This work would direct onto studies including signaling, directionality and cell morphology and would

offer the opportunity to identify the dominant surface parameter which gives rise to certain cell responses. It could be argued that cells such as fibroblasts or neuroblasts could have been studied as part of this research; however, like previously, on account of insufficient time to carry out further experimentation I have been unable to ascertain the effects of laser surface treatment on different cell types. In addition to this, it should be noted that not carrying out these experiments have not detracted from the results obtained using osteoblast cells and would only have allowed a more in depth study of the response of varying cell types to the laser surface treated nylon,6,6.

Another interesting study would be to investigate whether the same trends for both wettability and osteoblast cell response would arise as a result of the same laser processing of different polymeric materials. This would allow one to establish generic parameters for polymeric materials which would aid in the prediction of the wettability and biofunctionality of those materials. Such work to be carried out would require considerable time and resources which regrettably were not available.

Detailed Studies of Mechanical Attributes and in vivo Cell Response on Laser Modified Surfaces, along with Other Potential Applications

Once more studies have been carried out in vitro and confirmation of the enhancement of cell response attributed to the laser surface treatment has been achieved, then mechanical testing will be required to ensure that the surface treatment does not hinder the already sufficient mechanical properties for biological implantation. This would require studies such as tensile, friction, bending and compression testing. After the completion of mechanical testing *in vivo* experimentation can then be carried out to determine how laser surface treated polymeric materials perform in a real biological environment. Only then would a full applicability study of this research have been undertaken for the implementation of laser surface treated polymeric biomaterials in the human body. Another physical aspect to consider for future work is that of microstructure and its possible effects on wettability and bioactivity. Determining the microstructure of a polymeric material can prove to be difficult with specialist technology such as soft X-ray spectromicroscopy. On account of limited time and resources microstructure has not been studied as part of this work but would only add more insight into the results obtained.

On the other hand, it has been seen throughout this research that cell response could be hindered through laser surface modification and could be applied to bacterial applications. That is, where bacterial growth needs to be hindered (food packaging, clean rooms, surgical tools, etc.) laser surface treatment offers a convenient and effective means in being able to modify the surfaces to potentially stop bacterial growth. Leading on from this, if laser surface treatment was to ultimately enhance the bacterial growth, this could be applied to filtration systems which could attract the bacteria to the laser treated filter. What is more, laser surface treatment of polymeric materials also has the potential to be applied to other areas of research which are non-biomedical. For instance one can see that by changing the wettability characteristics through the use of laser technology, adhesion can be enhanced. Therefore, it is possible for this research to be applied to those subjects that involve the use of adhesion such as non-stick and self-cleaning applications.

References

1. Hecht J. (1992) *The Laser Guidebook: Second Edition*, USA: McGraw-Hill Inc., 1992.

2. Silfvast W.T. (1996) *Laser Fundamentals*, Cambridge, UK: Cambridge University Press.

3. Koechner W. (2006) *Solid-State Laser Engineering: Sixth Revised and Updated Edition*, New York, USA: Springer Sciences and Business Media.

4. Hao L., Lawrence J. (2005) *Laser Surface Treatment of Bio-Implant Materials*, New Jersey, USA: John Wiley & Sons Inc.

5. Bauerle D. (2000) *Laser Processing and Chemistry: Third Edition*, New York, USA: Springer-Verlag.

6. Gould R.F. (1964) *Contact Angle, Wettability and Adhesion*, Washington D.C., USA: Applied Publications.

7. Black J. (2006) *Biological Performance of Materials: Fundamentals of Biocompatibility: Fourth Edition*, Florida, USA: CRC Press.

8. Steen W.M. (2005) *Laser Material Processing: Third Edition*, London, UK: Springer-Verlag.

9. Ion J.C. (2005) *Laser Processing of Enigneering Materials: Principles, Procedure and Industrial Application*, Oxford, UK: Elsevier Butterworth-Heinemann.

10. Abbott C., Allot R., Bann B., Boehlon K., Gower M., Rumsby P., Stassen-Boehlen I., Sykes N. (2002) New techniques for laser micromachining MEMS devices. *Proceedings of the SPIE* **4760** 281

11. Boehlen K.L., Stassen-Boehlen I., Allot R. (2005) Advanced laser micro-structuring of super large area optical films. *Proceedings of the SPIE* **5720** 204

12. Canning J. (2006) Fibre lasers and related technologies. *Optics and Lasers in Engineering* **44** 647-676.

13. Li L., Lou Q., Zhuo J., Dong J., Wei Y., Du S., He B. (2007) High power single transverse mode operation of a tapered lare-mode-area fiber laser. *Optics Communications* **281** 655-657.

14. Li P., Zhu C., Zou S., Zhao H., Jiang D., Li G., Chen M.(2008) Theoretical and experimental investigation of thermal effects in a high power Yb^{3+}-doped double-clad fiber laser. *Optics and Laser Technology* **40** 360-364.

15. Beck T., Reng N., Weber H. (2000) Optical fibres for material processing lasers. *Optics and Lasers in Engineering* **34** 255-272.

16. Broderick N.G.R., Offerhaus H.L., Richardson D.J., Sammut R.A., Caplen J., Dong L. (1999) Large mode area fibers for high power applications. *Optical Fiber Technology* **5** 185-196.

17. Kirchhof J., Unger S., Schwuchow A., Grimm S., Reichel V. (2006) Materials for high-power fiber lasers. *Journal of Non-Crystalline Solids* **352** 2399-2403.

18. Quintino L., Costa A., Miranda R., Yapp D., Kumar V., Kong C.J. (2007) Welding with high power fiber lasers - a preliminary study. *Materials and Design* **28** 1231-1237.

19. Hecht E. (2002) *Optics: Fourth Edition*, San Francisco, CA: Addison Wesley, 2002.

20. Lynch W. (1982) *Implants: Reconstructing the Human Body*, New York, USA: Van Nostrand Reinhold Company Inc.

21. Tiaw K.S., Hong M.H., Teoh S.H. (2007) Precision laser micro-processing of polymers. *Journal of Alloys and Compounds* **449** 228-231.

22. Sarantopoulou E., Kollia Z., Cefalas A.C., Douvas A.M., Chatzichristidi M., Argitis P., Kobe S. (2007) Polymer self-assembled nano-structures and surface relief gratings induced with laser at 157nm. *Applied Surface Science* **253** 7884-7889.

23. Callewaert K., Martele Y., Breban L., Naessens K., Vandaele P., Baets R., Geuskens G., Schact E. (2003) Excimer laser induced patterning of polymeric surfaces. *Applied Surface Science* **208-209** 218-225.

24. Hegazy E.S.A., AbdEl-Rehim H.A., Kamal H., Kandeel K.A. (2001) Advances in radiation grafting. *Nuclear Instruments and Methods in Physics Research B* **185** 235-240.

25. Zhang J., Kang J., Hu P., Meng Q. (2007) Surface modification of poly(propylene carboante) by oxygen ion implantation. *Applied Surface Science* **253** 5436-5441.

26. Dadbin S. (2002) Surface modification of LDPE film by CO_2 pulsed laser irradiation. *European Polymer Journal* **38** 2489-2495.

27. Mao C., Zhao W., Zhu C., Zhu A., Shen J., Lin S. (2005) In vitro studies of platelet adhesion on UV radiation-treated nylon surface. *Carbohydrate Polymers* **59** 19-25.

28. Yu F., Mucklich F., Li P., Shen H., Mathur S., Lehr C.M., Bakowsky U. (2005) *In vitro* cell response to a polymer surface micropatterned by laser interference lithography. *Biomacromolecules* **6** 1160-1167.

29. Pfleging W., Bruns M., Welle A., Wilson S. (2007) Laser-assisted modification of polystyrene surfaces for cell culture applications. *Applied Surface Science* **253** 9177-9184.

30. Mirzadeh H., Dadsetan M. (2003) Influence of laser surface modifying of polyethylene terephthalate on fibroblast cell adhesion. *Radiation Physics and Chemistry* **67** 381-385.

31. Mirzadeh H., Katbab A.A., Burford R.P. (1995) CO_2-laser graft copolymerization of HEMA and NVP onto ethylene-propylene rubber (EPR) as biomaterial-(III). *Radiation Physics and Chemistry* **46** 859-862.

32. Wei Q.F., Gao W.D., Hou D.Y., Wang X.Q. (2005) Surface modification of polymer nanofibres by plasma treatment. *Applied Surface Science* **245** 16-20.

33. Kim M.S., Khang G., Lee H.B. (2008) Gradient polymer surfaces for biomedical applications. *Progress in Polymer Science* **33** 138-164.

34. Cui F.Z., Luo Z.S. (1999) Biomaterials modification by ion-beam processing. *Surface and Coatings Technology* **112** 278-285.

35. Paital S.R., Dahotre N.B. (2009) Calcium phosphate coatings for bio-implant applications: Materials, performance factors and methodologies. *Materials Science and Engineering R* **66** 1-70.

36. Rajesh J.J., Bijwe J., Venkataraman B., Tewari U.S. (2002) Effect of water absorption on erosive wear behaviour of polyamides. Journal of Material Science **37** 5107-5113.

37. Kishimoto A., Fujita H. (1957) Diffusion-controlled stress-relaxation in polymers, I. *Colloid and Polymer Science* **150** 24-34.

38. Hutcheon G.A., Messiou C., Wyre R.M., Davies M.C., Downes S. (2001) Water absorption and surface properties of novel poly(ethylmethacrylate) polymer systems for use in bone and cartilage repair. *Biomaterials* **22** 667-676.

39. Deb S., Braden M., Bonfield W. (1995) Water absorption characteristics of modified hydroxyapatite bone cements. *Biomaterials* **16** 1095-1100.

40. Monson L., Braunworth M., Extrand C.W. (2008) Moisture absorption by various polyamides and their associated dimensional changes. *Journal of Applied Polymer Science* **107** 355-363.

41. Kowalski J.B., Morrissey R.F. (2004) *Sterilization of implants and devices*. In: Ratner B.D., Hoffman A.S., Schoen F.J., Lemons J.E. (eds.) *Biomaterial Science: An Introduction to Materials in Medicine. Second Edition ed.*, San Diego, CA, USA: Elsevier Academic Press, pp. 754-760.

42. Benson R.S. (2002) Use of radiation in biomaterials science. *Nuclear Instruments and Methods in Physics Research B* **191** 752-757..

43. Zhu Z., Kelley M.J. (2005) Grafting onto poly(ethylene terephthalate) driven by 172nm UV light. *Applied Surface Science* **252** 303-310.

44. Ranby B., Yang W.T., Tretinnikov O. (1999) Surface photografting of polymer fibers, films and sheets. *Nuclear Instruments and Methods in Physics Research B* **151** 301-305.

45. Ranby B. (1999) Surface modification and lamination of polymers by photografting. International *Journal of Adhesion & Adhesives* **151** 337-343.

46. Arefi-Khonsari F., Tatoulian M., Bretagnol F., Bouloussa O., Rondelez F. (2005) Processing of polymers by plasma technologies. *Surface and Coatings Technology* **200** 14-20.

47. Milde F., Goedicke K., Fahland M. (1996) Adhesion behaviour of PVD coatings on ECR plasma and ion beam treated polymer films. *Thin Solid Films* **279** 169-173.

48. Abdul Majeed R.M.A., Datar A., Bhoraskar S.V., Bhoraskar V.N. (2007) Surface modification of polymers by atomic oxygen using ECR plasma. *Nuclear Instruments and Methods in Physics Research B* **258** 345-351.

49. Lai J., Sunderland B., Xue J., Yan S., Zhao W., Folkard M., Micahel B.D., Wang Y. (2006) Study on hydrophilicity of polymer surfaces improved by plasma treatment. *Applied Surface Science* **252** 3375-3379.

50. Wang X., McCord M.G. (2007) Grafting of poly(N-isopropylacrylamide) onto nylon and polystyrene surfaces by atmospheric plasma treatment followed with free radical graft copolymerization. *Journal of Applied Polymer Science* **104** 3614-3621.

51. Chu P.K. (2007) Plasma surface treatment of artificial orthopedic and cardiovascular biomaterials. *Surface and Coatings Technology* **201** 5601-5606.

52. Chu P.K. (2007) Enhancement of surface properties of biomaterials using plasma-based technologies. *Surface and Coatings Technology* **201** 8076-8082.

53. Chu P.K. (2006) Bioactivity of plasma implanted biomaterials. *Nuclear Instruments and Methods in Physics Research B* **242** 1-7.

54. Porte-Durrieu M.C., Brouillard B., Baquey C., Aymes-Chodur C., Le Moel A., Rouais F. (1997) Synthesis of biomaterials by swift heavy ion grafting: Preliminary results of haemocompatibility. *Nuclear Instruments and Methods in Physics Research B* **131** 364-375.

55. Lau WM. (1997) Ion beam techniques for functionalization of polymer surfaces. *Nuclear Instruments and Methods in Physics Research B* **131** 341-349.

56. Cho J.S., Beag Y.W., Han S., Kim K.H., Cho J., Koh S.K. (2000) Hydrophilic surface formation on materials and its applications. *Surface and Coatings Technology* **128-129** 66-70.

57. Aubry C., Trigaud T., Moliton J.P., Chiron D. (2002) Polymer gratings achieved by focused ion beam. *Synthetic Metals* **127** 307-311.

58. Iwanaga S., Akiyama Y., Kikuchi A., Yamato M., Sakai K., Okano T. (2005) Fabrication of a cell array on ultrathin hydrophilic polymer gels utilising electron beam irradiation and UV excimer laser ablation. *Biomaterials* **26** 5395-5404.

59. Lord M.S., Cousins B.G., Doherty P.J., Whitelock J.M., Simmons A., Williams R.L., Milthorpe B.K. (2006) The effect of silica nanoparticulate coatings on serum protein adsorption and cellular response. *Biomaterials* **27** 4856-4862.

60. Gross K.A., Berndt C.C. (1997) Thermal processing of hydroxyapatite for coating production. *Journal of Biomedical Materials Research Part A* **39** 580-587.

61. Harnett E.M., Alderman J., Wood T. (2007) The surface energy of various biomaterials coated with adhesion molecules used in cell culture. *Colloids and Surfaces B: Biointerfaces* **55** 90-97.

62. Song W., Jun Y.K., Han Y., Hong S.H. (2004) Biomimetic apatite coatings on micro-arc oxidzed titania. *Biomaterials* **25** 3341-3349.

63. Bloisi F., Vicari L., Papa R., Califano V., Pedrazzani R., Bontempi E., Depero L.E. (2007) Biomaterial thin film deposition and characterization by means of MAPLE technique. *Materials Science and Engineering C* **27** 1185-1190.

64. Mei Y., Kumar A., Gao W., Gross R., Kennedy S.B., Washburn N.R., Amis E.J., Elliott J.T. (2004) Biocompatiblity of sorbitol-containing polyesters. Part I: Synthesis, surface analysis and cell response in vitro. *Biomaterials* **25** 4195-4201.

65. Zhao Q., Wang C., Liu Y., Wang S. (2007) Bacterial adhesion on the metal-polymer composite coatings. *International Journal of Adhesion & Adhesives* **27** 85-91.

66. Davim J.P., Barricas N., Conceicao M., Oliveira C. (2008) Some experimental studies on CO_2 laser cutting quality of polymeric materials. *Journal of Materials Processing Technology* **198** 99-104.

67. Nielsen S.E. (1983) Laser material processing of polymers. *Polymer Testing* **3** 303-310.

68. Duncan A.C., Weisbuch F., Rouais F., Lazare S., Baquey Ch. (2002) Laser microfabricated model surfaces for controlled cell growth. *Biosensors & Bioelectronics* **17** 413-426.

69. David C., Wei J., Lippert T., Wakaun A. (2001) Diffractive grey-tone phase masks for laser ablation lithography. *Microelectronic Engineering* **57-58** 453-460.

70. Laude L.D., Martinez D., Dicara C.I., Hanus Fr., Kolev K. (2001) The ablation of polymers under excimer laser irradiation: The physics of the process and the polymer structure. *Nuclear Instruments and Methods in Physics Research B* **185** 147-155.

71. Chan C.M., Ko T.M., Hiraoka H. (1996) Polymer surface modification by plasmas and photons. *Surface Science Reports* **24** 1-54.

72. Yu F., Li P., Shen H., Mathur S., Lehr C.M., Bakowsky U., Mucklich F. (2005) Laser interference lithography as a new and efficient technique for micropatterning of biopolymer surface. *Biomaterials* **26** 2307-2312.

73. Aguilar C.A., Lu Y., Mao S., Chen S. (2005) Direct micro-patterning of biodegradable polymers using ultraviolet and femtosecond lasers. *Biomaterials* **26** 7642-7649.

74. Skordoulis C.D., Makropoulou M., Serafetinides A.A. (1995) Ablation of nylon-6,6 with UV and IR lasers. *Applied Surface Science* **86** 239-244.

75. Lawrence J., Li L. (2001) Modification of the wettability characteristics of polymethyl methacrylate (PMMA) by means of CO_2, Nd:YAG, excimer and high power diode laser irradiation. *Materials Science and Engineering A* **303** 142-149.

76. Lippert T., Wei J., Wokaun A., Hoogen N., Nuyken O. (2000) Polymers designed for laser microstructuring. *Applied Surface Science* **168** 270-272.

77. Losekrug B., Meschede A., Krebs H.U. (2007) Pulsed laser deposition of smooth poly(methyl methacrylate) films at 248nm. *Applied Surface Science* **254** 1312-1315.

78. Cristescu R., Stamatin I., Mihailescu D.E., Ghica C., Albulescu M., Mihailescu I.N., Chrisey D.B. (2004) Pulsed laser deposition of biocompatible polymers: A comparative study. *Thin Solid Films* **453-454** 262-268.

79. Chrisey D.B., Hubler G.K., (1994) *Pulsed Laser Deposition of Thin Films*, New York, USA: John Wiley & Sons Inc.

80. Rebollar E., Villavieja M.M., Gaspard S., Oujja M., Corrales T., Georgiou S., Domingo C., Bosch P., Castillejo M. (2007) Pulsed laser deposition of polymers doped with fluorescent probes. Application to environmental sensors. *Journal of Physics: Conference Series* **59** 305-309.

81. Shin D.S., Lee J.H., Kim T.H. (2006) Determination of the debris produced from poly(ethylene terephthalate) during KrF excimer laser ablation. *Applied Surface Science* **252** 2319-2327.

82. Niino H., Yabe A. (1996) Chemical surface modification of fluorocarbon polymers by excimer laser processing. *Applied Surface Science* **96-98** 550-557.

83. Laude L.D., Boutarek N., Kolev K. (1995) Excimer lasers for surface engineering of polymer-based composites. *Nuclear Instruments and Methods in Physics Research B* **105** 254-257.

84. Charbonnier M., Alami M., Romand M., Girardeau-Montaut J.P., Afif M. (1997) Laser-assisted grafting onto polycarbonate:application to metallization by chemical means. *Applied Surface Science* **109-110** 206-211.

85. Mirzadeh H., Katbab A.A., Khorsani M.T., Burford R.P., Gorgin E., Golestani A. (1995) Cell attachment to laser-induced AAm-and HEMA-grafted ethylene-propylene rubber as biomaterial: *in vivo* study. *Biomaterials* **16** 641-648.

86. Wu P.K., Ringeisen B.R., Callahan J., Brooks M., Bubb D.M., Wu H.D., Pique A., Spargo B., McGill R.A., Chrisey D.B. (2001) The deposition, structure, pattern deposition and activity of biomaterial thin-films by matrix-assisted pulsed-laser evaporation (MAPLE) and MAPLE direct write. *Thin Solid Films* **398-399** 607-614.

87. Ringeisen B.R., Chrisey D.B., Pique A., Young H.D., Modi R., Bucaro M., Jones-Meehan J., Spargo B.J. (2002) Generation of mesoscopic patterns of viable *escherichia coli* by ambient laser transfer. *Biomaterials* **23** 161-166.

88. Lawrence J., Li L. (2001) Laser Modification of the Wettability *Characteristics of Engineering Materials*, Suffolk, UK: Professional Engineering Publishing Limited.

89. Gotoh K., Nakata Y., Tagawa M., Tagawa M. (2003) Wettability of ultraviolet excimer-exposed PE, PI and PTFE films determined by the contact angle measurements. *Colloids and Surfaces A: Physiochemical and Engineering Aspects* **224** 165-173.

90. Dumitrascu N., Borcia G., Apetroaei N., Popa G. (2002) Roughness modification of surfaces treated by a pulsed dielectric barrier discharge. *Plasma Sources Science and Technology* **11** 127-134.

91. Ma M., Hill R.M. (2006) Superhydrophobic Surfaces. *Current Opinion in Colloid & Interface Science* **11** 193-202.

92. Cheng Y.T., Rodak D.E., Wong C.A., Hayden C.A. (2006) Effects of micro- and nano-structures on the self-cleaning behaviour of lotus leaves. *Nanotechnology* **17** 1359-1362.

93. Adamson A.W. (1973) Potential distortion model for contact angle and spreading II. Temperature dependant effects. *Journal of Colloidal and Interface Science* **44** 273-281.

94. De Connick J., Dunlop F. (1987) Wetting transitions and contact angles. *Europhysics Letters* **11** 1291-1296.

95. van Oss C.J., Good R.J., Chaudury M.K. (1986) The role of van der Waals forces and hydrogen bonds in hydrophobic interactions between biopolymers and low energy surfaces. *Interface Science* **111** 378-390.

96. Chibowski E. (2007) On some relations between advancing, receding and Young's contact angles. *Advances in Colloid and Interface Science* **133** 51-59.

97. Gerson D.F. (1982) An empirical equation-of-state for solid-fluid interfacial free energies. *Colloid and Polymer Science* **260** 539-544.

98. Whyman G., Bormashenko E., Stein T. (2008) The rigorous derivation of Young, Cassie-Baxter and Wenzel equations and the analysis of the contact angle hysteresis phenomenon. *Chemical Physics Letters* **450** 355-359.

99. Jakubczyk P., Napiorkowski M. (2004) The influence of droplet size on line tension. *Journal of Physics: Condensed Matter* **16** 6917-6928.

100. Bico J., Thiele U., Quere D. (2002) Wetting of textured surfaces. *Colloids and Surfaces A: Physiochemical and Engineering Aspects* **206** 41-46.

101. Jung Y.C., Bhushan B. (2007) Wetting transition of water droplets on superhydrophobic patterned surfaces. *Scripta Materialia* **57** 1057-1060.

102. Lee S.M., Kwon T.H. (2007) Effects of intrinsic hydrophobicity on wettability of polymer replicas of a superhydrophobic lotus leaf. J*ournal of Micromechanics and Microengineering* **17** 687-692.

103. Waugh D.G., Lawrence J., Morgan D.J., Thomas C.L. (2009) Interaction of CO_2 laser-modified nylon with osteoblast cells in relation to wettability. *Materials Science and Engineering C* **29** 2514-2524.

104. Waugh D.G., Lawrence J., Walton C.D., Zakaria R.B. (2010) On the effects of using CO_2 and F_2 lasers to modify the wettability of a polymeric biomaterial. *Optics and Laser Technology* **42** 347-356.

105. Jaycock M.J., Parfitt G.D. (1981) *Chemistry of Interfaces*, Chichester, UK: John Wiley.

106. Zisman W.A. (1964) *Chapter 1 - Relation of Equilibrium Contact Angle to Liquid and Solid Constitution*, In: Fowkes F.M. (ed.) *Contact Angle, Wettability and Adhesion*, Washington DC, USA: American Chemical Society, pp.1-51.

107. Zisman W.A. (1963) Influence of constitution on adhesion. *Industrial and Engineering Chemistry Research* **55** 19-38.

108. Rance D.G. (1982) *Chapter 6 - Thermodynamics of Wetting: From its Molecular Basis to Technological Application*, In: Brewis D.M. (ed.) *Surface Analysis and Pretreatment of Plastics and Metals*, Essex, UK: Applied Science Publishers, p.121.

109. Tavana H., Jehnichen D., Grundke K., Hair M.L., Neumann A.W. (2007) Contact angle hysteresis on fluoropolymer surfaces. *Advances in Colloid and Interface Science* **134-135** 236-248.

110. Chibowski E. (2005) Surface free energy and wettability of silyl layers on silicon determined from contact angle hysteresis. *Advances in Colloid and Interface Science* **113** 121-131.

111. Davies J.T., Rideal E.K. (1963) *Interfacial Phenomena*, New York, USA: Academic Press.

112. Michalski M., Saramango B.J.V. (2000) Static and dynamic wetting behaviour of triglycerides on solid surfaces. *Journal of Colloidal and Interface Science* **227** 380-389.

113. Sikalo S., Tropea C., Ganic E.N. (2005) Dynamic wetting angle of a spreading droplet. *Experimental Thermal and Fluid Science* **29** 795-802.

114. Wei Q., Liu Y., Hou D., Huang F. (2007) Dynamic wetting behavior of plasma treated PET fibers. *Journal of Materials Processing Technology* **194** 89-92.

115. Blake T.D., Bracke M., Shikhmurzaev Y.M. (1999) Experimental evidence of nonlocal hydrodynamic influence on the dynamic contact angle. *Physics of Fluids* **11** 1995-2007.

116. Wang X.D., Peng X.F., Lu J.F., Liu T., Wang B.X. (2004) Contact angle hysteresis on rough solid surfaces. *Heat Transfer - Asian Research* **33** 201-210.

117. McNutt J.E., Andes G.M. (1959) Relationship of the contact angle to interfacial energies. *Journal of Chemical Physics* **30** 1300-1303.

118. Adam N.K., Elliott G.E.P. (1958) The effects of high temperature variations on contact angle measurements of vitreous enamels. *Journal of Chemical Society* **18** 2206-2215.

119. Fowkes F.M. (1964) Attractive forces at interfaces. Industrial and Engineering Chemistry Research **56** 40-52.

120. Zenkiewicz M. (2007) Methods for calculation of surface free energy of solids. *Journal of Achievements in Materials and Manufacturing Engineering* **24** 137-145.

121. Johnson R.E. Jr., Dettre R.H. (1969) *Wettability and Contact Angles*, In: Matijevic E. (ed.) *Surface and Colloid Science*, New York, USA, Wiley-Interscience.

122. Johnson R.E, Dettre R.H. (1964) *Contact Angle Hysteresis. Contact Angle, Wettability and Adhesion*, Washington DC, USA: American Chemical Society, p.112.

123. Wenzel R.N. (1936) Resistance of Solid Surfaces to Wetting by Water. *Industrial and Engineering Chemistry Research* **28** 988-994.

124. Good D.J. (1952) A Thermodynamic Derivation of Wenzel's Modification of Young's Equation for Contact Angles; Together with a Theory of Hysteresis. *Journal of the American Chemical Society* **74** 5041-5042.

125. Schwartz A.M., Minor F.W. (1959) Contact Angle Hysteresis: The Effects of Surface Condition. *Journal of Colloid Science* **61** 1068-1078.

126. Cassie A.B.D., Baxter S. (1944) Wettability of Porous Surfaces. *Transactions of the Faraday Society* **40** 546-551.

127. Zhou X.B., de Hosson J.Th.M. (1995) The Influence of Surface Roughness on the Wetting Angle. *Journal of Materials Research* **10** 1984-1992.

128. Neumann A.W. (1974) Contact angles: Thermodynamic status, measurement, interpretation and application. *Advances in Colloid and Interface Science* **4** 105-191.

129. Neumann A.W., Good R.J. (1972) Thermodynamics of contact angles. I: Heterogeneous solid surfaces. *Journal of Colloid and Interface Science* **38** 341-358.

130. Chen X., Lu T. (2009) The apparent state of droplets on a rough surface. *Science in China Series G: Physics Mechanics and Astronomy* **52** 233-238.

131. Wu X., Zheng L., Wu D. (2005) Fabrication of superhydrophobic surfaces from microstructured ZnO-based surfaces via a wet-chemical route. *Langmuir* **21** 2665-2667.

132. Ma Z., Mao Z., Gao C. (2007) Surface modification and property analysis of biomedical polymers used for tissue engineering. *Colloids and Surfaces B: Biointerfaces* **60** 137-157.

133. O'Connell C., Sherlock R., Ball M.D., Aszalos-Kiss B., Prendergast U., Glynn T.J. (2009) Investigation of the hydrophobic recovery of various polymeric biomaterials after 172nm UV treatment using contact angle, surface free energy and XPS measurements. *Applied Surface Science* **255** 4405-4413.

134. Pimanpang S., Wang P.I., Senkevich J.J., Wang G.C., Lu T.M. (2006) Effect of hydrophilic group on water droplet contact angles on surfaces of acid modified SiLK and parylene polymers. *Colloids and Surfaces A: Physiochemical and Engineering Aspects* **278** 53-59.

135. Kim J., Chaudhury M.K., Owen M.J., Orbeck T. (2001) The mechanisms of hydrophobic recovery of polydimethylsiloxane elastomers exposed to partial electrical discharges. *Journal of Colloid and Interface Science* **244** 200-207.

136. Giliberti D.C. (2002) *Control of Cell-Biomaterial Interactions*, In: Dumitriu S. (ed.) *Polymeric Biomaterials: Second Edition*, New York, USA: Marcel Dekker, 2002. p. 361.

137. Xu L., Siedlecki C.A. (2007) Effects of surface wettability and contact time on protein adhesion to biomaterial surfaces. *Biomaterials* **28** 3273-3283.

138. Wirth C., Grosgogeat B., Lagneau C., Jaffrezic-Renault N., Ponsonnet L. (2008) Biomaterial surface properties modulate *in vitro* rat calvaria osteoblasts response: Roughness and or chemistry? *Materials Science and Engineering C: Biomimetc and Supramolecular Systems* **28** 990-1001.

139. Amin W.M., Ritchie G.M., Fletcher A.M. (1981) A mechanical analysis of the physical bonding properties of soft lining materials to PMMA. *International Journal of Adhesion and Adhesives* **1** 323-327.

140. Carew E.O. (2004) Chapter 1 - *Properties of Materials*, In: Ratner B.D. (ed.) *Biomaterials Science: Second Edition*, San Diego, California, USA: Elsevier Academic Press, p.23.

141. Vogler E.A. (1993) *Interfacial Chemistry in Biomaterials Science*, New York, USA: Marcel Dekker, p.184.

142. van Oss C.J., Gillman C.F., Neumann A.W. (1975) *Phagocytic Engulfment and Cell Adhesiveness*, New York, USA: Marcel Dekker.

143. Spijker H.T., Graaff R., Boonstra W., Busscher H.J., van Oeveren W. (2003) On the influence of flow conditions and wettability on blood material interactions. *Biomaterials* **24** 4717-4727.

144. Nuzzo R.G., Dubois L.H., Allara D.L. (1990) Fundamental studies of microscopic wetting on organic surfaces. I. formation and structural characterization of a self-consistent series of polyfunctional organic monolayers. *Journal of the American Chemical Society* **112** 558-569.

145. Laibinis P.E., Whitesides G.M., Allara D.L., Tao Y.T., Parikh A.N., Nuzzo R.G. (1992) Comparison of the structures and wetting properties of self-assembled monolayers of n-alkanethiols on the coinage metal surfaces, Cu, Ag, Au. *Journal of the American Chemical Society* **113** 7152-7167.

146. Botero A.E.C., Torem M.L., de Mesquita L.M.S., Surface chemistry fundamentals of biosorption of *Rhodococcus opacus* and its effect in calcite and magnesite flotation. *Minerals Engineering* **21** 83-92.

147. Van Oss C.J. (1989) Energetics of cell-cell and cell-biopolymer interactions. *Cell Biochemistry and Biophysics* **14** 1-16.

148. Sushko M.L., Shluger A.L. (2007) DLVO theory for like-charged polyelectrolyte and surface interactions. *Materials Science and Engineering C: Biomimetic and Supramolecular Systems* **27** 1090-1095.

149. Stewart M.G., Moy E., Chang G., Zingg W., Neumann A.W. (1989) Thermodynamic model for cell spreading. *Colloids and Surfaces* **42** 215-232.

150. Ratner B.D. (2004) Introduction: Degradation of Materials in the Biological Environment. In: Ratner B.D. (ed.) *Biomaterials Science: Second Edition*, San Diego, California, USA: Elsevier Academic Press, p.411.

151. Coury A.J. (2004) *Chemical and Biochemical Degradation of Polymers*, In: Ratner B.D. (ed.) *Biomaterials Science: Second Edition*, San Diego, California, USA: Elsevier Academic Press, p.411.

152. Coury A.J. (2004) *Degradation of Materials in the Biological Environment*, In: Ratner B.D. (ed.) *Biomaterials Science: Second Edition*, San Diego, California, USA: Elsevier Academic Press, p.411.

153. Schoen F.J., Levy R.J. (2004) *Pathological Calcification of Biomaterials*, In: Ratner B.D. (ed.) *Biomaterials Science: Second Edition*, San Diego, California, USA: Elsevier Academic Press, p.439.

154. Roach P., Eglin D., Rohde K., Perry C.C. (2007) Modern biomaterials: a review-bulk properties and implications of surface modifications. *Journal of Material Science: Materials in Medicine* **18** 1263-1277.

155. Hao L., Lawrence J., Li L. (2005) The wettability modification of bio-grade stainless steel in contact with simulated physiological liquids by the means of laser irradiation. *Applied Surface Science* **247** 453-457.

156. Nagano M., Kitsugi T., Nakamura T., Kokubo T., Tanahashi M. (1996) Bone bonding ability of an apatite-coated polymer produced using a biomimetic method: A mechanical and histological study *in vivo*. *Journal of Biomedical Materials Research* **31** 487-494.

157. Rey C. (1998) Orthopedic biomaterials, bioactivity, biodegradation; a physical-chemical approach. *Journal of Biomechanics* **31** 182.

158. Uchida M., Kim H., Kokubo T., Tanaka K., Nakamura T. (2002) Structural dependence of apatite formation on zirconia gels in a simulated body fluid. *Journal of the Ceramic Society of Japan* **110** 710-715.

159. Zhao Q., Liu Y., Wang C., Wang S. (2007) Evaluation of bacterial adhesion on Si-doped diamond-like carbon films. *Applied Surface Science* **253** 7254-7259.

160. Lawrence J., Hao L., Chew H.R. (2006) On the correlation between Nd:YAG laser-induced wettability characteristics modification and osteoblast cell bioactivity on a titanium alloy. *Surface and Coatings Technology* **200** 5581-5589.

161. Williams D.F. (2008) On the mechanisms of biocompatibility. *Biomaterials* **29** 2941-2953.

162. Chauvel-Lebret D.J., Auroy P., Bonnaure-Mallet M. (2001) *Chapter 13 - Biocompatibility of Elastomer*, In: Dumitriu S. (ed.) *Polymeric Biomaterials. 2nd Edition*, Boca Raton, FL, USA: CRC Press Taylor & Francis Group, pp.311-360.

163. Fauran-Clavel M.J., Oustrin J. (1986) Alkaline phosphatase and bone calcium parameters. *Bone* **7** 95-99.

164. De Renzo A., Micera V., Vaglio S., Luciano L., Selleri C., Rotoli B. (1990) Induction of alkaline phosphatase activity in chronic myeloid leukemia cells: *In vitro* studies and speculative hypotheses. *American Journal of Hematology* **35** 278-280.

165. Arwin H. (2000) Ellipsometry on thin organic layers of biological interest: characterization and applications. *Thin Solid Films* **377-378** 48-56.

166. Cuypers P.A., Hermens W.T., Hemker H.C. (1978) Ellipsometry as a tool to study protein films at liquid-solid interfaces. *Analytical Biochemistry* **84** 56-67.

167. Elwing H. (1998) Protein absorption and ellipsometry in biomaterial research. *Biomaterials* **19** 397-406.

168. Anderson J.M., Schoen F.J. (2004) *In Vivo Assessment of Tissue Compatibility*, In: Ratner B.D. (ed.) *Biomaterials Science: Second Edition*, San Diego, California, USA: Elsevier Academic Press, p.360. 163. Anderson J.M. (2004) *Biological Testing of Biomaterials*, In: Ratner B.D. (ed.) *Biomaterials Science: Second Edition*, San Diego, California, USA: Elsevier Academic Press, p.355.

169. Anderson, James M. et al. Biological testing of biomaterials. In: Ratner BD, editor. Biomaterials Science. Second ed. San Diego, California, USA: Elsevier Academic Press, 2004. p. 355.

170. Cheng Y.T., Rodak D.E. (2005) Is the lotus leaf superhydrophobic? *Applied Physics Letters* **86** 144101/1-144101/3.

171. Yoon T.O., Shin H.J., Jeoung S.C., Park Y.I. (2008) Formation of superhydrophobic poly(dimethysiloxane) by ultrafast laser-induced surface modification. *Optics Express* **16** 12715-12725.

172. Zorba V., Stratakis E., Barberooglou M., Spanakis E., Tzanetakis P., Anastasiadis S.H., Fotakis C. (2008) Biomimetic artificial surfaces quantitatively reproduce the water repellency of a lotus leaf. *Advanced Materials* **20** 4049-4054.

173. Kietzig A.M., Hatzikiriakos S.G., Englezos P. (2009) Patterned superhydrophobic metallic surfaces. *Langmuir* **25** 4821-4827.

174. Ross G.G., Chasse M., Bolduc M. (2003) Effect of ageing on wettability of quartz surfaces modified by Ar implantation. *Journal of Physics D: Applied Physics* **36** 1001-1008.

175. Li Y., Pham J.Q., Johnston K.P., Green P.F. (2007) Contact angle of water on polystyrene thin films: Effects of CO_2 environment and film thickness. *Langmuir* **23** 9785-9793.

176. Hansen G., Hamouda A.A., Denoyel R. (2000) The effect of pressure on contact angles and wettability in the mica/water/n-decane system and the calcite+stearic acid/water/n-decane system. *Colloids and Surfaces A: Physicochemical and Engineering Aspects* **172** 7-16.

177. Siemons N., Bruining H., Castelijns H., Wolf K.H. (2006) Pressure dependence of the contact angle in a CO_2-H_2O-coal system. *Journal of Colloid and Interface Science* **297** 755-761.

178. Lim J.Y., Hansen J.C., Siedlecki C.A., Runt J., Donahue H.J. (2005) Human foetal osteoblastic cell response to polymer-demixed nanotopographic interfaces. *Journal of the Royal Society Interface* **2** 97-108.

179. Hao L., Lawrence J., Lin L. (2005) Manipulation of the osteoblast response to a Ti-6Al-4V titanium alloy using a high power diode laser. *Applied Surface Science* **247** 602-606.

180. Nebe B., Luthen F., Lange R., Becker P., Beck U., Rychly J. (2004) Topography-induced alterations in adhesion structures affect mineralization in human osteoblasts on titanium. *Materials Science and Engineering C* **24** 619-624.

181. Sigma-Aldrich (2008) Nylon 6,6 Material Safety Data Sheet - Version 3.0. 2008.

182. Cook S.D., Ryaby J.P., McCabe J.R.N., Frey J.J., Heckman J.D., Kristiansen T.K. (1997) Acceleration of tibia and distal radius fracture healing in patients who smoke. *Clinical Orthopaedics and Related Research* **337** 198-207.

183. Karaca E., Hockenberger A.S. (2008) Analysis of the Fracture Morphology of Polyamide, Polyester, Polypropylene, and Silk Sutures Before and After Implantation In Vivo. *Journal of Biomedical Materials Research Part B: Applied Biomaterials* **2** 580-589.

184. Dadsetan M., Mirzadeh H., Sharifi-Sanjani N., Daliri M. (2001) Cell behaviour on laser surface-modified polyethylene terephthalate *in vitro*. *Journal of Biomedical Material Research* **57** 183-189.